Tires, Suspension and Handling

Second Edition

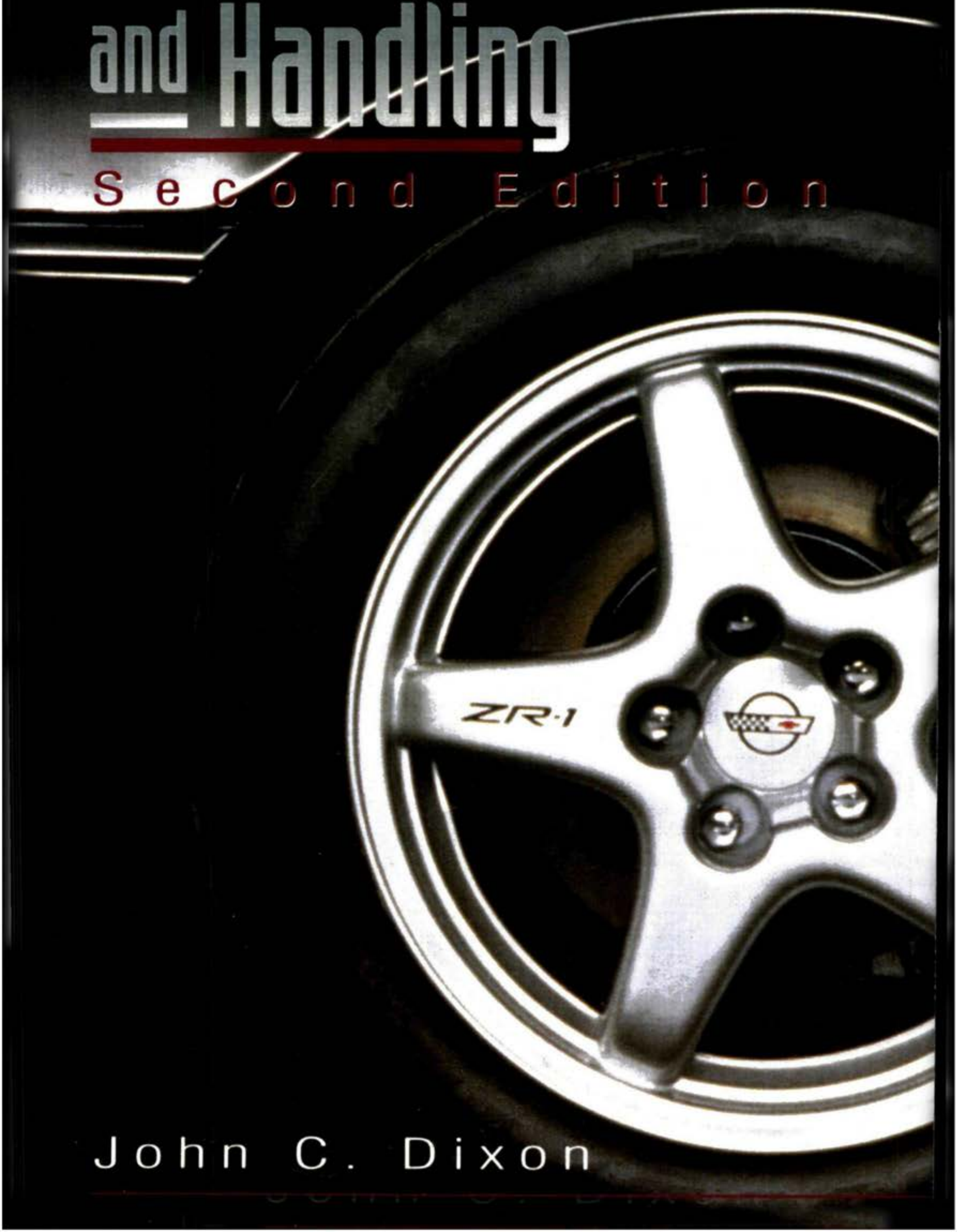

John C. Dixon

Tires, Suspension and Handling

Second Edition

John C. Dixon

Senior Lecturer in Engineering Mechanics
The Open University, Great Britain

Society of Automotive Engineers, Inc.
Warrendale, Pa.

A member of the Hodder Headline Group
London

Copyright © 1996 Society of Automotive Engineers, Inc. eISBN: 978-0-7680-6289-2

Disclaimer: This book is not intended as a guide for vehicle modification, and anyone who uses it as such does so entirely at his own risk. Testing vehicle performance may be dangerous. The author and publisher are not liable for consequential damage arising from application of any information in this book.

Copyright © 1996 Society of Automotive Engineers, Inc.

All rights reserved. Printed in the United States of America.

First edition published 1991 by Cambridge University Press, U.K.

Copublished in the rest of the World by
Arnold
A member of the Hodder Headline Group
338 Euston Road
London NW1 3BH

A catalogue record of this book is available from the British Library

Arnold ISBN 0 340 67796 1

Society of Automotive Engineers, Inc.
400 Commonwealth Drive
Warrendale, PA 15096-0001
Phone: (412) 776-4841 Fax: (412) 776-5760

Library of Congress Cataloging-in-Publication Data

Dixon, John C., 1948-
Tires, suspension, and handling / John C. Dixon. —2nd ed.
p. cm.
First ed. publisher under title: Tyres, suspension, and handling.
Includes bibliographical references and index.
ISBN 1-56091-831-4 (hardcover)
1. Automobiles—Handling characteristics. 2. Automobiles—Springs and suspension.
3. Automobiles—Tires. I. Dixon, John C., 1948- Tyres, suspension, and handling. II. Title.
TL245.5.D58 1996 96-27115
629.23'1—dc20 CIP

SAE ISBN 1-56091-831-4

Permission to photocopy for internal or personal use, or the internal or personal use of specific clients, is granted by SAE for libraries and other users registered with the Copyright Clearance Center (CCC), provided that the base fee of $.50 per page is paid directly to CCC, 222 Rosewood Dr., Danvers, MA 01923. Special requests should be addressed to the SAE Publications Group.
1-56091-831-4/96 $.50.

SAE Order No. R-168

To Anne

Contents

Preface to Second Edition xi

Preface to First Edition xiii

1 Introduction 1

1.1 Introduction and History 1
1.2 Control, Stability and Handling 6
1.3 Axis Systems and Notation 7
1.4 Vehicle Forces and Notation 12
1.5 Body Stiffness 15
1.6 Body Inertia 17
1.7 Loads 29
1.8 Engine and Brakes 32
1.9 Differentials 36
1.10 Wheels 41
1.11 Roads 46
1.12 Drivers 52
1.13 Testing 54
1.14 Problems 61
1.15 Bibliography 64

2 The Tire 67

2.1 Introduction 67
2.2 Construction 68
2.3 Rubber 72
2.4 Axes and Notation 76
2.5 Tire Radius 80
2.6 Speed Limitations 83
2.7 Rolling Resistance 85
2.8 Tire Models 87
2.9 Slip Angle and Cornering Force 90
2.10 Non-Dimensionalization 101
2.11 Improved Friction Model 104
2.12 Camber Angle and Camber Force 106
2.13 Experimental Measurements 109
2.14 Stiffness Measurements 111
2.15 Stiffness – Design Variables 116
2.16 Friction Forces – Design Variables 118
2.17 Longitudinal Forces 125
2.18 Combined Forces 129
2.19 Wet Surfaces 131
2.20 Tire Models 136
2.21 Tire Transients 137
2.22 Problems 138
2.23 Bibliography 143

3 Aerodynamics 145

3.1 Introduction 145
3.2 Atmospheric Properties 146
3.3 Wind and Turbulence 150
3.4 Principles 154
3.5 Forces and Moments 159
3.6 Coefficient Values 165
3.7 Competition Vehicles 171
3.8 Problems 178
3.9 Bibliography 180

4 **Suspension Components** 181

4.1 Introduction 181
4.2 Mobility Analysis 182
4.3 Straight-Line Mechanisms 185
4.4 Two-Dimensional Analysis 192
4.5 Independent Systems 194
4.6 Dependent Systems 199
4.7 Compliant Link Systems 202
4.8 Spring Types 204
4.9 Spring Linkage Geometry 206
4.10 Roll and Pitch Springing 209
4.11 Damper Types 211
4.12 Damper Characteristics 215
4.13 Parasitic Friction 219
4.14 Inertia 221
4.15 Gyroscopic Effects 223
4.16 Problems 223

5 **Suspension Characteristics** 225

5.1 Introduction 225
5.2 Bump and Heave 225
5.3 Roll 234
5.4 The Roll-Center 238
5.5 Independent Suspension Roll-Centers – Part 1 242
5.6 Independent Suspension Roll-Centers – Part 2 246
5.7 Solid-Axle Roll-Centers 252
5.8 Compliant-Link Roll-Centers 253
5.9 Experimental Roll-Centers 256
5.10 Suspension Load Transfer 257
5.11 Vehicle Load Transfer 263
5.12 Pitch 271
5.13 Wheel Vertical Forces 278
5.14 Steering 283
5.15 Turning Geometry 292
5.16 Bump-Steer and Roll-Steer 296
5.17 Compliance Steer 309
5.18 Ride Height 315

5.19 Problems 318
5.20 Bibliography 330

6 **Steady-State Handling** 331

6.1 Introduction 331
6.2 Parameters 332
6.3 Basic Handling Curve 335
6.4 Cornering Forces 342
6.5 Linear Theory 345
6.6 Vehicle Cornering Stiffnesses 351
6.7 Nonlinear Trim State 357
6.8 Nonlinear Theory 359
6.9 Understeer and Oversteer 361
6.10 Primary Handling 364
6.11 Secondary Handling 376
6.12 Final Handling 379
6.13 Differentials 387
6.14 Aerodynamics – Primary 391
6.15 Aerodynamics – Final 396
6.16 Path Radius 404
6.17 Banking 407
6.18 Hills 410
6.19 Loading 412
6.20 Wind 415
6.21 Testing 416
6.22 Moment Method 418
6.23 Desirable Results 420
6.24 Problems 422
6.25 Bibliography 429

7 **Unsteady-State Handling** 431

7.1 Introduction 431
7.2 1-dof Vibration 432
7.3 1-dof Sideslip 437
7.4 1-dof Yaw 439
7.5 2-dof Model (Vehicle-fixed Axes) 443
7.6 2-dof Model (Earth-fixed Axes) 447
7.7 2-dof Free Response 450

7.8 Improved 2-dof Model 461
7.9 Stability Derivatives 462
7.10 3-dof Model 464
7.11 Step-Steer Response 467
7.12 Oscillatory Steer Response 472
7.13 Power Steer 476
7.14 Disturbance Response 478
7.15 Testing 480
7.16 Desirable Results 481
7.17 Problems 484
7.18 Bibliography 486

Appendices

A Nomenclature 489
B Properties of Air and Water 501
C Example Car Specifications 507
D Selected Problem Solutions 515
E SAE J670e 521

References 557

Index 565

Preface to Second Edition

The first edition, published by Cambridge University Press in 1991, was well received in Europe but received limited exposure in the U.S.

I am therefore delighted that this edition has been adopted by the SAE who are ideal publishers for this subject matter.

The original policy was to give a thorough presentation of the principles of road vehicle handling theory, concentrating on the timeless core of the theory rather than elaborating temporary fancies. This approach seems to have been justified, as all the material continues to be relevant and useful.

The general contents of the second edition are therefore unchanged. However, the opportunity has been taken to make numerous detail additions and improvements. The small number of known errors have, of course, all been corrected.

I would like to express my appreciation to those who have offered suggestions for improvements to the earlier edition, and would like to invite readers to continue this process.

Finally, thanks to Rebecca McCormack, Sheila McBrearty, Morine Gordon and Sharon Lumbers for so patiently performing the text revisions, to the Faculty of Technology of The Open University for allowing me the time to continue developing this text, and to the SAE staff for final text preparation.

John Dixon, Faculty of Technology, The Open University
Milton Keynes, Buckinghamshire, England

Preface to First Edition

Some years ago I wanted to read a book explaining the principles of vehicle handling, with supporting information on tires and suspensions. Although there were two books available, they did not entirely meet my needs. This is my attempt to fill the gap.

I have emphasized physical understanding rather than mathematics, although I have been surprised by the number of equations that have been required in the chapters on handling.

I have included a fairly large number of questions, with answers for most of the quantitative ones. These questions should help self-organised study or act as stimulants for those using the book as a teaching aid.

I have been fortunate to have received constructive criticism of early drafts from a number of friends and colleagues. Thank you all. Especially I must mention John Dominy, Keith Martin, Rod Mansfield and John Whitehead. I have not always taken their advice. Of course, in a work of this kind one owes a great deal to the enormous number of authors of the vast research literature. No doubt there are still some technical faults in the material, for which I must remain responsible, and I would be delighted to be advised of corrections or to receive suggestions for possible improvements.

Certainly much more remains to be said on the subject area of this book, and I hope only that it will be seen as a reasonably thorough introduction.

Finally, thanks to Carla Walton, Mavis Beard and Rebecca McCormack for help with word processing, to David Greenway for the diagrams, and to Garry Hammond who performed the final text preparation and editing on behalf of Cambridge University Press.

1

Introduction

1.1 Introduction and History

The automobile, or horseless carriage, as it was originally known, appeared at the end of the 19th Century, approximately one hundred years ago, a direct consequence of the availability of suitable internal-combustion engines.

The design of automobiles evolved from that of the horse-drawn carriage, itself the culmination of several thousand years of slow evolution from early carts and chariots. At the time of arrival of the automobile, carriages already had suspension systems, very desirable in view of the poor roads at the time. There was therefore already a body of knowledge regarding ride quality and suspension systems. However, virtually no published material existed concerning investigation of handling qualities.

It is interesting to speculate what sort of concept of handling the earliest chariot engineers may have had. Perhaps the most obvious requirement of a high-performance chariot is a small mass. Certainly, the importance of this was appreciated at least 2000 years ago. The wheels were so light that they were removed when not in use (e.g., overnight) to obviate eccentricity and lack of roundness due to creep.

Early carts had steering in which the entire front axle pivoted about a vertical central pivot. Lightweight chariots were two-wheeled, so yawing could be achieved by relative rotation of the wheels, and the need for steering as such did not arise. The traditional horse-drawn carriage of the 18th and 19th Centuries had rigid axles front and rear; steering of the complete front axle about its central pivot naturally left the wheels perpendicular to radii from a notional center of the path arc. However, steering by movement of the complete axle was inconvenient, requiring large clearance around the wheels, so steering by pivoting the wheels separately on stub axles was introduced. In 1816 Georges Langensperger stated the geometric condition required for stub-axle steering to maintain the wheels perpendicular to their arc of motion. Such an arrangement was highly desirable to minimize friction at the wheels during low-speed maneuvering on small radii. This is still the case, although conditions are different at higher speeds. Ackermann recognized the importance of this invention; by agreement with Langensperger, acting as his agent in London, he took out British patents in 1817, and hence this arrangement is widely known as Ackermann steering. Some sixty years later, Amadée Bollée, in designs of 1873 and 1878, achieved a similar effect, possibly independently. From 1878 to 1881 Jeantaud arrived at the same arrangement, and performed some more scientific assessments. As a result, Langensperger's principle is known in France as the Jeantaud diagram. In 1893 Benz was granted a German patent for another arrangement, similar to Bollée's later type. By the time of the introduction of the automobile, then, stub axle steering was well established, and cars adopted this system from the beginning.

The above steering designs were all kinematic in concept, in that there was no recognition of a need for side forces or of the means by which such forces might arise. The dynamic concept of cornering began only at the start of the 20th Century. In 1907 Lanchester used the term "oversteer" in a paper to the Institution of Automobile Engineers (IAE):

> "In practice even the inertia of the hand and arm of the driver of a car with bath-chair steering tells its tale in the slightly zigzag course to which such cars are liable, each small steering effort becomes overdone, the car 'oversteers,' and its track is reminiscent of the motion of a water-fly."

The first significant steps toward a modern dynamic concept of cornering, rather than just a kinematic concept, had to be the recognition of the need for lateral forces and the presence of the slip angle that produces them. The term "slip" was used in an IAE paper by Kersey (1921)[1], in relation to toe-in and camber, with emphasis on the effective lateral velocity component. Healey (1924) included several pages on handling effects, but did not mention the terms understeer or oversteer. Credit for recognition of the concept of slip angle and its significance is usually given to Georges Broulhiet, who called it *envirage* in his 1925 paper to the French Institution of Civil Engineers.

---

[1] References are generally given at the end of the book; early historical references are not all given here, but may be found in Milliken & Whitcomb (1956).

Bradley and Allen (IAE 1930) investigated the friction properties of road surfaces and published what is probably the first graph of a tire side force against an angle, although the angle shown is not precisely that of the wheel relative to its ground motion, but the rigging angle of a motorcycle sidecar wheel. In fact, they were not interested in cornering *per se*, but in braking, and simply considered a rotating wheel at a large slip angle to be a good way to investigate the effects of road surface properties on maximum grip, the rotation preventing local overheating and excessive wear. This paper was conspicuously more scientific than much that went before regarding tire forces, and includes investigation of the effect of tread form and speed on tire friction with various surfaces.

In 1931 a study of steering vibrations by Becker, Fromm and Maruhn drew further attention to the mechanical properties of the tire. This included results of tests of tires on a rotating steel drum, and was the first paper to record some of the characteristics of tire cornering stiffness. Broulhiet presented a paper to the Society of Automotive Engineers (SAE) in 1933 on European ideas about independent suspension, including a description of his *envirage*. Olley (1934), describing work at Cadillac, included a diagram, Figure 1.1.1, and some discussion that indicates that the significance of the relationship between front and rear slip angles was understood, at least in principle.

It is interesting that the terms understeer and oversteer were not used in the 1934 paper, although they were used in an unpublished General Motors report by Olley in 1937, which indicated that in 1931 roll steer and tire pressures were known to be very important in controlling stability. Olley is generally given credit for the concept and interpretation of linear understeer and oversteer. Olley's 1934 paper shows that the basic relationships governing tire forces and slip angles were known, but it remained for Evans of Goodyear to make comprehensive investigations, which were published in 1935; Figure 1.1.2 shows his principal result.

In 1937, Bastow, giving a forward reference to Olley's 1938 paper, used the terms understeer and oversteer, and discussed roll steer effects on independent front suspensions and on leaf-spring supported axles. In 1938, in an IAE paper, Olley gave a more detailed description of handling behavior, including graphs of path curvature against speed, and of front wheel angle against lateral acceleration. The terms understeer and oversteer were included and described as "just coming into general use (oversteer was first used in 1932)" [sic]. (Statement in parentheses is incorrect.) Critical speed was included, with comments on the effect of lateral load transfer. Mathematical simulation results were claimed to be within 5%, presumably for steady state. Later in 1938, Law described factors affecting tire cornering stiffness, commented on handling behavior, and stated:

> "Automobile engineers have become familiar with the terms 'over-steering' and 'under-steering'..."

Thus, by the mid-1930s, all the important ingredients of a theory of handling were available, and by the late 1930s reasonable mathematical steady-state models were in use (Fox, 1937, and Olley, 1938) although details were not published. Attention soon turned to transient behavior (Stonex, 1941), although it was to be three decades before a comprehensive transient-response analysis was achieved, even for low lateral accelerations.

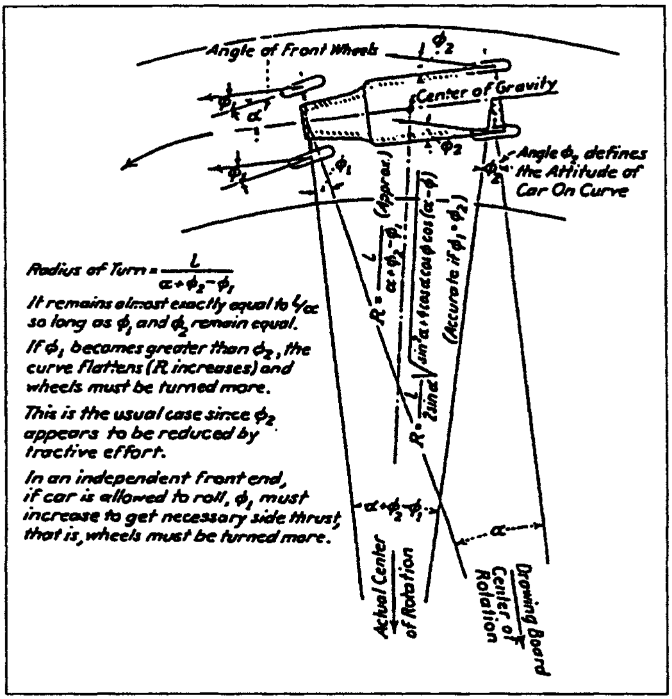
Angle of Front Wheels
ϕ_2
Center of Gravity
ϕ_1
α
ϕ_2
ϕ_1
Angle ϕ_2 defines the Attitude of Car On Curve
Radius of Turn = $\frac{L}{\alpha+\phi_2-\phi_1}$
It remains almost exactly equal to L/α so long as ϕ_1 and ϕ_2 remain equal.
If ϕ_1 becomes greater than ϕ_2, the curve flattens (R increases) and wheels must be turned more.
This is the usual case since ϕ_2 appears to be reduced by tractive effort.
In an independent front end, if car is allowed to roll, ϕ_1 must increase to get necessary side thrust, that is, wheels must be turned more.
$R = \frac{L}{\alpha+\phi_2-\phi_1}$ (Approx.)
$R = \frac{L}{2\sin\alpha}\sqrt{\sin^2\alpha+4\sin\alpha\cos\phi\cos(\alpha-\phi)}$ (Accurate if $\phi_1 = \phi_2$)
$\alpha+\phi_2-\phi_1$
α
Actual Center of Rotation
Drawing Board Center of Rotation

Figure 1.1.1. Early handling analysis (Olley, 1934).

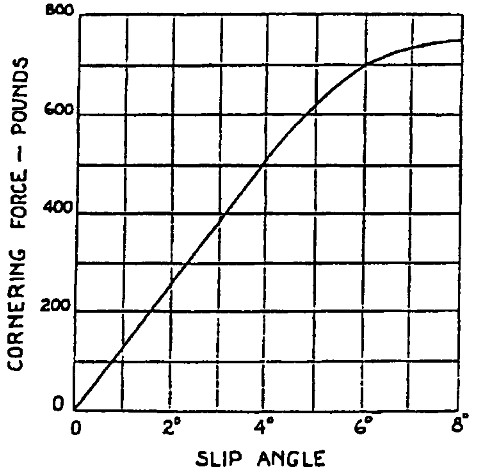

Figure 1.1.2. The first true tire cornering force curve (Evans, 1935).

German activity of the 1930s had a strong aerodynamic element. In 1938 Forster described a truck-towed tire tester and gave results, and in 1940 Rieckert & Schunk, Dietz & Harling, and Huber & Sawatzki all published details, mostly working under the direction of Kamm who reviewed this work in 1953. In 1941, von Schlippe published his model of the tire based on a stretched string analogy, successfully explaining the relaxation distance, relevant to the handling dynamics of the tires.

There was also activity in France during this period, with papers emerging from deSeze in 1937 and Gratzmüller in 1942, and then with substantial progress after the war, from Rocard in 1946, Julien in 1947 and 1948, and Lozano in 1951.

International political difficulties and language barriers obviously created problems, and the significance of the tire in vehicle behavior was not appreciated in Russia for a decade. By 1946, however, the European and American work was known to them, and, as examples, Pevsner in 1946 described testing techniques and Chudakov in 1947 included tire properties in his theoretical analysis. In the U.K., a number of papers appeared after the war (Olley 1947, Hardman 1949, Gough 1949). Progress became more rapid, not least in the area of tires (for example Joy *et al.*, 1956). The classic set of papers by Milliken, Segel and Whitcomb (I.Mech.E) in 1956 and 1957, thirty years after Broulhiet's introduction of *envirage*, applied linear control theory to give a frequency response analysis. This gave a description of the linear response regime corresponding to normal driving, with lateral accelerations of up to 3 m/s^2 (0.3g), completely apart from aerodynamics.

The following decades saw attention turning to the high lateral acceleration regime, requiring nonlinear analysis, and to the role of the driver, with closed-loop control analysis including the driver supplementing the driverless open-loop analysis. However, despite all this effort, there are still many interesting and unsolved problems in vehicle handling.

The fundamental problems have, however, largely been solved, and there is an accepted body of theory. This book presents the core theory of the subject. We shall be concerned principally with the four-wheeled vehicle – the car or light truck – operating on metalled roads. Vehicles with other than four wheels, and road surfaces of a loose or viscous kind such as gravel, mud or snow, will be mentioned only briefly. In the following part of this first chapter we shall gather together some of the ideas necessary for use in the detailed handling analyses to follow. The vehicle body will be examined for both structural stiffness and its contribution to inertia. The engine and brakes will be considered because acceleration and deceleration forces must be produced by the tire, and the call for these forces affects the ability of the tires to produce lateral forces for cornering. The various types of differential are considered, and road characteristics will be studied because this is one-half of the tire–road interaction, and on a large scale it is the principal cause of maneuvering requirements. The atmosphere will be considered because this affects aerodynamics, through density variations and wind and wind gusts, and affects the tire–road contact patch through the presence of water, ice and snow. This chapter then considers the driver, and finally introduces testing methods.

1.2 Control, Stability and Handling

Control is action by the driver intended to influence the motion of the car. The driver seeks to exercise control over the vector velocity of the vehicle, and hence over its path. Stability refers to the unwillingness of a car to be deflected from its existing path – usually a desirable trait, in moderation. Handling is the ability of a car to round corners successfully, the study of how this occurs, and the study of the driver's perception of the vehicle's cornering behavior. The vehicle as a whole can be influenced only by forces exerted by the road, by the atmosphere and by gravity, and as a consequence we shall be interested in the aerodynamic properties of the body and the cornering force characteristics of the tires. For most practical cases the tire forces are the dominant ones, with aerodynamics playing a secondary role in handling behavior.

The road vehicle, contrasted with the air-borne or water-borne vehicle, is characterized by the all-important presence of the tire; it is essentially for this reason that road vehicle dynamics can be regarded as a separate subject in its own right. The total force exerted on the tire by the road depends on many factors including the dimensions, structure and materials of the tire, and the angle of presentation of the tire to the road. Hence it is necessary to consider in detail the tire itself, and also the suspension system characteristics. Vehicle dynamics involves the study of both lateral and longitudinal motions. Lateral motions are the subject of interest here, so most of the standard results of longitudinal motion will be taken for granted. "Cornering," then, is the main subject. The term "roadholding" is used to mean the ultimate ability of a car to execute a given maneuver given a perfect driver. "Handling" is used in a narrow sense to mean the ease with which a real driver can realize desired maneuvers, including straight running when subject to disturbances, and is also used in a wider sense to mean the same as cornering. Handling, then, is a qualitative assessment of the "manners" of a car, and will depend on both the driver and the application. We shall deal here with roadholding and handling rather than with ride, which is the ability of a car to reduce the discomfort arising from road roughness.

Figure 1.2.1 shows the driver-vehicle system as a block diagram. The section to the right of the dotted line is the open-loop system; this represents the vehicle and its behavior in response to control inputs or disturbances from the road or atmosphere. The complete system includes the driver. Because the driver takes feedback information from the vehicle motion and the steering, this is called the closed-loop system. Handling analysis may be based on the open loop alone, where tests are intended to reveal the vehicle characteristics, or on the closed loop which also involves the performance of the driver.

1.3 Axis Systems and Notation

To study the response of a vehicle to control inputs or to disturbances it is necessary to specify one or more coordinate systems to measure the position of the vehicle. The method recommended by SAE will be described here (see SAE J670e in Appendix E). It was originally developed from aeronautical practice. Broadly similar methods are used throughout engineering dynamics analysis.

First there is an Earth-fixed axis system *XYZ* (Figure 1.3.1). Upper-case letters are used to denote Earth-fixed coordinates. For all ground vehicles the Earth may be considered to be stationary. This is not true in an absolute sense – the Earth spins about its own axis, and also moves around the Sun – but the associ-

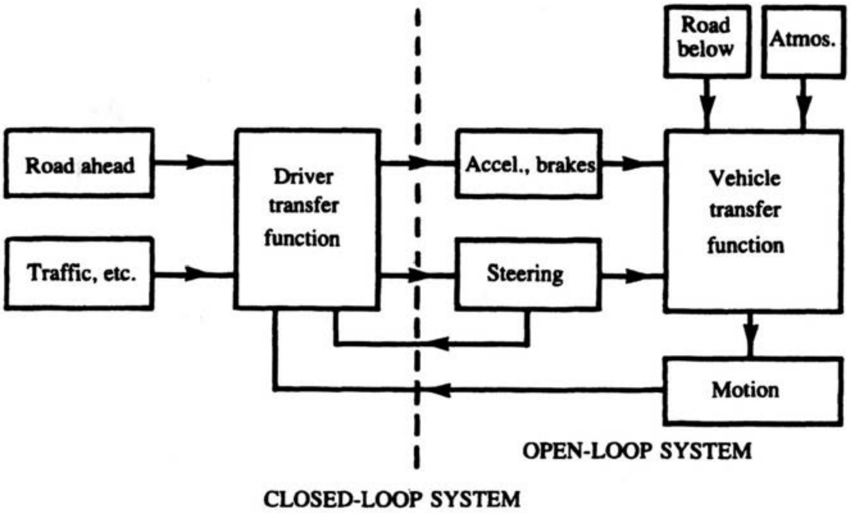

Figure 1.2.1. Driver-vehicle system block diagram

ated accelerations are small, so for our purposes the *XYZ* system is an inertial coordinate system, i.e., it has negligible acceleration. The *X*-axis is chosen longitudinally forward in the horizontal plane; *Y* is then 90° clockwise from *X* as viewed from above, and also in the horizontal plane. To form a right-hand coordinate system, the *Z*-axis is vertically downward, because this is the direction of motion of a right-hand screw turning *X* to *Y*. The origin of the *XYZ* system may be at any convenient point, typically in the ground plane. This is the SAE system. In the International Organization for Standardization (ISO) system, the *Y*-axis is to the left and the *Z*-axis is upward. There is also an axis system *xyz* (lower-case letters) fixed to the vehicle (Figure 1.3.2).

The use of upper-case *XYZ* for the Earth-fixed inertial system and lower-case *xyz* for the vehicle-fixed system follows widely accepted conventions. The origin of the *xyz* system is usually placed at the vehicle center of mass. The *x*-axis is approximately in the central plane, pointing forward, and is horizontal when the vehicle is in its usual pitch attitude; thus the pitch angle is the angle of *x* to the horizontal plane. The *y*-axis points to the driver's right, and is horizontal when the vehicle has zero roll angle; thus the roll angle is the angle between the *y*-axis and the horizontal plane. The *z*-axis is downward, again to give a right-hand system of mutually perpendicular axes. In general the vehicle has some acceleration, so the *xyz* system is a non-inertial system.

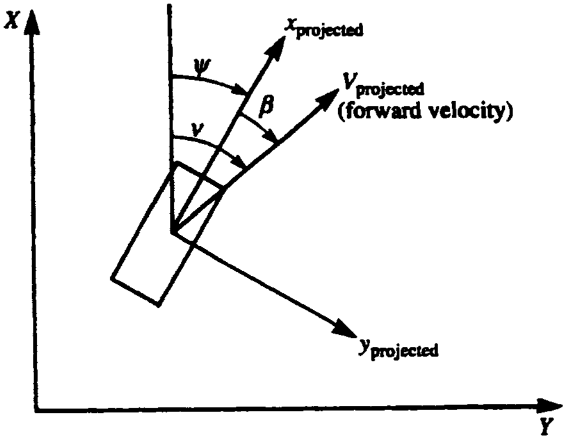
X
$x_{\text{projected}}$
ψ
$V_{\text{projected}}$
(forward velocity)
β
ν
$y_{\text{projected}}$
Y

Figure 1.3.1. Axis systems.

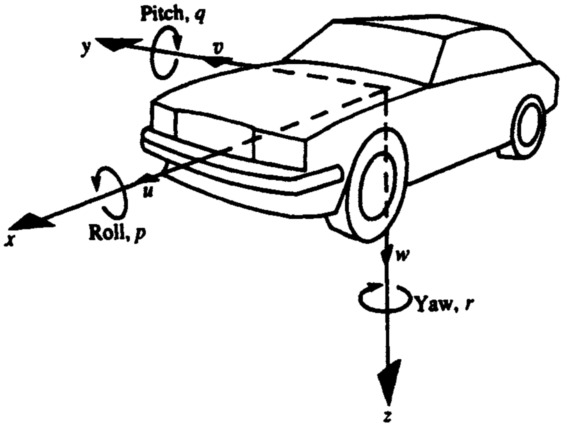
Pitch, q
y
v
x
u
Roll, p
w
Yaw, r
z

Figure 1.3.2. Vehicle-fixed axes.

The position of the vehicle, i.e., of the moving xyz axes, relative to the Earth-fixed XYZ axes, is measured by three coordinates giving the position of the origin of xyz in XYZ, and three rotations of xyz in XYZ. Angular rotations are taken as right-handed by convention, so a positive rotation corresponds to the rotation of a right-hand screw when advancing in the positive direction of the corresponding axis. The three rotations defined as standard by the SAE, starting from a position with xyz aligned with XYZ, are, in sequence:

(1) A yaw rotation ψ about the z-axis

(2) A pitch rotation θ about the y-axis

(3) A roll rotation ϕ about the x-axis

Note that the rotations are taken about the vehicle-fixed axes. (A nomenclature list for each chapter appears in Appendix A.) Roll angle ϕ is positive for a clockwise rotation seen from the rear. Pitch angle θ is positive for a nose-up position.

The translational velocity of the vehicle is taken as the velocity of its center of mass G, at the origin of xyz, measured in the system XYZ. For convenience the velocity is resolved into components along each of the xyz axes (Figure 1.3.2). There is:

(1) A longitudinal velocity u along the x-axis

(2) A side velocity v along the y-axis

(3) A normal velocity w along the z-axis

Because the x and y axes are not generally exactly parallel to the ground plane, other terms are also defined as follows. Forward velocity is the velocity component in the ground plane perpendicular to y; essentially this is the longitudinal velocity resolved into the ground plane. Lateral velocity is the velocity component in the ground plane perpendicular to the x-axis; essentially this is the side velocity resolved into the ground plane. The total velocity in the horizontal plane is the velocity tangential to the path of the vehicle center of mass. It is also convenient to define the heave velocity as the velocity component perpendicular to the ground plane, positive away from the ground ($-V_Z$). Special care is required with definition of terms if the ground plane is not horizontal.

It is sometimes convenient to use the terms heave and sway from ship dynamics. These refer, respectively, to vertical and lateral motions in linear translation without rotation.

Because the xyz axes are attached to the vehicle, the position of G is constant and it has zero velocity and acceleration in these axes. The actual acceleration of the vehicle in the XYZ system is again resolved into components parallel to the xyz axes, there being a longitudinal acceleration $\dot{u}$ along x, a side acceleration $\dot{v}$ along y, and a normal acceleration $\dot{w}$ along z. There are also lateral, forward and heave linear accelerations. Figure 1.3.3, with exaggerated attitude angle, shows how the total horizontal acceleration may be resolved into forward and lateral components, or into tangential and centripetal components. The centripetal acceleration is the component parallel to the road plane and perpendicular to the vehicle path, i.e., directed toward the path center of curvature.

The angular velocities of the vehicle are naturally measured relative to the inertial XYZ system, but are resolved about the xyz axes for convenience, to give:

(1) The roll angular speed p

(2) The pitch angular speed q

(3) The yaw angular speed r

These are expressed as rad/s or deg/s. In rotation there are roll ($\dot{p}$), pitch ($\dot{q}$) and yaw ($\dot{r}$) angular accelerations.

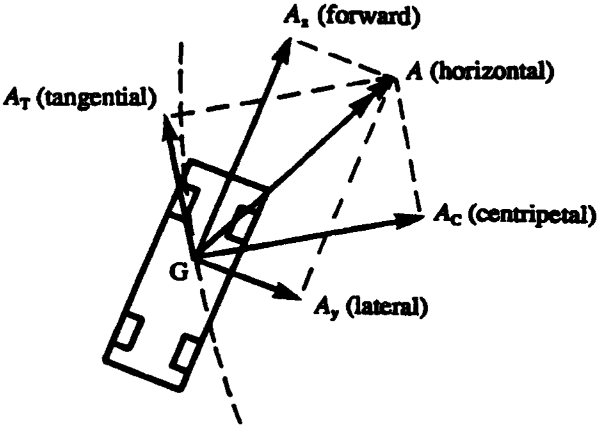

Figure 1.3.3. Acceleration components.

Referring again to Figure 1.3.1, looking down on the horizontal XY plane, we have:

(1) The angular position ψ (psi) of the projected x-axis relative to the X-axis, called the heading angle, measured positive clockwise.

(2) The angular position β (beta) of the forward velocity, relative to the projected x-axis, called the attitude angle (sometimes sideslip angle), again positive clockwise.

(3) The angular position of the velocity vector, which is tangential to the path and denoted by ν (nu), called the course angle.

Consequently

$$\nu = \psi + \beta$$

The terminology introduced here becomes familiar only with regular use. Its complexity reflects the fact that the vehicle motion is itself complex. The complete system of notation is called for only in the general approach to vehicle dynamics. Happily, many problems can be treated without the full generality, and therefore in a more easily understood form; this latter approach is the one that will be adopted throughout most of this book.

1.4 Vehicle Forces and Notation

The motion of the vehicle is governed by:

(1) The total resultant force acting on the vehicle,

(2) The total resultant moment acting on the vehicle,

(3) The translation and rotational inertial properties of the vehicle.

Expressed in its most general form we have two vector equations that can be written for the vehicle motion: force equals rate of change of linear momentum, and moment about the center of mass equals rate of change of angular momentum:

$$\mathbf{F} = \mathbf{G}$$

$$\mathbf{M} = \dot{\mathbf{H}}$$

These are the basic laws of motion as expressed by Euler. Newton's three laws of motion can all be deduced from the first of these. In practice in three-dimensional mechanics the first of Euler's two equations is much easier to apply than the second. Considering $\mathbf{F} = \dot{\mathbf{G}}$ first, by approximating the vehicle as having constant mass, this can be expressed as $\mathbf{F} = m\mathbf{A}$, or as applied in practice in a coordinate system, in three equations of the form $F_X = mA_X$ where F_X is the sum of all force components in the x-coordinate direction. Thus if all the forces on the vehicle are known with reasonable accuracy, the vehicle acceleration can be determined. In practice, in most cases the center of mass can be taken as having a fixed location relative to the vehicle body. However, this is not exact, as discussed in Section 1.6 on body inertia. The total force acting is a combination of the forces exerted by the ground on the tires, detailed in Chapter

2, of the forces exerted by the air on the body, Chapter 3, and of the weight force exerted by gravity.

The response of the vehicle to the total moment acting about the center of mass is much more difficult to determine. This is because of several factors. By neglecting the fact that there are rotating wheels, engine and drivetrain, i.e., neglecting associated gyroscopic effects (which is not necessarily a good approximation), and by using the same approximations as for the translational analysis, the vehicle can be treated as a rigid body. However, the detailed equations of motion are still complex, not least because the principal axes of inertia of the vehicle do not in general coincide with the body-fixed axes. Fortunately, most practical handling problems are adequately analyzed by dealing with simplified cases, for example by treating the vehicle as being in approximately plane motion parallel to the ground plane, so that the full generality of the equations is not required. For those readers interested in the general approach, the bibliography at the end of this chapter gives references.

Notation for forces on the vehicle follows a similar pattern to kinematic notation, including the use of the various subscripts for axis directions, and terms such as longitudinal force and side force. Notation for forces in the ground plane follows the acceleration notation of Figure 1.3.3. The centripetal force F_{C} gives the centripetal acceleration that causes path curvature. The tangential force F_{T} controls the acceleration along the path.

Figure 1.4.1(a) shows the free-body diagram of the vehicle in the ground plane, viewed in the *XYZ* inertial coordinate axes. The free-body diagram shows the chosen free body with the relevant forces that act on it. As a result of the net forces in Figure 1.4.1(a) the vehicle experiences accelerations A_{T} and A_{C} according to $\mathbf{F} = m\mathbf{A}$ in the inertial *XYZ* system. For example, the equation of motion perpendicular to the path is

$$F_{\mathrm{C}} = mA_{\mathrm{C}}$$

If we now view the vehicle in a non-inertial coordinate system, having an acceleration relative to *XYZ*, the measured vehicle acceleration in this system will be different. Thus the acceleration calculated from $\mathbf{F} = m\mathbf{A}$ will be wrong – Newton's second law fails in an accelerating coordinate system. This difficulty may be overcome by "adjusting" the free-body diagram, by adding compensation forces, or fictitious forces or d'Alembert forces as they are sometimes known, to bring the value of $\mathbf{F}$ into agreement with the measured $m\mathbf{A}$ in the accelerating coordinate system. The value of the compensation force needed equals the mass of the body times the acceleration of the coordinate system seen in non-accelerating coordinate axes. The compensation force must be added to the free-body diagram acting in the opposite direction to the true acceleration of the free body.

This method is shown applied in Figure 1.4.1(b) for the special case of the body-fixed axes. The true centripetal acceleration requires that we add the force mA_C opposing the true acceleration. Similarly mA_T is added. Because xyz is a body-fixed system, the vehicle has no acceleration in this system. From this free-body diagram the equation of motion perpendicular to the path is

$$F_C - mA_C = 0$$

because there is no acceleration of the vehicle in the vehicle-fixed axes. Comparing this with the equation from the XYZ system free body, we see it to be correct: the acceleration in inertial axes is $A_C = F_C/m$.

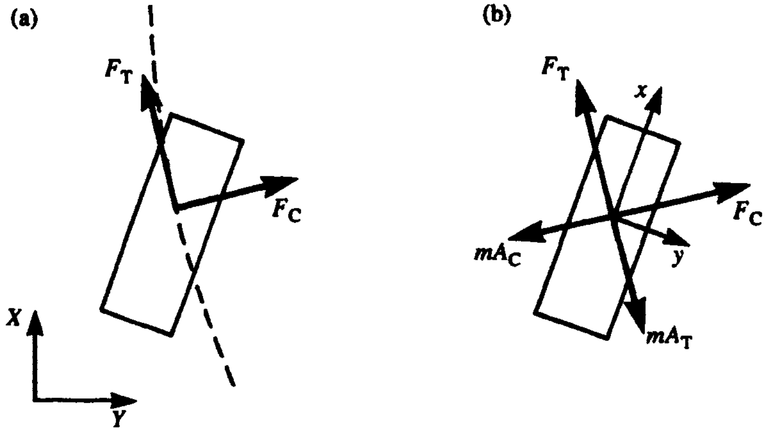

Figure 1.4.1. Plan-view free-body diagram: (a) in XYZ, (b) in xyz.

The force mA_C, balancing the centripetal acceleration, is called the centrifugal force because it acts outward from the center of curvature. This centrifugal force is a compensation force, and appears only in order to make Newton's second law valid in the accelerated reference frame. Unfortunately, this special nature of compensation forces is often overlooked, and they are believed to act even in inertial coordinates such as XYZ, which leads to great confusion.

Figure 1.4.2(a) shows the rear elevation of the same vehicle in the inertial axes *XYZ*, simplified to one axle. Here F_C gives the real centripetal acceleration A_C. Also there is lateral load transfer: N_1 exceeds N_2 to balance the moment of F_C about G because there is no angular acceleration in roll in the steady state. Figure 1.4.2(b) shows the corresponding free-body diagram viewed in the accelerating body-fixed axes, and therefore including the compensation centrifugal force mA_C. By definition, in this axis system the vehicle has no acceleration, i.e., it is in equilibrium.

Both inertial and body-fixed accelerating coordinate systems will be used here, according to which is more convenient at the time. In accordance with the usual conventions, the inertial coordinate system *XYZ* is in use unless otherwise stated.

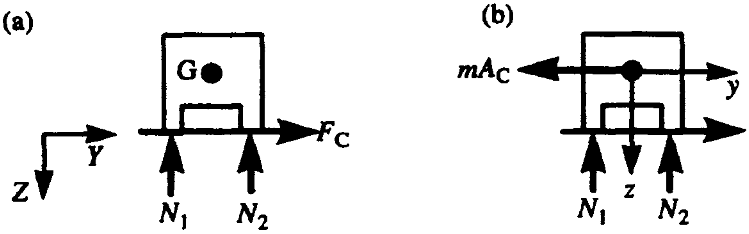

Figure 1.4.2. Rear-view free-body diagram for a right-hand turn: (a) in XYZ, (b) in xyz.

1.5 Body Stiffness

From a handling perspective, a high stiffness of the body or chassis is nearly always preferred so that handling control may be realized by the design of the suspension and tires. The body is loaded by the suspension at the transverse planes of the axles, so it is the effective stiffness between these planes that is significant. The principal loads are the vertical ones, applied primarily through the springs, dampers and suspension links, and essentially equal to the vertical tire forces. If the sums of the vertical forces on the two vehicle diagonals are not equal then the body is in torsion. For cornering, the suspension is generally designed to create such an effect, for example by anti-roll bars, so that the tire normal forces influence the lateral forces in a desirable way. Because of this, the body torsional stiffness can influence handling behavior, in particular if the stiffness is inadequate, which prevents the suspension from acting in the desired manner.

The torsional stiffness of the body or chassis is measured by applying appropriate forces and torques in the vertical transverse planes of the two suspensions. The most satisfactory way to do this is perhaps to support each axle wheel pair on a transverse beam that can be inclined laterally, so that the torsion-causing forces are fed into the body in a realistic way, and to measure the body distortion with dial gauges.

The torsional stiffness of the body or chassis is not easily calculated because of the complexity of the structure, and because of the difficulty of allowing for the influence of imperfect connection between panels, which may have a large effect. Since the 1950s most passenger vehicles have been based on an integral monocoque stressed-skin structure, as opposed to the previous method of having a chassis with a separate and relatively unstressed body, as is still used on trucks. Because of the greater enclosed cross-sectional area of a body compared to that of a chassis, torsional stiffness is much greater, e.g., 10 kNm/deg, and modern car bodies can generally be treated as torsionally rigid for handling analysis. For example, a vehicle of 12 kN weight in the most extreme possible steady-state case would have vertical forces of 6 kN at each end of one diagonal, giving a torque on the body about a longitudinal axis on the centerline of 4 to 5 kNm, but the angular deflection would be only about 0.4°. In normal use it is even less. Although the stiffness is measured between the suspension planes, the bodywork beyond the suspensions can also contribute significantly to the stiffness.

Where a separate chassis is used, as on most trucks, the torsional compliance is substantial, and certainly enough to influence handling. Many trucks and tractor units tend to instability because of the stiff rear springs that are required, and because there is insufficient torsional stiffness in many current designs to allow this to be compensated effectively by front anti-roll bars. The typical truck chassis construction uses a ladder-like assembly – a pair of side rails with connecting crossmembers. The rails are typically steel or aluminum channels with the flanges pointing inward, typically 200 mm × 70 mm, 6 mm thick. Such open channels have much poorer torsional rigidity than closed tubes or boxes. Because they pass just over the axle, and hence between the wheels, they are usually rather close together, especially where double rear wheels are used, and this further limits the rigidity that is achieved.

Truck chassis side rails also bend as beams in side view; in steady state this has little effect on handling, although it can influence the steering mechanism. In plan view there may be bending or lozenging; this may influence the geometric relationship between the wheels and hence alter handling to some extent, although probably less than torsional effects.

1.6 Body Inertia

The inertia properties of a vehicle are usually represented by:

(1) The mass, m

(2) The position of the center of mass, G

(3) The second moment of mass about each axis

(4) The cross products of inertia

In practice, because of near symmetry, the cross products of inertia I_{xy} and I_{yz} are usually taken as zero; I_{xz} is also small but sometimes considered. This is equivalent to saying that the principal inertia axes are close to the xyz axes, although the longitudinal principal axis is often slightly inclined, usually down at the front.

The inertia properties depend on the loading condition, which can best be dealt with by establishing values for the unloaded vehicle, and then incorporating any particular loading condition as required. In general the vehicle is treated as a rigid body, but in some cases it is desirable to include load shifting effects, for example for large fluid loads.

The mass and center of mass may be found theoretically if the masses and positions of the centers of mass of the component parts are known. In view of the large number of parts this may be inconvenient, even if computerized, but is the only way available at the design stage. In this method a coordinate system is defined, typically measuring x back from the front suspension plane, y laterally from the center plane, and z vertically upward from ground level. The total mass moment for each axis may then be calculated by summing the contributions, e.g., $\Sigma x_k m_k$ where m_k is the mass of the kth component. The center-of-mass position is then

$$X_G = \frac{\sum x_k m_k}{m}$$

where m is the total mass. The second moment of mass can then be found for axes through the center of mass. Considering now the standard body-fixed axes xyz, using the parallel axes theorem gives, for example,

$$I_{xx} = \sum \left(I_k + m_k x_k^2 \right)$$

where m_k is the mass of each component and I_k is the second moment of mass of the component about an axis through its own center of mass parallel to, in this case, the x-axis. The second moment of mass of a uniform rectangular solid of dimensions a by b by c about an axis through its center of mass perpendicular to the side a by b is

$$I = \frac{1}{12} m \left(a^2 + b^2\right)$$

The products of inertia can also be found, and then the principal axes and principal moments of inertia follow from the usual transformation equations (e.g., McLean & Nelson, 1962). This can all be rather laborious unless computerized. However, steady-state handling problems depend only on the total mass and the position of the center of mass.

If the vehicle already exists, the mass and center of mass are perhaps most easily found by weighing. Each wheel vertical reaction can be measured, for example the front-left reaction denoted by F_{VfL}. The front axle reaction is then

$$N_{\mathrm{f}} = F_{\mathrm{VfL}} + F_{\mathrm{VfR}}$$

Figure 1.6.1 shows the weight and axle reactions. For ground vehicles the center of gravity (the point at which the weight force acts) and the center of mass (the mean position of the mass elements) can be taken as coincident, although this is not always an adequate approximation, for some space satellites for example. This effectively common point will be denoted G.

From the free body of Figure 1.6.1, which is in equilibrium, it follows that $W = N_{\mathrm{f}} + N_{\mathrm{r}}$. Of course, this is with zero vertical aerodynamic force. In the International System of Units (S.I.), the reaction forces should be expressed in newtons, giving a weight force in newtons. The mass is then $m = W/g$ where g, although varying slightly over the Earth at ground level, is often standardized as 9.81 m/s^2, and m is in kilograms. In the most commonly used version of the Imperial system, the forces are in pounds force (lbf, equals the weight of one pound mass in the standard gravitational field), the mass is in slugs (1 slug equals 32.2 pounds mass), and the standard gravitation is 32.2 ft/s^2. Commercial spring-balance type weighing devices may be calibrated in kg, intended to indicate mass directly, a liberty that is allowable because they are used in a gravitational field that is close to constant. Really they indicate forces in units of kilograms force (kiloponds), the weight of one kilogram in the standard gravity, so in a scientific context the force value in newtons should be found by multiplying by 9.81 N/kg.

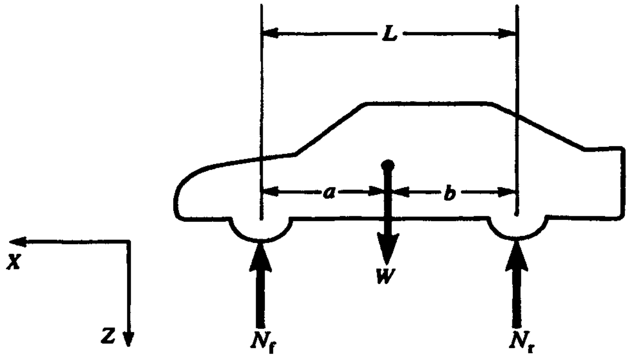

Figure 1.6.1. Side view static free-body diagram.

As a matter of interest, Figure 1.6.1 is, strictly, incomplete because it neglects the atmospheric buoyancy force which acts vertically upward at approximately the center of volume. If we include this, taking it to act at approximately the center of mass, we then see that the sum of the measured reaction forces is actually

$$N_f + N_r = W - B$$
$$W = N_f + N_r + B$$

Thus the weight is really slightly greater than $N_f + N_r$. The buoyancy force is $B = \rho Vg$ where ρ is the air density and V is the volume. Considering the enclosed air to be part of the vehicle, the total enclosed volume for a large car is about 8 m^3, giving $B \approx 100$ N. Thus the mass calculated in the ordinary way from the apparent weight $N_f + N_r$ is too small by about 10 kg. This is under 1%, although up to 3% in the case of some light vehicles with abnormally large enclosed volume. Normally this is neglected.

Returning to the simplified Figure 1.6.1, the longitudinal position of G follows by taking moments, for example about the front wheel contacts, neglecting tire rolling resistance moment, the total moment being

$$\sum M_f = aW - LN_r = 0$$

$$a = \frac{N_r L}{W}$$

The lateral position of G follows similarly from the left and right totals of the vertical tire forces on an end-view free body.

In determination of the vertical forces it is not essential, although it is convenient, to have four load cells. One pair, adjustable for the track, is suitable; a single cell is possible, but less convenient. At the time of measurement, all wheels must be acting against a flat plane, i.e., the load cell must be recessed into the effective floor plane, or the suspension and tire stiffnesses will combine with the wheel deflection to distort the results. The vehicle must be in its standard loading condition, for example dry or fueled, with or without passengers, as appropriate.

Determination of the height of G is more difficult. One method is to hoist one end of the vehicle, for example as in Figure 1.6.2, with a force *F* at point P, to an angle θ. The vehicle may be rested on its rear wheels on columns mounted on ground-level load cells, as an alternative to a hoist with a load cell. Because the suspension forces change from their values in the horizontal position, the suspension should be locked in its normal standing position before hoisting, for example by pinned-through dampers or screwed rods replacing the normal dampers. Applying moment equilibrium to the free body of Figure 1.6.2 gives

$$Wc - F(c + d) = 0$$
$$Wd - N_f (c + d) = 0$$

Thus dimension *c*, from the front wheel center to the line of action of *W*, may be determined, depending on the actual parameters measured. In conjunction with the angle θ the line of *W* is determined, and in conjunction with the already known value of *a* the height of G may be found using the geometric relationship

$$c + H \sin\theta = a \cos\theta + R_L \sin\theta$$

where R_L is the loaded wheel radius, and *H* is the normal height of the center of mass above the ground plane. This gives

$$H = R_L + \frac{a \cos\theta - c}{\sin\theta}$$

so in this test the forward load transfer really indicates the height of G above the wheel center. Hence, for some racing cars the load transfer in this test will be small, or even negative.

The accuracy of this method depends on achieving an adequate value of θ, preferably about 30°. Great care is required to achieve reasonable accuracy in *H*.

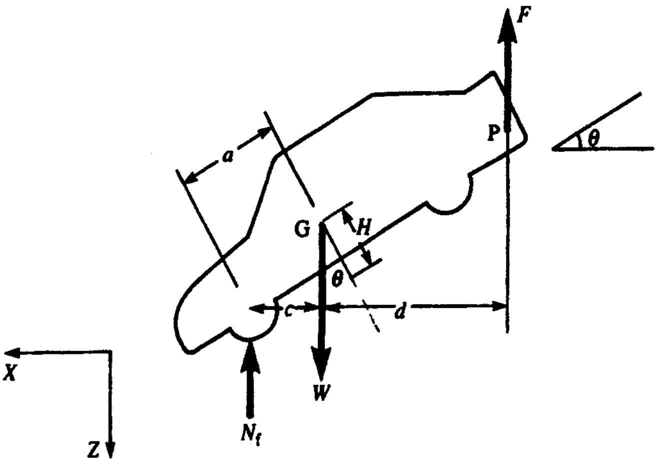

Figure 1.6.2. Determination of height of the center of mass.

Because of the difficulty of doing this, particularly with large trucks, other methods are sometimes adopted. In some cases (e.g., trucks without their rear bodies) it is feasible to rest the vehicle on knife edges at a point directly above G by an unknown amount (Figure 1.6.3), the dimension a already being known, at which point the vehicle hangs level. The addition of a known load m_e at the front or rear will cause a measurable pitch angle position change θ, from which the distance of the vertical center of mass position below the pivot is easily found by

$$z = \frac{m_e e}{m \tan \theta}$$

Alternatively, if the knife edges are below the center of mass, for example under the chassis rails, then in a pitched position there is a destabilizing moment from W, which can be resisted by a load cell or balanced at the other end by a weight. Alternatively, with appropriate precautions, using sharp-edged solid disc wheels it is possible to incline the vehicle laterally until it is balanced on the wheels of one side. In all of these methods, caution must be exercised in locking the suspension, and in preventing or making allowance for fluid load shifting.

The part of the vehicle on the road side of the suspension is called the unsprung mass, discussed in more detail in Section 4.14. It is usually summarized as front and rear total unsprung masses designated m_{Uf} and m_{Ur}, basically found by weighing with proportions of the partly moving elements, for example links.

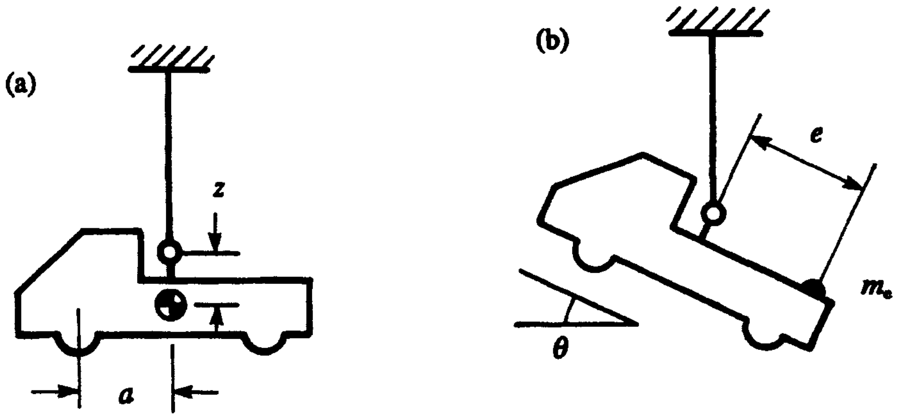

Figure 1.6.3. Alternative measurement of vertical C.G. height.

The unsprung masses may be a significant proportion of the total mass, especially for solid axles, so they are generally treated separately. The basic measured data are total mass at height H positioned a distance a behind the front axle and b in front of the rear axle on wheelbase

$$L = a + b$$

and also the unsprung masses m_{Uf} and m_{Ur} at heights H_{Uf} and H_{Ur} often taken as equal to the wheel radius. From these may be deduced the total front and rear end-masses:

$$m_{\mathrm{f}} = \frac{mb}{L}$$

$$m_{\mathrm{r}} = \frac{ma}{L}$$

The total unsprung mass is

$$m_{\mathrm{U}} = m_{\mathrm{Uf}} + m_{\mathrm{Ur}}$$

The sprung mass is

$$\begin{aligned} m_S &= m - m_U \\ &= m - m_{Uf} - m_{Ur} \end{aligned}$$

The front and rear sprung end-masses are

$$m_{Sf} = m_f - m_{Uf}$$
$$m_{Sr} = m_r - m_{Ur}$$

and, of course, the total sprung mass is

$$m_S = m_{Sf} + m_{Sr}$$

The distance of the sprung center of mass behind the front axle is a_S, for which

$$a_S = \frac{m_{Sr}}{m_S}L$$

$$b_S = \frac{m_{Sf}}{m_S}L$$

It is sometimes convenient to think of the front and rear unsprung masses combined as one unit. Then

$$a_U = \frac{m_{Ur}}{m_U}L$$

$$b_U = \frac{m_{Uf}}{m_U}L$$

The wheelbase is of course,

$$L = a + b = a_S + b_S = a_U + b_U$$

The sprung center of mass height H_S follows by mass moments from ground level, giving

$$mH = m_S H_S + m_{Uf} H_{Uf} + m_{Ur} H_{Ur}$$

$$H_S = \frac{mH - m_{Uf}H_{Uf} - m_{Ur}H_{Ur}}{m_S}$$

The measurement of second moment of mass must be done by investigating the inertia directly rather than by weighing. The vehicle is put into oscillation about a fixed axis, with a restoring moment due to the weight force or a spring, and the natural frequency is measured. Knowing the restoring stiffness, the second moment of mass about the fixed axis may be deduced, and from that the second moment of mass about an axis through G parallel to the fixed axis can be calculated using the parallel axes theorem. Appropriate fixed axes are therefore chosen to investigate the inertia in yaw, pitch and roll oscillations.

For yaw, using the standard trifilar pendulum (Figure 1.6.4), the vehicle is supported on a platform suspended by three equally spaced pendulum wires of length L_P. The vehicle G must be directly over the platform G, which must be centrally positioned. Each wire has a tension $W/3$, where W is the total weight, so when the platform is rotated by θ there is a restoring moment, because of wire inclination, of

$$M = 3 \times \frac{W}{3} \times \frac{R\theta}{L_P} \times R = \frac{WR^2\theta}{L_P}$$

so the torsional stiffness is

$$\frac{\mathrm{d}M}{\mathrm{d}\theta} = \frac{WR^2}{L_P}$$

It is usually acceptable to neglect the wire torsional stiffness in this method, although a correction is easily added if desired. The natural frequency of torsional vibration is therefore

$$f = \frac{1}{2\pi}\sqrt{\frac{WR^2}{I\,L_P}}$$

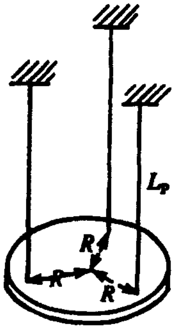

Figure 1.6.4. Trifilar pendulum.

By observing the natural frequency, first for the platform alone, then for the vehicle plus platform, I may be found for each case, and hence deduced for the vehicle, using

$$I = \frac{K}{\omega^2} = \frac{WR^2}{4\pi^2 f^2 L_P}$$

The final result for the vehicle yaw inertia is

$$I_V = \frac{(m_V + m_P)gR^2}{4\pi^2 f^2 L_P} - I_P$$

The advantage of the trifilar pendulum over the quadrifilar pendulum is that the individual tensions are statically determinate. However, it may be more convenient to use a quadrifilar pendulum. For this case, or for a trifilar pendulum with non-centralized load,

$$K_\theta = \frac{\mathrm{d}M}{\mathrm{d}\theta} = \sum \frac{T_k R_k^2}{L_P}$$

where T_k is the tension of the wire at radius R_k from the vertical line of the center of mass. For a quadrifilar pendulum with lateral symmetry

$$K = \frac{mg}{L_P}(bR_f + aR_r)$$

If the vehicle is centralized so that all the radii are the same, then the indeterminacy does not matter, i.e., it is not necessary to know each tension individually. One practical advantage of the quadrifilar pendulum is that each wire can be attached directly to each end of an axle; the effect of the center of mass position on the various R values and tensions must then be allowed for. The quadrifilar pendulum's natural frequency may be found from the general formula

$$\omega_N^2 = \frac{K}{I}$$

$$f_N = \frac{1}{2\pi}\sqrt{\frac{\mathrm{d}M/\mathrm{d}\theta}{I}}$$

Pendulum methods require a strong and rigid overhead structure, which may be problematic for very large or massive vehicles. An alternative method is to support the vehicle from below on a spherical air bearing, a hydrostatic oil bearing, or a small steel ball of say 20 mm diameter. By placing this support a small distance d behind the vertical line of G, a small supporting reaction is required at the front wheels, met by a plate resting on balls or an air bearing. Thus the vehicle is constrained to rotate about a vertical axis just behind G. A horizontal spring with moment arm R and stiffness K provides a restoring moment at deflection θ of

$$M = K R^2 \theta$$

The natural frequency is therefore

$$f_N = \frac{1}{2\pi}\sqrt{\frac{KR^2}{I_0}}$$

where I_0 is the second moment of mass about the fixed axis, which by the parallel axes theorem is

$$I_0 = I_Z + mx^2$$

where x is the distance of the axis from G, allowing I_Z to be deduced. A correction may be made for the inertia contribution of the plates under the front wheels.

Experimental determination of the pitch or roll second moments of mass is usually performed by holding the vehicle in a cradle to form a pendulum, shown for pitch in Figure 1.6.5. The restoring moment at deflection θ is

$$M = WZ\theta$$

where W is the total weight and Z is the distance from the axis to the total center of mass. By the parallel axes theorem the observed second moment of mass is

$$I_0 = I_P + m_V Z_V^2 + I_C$$

where I_P is the desired vehicle pitch inertia, I_C is the cradle inertia about the pivot, and Z_V is the pendulum length to the vehicle center of mass. The natural frequency of pendulum motion is

$$f = \frac{1}{2\pi}\sqrt{\frac{WZ}{I_0}}$$

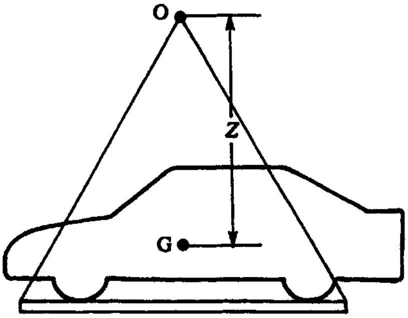

Figure 1.6.5. Conventional pendulum

The cradle inertia is found by testing the cradle alone; then $I_P + m_V Z_V^2$, and hence I_P may be deduced. It may be easier to pivot the cradle on knife edges lower down nearer to the center of mass, in which case additional restoring stiffness may be provided by a suitable spring. This may also be more accurate, because the $m_V Z_V^2$ term is much smaller.

As a matter of interest, by finding the pitch frequency for two pendulum lengths, in principle both I_P and the height of G may be deduced. However, this requires great precision, and it is necessary to allow for inertia of the vehicle's added mass arising from external air motion, for the internal air mass, and for buoyancy forces. It is therefore not a practical method.

Because of approximate lateral symmetry, the only product of inertia that is significant is I_{XZ}. This may be measured in the following way. The vehicle is again tested for yaw inertia, but this time with the x-axis inclined upward at the angle θ, say 30°, giving a result I_r. Then

$$I_{XZ} = \frac{I_r - I_X \sin^2\theta - I_Z \cos^2\theta}{\sin 2\theta}$$

The inclination of the principal axes from the xz axes is θ_P where

$$\theta_P = \frac{1}{2}\tan^{-1}\left(\frac{2I_{XZ}}{I_X - I_Z}\right)$$

Denoting the second moment of mass about a vertical axis through G, i.e., the yaw inertia, as I_Y, the radius of gyration for yaw is

$$k_Y = \sqrt{\frac{I_Y}{m}}$$

and has a typical value of about 1.4 m. Similar radii of gyration are defined for the other axes.

In analysis of transient dynamics, it is found that the significance of the yaw radius of gyration depends on how it compares with the distance of the axles from the center of mass. Specifically, where a is the distance from the front axle to the vertical line of G, and b is the distance of the rear axle (Figure 1.6.1), the ratio

$$i_Y = \frac{I_Y}{mab} = \frac{k_Y^2}{ab}$$

is called the yaw dynamic index, or just the dynamic index. The value is around 1.0 for a passenger car, but as low as 0.6 for a formula racing car.

The corresponding pitch dynamic index is

$$i_P = \frac{I_P}{mab} = \frac{k_P^2}{ab}$$

where k_P is the pitch radius of gyration.

The roll dynamic index may be defined as

$$i_R = \frac{I_R}{\frac{1}{4}mT^2} = \frac{4k_R^2}{T^2}$$

where k_R is the roll radius of gyration and T is the mean track. Here $\frac{1}{2}T$ has been preferred to T for the reference length so that the numerical values of i_R can be related better to those of i_Y and i_P.

The influence of yaw dynamic index will be discussed in Chapter 7 on unsteady-state handling, but briefly a high dynamic index, which tends to be associated with large cars because of their proportionally greater front and rear overhang, tends to lengthen the time constants of the response.

In rolling and pitching it is often the angular inertia of the sprung mass alone that is of interest, which may be deduced by standard techniques found in mechanics textbooks, mainly involving transformation to new axes and the addition or deletion of components. In yaw, the inertia of the whole vehicle is appropriate.

1.7 Loads

For a normal passenger car, addition of the driver, passengers and luggage will have a substantial effect on the total mass, on the position of the center of mass, and on the second moments of mass.

The process of finding the loaded properties is the same for all axes. The mass is simply the sum of the masses, of course. The new center of mass is the point about which the first moment of mass of the vehicle plus load is zero. The second moment of mass about axes through the new center of mass is the sum of contributions from the vehicle and the load, each found by the parallel axes theorem,

$$I_0 = I + mx^2$$

The second moment of mass of a uniform rectangular load, *a* by *b*, about its own center of mass, is $m(a^2 + b^2) / 12$.

For a typical sedan (saloon) the driver and front passenger are near the longitudinal center of mass and so have relatively little effect on the longitudinal properties. Two rear seat passengers have a total first moment of mass about the center of mass of about 140 kg m, moving the center of mass back about 100 mm. A full fuel tank may move G by 70 mm. A loaded trunk (boot) may move G by 100 mm rearward. The total movement of 250–300 mm is about 10% of the wheelbase, and of considerable significance in influencing behavior.

Loading of a small or large commercial vehicle may have an even greater effect on the inertia properties. Because of the large effect, each case must be considered individually. The usual effect of adding load is to move G backward and slightly upward.

The repositioning of even supposedly minor components may be significant. Moving a battery from the engine bay to the trunk may move the center of mass by 30 mm, changing the front–rear load distribution by 1%. On front-drive vehicles, which are very light at the rear, this may be a useful improvement. Alternatively, for rear-engine vehicles, which are often light at the front, a useful improvement may be achieved by moving components forward, or even by adding dead load as trim as far forward as possible, for example lead in the front fenders in one well-known case.

The influence of fuel load may be a considerable problem on certain specialized vehicles. For example, the standard layout of racing cars before 1959 was a front engine, followed by the driver, with the fuel tank placed over and behind the rear axle. Because of the small total mass and the large fuel mass, there was a marked change of center of mass position during a race. One Indianapolis racer of the early 1950s carried 380 kg (115 gallons) of fuel, moving the center of mass by almost 20% of the wheelbase. In an attempt to overcome this problem, one European manufacturer put the fuel in outboard tanks filling the longitudinal space between the wheels, also reducing wheel drag. This placed the fuel load close to the longitudinal position of G, but the method proved inferior to the standard layout of the period, apparently because it greatly increased the roll inertia, which reduced the roll natural frequency and spoiled the transient dynamics.

With the change to rear engines in racing in 1959, the fuel was placed in various tanks including at the sides, but this time close in to the flanks. With the ground-effect aerodynamics revolution of 1978, it became essential to minimize the width of the true body in order to maximize the width of the ground-effect tunnels on each side. For this reason the fuel was placed in a single central tank between the driver and the rear engine. This was also ideal for minimizing the shift of center of mass, especially with the large fuel loads, up to 200 kg of fuel with a dry vehicle mass of 600 kg or less.

The lateral position of the center of mass is usually taken in the longitudinal plane of symmetry, because usually the vehicle itself has only minor asymmetries when unloaded and dry. However, loading may offset G significantly. Often the fuel tank is on one side, and this may offset the center of mass by 30 mm, 2.5% of the track. Each driver or passenger may cause an offset of 20 kg m, giving 20 mm offset (1.5% of the track). On some vehicles the tank and driver are on the same side, so an offset of 50 mm may commonly arise. A worst case would be with one passenger on the same side in the rear, giving 70 mm offset, 5% of the track.

The center of mass is considered to be a fixed point in the sprung body in most cases, for a given loading condition, and usually on the center plane, and the total mass is treated as constant. The constant total mass approximation is a good one because the mass rate of change is small, e.g., fuel consumption. The constant position approximation is less accurate because of the possibility of shifting of the load or passengers, i.e., there are inaccuracies in the rigid-body model, although again these are usually small. For example, the leaning of four passengers in severe cornering moves their center of mass typically 15 mm, giving a total center of mass movement of about 3 mm. Shifting of fuel in the tank of a typical sedan may also give a center of mass movement of about 3 mm, so when combined with the passengers the total movement is about 6 mm or 0.5% of the track, and normally negligible.

For some specialized vehicles the shiftable load may be a much larger proportion of the total mass, tankers for liquids providing an obvious extreme example, and in such cases special precautions are required, for example, baffling of the tank. Load shifting is at its worst for a range of part loads around 50%, depending on the tank shape and the lateral acceleration. In all cases of fluid load shifting, in steady-state cornering the fluid surface is at an angle to the horizontal of $\theta = \tan^{-1}(A_y/g)$, where A_y is the lateral acceleration, which in the vehicle-fixed axes we may explain as the consequence of centrifugal force on the liquid. Such vehicles are also characterized by a high ratio of center-of-mass height to track, and when tire and suspension compliance are included, the steady-state rollover lateral acceleration is as low as 4 m/s^2 (0.4g). When dynamic response of the liquid and the behavior of trailer units is included, the limit may be only 2 m/s^2 (0.2g). Hence it is understandable that rollovers are a significant contributor to accidents for such vehicles.

1.8 Engine and Brakes

The engine and brakes are the means by which tire longitudinal forces are controlled, the longitudinal force being the force in the direction in which the tire points. Because of the steering on front-drive vehicles, and because of the vehicle attitude on rear-drive vehicles, in general the longitudinal tire forces have components contributing to, or detracting from, the vehicle centripetal acceleration; but primarily the engine and brakes control the acceleration tangential to the path.

In steady-state cornering on a level surface, the engine must provide the net power to overcome the aerodynamic drag and tire drag forces. Also the longitudinal forces on the driven tires influence the lateral forces at a given slip angle because of the tire characteristics, and hence the longitudinal forces have an effect on the handling.

Approximate values for the cornering thrust and power requirements can be found by considering the vehicle to be concentrated at a single tire with a mean slip angle. Figure 1.8.1 shows an unpowered tire with slip angle α, and with the forces exerted on the tire by the road. These are the lateral force F_Y, and the rolling resistance force $\mu_R F_V$, where F_V is the tire vertical force. To provide the vehicle centripetal acceleration, and neglecting aerodynamic forces, at path radius R,

$$F_Y \cos\alpha - \mu_R F_V \sin\alpha = mA = mV^2/R$$

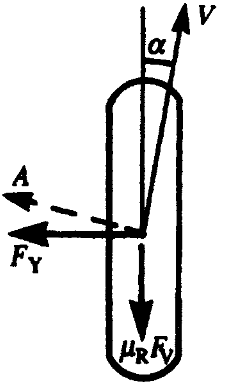

Figure 1.8.1. Plan view of unpowered cornering tire.

Because μ_R is small ($\mu_R < 0.02$ typically)

$$F_Y \approx \frac{mV^2}{R\cos\alpha}$$

The tire drag is the sum of cornering drag and rolling resistance

$$\begin{aligned} F_{TD} &= F_{TCD} + F_R \\ &= F_Y \sin\alpha + \mu_R F_V \cos\alpha \end{aligned}$$

Because α is reasonably small,

$$F_{TD} \approx F_Y \sin\alpha + \mu_R F_V$$

Substituting for F_Y,

$$F_{TD} = \frac{mV^2}{R}\tan\alpha + \mu_R mg$$

The power dissipation at the tire is

$$\begin{aligned} P_T &= F_{TD}V \\ &= \frac{mV^3}{R}\tan\alpha + \mu_R mgV \end{aligned}$$

The aerodynamic drag (Chapter 3) is given by

$$F_{AeD} = \tfrac{1}{2}\rho V^2 A_D$$

where A_D is the drag area, typically 0.6 m^2 for a small to medium sedan, and actually influenced somewhat by the attitude angle.

The aerodynamic power dissipation is

$$\begin{aligned} P_{Ae} &= F_{AeD}\,V \\ &= \tfrac{1}{2}\rho V^3 A_D \end{aligned}$$

The thrust power required to overcome these resistances is

$$\begin{aligned} P &= P_{\mathrm{T}} + P_{\mathrm{Ae}} \\ &= \left(F_{\mathrm{TD}} + F_{\mathrm{AeD}}\right) V \end{aligned}$$

On level ground, the engine must provide this, plus losses in the transmission.

Steady-state testing is normally performed at a sufficiently small radius for a moderate power requirement, for example 32.9 m (108 ft). For a centripetal acceleration of 8 m/s^2 the speed is 16.22 m/s (36.5 mph). With a mean tire slip angle of 8°, a vehicle mass of 1200 kg, and $\mu_{\mathrm{R}} = 0.017$, the total tire drag is

$$\begin{aligned} F_{\mathrm{TD}} &= (mV^2/R) \tan \alpha + \mu_{\mathrm{R}}\, mg \\ &= 1349 + 200 = 1549 \text{ N} \end{aligned}$$

The aerodynamic drag, for 0.6 m^2 drag area, is

$$F_{\mathrm{AeD}} = \tfrac{1}{2} \rho V^2 A_{\mathrm{D}} = 96 \text{ N}$$

This is much less than the tire drag. The thrust power required at the wheels is

$$P = (F_{\mathrm{TD}} + F_{\mathrm{AeD}})\, V = 27 \text{ kW} \quad (36 \text{ bhp})$$

This is well within the capabilities of the average vehicle. On the other hand, if the test radius is increased to 100 m, for the same lateral acceleration the speed is 28.3 m/s (63.3 mph). With the same slip angle, which will be approximately true, the tire drag is still 1549 N, but the aerodynamic drag is up to 343 N, and, mostly because of the increased speed, the total thrust power is now 53.5 kW (71 bhp). Not all vehicles could achieve this. This also implies a power dissipation of 11 kW at each tire, with a corresponding temperature increase.

The dependence of the tire power dissipation on vehicle speed during cornering is of interest. We have

$$P_{\mathrm{T}} = F_{\mathrm{TD}} V$$

which in the linear cornering regime is

$$P_{\mathrm{T}} = \left(F_{\mathrm{Y}} \alpha + \mu_{\mathrm{R}} F_{\mathrm{V}}\right) V$$

Considering a small rolling resistance, and a total vehicle cornering stiffness $C_{\alpha V}$ equal to the total for four tires,

$$\begin{aligned} C_{\alpha V} &= 4C_\alpha \\ P_T &= F_Y \alpha V \\ &= \frac{F_Y^2 V}{C_{\alpha V}} \end{aligned}$$

Hence,

$$P_T = \frac{m^2}{R^2 C_{\alpha V}} V^5$$

exhibiting a remarkable sensitivity to the velocity.

The actual total tire cornering drag is

$$F_{TCD} = \frac{m^2}{R^2 C_{\alpha V}} V^4$$

arising because both slip angle α and lateral force F_Y are proportional to V^2 at a given path radius.

From the above example we may conclude that in typical steady-state testing the power requirement depends primarily on the tires rather than on the aerodynamics, and that the power output is usually adequate for testing at a moderate radius, but that at larger radii the engine power may be a limiting factor. In other words, the engine power defines a limit to the steady-state cornering performance envelope. The maximum steady-state centripetal acceleration at any given speed is shown in Figure 1.8.2. Section AB of the curve is limited by steering lock, section BC by tire friction limits, generally declining slightly with speed, and section CD by engine power. At D all of the engine power is required to sustain forward speed in a straight line, and steady-state centripetal acceleration is not possible. For a racing car, the intermediate region BC, tire friction limited, will generally rise from B to C because of increasing aerodynamic downforce.

It is sometimes stated that the total tire drag on a vehicle is greater on a small test radius because of the increased steer angle. This is incorrect. The vehicle is traveling in a slightly different direction at the two axles, and part of the steer angle compensates for this (Section 5.15 discusses turning geometry). The drag

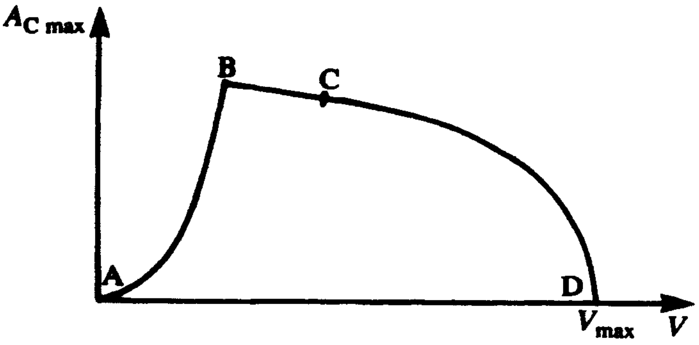

Figure 1.8.2. Cornering performance envelope.

and power dissipation depend on the tire slip angles, not on the steer angle. This is confirmed by considering the energy dissipation.

For an uphill corner the steady-state power requirement is increased because of the rearward component of the weight force, and for a downhill corner the power is reduced. For example, on the 32.9 m radius condition discussed above, a downhill spiral slope of about 1 in 7 would eliminate the need for engine power, although there would then also be other effects such as forward load transfer.

Clearly then, for transient maneuvers in acceleration the engine power limit may be significant. Most modern cars have brakes capable of locking the wheels if required, so braking capability is not generally a limitation, although the front-to-rear balance is important.

An interesting common case is that of engine overrun without braking, which applies a torque to the driven wheels. This torque depends on the gear and the engine rotational speed. The actual engine resistance is zero at a vehicle speed giving tickover rpm, and increases in a way that is sensitive to the tickover setting, i.e., a small increase in tickover speed setting may considerably reduce the engine overrun braking effect at higher vehicle speeds.

1.9 Differentials

The basic types of differential are:

(1) Free

(2) Solid

(3) Locking

(4) Limited-slip

Most road vehicles are fitted with a free differential. Some utility vehicles, for example tractors, have a free differential that can be manually locked when required, as distinct from the automatic locking type above.

The free, or open, differential is a mechanical force balancer that applies equal torques to the two driveshafts while allowing them to rotate at different speeds. This is the usual equipment of most road vehicles. The speed difference is required because in a corner the outer wheel is on a larger radius from the center of curvature and must travel farther, and it therefore wishes to rotate faster. The ratio of the outer speed to inner speed, with zero longitudinal slip, is

$$\frac{\Omega_o}{\Omega_i} = \frac{R + T/2}{R - T/2} \approx 1 + \frac{T}{R}$$

where R is the mean path radius and T is the track. Hence the proportional speed difference is most marked for small-radius corners, and may be as great as 30%.

The disadvantage of a free differential is that if one wheel can withstand only a small torque, then the other wheel is also restricted to this torque. This can badly affect the traction in patchy or low-friction conditions. It also occurs in cornering, where the load transfer reduces the vertical force on the inner wheel, and hence reduces the limiting friction force. Although the driveshaft torques are equal, the tire longitudinal forces may not be exactly so; this can occur if one wheel is spinning and accelerating, when the acceleration torque $I\alpha$ on that wheel will be matched by a thrust at the other tire. For example, with $I = 0.4$ kg m^2 and $\alpha = 100$ rad/s^2, at $r = 0.32$ m the opposite longitudinal force from this effect will be 125 N, which is small.

Because the longitudinal forces produced by a free differential are normally equal, these forces do not have a net moment in plan view about the center of mass, and in this sense the free differential is neutral in its influence on handling.

The opposite of a free differential is a solid differential. This is interesting as a limiting case of differential types, and although not found on road vehicles it is not unusual in racing, where it may be preferred over a limited-slip differential because of strength, reliability, availability or cost, and over a free differential because of performance. In the locked differential the driveshafts are connected rigidly so that they are constrained to have the same angular speed. Evidently in a corner there must be some elastic slip or actual sliding of the tires on the ground. The total discrepancy in the advance of the two tires, over a corner arc of θ, is

$$R_o\theta - R_i\theta = T\theta$$

If this is distributed evenly on each tire, then each tire has a longitudinal slip of approximately

$$S = \pm\frac{T\theta/2}{R\theta} = \pm\frac{T}{2R}$$

This slip gives rise to longitudinal tire forces, and evidently is of increasing severity as the corner radius becomes smaller. Because the inner wheel wants to go faster, and the outer slower, the longitudinal forces on the tires are forward on the inner wheel and backward on the outer wheel, hence trying to turn the vehicle out of the corner, a so-called understeering effect. Such an effect will certainly be significant at a longitudinal slip of 1% (see Chapter 2), which for a typical vehicle track occurs at a radius of 60 m. The steer effect and the high rate of tire wear caused by the slip mean that the solid differential is unsuitable for normal road use.

The solid differential does sometimes find application in racing, particularly and understandably on those circuits with only large-radius corners or superelevated banking where the disadvantages are minimal: this means that it appears on the large oval circuits of America rather than the intricate road circuits of Europe. Because the ovals have turns of only one direction the solid differential is used in conjunction with a slightly larger-diameter outer tire ("tire stagger") alleviating the slip discrepancy on the corners at the cost of introducing some acceptable steering effect on the straight.

The locking type of differential has an overrun device on each driveshaft, ensuring that each is free on the overrun, but when power is applied the differential becomes solid. In corners, because the outer wheel has a greater angular speed, under power all the tractive force occurs at the inner wheel, steering the vehicle out of the corner, an understeer effect. Also, if one wheel slips because of a low-friction area of road, all the torque is applied to the other wheel.

Limited-slip differentials, also known as torque-bias and torque-proportioning differentials, act as free differentials on the overrun, or when moderate driving torques are applied, but partially lock up when one wheel tries to spin, so that the torque is directed to the other wheel. In this way the total longitudinal force at the driven wheels is improved, and with sufficient slip limitation (torque transfer) at the differential it may be limited only by the total friction force at the tires, rather than by that at the worse side only. In a corner, the outer wheel tries to run faster, which the limited-slip differential interprets as wheel spin and therefore partially locks, giving more tractive force on the inside wheel; this is a similar understeer effect to the locking differential under these circumstances, but less severe.

There are various designs of limited-slip differential, including the cam and the pawl, the friction clutch and viscous coupling types. In the cam and pawl type, power is applied to the pawls which wedge between ramps on the "cams" that drive the driveshafts. The mechanical friction of the wedging action, produced by the input torque, means that even when one driveshaft runs free, some torque can be applied to the other one. Without input torque, the differential is virtually free. The degree of locking that is achieved under power, usually about 75%, depends on the design angles and dimensions. This type is light and compact but is subject to wear, particularly when heavily loaded, and the locking action reduces as the critical dimensions are changed by the wear pattern.

In the clutch type, the two driveshafts are connected together through clutch plates, the clutches generally having some spring preload, and are further loaded by wedging action of the input torque. Thus if one driveshaft slips, the clutch pack returns the torque to the other driveshaft. The clutch loading can also be done hydraulically, so that the limited-slip action can be controlled electronically, for example with wheel speed sensors, giving any desired characteristic.

The viscous coupling type transfers torque from the faster to the slower driveshaft simply by the viscous effect with the speed difference, and is not controlled by the input torque.

One disadvantage of limited-slip differentials is that during locking operation there is power dissipation, which may lead to heating problems in continuous operation. Actually, a limited-slip effect may be achieved by any system that introduces inefficiency if slipping occurs. Thus there are other types based on various arrangements of gears, including worm-gear systems, which can be arranged to provide the desired inefficiency, i.e., friction, under the appropriate operating conditions.

One difficulty that may be experienced with locking and limited-slip differentials is that although the design may, under given conditions, have an equilibrium state with the desirable transmission of torque, the equilibrium may be dynamically unstable so that the differential locks and unlocks in rapid sequence, leading to an oscillating torque application to the wheels which may lead to an erratic response from the vehicle.

Figure 1.9.1 illustrates differential characteristics; the total tractive force $T_1 + T_2$ is shown as a function of the tractive force limit at the low-friction side, T_1. For a free differential, $T_2 = T_1$ up to the point where both are limited by the input torque. For a solid or locked differential, T_2 is independent of T_1. Each design of limited-slip differential has some kind of intermediate characteristic, being virtually free at small T_1 but becoming virtually solid at higher values of

T_1. The viscous-friction type is not well represented on such a graph because the torque transfer is speed dependent.

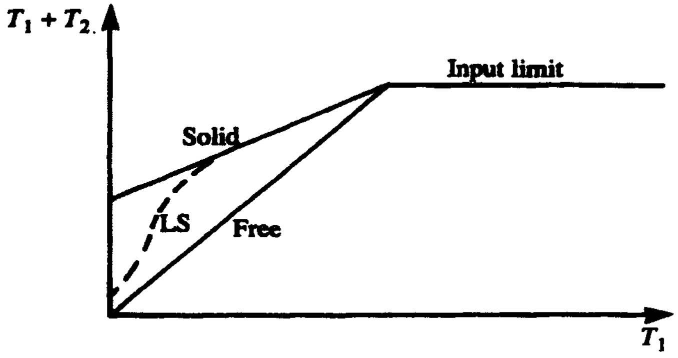

Figure 1.9.1. Differential traction characteristics.

Limited-slip differentials are quite commonly fitted to more expensive or sporting vehicles, although they are a significant extra cost. From the point of view of conventional motoring, their value is in discouraging wheel spin in adverse conditions in plain longitudinal motion. Unfortunately, in cornering they may cause more sudden breakaway. On front-drive vehicles the difference between the torque in the driveshafts means that there can be considerable steering wheel reaction ("wheel fight") when the locking comes into play. In good road conditions and normal driving, the free differential seems to be quite adequate. Therefore, for passenger cars the real value of a limited-slip differential is seen only in adverse conditions such as ice or snow. In racing, some form of locking or limited-slip differential is essential for realizing the maximum performance, in this case because of the requirement for excellent traction when leaving a corner, while still with considerable lateral load transfer. Of course, for wheeled military vehicles and for rally cars on muddy or loose gravel surfaces, the limited-slip differential may be of great value.

Four-wheel-drive systems are common on off-road, mixed-use and military vehicles, and are recently becoming more common on passenger cars. This requires some sort of central differential to distribute torque between front and rear axles. Typical mixed-use vehicles have an open center differential that can be manually locked, sometimes combined with a locking or limited-slip differential for the rear axle. Except when the most difficult conditions will be encountered, an open differential is generally used for the steered front axle because of adverse effects on the steering feel, although the viscous coupling type is attractive here. Some military vehicles have four-wheel drive with a solid center differential. Although this is obviously useful for obtaining maximum traction in poor conditions, it may have serious adverse effects on the behavior on surfaced roads, especially if the tire diameters are slightly different front to rear because of wear.

1.10 Wheels

The term "wheel" may be used in a wide sense to include the whole of the rotating element including the tire, or in a narrow sense to mean the part that connects the tire to the hub. The wheel probably originated at least 5000 years ago. The first wheels were presumably developed from the older idea of using a tree trunk as a roller, and possibly made by cutting discs from a trunk; such wheels are weak because of the grain direction. Fabricated wooden wheels are probably almost as old, and would have been very satisfactory on agricultural carts. With higher performance demands from military chariots, it may well have been the military engineers who devised the spoked wheel, which was certainly in common use at least two thousand years ago. The wooden-spoked wheel with wooden felloes and steel rim became very highly developed by the end of the 19th Century. However, the arrival of the bicycle, the motor vehicle and the airplane all created a demand for improved wheels.

In fact, today there is a wide variety of wheel types for cars and commercial vehicles, the main types being:

(1) Steel disc

(2) Spoked

(3) Light alloy

(4) Flat-base and wide-base

(5) Divided

(6) Modular

The steel disc wheel is the standard fitting on most cars today. The wheel size is usually specified by the rim diameter and rim width, and a letter defining the rim section shape, for example 14×5J. The wheel rim dimensions must of course match those of the tire. The outset is the distance from the mounting surface, on the central disc, out to the rim/tire centerline. Inset is the negative of outset, outset being more common. The tire bead seats against the flanges, which are curved outward to provide a smooth edge and a progressive contact surface for the tire as it distorts because of bumps or cornering. The inside of the wheel must be clear of the brakes and suspension components. To improve brake cooling, holes are usually provided in the central disc, and so this standard wheel is often known as a ventilated disc wheel.

The steel disc wheel is constructed from two components – the rim and the disc or dish. The rim is formed from steel strip by cutting, rolling and butt-welding. The disc is pressed to a dished shape, typically from an octagonal blank, to give the inset, and is contoured to improve stiffness compared with a flat disc, and then usually spot-welded to the rim. This is a very economical method of wheel manufacture.

Although the spoked or wire wheel of early sports cars offered at that time a lower unsprung mass, nowadays it is selected for appearance only. The rim and a small hub are connected by about seventy spokes. These are arranged at various angles to enable the driving and cornering forces to be transmitted. The setting up of such a wheel with an even distribution of spoke tension and with the rim accurately located requires a systematic procedure and can be time-consuming. Unfortunately the wire wheel requires a good deal of attention to maintain its appearance and adjustment, and so is now virtually obsolete.

The light-alloy wheel has, for quite a long period, enjoyed success as an aircraft wheel and also for car rallying and racing. More recently it has enjoyed a considerable vogue on passenger cars, essentially for appearance, and is becoming a common option rather than just the province of after-market suppliers. Either aluminum or magnesium alloys are used, cast or forged. The best strength is achieved by forging, although this is much more expensive. Magnesium alloys, of density about 1800 kg/m^3, are potentially lighter than aluminum alloys, of density about 2800 kg/m^3, and although they require larger sections they are usually preferred where performance is paramount. Most road vehicle light-alloy wheels are made of aluminum, and are hardly any lighter than a good steel wheel. In all cases precise alloy selection is critical for strength, fatigue resistance and corrosion resistance.

Flat-base and wide-base wheels are variations on the steel wheel for use on commercial vehicles. For cars, the tire is fairly flexible and the rim well is adequate to allow assembly. The tires of trucks and commercial vehicles are much more rigid, so in some cases it is necessary to completely remove one flange; the removable flange has a joint so that it can be sprung into position after the tire is slid onto the rim. The well is then no longer required. There are several methods of locating the removable flange. On some light trucks with tires of intermediate stiffness, a rim is used which combines a removable flange with a shallow well.

In the divided wheel, the flanges are integral with the rim, but the rim is split circumferentially at its center where it has additional turned-in flanges to allow the whole wheel to be bolted together. This method is favored for military vehicles using run-flat tires. Although normally run with air pressure, these have very stiff sidewalls which are trapped between the flanges and a spacer between the beads, so that in the event of tire damage the sidewalls act essentially as cantilevers supporting the remains of the tread, if any, and in any case allow some mobility until the tire can be replaced.

In the modular wheel, which has become popular in racing, there is a cast or forged light-alloy center or spider which is bolted in between two spun or pressed aluminum rim halves. This design has various advantages: it is light, it has good crash energy absorption, various total rim widths and offsets can be made up, minor rim damage is often repairable unlike a completely cast wheel, and even if not, then only a part of the wheel may need replacing. This type has not so far found significant application on road vehicles.

In addition there are innumerable special wheel designs for specialized vehicles, for example agricultural equipment such as tractors, and construction equipment; solid-tired wheels are used for forklift trucks; and so on. One interesting development is on land speed record vehicles, where the very high speeds, about 300 m/s, mean that it has become very difficult to produce tires that will withstand the centrifugal forces arising from wheel rotation, even when these are minimized with large-radius wheels. For example, at 300 m/s, a wheel of radius 1 m has a centripetal acceleration at the edge of 90 km/s^2, or about 9000g. Consequently the current jet reaction vehicles use solid metal wheels. These vehicles run on salt flats or mud playas rather than hard metalled surfaces, so the wheel is harder than the road.

One method of mounting road vehicle wheels to the hub is by several studs, typically four on cars. To improve vibration resistance it is desirable to have some compliance of the wheel at the place where the stud nuts bear against it. Therefore on a steel wheel these parts of the wheel are stood forward from the plane of the mounting face. The nuts are tapered on the bearing face so that the wheel locates on the nuts rather than the studs. For normal use it is more accurate to locate the wheel on its center bore, and to use the nuts for retention only.

The alternative method of wheel retention is the center-lock. The wheel is trapped and centralized between two tapers, one on the hub and one on a single large nut that screws onto the protruding hub center. In order to provide selftightening, it is usual to have left-hand threads on the left of the car. This method is more expensive than the multi-stud method, although aesthetically more appealing. It was often associated with spoked wheels, and similarly is becoming obsolete. One advantage is that rapid wheel changes are possible, and for this reason it still finds regular application in racing.

The manufacturing process naturally leaves the wheel with dimensional imperfections. The important feature is how the wheel locates the tire relative to the hub, so dimensional tolerances are specified for radial and axial run-out of the rim at the tire bead locating point. Cast and machined alloy wheels tend to be more accurate than fabricated steel wheels. Additional inaccuracy can arise because of inconsistent location of the wheel on the hub.

The wheel is generally slightly out of balance both statically and dynamically, i.e., the center of mass may be off-axis and the principal axes may be misaligned, and this is usually dealt with by balancing the combined wheel and tire by adding appropriate counter-masses.

In Figure 1.10.1(a), an off-center mass, considered in the coordinate system rotating with the wheel, has a centrifugal imbalance force

$$F_\mathrm{I} = m\omega^2 r$$

This is static imbalance. In Figure 1.10.1(b), two such masses, diametrically opposed but axially displaced, have zero total force, but there is an imbalance moment

$$M_\mathrm{I} = m\omega^2 r e$$

This is dynamic imbalance.

The wheel is subject to quite a complex load distribution in transmitting the tire forces to the hub. Although these can be analyzed, wheels are largely designed by experience. Mounting the tire on the rim puts the rim transverse section into bending. Inflation results in a tension of the rim, and also some bending stresses. The standing vehicle load is transmitted to the rim by redistribution of the compressive force of the bead on the rim. When the vehicle runs, this gives a fatiguing stress. Braking and driving apply an axial moment to the wheel, and tend to make the tire slip around the wheel. Hence substantial normal forces are required at the bead to provide adequate frictional forces. In cornering, the center dish or spider is put into substantial bending, the whole wheel being effectively subject to a bending moment about a diametral axis of value approximately equal

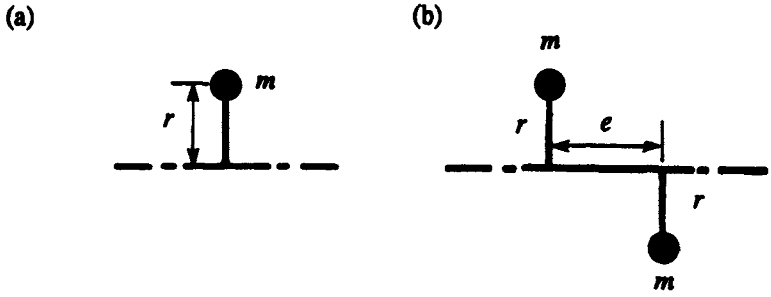

Figure 1.10.1. Imbalance: (a) static, (b) dynamic.

to the product of lateral force and tire loaded radius, $F_Y R_1$, with a typical value up to 1000 Nm. This gives substantial fatiguing stresses on the dish as the wheel rotates. The wheel must have sufficient fatigue strength to withstand these, and so, because the fatigue strength of light alloy is lower than that of steel, larger sections must be used.

The applied forces also cause wheel deflections. Although there does not seem to have been any directly observed measurement of the influence of wheel flexibility on handling, there is some anecdotal evidence that it can be detectable in some circumstances, especially on the race track where racing tires produce large lateral forces, where wheels are designed for lightness, wide tires are camber-sensitive, and vehicles are finely balanced.

The maximum moment about an axis on a vertical diameter is the maximum self-aligning torque, about 50 Nm, much less than the moment of 1000 Nm found about a horizontal axis. Hence, although the tire lateral force is much more sensitive to slip angle than camber angle, the wheel deflection in camber is significant. Considering a wheel diametral torsional stiffness of 500 Nm/deg, 1000 Nm will give a camber deflection of 2°, which is not negligible. Because it is necessary to provide adequate stiffness, there is little incentive to use high-strength steel in wheels, because the moduli of elasticity of various steels are virtually the same, and so a section reduction allowable because of high-strength material would result in excessive flexibility unless an improved shape could be found. Plastic wheels, with their low modulus, are also subject to this problem even if they are strong enough. Fiber-reinforced plastic wheels would be expensive for production road vehicles, although their properties might be acceptable; however, they have not found application so far. Plastics are generally prone to fatigue. The mass of a typical car wheel, using current materials, is approximately 10 kg.

Alternative wheel concepts have been proposed at various times, for example the now defunct Dunlop Denovo "run-flat" system. Currently in limited use are the Michelin/Dunlop TD system and the Pirelli/Goodyear asymmetric-hump tire-retention rim. Various other new systems are under development.

1.11 Roads

The ground surface is naturally a very important element in the environment of a vehicle. In some cases vehicles are required to be able to traverse a very wide range of terrain, for example military vehicles and to a lesser extent agricultural, construction and mining vehicles. However, a great majority of vehicles are designed to operate almost exclusively on specially prepared roads. As a minimum, the surface shape is controlled, basically by smoothing, and usually a gravel substructure (for strength) and a hard-wearing surface are provided, for example tarmacadam or concrete. The provision of roads is more or less as old as civilization itself.

Road density correlates well with industrial development and population density. The world average is about 0.14 km/km^2 of land area. Assuming an average road width of 10 m suggests that 0.14% of the world's land surface is road. The figures are highest in Western Europe, with an average of about 1.2 km/km^2, 1.2% of the land surface. A road density of 2 km/km^2 would be equaled by a square mesh of roads at 1 km intervals. Such high road densities imply a large number of road junctions, so vehicles must often negotiate the sharp corners that are characteristic of junctions.

Car ownership in Europe is approximately 0.2 car per person, against a world average of about 0.05. This means that in Europe there are about 50 vehicles per kilometre of road, or the amount of road is 20 m per car. Fortunately, at any one time most cars are off the road, but nevertheless this low figure does mean that the driving environment is often characterized by the presence of other vehicles, which may greatly constrain a driver's maneuvering options. In a direct sense, the presence of the other vehicles only impinges on a vehicle when there is a collision. Happily this is relatively rare, European insurance statistics indicating that the average car and driver has an accident claim at intervals of about eight years. Adapting a concept from statistical thermodynamics, we could say that the average car has a mean free path on the order of 10^8 m between significant collisions.

The kinematic design of a road depends on the service that it is required to provide. The number of lanes depends on the traffic density; one lane can handle an uninterrupted flow of about 1200 vehicles per hour, although this can be influenced by many factors including slope, curvature, sight distances, width, frequency of interruptions such as junctions or bus stops, lighting, speed limits, weather, etc.

The mechanical design of a road depends on the size and frequency of the imposed traffic loads. A road may be likened to a cyclically loaded metal component, having a fatigue life. For loads below some threshold the life is virtually infinite, but larger loads rapidly cause damage and consume the fatigue life. The important load is not the total vehicle weight but the individual tire loads. In practice, in road design lateral load transfer is neglected, and the axle load is considered as the vital parameter. Tire lateral forces certainly increase the surface wear rate, but the road structure is designed around the distribution of vertical forces to be accommodated with an acceptable life. Any undulations of the road considerably increase the peak dynamic vertical forces above the mean value, and this must be allowed for.

From the civil engineering point of view, the basic structure of a road is considered to be either flexible or rigid. In either case, there is a sublayer of typically 250 mm of gravel placed over the compacted subsoil. For a so-called flexible pavement the top layer is about 70 mm of tarmacadam or similar tar-coated gravel. A rigid pavement has a top layer of about 250 mm of concrete, often reinforced; this is in sections with expansion joints. The rigid type has substantial bending strength, and distributes the load more widely, although both types may accommodate heavy loads with appropriate thickness of material. Even the flexible type has only a small deflection under the actual loads, and for vehicle dynamic analysis on road surfaces it is usual to treat the road as completely rigid; this is a very helpful simplification, which would be quite inappropriate for many off-road analyses. There is of course a wide variety of other surfaces, rarely laid new today, such as cobbles and pavé.

For handling analysis, the surface character of the road must be represented in some way, i.e., we must consider deviation of the road from the simplest possible case of perfectly smooth, horizontal and straight. Much of the character of the road can be represented by considering a spectral analysis of the road surface deviations. Table 1.11.1 shows one possible way of partitioning the wavelengths, and how they bear upon handling analysis.

Table 1.11.1. Road Spectral Analysis

Characteristic		Wavelength	Influence on:
Slopes		50 m < λ	Pseudo-static
Undulations		1 m < λ < 50 m	Dynamic (ride)
Roughness		10 mm < λ < 1 m	Dynamic (NVH)
Texture	Macro	1 mm < λ < 10 mm	Friction and noise
	Micro	10 µm < λ < 1 mm	Friction
Material		Molecular	Friction

For wavelengths exceeding 50 m, i.e., hills and slopes, at an example speed of 20 m/s the forcing period exceeds 2.5 s, which is slow enough for the vehicle to be in effective equilibrium on its supension. Thus in this range the effect may be dealt with by a static analysis; in other words, to the vehicle a hill is essentially a sequence of steady-state conditions, each of constant slope.

Wavelengths from 1 m to 50 m, i.e., periods of 50 ms to 2.5 s, called "undulations" here, are dealt with primarily by the suspension, and stimulate a dynamic response. This includes the basic sprung mass resonance at about 1 Hz, which must be controlled by the damping. Wavelengths of 10 mm to 1 m, with periods 0.5 ms to 50 ms, called "roughness" here, are dealt with largely by tire deflection, and again require a dynamic analysis of the vehicle response. Some roads, for example cobbles and pavé, exhibit a large spectral peak at a wavelength corresponding to the dimension of the constructing elements, around 100 mm.

For wavelengths under 10 mm there is little dynamic response from the vehicle, the forcing period being under 0.5 ms. The main effect is on the frictional behavior of the tire. The division into macrotexture and microtexture is a result of analysis of actual roads and their influence on friction, where it has been found that the road can be well represented by giving it roughness values on the macrotexture and microtexture scales, or simply defining it as rough or smooth on each scale (Figure 1.11.1). Macrotexture is described as rough or smooth, whereas microtexture is described as harsh or polished. Older, obsolete terms for macrotexture were open and closed, respectively. Macrotexture corresponds essentially to the size of gravel used in the tarmacadam, size range 1 to 10 mm, and in a sense measures the extent to which the gravel protrudes or has been rolled-in flat with the tar, while the microtexture corresponds to the surface finish of the gravel elements. Their influence on wet roads is somewhat similar to the influence of tire tread design, in that a rough macrotexture assists water clearance

	Macro-texture	Micro-texture
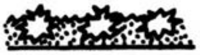	Rough	Harsh
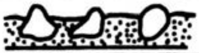	Rough	Polished
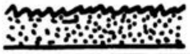	Smooth	Harsh
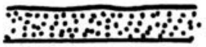	Smooth	Polished

Figure 1.11.1. Macrotexture and microtexture of road surface.

in the tire footprint like the tread grooves, while a rough microtexture, like sipes, gives high local pressures to clear the final film. In wet conditions the porosity of the upper layer is important in providing additional drainage paths below the tire, whereas on a smooth impervious surface such as concrete, tire footprint clearance must be achieved exclusively by the tire tread design. This topic is explored more extensively in Section 2.19. Attempts have been made to improve concrete road drainage below the tire by introducing lateral grooves in the road surface; this is effective but causes substantial tire noise.

At a molecular scale, the actual road material has a considerable influence on the frictional characteristics. Also, the variation of frictional coefficient with temperature is quite different for tarmacadam and concrete (Section 2.16).

The above spectral analysis of road deviations can be performed for three directions, i.e., we can analyze the road shape in plan view, in lateral section and in longitudinal section. The comments made above are mainly concerned with the last of these. In plan view the analysis would be significant only for wavelengths of undulation size or larger; i.e., in this case the class "slopes" corresponds to the direction of the road, and the class "undulations" corresponds to curves or corners. Smaller deviations are not meaningful in this case. In lateral section the terminology used for longitudinal sections is generally appropriate. However, lateral slope and undulations are normally given the special names of "road camber" and "road camber curvature." Lateral section roughness influences the vehicle in a similar way to longitudinal roughness, but through tire camber effects. It is possible in principle for lateral section texture to be different from longitudinal texture, for example because of fine lateral grooves in concrete or because of the longitudinal rolling process in road manufacture, but in practice such differences are usually neglected.

As far as handling analysis is concerned, road factors of type texture and material are dealt with as part of the tire properties for a particular surface; frictional properties are always a property of the combination of surfaces, so the expression tire properties should really be considered as an abbreviation for tire–road properties.

Road factors of type roughness and undulations stimulate a dynamic vehicle response and are generally regarded as constituting part of the field of unsteady-state response. The mean response of a cornering vehicle to a systematic form of roughness might, however, in some cases be considered to be an effectively steady-state response. Lateral undulations, i.e., successive corners, will generally constitute a continuous unsteady state. However, the special case of a constant-radius corner, neglecting entry and exit transients, obviously constitutes a steady state, as does the true fixed-radius standard test. Road slopes, or direction in plan view, clearly constitute steady-state problems.

For handling analysis it is often convenient to represent the road at a given point by its direction and curvature, and possibly rate of change of curvature, in each of its three sections (Figure 1.11.2). In plan view the road, or more precisely the vehicle path, has direction and corner curvature. The direction of a road is not significant in a handling sense, other than in the context of a wind of specified direction; but as stated in Section 1.3, the direction of the path, i.e., of the projected vehicle velocity, is measured from the X-axis of an arbitrarily selected inertial XYZ system, clockwise positive in plan view, and represented by ν (nu). A positive radius of corner curvature will be considered to have a center in positive y of the vehicle-fixed axes in normal running, i.e., Figure 1.11.2(a) shows positive curvature. Positive curvature, and a positive radius, correspond to a right-hand turn.

Positive camber will be increasing height toward positive y; camber is expressed in radians or degrees or as a gradient, typically 2° or a gradient of 0.035 or 3.5%. For large gradients, the distinction between the use of $\sin\theta$ and $\tan\theta$ becomes significant; $\sin\theta$ will be used here. Positive camber radius will be with the center of curvature in positive z. Figure 1.11.2(b) shows positive camber slope and positive camber curvature.

Positive longitudinal slope will be increasing height toward positive x, i.e., uphill, expressed as radians or degrees or as a gradient. Positive longitudinal radius will be with the center of curvature in positive z. Thus a humpback bridge

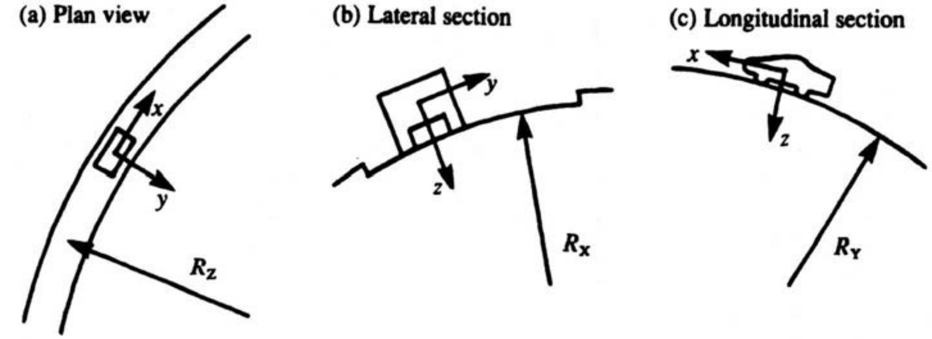

Figure 1.11.2. Road slope and curvature.

has positive curvature and radius at the center, and negative curvature and radius at its entry and exit. Figure 1.11.2(c) shows positive slope and positive curvature.

The influence of these road shapes on handling will be discussed in the chapters on handling. Briefly, however, corner curvature evidently demands lateral forces to provide the centripetal acceleration. Camber slope demands a lateral force on a straight road, to balance the side component of the weight force, and also causes lateral load transfer. Camber curvature introduces camber angles to the tires. Longitudinal slope influences the thrust requirement in steady state, and causes longitudinal load transfer. Longitudinal curvature influences the tire normal forces, which in the vehicle-fixed axes can be explained as the consequence of a vertical centrifugal (compensation) force. The influence of slopes is particularly significant in low-friction conditions. For example, with a camber gradient of 5% and an ice-covered road with a tire friction coefficient of 0.1, half of the available friction force is required simply to drive straight ahead.

In practice these road deviations are often combined, for example camber in a corner, or a corner on a crest, posing interesting handling problems.

The surface of a road is often at variance with its basic design condition, through damage, e.g., potholes, or contamination, e.g., rain, ice or fallen leaves. Rain is dealt with by having a camber, the slope of which depends on the water thickness that is tolerable for a given rainfall rate. For example, at a rainfall rate of 20 mm/h, which is 5.5 g/m^{2}s, a 10 m wide carriageway draining to both sides will have a flow of 28 g/s for each metre of length at the edges, and proportionately less toward the center. Thus greater camber is needed at the edges; typically 2% is used. The necessary camber depends on the acceptable depth of water, which is a function of vehicle speed and tire tread design (Section 2.19), so safe vehicle speed is directly related to rainfall rate.

Ice is a serious hazard because of its low friction properties. It is white when broken or frozen unevenly, for example frost, because of refraction and scattering of light by the facets of the ice fragments. So-called black ice is water that has frozen *in situ*, and is therefore transparent, appearing to be the color of the underlying road. This is particularly dangerous because it is difficult to see.

1.12 Drivers

In any particular situation, the motion of the car depends on the performance of the complete car–driver system. Figure 1.2.1 showed the principal interrelationships. The driver accepts feedback information, mainly from the vehicle motion including position on the road and steering feel, and hence this is a closed-loop system. A large part of handling theory is concerned with expressing the vehicle transfer function in terms of its detailed design, for example tire and suspension parameters. This is conventional engineering, and considerable progress has been made in this area (Chapters 6 and 7), although the process is not yet complete.

When we consider the closed-loop system, which includes the driver, many new questions arise. What is the optimum vehicle transfer function to enable the driver–vehicle system to achieve optimum performance? Indeed, does such an optimum exist, or does it vary considerably between various drivers and roads? If there is no optimum, can limits be set on acceptable vehicle open-loop characteristics? In the interests of safety, should these be the basis of legal requirements? These have proved to be very awkward questions – the identification and objective specification of good handling qualities are extremely difficult. One aspect of the problem is that in practice a vehicle must be suitable for a range of activities and conditions. Another reason for difficulty lies with the driver, because the driver transfer function is highly complex, variable between drivers, and with time for a given driver; the driver is a highly adaptable control system and to a considerable degree the driver adjusts according to the vehicle characteristics to give a satisfactory overall system characteristic. Also, it is difficult to keep constant the experimental conditions such as mental and physical state and skill of the driver.

The driver uses most of his senses in driving; in some respects the human is far superior to the machine in processing data at present, for example in sight and visual field processing, i.e., pattern recognition, but inferior in other respects, for example the inner ear for inertial navigation. Sight is used primarily to examine the road shape ahead including obstacles such as other vehicles, and to assess some of the vehicle motion variables, particularly vehicle position on the road, path curvature, speed, yaw speed and roll angle. Tactility, i.e., external feeling over the body, is used to detect linear accelerations, as perhaps is feel at the hands indicating steering torque, and at the feet for pedal forces. Kinaesthetics, i.e., the internal feeling of muscular effort, is used to assess steering torque and pedal loads, and also lateral acceleration in those cases where the seat does not adequately locate the body. The inner ear also contributes to acceleration assessment. Hearing gives occasional information, including speed cues such as wind and engine noise and tire squeal, but is perhaps most important as a warning channel, for example other vehicles' horns. In certain military and competition activities, hearing is important as the communication channel with a navigator. With the advent of the talking microprocessor, this channel can be used to advise the driver of road hazards or of inadequate distances from other vehicles, detected by suitable sensors.

The data are transmitted to the brain and processed, and then suitable muscles are activated, thus introducing a time delay. In a simple tracking problem this is typically 0.15 s, and associated largely with the transmission speed in the motor neurons from brain to hand. This compares with a total time of about 1.0 s for a realistic braking or swerving situation, requiring about 0.5 s for recognition of the need for action and about 0.5 s to activate the muscles. Thus human response time constants are typically 0.15 to 1.0 s, provided that deliberation is not required. This compares with typically 0.2 s for the time constant of a car in yaw.

The driver judges much of the vehicle's behavior through the seat. Experiments have been performed with the seat pivoted about a vertical axis so that any lateral acceleration of the vehicle causes a slight rotation of the seat. This strongly influences the driver's perception of the vehicle's behavior, with a forward pivot making the vehicle seem unstable and giving the driver a low confidence, and a rearward pivot giving a good stability feeling and possibly overconfidence. A forward pivot results in the driver's body having an increased attitude angle, so this is consistent with the general result that it is subjectively good for attitude angles to be small. For those commercial vehicles with isolated cabs there may be significant motion of the cab relative to the chassis, so if the driver's perception is being considered then it is necessary to instrument the cab in addition to the chassis.

On the whole it seems that the driver is remarkably sensitive to minor cues regarding the behavior of the vehicle. In open-loop handling tests the path of the vehicle can be quite well predicted, even from steady-state data, but the reaction of a driver to a vehicle, i.e., favorable or unfavorable, is much more difficult to predict. This is important; minor changes that would normally be regarded as negligible from the engineering perspective and which hardly affect the vehicle response at all may have a substantial effect on the driver's perception of the vehicle, and may make the difference between a vehicle that is subjectively good or bad. Thus in answering the question of what design features lead to good handling, it is essential to distinguish clearly between the problem of achieving a good vehicle response, i.e., a fast stable response to control inputs, and the problem of achieving a good "driver feel."

Attempts to find specific vehicle parameters that give favorable subjective assessment have met with only limited success, with different and sometimes opposite results from various studies, and with a wide variety of driver preferences and ability to discriminate between different vehicles. Typically, drivers can discriminate approximately 10% changes in steering gear ratio G, in the understeer gradient k, and in the yaw response time τ, when driving vehicles at intervals of a few minutes. Chapters 6 and 7 give information on the best values for design variables.

Actual driver behavior on the road, in terms of frequency of lateral acceleration demand, varies considerably between roads and drivers. Figure 1.12.1 shows percentage distance traveled against lateral acceleration for an average driver. For example, from this figure we can read that on rural roads an average driver exceeds $0.25g$ lateral acceleration for 1% of distance traveled, and that in all cases about 90% of distance traveled is covered at less than $0.07g$. Note that speed alone is not a good indicator; motorways, with their absence of small-radius bends, have high speeds but a small lateral acceleration demand. Rural roads have the highest lateral acceleration demands. Trunk and urban roads are similar, although mean speed on the former was twice that on the latter. As an example of the differences between drivers, on rural roads relatively slow, medium and fast drivers produced results with a similar pattern to Figure 1.12.1, but the demands for $0.3g$ were zero, 0.2% and 1.0%, respectively.

1.13 Testing

Vehicle testing is performed for various purposes, for example to confirm that a proposed vehicle design is acceptable, or to test proposed changes, or to test theory in the hope of gaining improved understanding which should in turn lead to better vehicle behavior. Referring back to Figure 1.2.1, which defines the open-loop system as the vehicle response only and the closed-loop system as the vehicle plus driver, the tests can be subdivided into:

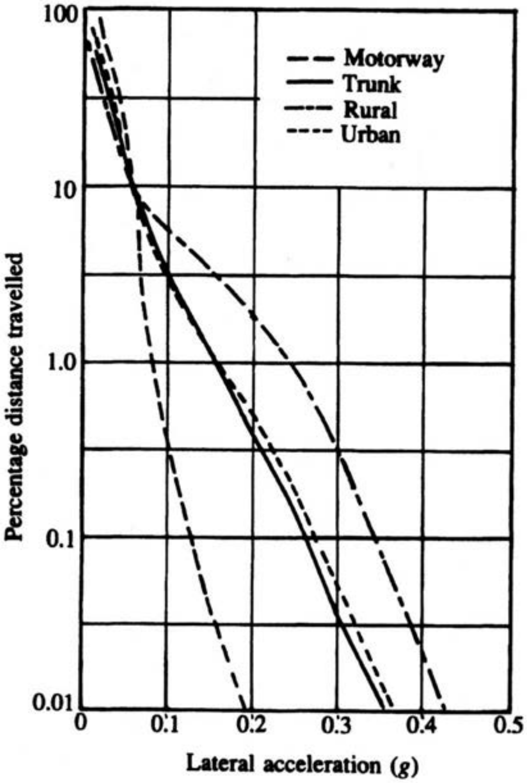

Figure 1.12.1. Average driver behavior. (Reproduced by permission of the Council of the Institution of Mechanical Engineers, from Smith, J.G., and Smith, J.E., "Lateral Forces on Vehicles During Driving," Automobile Engineer, *December 1967.)*

- (1) Open-loop
  - (a) Position control
  - (b) Force control
  - (c) Disturbance response
- (2) Closed-loop
  - (a) Task performance
  - (b) Subjective evaluation
  - (c) Disturbance response

Position control means that the control positions are specified, for example a ramp-step or sinusoidal steering input. Force control tests are unusual for road vehicles, although common for aircraft in the special case of zero force, known as the "stick-free test." Disturbance response includes tests such as side wind gusts. For vehicle plus driver closed-loop tests, specific tasks may be set, for example to perform a maneuver at the maximum speed or in the shortest time, giving an objective measure of performance in speed or time. Alternatively, in subjective assessment the driver's opinion of the vehicle's behavior is solicited.

The ultimate test of handling is to expose a vehicle to experienced test drivers over a wide range of road types and weather conditions. The drivers can then score the vehicle on various qualities, and in particular can point out any problem areas; i.e., this is a subjective test. The advantage of this method is that it is comprehensive and realistic. However, it may also be time-consuming, and because it is subjective it is necessary to have several test drivers.

Although it may be possible to correlate test driver ratings with objective performance measures and with the detail design of the vehicle, this is not easy and not always successful. In order to understand handling and to relate it to design features it is normal to use various standard open-loop tests. These tests are of a relatively simple nature so that the vehicle response is measurable objectively, and can be directly and causally related to design. With the present state of knowledge, there is a substantial gap between the idealized tests and the broader road behavior of the vehicle, i.e., although there has been some progress in this area it is not yet possible to define a series of standard tests that adequately encompass road behavior.

The basic steady-state test is to operate the vehicle in steady cornering, i.e., constant speed and constant radius. Other steady-state test conditions include operation on a cambered, i.e., laterally sloping road, and operation in a side wind. The most fundamental unsteady-state test is perhaps one of constant speed with varying path curvature, which for a given curvature can be compared with the corresponding steady state; this is a test at a point condition. In practice, manufacturers and independent testers use various other more specific tests, for example capability of a lane change, or maximum speed through a chicane, i.e., a double lane change, specific corner entry and exit tests, and speed through a slalom; these are task performance tests and are closed-loop tests over a given path, as opposed to tests at a given point condition. Open-loop tests measure response to a given steer input, for example step, ramp, sinusoidal or random input. In addition there are unsteady wind response tests, for example exposure to a gust or to a step change of side wind. Among given-path unsteady-state tests there is little standardization of the details, e.g., of chicane dimensions, although there are ISO drafts for a number of open-loop tests.

The steady-state test has been subject to some standardization, for example ISO 4138. The purpose is to explore the relationship between each of steering wheel angle, steering wheel torque, sideslip angle and roll angle with the lateral acceleration; the primary result is the one for steering wheel angle. The test is performed on a fairly smooth area of a hard high-friction surface, for example asphalt or concrete, with a radial slope of up to 2% for drainage. The radius should be at least 30 m; for example the Motor Industry Research Association (MIRA) pad course is 32.9 m (108 ft). A large radius means a higher speed for a given lateral acceleration, so for a larger radius aerodynamic forces may become significant. At 30 m radius, 8 m/s^2 lateral acceleration occurs at a speed of 15.5 m/s (34.7 mph); typically $C_DA < 1$ m^2 and $C_LA \approx 1$ m^2 giving drag and lift forces of about 150 N, about 1% of the weight, and just about negligible. At a 300 m radius the required speed is 49 m/s, giving drag and lift of about 1.5 kN, about 10% of the weight. The side forces will generally be of the same order. Thus the test radius can be chosen to include or exclude aerodynamic effects, within limitations of engine power and track facilities. Lift and pitch are basically proportional to speed squared for constant coefficients, and hence to lateral acceleration at a given radius. On the other hand, because yaw angle grows with lateral acceleration, the aerodynamic side force and yaw moment, which depend both on dynamic pressure $\left(\frac{1}{2}\rho V^2\right)$ and on the aerodynamic yaw angle, are basically proportional to speed to the fourth power, and to lateral acceleration squared (Chapter 3). Engine power demands were discussed in Section 1.8. This can be a particular limitation for commercial vehicles. For large radii only partial circuits are used, but sufficient to allow steady state to be established; this should be for at least 3 s, with a path deviation not exceeding 0.3 m.

Wind speed should not exceed 7 m/s for 30 m radius, and less for larger radii where the vehicle speed will be higher and wind sensitivity greater. Tires are warmed up for 500 m at 3 m/s^2. Data points are taken at lateral acceleration intervals of no more than 0.5 m/s^2, and less if the results are sensitive to lateral acceleration, which may be so for small values, e.g., under 1 m/s^2, and is always so for large values, e.g., over 6 m/s^2. Increasing values of lateral acceleration are used until steady state can no longer be maintained. Data are taken and presented for both directions, because in some cases this makes a considerable difference.

The actual speed V, yaw velocity r and centripetal acceleration A can be measured and calculated from each other in various ways, for steady state, since we have:

$$V = rR$$

$$A = r^2 R = rV = \frac{V^2}{R}$$

Data may be taken from:

(1) A y-aligned accelerometer

(2) A yaw-rate gyro measuring r

(3) An inertial velocity transducer

(4) Elapsed time over a given path, for example one lap

Table 1.13.1 shows suggested ranges and maximum errors for the complete measurement system employed, and gives some idea of the accuracy that can realistically be achieved. The frequency bandwidth should be at least 3 Hz for steady-state measurements, to indicate fluctuations and to allow automatic sensing of when an acceptable duration of effective steady state has been achieved. For vehicles with significant chassis torsional compliance, for example commercial vehicles, it is necessary to measure the roll angle at at least two points, for example over the axles. The use of vehicle transducers means that the data are measured in the vehicle-fixed axes, so appropriate transformations must be applied to obtain the desired plotting values, for example acceleration from a transducer aligned with the y-axis will need consideration of both roll and sideslip angles.

Table 1.13.1. Transducer and Recorder Specifications

Variable	Symbol	Min. range	Max. error
Steering wheel angle	δ_{SW}	±360°	±2° (<180°) ±4° (>180°)
Lateral acceleration	A	±15 m/s^2	±0.15 m/s^2
Yaw angular speed	r	±50°/s	±0.5°/s
Speed	V	+50 m/s	±0.5 m/s
Attitude angle	β	±15°	±0.5°
Steering wheel torque	T_{SW}	±30 Nm	±0.3 Nm
Roll angle	ϕ	±15°	±0.15°

Instead of using transducers in the vehicle, some parameters can be measured by using a small trailer, e.g., the MIRA roll/slip trolley. This was a small trolley of mass 18 kg, with two small cycle wheels usually attached to the rear of the vehicle. Being light and balanced, it corners with small roll and sideslip, thereby providing a reference from which the vehicle roll and sideslip can be measured at the connection to the vehicle. A geometrical allowance must be made for the trolley position relative to the vehicle center of mass. This method has proved to be more suitable for steady-state response investigations. Laser distance meters can be used for ride height and roll angle measurement, and laser-doppler devices for accurate speed measurement. These are effective, but expensive.

An unusual alternative form of steady-state testing developed at MIRA, now no longer used, was tethered testing. Here the vehicle was firmly displacement-located, at a point close to its center of mass, from a rigid arm cantilevered sideways from a large truck. The test vehicle could rotate freely, and hence adopt steady-state yaw, pitch and roll angles according to the steer and throttle positions. Extensive data acquisition and processing equipment could be carried in the truck, avoiding the problem of loading the vehicle.

In steady-state testing a human driver is normally used, attempting to maintain constant radius, constant steering and constant accelerator position. Near to the maximum lateral acceleration it proves increasingly difficult to maintain steady conditions. Thus an open-loop test of the vehicle only becomes to some extent a closed-loop test.

When studying the unsteady response to a specified steering input, it is very difficult for a driver to control the wheel position accurately, for example over a ramp change at a specified rate to a particular value. In some cases, therefore, steering wheel control has been automated, driven by a stepper motor. This gives much better repeatability.

The random steer input test is typically performed over a straight of at least 1 km at several speeds, e.g., 50, 80 and 120 km/h. After analysis, the basic result is a transfer function for the vehicle.

The results of testing can be expressed in many different ways; these are discussed in Chapters 6 and 7. Typically, the steady cornering result is a plot of the various parameters against lateral acceleration. Although the centripetal acceleration should really be used, it has become common practice to use the lateral acceleration. The difference is usually small because it is a cosine difference in β, e.g., 1% at 8°. Often the steering wheel angle is divided by the effective steering gear ratio between the hand wheel and the road wheels to give the reference steer angle δ_{ref}, and then this and the sideslip and roll angles are all plotted on one figure, as for example in Figure 1.13.1. The transient response is often summarized by plotting the steering response gain and the phase against frequency.

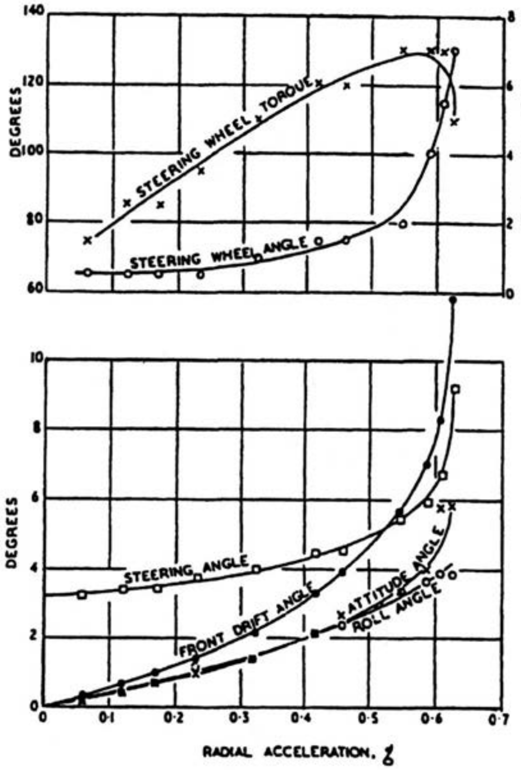

Figure 1.13.1. An early steering pad result (Porsche 911, Mark 1).

Figure 1.13.2 shows the Dunlop–MIRA handling and stability circuit, designed to provide preliminary assessment of handling qualities of vehicles or tires before more extensive road testing. A variety of radii are provided, each long enough for the steady state to be established, so that all phases of cornering can be studied. There is also an area for chicanes and small-radius tests. Part of the circuit passes in front of the MIRA wind generator, for wind response tests.

MIRA also has a ride and handling circuit for suspension evaluation, including pavé, corrugated track, long-wave pitching track, single bump, 1.5-inch dip, manholes, broken edges, corrugated bend, level crossing, hills and dips, adverse camber, road intersection, spoon drain and Australian Creek, and other "standard" challenges to the suspension, some rarely used nowadays.

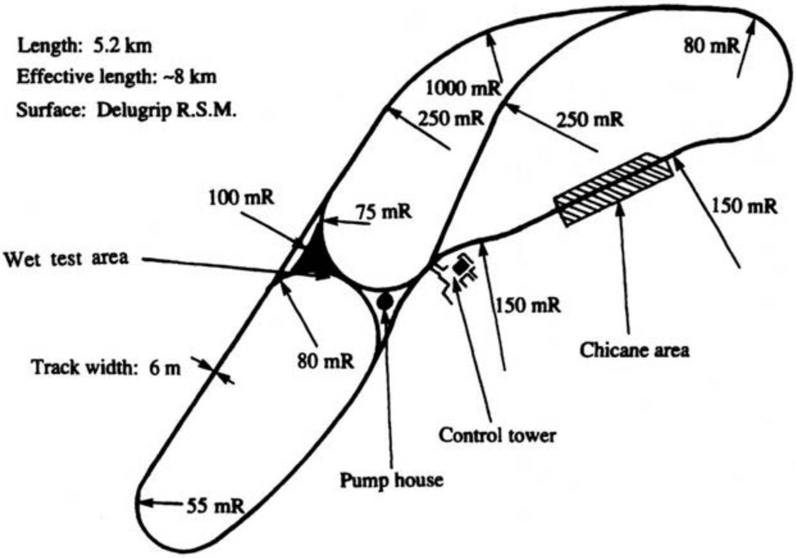
Length: 5.2 km
Effective length: ~8 km
Surface: Delugrip R.S.M.
1000 mR
250 mR
250 mR
80 mR
100 mR
75 mR
150 mR
Wet test area
150 mR
Chicane area
Track width: 6 m
80 mR
Control tower
Pump house
55 mR

Figure 1.13.2. Dunlop-MIRA handling and stability circuit.

1.14 Problems

Q 1.1.1	Explain the meaning of the terms cornering, road-holding and handling.
Q 1.2.1	Give a 1000-word review of the history of the theory of handling.
Q 1.3.1	Explain the differences between longitudinal, side, normal, forward, lateral, heave, tangential and centripetal accelerations.
Q 1.3.2	Explain the relationship between the heading angle, sideslip angle, attitude angle and course angle.
Q 1.4.1	Discuss the validity of treating the vehicle as a rigid body, with regard to wheel rotation.
Q 1.4.2	Explain the term "compensation force."
Q 1.5.1	Describe in some detail how you would measure the torsional rigidity of a chassis.

Q 1.6.1 Four wheel reactions are measured as $F_{\mathrm{VfL}} = 4.1$ kN, $F_{\mathrm{VfR}} = 4.9$ kN, $F_{\mathrm{VrL}} = 4.1$ kN and $F_{\mathrm{VrR}} = 4.3$ kN on a wheelbase of 3.20 m and track of 1.40 m. Where is the center of mass?

Q 1.6.2 On the Moon ($g = 1.60$ m/s^2) a spring balance intended for use on the Earth is used, and indicates 4.300 kg. Calculate the weight and mass of the object.

Q 1.6.3 A 3.50 m wheelbase vehicle has a wheel radius of 0.30 m, and has $N_{\mathrm{f}} = 9.20$ kN and $N_{\mathrm{r}} = 7.80$ kN when level. When inclined at 30°, still resting on its wheels, $N_{\mathrm{r}} = 6.3$ kN. Find the longitudinal position and height of G.

Q 1.6.4 In a trifilar pendulum test, with wires of length 3 m at radius 2 m, the platform alone has a mass of 220 kg and a frequency of 0.270 Hz, and the platform plus vehicle is 0.256 Hz. The vehicle mass is 1640 kg. Calculate the vehicle yaw inertia.

Q 1.6.5 A vehicle of wheelbase 2.500 m with mass 1540 kg and $a = 1.100$ m is suspended on a quadrifilar pendulum, supported directly at each axle at a width of 2.100 m, on wires of length 2.00 m. The natural yaw frequency is 0.290 Hz. Calculate the yaw inertia.

Q 1.6.6 A 1760 kg vehicle of wheelbase 3.00 m ($a = 1.50$ m) is mounted on a hydrostatic pivot bearing 0.52 m behind G, and put into fixed-axis oscillation about a vertical axis. The restoring moment is from a 20.0 kN/m spring acting with a moment arm of 1.620 m. The natural frequency is 0.411 Hz. Calculate the vehicle yaw inertia and corresponding radius of gyration and dynamic index.

Q 1.6.7 A vehicle of mass 1330 kg and center of mass height 0.580 m rests on a pendulum plate with upper surface 3.00 m below the pivot. The plate center of mass is 3.05 m below the pivot, and the plate mass is 210 kg. The plate alone is found to take 41.84 s for 10 cycles; the plate plus vehicle takes 37.04 s for 10 cycles. Calculate the vehicle pitch inertia and corresponding radius of gyration.

Q 1.6.8 Obtain an expression for the lateral distance of G from the centerline in terms of the static wheel reactions.

Q 1.6.9 For Figure 1.6.2, by drawing a suitable diagram, show that

$$c + H \sin \theta = a \cos \theta + r \sin \theta$$

Q 1.6.10 The height and lateral position of the center of mass of a vehicle are to be investigated by fitting it with thin disc wheels and inclining it laterally until balance is achieved. The angles from the horizontal are found to be θ_l and θ_r for left and right wheels on the ground, respectively. Obtain equations for the desired values.

Q 1.6.11 A complete vehicle has mass 1750 kg with G at height 720 mm, 1.420 m back on a 2.920 m wheelbase, and has front and rear unsprung masses of 130 kg and 270 kg both at height 340 mm. Find the front and rear end-masses, and sprung G position behind front axle and height.

Q 1.6.12 Explain how the value of the sprung mass and the longitudinal and vertical position of the center of sprung mass may be calculated from the properties of the complete vehicle and the unsprung masses. State exactly what information is required, and give all relevant equations in the order in which they will be used.

Q 1.7.1 An unloaded vehicle has mass 1800 kg, with G at a point 1.422 m behind the front axle and 0.630 m above ground level. $I_P = 3400$ kg m^2. A uniform load of mass 340 kg is added, with its center of mass 2.413 m behind the front axle, and at a height of 1.104 m. The load dimensions in side view are length 2.142 m and height 1.010 m. Find the combined center-of-mass position and the pitch inertia.

Q 1.8.1 Describe how the engine power requirement depends on test radius for a given lateral acceleration, and on lateral acceleration at a given radius.

Q 1.9.1 Explain the functional difference between open, solid, locking and limited-slip differentials.

Q 1.10.1 Describe briefly the different types of wheels.

Q 1.10.2 Describe the influence that the geometric and stiffness properties of the wheel has on handling.

Q 1.11.1 Describe how the longitudinal fluctuation of road shape may be considered in terms of a spectral analysis, and how the wavelengths may be grouped.

Q 1.11.2 Describe how road texture influences tire characteristics in wet road conditions.

Q 1.11.3 Sketch the three cross-sections of a road which has positive slope and curvature in each case. What part does each play in handling?

Q 1.12.1 Discuss the reasons for the difficulty in determining vehicle design features that optimize closed-loop system performance, and that give good subjective assessment of vehicle dynamics.

Q 1.12.2 Describe how a driver perceives vehicle motion.

Q 1.12.3 With what percentage probability, based on distance, does an average driver call for a lateral acceleration exceeding 2 m/s^2 on typical rural roads and trunk roads in Europe?

Q 1.13.1 Discuss the relative merits of subjective, task performance and vehicle response tests.

Q 1.13.2 Describe the most common forms of unsteady-state tests.

Q 1.13.3 Sketch a typical graphical result of a steady-state circular test, and briefly describe its main features.

Q 1.13.4 Describe the various ways in which speed, yaw velocity and lateral acceleration can be measured and calculated from each other for a circular pad test.

1.15 Bibliography

There are only a few books on vehicle dynamics, mentioned as appropriate below and in other Chapter bibliographies. There is, however, an extensive research literature, of which it is possible to mention only a limited number of the more salient and useful papers.

Most of the useful papers appear in the following publications: *Automobiltechnische Zeitschrift* (in German), *Bulletin of the Japanese Society of Mechanical Engineers* (in English), *Proceedings of the Institution of Mechanical Engineers*, Society of Automotive Engineers technical paper series, *Transactions of the SAE, Transactions of the American Society of Mechanical Engineers*, and the journals *Vehicle System Dynamics* and the *International Journal of Vehicle Design*. There have also been many relevant conference proceedings, mostly sponsored by the above bodies, including, for example, the long-running IAVSD symposium series "Dynamics of Vehicles on Roads and Tracks."

To put road vehicles into context, the broader background of ground vehicles in general may be found in Bekker (1956, 1960, 1969) and Wong (1978). (References can be found in the references section near the end of the book.) A good general introduction to the mechanical design of vehicles is that by Korff (1980). A useful general introduction to the analysis of vehicles is that by Artamonov *et al.* (1976). For a general introduction to vehicle dynamics, see Gillespie (1992). For a qualitative description of vehicle components, see Heisler (1989) or Newton, Steeds and Garrett (1989).

For a useful general perspective on road-vehicle handling and suspension design, see Bastow (1980 or 1987) and Giles (1968). Another general work on suspension and handling is that by Steeds (1960). A largely practically oriented overview of the subject is the useful popular work by Puhn (1976, 1981). For a theoretical approach in a mathematical vein, see Ellis (1969), now out of print, or more recently Ellis (1989) or Ellis (1994). The latter has some overlap with this book (perhaps 30%), but is generally different in approach and coverage, and is recommended as a second opinion on those areas that are in common. Extra material there includes more extensive linear analysis, ride, steering oscillations, and articulated vehicles. Smith (1978) gives an interesting discussion of the optimization of racing car handling. Truck handling is dealt with extensively in Segel, Ervin & Fancher (1981). This also discusses load shifting.

The history of early handling, with extensive references, is given in Milliken & Whitcomb (1956). Details of the historical papers can be traced there. Figure 1.1.1 comes from Olley (1934). Figure 1.1.2 comes from Evans (1935). For more details on measurement of body inertia, see Winkler (1973) and Goran & Hurlong (1973). For details of the macrotexture and microtexture of roads see Sabey (1969). Driver behavior on the road is examined in Smith & Smith (1967). For a description of limited-slip differentials, see Lewis & O'Brien (1959), Hall (1986) and Garrett (1987).

2

The Tire

2.1 Introduction

Motion of the vehicle is controlled almost entirely through the forces exerted on the tire by the road. The tire characteristics therefore have a major effect on handling problems. This chapter presents the necessary information on the handling properties of tires. To put this in context, some general background information is also given. The essential function of a tire is to interact with the road in order to produce the forces necessary for support and movement of the vehicle body. Forces must be created to cause forward acceleration, braking, and cornering. The tire is also required to cushion the vehicle against road irregularities and to operate for many miles with great reliability. We shall be concerned here only with the vehicle control forces produced on the tire by the road; this is not to suggest that other factors, such as vibration isolation, are unimportant in the wider view.

In the production of the forces required to give the vehicle its desired kinematic behavior, it is the contact patch – the "footprint" – that is the focus of attention. To quote the first paper on tire cornering properties, by Evans in 1935, "The areas of contact between tires and road ... are the very front line trenches in the furious battle between space and time." The rubber-carcass pneumatic tire is uniquely adapted to this evolutionary niche. In the more than 100 years since the invention of the pneumatic tire, various alternative ideas have been investigated and some have even been tried on the road, but there has not been a significant commercial success for any alternative. This dominance by the rubber tire is the result of a remarkable combination of properties that enables the tire to provide support and control with good durability in difficult conditions, while being highly adaptable to specific applications.

For a given tire and road surface, the lateral force produced by road contact depends on many factors, especially the angular position of the tire relative to its direction of travel (the slip angle, sometimes called drift angle), its angle of lean to the vertical (the camber angle), the vertical force, the inflation pressure, and the rolling angular speed (associated with any tractive or braking forces also demanded). Many other factors have a secondary influence, including for example the speed of travel. When various tire designs and various road surfaces are considered, then a whole host of further factors are introduced. It is impossible to predict with high accuracy the tire force that will result in any real conditions. This is so for several reasons, including tire production variations, tire wear, road surface variation, and so on. Even in the laboratory, testing causes such rapid wear that a tire is likely to change its characteristics very quickly, and a tire will certainly wear out before a truly comprehensive set of results can be obtained. Nevertheless, characteristics of engineering accuracy can be achieved. These are reasonably accurate in relation to natural road variations. This chapter attempts to provide a qualitative, and to some extent a quantitative, understanding of the behavior of the tire and of the factors that influence it, and to provide some insight into the modeling of tire behavior for vehicle dynamic simulations.

2.2 Construction

The feature peculiar to a road vehicle, in contrast to a fluid-borne vehicle such as a ship or an aircraft, is the wheel. Since there is no fluid to provide the compliance necessary for both comfort and control, then compliance must be engineered into the vehicle. In practice this is provided by the tire, the suspension and the seat.

The essential constructional feature of the modern pneumatic tire is the carcass – a molding of rubber reinforced by several layers of cords or fabric, each layer called a ply. The carcass makes contact with the wheel at the bead. Multiple beads are sometimes used if there are more than eight plies, for example on trucks or aircraft. The bead is an interference fit on the rim which has a taper of about 5°. The carcass is inflated with air, sometimes using a thin inner tube for sealing, thus tensioning the carcass. Pressures are typically 120 to 200 kPa for cars, 300 to 600 kPa for trucks. These are, of course, gauge pressures; absolute pressures are 1 atmosphere (around 101 kPa or 1 bar) higher. The reinforcing cords, typically nylon, rayon or terylene, have a higher modulus of elasticity than the rubber, and their creep is less, so they carry the tension while the rubber acts essentially as a gas sealant. The alignment of the cords is an important feature affecting the vehicle handling behavior. In the radial-ply tire, the cords are radial in side view, running directly across the tread area (the crown) at 90° to the centerline. This is described as a crown angle of 90°, i.e., the crown angle is measured from a peripheral line around the tire. On the bias-ply (also called diagonal-ply or cross-ply) tire, the cord crown angle is typically 40°, alternate plies being angled left and right from the centerline, and they are no longer simply radial or, indeed, even straight, in side view.

The rubber of the carcass is fairly soft to give it good fatigue resistance. Various materials have been used for the cords. Dunlop's original tire used flax. Cotton was dominant up to 1945, then rayon up to 1960, and then nylon. Since about 1975 polyester has been most common. Steel, glass fibers and aramid fibers have also gained ground since 1970. These changes are directly related to the mechanical properties of the candidate materials. Brass-plated steel wire is favored for commercial vehicles and off-road applications. Laying up the cords is an expensive manual operation, but cordless tires have not yet come to commercial fruition. The density of the reinforcement varies considerably, e.g., nylon 1100 kg/m^3, glass fiber 2500 kg/m^3, steel 7800 kg/m^3.

On radial-ply tires, the crown has a circumferential reinforcing belt of nylon or steel cords. Some bias-ply (diagonal-ply) tires have been manufactured with belts (the belted-bias type) but these are no longer produced. All radial-ply tires are belted, so the simple term radial always implies this. The cord direction in a belt is relatively close to circumferential, i.e., the belt itself has only a small crown angle, typically 20°. Sometimes a breaker is used on a bias-ply tire – this is like a belt but with a crown angle close to that of the main carcass cords. A belt is sometimes known as a rigid breaker. The carcass construction so far described plays a dominant role in determining the tire characteristics and vehicle dynamics as far as normal driving is concerned, i.e., for lateral and longitudinal accelerations up to about 3 m/s^2 (0.3g).

On the outside of the crown, the perimeter of the tire, is the tread – the wearing course of rubber that actually contacts the road. This is patterned with grooves, slots and sipes (cuts), typically to a depth of about 8 mm when new (12 to 14 mm on truck tires) to encourage drainage in wet conditions. The tread pattern also assists cooling in dry conditions. When large accelerations in any direction are required of the car, then the frictional properties of the tread become most important. The tread rubber must be quite hard to give good wear characteristics, and therefore in choosing the rubber blend there is a conflict between wear and grip. Sometimes a softer cushion layer is used beneath the tread.

Tire size is normally specified by two primary dimensions: the wheel rim diameter and the section width (Figure 2.2.1). The section width is specified in millimetres for radial-ply tires. The safe load-carrying capability of a tire is primarily dependent on its size. The outer diameter is independently variable from the rim diameter, giving rise to various cross-section proportions normally expressed by the aspect ratio or profile, which is the section height divided by the section width. The tendency is toward greater width and less height, giving a lower aspect ratio, led by the extremely low profiles in racing. Modern passenger car tires have aspect ratio values of 50, 60, 70, 78 and 82%; in racing it may be as low as 30%. Low aspect ratios (65%) are now also used on trucks. For a bias-ply tire the natural aspect ratio depends on the cord crown angle, whereas for the radial it depends on the restricting effect of the belt. The structural design and materials selection for a tire is a delicate balance, and although it is known how to improve each separate property of a tire, the problem is to achieve this without an even greater sacrifice in some other property.

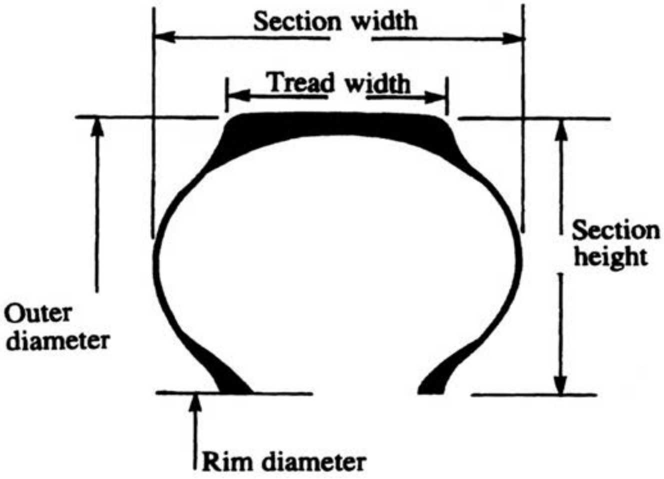

Figure 2.2.1. Tire cross-section

Although a design load may be quoted for a tire, its load-bearing capability depends in practice on the service conditions. The combination of load and inflation pressure results in a vertical deflection which causes bending of the carcass and tread, and hence fatigue stresses while running. There is also a consequential power dissipation and temperature increase. Hence the optimum pressure is load-dependent. This also implies that in severe cornering with substantial load transfer the interests of the dominant outside tires are better served by a higher pressure than is ideal for straight running. The acceptable deflection, and hence load, depends on the load-time duration, so that a load acceptable briefly in extreme cornering is not acceptable on a continuous basis. The sidewalls are normally expected to outlive the tread, although at very low wear rates embrittlement and sidewall cracking may occur first. The effect of operation at excessively high material temperatures (unacceptable combination of load, speed and environment) typically manifests itself as blistering (delamination), tread chunking (loss of small pieces of tread), tread stripping (loss of large pieces of tread), and roughness caused by loss of homogeneity.

The choice of a tubed or tubeless tire depends to some extent on the service conditions, although for road use it is largely a matter of local custom, with habits varying greatly between different countries. The tubeless tire is initially more economical and is more puncture-resistant; both types have a typical road distance between carcass penetrations of 30000 km, but the tubeless type requires a roadside wheel change in only about one penetration in five. In rough conditions such as rallying or other off-road activities, the tubeless type may lift from the rim under severe impact, with immediate deflation. For a normal road puncture, however, it deflates more slowly than a tubed type. The tubeless type is also a little lighter.

Charged with producing a new tire for a new vehicle, the tire designer is usually faced with basic dimensional restrictions – sufficient wheel diameter to accommodate suitable brakes, plus maximum outer diameter and section width for reasons of body clearance. The load-carrying ability is governed by the dimensions and the inflation pressure. Once the diameters and section width are determined, the cross-sectional shape must be decided. For an unbelted tire this is a function of the angle of the carcass cords. There being little bending stiffness, the cord tension must provide equilibrium against the inflation pressure and only one crown angle is compatible with a given set of values of rim radius, rim width, tire radius and section width. The cord crown angle of an unbelted tire governs many of the basic performance properties. For a larger crown angle (i.e., nearer to radial) the section width is lower, tread radius lower, rolling resistance lower,

shear stresses lower, bead stresses higher, cord tension lower, loaded deflection greater, contact length greater, lateral stiffness less, tread wear worse, sidewall cracking worse, tread cracking less, cornering stiffness less, ride softer, and bursting strength higher.

The carcass constructional details are much more complex and subtle than may appear from this terse description, and the properties of the tire can be markedly changed by quite small design alterations, especially of cord angles.

Although the bias-ply tire will no doubt continue in some specialized uses, for most applications the radial-ply tire is superior, especially for wear rate, and can be expected to continue to dominate in road vehicle use.

2.3 Rubber

The density of commercial rubber is 1100 to 1200 kg/m^3. Tire rubber includes other constituents such as carbon black and oil, and has an average density of about 1200 kg/m^3. Rubber, whether natural or synthetic, is a visco-elastic material. Essentially this means that when a piece of rubber is distorted, it will resist with a force, but the rubber relaxes because of the viscous effects, and the force diminishes. Figure 2.3.1 shows a very simple model that exhibits this kind of behavior. If a sinusoidally varying displacement is applied to the top point A, then the consequent force amplitude at A will depend on the frequency. At low frequency the damper will exert negligible effect, and the apparent stiffness will be that of the two springs in series. At high frequency the damper will have a large resistance and hardly move at all, so the stiffness will be greater, being that of the upper spring only. At both these frequency extremes, the damper will dissipate little energy. However, there is an intermediate frequency at which the energy dissipation is at a maximum.

If pure rubber is given a laboratory friction test against glass in clean conditions, then the frictional coefficient is found to depend on the sliding speed and the temperature (Figure 2.3.2). The peak friction coefficient observed may be very high, well in excess of 2.0. To avoid any confusion on this point, let it be clear that the coefficient of friction is not limited to values less than 1.0. The curves for various temperatures can be reduced to a single one, the master curve (Figure 2.3.3), by the Williams–Landel–Ferry (WLF) transformation which is based on a visco-elastic model of rubber. This very strong correlation between the equations of visco-elastic behavior and of rubber friction suggests that at least the phenomena have a common origin, and possibly that visco-elasticity is the cause of rubber friction.

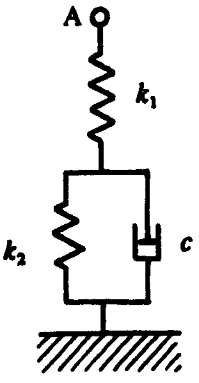

Figure 2.3.1. A mechanical model of rubber, with frequency-dependent damping.

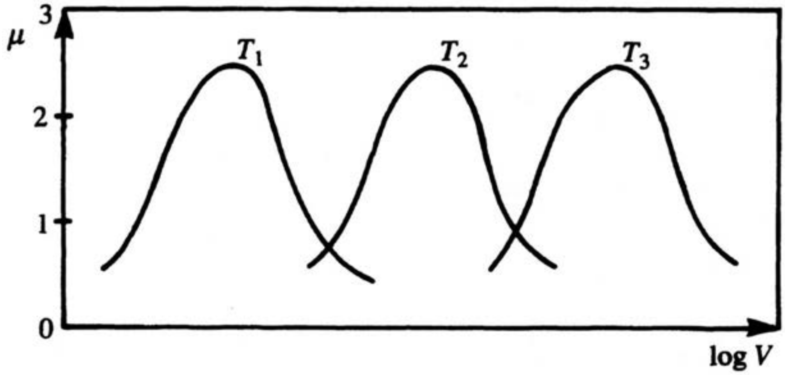

Figure 2.3.2. Rubber friction against sliding speed.

If the rubber is tested instead against a rough surface such as silicon carbide, then the WLF transformation is still successful, but the master curve is now shaped differently (Figure 2.3.3). The new and rather sharp peak is due to rubber distortion around the rough asperities, while the previous, much smaller-scale molecular effects are of diminished importance..

The addition of carbon black to improve wear resistance smooths out the curve and lowers the average value, giving friction values closer to the practical values of normal tires. This is part of the reason for the temperature sensitivity of racing tires, where the maximum frictional coefficient is sought. There are some

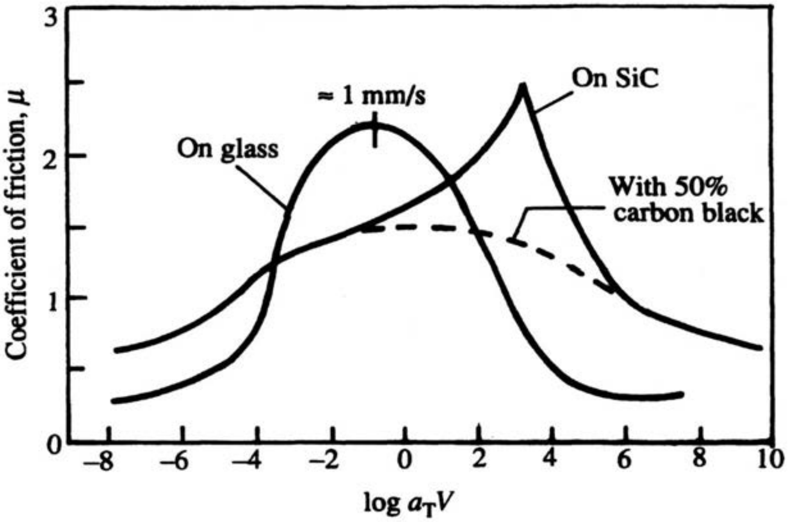

Figure 2.3.3. Friction of rubber on glass and silicon carbide.

thirty basic types of carbon black with various properties, the particle size and the chemical interaction with the rubber being important – it is not just a filler. Most widely used is high-abrasion furnace black (HAF black). In addition to wear resistance, benefits include improved tensile strength and tear strength. The addition of carbon black was first proposed by Mote in 1904. It was first used by Pirelli in 1907, when it was found to improve tread life by a factor of two or three. The hardening of rubber by vulcanization with sulfur was invented by Goodyear, and first performed in 1839.

Another constituent of tread rubber is oil; the result of including oil is to increase friction, shifting the master curve upward and toward lower sliding speeds. There is, however, a region of reversal, so that under particular conditions of temperature or skidding speed an oil-extended rubber can be inferior.

When tested on ice, rubber friction is found to undergo rather sudden changes. Very cold ice is just a smooth surface, with the rubber behaving normally. High friction can be achieved by using a rubber that is at the peak of its master curve at, say, −10°C. In laboratory conditions, ice can give higher friction than glass. Just below the melting point of ice, however, there is a depression in the curve of friction coefficient versus temperature, presumably due to some melting of the ice caused by frictional heating and pressure.

For many pairs of materials, the coefficient of friction can be considered to be independent of the apparent contact area. However, this is far from accurate when rubber is involved. Figure 2.3.4 represents a rubber slider on an idealized rough road. If the surface is lubricated and offers no shear force, there can still be a friction force because of different pressures normal to the inclined surfaces arising from rubber hysteresis, i.e., the visco-elastic effect. Increasing the vertical load will increase the area of contact between rubber and road, although in a nonlinear manner. Hence the friction force would increase, but the friction coefficient would decrease, as is found in practice, typically in proportion to the mean contact pressure to the power -0.15. Detailed analysis of the model of Figure 2.3.4 shows that the friction coefficient does not depend on the scale of the serrations, but does depend on their angle. From Figure 2.3.5, this is because the element contributes a friction force $P_hA \sin\theta$, where P_h is the hysteresis pressure difference. Evidently the angle is important, and a surface with a microscale roughness of larger average angle can produce better friction. This outline explanation gives a possible illustration of why the coefficient of friction of rubber is load-dependent, and hence why a greater rubber area for a given load can result in a higher limiting friction force.

Equally important is the adhesive component of the total friction. This is due to molecular bonding between tire and road. The formation of the bond does not provide useful energy, but the breaking of the bond requires an input of energy, hence causing energy dissipation in sliding or rolling. This adhesion component is most important in dry conditions, whereas the hysteresis component is more important in wet conditions.

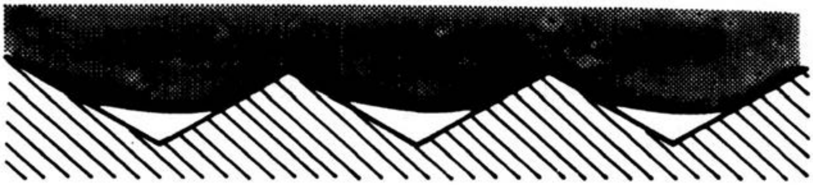

Figure 2.3.4. Idealized tire-to-road contact, showing draping of rubber over asperities.

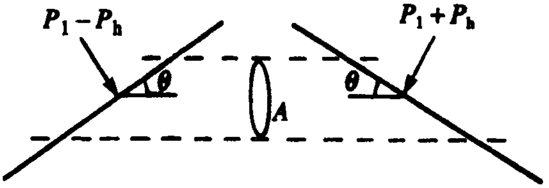

Figure 2.3.5. Idealized tire-to-road contact (detail).

A complete tire contains several different blends of rubber, each optimized for properties and cost according to its specific application, e.g., tread, carcass wall, bead filler, inner liner. One important parameter is hardness, governed largely by the quantity of carbon black and the degree of vulcanization. This is usually measured by a dial gauge pressing a conical tip a fixed distance into the rubber (Shore A Durometer) giving a hardness reading from 0 to 100. A typical tread hardness value is about 60.

A modern passenger car tire has a mass of about 12 kg, comprising about 4 kg of rubber, 2 kg of carbon black, 2 kg of oil extenders, 3 kg of steel and 1 kg of rayon, and therefore is, surprisingly, only about one-third real rubber.

Natural rubber has a specific thermal capacity c_P of 1900 J/kg K, and synthetic rubbers tend to be around 1700 J/kg K. Carbon, in graphite form at least, is 710 J/kg K. This suggests that for tire rubber, including carbon black and oil extenders,

$$c_P \approx 1200 \ \text{J/kg K}$$

Rubber has a low thermal conductivity, which is problematic. The carbon black improves the conductivity, but more so at lower temperatures, so typical tire compounds have a thermal conductivity which is temperature sensitive. The value at 20°C is around

$$k_{20} \approx 0.23 \ \text{W/m K}$$

The temperature variation over the range of interest (0°C to 150°C) can generally be well represented by

$$k = k_{20}\left(\frac{T_K}{293}\right)^n$$

where n is close to -1.0. Hence the conductivity of real tire rubbers is roughly inversely proportional to the absolute temperature.

2.4 Axes and Notation

Figure 2.4.1 shows the SAE axis system. It is expected that the ISO will soon publish a standard, also using a right-hand set of axes, and with X forward, but with Y to the left and Z upward.

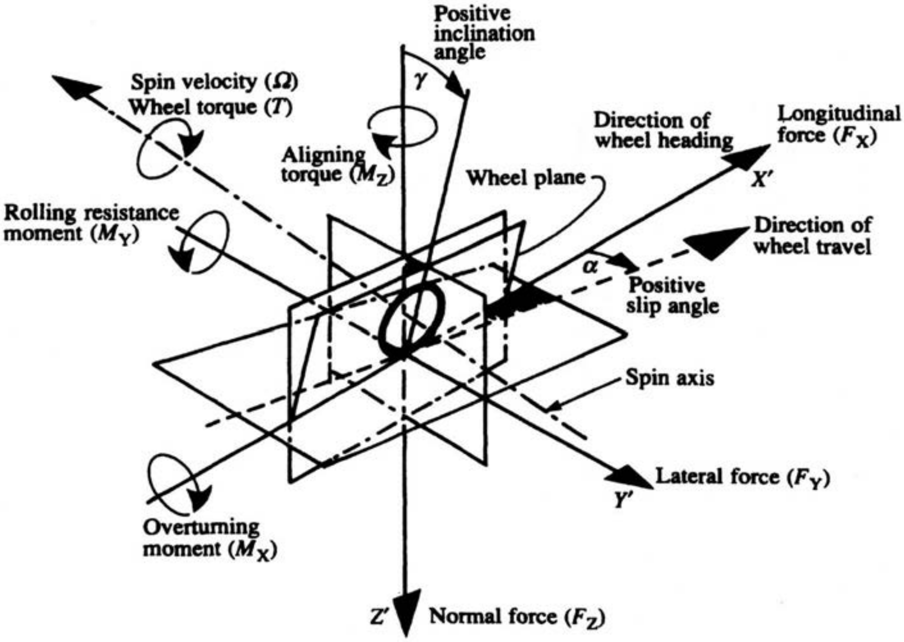
Positive inclination angle
γ
Spin velocity (Ω)
Wheel torque (T)
Aligning torque (M_Z)
Direction of wheel heading
Longitudinal force (F_X)
X'
Wheel plane
Rolling resistance moment (M_Y)
Direction of wheel travel
α
Positive slip angle
Spin axis
Lateral force (F_Y)
Y'
Overturning moment (M_X)
Z'
Normal force (F_Z)

Figure 2.4.1. SAE tire axes and terminology.

In its simplest state, the wheel stands vertically and rolls in its plane of symmetry. If the direction of travel is other than in the plane of symmetry then there is a non-zero slip angle α, with an associated cornering force (Figure 2.4.2(a)). Regardless of slip angle, the wheel may also be inclined (Figure 2.4.2(b)). Inclination is measured positive for right-hand rotation about the X'-axis. In keeping with common use, SAE camber angle equals inclination in magnitude, but takes a positive value when the top of the wheel leans outward from the car centerline. Hence, for a wheel on the right-hand side the camber angle equals the inclination angle; on the left, camber angle equals the inclination angle with reversed sign. Camber angle results in a camber force, directed toward the low axis side. It is sometimes known as the camber thrust (an obsolescent term).

Figure 2.4.3 shows combined slip and camber, plus axes and forces. The $X'Y'$ axes are in the ground plane, parallel and perpendicular to the wheel. The Z'-axis is downward in order to form a right-hand set. The force exerted on the tire by the road along X', denoted by F_X, is called the longitudinal force, and is negative for braking. The force along Y', denoted by F_Y, is called the cornering force (slip

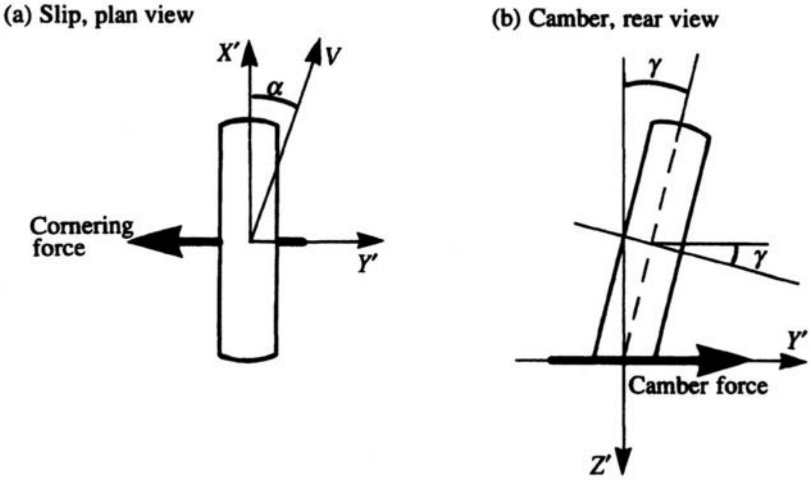

Figure 2.4.2. Tire angle and the force exerted by the ground on the tire: (a) slip, (b) camber.

angle force) when caused by the slip angle only, camber force when caused by camber angle only, or more generally the lateral force. The force on the tire along Z', F_Z, is called the normal force; this is negative, so for convenience the upward force on the tire is called the vertical force, F_V. Hence

$$F_V \equiv -F_Z$$

The aligning moment M_Z and the overturning moment M_X act in the right-hand positive sense relative to their associated axes. It is best to treat the rolling resistance as a force acting at spin axis height, opposing motion (Section 2.7).

In summary, the force components and moments exerted on the tire by the road are:

(1) F_Z, normal force positive downward

(2) F_V, vertical force, $\equiv -F_Z$, positive upward

(3) F_X, longitudinal force, positive for driving

(4) F_Y, lateral force (cornering force F_α plus camber force F_γ)

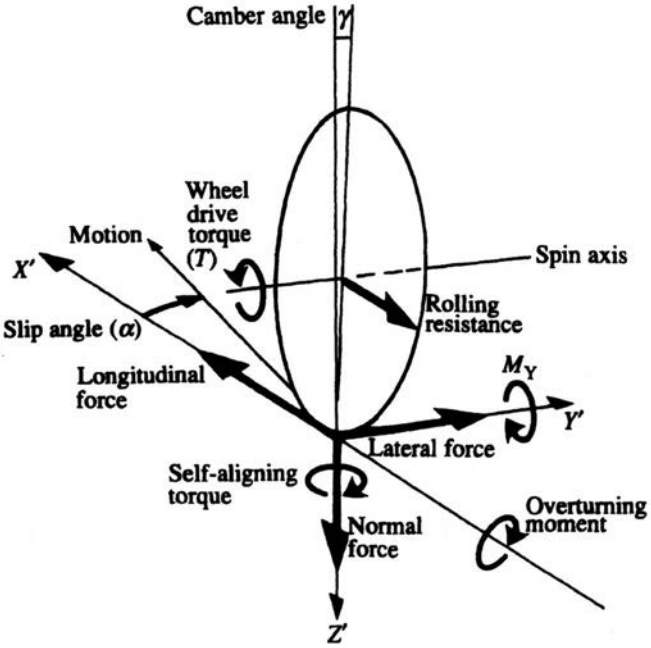
Camber angle
γ
Wheel drive torque (T)
Motion
X'
Spin axis
Rolling resistance
Slip angle (α)
Longitudinal force
M_Y
Y'
Lateral force
Self-aligning torque
Overturning moment
Normal force
Z'

Figure 2.4.3. Tire forces.

(5) M_X, overturning moment

(6) M_Y, rolling resistance moment

(7) M_Z, aligning moment (self-aligning torque)

All of the forces and moments mentioned so far are those exerted on the tire by the road. In addition there are forces exerted on the wheel by the suspension components, the driveshaft and the brakes, which will be considered later.

The term "tire force" generally means the total force exerted by the ground on the tire. Where the context makes it clear, it is also used to mean the total force parallel to the ground plane (Figure 2.4.4(a)). Here the tire force is resolved into lateral and longitudinal components. Note that the $X'Y'$ axes rotate when the wheel is steered, so the force along X' is the result of engine or brake action, together with the rolling resistance if significant. The force along Y' is the lateral force, which is the cornering force because of slip angle plus the camber force because of camber angle.

The term "lateral force" was used differently in early SAE papers to mean the force perpendicular to motion, which is now known as the central force. For the analysis of the vehicle, rather than the tire, it is in fact more useful to know the forces along and perpendicular to the vehicle motion. This is not quite the same as the tire motion because of other effects such as vehicle rotation. The *XYZ* (unprimed) axes are used for the vehicle. The $X''Y''Z''$ axes are the axes aligned with the motion of the individual wheel (Figure 2.4.4(b)). They are usually fairly close in direction to the vehicle *XY*. If the tire forces are resolved into X'' and Y'' components, then these are called the tractive force F_T and the central force F_S. In the absence of engine or brake action, neglecting rolling resistance the longitudinal force is zero and the tire force is perpendicular to the wheel, so the tractive force is then negative and called the tire drag force.

It is essentially the central force that provides the cornering centripetal acceleration of the vehicle. As Figure 2.4.4(b) illustrates, it is the tractive force that determines whether the vehicle rounds a curve at constant speed or not, i.e., the tractive force governs the tangential acceleration. However, for a freely rolling tire the longitudinal force is small, so tire cornering force data are most simply and conveniently expressed in terms of the lateral force.

In summary, the tire force on the ground plane can be resolved into two main pairs of components:

(1) Tire aligned: longitudinal force F_X plus lateral force F_Y.

(2) Motion aligned: tractive force F_T plus central force F_S.

2.5 Tire Radius

Three types of tire radius are generally recognized: the unloaded radius R_u, the loaded radius R_l and the effective rolling radius R_e.

(1) The unloaded radius R_u, in practice measured through the unloaded tire circumference C_t with a tape measure, is defined by

$$R_u = \frac{C_t}{2\pi}$$

(a) Tire force is lateral force plus longitudinal force

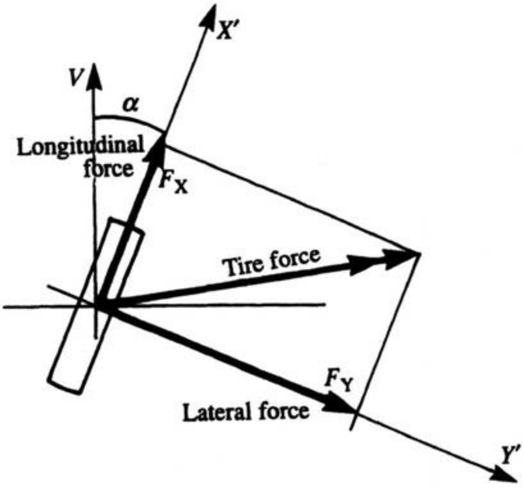
X'
V
α
Longitudinal force
F_X
Tire force
F_Y
Lateral force
Y'

(b) Tire force is central force plus tractive force

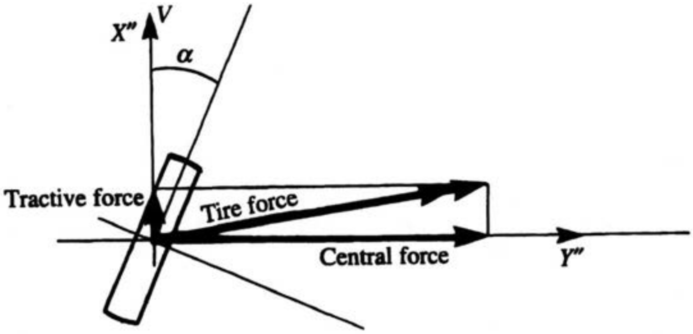
X''
V
α
Tractive force
Tire force
Central force
Y''

Figure 2.4.4. Tire force components: (a) in $X'Y'$, (b) in $X''Y''$.

(2) The loaded radius R_l, dependent on the particular load, is the distance of the wheel axis from the ground, in the wheel center plane, or loosely, the height of the wheel axis.

(3) The effective radius R_e (also called rolling radius) is defined as the translation velocity of the wheel axis divided by the wheel angular speed:

$$R_e = \frac{V}{\Omega}$$

Note that for a locked sliding wheel R_e is infinite, while for a spinning, non-translating wheel R_e is zero.

The loaded radius R_l depends on the vertical deflection under vertical load. The tire vertical deflection δ_t is defined as

$$\delta_t = R_l - R_u$$

Under normal load this deflection is typically 18–24% of the section height. The footprint length is typically about 0.5R (150 mm) for an average car tire, subtending about 30° at the wheel center. Therefore the crown undergoes a fairly sharp bend of 15° at each end of the footprint. Vertical deflection is about 0.035R (10 mm) and is quite closely proportional to vertical force, so it is meaningful to refer to the vertical stiffness. Hence

$$\delta_t = \frac{F_V}{K_t}$$

where the tire vertical stiffness K_t depends on size, construction and inflation pressure. A typical value is 250 N/mm. Over 80% of the total stiffness is due to the inflation pressure (over 90% for aircraft tires) so the pressure has a large effect on stiffness. The unpressurized carcass has some stiffness arising from bending of the tread and sidewalls, but this is relatively small. Tire vertical stiffness generally increases with load capacity, rim width, and decreasing cord crown angle. There is a variation of typically ±10%, for a given size and pressure, from various manufacturers. Increasing speed increases the stiffness at about 0.4% per m/s. Hence

$$K_t = K_{t0}\left(1 + k_{\mathrm{KtV}} V\right)$$

with

$$k_{\mathrm{KtV}} \approx 0.004/\mathrm{m\ s}^{-1}$$

When large cornering forces are induced, the vertical stiffness may reduce by about 20%. Hence

$$K_{\mathrm{t}} = K_{\mathrm{t0}}\left(1 - k_{\mathrm{KtCy}} C_{\mathrm{Y}}\right)$$

where

$$C_{\mathrm{Y}} = F_{\mathrm{Y}}/F_{\mathrm{V}}$$
$$k_{\mathrm{ktCy}} \approx 0.20$$

At a given deflection, the increase of vertical force with increasing speed is due to impact of the tire periphery on the ground. Hence, for a given vertical force, the deflection reduces. This is not important for passenger cars, but is important for ground-effect racing cars.

The effective radius R_{e} is not equal to R_{l} even in free running; in fact R_{e} is closer to R_{u} in such conditions. Approximately

$$R_{\mathrm{e}} = R_{\mathrm{u}} - \tfrac{1}{3}\delta_{\mathrm{t}}$$

Damping in a tire is nonlinear, being a function of amplitude, but it is small and for many purposes it may be neglected. It is generally insensitive to inflation pressure because it arises from carcass hysteresis and ground friction. One published result for a typical car tire gave a damping coefficient of 200 N s/m at 6 mm amplitude, varying as amplitude to the power –0.64. Another result showed a hysteretic deflection δ_{tH} of 1.5 mm each side of the mean, equivalent to a Coulomb type friction force F_{tH} of about 350 N, i.e.,

$$F_{\mathrm{V}} = K_{\mathrm{t}}\delta_{\mathrm{t}} \pm F_{\mathrm{tH}}$$

$$F_{\mathrm{tH}} = K_{\mathrm{t}}\delta_{\mathrm{tH}}$$

2.6 Speed Limitations

Aircraft speed is often characterized by the Mach number, relating the vehicle speed to the speed of sound waves in the air, arising from the elasticity of that medium. The road vehicle is also supported by a flexible medium, namely the tire, which is therefore capable of supporting wave phenomena. Such waves were in fact first studied by Gardner & Worswick (1951), beginning at a speed of around 40 m/s. Instead of leaving the ground and smoothly taking up its normal circular form, the crown goes through a wave behind the footprint. At constant speed the wave is static, i.e., it does not pass around the wheel. The wave amplitude may be 10 mm or more, and the wavelength is typically 100 mm; the waves may extend around one-quarter or more of the tire circumference with gradually reducing amplitude.

A successful theory of such waves in tire treads was provided by Turner in 1954, who showed that the wave speed was

$$C_W = \sqrt{\frac{t_C}{\rho_C}}$$

where t_C is the crown circumferential tension per unit width, itself depending on inflation pressure and speed, and ρ_C is the crown density per unit area. Once the wheel peripheral speed reaches this value then the tire periphery, before arriving at the ground at the front of the contact patch, can no longer receive by elastic transmission any advance warning of the impending impact. Also, the tread leaving the ground with a radial speed component carries a great deal of energy which is dissipated by the wave action behind the contact patch. The predicted wavelength is theoretically dependent on speed:

$$\lambda = \lambda_1\sqrt{\left(\frac{V}{C_W}\right)^2 - 1}$$

where λ_1 is a constant, being the value of λ at $V = \sqrt{2}\, C_W$, which agrees with the experimental data. The analogy of this wave with the Mach number for fluids seems apt, giving the Turner number for tires, being the ratio of speed V to the wave speed C_W:

$$N_T = \frac{V}{C_W}$$

For a freely rotating wheel, V is the vehicle translational speed. More generally

$$N_T = \frac{\Omega R_u}{\sqrt{(t_C/\rho_C)}}$$

where V is the peripheral speed of the tread (ΩR_u); this should be correct for both slipping (spinning or locked) or non-slipping wheels.

The presence of such waves dissipates energy, increases the rolling resistance, and raises the temperature of the carcass, soon causing damage. Because of carcass flexing and tread scrubbing, even at lower speeds there may be a substantial temperature rise in the tire, so for sustained operation this sets acceptable limits to speed and load combinations. A thick tread may cause heat dissipation problems, although the tread pattern itself helps cooling. Also, at high speed there are significant centrifugal stresses on the outer tread elements. Therefore, for high-speed tires the crown density per unit area must be small. For land speed record vehicles the tire tread thickness has been as little as 0.4 mm.

2.7 Rolling Resistance

Considering a notional isolated wheel rolling at constant speed down a ramp in a vacuum, forces and moments on the wheel must be in equilibrium. This determines the nature and value of the rolling resistance force and moment. There must be zero moment about the wheel axis (center of mass) to maintain zero angular acceleration, so the total rolling resistance must act through that axis. At the footprint it must comprise a drag force plus a moment, or a drag plus a forward shift of the normal force, which actually arises from changes in the footprint pressure distribution. Figure 2.7.1 shows some possible representations.

The rolling resistance is a relatively small force and not of decisive importance in most handling problems; it will be treated as acting at the axis if it is included at all. Its main effect in the context of handling is on steering feel; effects arise from lateral load transfer in steady cornering, or from vertical force variation due to bumps. Practical measurements of rolling resistance show it to be reasonably constant with speed, possibly increasing slightly, up to a Turner number of about 0.8, beyond which it increases rapidly because of the wave energy loss. These losses effectively limit the permissible speed of tires because of the danger of overheating and tread separation. Tires are speed rated; for example, SR not to exceed 180 km/h, TR 190 km/h, HR 210 km/h. For high-

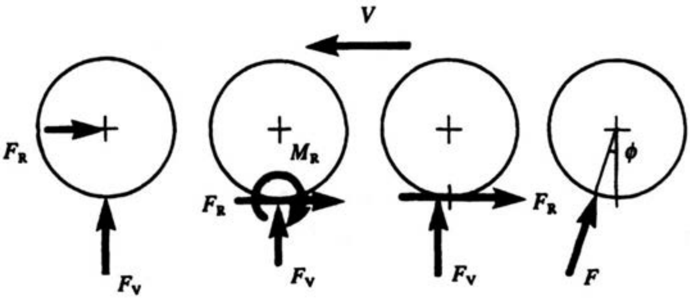

Figure 2.7.1. Alternative representations of rolling resistance with vertical force.

speed running, the Turner number can be minimized by increasing the tread tension which results from an increase in inflation pressure. In steady state the cavity air temperature and pressure themselves depend on speed. There is a rise of typically 35°C and 40 kPa in steady state at 30 m/s compared with cold static conditions. Provided the Turner number is less than about 0.8, speed does not normally play a primary role in tire handling effects, although there are some secondary effects through visco-elasticity, changing of the tension in the carcass, and changes of the friction of the tread.

For a static or freely rolling weightless tire with a perfectly compliant tread and carcass, the footprint contact pressure would equal the inflation pressure. This first estimate is a better approximation for the radial-ply than for the bias-ply tire. For a radial tire, the normal force distribution along the footprint is correspondingly roughly constant. For the bias-ply tire it is trapezoidal, one-quarter of the footprint length being required for the increase and one-quarter for the decrease. The normal force is slightly greater over the front half, associated with the rolling resistance. In tire modeling, rectangular, parabolic and elliptical distributions have been used as analytical models. The longitudinal shear force distribution, associated with tread shear strains, has small fore–aft asymmetries that are manifestations of the rolling resistance. The lateral distribution is non-uniform, especially for the bias-ply type, i.e., separate thin strips parallel to the centerline can have longitudinal force distributions differing markedly from each other. Even for a freely rolling tire, the average longitudinal shear stress at the road surface is typically 30 kPa, and peak values often exceed 100 kPa. These are significant in the context of a mean contact pressure of about 200 kPa. The normal pressure distribution is, in fact, similarly complex, peaking at typically 800 kPa (five times the inflation pressure) for bias-ply, and 300 kPa for radial-ply. Lateral shear stresses are likely to exceed 400 kPa locally. These figures, generally more extreme for bias-ply than radial, suggest that some local sliding will occur even for a freely rolling tire, and are the principal reason for the radial-ply type exhibiting less wear and lower rolling resistance.

The rolling resistance coefficient μ_R is defined by the equation

$$F_R = \mu_R F_V$$

where F_R is the rolling resistance force and F_V is the vertical force. The rolling resistance coefficient ranges from 0.01 to 0.025 for cars. For trucks the range is somewhat lower at 0.005 to 0.012 because of higher inflation pressures and harder tread compounds. The total rolling resistance of a good tire is apportioned typically as 90% material hysteresis, 8% surface friction, and 2% air friction, at moderate speed.

2.8 Tire Models

In vehicle handling analysis, the tires are generally represented by empirical models; these are non-phenomenological, that is, the tire behavior is not derived from the material properties and structure of the tire. The material of a tire is a multi-layered, non-uniform, anisotropic, cord–rubber composite, so to understand tire behavior there is a pressing need for simplification. There are three principal models used to understand tire forces and deflections in cornering and to give some insight into footprint behavior: the elastic foundation model, the string model, and the beam model.

In the elastic foundation model, each small element of the contact patch surface is considered to act independently; if forced by the ground it can be displaced from its null position relative to the foundation and resists with a given stiffness. Figure 2.8.1(a) represents a plan view of a tire during cornering, showing the lateral deflection of the tire centerline in the footprint. Figure 2.8.1(b) is a representation of this, with the various elements each constrained by a foundation stiffness spring, attempting to restore the element to its central position. This is the simplest model. In the string model, lateral displacement of each element is also resisted by tension between the elements because of changes in the displacement slope. In the beam model, each element exerts bending moments on its neighbors. The foundation stiffness model allows a discontinuous distribution of displacement and slope of the centerline. The string model allows discontinuous changes of slope, but not of deflection. The beam model does not allow discontinuities of either. The string and beam models are sometimes combined. None of these models reflects directly, in a physical sense, the true complexity of a real tire, and the various stiffness values are selected empirically to obtain realistic results. For radial-ply or belted bias-ply tires, the beam model is generally found to be superior. The implication is of course that the bending stiffness is largely associated with the belt.

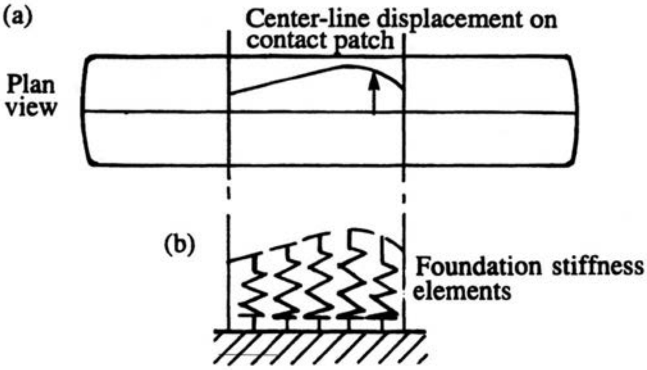
(a)
Center-line displacement on contact patch
Plan view
(b)
Foundation stiffness elements

Figure 2.8.1. (a) Tire displacement, (b) Foundation stiffness model.

There have been various attempts to use finite-element techniques to model tires. These do go some way toward predicting tire characteristics, but they are generally unsuitable for vehicle handling simulations because of their complexity, i.e., because of the large number of parameters or degrees of freedom, which means that the program is too slow except perhaps for the very fastest computers.

Even the simplest model, the elastic foundation alone, produces many of the interesting characteristics of a real tire, and this model will be used here to "predict" various properties of tires and to illustrate frictional behavior in the footprint. For simplicity, a displacement graph can be constructed to show only the tire centerline, not the whole tread width; Figure 2.8.2 illustrates this, with a view down through a "transparent" idealized tire with foundation stiffness only, and its corresponding centerline displacement graph at a small slip angle. Each element touches the ground at the front of the contact patch, and is then deflected laterally at the angle α as it passes through the contact patch. At the rear, having reached a deflection $l \tan\alpha$, it suddenly leaves the ground and can jump back to the centerline. This is, of course, a highly simplified representation, and the deflection is really much smoother. Because of the foundation stiffness, this distortion of the tire requires a force to be exerted on the tire by the road; this is the lateral force to be determined.

In Figure 2.8.3, the element of length δx and centerline displacement d, according to the elastic foundation model, gives a force on the tire of

$$\delta F = c d\, \delta x$$

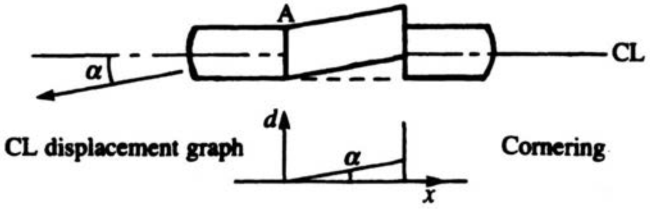
A
α
CL
d
CL displacement graph
α
Cornering
x

Figure 2.8.2. Model tire and displacement.

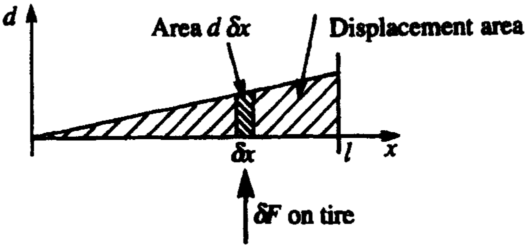
d
Area d δx
Displacement area
δx
l
x
δF on tire

Figure 2.8.3. Model tire centerline displacement.

where c is the foundation stiffness. Hence the effective foundation stiffness c has units of pascals (Pa), the total force being the stiffness times the displacement area. The lateral stiffness of a particular element of length δx is $c\,\delta x$ N/m of lateral displacement. The lateral force concentration, in newtons/metre, is

$$\frac{\mathrm{d}F}{\mathrm{d}x} = cd$$

For any given distribution of centerline displacement, the total force magnitude is

$$F = \int_0^l cd\,\mathrm{d}x$$

and the moment about the contact patch centerpoint is

$$M = \int_0^l cd\left(x - \frac{1}{2}l\right) \mathrm{d}x$$

For realistic results, the foundation stiffness c must be given a suitable empirical value, not simply that measured from the actual overall lateral stiffness of the tire tread relative to the wheel.

The purpose of this exercise is simply to give some physical insight into tire characteristics, rather than to produce accurate real characteristics. However, with suitable choice of the effective foundation stiffness c and the friction coefficient, quite realistic performance curves are produced. For accurate numerical handling predictions it is necessary to measure the actual tire characteristics.

2.9 Slip Angle and Cornering Force

An example variation of cornering force with slip angle was shown in Figure 1.1.2. It is characterized by an initial approximately linear region with force proportional to angle, and a final friction-limited value. This section will show how such a characteristic results from the simple elastic foundation model.

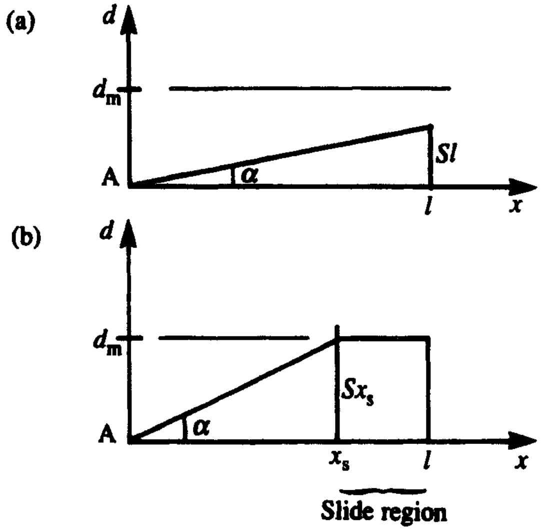

Figure 2.9.1. Model tire centerline displacement: (a) small slip angle, (b) larger slip angle.

For a small slip angle, the centerline deviation is that of Figure 2.9.1(a). The tire contacts the ground at A. The tread is supported by the ground, which exerts the vertical force F_V. The normal force concentration, considered to be distributed uniformly, is F_V/l (N/m). To avoid sliding, the highest lateral force concentration allowable is $\mu F_V/l$. The previous section showed that the lateral force concentration is cd where c is the effective foundation stiffness. Hence, for no sliding,

$$cd \le \frac{\mu F_V}{l}$$

at all points along the footprint. The maximum possible displacement for no sliding is therefore

$$d_M = \frac{\mu F_V}{cl}$$

Denoting the lateral slip as S,

$$S = \tan\alpha$$

For small slip angles, with α in radians,

$$S \approx \alpha$$

For small α and S, the largest d is at $x = l$ (Figure 2.9.1(a)), where

$$d = l\tan\alpha = Sl$$

and the condition for no sliding is that d must not exceed d_M, giving

$$S \le d_M/l$$

Substituting $d_M = \mu F_V/cl$ gives

$$S \le \frac{\mu F_V}{cl^2} = S_1$$

Realistic figures are: contact patch length 180 mm, normal force 5 kN, friction coefficient 1.0, and effective foundation stiffness 3 MPa. This gives a slide-free maximum slip $S_1 = 0.051$ ($\alpha_1 = 2.95°$). The corresponding maximum tread displacement is

$$d_M = \mu F_V / cl = 9.3 \text{ mm}$$

In this small slip angle regime, the triangular displacement graph as in Figure 2.9.1(a) is valid. The total force magnitude is

$$F_Y = \int_0^l cd \,\mathrm{d}x$$

This is just the stiffness times the area of the displacement diagram,

$$F_Y = \tfrac{1}{2} cl^2 S$$

so the force is proportional to the slip. For small α, with α in radians,

$$F_Y \approx \tfrac{1}{2} cl^2 \alpha$$

The cornering stiffness is

$$C_\alpha = \frac{\mathrm{d}F_Y}{\mathrm{d}\alpha} = \tfrac{1}{2} cl^2 \quad \text{(per radian)}$$

The maximum non-slide force is

$$\tfrac{1}{2} cd_M l = \tfrac{1}{2} cl \left(\frac{\mu F_V}{cl} \right) = \tfrac{1}{2} \mu F_V$$

Thus the model predicts a lateral force proportional to slip angle, for a force up to half of the maximum total friction limit force μF_V. For the example values, the cornering stiffness is 49 kN/rad (848 N/deg) and the maximum non-slide force is 1500 N.

The force acts through the triangle centroid, a distance $2l/3$ from the first contact, and therefore $l/6$ behind the mid-point. So the self-aligning torque is

$$M_Z = \frac{F_Y l}{6} = \frac{cl^3 S}{12}$$

which is proportional to the slip. The pneumatic trail (the moment arm) is

$$t = \frac{M_Z}{F_Y} = \frac{l}{6}$$

which is constant. Hence this model successfully predicts the existence of a pneumatic trail. In practice larger values are usually found at small slip angles, t/l being typically 0.2 to 0.35.

It is important to appreciate that the relationship between lateral force and slip, i.e., the slope of the F against S (or α) curve, depends not on the friction coefficient but on the foundation stiffness, i.e., the tire compliance which is due to the carcass and tread compliance. The available friction does, however, define the limit of the non-slide linear operating regime.

If the slip angle is increased further, then there will no longer be sufficient friction to keep the rear of the contact patch fixed on the road. Considering a simple model in which the friction coefficient is independent of sliding speed, then at larger slip angles the rear of the contact patch will reach the friction limit displacement (Figure 2.9.1(b)), and remain there until lifted from the road at $x = l$. The position at which sliding begins is denoted by x_s.

$$S = \tan\alpha = \frac{d_M}{x_s}$$

$$d_M = \frac{\mu F_Y}{cl}$$

$$x_s = \frac{d_M}{S} = \frac{\mu F_Y}{clS}$$

The lateral force is the stiffness times the displacement area, integrated from the displacement graph:

$$\begin{aligned}F_Y &= \int cd\,\mathrm{dx}\\ &= \tfrac{1}{2}cd_M x_s + cd_M(l - x_s)\\ &= cd_M\left(l - \tfrac{1}{2}x_s\right)\end{aligned}$$

Substituting $x_s = \mu F_V/clS$ and $d_M = \mu F_V/cl$ gives a lateral force

$$F_Y = \mu F_V - \frac{\mu^2 F_V^2}{2cl^2 S}$$

and a lateral force coefficient

$$C_Y = \mu - \frac{\mu^2 F_V}{2cl^2 S}$$

Hence, as the lateral slip S continues to increase beyond initiation of sliding at the rear of the footprint, the lateral force approaches the limit μF_V asymptotically. Since $S = \tan\alpha$, the ultimate limit force is actually reached at a slip angle of 90° when the tire is sliding fully sideways. Figure 2.9.2(a) shows the graph of lateral force against slip angle for the example values. Real tires do indeed have a characteristic of this nature, as may be seen by comparison with Figure 1.1.2.

The self-aligning torque after sliding begins is:

$$\begin{aligned}M_Z &= \int_0^l cd\left(x - \tfrac{1}{2}l\right)\mathrm{dx}\\ &= \frac{cld_M x_s}{4} - \frac{cd_M x_s^2}{6}\end{aligned}$$

Substituting $x_s = d_M/S$ gives

$$M_Z = \frac{cld_M^2}{4S} - \frac{cd_M^3}{6S^2}$$

Thus for a slip angle greater than the non-slide limit, the self-aligning torque eventually reduces. Substituting for d_M gives

$$M_Z = \frac{\mu^2 F_V^2}{4clS} - \frac{\mu^3 F_V^3}{6c^2 l^3 S^2}$$

The pneumatic trail is:

$$t = \frac{M_Z}{F_Y}$$

$$= \frac{3\mu F_V c l^2 S - 2\mu^2 F_V^2}{12c^2 l^3 S^2 - 6\mu F_V clS}$$

Physically, from Figure 2.9.1(b), we can see that increasing the slip angle reduces the length x_s, and therefore the pneumatic trail reduces once sliding begins at the rear, and goes to zero as the slip angle approaches 90°. Hence the self-aligning torque reduces even though the force increases. Figure 2.9.2(b) shows the self-aligning torque variation for this model. The reduction of aligning moment and hence of steering-wheel torque as the lateral force approaches its limit is a valuable form of feedback to the driver. It is especially important in giving warning of a poor friction surface.

The general form of the curves of both lateral force and self-aligning torque derived from this simple model are in accordance with experimental data, although in the case of experimental self-aligning moment negative values are often observed at high slip. This arises because of a decline of friction with sliding speed, because of sideways shifting of the rolling resistance caused by carcass distortion, and because of the fore–aft asymmetry of the vertical force distribution which allows greater friction in the front half of the contact patch.

Since $\alpha = \arctan S$, the graphs of force and moment are not strictly linear even at first, although this error is negligible because of the small angles obtaining in this region. The initial slope of the force curve is denoted the cornering stiffness and given the symbol C_α. Synonyms for cornering stiffness are cornering rate and cornering power, but these terms are obsolete and will not be used here. A typical value of cornering stiffness for a car tire is 50 kN/rad (870 N/deg). To improve comparability between tires of different load ratings it is often convenient to divide the cornering stiffness by the normal force F_V to give the corner-

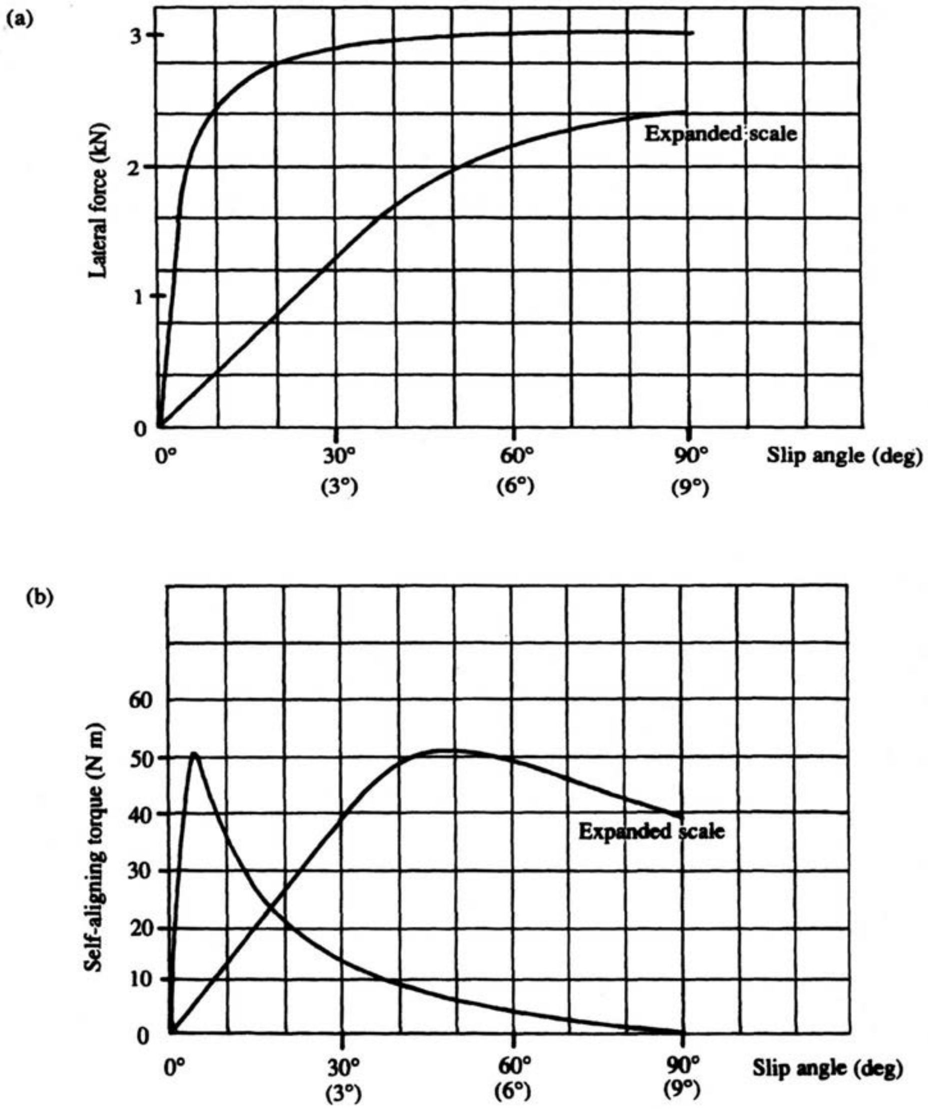

Figure 2.9.2. (a) Tire cornering force against slip angle, (b) Tire self-aligning torque against slip angle.

ing (stiffness) coefficient C_S (subscript S for slip angle), which has a typical value of 0.16/deg or 10/rad for radial-ply, and some 20% less for bias-ply.

For small α (in the non-slide regime),

$$F_Y = F_\alpha = C_\alpha \alpha = C_S F_V \alpha$$

The lateral force coefficient is

$$C_Y = F_Y / F_V = C_S \alpha$$

The meaning of these equations is clear enough for experimental conditions, but in application to vehicle handling the vertical force is itself a variable, and some caution must be exercised.

It is of course essential to distinguish carefully between cornering force, cornering-force coefficient, cornering stiffness, cornering-stiffness coefficient, maximum cornering force, and maximum cornering-force coefficient (Figure 2.9.3). (In addition, if camber is not zero, there are camber force, camber-force coefficient, camber stiffness, camber-stiffness coefficient, maximum lateral force and maximum lateral force coefficient [Section 2.12].) In every case the word "coefficient" is added where the variable has been normalized against F_V.

The force that provides the vehicle's centripetal acceleration is not actually the tire cornering or lateral force. It is the tire force perpendicular to the vehicle path; depending on the angle of the tire relative to the vehicle this is approximately the tire central force (Figure 2.9.4). Note that, for an undriven wheel, in addition to the desirable central force there is also a tire drag force F_D which will reduce the vehicle's speed. If compensating forces are provided by the engine, then the drag force may be overcome and a positive tractive force created (Figure 2.4.4(b)). Resolving the lateral force into central and drag forces results in Figure 2.9.5. Note that the central force has a well-defined maximum value, at a slip angle of 20° for this model, and that excessive slip angles produce inferior centripetal forces on the vehicle. The effect of the drag force in these conditions is readily observed by cornering sharply with the clutch depressed, when a marked loss of speed will be observed, far in excess of the speed loss over the same distance in a straight line.

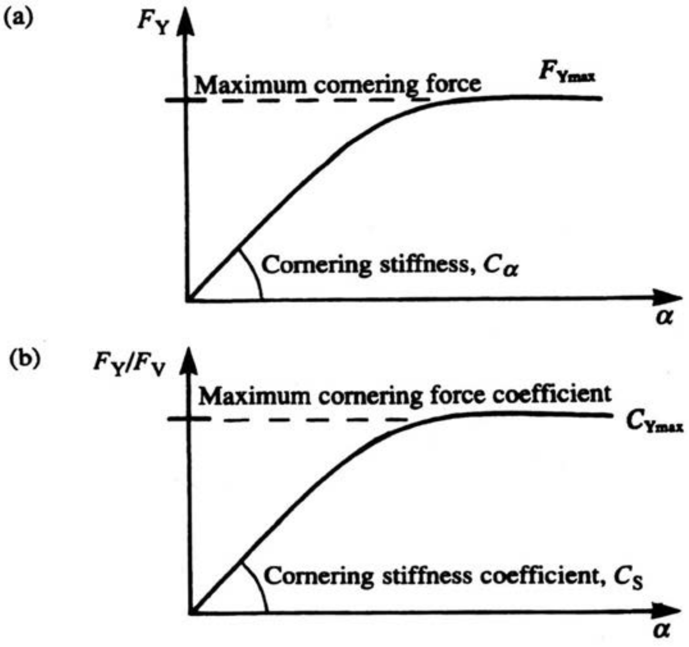

Figure 2.9.3. (a) F_Y against slip angle, (b) F_Y/F_V against slip angle.

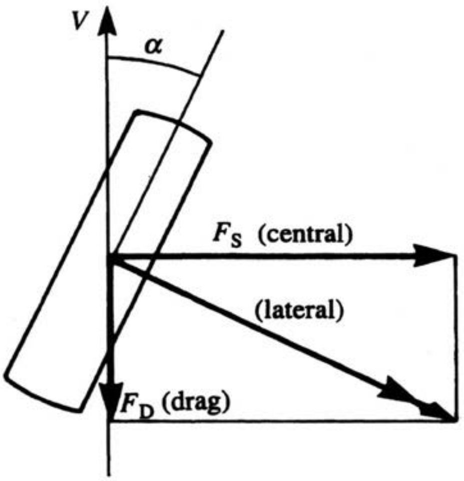
V
α
F_S (central)
(lateral)
F_D (drag)

Figure 2.9.4. Force components for undriven tire.

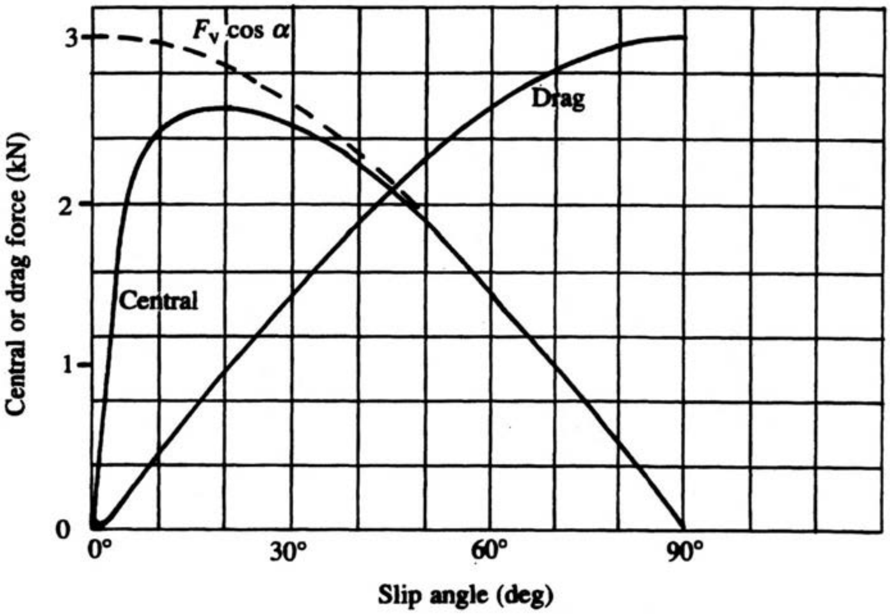

Figure 2.9.5. Tire central and drag force against slip angle.

In summary, we have the following tire slip parameters:

(1) F_V, vertical force

(2) α, slip angle

(3) C_α, cornering stiffness

(4) $C_S = C_\alpha / F_V$, cornering stiffness coefficient

(5) F_Y, lateral force

(6) F_S, central force

(7) F_D, drag force

(8) $C_Y = F_Y / F_V$, lateral force coefficient

(9) $C_{FS} = F_S / F_V$, central force coefficient

(10) $C_{FD} = F_D / F_V$, drag force coefficient

(11) F_{Ymax}, maximum lateral force

(12) F_{Smax}, maximum central force

(13) $\mu_{\mathrm{Y}} \equiv C_{\mathrm{Ymax}} = F_{\mathrm{Ymax}}/F_{\mathrm{V}}$, maximum lateral force coefficient

(14) $\mu_{\mathrm{S}} \equiv C_{\mathrm{Smax}} = F_{\mathrm{Smax}}/F_{\mathrm{V}}$, maximum central force coefficient

Note that μ has traditionally been used in physics and engineering for the coefficient of limiting friction (not just the ratio of transverse force to vertical force) and so is reserved here for the maximum force coefficients.

The central/drag force ratio is analogous to the lift/drag ratio for a wing. Neglecting rolling resistance this is simply $\cot\alpha$, which reduces continuously with slip angle. Higher cornering stiffness therefore has merit, especially for competition vehicles, because a given central force will be achieved at smaller slip angle and therefore with a smaller tire drag force. Including rolling resistance gives the central/drag force ratio, within the range of linear cornering force, as

$$\frac{F_{\mathrm{S}}}{F_{\mathrm{D}}} = \frac{C_{\alpha}\alpha \cos\alpha}{\mu_{\mathrm{R}}F_{\mathrm{V}} + C_{\alpha}\alpha \sin\alpha}$$

For realistic values this typically peaks at a value between 10 and 12, at 2° to 3° slip angle.

Figure 2.9.6 shows lateral force plotted against self-aligning torque for the simple foundation model; this is known as the Gough plot, and is of particular interest with regard to feel at the steering wheel. For real tires, because the self-aligning moment goes negative, the curve actually goes off to the left beyond a slip angle of 20°.

Cornering force causes tire distortions that give an overturning moment. This can be conceived as a lateral shift y of the vertical force position, where

$$y = M_{\mathrm{X}}/F_{\mathrm{V}}$$

This has significant effects on lateral load transfer.

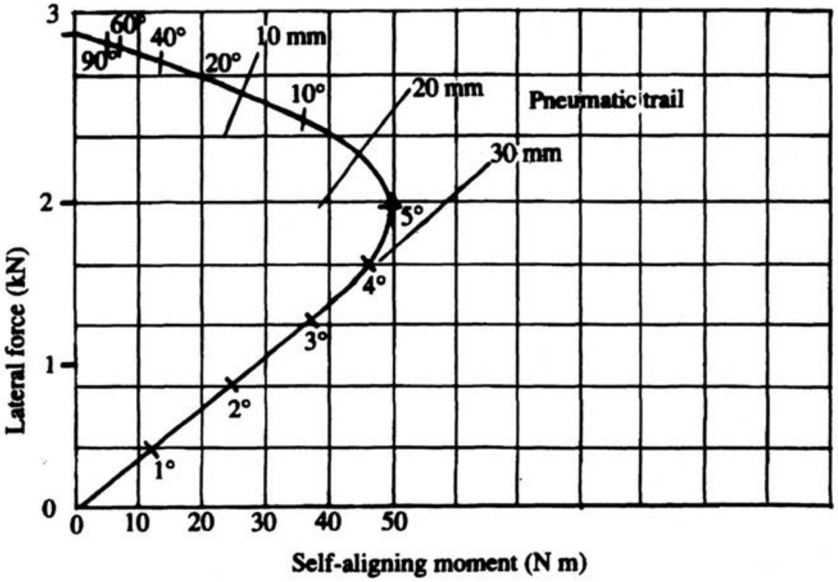

Figure 2.9.6. Gough plot for simple model tire.

2.10 Non-Dimensionalization

It is often helpful to non-dimensionalize the tire characteristics. The lateral or cornering force is easily non-dimensionalized by dividing by F_{Ymax}, in which case the force coefficient is

$$C_{\mathrm{Y}} = \frac{F_{\mathrm{Y}}}{F_{\mathrm{Ymax}}} = \frac{F_{\mathrm{Y}}}{\mu_{\mathrm{C}} F_{\mathrm{V}}} \qquad \text{(abnormal definition)}$$

When the lateral force has been non-dimensionalized like this, all graphs have a maximum value of 1.0. Alternatively, and more usually, the forces are non-dimensionalized by dividing by F_{V}. The lateral force coefficient is then

$$C_{\mathrm{Y}} = \frac{F_{\mathrm{Y}}}{F_{\mathrm{V}}}$$

The maximum value is then the maximum lateral force coefficient μ_{Y}.

The slip can be non-dimensionalized by defining a characteristic slip S^* (and characteristic slip angle α^*), and then plotting forces against S/S^* or α/α^*. The characteristic slip angle is the angle at which the tangent from the origin meets the lateral force value F_{Ymax}. Thus

$$S^* = \frac{F_{\mathrm{Ymax}}}{C_\alpha} = \frac{\mu_{\mathrm{Y}}}{C_{\mathrm{S}}}$$

which for this model is

$$S^* = \frac{2\mu F_{\mathrm{V}}}{cl^2}$$

It has a typical value of 6° or 0.1 rad. Thus the slip coefficient (non-dimensionalized slip) is

$$s = S/S^*$$

In terms of angles,

$$\alpha^* = \arctan S^*$$

$$s = \frac{\tan\alpha}{\tan\alpha^*}$$

The non-dimensional slip angle is

$$\theta = \arctan s \approx \alpha/\alpha^*$$

Now, for the simple tire model, for no sliding ($S < S_1$)

$$s < \tfrac{1}{2}$$

The side force is

$$F_{\mathrm{Y}} = \tfrac{1}{2}cl^2 S$$

The side force coefficient is

$$C_Y = \frac{F_Y}{F_V} = \left(\frac{cl^2}{2\mu F_V}\right)\mu S$$

$$= \frac{\mu S}{S^*} = \mu s$$

which introduces a rewarding simplicity.

Defining a self-aligning moment coefficient C_{MZ} as (not non-dimesional, but the usual definition),

$$C_{MZ} = \frac{M_Z}{F_V}$$

$$= \frac{cl^3 S}{12F_V}$$

$$= \left(\frac{cl^2}{2\mu F_V}\right)\frac{\mu l S}{6}$$

$$= \frac{\mu l S}{6S^*}$$

$$= \frac{\mu l s}{6}$$

The non-dimensional pneumatic trail is t/l, which for this model is simply

$$\frac{t}{l} = \frac{1}{6}$$

Beyond the point of sliding

$$C_Y = \mu\left(1 - \frac{S^*}{4S}\right)$$

$$= \mu\left(1 - \frac{1}{4s}\right)$$

$$C_{MZ} = \mu l \left(\frac{S^*}{8S} - \frac{S^{*2}}{24S^2} \right)$$

$$= \mu l \left(\frac{1}{8s} - \frac{1}{24s^2} \right)$$

$$\frac{t}{l} = \frac{3s - 1}{24s^2 - 6s}$$

Evidently, by using non-dimensionalization, the equations become more manageable. More importantly, all the model tires now have the same characteristic shape, with an initial gradient of 1 and maximum value of μ_C. Consequently, any particular example can be fully represented by only two parameters, μ_C and S^*, which define the actual scales of the two axes.

The process of non-dimensionalization can usefully be applied to real tire experimental data. Usually the cornering force is simply non-dimensionalized against vertical force, so peak values vary somewhat, equaling the maximum cornering force coefficient μ_C. There remain some other differences. The graph curvature in the transition region (slip around 6°) is the main one, radial-ply generally having a sharper knee to the curve than bias-ply, giving less progressive final handling. Also, there may be a decline of cornering force beyond a peak, especially at high speed.

2.11 Improved Friction Model

Tire experiments show that the friction coefficient depends on speed, but also depends on skid duration preceding measurement at a given speed. As described in Section 2.3, the coefficient of friction of any particular rubber on a given surface depends on the sliding speed and temperature. Once the rear of the footprint is sliding, the rubber temperature will rise in a way that is rather hard to quantify. However, the practical consequence is that there is a reduction of frictional coefficient because the temperature exceeds the optimum. As shown in Figure 2.3.3, the friction value actually rises and then falls with sliding speed. For realistic tires and sliding speeds, friction is past the peak and therefore reduces with speed.

There are four commonly used analytic friction–speed models:

(1) Constant μ

(2) Different static and dynamic values μ_S and μ_D

(3) $\mu_D = \mu_S(1 - KV)$

(4) $\mu_D = \mu_S\, e^{-V/V_1}$

In model (2) $\mu_D/\mu_S \approx 0.8$. In model (3) $K \approx 0.012$ s/m. In model (4) $V_1 \approx 60$ m/s. The low-speed friction coefficient μ_S can be as high as 1.2 for standard car tires, but is much less for trucks; Figure 2.11.1 shows results for locked-wheel braking tests. The lower value for trucks is due to harder tread compounds for low wear and to high contact pressures. The high values for racing tires are achieved by using special compounds and low contact pressures. The values are only roughly indicative and may vary substantially according to the particular tire, vertical force, temperature and other conditions.

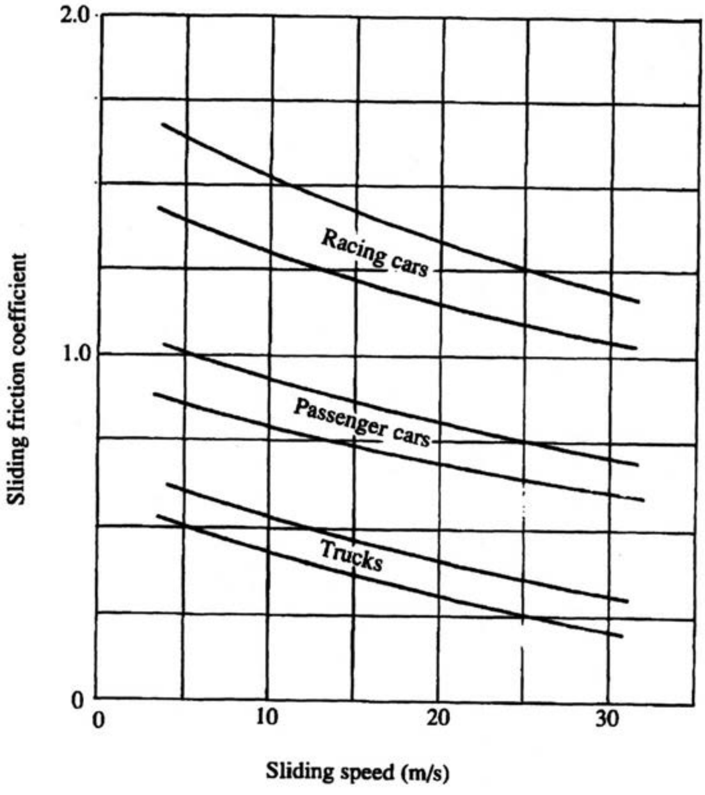

Figure 2.11.1. Friction against speed for locked-wheel braking.

Although the more complex models are needed for accurate analysis, model (2) is sufficient to understand the effect of speed dependence of friction by defining one static coefficient of friction applicable to and limiting the non-sliding part of the footprint, plus a lower dynamic coefficient of friction applicable to the sliding part of the footprint.

The consequences of this on cornering force can be seen fairly easily. At high slip angles the sliding part of the footprint, at the rear, will have a reduced friction coefficient, so the cornering force will peak at a moderate value of slip angle and then decline. However, the decline of maximum cornering force with speed will be less dramatic than that of locked wheel braking because the actual relative sliding speed is only $V \sin\alpha$, and the wheel continues to rotate so the local temperature rise is less. The reduced coefficient of friction behind the footprint center contributes to the negative self-aligning moments that are observed in practice.

2.12 Camber Angle and Camber Force

Camber is the inclination of the tire in front or rear view (Figure 2.4.2(b)). The SAE defines positive rotation about the X-axis, as shown, as the inclination angle and defines camber as the modulus of the inclination, with a positive value if the top of the wheel is outward from the vehicle centerline. In practice, the term camber angle is frequently used to mean inclination angle, especially in the context of an isolated tire or wheel, when the SAE definition of camber is not applicable. Single-track two-wheeled vehicles operate at extreme camber angles in cornering; four-wheeled vehicles usually have angles less than 10°. Figure 2.12.1 represents a view down through a transparent cambered wheel showing the tread area distortion caused by the camber. The consequence is a lateral force. There is also a camber aligning moment about the Z-axis, often negative (associated with a negative camber trail), but this is small and usually neglected.

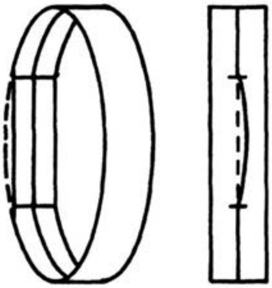

Figure 2.12.1. Tire camber distortion.

The lateral force produced is called the camber force, sometimes the camber thrust (an obsolescent term); because camber angles are fairly small, friction effects are generally secondary and the camber force is a function of the stiffness properties of the tire, of the camber angle and of the vertical force. It acts toward the low axis side and is typically found to be proportional to the camber angle; hence the camber stiffness C_γ is defined as the rate of change of camber force with camber angle. It has a typical value for a modern radial car tire of 35 N/deg (2 kN/rad). The camber force is approximately proportional to the vertical force, so dividing by the vertical force gives the approximately constant camber stiffness coefficient C_C. (The analogous cornering stiffness coefficient was denoted C_S.) Hence, at zero slip angle

$$F_Y = F_\gamma = C_\gamma \gamma = C_C F_V \gamma$$

The value of C_C is typically 1.0 for a bias-ply tire and about 0.4 for a radial-ply tire. Hence in the case of a bias-ply tire, the normal force plus camber force acts approximately up the tire centerline, which is desirable for a two-wheeled vehicle. Radial-ply tires for motorcycles are given a large section radius to move F_V laterally to compensate for the low value of C_C.

Interestingly, in contrast to cornering force from slip angle, there is no simple theoretical basis for any drag force to occur in conjunction with camber force. Also, experimentally it is found that associated drag forces are indeed small.

The camber angles found on four-wheeled vehicles are typically 0 to 1° in the static position, increasing to a limit of ±10°, usually less, under extreme cornering. The forces caused by camber angle are therefore generally less than those caused by slip angle. However, they can have a significant effect on handling behavior because of camber changes during suspension movement, which may be different front and rear; for example, many vehicles have independent suspension at the front with a solid axle at the rear.

Early tire force experiments were interpreted as implying that camber angle affected the slip-angle cornering stiffness. However, it is now generally accepted that for car analysis, for small angles, the two can be treated as independent, i.e.,

$$\begin{aligned} F_Y &= F_\alpha + F_\gamma \\ &= C_\alpha \alpha + C_\gamma \gamma \\ &= C_S F_V \alpha + C_C F_V \gamma \\ &= F_V (C_S \alpha + C_C \gamma) \end{aligned}$$

The lateral force coefficient is

$$\frac{F_Y}{F_V} \equiv C_Y = C_S\alpha + C_C\gamma$$

The camber coefficient diminishes for large slip angles. This is necessarily the case because at high slip angles, near to peak F_Y, camber has only a relatively small effect on F_Y. Some experiments indicate that C_γ reduces significantly with speed beyond about 30 m/s. The effect of camber on force generation at high slip angles is discussed under tire experimental data.

Lateral force is cornering force (from α) plus camber force (from γ). This is clear for small angles, but the distinction ceases to be clear in the nonlinear regime where the simple summation is no longer valid. At large camber angles, as achieved on motorcycles, the cornering stiffness is reduced significantly. The reduction in C_α is generally in the range 0.3 to 0.7% per degree of camber angle, and is virtually linear up to very large camber (60°). Hence

$$C_\alpha = C_{\alpha 0} - k_{C\alpha\gamma}\gamma$$

with

$$k_{C\alpha\gamma} \approx 0.005/\text{deg} \approx 0.3 \text{ rad}$$

The path curvature

$$\rho = \frac{1}{R}$$

also has an effect on tire lateral force. The contribution to F_Y from path curvature alone, in the linear region, is

$$F_Y = F_\rho = C_\rho \rho$$

where C_ρ is the path curvature stiffness of the tire. Now a tire of loaded radius R_l with camber angle γ, rolling freely, and hence with no lateral force, moves approximately as a cone following a path radius R, where

$$\gamma \approx sin\gamma = R_l/R = \rho R_l$$

However, for free rolling $F_Y = 0$, so with $\alpha = 0$ the result is

$$F_Y = C_\gamma \gamma + C_\rho \rho = 0$$

$$C_\rho = -\frac{\gamma}{\rho} C_\gamma$$

$$= -R_1 C_\gamma$$

A representative value of C_ρ is 600 Nm. The effect of path curvature on tire force is usually neglected in ordinary handling problems, although it is important in some steering vibration problems where the high frequency of oscillation results in a small path radius for the individual tire.

In summary, we have the following additional tire camber parameters:

(1) F_γ, camber force

(2) F_Y, lateral force including camber force

(3) C_γ, camber stiffness

(4) $C_C = C_\gamma / F_V$, camber stiffness coefficient

and for path curvature effects:

(1) ρ, path curvature for the tire

(2) F_ρ, path curvature force

(3) C_ρ, tire path curvature stiffness

2.13 Experimental Measurements

The complexity of tire construction and the notorious variability of friction mean that it is not at present possible to predict tire performance very successfully by direct theoretical means. However, the simple models already examined show that there are two principal parameters of tire behavior: the cornering stiffness coefficient and the maximum cornering-force coefficient. The former governs behavior in normal driving and depends primarily on the stiffness properties of the tire. The latter governs the behavior during extreme driving and depends primarily on the frictional properties of the tread on the relevant road surface. Even if conditions are restricted to dry hard road surfaces, the friction forces are rather variable. There are relatively few published measurements of maximum forces, although fairly extensive investigations have been made of cornering stiffness and camber stiffness values.

There are various possible ways to measure tire characteristics. The most convenient is to operate the tire on the outside surface of a circular cylindrical drum, typically of 4 m diameter. Such results are good for comparative purposes, but must be treated with some caution because the drum curvature influences the results, especially the self-aligning torque. The inaccuracies are generally proportionately worse at small slip angles. Adjustments on the order of 10% can be made to correct the cornering force data to flat conditions although these are not really reliable; the cornering stiffness coefficient needs to be increased according to the tire and drum radii:

$$C_\alpha = C_{\alpha \mathrm{D}}\left(1 + 0.4\frac{R_\mathrm{u}}{R_\mathrm{D}}\right)$$

Measurements have also been made on the inside surface of drums and on discs. The best laboratory arrangement is the continuous belt, supported from below by an air bearing. A remaining limitation of this method is the problem of simulating the road surface. This can be overcome by running the tire along a suitably prepared floor, but then only rather low speeds are practical. Each method therefore has its advantages and disadvantages.

An attractive alternative to laboratory measurement is to make mobile tests on the road, typically done by cantilevering the tire out from the rear of a lorry. While offering realistic results, this method obviously has problems of environmental and surface control and repeatability.

The results of a tire test depend on the usage history of the tire, especially carcass conditioning and tread wear. Changes can be especially rapid on a new tire during its first few runs, seemingly from two effects. First, flexing of the carcass results in some stiffness changes. Second, a new tread surface has a mold sheen which quickly wears off. This is a surface unrepresentative of the rubber below, and it is also likely to be contaminated with mold lubricant. These effects are quite different from those of gross tread wear. Specific tests have been performed to investigate this running-in effect on the tire. Generally, the effects on peak side force, which tends to increase, are

(1) A sharp and often erratic change in the first run due to wearing away of the mold sheen.

(2) An upward exponential decay, with a distance constant of typically 1 km eventually resulting in a total coefficient increase of about 0.08.

(3) A steady coefficient change of about 0.015/km caused by uniform wear of the tread during initial operation at high slip angle.

On the other hand, cornering stiffness coefficient is often reduced by conditioning. The effects are:

(1) A recoverable effect because of rise of carcass temperature (–0.0007/°C).

(2) Typically about 10% reduction because of visco-elastic effects in the carcass, of which 7% is permanent, and 3% recovered when resting with a time constant of about 1000 s.

The tread is likely to be worn away completely in 10 to 20 km of hard testing, reflecting the severe operating conditions. Even after initial transient effects, the steady variation can give a total change of 20% in cornering stiffness during the life of the tire – sufficient to have a major effect on vehicle handling.

Even when using flatbed belt testers with agreed conditioning procedures, there remain significant differences between cornering stiffness results from different machines, on the order of 5% or more.

Carcass flexing and initial tread wear often result in a marked increase of aligning torque stiffness, of typically 30%, with a modest increase during the remainder of the life. On the road, the full carcass conditioning period corresponds to typically 1000 km.

Conditioning effects are generally inconsistent, varying between tire types. Some investigations have found little or no statistical significance for the results of various conditioning procedures in relation to the random variation between tire samples.

2.14 Stiffness Measurements

Even if a new tire is tested against a smooth (but frictional) surface, because of minor variations in structure such as cord angles and rubber thicknesses around the perimeter, there are small variations in lateral forces as the tire rotates. These variations have an amplitude on the order of $0.01F_V$. Also, the average forces and moments are not zero for zero angles; in fact, some tires are produced with deliberate such asymmetry of carcass or tread or both. The force and moment values at zero slip and camber angles are called the residual cornering force and residual aligning moment.

The average lateral force at zero slip angle results from two factors: conicity and ply-steer. These are more significant for radial-ply tires than for bias-ply. Ply-steer forces result from the angle of the belt plies; for an equal number of plies of alternate angles each side of the centerline, the outer ply exerts the dominant effect. The direction of the ply-steer lateral force depends on the direction of rolling. This is also true of slip angle, so ply-steer is also known as pseudo-slip. A typical ply-steer force value is equivalent to 0.3° of slip angle, or about 250 N. For a given design of tire, the ply-steer force is a fairly constant value with small variations between samples, but, of course, there is considerable variation between tire designs.

Conicity force is so-called by analogy with a rolling cone, and results in a lateral force that has the same direction whether the tire is rolling forward or backward. This is also a property of camber force, so conicity is also known as pseudo-camber. Eighty percent or more of conicity forces are caused by the belt being off-center, the force sensitivity being typically 30 N/mm of belt offset. For a given design of tire, the conicity forces occur randomly. The production tolerance for belt position is typically around 3 mm, equivalent to 100 N lateral force.

A real tire has both types of force together, hence exhibiting different forces according to the direction of rolling. By testing in both directions these can be resolved into conicity and ply-steer, conicity being the mean force, and ply-steer being half of the difference.

The cornering stiffness itself also varies from tire to tire, even among those nominally of the same type from a given manufacturer, with a typical standard deviation of 3%, and 6% for aligning torque stiffness. This is simply a matter of the economics of quality control.

Tire designs of a given nominal size and type from various manufacturers have a standard deviation of about 15% on cornering stiffness. The random variations, although not always negligible, are therefore much less than the systematic differences between designs. The main controlling factor in the cornering stiffness is the carcass structure; basically whether it is radial-ply or bias-ply. Belted bias-ply tires have a cornering stiffness typically 5% greater than normal bias-ply; radial-ply average typically 40% stiffer than basic bias-ply. Aligning coefficients are ordered similarly, with bias-belted 15% stiffer than bias-ply, and radial 30% stiffer than bias.

Some tires used to exhibit a reduced cornering stiffness for very small slip angles. This caused unresponsive straight-line handling and a deadband in the steering ("wide-center" feel). It is insignificant on most modern tires because of better design and quality control.

In examining the effect of tire structure, a rather different picture emerges for camber coefficient. Belted-bias and bias are much the same, both having coefficients giving a camber thrust resulting in the total force acting approximately directly up the tire centerline, corresponding to a camber coefficient of 1/rad or 0.018/deg. For radial ply it is typically 0.4/rad or 0.008/deg. Since radial-ply tires, compared with bias-ply, exhibit a high cornering coefficient and low camber coefficient, then the different carcass constructions are strongly characterized by the ratio of camber stiffness to cornering stiffness, which of course also indicates the slip angle needed to overcome the force caused by one degree of camber angle. This ratio is typically 0.15 for bias-ply and 0.05 for radial-ply.

Speed has been found to have some effect on force coefficients. Beyond about 8° slip angle, the frictional effects usually dominate, and high speed gives lower forces. At less than 8°, the main effect of higher speed is to stiffen the carcass, increasing the cornering forces. Plotting the cornering stiffness coefficient against the logarithm of speed, a straight line is obtained. The speed sensitivity k_V is defined as the stiffness increase resulting from a factor of ten speed increase; it has a value of 0.06 to 0.10. Hence

$$C_S = C_{S0}\left[1 + k_{CSV}\log_{10}(V/V_0)\right]$$

A limited amount of data suggests that speed tends to reduce the camber coefficient, particularly beyond 30 m/s.

Lateral force coefficients also depend on vertical load. The three common models are (1) linear, (2) power, (3) exponential.

(1) Linear: A simple model of the variation is a linear one, declining with load:

$$C_S = C_{S0}\left[1 + k_1\left(1 - \frac{F_V}{F_{V0}}\right)\right]$$

where subscript 0 is the reference point (standard load), and k_1 is the load sensitivity. At zero load C_S goes to $(1 + k_1)C_{S0}$. Typically k_1 is 0.6. This gives realistic characteristics provided that the loads are not too large, i.e., not approaching those for which C_S goes to zero.

(2) Power: This expresses the cornering stiffness as

$$\frac{C_\alpha}{C_{\alpha 0}} = \left(\frac{F_V}{F_{V0}}\right)^f$$

which is equivalent to

$$\frac{C_S}{C_{S0}} = \left(\frac{F_V}{F_{V0}}\right)^{f-1}$$

The exponent f varies widely, especially with F_{V0}, but is typically 0.5.

(3) Exponential: The above models are conveniently simple, but for computer simulations a more accurate model has the cornering stiffness coefficient declining exponentially with load (Figure 2.14.1):

$$C_S = C_{S1}\, e^{-k_{CSFV}(F_V/F_V-1)}$$

$$C_\alpha = C_{\alpha 1} \frac{F_V}{F_{V1}} e^{-k_{CSFV}(F_V/F_{V1}-1)}$$

The vertical force for maximum C_α is equal to F_{V1}/k_{CSFV}. If F_{V1} is chosen equal to this value, then k_{CSFV} is 1.0.

This model is particularly good for wide variation of load, and agrees well with data. In view of this, it is apparent why the simpler models above fit over only a limited range of load, and why their parameters vary with reference load. In Figure 2.14.1(b), the variation of C_α increasing and then decreasing with load shows how the variation of C_α with load around the operating point depends very much on the reference load, and hence on the size of tires in relation to the vehicle mass.

It is clear from all of the above that the broad specification of a tire structure is indicative of its properties, but that marked variations can occur because of the details of its design or operating conditions. As a very rough guide, the cornering stiffness coefficient is typically 0.12/deg for bias-ply, 0.16/deg for radial-ply, and the camber stiffness coefficient is 0.018/deg for bias and 0.008/deg for radial. Camber-to-cornering stiffness ratios are typically 0.15 for bias-ply and 0.05 for radial-ply.

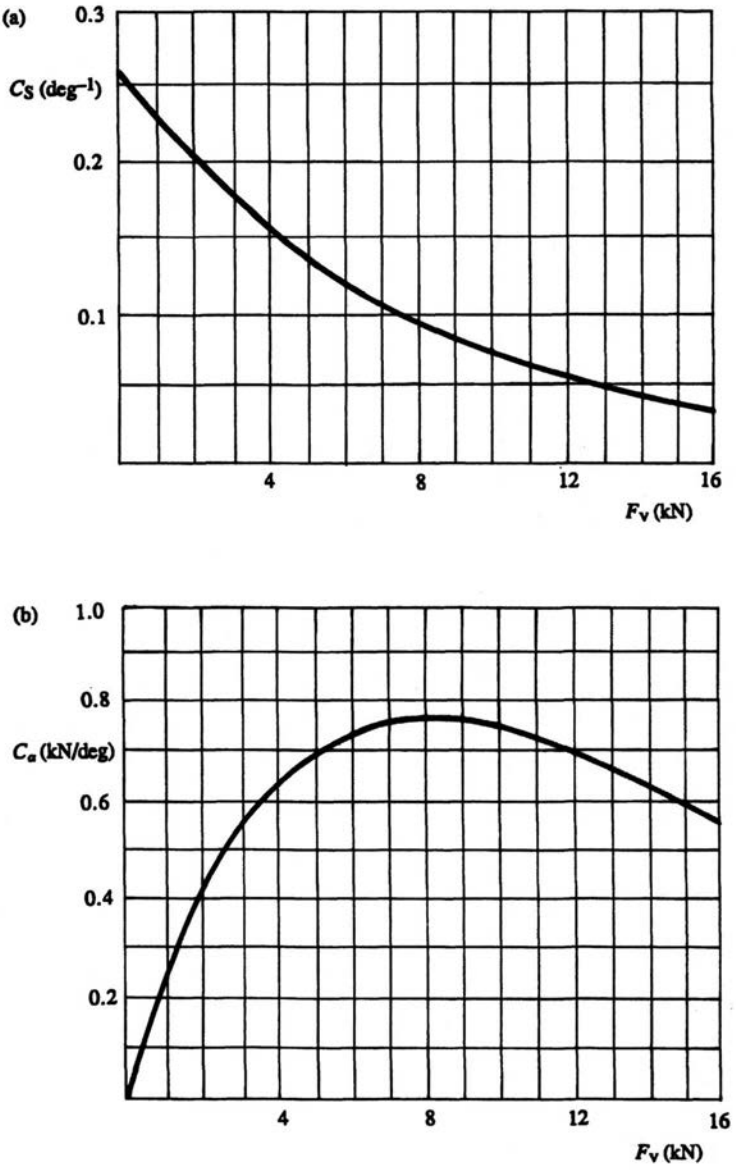

Figure 2.14.1. The effect of vertical force on C_S and C_α.

2.15 Stiffness – Design Variables

Even given a specific tire construction, the cornering and camber stiffnesses are found to depend on the tire size, section height, section width, tread width, rim width, tread depth and form, inflation pressure, load, and so on. The following is offered only as an approximate guide to likely effects, since there is considerable variation between designs.

2.15.1 Design Load (Size)

Cornering stiffness when carrying the design load is more or less proportional to design load (i.e., the cornering coefficient is independent of size). Cornering aligning stiffness, if expressed as Nm/deg, increases with size. This is reasonable because the pneumatic trail would be expected to increase in proportion to footprint size, and hence with design load and diameter. At constant load, pressure and rim width, the cornering stiffness varies typically as rim diameter to the power 0.5. The cornering aligning coefficient, normally defined as aligning moment stiffness divided by normal load (Nm deg^{-1}/N = m/deg), might logically be better defined by also dividing by a linear dimension such as rim diameter. It varies typically as rim diameter to the power 0.8. Camber stiffness coefficient is roughly proportional to design load (camber coefficient independent of size). Camber aligning stiffness (as Nm/deg) is rather widely scattered, but small and usually neglected. The constancy of cornering coefficient with size is of course related to the practical observation that the operation of a vehicle in terms of maximum cornering ability and of tire slip angles does not have a first-order dependence on size.

2.15.2 Construction

Increasing the number of plies seems to have little effect on cornering stiffness, but seems to reduce aligning torque (number of plies to the power −0.3). A large crown angle for bias-ply cords gives reduced cornering stiffness.

2.15.3 Section Width

Cornering stiffness coefficient varies typically as section width to the power 0.3 (constant load, pressure, rim width), although if an appropriately reduced inflation pressure is used, about half of the increase is lost. The self-aligning torque is affected increasingly as slip angle increases, but typically varies with section width to the power 1.0 at 6° slip angle.

2.15.4 Section Height

An increased section height implies a larger outer diameter, and typically a lower design inflation pressure for a given design load, with a longer footprint and more flexible sidewalls. The expected result would be reduced cornering stiffness.

2.15.5 Tread Width and Contour

Increased tread width increases the cornering stiffness slightly. A rounded contour generally increases the stiffness, possibly owing to a longer contact patch length.

2.15.6 Rim Width

Increasing the rim width upon which a given tire is mounted also incidentally increases the section width, which should be distinguished from a design change to the section width with a corresponding increase of design rim width. Cornering stiffness is roughly proportional to the rim width to the power 0.5, which therefore offers a useful degree of control – there is, of course, a limit to the rim width that a given tire can safely accept.

2.15.7 Inflation Pressure

At very low pressure the cornering stiffness is correspondingly small because it depends mainly on the inflation pressure rather than on inherent carcass stiffness. Moderate increases in inflation pressure above the design value generally raise the cornering stiffness because of an increase in carcass tension. The stiffness typically peaks at about 20% more than the design value for a pressure 70% more than design. It then reduces, probably because of contact-patch shortening. Increasing pressure usually causes a reduced aligning stiffness because of the shorter contact patch, and tends to increase the camber stiffness. Low pressures are desirable to improve the ride, but there is a corresponding loss of tire life, increase of self-aligning torque, and increase of squeal. The loss of stiffness generally causes poorer handling and feel. The warmed-up operating pressure is typically 30 kPa higher than the cold-set value. This is a 15% gauge pressure increase, 10% absolute. The more water vapor there is in the tire, the greater is the temperature sensitivity, so dry air is generally preferred.

2.15.8 Load

Cornering stiffness is zero at zero load, and initially increases in proportion to load, but it then peaks and declines for larger loads (see Section 2.14). High inflation pressures and wide rims tend to result in an increase in stiffness sensitivity to load. This can be important because if the cornering stiffness increases with load, the sensitivity of the vehicle handling to load changes is reduced. The cornering stiffness coefficient is greatest at "zero" load, declining smoothly and exponentially, as discussed in the previous section. The aligning coefficient shows a continuous increase due to the lengthening contact patch. Camber coefficient usually shows a reduction away from the design load.

2.15.9 Tread Depth

The introduction of tread grooves for drainage in wet conditions increases the lateral compliance of the tread part of the tire, although it is too simplistic to consider the tread simply as a compliance added to the carcass. Evidently this depends to some extent on the tread pattern, and where possible the width of circumferential ribs is at least twice the groove depth, i.e., 16 mm for a typical new groove depth of 8 mm. Wide ribs, although aiding tread stability, cause water clearance difficulties. The cornering stiffness of a bias tire with the tread worn almost entirely away is typically 15% higher, and sometimes as much as 50% higher, than for the new tire, the difference being pressure- and load-sensitive. Radial-ply tires often show a reduced stiffness after wearing. The corner aligning torque coefficient generally increases with wear for all types, and may double over the tire life.

2.16 Friction Forces – Design Variables

The second principal variable controlling the shape of the cornering force versus slip angle curve is the maximum available force. This occurs at 90° slip angle for the simple model, but at perhaps 10° in reality according to the particular tire and operating conditions, especially vertical force. The maximum cornering force is controlled to a large extent by the tread rubber material and the road surface, but other factors play a part, particularly the surface area of rubber presented to the road in relation to the load, i.e., the mean contact pressure. A harder rubber has been known to result in a higher maximum cornering force but in a smaller maximum braking force. This cannot be simply a friction effect. Presumably it is related to the different distortions experienced by the tread in these two modes of operation. The maximum central force is influenced by both friction and stiffness characteristics because of the $\cos\alpha$ factor. In practice there is found to be a scale effect, with truck tires exhibiting a friction coefficient typically 40% lower than that of passenger cars (Figure 2.11.1). This is probably attributable to the higher inflation pressures and to the harder tread materials used, because of the service requirement for low wear rate.

Changes of road conditions have a major effect, the most extreme case being surface ice. However, even in dry conditions road characteristics vary through a wide range, and this is emphasized by damp conditions (wet conditions are considered later). The self-aligning torque is also affected by low friction, so the driver is able to detect this through light steering at quite low steering angles. The temperature of the road surface affects maximum friction, but in a way that depends on the road material. In one investigation on asphalt the maximum cornering force coefficient μ_C was 0.9 at 0°C, declining linearly at 0.0025/°C to 0.8 at 40°C. On concrete it was also 0.9 at 0°C, but increased to a peak of 1.06 at 26°C and then declined to 1.0 at 40°C in a smooth curve.

Increase of load shows an increase of limiting force, but not in full proportion. The variation of maximum cornering force may be modeled well by

$$F_{\mathrm{Y\,max}} = F_{\mathrm{Y\,max\,0}}\left(\frac{F_{\mathrm{V}}}{F_{\mathrm{V0}}}\right)^{1+p}$$

$$\frac{\mu_{\mathrm{C}}}{\mu_{\mathrm{C0}}} = \left(\frac{F_{\mathrm{V}}}{F_{\mathrm{V0}}}\right)^{p}$$

The limited amount of actual tire maximum force data indicates a value of $p = -0.15$ for the typical tire maximum cornering force coefficient sensitivity to vertical force for passenger car tires. Racing tires seem to be more sensitive at −0.20 to −0.25. This relationship is an important one in the investigation of limit handling, for example in considering the effect of center of mass position or load transfer.

This power expression represents real tire data very well over the important range of vertical force. At very small F_{V}, however, it overpredicts F_{Ymax} slightly, and indicates a maximum lateral force coefficient going to infinity.

Therefore in computer simulations it is desirable to represent μ_C by a linear section for small F_V, e.g., less than one-quarter of the reference value (Figure 2.16.1).

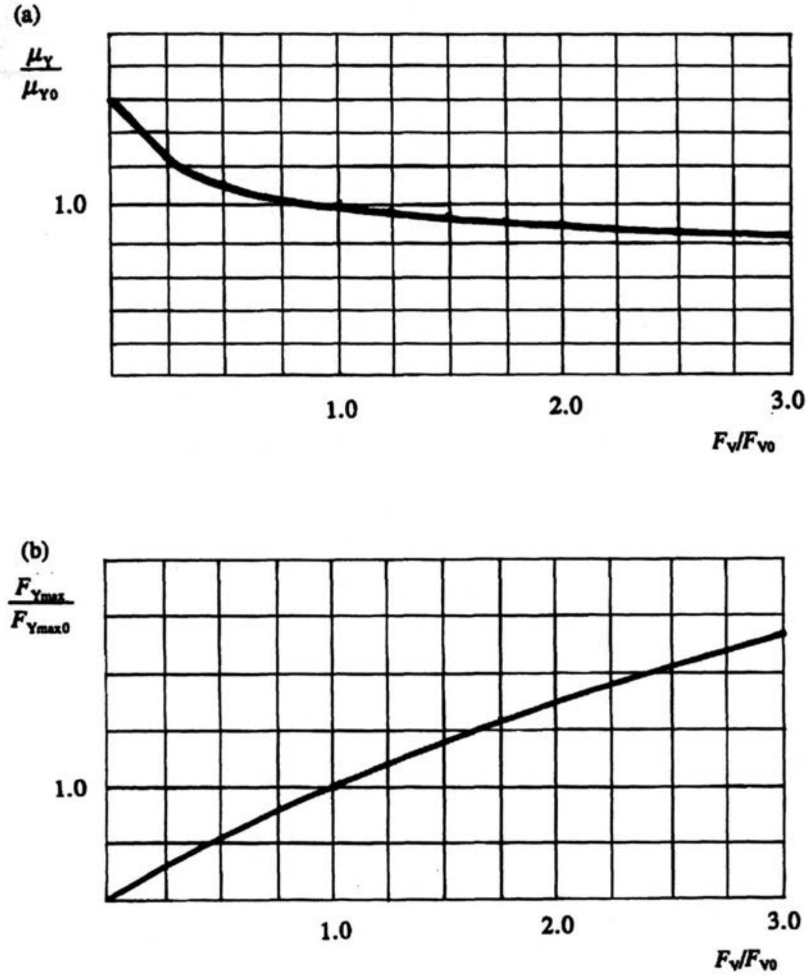

Figure 2.16.1. The effect of vertical force on μ_y *and* F_{Ymax}.

This suggests that an exponential model might be good, as used for the variation of C_S with load. However, such a model is a much inferior fit to the data over the important range of F_V.

An increase of contact area gives a higher limiting force – this has contributed to the trend to very wide racing tires with some tendency in the same direction for passenger cars. This suggests a maximum force coefficient rising as the 0.15 power of tire tread width, for constant footprint length. The introduction of drainage channels reduces the contact area and hence reduces the limiting force in dry conditions. The racing "slick" tire has no tread pattern at all to give maximum contact area. The rubber area in direct contact with the road is normally less than the nominal footprint area, and also the pressure distribution is likely to be highly variable due to the distorting effects of the forces applied by the road. Wider rims seem to help a little in this respect. There is an optimum inflation pressure that gives the most uniform footprint pressure, and this optimum inflation pressure increases with increasing normal load. Too low an inflation pressure gives high contact pressure at the tread edges because of the carcass stiffness, whereas too high a pressure loads the center. A tire pressure optimum for wear in normal straight running is therefore rather low for extreme cornering because of severe load transfer in this condition. High pressures can create difficulties for the tire in adapting to road roughness. An interesting racing development that has found application on road tires is the depressed crown, which becomes flat once correctly inflated.

The effect of camber angle on maximum force seems to depend on the tire crown shape. A very round profile seems to develop maximum lateral force with a large negative camber, the optimum slip angle then being quite small. A flatter crown tire seems to be best in the 0–4° negative camber range. Possibly in some cases negative camber compensates for slip-angle distortions to help keep a flat crown on the road. The camber tolerance range seems to increase with increasing normal force, presumably because the mean contact pressure is increased, so that the proportional pressure variation is reduced.

The tire speed can affect maximum force measurements. First, this will occur if the Turner number exceeds about 0.8 because of wave effects. Normally vehicle conditions are comfortably below this, and test conditions lower still. Second, a speed influence may be exhibited when sliding occurs because the friction coefficient is speed-dependent. Hence for small slip angles, where elastic effects dominate, tests can be conducted at relatively low speed, although corrections should be applied (see Section 2.14). For large slip angles this cannot be taken for granted. Fortunately the actual contact patch sliding speed, even at maximum lateral force, is usually quite small. According to the simple tire model advanced in Section 2.9, the rear of the contact patch will slide, giving a relative speed of $V\sin\alpha$. Hence for a slip angle of 15°, at a vehicle speed of 60 m/s, the sliding speed is about 15 m/s. The effect of speed-sensitive friction on lateral force is therefore generally less than it is on locked-wheel braking. Nevertheless, low-speed tests are not entirely adequate in this respect.

The periphery of the tire strikes the ground at the front of the contact patch. At high speed this gives an impact force which increases the vertical force at a given deflection. It also moves the vertical force forward. This increases the rolling resistance. It also results in the pneumatic trail going to a large negative value at very high speed.

A second major difficulty of all force measurements is that they are rather sensitive to the tread contour, as modified by use and wear. The idea of the performance of an engine changing as the parts wear to fit each other is a familiar one – the tire too behaves like this. Hence a tire conditioned by gentle driving, suddenly called upon to provide a large lateral force, will not be matched to the road in its new distorted shape and will present a highly non-uniform pressure in the contact patch. If the demand for this new force is maintained, the tire will wear the highly loaded regions, and hence adapt, and in due course would be expected to be able to give a higher force. In high wear-rate tests this effect is sometimes observed, but sometimes the opposite occurs. Presumably the tire force is best assessed as the one immediately available on a tire with a wear history typical of the relevant application. Obviously the normal tire testing machine tends to operate at higher average slip angles than the usual driver – it would be uneconomic to do otherwise. Hence some doubt about the applicability of the results must remain.

Vertical load is important because handling in the high lateral acceleration regime causes large lateral load transfers. Figure 2.16.2 shows some example lateral force results, plotted against slip angle for various loads.

Figure 2.16.3 shows lateral force plotted against vertical force. An increase of vertical force at fixed slip angle does not give a proportionately greater lateral force. The rate of change of lateral force with vertical force at a particular slip angle is called the vertical force sensitivity (load sensitivity), mathematically defined as:

$$C_{\mathrm{FV}} = \left(\frac{\partial F_{\mathrm{Y}}}{\partial F_{\mathrm{V}}}\right)_{\alpha}$$

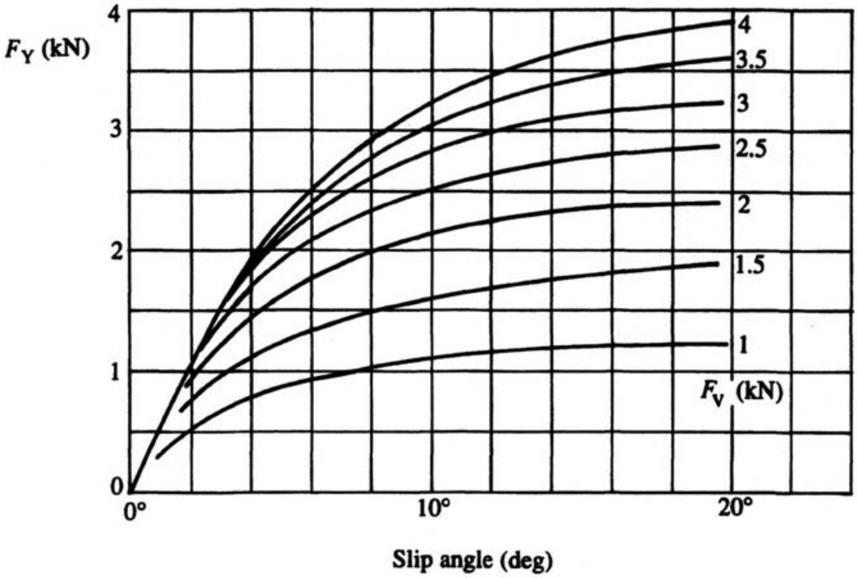

Figure 2.16.2. Tire lateral force against slip angle.

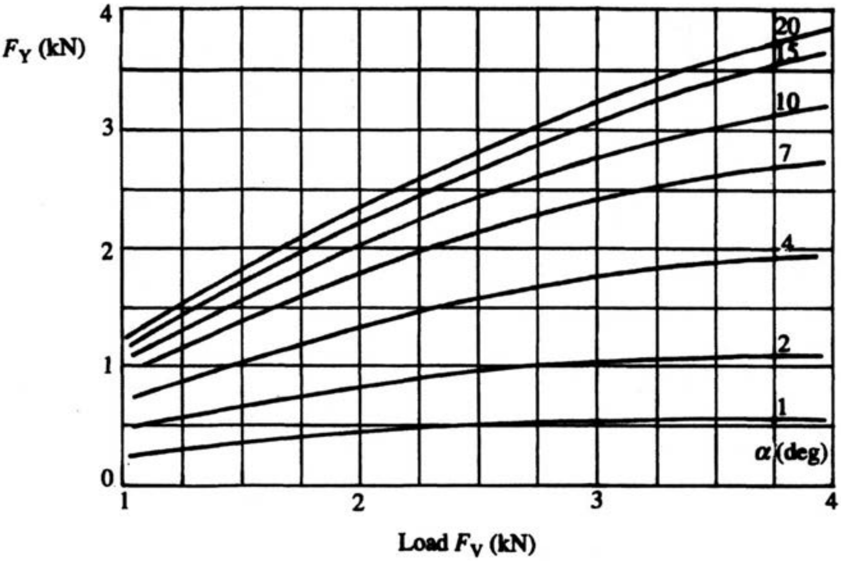

Figure 2.16.3 Tire lateral force against vertical force.

For two wheels of fixed total load, for example at the ends of an axle, the more unevenly the load is distributed by load transfer, then the less the total lateral force (Figure 2.16.4). This can strongly affect handling at large lateral accelerations. The sensitivity of the lateral force of a pair of wheels to load transfer, at constant total load $2F_V$ with transferred load F_{VT}, is the load transfer sensitivity:

$$C_{FT} = \left(\frac{\partial F_{Y2}}{\partial F_{VT}}\right)_{\alpha, F_{V2}}$$

The normalized load transfer sensitivity is

$$C_T = \frac{\left(\dfrac{\partial F_{Y2}}{\partial F_{VT}}\right)_{\alpha}}{\dfrac{F_{Y2}}{F_{VT}}}$$

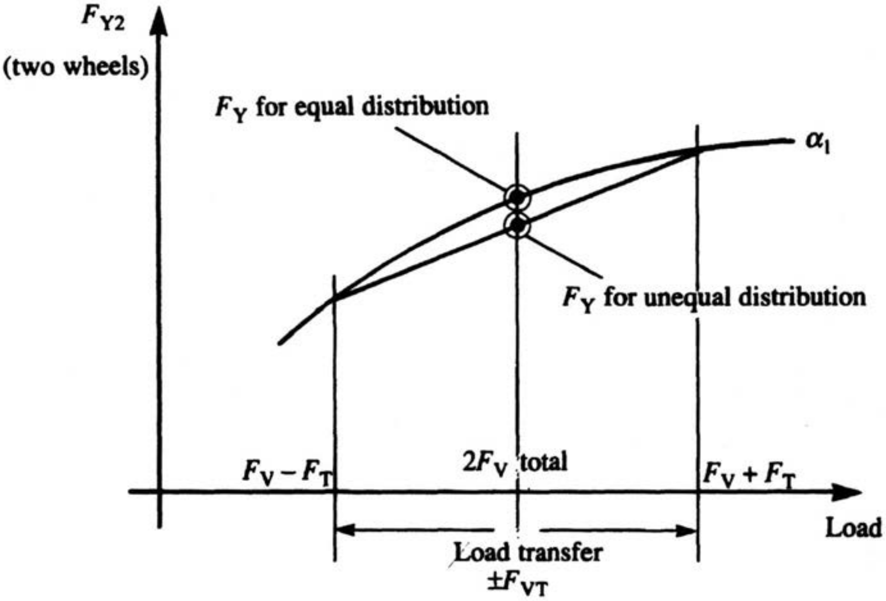
F_{Y2}
(two wheels)
F_Y for equal distribution
α_1
F_Y for unequal distribution
$F_V - F_T$
$2F_V$ total
$F_V + F_T$
Load
Load transfer
$\pm F_{VT}$

Figure 2.16.4 Effect of load transfer on axle lateral force.

where F_{Y2} is the side force for two wheels, and F_{VT} is the transferred vertical force. Because this is a second-order effect (i.e., locally, a line curvature), it is normally evaluated for a fairly large normalized load transfer, typically $F_{VT}/F_V = 0.6$, and has a typical value of 0.2. In other words, 60% load transfer gives 12% reduction of F_{Y2}, the reduction depending on the square of the load transfer.

Using the vertical force transfer factor (load transfer factor),

$$e_V = \frac{F_{VT}}{F_{V0}}$$

an adequately realistic model of the variation of F_Y with F_V for one wheel is the quadratic expression

$$\frac{F_Y}{F_{Y0}} = 1 + C_1 e_V + C_2 e_V^2$$

To give $F_Y = 0$ at $e_V = -1$, then

$$\frac{F_Y}{F_{Y0}} = 1 + (1 + C_V)e_V + C_V e_V^2$$

where C_V is then a single parameter for the load sensitivity, with a realistic value of

$$C_V = -0.333$$

For the two wheels of an axle, one seeing transfer factor $+e_V$ and the other seeing the negative of that value, this gives

$$\frac{F_{Y2}}{F_{Y20}} = 1 + C_V e_V^2$$

Hence the linear dependence on load transfer disappears, leaving the second-order variation.

2.17 Longitudinal Forces

Whereas lateral forces are achieved by steering the wheels, longitudinal forces are created by applying torques about the wheel spin axis; in the latter case, unless the wheel is not rotating, there must be a corresponding power flow either providing kinetic energy (engine) or dissipating it (brakes). SAE uses "longitudinal" to refer to tire forces along the tire X'-axis (Figure 2.17.1), and also for the heading vector direction of the vehicle as a whole. Driving will be used for positive forward (X'-axis) tire forces, braking for negative (backward) forces, and longitudinal for either.

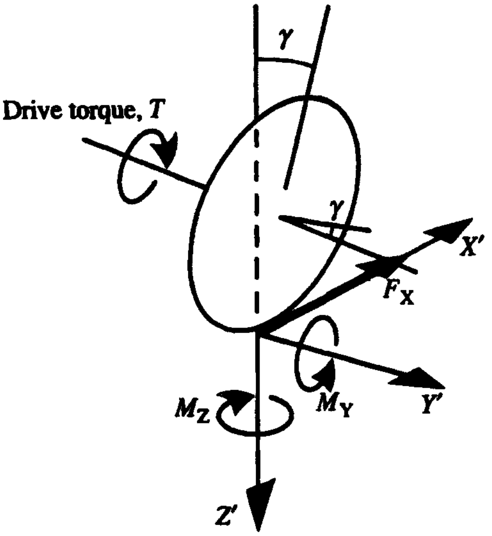

Figure 2.17.1. Forces and moments on a driven wheel.

In the SAE system, a positive applied torque T, from the driveshaft or brake, is defined to cause a positive longitudinal force. Figure 2.17.1 shows the corresponding wheel free-body diagram with forces. For moments about the wheel axis:

$$-T + F_X R_1 + M_Y \cos\gamma + M_Z \sin\gamma = I\dot{\Omega}$$

For small camber angles, wheel accelerations and rolling resistance,

$$T = F_X R_1$$

For forward acceleration a torque T is applied through the driveshaft; the brakes may apply a couple to the wheel, but of course the result at the tire is dependent simply on the effective torque.

If a braking torque is applied to a wheel that is maintained at constant translational speed, then the wheel rotational speed changes slightly. This means that there is an effective difference of speed between the tire at the contact patch and the road, ΩR_1 and V, respectively, relative to the wheel axis. However, there is not necessarily any actual sliding. The nominal speed difference is $V-\Omega R_1$. This can be non-dimensionalized to give a longitudinal slip S:

$$S = \frac{(V - \Omega R_1)}{V} = 1 - \frac{\Omega R_1}{V}$$

The effective rolling radius is $R_e = V/\Omega$, so the slip can be expressed as

$$S = 1 - \frac{R_1}{R_e}$$

Longitudinal slip is analogous to lateral slip: a small longitudinal slip produces forces by elasticity, and a large slip results in frictional effects coming into play. Again we can introduce a foundation stiffness model which can be pictured as short cantilever "spokes" (the "brush" model) which are stressed in the contact patch.

During road contact, the displacement of the wheel side of the foundation stiffness (Figure 2.17.2) is

$$l = t\,\Omega\,R$$

where t is the time that any element is in contact with the road. The displacement at the road side, for zero sliding, is

$$l' = tV$$

Hence the total deflection is

$$d_1 = (V - \Omega R)\,t$$

and the deflection at a distance x along the contact is

$$d = \left(\frac{x}{l}\right)(V - \Omega R)\,t$$

Noting that $l = \Omega R t$, then

$$d = \frac{xS}{(1-S)}$$

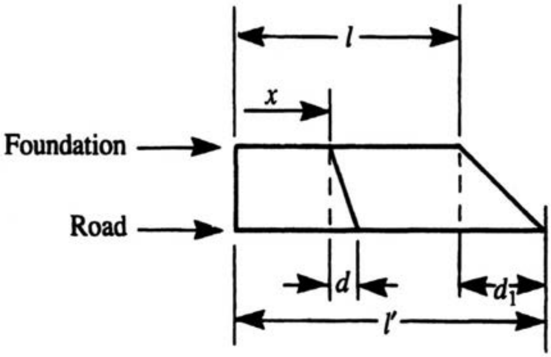

Figure 2.17.2 Displacement of brush model.

Figure 2.17.3(a) illustrates this deflection for a non-slide condition, i.e., small slip; its similarity to the lateral displacement model is apparent. Once again we can introduce a foundation stiffness, which when multiplied by the displacement area gives the retarding force. It may seem rather anomolous that the wheel can have an angular speed not equal to V/R_1 without there being any sliding, but this is possible because the elastic strain that occurs in the contact patch can be recovered when the tread elements leave contact with the road.

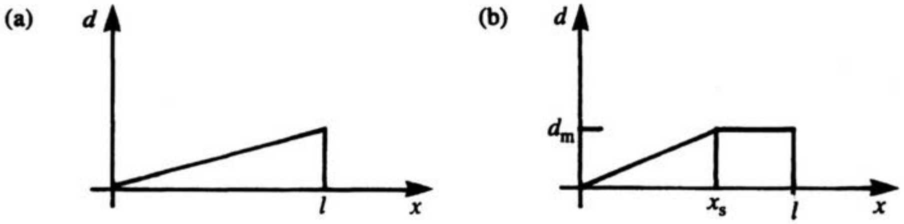

Figure 2.17.3. Longitudinal displacement: (a) small slip, (b) larger slip.

When a large slip is called for, the model predicts that, because of friction limitations, sliding will begin at the rear of the contact patch, the sliding area growing with slip (Figure 2.17.3(b)), as in the case of lateral force generation. The force versus slip curve, according to this model, gives maximum retarding force at a slip of 1.0 (locked wheel). This model can be refined by admitting reduction of friction coefficient with sliding speed, which gives realistic results, with the retarding force reaching a maximum at a slip of about 0.15 and then declining, the rate of decline being greater for high speed.

This incidentally reveals a limitation of the use of slip. The concept of longitudinal slip arises essentially from non-dimensionalization of the apparent speed differential at the contact patch. If we consider a locked wheel, it is evident that the slip is 1.0 regardless of the wheel translational speed, but since the rubber friction will really depend on the actual speed of sliding, the use of slip clearly has its limitations.

If a tractive force, rather than braking force, is required of the tire, then the behavior of the contact patch is similar, with stress and strain both adopting opposite signs from the braking case. Hence sliding will still begin from the rear of the contact patch.

2.18 Combined Forces

Combined longitudinal and lateral accelerations are of practical importance because they are likely to occur during accident avoidance maneuvers. Basically, the longitudinal and lateral forces are a combined function of the lateral and longitudinal slip. Longitudinal forces can generally be achieved only at some cost in lateral force, and lateral force exerts a price on longitudinal force. For $S = 1$ the wheel is locked, so curves of F_X and F_Y against slip angle are basically sine and cosine curves representing the resolution of a roughly constant total force into the $X'Y'$ coordinate directions. The most convenient presentation of such force combinations is probably the plot of lateral force coefficient against longitudinal force coefficient (Figure 2.18.1). This is roughly symmetrical for the radial-ply tire, although sometimes for bias-ply it is found that braking can initially give a small increase of the cornering force. Evidently, especially in the case of the bias-ply, elastic effects in the carcass play a significant part. The dominant controlling factor is, however, the tire-to-road friction.

For a foundation stiffness model tire, operating at a moderate slip angle, the contact patch is laterally stressed, especially at the rear; the lateral displacement from cornering is denoted by d_C. This corresponds to the shear stress to be resisted by friction. If a longitudinal force is also called for, there is a longitudinal (braking) strain d_b. Neglecting interactive strain effects in the carcass, which of

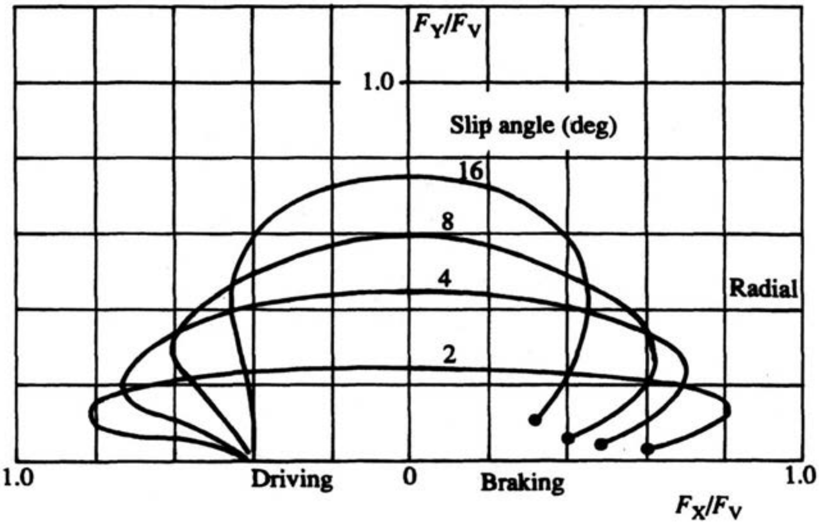

Figure 2.18.1. F_Y/F_V against F_X/F_V for various slip angles.

course the simple model does not admit, increasing d_b will result in sliding at the rear when

$$d_b^2 + d_c^2 = d_M^2$$

where d_M is the maximum (friction-limited) stress. As written, this corresponds to equal foundation stiffnesses in both directions, but this could easily be generalized if required. The qualitative conclusion is evident: except at low slips in both directions, the available friction force must be shared. Increasing the longitudinal force will reduce the lateral force. To follow this implication through in detail requires consideration of the operating conditions throughout the contact patch. The force variation of Figure 2.18.1 is the practical result.

There is an asymmetry of this figure that is of interest: under driving, F_Y ultimately goes to zero, whereas under braking it does not. A wheel locked in braking will have a total force on it governed kinematically: the force will act in the direction of motion of the ground relative to the tire. Hence the cornering force does not go to zero, but the central force does. For a wheel spinning due to gross excess power input, the limiting kinematic case of very-high-speed spinning gives the force in the direction of wheel heading rather than wheel motion. In this case the cornering force goes to zero, but there is a residual central force which may be significant at high slip angles. For example, the accepted rear-wheel-drive cornering technique for rally driving on loose surfaces is with spinning rear wheels at very large yaw angle.

The shape of these curves has given rise to the ellipse model, of attractive simplicity, in which the shape for each particular slip angle is approximated as half of an ellipse. The degree of precision available from such a model is limited by the frictional representation, since it is tantamount to adopting a friction value independent of sliding speed. Incorporation of this variation adds greatly to the accuracy, but also to the complexity of the model. Hence, for small forces the ellipse model is often adopted or the interaction is neglected completely. For accurate results at high forces it is essential to include the friction sensitivity to sliding speed.

There is a close relationship between the shape of the lateral–longitudinal force curve and the friction–speed curve. This is perhaps best seen by considering the limiting F_Y versus F_X curve for small slip angles which lies close to the F_X axis in Figure 2.18.1. Viewed sideways, this corresponds to the shape of the force–speed friction curve for the rubber.

The self-aligning torque when cornering is usually increased by moderate braking and decreased by driving. This is because the tire distortion shifts the lateral force line of action, i.e., it changes the pneumatic trail.

The complexity of Figure 2.18.1, applicable to only one speed, with zero camber for one tire type in a given state of wear on a given wheel and road surface, illustrates the problem of acquiring comprehensive data for the performance of even one tire design.

2.19 Wet Surfaces

During severe braking or cornering in damp conditions, sufficient heat is produced at the footprint for a very thin water film (i.e., dampness, 0.01 μm) to be boiled away. Even under nominally dry conditions, the atmospheric humidity will result in such a film.

Faced with a wet surface, i.e., 1 or 2 mm depth of water rather than just a damp film, the tire must clear away the water in order to establish contact with the solid road below. This is obviously a much more difficult fluid to clear than air because of the density and viscosity of water (see Table 2.19.1). Hence the tire is provided with a tread pattern, i.e., channels, slots and sipes (cuts) to provide passages for water movement. The footprint area is considered to operate in three sections: in the first the bulk water is cleared from beneath the ribs, in the second the residual film is cleared, and in the third the tire rubber is in good contact with the road surface.

Table 2.19.1. Comparison of Air and Water (at 15°C, standard pressure)

Property	Symbol	Units	Air	Water	(Ratio W/A)
Density	ρ	kg/m^3	1.225	999.2	(816)
Viscosity	μ	Ns/m^2	17.8×10^{-6}	1.14×10^{-3}	(64.0)
Kinematic viscosity	v	m^2/s	14.5×10^{-6}	1.14×10^{-6}	(0.079)

The basic mode of operation is that the water is first squeezed sideways from beneath the tread elements either out of the side of the footprint or into the longitudinal channels, where it then passes through the footprint within the channels. Operation of the channels depends on the depth of water ahead of the tire and the degree of wear of the tire. The cross-sectional area of the channels in front view, divided by the cross-sectional area of the approaching water, within the footprint width, gives a non-dimensional measure of the water drainage problem, i.e., a "drainage" number, N_{Dr}. Provided this is less than about 1.0, the approaching water, if shifted sideways into the channels, will not fill them up. In this case there is simply a lateral flow of water. If the approaching water is too deep and more than fills the channels, then they operate in a new role, acting genuinely as channels rather than reservoirs, allowing the water to flow relative to the tire through the contact patch and to emerge at the rear. If the wheel is locked, the channels are obliged to operate in this mode anyway. For water approaching the tires near the outer edges, it may be preferable to use lateral drainage to the edge of the tire, especially for a convex tread. A porous road surface can also contribute to footprint clearance for all tires. The details of optimization of tread design for drainage vary considerably between manufacturers and according to application. Evidently a racing tire, with a footprint aspect ratio (width/length) of three or more, may require a different solution to a conventional road tire with footprint aspect ratio of one or less, where moving the water out from the side of the footprint can make a proportionately greater contribution.

Once the bulk drainage is essentially complete, it remains to remove the thin residual water film. Both of these operations are facilitated by high contact pressure and the presence of a good road texture. Lateral slots help to reduce resistance to fluid flow into the main channels; sipes (small cuts) aid final wiping by producing high local contact pressures through local distortion under stress.

Hydroplaning (aquaplaning) can occur in two different ways. Dynamic hydroplaning occurs when the dynamic pressure of the oncoming water is sufficient to support the tire. Viscous hydroplaning occurs when the water viscosity prevents the water from being successfully squeezed from beneath the tread elements. The total time that any rubber element is in the footprint is inversely proportional to speed, and is typically 6 ms at a speed of 30 m/s (footprint length 180 mm). Hence water clearance must be achieved in only 2 or 3 ms.

In wet conditions the influence of vehicle speed and tread depth on maximum braking force is considerable. In one investigation with 2.5 mm of water, at very low speed all tread depths had a maximum braking coefficient μ_B of 1.0, but at 20 m/s it was down to 0.77 for 8 mm tread, 0.58 for 4 mm tread and 0.20 for zero tread. At 40 m/s it was 0.48 for 8 mm, 0.22 for 4 mm and only 0.05 for zero tread. Evidently at higher speeds much of the tire is resting on the water.

Because the part of the footprint that contacts the road is the rear part of the usual contact area, this is equivalent to a short footprint tire with a large mechanical trail (large caster angle). The behavior is therefore quite unlike a low-friction ice surface. The large total trail means that aligning torques stay high so the driver does not receive the same warning through the steering as on a low-friction surface.

The relative values of track front and rear can affect handling in wet conditions. If the tracks are equal, when running straight, the rear tire has the benefit of a partially cleared surface. Once rounding a corner, the front-to-rear alignment changes; at an attitude angle of 6° on a large radius the off-tracking is about 300 mm, moving the rear tires onto an uncleared surface. With narrower rear track, as on some vehicles, the rear tires will run on the cleared surface at some particular lateral acceleration depending on the tire cornering stiffness.

The gross area within the contact patch periphery is A_{CP}. The pattern of the tread reduces this to the net area A_{TP}. The tread pattern area coefficient is

$$C_{TP} = \frac{A_{TP}}{A_{CP}}$$

One investigation of how the maximum cornering force coefficient varied with speed for two tread designs of pattern area coefficient 60% and 80% (i.e., pattern void area 40% and 20%, respectively) on a low-macrotexture surface, where the road contributes little drainage beneath the footprint, gave for speeds up to 35 m/s:

$$\mu_C = 0.62 - 0.013V \quad \text{(for 80\% solid)}$$
$$\mu_C = 0.50 - 0.005V \quad \text{(for 60\% solid)}$$

At low speed, gross drainage is easily achieved and the higher-solidity tread, offering more rubber area to the ground, achieves a higher maximum coefficient, as for dry conditions. However, the low-solidity tread provides better drainage, so it deteriorates more slowly with speed. Hence there is a performance crossover, in this case at 15 m/s. The linearity suggests that the fraction of the footprint supported by the water is proportional to speed. This is compatible with the notion that drainage rate is more or less a constant, or that, for a given tread and water depth, a fixed time is required for a tread element to make effective contact. The corresponding times calculated for the above equations are 4 ms and 2 ms. The same tires on a good drainage surface exhibited time factors of about 1.6 ms and 0.8 ms. Evidently the road surface drainage can play as great a part as the tread itself, although a good tread is still helpful even on a good surface.

For a freely rolling tire, the time that a point on the tire is in the footprint is l/V where l is the footprint length. Representing the effective clearance time constant by τ, we can define a viscous hydroplaning number

$$N_{VH} = \frac{\tau}{l/V} = \frac{\tau V}{l}$$

which indicates the fraction of the footprint that is effectively supported off the ground. Full viscous aquaplaning would occur for $N_V = 1.0$.

Figure 2.19.1 shows how the maximum cornering coefficient varied with speed at 6 mm water depth in one investigation. Depending on detailed conditions of tire and road, the linear relationship arising from viscous resistance to flow breaks down as a transition occurs to full dynamic hydroplaning, caused by inertial (dynamic pressure) effects, at 22 m/s in this case. Even in the absence of inertial hydroplaning, full separation would still occur eventually due to viscous effects. Inertial (dynamic) hydroplaning occurs when the tire is fully supported by the dynamic pressure of oncoming water. Defining a dynamic hydroplaning number

$$N_{DH} = \frac{\frac{1}{2}\rho_W V^2}{p_i}$$

where ρ_W is the water density and p_i is the tire inflation pressure, then full dynamic flotation occurs at typically $N_D \approx 1.5$.

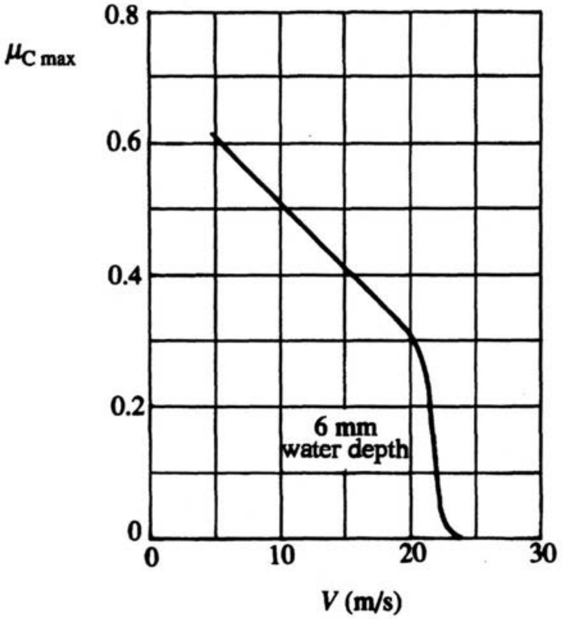

Figure 2.19.1 Maximum cornering force.

Different tread rubbers have different frictional–speed dependence in wet conditions. At low speeds the normal friction coefficient effects are dominant. However, at high speed, elastohydrodynamic lubrication effects discriminate against a soft tread surface, so the rather soft butyl rubber deteriorates more rapidly with speed than most. The performance of a blended compound is not merely an average of its constituents, so in fact butyl rubber can still play a useful role in tire blends that must perform well in wet conditions.

Moderate water depth affects maximum cornering force rather than cornering stiffness. In one investigation with 1 mm of water, the very small angle cornering stiffness was independent of speed, but the maximum cornering force coefficient was 0.7 at 10 m/s, 0.5 at 20 m/s and 0.25 at 30 m/s, the optimum slip angles being 7°, 5° and 1.5°, respectively.

The slight increase of cornering stiffness with speed for a dry or damp surface becomes a very marked reduction with speed when the water is deep. For example, in one investigation, at 10 m/s there was little effect, but at 20 m/s a 2 mm depth of water reduced the cornering stiffness by 20%, 5 mm by 45% and 10 mm by 70%. At the speed of full hydroplaning, the cornering stiffness goes to zero. Water depth typically affects traction and cornering friction in an equal way.

The presence of a layer of water can considerably increase the effective rolling resistance. Considering a tire width *w* and water depth *d*, at velocity *V* the momentum flux of the water approaching the tire is

$$\begin{aligned}\dot{M} &= \dot{m}V \\ &= \rho w d V^2\end{aligned}$$

In a similar manner to the force exerted on a Pelton wheel bucket, this can exert a force on the wheel, according to the exit angle. Considering a width of 100 mm, a water depth of 5 mm and a speed of 30 m/s, the momentum flux is 450 N, compared with a dry rolling resistance of around 60 N.

2.20 Tire Models

For handling analysis, it is necessary to represent the tire characteristics in some way. It is not practical to calculate the properties from the basic tire constructional data, and finite element models are too computationally intensive. Therefore the representation is achieved by:

(1) Interpolation of a data table

(2) Empirical equations

Use of a data table is reasonably straightforward, but there is a problem with creating the table because a fully comprehensive set of data is rarely, if ever, available. Hence some of the table values may need to be generated by empirical equations fitted to the available data.

In the case of direct use of empirical equations, the form of the equations is in general accord with the character of tires, and a series of parameter values is used to represent any particular tire.

Examples of such parameters would be a reference vertical force, cornering stiffness in reference conditions, maximum cornering force at reference vertical force, etc. There will also be variational parameters to show how the prime parameters vary, e.g., the load sensitivity of maximum cornering force, load sensitivity of cornering stiffness, etc. This chapter has considered the behavior of tires largely in terms of simple empirical equations using such parameters, which are comprehensible in the sense that any particular parameter has a definite physical meaning. Another advantage of this approach is that the model is applicable not just to computer analysis, but also to direct analytical work that can provide great insight into vehicle behavior. An example of this is the parameter p representing the variation of tire maximum cornering force coefficient with vertical force, which can be used to great effect in analysis of limit handling.

In an alternative approach, empirical equations are used, but no real attempt is made to maintain a direct relationship between particular parameters and particular physical effects. Such an approach is unsuitable for analytic work or for direct human understanding, but is acceptable for computer work. The Bakker-Nyborg-Pacejka model is of this type, and produces realistic tire behavior that generally fits data well; so well in the original paper that it was given the unfortunate name of the "Magic Formula." The BNP model has been used quite widely for numerical work.

2.21 Tire Transients

If a step change is made to the slip angle of a rolling tire, the new steady-state value of cornering force is not developed immediately, but in an exponential manner which depends on the distance x rolled, i.e., the lateral force deficit from the final value decays exponentially. The relaxation distance of rolling, l, is the distance required to give $1-1/e$ (= 0.632) of the response change.

$$\frac{F}{F_\infty}=1-e^{-x/l}$$

The length l has a value of approximately one tire radius. It is not very sensitive to load, and tends to decrease with increasing inflation pressure. A useful rule of thumb for assurance of approximate equilibrium conditions is a roll distance of one revolution.

If the slip angle is oscillated sinusoidally, then the amplitude of the force developed depends on the distance traveled per cycle. For a small distance per cycle, the lateral force amplitude tends to zero; for a long distance it tends to the steady-state value. The force has a phase lag of 90° at high frequency, zero at low frequency. This can be analyzed using the relaxation distance concept given above.

During a ramp input of steering angle, passing through zero slip angle, the lateral force will not be zero at the time when the slip angle is zero. For a ramp steer gradient of a (deg/s), speed V and relaxation length l, the spatial steer gradient is

a/V deg/m, and the angle lag will be al/V deg. The force lag will be $C_\alpha al/V$ newtons. For most practical cases these are small effects, although they may be significant during severe evasion maneuvers when the steer input may be 500 deg/s or more. To consider it another way, at any speed, neglect of the tire transient can be expected to introduce a longitudinal path error of size equal to the relaxation length.

Subjective evaluation of handling behavior suggests that tire transients may be more important in influencing the perceived vehicle behavior than would be expected from the vehicle dynamic analysis.

Analysis of the effect of road roughness requires consideration of transient effects. Obviously the relaxation length is important in smoothing out the effect of road irregularities on cornering forces. On the other hand, a tire making irregular road contact would relax rather rapidly when off the road, but then recover its proper lateral force generating shape only over the normal relaxation length, resulting in a reduced average cornering force. A larger tire of lower inflation pressure often exhibits better cornering ability on knobbly surfaces, owing to improved ground contact.

2.22 Problems

Q 2.2.1 Describe the differences between radial-ply and bias-ply tire constructions.

Q 2.2.2 Summarize the difference in handling characteristics between radial-ply and bias-ply tire constructions.

Q 2.2.3 Describe the features of a typical tread pattern, and explain their function.

Q 2.3.1 Describe how the visco-elastic properties of rubber may explain the friction of rubber on a lubricated but rough surface.

Q 2.4.1 Define wheel angular position and related terms, and all the wheel forces and moments, giving appropriate diagrams.

Q 2.5.1 Define and describe the various kinds of wheel radius.

Q 2.5.2 Explain the meaning of the "vertical stiffness" of a tire. To what extent is this a justifiable model of the tire vertical characteristic? What parameters affect this stiffness?

Q 2.5.3 Considering a thin-walled toroidal tire, whose stiffness is the result only of the contact patch area and inflation pressure, find an expression for the vertical force as a function of the deflection, the unloaded radius and section radius. Obtain an algebraic expression for the stiffness for small deflections.

Q 2.5.4 Considering a thin-walled cylindrical (racing) tire otherwise as for Q 2.5.3, analyze the vertical force. Draw graphs of vertical force and vertical stiffness against deflection.

Q 2.5.5 At speed, the tire vertical force at a given deflection increases because of the impact of the perimeter against the road at the front of the contact patch. This can be important on cars with underbody venturis because it tends to increase the ground clearance, or at least offsets the reduction of ground clearance with aerodynamic downforce as speed increases. Because it gives a vertical force toward the front of the contact patch where it can increase friction, it also contributes to the negative aligning moment at high slip angles.

(1) Obtain an expression for the impact force for the simple case of a cylindrical (racing) tire, in terms of the peripheral mass, the unloaded radius, the wheel spin speed and the impact angle θ equal to half of the angle subtended by the contact patch.

(2) Use the intersecting chords theorem to show that the tire deflection is approximately $l^2/8R_\mathrm{u}$.

(3) Obtain an approximate expression for the impact force in terms of the vertical deflection, as a function of vehicle speed (with no wheel slip).

Q 2.5.6 A racing car tire has a peripheral mass of 2.0 kg, a radius of 0.340 m, and footprint length 0.170 m. Calculate the vertical impact force at the front edge of the contact patch at a vehicle speed of 80 m/s, with negligible wheel slip.

Q 2.6.1 Describe the formation of waves in a tire perimeter at high speed, including a sketch. Give relevant equations, and explain the Turner number.

Q 2.6.2 Modeling the tire as a crown only, neglecting side walls, obtain an equation relating crown tension per unit width to the radius, peripheral speed, crown density per unit area, and inflation pressure (analyze a small segment of length $R\theta$). Investigate realistic values. Neglecting pressure, evaluate the Turner number.

Q 2.6.3 Consider an isolated tread element of height h (8 mm), area A, and density ρ (1300 kg/m^3). Obtain an expression for the base tension from centrifugal stress. Calculate the stress for $R = 0.3$ m at 50 m/s.

Q 2.7.1 Explain the different ways of representing rolling resistance on a wheel free-body diagram.

Q 2.7.2 Explain how the rolling resistance of a tire arises.

Q 2.7.3 A vehicle has wheels with a mean rolling resistance coefficient of 0.021. On what angle of slope will it just move?

Q 2.8.1 Describe briefly the differences between the foundation stiffness, string and beam models of the tire.

Q 2.9.1 Define and explain the difference between cornering force, cornering force coefficient, cornering stiffness, cornering stiffness coefficient, maximum cornering force, and maximum cornering force coefficient. Why is cornering power a bad name?

Q 2.9.2 Explain the difference between tire force, lateral force, cornering force, camber force, tractive force, central force, drag force, and longitudinal force. Draw appropriate figures.

Q 2.9.3 A simple foundation stiffness tire model has the following parameters: contact patch length 200 mm, vertical force 4.8 kN, friction coefficient 1.2, foundation stiffness 2.8 MPa. Calculate:

(1) The slide-free maximum slip and slip angle.

(2) The cornering stiffness.

(3) The cornering stiffness coefficient.

(4) The slide-free maximum force.

(5) The lateral force at 5° slip angle.

(6) The maximum lateral force.

Q 2.9.4 Draw a polar diagram of tire cornering force against slip angle. Show the central and drag components for a typical cornering force. Show the maximum central force.

Q 2.9.5 Plot a graph of central/drag force ratio including rolling resistance, for $\mu_R = 0$, 0.015 and 0.030, for a cornering stiffness coefficient of 0.16/deg.

Q 2.10.1 Discuss the relative merits of non-dimensionalizing tire lateral forces (1) by dividing by F_V, (2) by dividing by $F_{Y\max}$.

Q 2.10.2 Explain non-dimensionalization of tire forces (1) for the force, (2) for the slip angle. Draw example graphs.

Q 2.11.1 At approximately what sliding speed is typical tire friction halved from its low-speed value?

Q 2.12.1 Explain the difference between lateral force, cornering force and camber force.

Q 2.12.2 Explain how tire camber forces arise, giving example values of camber stiffness and coefficients.

Q 2.12.3 A mad inventor has devised a scheme for perpetual motion of his car. It weighs 12 kN, equally distributed. The tires all have camber stiffness coefficient 0.016/deg and cornering stiffness coefficient 0.16/deg. He plans to set all the wheels at 20° positive camber to generate camber forces, and at 1° toe-in, to point the camber forces slightly forward to drive the car along. Give a calculation of the effect of this arrangement, supporting his view, and discuss it in relation to the principle of conservation of energy.

Q 2.12.4 Explain the path curvature stiffness of a tire and how it may be related to C_γ.

Q 2.13.1 Describe the various possible types of tire force testing methods, and discuss their relative merits.

Q 2.14.1 Describe and explain typical tire conditioning effects.

Q 2.14.2 Describe and explain the influence of production tolerances on tire handling parameters.

Q 2.14.3 At a reference load of 3 kN a tire has a cornering stiffness coefficient of 0.160/deg. Estimate the cornering stiffness coefficient and cornering stiffness at a vertical load of 3.3 kN.

Q 2.14.4 A tire has a speed sensitivity of 8%, and a cornering stiffness of 700 N/deg at 5 m/s, found by testing. Estimate the cornering stiffness at 40 m/s.

Q 2.14.5 Give equations for three models of the load sensitivity of tire cornering stiffness coefficient, and show how the various load sensitivity parameters are related for small load changes.

Q 2.14.6 The cornering characteristics of a tire are to be modeled by an exponential cornering stiffness coefficient with $C_{\alpha 1} = 820$ N/deg at $F_{V1} = 4000$ N, and $k_1 = 0.74$. Evaluate (1) C_{S1}, and (2) C_{S0} (at $F_V = 0$). Draw graphs of C_S and C_α versus F_V, for F_V taking values from zero to 10 kN.

Q 2.14.7 For the tire model of the last question, determine analytically (1) F_V for $C_{\alpha\max}$, (2) $C_{\alpha\max}$.

Q 2.14.8 Describe the exponential decay model of tire cornering stiffness coefficient variation with vertical force. Give equations, and develop expressions for any significant values of C_S or C_α.

Q 2.14.9 A tire is found to have a maximum cornering stiffness $C_{\alpha 2}$ of 1195 N/deg at a vertical force F_{V2} of 4780 N. It is to be used at a standard load F_{V1} of 2868 N. Calculate (1) the cornering stiffness coefficient C_{S2}, (2) the load sensitivity, (3) the cornering stiffness coefficient C_{S1}, (4) the cornering stiffness $C_{\alpha 1}$, according to the exponential cornering stiffness coefficient model.

Q 2.14.10 Using the exponential cornering stiffness coefficient model, a tire has a standard vertical force of 3800 N, a load sensitivity of 0.722, and a standard cornering stiffness of 810 N/deg. Calculate (1) the vertical load for maximum cornering stiffness, (2) the maximum cornering stiffness.

Q 2.14.11 For the exponential cornering stiffness coefficient model, obtain an algebraic expression for the ratio of the peak cornering stiffness to the standard value, in terms of the load sensitivity.

Q 2.14.12 Explain the load dependence of tire cornering force at small slip angles. Give appropriate equations and example values.

Q 2.16.1 Describe the effect of variation of vertical force on tire maximum lateral force coefficient.

Q 2.16.2 Describe the effect of lateral load transfer on the total cornering force generated by an axle at a given slip angle.

Q 2.16.3 Using the exponential model for variation of C_α with F_V, investigate the effect of lateral load transfer on the cornering coefficient of an axle.

Q 2.17.1 Describe the generation of longitudinal forces in the contact patch, according to the simple foundation stiffness model.

Q 2.18.1 Describe, and explain by reference to the simple foundation stiffness model, the interrelationship of lateral and longitudinal force.

Q 2.18.2 "A locked braking wheel will have a cornering force but no central force. A severely spinning driven wheel will have a central force but no cornering force." Discuss, with plan-view wheel force diagrams.

Q 2.19.1 Describe the role of the tread pattern in clearing water from beneath a tire.

Q 2.19.2 A tire takes 2 ms to clear the approaching water depth, and has a footprint length of 200 mm. At what speed will half of the footprint be supported by viscous hydroplaning?

Q 2.19.3 Describe and explain the process of hydroplaning.

Q 2.19.4 A vehicle has a wheelbase of 3 m, front track 1.7 m, and rear track 1.5 m. At what attitude angle and approximately what lateral acceleration will the rear outer wheel run on the same line as the outer front?

Q 2.21.1 Describe tire transients, and their influence on handling on smooth and knobbly surfaces.

Q 2.21.2 A tire has a distance constant of 0.25 m, and a cornering stiffness of 800 N/deg. When stationary it is set at a slip angle of 1.5°. Estimate the side force after it has rolled (1) 0.1 m, (2) 1 m.

Q 2.21.3 Using the rule of thumb that the tire relaxation distance is one radius, after a tire has rolled one revolution what is the fractional force deficit?

2.23 Bibliography

The information in this chapter has been gleaned from a large number of papers from the SAE, I.Mech.E. and various journals, too numerous to list usefully here. For elaboration of any particular points, SAE is the best single source of papers. For a general introduction to the tire, refer to Setright (1972), Shearer (1977), Tompkins (1981), Norbye (1982) and French (1989). None of these, however, considers lateral forces in detail.

Clark (1981) provides a massive compilation of tire theory and data in one volume, including innumerable references. See also Clark (1996). An interesting reference on the theory and data of rubber friction is Hays & Browne (1974). For a more extensive discussion of tire properties relevant to vehicle handling, see Moore (1975). A full definition of terms is provided in SAE J670e (1978) (see Appendix E). For non-dimensionalized experimental tire data refer to Radt & Milliken (1983). Sakai (1981) provides a detailed discussion of advanced tire models. Some 280 references, including many foreign language ones, are given in Frank & Hofferberth (1967).

SAE has a new standard in draft for tire terminology and axis systems (J2047) due in 1997.

3

Aerodynamics

3.1 Introduction

In most circumstances, the aerodynamic forces on a vehicle are much less than the tire forces. However, aerodynamic forces are always important at high speed, and it is essential to consider this at the design stage. For racing cars, of course, aerodynamic forces are of major importance.

Analysis of the response of a vehicle to aerodynamic effects may be considered in two parts:

(1) Determining the forces acting on the vehicle

(2) Finding the response of the vehicle to those forces

This chapter considers the determination of the forces, and therefore gives information on the atmosphere and some related topics. The consequences of the forces are dealt with in Chapters 6 and 7. Drag is a major factor in the fuel economy of a vehicle, although the influence of aerodynamics is in general secondary to that of the tires as far as handling and stability are concerned.

Atmospheric properties may influence the handling of a vehicle in various ways. First, they affect the aerodynamic forces on the vehicle. This depends primarily on the density of the air, but also in principle on the Reynolds number and the Mach number, and hence also on the viscosity and the speed of sound. Engine power is also affected. The tire–road interface is affected by dampness or depth of free water depending on the rate of rainfall, or by snowfall or ice if the temperature is low. Ambient air temperature and solar radiation can affect the tire–road friction. The vehicle is also affected by existing motions of the atmosphere. The worst cases of wind effects are usually where a vehicle passes from a sheltered region into a strong side wind, i.e., where there is a spatial variation of side wind. Another common problem is the disturbance caused by other vehicles, especially large ones on motorways.

The genesis of aerodynamic forces on the vehicle is described in this chapter, and examples are given for the various force and moment coefficients. Finally, an overview is given of the development of aerodynamics in competition, where it has become a major factor because of the great advantages of downforce in enhancing the forces at the tires.

3.2 Atmospheric Properties

It is desirable to specify a standard set of atmospheric conditions so that different studies are made on a comparable basis. On the other hand, the influence of variations of the real atmosphere from the standard should be recognized. Many standard atmospheres have been proposed, including the International Standard Atmosphere, the ISO Standard Reference Atmosphere, the ICAO atmosphere, the U.S. Standards (NASA, USAF, USN, etc.), ASME, NIST, SAE Engine Testing, and so on. The ISO Standard Reference Atmosphere is somewhat unusual in specifying a 65% relative humidity, where all the others specify dry air, i.e., no water vapor whatsoever. Table 3.2.1 gives a representative specification for sea level..

The provision of such accurate standard values, for example a density to five significant figures, is in a sense misleading because there are considerable variations in the real atmospheric properties arising from variation of pressure, temperature and humidity. The properties are not significantly influenced by changes of the proportions of dry constituents within the altitude range of roads, up to 5000 m. Appendix B gives more detailed information, including variations with temperature.

The presence of the small amount of water vapor in the real atmosphere has a considerable effect on weather patterns because of the large latent heat of vaporization of water (see Table 3.2.2). There is a small effect on density because the molecular weight of water is only 18, which displaces dry air of molecular weight about 29. The density corrections, although small, are nevertheless made in wind-tunnel testing. The absolute humidity is the water content of the air expressed as a density, i.e., as kg/m^3. The water content is normally expressed as the relative humidity, which is the absolute humidity divided by the maximum amount of water that the air can carry in uniform mixture, i.e., without condensation, at that temperature. This maximum varies rapidly with temperature, which is why cooling often leads to condensation, i.e., fog or rain, the relative humidity rising to 100% or more at constant absolute humidity. At 15°C and 100% relative humidity the absolute humidity is 0.0128 kg/m^3. Thus a typical 65% relative humidity corresponds to 0.0083 kg/m^3, or about 0.7% of the total air mass. In the British Isles, humidity is usually 40 to 95%. Over the continental U.S., the variation is extremely wide, according to local conditions.

Table 3.2.1. Standard Properties of Dry Air at Sea-Level, 15°C.

Constituents by mass:	Nitrogen	(N_2)	0.7553
	Oxygen	(O_2)	0.2314
	Argon	(Ar)	0.0128
	Carbon dioxide	(CO_2)	0.0005
Temperature	T_C	15	°C
	T_K	288.15	K
Pressure (absolute)	P	101325	Pa
Density	ρ	1.2256	kg/m^3
Dynamic viscosity	μ	17.83×10^{-6}	Ns/m^2
Kinematic viscosity	ν	14.55×10^{-6}	m^2/s
Molar mass	m_m	28.965	kg/kmol
Specific gas constant	R_A	287.05	J/kg K
Specific heats	c_p	1005	J/kg K
	c_v	718	J/kg K
Ratio of specific heats	γ	1.400	
Thermal conductivity	k	0.02534	W/m K
Speed of sound	V_s	340.6	m/s

Table 3.2.2. Properties of Water Substance

Compound H_2O			
Constituents by mass:	Hydrogen		0.0119
	Oxygen (O_2)		0.8881
Freezing point	T_F	0.0	°C
Boiling point (1 Ata pressure)	T_B	100.0	°C
Density of ice at 0°C	ρ	0.917	kg/m^3
Density of water at 4°C	ρ	1000.0	kg/m^3
Density of water at 15°C	ρ	999.2	kg/m^3
Density of water at 30°C	ρ	995.7	kg/m^3
Dynamic viscosity at 15°C	μ	1.139	mNs/m^2
Kinematic viscosity at 15°C	ν	1.140	mm^2/s
Molar mass	m_m	18.015	kg/kmol
Specific gas constant	R_W	461.51	J/kg K
Specific thermal capacity (at 50°C)	c_p	4178	J/kg K
Thermal conductivity of water (50°C)	k	0.643	W/m K
(Latent) Energy of melting	h_{sf}	333	kJ/kg
(Latent) Energy of boiling (100°C)	h_{fg}	2257	kJ/kg
Thermal conductivity of ice	k	2.2	W/m K
Specific thermal capacity of ice	c_p	2090	J/kg K

Even in temperate climates at low altitude, there are substantial variations in temperature and pressure, and hence in density. Dry air, considered as an ideal gas, obeys the perfect gas equation

$$P = R_A \rho T_K$$

where $R_A = 287.05$ J/kg K is the specific gas constant for air, ρ is the density and T_K is the absolute (kelvin) temperature. Thus the density is proportional to the pressure and inversely proportional to the absolute temperature. The ambient pressure varies typically ±3 kPa from the mean, i.e., by about 3%. The ambient temperature varies by typically 15 K from the mean, 5% of the absolute temperature. Thus at sea level the density can vary by 8% or more from the mean, with more variation with altitude, and with temperature range variations with geographical location. The standard conditions should be seen in this light. These variations are, of course, one of the reasons for the different atmospheric standards in different countries. The extremes of recorded pressure are 87.6 to 108.4 kPa for the world, and 92.6 to 105.5 kPa for the British Isles. The recorded temperature extremes for the British Isles are –27°C to +37°C in the shade, and, again, even wider for the U.S.

Appendix B gives an accurate method for calculation of density and other properties. Where a more approximate value of density will suffice, as is normally the case in the dynamics of handling, then it is usual to neglect the water vapor content and to treat the air as a simple ideal gas, giving, in SI units,

$$\rho = \frac{P}{R_A T_K}$$

Within the ambient temperature range the dynamic viscosity is often taken as having a constant value, for example $\mu = 17.8 \times 10^{-6}$ Ns/m², and the speed of sound, if required, is often taken as constant at $V_s = 340$ m/s.

The typical variation of atmospheric properties with altitude is recognized directly in the aeronautical standards by specifying the temperature variation with height, which when combined with a value for the gravitational field g allows the properties to be calculated. In the troposphere (below 11 km) the standard temperature declines with altitude at the temperature lapse rate $r = 6.5$ K/km, from a standard sea level temperature $T_0 = 15$°C, giving

$$T_C = T_0 - rz$$

This results in a density relative to sea level of

$$\frac{\rho}{\rho_0} = \left(1 - \frac{z}{z_0}\right)^n$$

where z is the altitude and z_0 is a constant of value 44,300 m. The exponent n has the value

$$n = \left(\frac{g}{rR_A} - 1\right) = 4.256$$

Thus at 1500 m (about 5000 ft), which is a typical operating height in some parts of the world, the density is reduced by 14%. If this occurs in the tropics then the density will be even lower because of high temperature.

The standard recommended by SAE J670e (in Appendix E) is dry air of density 1.226 kg/m^3 (2378 × 10^{-6} slug/ft^3), pressure 101 kPa (29.92 in Hg) at 15°C (59°F), with a viscosity of 17.9 × 10^{-6} Ns/m^2 (373 × 10^{-9} slug/ft s).

Water is of relevance in several respects (see Table 3.2.2; see also Appendix B). The main influence of rain is to give a layer of water on the road, depending on road camber and the quality of drainage. Drop sizes and terminal speeds for drizzle are 0.05 to 0.5 mm diameter at 0.7 to 2.0 m/s, and for rain 0.5 to 2.5 mm diameter at 3.9 to 9.1 m/s. The intensity of rain, as coverage, is less than 0.5 mm/h for light rain, 0.5 to 4 mm/h for moderate rain, and over 4 mm/h for heavy rain. A coverage of 10 mm/h is 10 kg/m^{2}h, or about 3 g/m^{2}s. With a terminal speed of 8 m/s, the rain density is then 0.4 g/m^3, increasing the mean density of the atmosphere by only about 0.03%. Because of the arrangements for drainage, the depth of water on a road is mainly a function of the rainfall rate.

In contrast, because snow is not drained until it melts, the depth of snow is a cumulative effect and can therefore be a particular problem, not least because in some countries there are floods when it melts. There are various types of snow. On continental land masses far from the sea, dry snow is common, of density 100 kg/m^3. This has small powdery crystals that do not easily bond under pressure and can be cleared by blowers. For the maritime borders of continents in latitudes 40° to 60°, wet snow is most common, with density up to 300 kg/m^3, for which the crystals are bonded into flakes which easily stick together. This must be cleared by plow or shovel. In snow or ice conditions, of course, special tires, sometimes with chains or studs, may be used.

3.3 Wind and Turbulence

A vehicle moves in a non-stationary mass of air. Although time-stepping computer simulations can deal with the complex situation of a cornering vehicle in a turbulent windy air, investigations of the effect of air movement are mainly related to the straight running condition. This is because vehicles are most critically sensitive to wind disturbance when running at high speed, for example on a motorway, when a small angular deflection of the path can quickly lead to a collision.

Movements of the atmosphere can best be considered in two parts. More than about 600 m above the surface is the geostrophic wind. Below 600 m is the atmospheric boundary layer, in which air movements are driven by the geostrophic wind but reduced by the friction of the land or sea surface. The geostrophic wind arises from non-uniform heating of the air, which gives the pressure differences that result in the wind. The geostrophic wind in any particular region is a combination of two contributions. The first is the regular global wind pattern; for example, Great Britain is in the "Westerlies" of the temperate zone, with regular southwesterly winds. In addition there are cyclones and anti-cyclones, familiar from the weather reports, which introduce a low-frequency (i.e., period of about four days), more or less random fluctuation to the wind at any point. The total of these two effects is the geostrophic wind.

The speed in the atmospheric boundary layer varies from zero at the ground to the full geostrophic value at the top. Except for very slow winds, less than about 5 m/s at 10 m height, the boundary layer flow is turbulent, giving random speed fluctuations, the period of which is typically a few seconds but which can be as slow as five minutes. Thus it is convenient to refer to a sustained wind speed averaged over some period between ten minutes and an hour, which is free of the turbulent fluctuations. In engineering applications the sustained wind is represented as a function of height by a power model

$$\frac{U}{U_{\mathrm{r}}} = \left(\frac{h}{h_{\mathrm{r}}}\right)^{a}$$

where U_{r} is the speed at a reference height h_{r}. The standard reference height is 10 m, and this is often referred to, perhaps illogically, as the ground level wind. The exponent a varies according to the effective friction of the surface, being typically 0.1 for sea or for land flats, 0.15 for open terrain, 0.25 for suburban conditions, and 0.35 for a city center. Thus a car, with a characteristic height of about 1 m, is in a strongly shearing wind distribution, the air speed increasing rapidly with height from zero at ground level.

The likelihood of a given wind speed being exceeded is usually calculated from a Weibull equation. The fraction of the time that the wind speed U will exceed V is given by the long-term probability

$$P_{U>V} = \exp\left[-(V/V_{ch})^{\beta}\right]$$

where V_{ch} is the characteristic wind speed, which is typically 3 to 5 m/s for normal land sites at 10 m height, and β is the wind shape factor, typically 2 and normally in the range 1.5 to 2.5. The relationship between V_{ch} and V_{mean} varies with β, but for $\beta = 2$, $V_{ch} = 1.128\ V_{mean}$. For exposed sites, for example high bridges, the characteristic speed will be high, giving a correspondingly high probability of winds that are sufficient to disallow certain types of vehicle from using the road because of handling problems or the danger of overturning. For a typical inland site, with a characteristic speed of 4 m/s and shape factor of 2, the probability of exceeding 12 m/s is only 0.012%, and hence wind speeds are usually much less than road vehicle speeds.

The actual instantaneous speed, measured with fast-response instruments, is found to vary erratically about the sustained speed; i.e., the actual instantaneous speed is the sustained speed U plus a random turbulent component V. These random fluctuations have a period of typically a few seconds. The probability distribution of the instantaneous speed about the sustained speed is found to be well modeled by a Gaussian distribution, which is characterized by the turbulent speed deviation W (Figure 3.3.1). The instantaneous speed is within W of the sustained speed U for 68.3% of the time, within $2W$ for 95.5%, and within $3W$ for 99.7%.

The turbulence of an airflow is usually specified by the turbulent intensity, which is the ratio of the statistical deviation of the turbulent speed, W, to the sustained speed V_S:

$$I = W/V_S$$

Considering the flow relative to a moving car instead of relative to the ground, the relative sustained speed will be different but the turbulent deviation W will be the same. We are considering here the properties of the natural atmospheric turbulence, not the turbulence created by the car. Because of this change of relative sustained speed, the turbulent intensity depends on the coordinate system in which the flow is observed, for example relative to the car or ground, although the actual turbulent fluctuations are of the same value. The typical turbulent

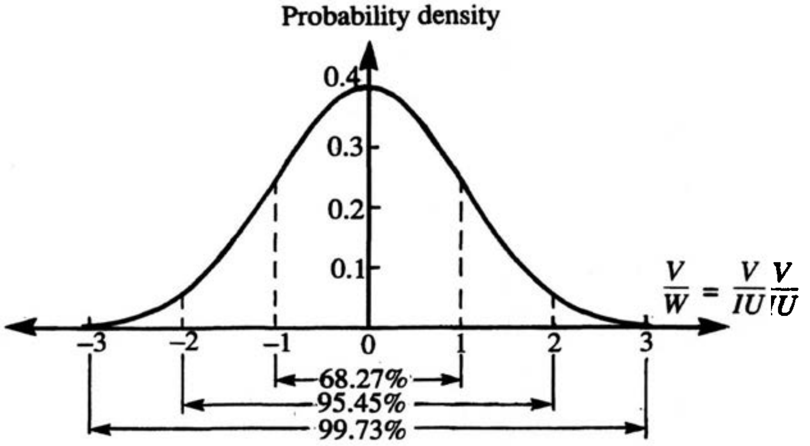

Figure 3.3.1. Probability distribution of the speed deviations of a turbulent wind.

intensity of the wind, measured relative to the ground, is about 20%, varying somewhat with height and tending to be smaller at sites where the speed–height exponent is smaller. Relative to the moving car, the typical turbulent intensity is usually less because of the car speed; e.g., in a wind of 10 m/s with $I = 0.20$, the turbulent deviation is 2 m/s, so relative to a car moving at 30 m/s directly into the wind the turbulent intensity is only $2/(30 + 10) = 0.05$. Modern wind tunnels tend to have extremely low levels of turbulent intensity, e.g., 0.1% or less. In some cases special facilities are provided to generate turbulence, for example by air jets directed radially inward.

The typical state of the atmospheric boundary layer, when the wind speed is high enough to be of significance, is a turbulent one, so the vehicle is in a turbulent, shearing flow. There is also likely to be additional turbulence caused by vortex shedding or trailing vortices from other vehicles, or from obstructions to the wind at the roadside. These are all variations of speed at a given point, i.e., unsteady flows.

Another effect that can have a major influence on a vehicle is the spatial variation of speed because of steady flow patterns as the wind passes around objects at the roadside. The most familiar example of this is when a vehicle emerges from a sheltered region, such as a row of houses, into a strong side wind. This kind of flow is difficult to predict analytically and is usually studied in wind tunnels. The response of vehicles can be investigated by specifying a side wind distribution for the vehicle to pass through, either in theory or in a wind tunnel or in a full-size test. The side wind distributions are typically either a sharp step change, a ramp step change, or a sinusoidal step change.

One classic problem for cars is disturbance when passing, or being passed by, large vehicles at speed, for example on a motorway. In this case the car is subject to an airflow that varies systematically in both space and time.

3.4 Principles

The handling response of a vehicle to aerodynamic influences involves determination of the force acting on the vehicle, and finding the response of the vehicle to that force. The first of these will be introduced in this chapter.

The aerodynamic influences on ordinary vehicles as far as handling is concerned are generally secondary to the tire forces. This is fortunate because accurate determination of the aerodynamic forces in any particular case is rather difficult because the forces are sensitive to detailed changes in body shape. To date, theory is rather limited in its ability to predict the forces from first principles; however, theory is essential in interpreting and using the results of the extensive wind-tunnel tests that are required to assess the aerodynamic properties of a vehicle.

The aerodynamics of a ground vehicle are fundamentally different from those of an aircraft in flight for a variety of reasons, including:

(1) There are severe practicality constraints.

(2) A ground vehicle is a bluff body.

(3) The flow around a ground vehicle separates.

(4) Ground proximity has to be taken into account.

(5) The presence of wheels has to be taken into account.

These factors are of course interrelated. The practicality constraints disallow a long streamlined tail which means that the body is a bluff one, with separating flow, for which the drag is largely the consequence of trailing vortices and shed vortices. In contrast, an aircraft is basically streamlined with a substantial skin drag, some form drag and trailing vortex drag, but relatively little flow separation. The aerodynamic forces on an aircraft with its attached flow are more amenable to theoretical analysis than those on a ground vehicle with its largely separated flow. The presence of the ground is an additional complexity, encountered by aircraft only at take-off and landing. Thus the very extensive knowledge of aircraft aerodynamics has only limited application to ground vehicle aerodynamics, which forms a separate subject in its own right.

The aerodynamic forces are found to depend primarily on the vehicle size, the vehicle shape, the vehicle attitude to the airstream, the air density, and the square of the relative air speed. The influence of size is such that the forces are proportional to areas, because the other factors combine to give resulting pressures at the vehicle surface. Hence the total forces are usually expressed in terms of force coefficients:

$$F = qCA$$

where

$$q = \tfrac{1}{2}\rho V^2$$

is the dynamic air pressure, F is the force magnitude, C is the force coefficient, and A is the reference area. Different force magnitudes will result from a given coefficient value if different reference areas are used, so it is essential to specify the reference area in each case. In ground vehicle aerodynamics, it is most common to use the total vehicle frontal area, i.e., the area inside the vehicle front profile. Alternatively, the product CA is used, for example the drag area

$$A_D = C_D A \quad [\mathrm{m}^2]$$

Sometimes a reference area of one square metre is used, which gives a drag coefficient numerically equal to the drag area:

$$C_{D1} = \frac{A_D}{1\ \mathrm{m}^2}$$

which is dimensionless.

The frontal area will be used as the reference area here except where some other area is declared in some special cases. When modifications to a vehicle are being tested, the frontal area may be changed by the modifications; in such cases the usual policy is to relate all the coefficients to the frontal area of the baseline vehicle; otherwise comparison of the coefficients is not meaningful.

The great utility of force coefficients is that they remain approximately constant with variations of speed and size and of fluid density, provided that the vehicle shape and attitude are the same. This allows wind-tunnel tests to be made on a smaller vehicle, often quarter size, to find the coefficients which then predict the real vehicle forces. However, the coefficients are not truly constant unless the Reynolds numbers (Re) and Mach numbers (Ma) of the flows are the same for the two cases, where

$$\mathrm{Re} = \frac{\rho V x}{\mu}$$

$$\mathrm{Ma} = \frac{V}{V_\mathrm{s}}$$

The parameter x is some vehicle characteristic dimension, μ is the fluid dynamic viscosity, ρ is the density and V_s is the speed of sound. In practice, unless a full-scale test is performed then the Reynolds numbers and the Mach numbers are not both correct. Also, of course, the force coefficients are used for a range of speeds of the real vehicle and so over a range of Reynolds and Mach numbers.

The problem is usually dealt with in the following way. First, model test Reynolds numbers are generally smaller than real because the model is small, so if possible the test speed is increased to compensate. This makes the Mach number too high, but in practice this is less important for normal vehicles. Corrections may be applied for Mach number. For a typical wing, the lift force coefficient is influenced by the Mach number Ma, according to Prandtl's correction, by

$$\frac{C'}{C} = \frac{1}{\sqrt{\left(1 - \mathrm{Ma}^2\right)}}$$

Thus, relative to Ma = 0, there is a 1% correction at Ma = 0.14, which is a speed of 48 m/s (107 mph). Thus Mach corrections are negligible in ordinary road vehicle use but may be significant in the wind tunnel, or for racing cars, which may reach 100 m/s in some cases. For transonic conditions, as experienced by land speed record vehicles, this method of correction is no longer appropriate. The forces are then highly sensitive to Mach number, and the best that can be done is for wind-tunnel testing to be performed at the correct Mach number with Reynolds number playing a secondary role, possibly with roughness strips to induce transition in the boundary layer at the required position.

The influence of variation of Reynolds number on force coefficients is potentially complex, but fortunately the effect is usually small. Basically the Reynolds number indicates the relative significance of the viscous and inertial forces in the fluid, and indicates the state of the boundary layer, which in turn controls any separation of the flow. Thus where flow separation is well located by sharp edges, Reynolds number will have little effect. Where separation occurs from a curved surface, the separation point, and hence force coefficients, may change significantly with Reynolds number. If the flow is fully attached, for example as on a wing at low incidence, then the Reynolds number usually has a progressive effect because of change in the boundary layer thickness. In practice for a typical car, an increase of flow speed and hence of Reynolds number in the usual range of operating conditions can sometimes give a sudden change of flow pattern with a step change of force coefficients of perhaps 10%.

In studying the response of a vehicle to gusts it may be necessary to consider the vehicle to be subject to a non-uniform wind, for example a side wind that varies along the length of the car. In most cases, however, it is adequate to consider the vehicle to be in a uniform wind.

The ambient wind is measured by the magnitude and direction of the bulk air velocity relative to the ground, i.e., measured in the Earth-fixed axes *XYZ*. Because of the atmospheric boundary layer, this varies with height. Vertical components are normally neglected. Following SAE terminology, the magnitude of the ambient wind speed is v_a. (Speeds are denoted by v (vee) and angles by ν (nu).) The direction, measured clockwise from the *X*-axis direction, is the ambient wind angle ν_a. The relative air velocity may be found by the velocity diagram of Figure 3.4.1, by plotting the vehicle's velocity relative to the ground, v_V at ν from the *X*-axis direction, to give point V, and plotting the air velocity relative to the ground, v_a at ν_a, to give point W. The air velocity relative to the vehicle is then given by the position of W relative to V, with magnitude v_r and direction ν_r. The actual evaluation of the relative velocity is done by considering the *X* and *Y* components and using Pythagoras' Theorem. The speed of the vehicle relative to the air may conveniently be referred to as the air speed, as distinct from the wind speed or the ground speed of the vehicle.

Figure 3.4.2 shows the air impinging on the vehicle. In this figure, the air approaches the vehicle at the angle $\nu_r - 180°$. The path angle ν, vehicle heading angle ψ, and sideslip angle β are as defined in Section 1.3. The aerodynamic sideslip or yaw angle is

$$\begin{aligned}\beta_{Ae} &= \nu_r - 180° - \psi \\ &= \nu_r - 180° - \nu + \beta\end{aligned}$$

In still air $\beta_{Ae} = \beta$.

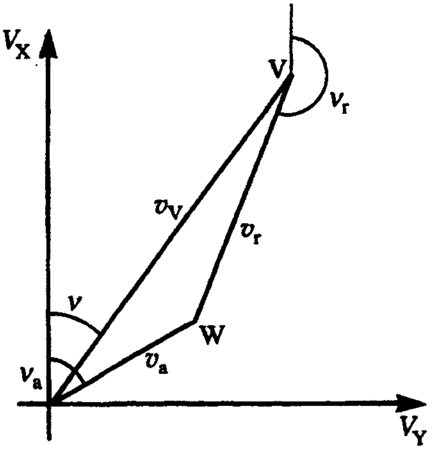
V_X
V
ν_r
v_V
v_r
ν
W
ν_a
v_a
V_Y

Figure 3.4.1. Velocity diagram for vehicle and wind.

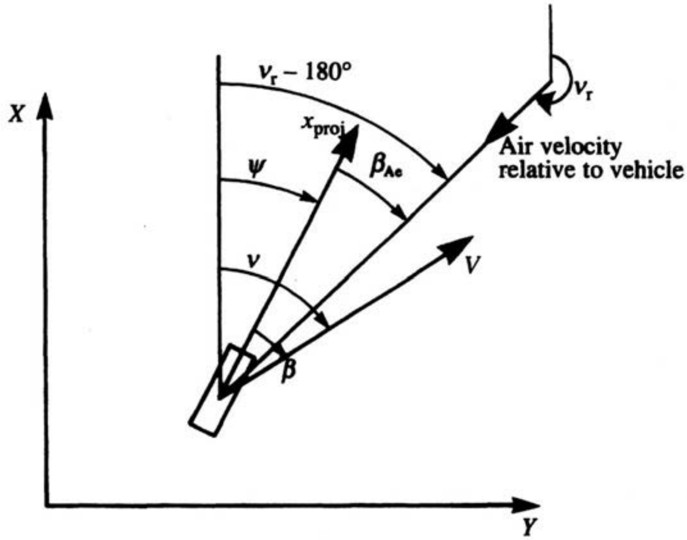
X
$\nu_r - 180°$
ν_r
x_{proj}
ψ
β_{Ae}
Air velocity
relative to vehicle
ν
V
β
Y

Figure 3.4.2. Vehicle and wind angles.

The other angle required to specify the vehicle's aerodynamic attitude is the aerodynamic angle of attack, α_A. Because the air velocity is essentially parallel to the ground, this is simply the angular position of the vehicle's x-axis. This can easily be extended to other cases, for example a non-horizontal wind because of sloping ground.

In principle it is also necessary to specify the roll angle of the vehicle. However, experiments have shown that for normal vehicles the roll angle has only a rather small effect on the aerodynamic forces, so this effect is generally neglected.

3.5 Forces and Moments

The air exerts one single total force on the vehicle, but for convenience of analysis this is usually considered to be resolved into rectangular components of force at a given point, plus moments about the axes. Therefore there are three forces and three moments. These are usually expressed as coefficients. The forces are reduced to coefficients by using

$$C_F = \frac{F}{qA}$$

where $q = \frac{1}{2}\rho V^2$ is the dynamic pressure and A is the reference area, as already mentioned. To reduce the moments to coefficients, an extra length dimension is required. Ideally an aerodynamically significant length would be used, such as the overall length, but in practice the wheelbase is usually preferred, giving

$$C_M = \frac{M}{qAL}$$

This means that in comparing coefficients between vehicles, differences of the aerodynamically irrelevant wheelbase may create problems; in practice this is not a serious handicap. It has the considerable virtue of relating pitching and yawing moments to the wheelbase, over which they are reacted by the wheels, and is therefore a very convenient system when applied to handling analysis.

The coordinate system chosen for resolving the aerodynamic force may be the vehicle-fixed axis system xyz, giving force coefficients for longitudinal force C_x, side force C_y, and normal force C_z, and moment coefficients C_{Mx} for roll, C_{My} for pitch, and C_{Mz} for yaw.

It is often preferred to express the total aerodynamic force in components related to the direction of the airflow. In this case the coefficient in the actual direction of the airflow relative to the vehicle is the drag coefficient. The force perpendicular to the flow is generally called the lift; however, there is some consequent ambiguity because the term lift may be applied to the total perpendicular force, the vertical force or the lateral force. The term lift or vertical lift is normally used for the component perpendicular to the ground, and the term lateral lift or side lift is used for the component parallel to the ground. The coefficients will be denoted C_D, C_L, and C_S, and the moment coefficients about the corresponding axes are C_R for roll, C_Y for yaw, and C_P for pitch. C_S is taken positive to the right, i.e., approximately as the y-axis, with C_P positive for pitch up. C_Y is positive when it tends to increase the yaw angle. To clarify these coefficients in the case of possible confusion with tire coefficients, the subscript Ae for aerodynamics may be added, e.g., C_{AeS}. With these coefficients, β_{Ae} is usually taken for a direction such that $dC_S/d\beta_{Ae}$ is positive.

The majority of aerodynamic investigations are concerned with drag, lift and pitch in straight running, in which case the directions of these axes essentially coincide with the vehicle-fixed axes xyz, although $C_D = -C_x$ and $C_L = -C_z$, i.e., C_D is positive to the rear, and C_L is positive upward.

The use of front and rear lift, instead of lift and pitch, is convenient because this shows directly the influence on the tire vertical forces, and also because the lift is usually measured in practice by the reactions at the wheels. If the stated front and rear lifts are to be applicable to the real steady-state operating condition then the drag must be taken to act at ground level, because the drag is overcome by a wheel thrust at ground level.

The selection of the vehicle center of mass as the axis center would be somewhat arbitrary in an aerodynamic sense, since the position of the center of mass is not aerodynamically significant. Also, the center of mass will be changed in the real vehicle by loading conditions. Hence, in vehicle aerodynamics, the standard axes are taken at the center of the wheelbase at ground level; Figures 3.5.1(a) and (b) show the partial vehicle free-body diagram in side view, with two alternative representations of the standard aerodynamic forces. In particular, in Figure 3.5.1(b) note that, for example, F_{AeLf} is not a wheel reaction, it is an effective aerodynamic force exerted on the vehicle, and when it is positive it will reduce the force exerted by the ground on the wheel.

Because of the use of the wheelbase as the reference length for non-dimensionalizing the moments, there are particularly simple relationships between the coefficients:

$$\begin{aligned} C_{Lf} &= \tfrac{1}{2}C_L + C_P \\ C_{Lr} &= \tfrac{1}{2}C_L - C_P \\ C_L &= C_{Lf} + C_{Lr} \\ C_P &= \tfrac{1}{2}(C_{Lf} - C_{Lr}) \end{aligned}$$

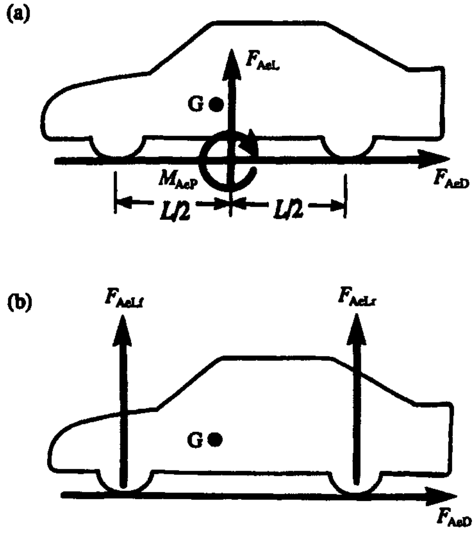

Figure 3.5.1. Standard aerodynamic axes for road vehicles, side view (only aerodynamic forces shown).

The side force and yaw moment, which occur when the vehicle is yawed (Figure 3.5.2(a)), can be handled in a similar way. The standard axis origin is on the centerline, still at the mid-point of the wheelbase, and of course the drag is deemed to act at the origin. Alternatively the side force may be treated as forces at the front and rear axles. This gives similar relationships as for lift:

$$C_{Sf} = \tfrac{1}{2}C_S + C_Y$$

$$C_{Sr} = \tfrac{1}{2}C_S - C_Y$$

$$C_S = C_{Sf} + C_{Sr}$$

$$C_Y = \tfrac{1}{2}(C_{Sf} - C_{Sr})$$

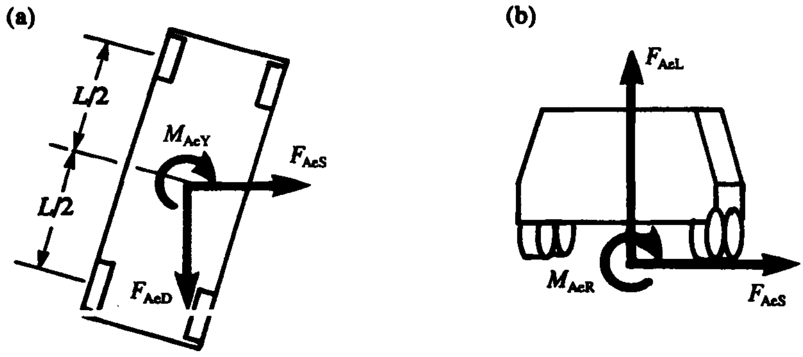

Figure 3.5.2. Standard aerodynamic axes: (a) plan view, (b) rear view (only aerodynamic forces shown).

The side force plus yawing moment can be combined to give the side force a new line of action, no longer at the axis center. The distance of the line of action of the single total side force behind the axis center (the static margin from the wheelbase mid-point), h_A, is given in terms of the wheelbase by

$$\frac{h_A}{L} = -\frac{C_Y}{C_S}$$

We must distinguish here between the position of the line of action of this side lift and the position of the next increment of side lift, analogous to the center of pressure and aerodynamic center of a wing. Rearward movement of the side lift with increasing yaw angle implies that the increments are farther back than the side force. In a steady-state handling analysis, it is the position of the side lift that is involved in determining the trim state, i.e., the required tire slip angles, and hence the steering wheel position, but it is the position of the next force increment that determines the stability of that trim state. Thus it is not correct to say that a side lift in front of the center of mass necessarily tends to destabilize a steady state. It really depends on the position of the aerodynamic force increment in relation to the position of the tire force increment (see Chapter 6). The position of the force increments behind the axis center is given in terms of the wheelbase by

$$\begin{aligned}\frac{h'_\mathrm{A}}{L} &= -\frac{\mathrm{d}C_\mathrm{Y}}{\mathrm{d}C_\mathrm{S}}\\ &= -\frac{\mathrm{d}C_\mathrm{Y}/\mathrm{d}\beta_\mathrm{Ae}}{\mathrm{d}C_\mathrm{S}/\mathrm{d}\beta_\mathrm{Ae}}\\ &= -\frac{C'_\mathrm{Y}}{C'_\mathrm{S}}\end{aligned}$$

In aeronautical engineering, the distance of the force increment behind the center-of-mass position is called the static margin.

In rear view (Figure 3.5.2(b)) the origin of coordinates is at ground level at the center of the track. The side lift acts at ground level. Because of the attitude angle in cornering, nose inward at higher lateral accelerations, the aerodynamic roll moment generally opposes normal body roll.

Using coefficient values from the next section as estimates or, preferably of course, using vehicle-specific wind tunnel data and the following equations, the drag force, lift force, side lift force, pitch moment, yaw moment and roll moment may be found:

$$\begin{aligned}F_\mathrm{AeD} &= C_\mathrm{D}qA\\ F_\mathrm{AeL} &= C_\mathrm{L}qA\\ M_\mathrm{AeP} &= C_\mathrm{P}qAL\\ F_\mathrm{AeS} &= C_\mathrm{S}qA \approx C'_\mathrm{S}\beta_\mathrm{Ae}qA\\ M_\mathrm{AeY} &= C_\mathrm{Y}qAL \approx C'_\mathrm{Y}\beta_\mathrm{Ae}qAL\\ M_\mathrm{AeR} &= C_\mathrm{R}qAL \approx C'_\mathrm{R}\beta_\mathrm{Ae}qAL\end{aligned}$$

In principle, the angular speed of the vehicle in yaw, pitch and roll may also influence the forces and moments. This is important for aircraft, where the fin and tail provide the pitch and yaw damping, and the outer wings provide the roll damping. Such effects seem to be rather small for cars, where roll and pitch damping are primarily provided by the dampers, and yaw damping by the tires (see Chapters 6 and 7). Path curvature is also an insignificant effect.

For example, approximately, we have for a given path radius

$$A = V^2/R$$

and dynamic pressure

$$q = \tfrac{1}{2}\rho V^2$$

The aerodynamic side force is

$$\begin{aligned} F_{\mathrm{AeS}} &= \tfrac{1}{2}\rho V^2 S_{\mathrm{ref}} C_{\mathrm{AeS}} \\ &= \tfrac{1}{2}\rho V^2 S_{\mathrm{ref}} C'_{\mathrm{AeS}} \beta_{\mathrm{Ae}} \end{aligned}$$

The aerodynamic yaw angle is

$$\begin{aligned} \beta_{\mathrm{Ae}} &\approx \beta \\ &\approx \frac{F_{\mathrm{Y}}}{4C_\alpha} \\ &\approx \frac{mV^2}{4RC_\alpha} \end{aligned}$$

Hence the aerodynamic side force is

$$F_{\mathrm{AeS}} = \frac{\rho\, S_{\mathrm{ref}}\, C'_{\mathrm{AeS}}\, m}{8RC_\alpha} V^4$$

This is proportional to V^4. Interestingly, it is also proportional to the mass.

Although the aerodynamic forces and coefficients are usually referred to axes with origin at the center of the wheelbase, it may be of interest to consider them based on axes with origin at the center of mass. This is a distance

$$x_{\mathrm{G}} = \tfrac{1}{2}L - a$$

in front of the wheelbase mid-point. The forces are unchanged, but the yaw moment is different.

$$M_{\mathrm{AeY,G}} = M_{\mathrm{AeY}} - F_{\mathrm{AeS}}\left(\tfrac{1}{2}L - a\right)$$

Hence the yaw moment coefficient about *G* becomes

$$C_{Y,G} = C_Y - C_S\left(\frac{1}{2} - \frac{a}{L}\right)$$

and the moment gradient coefficient becomes

$$C'_{Y,G} = C'_Y - C'_S\left(\frac{1}{2} - \frac{a}{L}\right)$$

3.6 Coefficient Values

The forces, and even force coefficients, vary considerably between vehicles, even of similar design. This section will give some examples. For a given vehicle all forces and moments depend on the three rotations, i.e., the aerodynamic pitch, yaw and roll. The effect of roll angle on the aerodynamic forces is generally small and usually neglected. The height position of the vehicle, i.e., the ground clearance, is significant. This complex interrelationship can be simplified somewhat in practice because a vehicle is roughly prismatic, i.e., vertical longitudinal sections are roughly the same, and also the vehicle has lateral symmetry. If we consider the vehicle to be truly prismatic, and considering that pressure forces dominate over skin friction shear forces, then drag and lift forces and the pitching moment must be produced by the upper and lower and front and rear faces of the body. In handling analysis, these forces affect the tire vertical reactions and also the tractive force requirements. On the other hand, lateral forces, and the yawing and rolling moments, are produced primarily by pressures on the vehicle sides. These forces directly affect the lateral dynamics.

First, consider the flow over the top of the vehicle. The vehicle body acts somewhat like a wing section, giving flows of increased speed and low pressure, giving a lift force and a pitching moment. The actual flow around a vehicle is very much a three-dimensional phenomenon, so the drag, lift and pitching moment cannot be calculated satisfactorily from the centerline pressure distribution. By adding a spoiler at the rear of the trunk (boot), a positive pressure increment can be produced over the trunk and rear window, and possibly even on the roof. The positive pressure increment on the rear window tends to reduce drag and usually more than offsets the drag on the spoiler itself for spoiler heights up to about 20 mm. The pressure increment also reduces lift at the rear, i.e., it gives a negative lift increment and a pitch-up increment. This effect can be made quite large with a large spoiler, beyond the drag optimum. The pressures are sensitive to the shape, for example to the screen inclinations, and satisfactory results can often be achieved without extraneous devices.

The actual flow pattern is characterized by flow separation at the rear. The pattern depends largely on the angle of the rear window because in the range 20°–40° to the horizontal there are strong trailing vortices, so the drag has a peak at 30° rear-screen angle. Typically, less than 20° is called fastback, 20° to 40° is hatchback, and more than 40° is squareback. The so-called K-tail, sometimes Kamm tail, in which the rear is sharply truncated with only limited tapering of the body, originated around 1935. It was possibly invented by Everling in 1934; Kamm made extensive studies in 1935, and it was patented by Koenig-Fachsenfeld in 1936. Although the flat rear has a base drag because of its low pressure, the avoidance of the strong trailing vortices means that it is often better than an apparently more streamlined shape of the same length.

At the front of the vehicle the trend is toward low hood (bonnet) fronts, and raked windshield, with a rather small angular deflection between the hood and windshield. This wedge-shaped front may help to reduce front lift. A low stagnation point at the front means that the air flows over rather than under the vehicle, which is generally favorable.

On commercial vehicles, which are basically box-shaped, even quite modest radiusing of the front edges can have a considerably beneficial effect; for example, for a typical box the C_D is better than halved if the leading edges are given a radius of 5% of the box height.

Underneath the vehicle the influence can be considered in two parts: first the mean pressure and then the effect of flow. The higher the mean pressure underneath, the greater the lift. The mean pressure is a compromise between the high stagnation pressure at the front of the vehicle and the low base pressure at the rear because of flow separation. Thus a minimal pressure will be achieved underneath with a large flow resistance at the front edge of the underside and a small one at the rear. This will be achieved with a front air dam (spoiler) and with the underbody open to the low pressure at the rear. Side skirts can help if the average pressure is below atmospheric. The practicalities of ground clearance, and especially curb clearance, limit the effectiveness of such devices on passenger vehicles, although they are applied in racing. The mean underpressure can also be influenced by suction at the wheel side apertures.

The flow under a vehicle can be used to great advantage in racing (Section 3.7). On normal vehicles the underbody flow seems principally to increase the drag because the underside of most vehicles is extremely irregular. With suspension and exhaust components to be accommodated, this is clearly a problem, but improvements have been made. The front air dam is helpful in minimizing the flow beneath the vehicle. Also it tends to give a pitch-down increment so it can be balanced against a rear spoiler.

The aerodynamics of cars have long been a consequence of packaging and aesthetic requirements rather than a decisive influence on design. In general, drag coefficients have been lower in Europe than in the U.S., possibly because of the higher price of fuel. The fuel price rises since 1970 have triggered considerable attention to drag and hence also to other aerodynamic aspects, and there have certainly been dramatic improvements. Some of these have been without significant styling repercussions; others do influence styling, but many would say favorably.

In the 1920s, for typical cars C_D was about 0.8. Improved metal forming in the 1940s gave better shapes and C_D reduced to typically 0.65. In the 1970s it was typically 0.55 in the U.S., somewhat under 0.5 in Europe. In 1990, some production vehicles are below 0.30, with research vehicles below 0.25. Various studies suggest that the aerodynamic drag is typically distributed 65/15/5/5/10 in form drag, interference drag, internal (engine and cabin cooling) drag, skin drag, and lift-associated drag, but this will vary substantially between vehicles. Skin roughness has negligible effect, although mismatch of panel edges may be significant.

High-speed, piston-engined aircraft can obtain some positive thrust from the cooling heat, or certainly largely eliminate the drag, by operating the cooling duct on the principle of a ram jet, with the waste cooling heat as the energy source. This cannot be achieved on cars because of the lower speed.

Table 3.6.1 gives typical drag figures for a range of vehicles, showing the frontal area A, the drag coefficient C_D and the drag area C_DA. The frontal area of a typical car is 0.81 of its width times its height, and is about 1.8 m^2 (European medium or U.S. compact). A good modern sedan has a drag area of 0.5 to 0.6 m^2; it is remarkable that this is barely any more than that of a touring cyclist.

Values for a racing car vary considerably with the set-up for any particular circuit, as may be seen by comparing the Sports Prototype Le Mans figures (high-speed circuit) with those for a more intricate circuit. The Formula 1 values are average ones. The very high drag coefficient (0.90) occurs because this is a justifiable penalty for the considerable downforce.

The figures above refer to the vehicle in standard condition, at zero incidence and yaw, and at standard ground clearance. For a typical car

$$\frac{dC_D}{dh} \approx 0.5/\text{m}$$

$$\frac{dC_D}{d\alpha} \approx 0.015/\text{deg}$$

This latter figure is largely the consequence of increased airflow beneath the car. Thus pitch moment is of interest in maintaining correct attitude, to control drag. The drag itself has some influence on handling because it must be overcome by a tractive force, which affects the tire lateral force characteristics. Lift and drag coefficients may vary with speed because of changing height or pitch angle. In particular, this can lead to a rapid increase of front lift on fast cars.

Table 3.6.1. Example Drag Coefficients and Drag Areas

Vehicle		Frontal area A (m^2)	Drag coefficient C_D	Drag area A_D (m^2)
Motorcycle	– touring	0.7	0.90	0.63
	– racing	0.48	0.67	0.32
Kart		0.35	0.80	0.28
Good car		1.80	0.30	0.54
Poor car		1.80	0.50	0.90
Larger car		2.3	0.46	1.06
Small commercial vehicle		5	0.50	2.50
Light truck		7	0.73	5.10
Coach		7	0.66	4.60
Heavy truck		9	0.78	7.00
Heavy truck + trailer		9	0.90	8.10
Formula 1 racing		1.6	0.90	1.44
Sports prototype racing		1.7	0.50	0.85
Le Mans racing		1.7	0.38	0.65
Light aircraft		5	0.12	0.60
Cyclist	– touring	0.50	1.00	0.50
	– racing	0.33	0.90	0.30

Representative main aerodynamic coefficients for a car are summarized in Table 3.6.2. The total lift coefficient of a typical car is about 0.3, ranging widely from 0 to 0.6 or more. The lift coefficient is quite sensitive to height and incidence, with typically

$$\frac{dC_L}{dh} \approx -0.2/\mathrm{m}$$

$$\frac{dC_L}{d\alpha} \approx 0.06/\mathrm{deg}$$

Table 3.6.2. Typical Aerodynamic Coefficients for a Passenger Car

Lift	C_L	0.30
Drag	C_D	0.35
Pitch moment	C_P	−0.05
Side force	$C'_S = \mathrm{d}C_S/\mathrm{d}\beta$	0.040/deg
Yaw moment	$C'_Y = \mathrm{d}C_Y/\mathrm{d}\beta$	0.005/deg
Roll moment	$C'_R = \mathrm{d}C_R/\mathrm{d}\beta$	0.005/deg

The pitching moment coefficient should preferably be small. It is typically −0.05 and varies considerably between vehicles. It varies with incidence, typically at

$$\frac{\mathrm{d}C_P}{\mathrm{d}\alpha} \approx 0.03/\mathrm{deg}$$

The lift force and pitching moment, or front and rear lift, can have a substantial effect on high-speed handling because by changing the tire vertical forces the cornering stiffness of the tires is altered. Front lift leads to unpleasantly light steering with low limit lateral forces, and rear lift leads to directional instability, discussed in more detail in Chapter 6. Passenger car designers aim for zero lift and pitch or a small amount of balanced downforce. Positive lift can be dangerous at high speeds.

It remains now to consider the influence of pressures on the sides of the vehicle, i.e., to look at the lateral lift, the yawing moment and the rolling moment. Although there may be significant pressures on the sides in straight running, they balance out. A net resultant force occurs only when there is an aerodynamic yaw angle β_{Ae}. In normal conditions the vehicle speed is substantially greater than the wind speed, so it is yaw angles up to about 30° that are of most interest. The following comments are restricted to that range, and should not be extrapolated beyond 30°.

The principal effect of yaw is to give a lateral lift and a yawing moment. Various theories of lateral lift have been proposed, none entirely satisfactory because of the complex flow pattern. In practice a typical experimental value of the lateral lift coefficient variation with yaw angle is 0.04/deg, with individual examples ranging from 0.02 to 0.05/deg. This is usually fairly constant up to 30° yaw.

The yawing moment is the consequence of the lateral lift and its line of action. The yaw moment coefficient C_Y usually increases fairly linearly up to 15° yaw angle at a rate of about 0.005/deg, i.e., $dC_Y/d\beta_A = 0.005/\text{deg}$, but then peaks at a value of typically 0.10 at an angle of 25°, and then declines. This can typically be modeled by

$$C_Y = C_{YB1}\,\beta_{Ae} - C_{YB5}\,\beta_{Ae}^5$$

This reflects the fact that the line of action of the lateral lift starts well forward, but moves back toward the axis center, tending to reduce the moment. The yaw moment is normally positive, and hence tends to increase the yaw angle. Better aerodynamic directional stability is afforded by vehicles with a smaller yaw coefficient, i.e., greater side area at the rear such as station wagons (estate cars), or those with a high trunk profile and with a low hood line.

An aerodynamic yaw angle also causes a roll moment coefficient. Typically this increases smoothly with β_{Ae} up to 30°, at 0.005/deg. This is because the side lift really acts above the ground level, actually at a height $(C_R/C_S)L$ which is surprisingly low, being about equal to the wheel radius, presumably because the flow can easily pass around the upper edges.

The yaw angle also causes an increase of drag, typically quadratic in nature, i.e.,

$$C_D = C_{D0} + k\beta_{Ae}^2$$

where in one case $k = 1.6 \times 10^{-4}\ \text{deg}^{-2}$. Yaw also causes a quadratic increase of lift coefficient up to about 20°, beyond which it levels off and then declines beyond 30°. In this case typically $k \approx 1.2 \times 10^{-3}\ \text{deg}^{-2}$. The pitch coefficient also tends to increase, typically in this case with $k \approx 1.2 \times 10^{-4}\ \text{deg}^{-2}$.

The angle of the steered wheels will have some effect on the side lift and yaw. Measurements on one Formula 1 racing car, with exposed wheels at steer angle δ, gave

$$\frac{dC_S}{d\delta} = 0.008/\text{deg}$$

$$\frac{dC_Y}{d\delta} = 0.024/\text{deg}$$

The effects are probably very small for a normal sedan with almost enclosed front wheels.

3.7 Competition Vehicles

The aerodynamics of competition vehicles, like their other features, is more extreme than for normal passenger or commercial vehicles. For land speed record vehicles, drag has always been important, and lift/downforce has been considered since the 1920s. The role of aerodynamics in racing-car design has increased dramatically since the mid-1960s, and is now of great importance. The history of competition vehicle aerodynamics will be treated briefly here because of its technical interest. Also, road vehicle design has been influenced to a limited extent by competition experience, for example by underbody shape and ground effects.

Early racing and land speed record vehicles appear crude by modern standards. In many cases aerodynamics was influential in the layout because frontal area, governed by the large engines mounted high on rigid axles, was generally minimized within the perceived options. Streamlined body forms, although with many excrescences including the driver, were naturally applied to land speed record vehicles in the very early days, for example Chasseloup–Laubat and Jenatzy in 1899, both with battery electric vehicles at about 25 m/s (56 mph). Much improved streamlining was achieved by the Baker Electric Torpedo in 1902 and the steam-driven Stanley Rocket in 1906. In view of the limited aerodynamic knowledge of the day, these were quite respectable efforts, and in marked contrast to most of their competition.

In 1927 the rocket-powered Opel Rak 1 appeared, of uncompetitive performance but of historical interest because it featured small wings mounted on the body behind the front wheels. The Rak 2 of 1928 had larger wings of about 1 m^2 each. Judging from photographs, however, the design was very odd, using a fairly thin, well-cambered section fitted as if to give lift, but then set at a negative incidence that would have resulted in little vertical force at all. It is doubtful that either of these two vehicles could be considered to be serious contenders; more likely, they were just publicity vehicles.

Prevost (1928) first described proposals for a venturi-bodied land speed record car (Figure 3.7.1), with the stated intention of preventing lift. In 1929, the Irving-designed Golden Arrow set a land speed record of 103 m/s (231 mph). This used a venturi-shaped underbody (Figure 3.7.2), which according to wind-tunnel tests, would give 2440 N downforce at the design speed of 112 m/s (250 mph) (Irving 1930). In Prevost's proposal the venturi had a large entry depth, but in Irving's design the venturi had acquired its modern form, with the entry barely any deeper than the throat, necessary because a deep entry gives front lift.

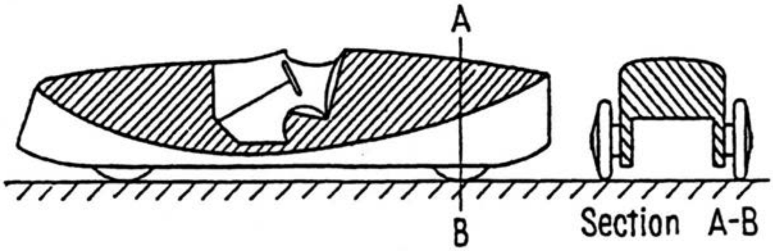

Figure 3.7.1. Proposal for a venturi underbody by Prevost. (Reproduced by permission of the Council of the Institution of Mechanical Engineers, from Automobile Engineer, *letter from R. Prevost, September 1928.)*

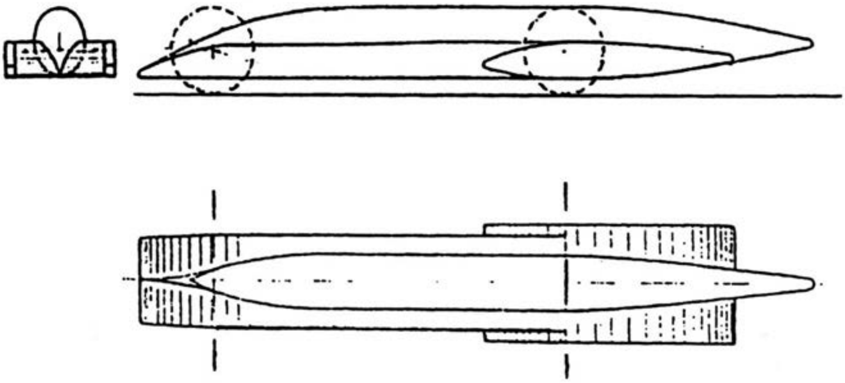

Figure 3.7.2. Basic body shape of Irving's Golden Arrow. (Reproduced by permission of the Council of the Institution of Mechanical Engineers, from Irving, J.S., "The Golden Arrow and the World's Land Speed Record," Automobile Engineer, *May 1930.)*

The massive Eyston–Andreau Thunderbolt of 1938 had the eight wheels enclosed within the body using a narrow front track to allow this, and achieved 154 m/s (345 mph) on 3500 kW. In contrast, in 1939 the smaller and highly streamlined Railton Mobil Special achieved 166 m/s (370 mph) on only 930 kW, with the emphasis on low drag including ice cooling to reduce the internal flow losses. In contrast to the later thrust reaction types, it was common in that period of wheel-driven speed vehicles to have traction problems, and this led to the use of heavy vehicles and in some cases to multiple drive axles. For example, Thunderbolt required a thrust of 23 kN with a weight of 70 kN, for a traction requirement of 0.33 even if all eight wheels had been driven, and a much higher value with only the rear four driven, as actually used. It should also be borne in mind that record runs were mainly made on natural surfaces, such as sand or salt, with less friction available than on a prepared hard surface. Inadequate traction has certainly been the downfall of many wheel-driven record contenders.

The possible application of aerodynamic downforce to improve traction was recognized in the 1939 Daimler Benz T80 speed record contender, which was built but never ran. This featured tapered stub wings of low aspect ratio and area about 0.8 m^2 each, positioned on the body sides in front of the rear wheels. However, in marked contrast to the earlier Opel, this time the wing section was properly arranged to give downforce, with a cambered section having a flat upper surface and appropriate incidence, and therefore this should perhaps be admitted as the first true winged downforce vehicle. An adjustable-incidence rear airfoil on struts was also proposed, but not used. The drag coefficient was 0.18 on 1.7 m^2 frontal area.

It seems that the potential for downforce to improve racing vehicles (as opposed to speed record vehicles) remained unrecognized, with aerodynamic attention limited to drag and engine cooling, and provision of a cool buffet-free cockpit. The next interesting development was the use of a hydraulically operated air brake on the Mercedes 300SLR sports racer, tested in 1952 and used at Le Mans in 1955. This was intended to relieve the brakes on fast circuits, but it was found that cornering also improved if the brake was kept open. This was because the air brake, a rear-hinged trunk lid that rose to about 60°, acted as a half-metre-high spoiler that gave downforce.

At Indianapolis in this period there was a vogue for full bodywork which dramatically reduced drag compared with the usual fully exposed wheels, but the extra mass and the adverse aerodynamics in lift and yaw, not yet adequately understood, were sufficient to halt the trend. Compared with most European circuits which have a wide variety of corners and a wide speed range, at Indianapolis speeds are relatively uniform and high, for example a minimum more than 75% of the maximum (about 90 m/s), so aerodynamic effects are particularly strong. However, even in Europe the Mercedes W196 of 1954 used full streamlining to good effect on some circuits.

In 1956 a Porsche sports racer operated by M. May appeared at the Nurburgring with a downforce aerofoil over the body at mid-wheelbase. It was used in practice, but disallowed from racing by the scrutineers, rejected as being dangerous. Over the next ten years up to the mid-1960s there seems to have been no development of the concept. Perhaps in the early 1960s designers were too busy coming to terms with the rear-engine revolution, which itself improved aerodynamics by reducing drag because of the lower driver position.

In 1960 spoilers appeared at the rear of Porsche and Ferrari sports racers, giving some rear downthrust, better high-speed stability and slightly better cornering. In 1965 Herd for McLaren in England and Hall in the U.S. made preliminary tests on downforce wings, with encouraging results. In 1966, Hall started to use a downforce wing on his Can-Am series Chaparral, placed high on struts above the rear wheels. The original intention was apparently to improve high-speed stability. In 1967 the wing was of roughly symmetrical section, but had pitch control from a driver's pedal, and was used to give large downforce in corners but smaller downforce and drag on the straight. In Formula 1, in 1967, limited aerodynamic devices were tried, especially small front "bib" or "ear" spoilers on the nose, but these were often removed because of lack of pitch balance. The existence of body lift and the variation of lift and pitch moment with pitch angle were proving a problem, and the Lotus answer was the wedge body that also did well at Indianapolis in 1968. This then acquired front stub wings and an upswept engine-cover rear spoiler.

Then, in mid-1968, the wing idea was widely adopted in Europe, and high-mounted wings appeared on many cars, some acting on the body but most acting directly on the hub carriers to avoid loading the suspension. Balance was achieved by a variety of front devices from bib spoilers to stub wings. In 1969 front wings were also mounted high and on the hub carriers, and many wings had pitch control. However, the severe vibration and aerodynamic load reversals caused some dramatic accidents. After a period of uncertainty, new rules limiting wing design were introduced throughout most of motor racing, including Formula 1 and Indianapolis. Essentially these limited the size and height of wings, and required the wings to act on the sprung mass, not directly on the carriers. Wings were still not universally used; an alternative is to try to use the whole of the body's upper surface as a wedge. The wedge body shape usually produces good front downforce, so it is well suited to combination with a large rear wing, with front wings used just for trimming. A wedge body with hydraulically controlled incidence has also been used. A shallow spoiler was used across the front of bodies to reduce body lift or improve downforce. Generally, 1970 saw improved understanding of wings and their use, and the slatted rear wing appeared.

In sports car racing around 1970 the vehicle front profile underwent a notable change from rounded to vertical, i.e., the air dam front arrived to reduce underbody pressure. Sometimes a "splitter" plate was added – a thin horizontal lip protruding forward at the bottom of the air dam. The splitter helped the downforce but tended to increase pitch sensitivity (sensitivity of the downforce distribution to pitch angle). The sides also became flatter and closer to the ground.

Concave longitudinal section front and rear decks were found to be worthwhile to minimize sensitivity to pitch angle, although increasing drag by 10%. As an example of the influence of bodywork on drag, wind-tunnel tests to attempt to purge the drag of one Porsche open sports racer reduced C_D from 0.70 to 0.49, and to 0.36 with a long tail. The better short-tail version gave its best track performance with the addition of front and rear spoilers that increased C_D to 0.58. Twin rear fins were found to reduce drag, as was a wing mounted between them, because this prevented flow separation from the body. Front-edge fences can considerably increase front downforce without increasing drag. Full-length edge fences were briefly popular. Before movable aerodynamic devices were banned, flaps at the rear operated by the suspension were used to minimize pitch changes. Separate left and right flaps can in principle reduce roll, but in practice this did not prove helpful.

More revolutionary, in 1970, Hall in the U.S. produced the fan car for sports racing. This had flexible sealing skirts all around the edges of the body, with twin fans that extracted the air and blew it backwards, reducing the underpressure. One advantage of this system over wings is that it functions at full effectiveness at low speed, so low-speed cornering and low-speed traction are greatly improved. With 6 m^2 of enclosed area, only 1 kPa pressure reduction would give 3 kN downforce, about half the vehicle weight. The principle was very successful, and was promptly banned. The same idea appeared briefly in Formula 1 in 1978, with the same results.

1971 saw a marked improvement in the application of wings. Previously the rear wing was mounted rather low over the engine, with very restricted flow to its underside so that it really acted as a large spoiler. On the 1971 McLaren for Indianapolis, which was basically a wedge with wings and side radiators, the rear bodywork was improved to give a good airflow below the wing, greatly increasing the downforce. The downforce was equal to about half the car's weight at maximum speed, about 3 kN at 90 m/s or a total lift area C_LA of about 0.6 m^2. In Formula 1 tall air boxes also appeared to deliver air to the engine, although there was disagreement about whether they made airflow to the rear wing better or worse. In 1972 there were further dramatic cornering speed increases, with the rear wing going further to the rear. Total downforce increased to about 6 kN at 90 m/s, a lift area of 1.2 m^2. The actual wing areas were about 0.6 m^2 at the rear and 0.25 m^2 at the front, these being limited by the rules. One advantage of the rearward wing is that the suction on the wing undersurface is not compromised by suction on the top surface of the body beneath, because the wing is over the road instead. Also, because the rear wing is of low aspect ratio and in turbulent air, its maximum lift is limited, so moving it back while retaining overall aerodynamic balance allows a larger downforce at the front giving an increased total downforce.

The period 1973 to 1977 saw refinement of the aerodynamics with increasing lift coefficients from improved airfoil contours, tip plates, adjustable flaps, slots, trailing-edge lips, and so on.

The next revolution in racing was to use the underbody to produce downforce, i.e., ground-effect venturis as used on speed record cars in the 1920s, introduced to racing by Lotus in 1977. The essential concept of the car was a very wide chord wing on each side of the body. The conceptual improvement was large end-plates with brushes that rubbed against the ground to provide an air seal. The wing span was severely limited by the body width regulations, but despite the very low aspect ratio and the poor seal of the brushes, considerable downforce was generated at a good lift/drag ratio. The cooling radiators were buried in the wings. The wing and ground considered in longitudinal section act as a venturi. The wing to ground clearance (the venturi throat) is about 100 mm. The large exit draws a maximum of air through the throat where the correspondingly high air speed results in a low pressure on the wing undersurface giving an effective downforce. A later development was to have a long parallel throat to maximize the area where the pressure is very low. This effect is assisted by the extractor effect of the rear wing which helps to draw air through the venturi. The Lotus 79, for 1978, developed the idea further, the whole layout being governed by optimization of the ground effects; this included minimizing the width of the true body to maximize the width of the venturi tunnels. To do this the driver was moved forward, and the fuel was placed in a single cell behind the driver. This car firmly established the ground-effect concept.

In 1979 ground-effect cars also appeared at Indianapolis and, wherever it was allowed, ground effect became essential. Optimization of the ground-effect tunnels affected many other features; for example, where previously the flat opposed-cylinder engine layout was considered ideal because of the low center of mass, the V8 became preferable because it is narrower and matches the front profile of the driver with narrow hips and wide shoulders, giving more room for the tunnels.

Front wings were often omitted because the downforce from underbody tunnels was already well forward, tending to give limit oversteer at high speed. To help correct this, front wings were sometimes used to give an upward force. It is important to position the downforce correctly; fine balance is usually achieved by adjusting the rear wing flap. Front suspension was revised, moving the springs and dampers into the body to improve airflow to the tunnels.

The downforce did create problems in demanding extremely stiff suspension springing to minimize height and attitude changes, even with sliding or flexible sealing skirts. In 1981, in Formula 1, a 60 mm ground clearance was required, but this rule was circumvented by hydraulic suspension lifters. Flat bottoms between the axles and greater clearance were required for 1983, which reduced downforce and allowed suspension action to be restored. The body can still produce some downforce, but less than the wings.

1981 was also the year of the abortive Lotus 88, an imaginative concept that fell foul of the rules. This had two chassis, the inner one being the main chassis with conventional suspension, and the outer one being an aerodynamic shell with much stiffer connection to the wheels allowing good control of the ground clearance. It was disallowed on the basis that the outer shell was a movable aerodynamic device.

At their peak, ground effects were such that downforces of about 22 kN were being achieved in Formula 1 at 75 m/s, corresponding to a lift area of 6.4 m^2. Of this, about 20% came from the wings and 80% from the body. On a vehicle mass of 660 kg and with a tire friction coefficient of over 1.0, this allows lateral and braking accelerations of about 40 m/s^2 ($4g$). Also, the position of the center of mass becomes critical. The drag area was about 1.4 m^2, giving a lift/drag ratio of 4.6. The current restrictive rules, specifying maximum wing sizes and calling for flat-bottomed areas under the body, considerably reduce the downforce values, although some favorable underbody effect is achieved by swept-up diffuser areas at the rear. The engine exhaust is often fed to the diffusers, possibly "blowing" an improved airflow beneath, and also helping the engine by reduced exhaust back pressure, although often compromising the length of the exhaust pipe secondaries for optimum pressure pulse tuning.

An interesting aspect of downforce is that for a given force the performance becomes more sensitive to the total mass. This is because for a large downforce the tire vertical forces are almost independent of weight, so the maximum lateral acceleration becomes inversely proportional to mass.

Over recent years there has been detailed optimization rather than revolution, and aerodynamics is now just a large part of the picture, rather than completely dominating it. Continuing detailed optimization and improvement is offset by gradually more restrictive rules.

Wind-tunnel tests of ground-effect vehicles have sometimes shown considerable discrepancies from track behavior. This is caused by the boundary layer on the floor of the wind tunnel. Nowadays it is considered highly desirable to have a moving-belt floor in the wind tunnel, the speed of which matches the air speed. Corrections can be applied for static floors, but this is not completely satisfactory.

Downforce has been used in other competition motoring events, including rallying, drag racing and kart racing. Small stub wings have even been used on motorcycles to discourage lifting of the front wheel in acceleration, but wings are now banned. In any case, because a motorcycle leans considerably in a corner, downforce wings would be of limited effectiveness in cornering. Racing sidecar motorcycles have more extensive bodywork, so some downforce can be produced.

3.8 Problems

Q 3.2.1 What is the standard atmospheric density at 500 m above sea level?

Q 3.2.2 Temperature, pressure and relative humidity are measured as 22.3°C, 99.4 kPa, and 54%. Calculate the density according to the approximate method of Section 3.2.

Q 3.3.1 In open terrain the 10 m wind is 8.4 m/s. Estimate the wind speed at 1 m height.

Q 3.3.2 An airflow has a mean speed of 14 m/s and turbulent intensity of 24%. What speed range will the instantaneous speed be within for 95.5% of the time?

Q 3.3.3 In a wind of 8 m/s and turbulent intensity 28%, a car drives crosswind at 27 m/s. What turbulent intensity does the car experience?

Q 3.3.4 The wind at a high bridge may be modeled by a Weibull distribution with a characteristic speed of 7 m/s and a shape factor of 1.9. What is the probability for winds exceeding 10 m/s? If sustained winds exceeding 20 m/s make the bridge unsafe for use, what proportion of the time is it likely to be closed?

Q 3.4.1 Describe the differences between aircraft aerodynamics and ground vehicle aerodynamics.

Q 3.4.2 Describe the problems of obtaining accurate force prediction for a real car by testing a small model in a wind tunnel.

Q 3.4.3 Describe how force coefficients are likely to change with Reynolds number for various types of body.

Q 3.4.4 A vehicle travels at 26 m/s at a heading angle of 40° with a sideslip angle of 4° in a wind of 16 m/s at 160°. Calculate the air velocity relative to the vehicle. Calculate the aerodynamic yaw angle.

Q 3.5.1 A vehicle has mass 1200 kg, center of mass 1.350 m back on a 3.000 m wheelbase, and $C_L = 0.412$, $C_P = 0.083$, $C_S = 0.160$, $C_Y = 0.020$, and $C_D = 0.392$, based on standard vehicle aerodynamic axes. The air density is 1.200 kg/m^3. The frontal area is 2.35 m^2 and the speed 29 m/s. Calculate the actual forces and moments.

Q 3.5.2 For the vehicle of the last question, calculate the C_{Lf} and C_{Lr}.

Q 3.5.3 The vehicle of Q 3.5.1 has a lateral acceleration of 4 m/s^2 at a speed of 45 m/s. Calculate the front and rear axle cornering force coefficients.

Q 3.6.1 Summarize typical values of car aerodynamic coefficients.

Q 3.6.2 A typical car is given a steady-state cornering test at 8 m/s^2 on a 50 m radius, at which it has an attitude angle of 8°. Make an estimate of the aerodynamic forces and moments, and investigate their significance.

Q 3.6.3 Explain the concepts of center of pressure and aerodynamic center in the context of lateral aerodynamic force and yaw moment on a vehicle, including any relevant equations.

Q 3.7.1 The Daimler Benz T80 land speed record contender had a mass of about 2000 kg and a probable design speed of 200 m/s, with a drag area of 0.306 m^2. Discuss the possible value of the wings (total area 1.6 m^2) in enhancing traction, giving calculations.

Q 3.7.2 Describe the features of the bodywork of a typical modern sports racer, and discuss the reasons for it.

Q 3.7.3 Describe the evolution of Formula 1 or Indianapolis racing car design in the light of aerodynamic effects and rule changes.

Q 3.7.4 Consider a motorcycle with a downforce wing. Considering the angle of lean and a constant tire maximum cornering force coefficient, under what conditions is such a wing advantageous in increasing maximum cornering speed?

Q 3.7.5 Repeat the last question, but incorporating variation of μ_Y with F_V.

Q 3.8.1 See Q 5.19.3 – 5.19.7 at the end of Chapter 5.

3.9 Bibliography

A general introduction to automobile aerodynamics is provided by Howard (1986). Ludvigsen (1970) reviewed historical developments in vehicle aerodynamics. A good overview of vehicle aerodynamics, with innumerable references, can be found in Dorgham & Businaro (1983). An excellent condensation and systematization of the extensive experimental data on drag and lift is given in Hoerner (1965) and Hoerner & Borst (1975) (generally, not just for ground vehicles). Robinson (1990) gives information on motorcycle drag areas.

From the many books on competition motor vehicles, four that can be recommended (not just for aerodynamics) are: Frere (1973), Nye (1978), Huntingdon (1981) and Posthumus & Tremayne (1985).

For those interested in the application of wings to competition vehicles, the basic theory of wings may be found in fluid dynamic texts, for example Hoerner (1965). A basic introduction is provided by Massey (1983). Detail is given in more specialized texts such as Houghton & Brock (1970). For theory and extensive wind-tunnel results of wing sections see Abbott & von Doenhoff (1959). Rae & Pope (1984) is a useful reference on testing techniques. For technical analysis of some aerodynamic aspects of competition vehicles see Pershing (1968 and 1974). Benzing (1991) gives information on racing car wing performance. Simiu & Scanlan (1971) give information on wind behavior.

4

Suspension Components

4.1 Introduction

The lateral force exerted by the road on a tire depends on many factors; principal among these are the slip angle, the camber angle, the vertical tire deflection and the longitudinal slip (or the vertical force and the longitudinal force). The angular positions and the vertical force depend on the suspension system, which locates the wheel relative to the vehicle body. Thus the suspension system design plays an important role in the cornering and handling characteristics and requires detailed consideration. In analyzing the suspension, our main interests are in the geometry in order to find the wheel camber and steer angles, and in the distribution of vertical force between the four wheels. This chapter looks mainly at the properties of individual suspension components. Chapter 5 then looks at the complete suspension and at suspension analysis in the context of handling, including ideas such as the roll center and roll axis.

In a practical suspension system, the wheel is connected to the body through various links; these permit an approximately vertical motion of the wheel relative to the body, controlled by the spring and damper. The steering system controls a different type of wheel motion – rotation about an approximately vertical axis. For a normal road vehicle, the suspension links include rubber bushes. These reduce the transmission of noise, vibration and harshness into the passenger compartment. The compliance in the links, bushes, steering system and chassis has the result that the slip angle and camber angle of the wheel are to some extent dependent on the forces acting. However, in order to obtain a clear picture of the operation and behavior of suspensions, it is easiest to begin by analyzing them as though all links were perfectly rigid, and to add the effects of compliance later. Thus we should consider:

(1) The geometry of idealized suspensions, investigating possible arrangements of the links and the consequent implications for the wheel motion relative to the chassis.

(2) The compliance of suspension components, in particular those that are specifically provided to control the wheel motions, such as springs and anti-roll bars, but also the compliance of links and rubber bushes.

(3) Friction, both that deliberately introduced by dampers, and residual friction in the joints.

(4) Inertia of the components in the types of motion relevant to suspension action.

The intention of this chapter is not to provide a comprehensive systematization of all possible suspensions; rather it is to reveal some order among the wide range of types, and to outline the features that influence handling.

4.2 Mobility Analysis

The following few pages attempt to place some systematic order on suspension systems by using a degrees-of-freedom (mobility) analysis. Mobility analysis can be very helpful in the design of precise mechanisms, but there are some difficulties in applying it to vehicle suspensions. Most suspensions include many compliant rubber bushes so that changes of link lengths are possible, contrary to the geometrically ideal rigid bodies of mobility analysis. Even worse, sometimes the link itself is highly compliant, such as a leaf spring supporting an axle or a trailing twist axle. Such cases must be dealt with by finding geometrically equivalent rigid linkages. Further, some suspensions are redundant, i.e., they contain "too many" links, because in the idealized analysis one or more of the links merely confirms rather than controls a particular motion. Finally, a suspension that in an idealized analysis appears to be a structure rather than a mechanism may function adequately because of compliance in the bushes or in the links themselves.

Notwithstanding the above limitations, most suspensions are amenable to analysis, and a degrees-of-freedom analysis does provide a helpful framework for categorizing the wide range of real suspension designs. Even if it does not point directly to an optimum design, it provides an appreciation of certain limitations of the simple mechanisms that are met in practice.

Every real suspension works in three spatial dimensions. A full kinematic analysis of the required generality to cope with the range of practical suspensions is highly complex. Therefore, the presentation here is based on an appeal to relatively simple notions in common engineering usage. Computer software packages now make possible advanced three-dimensional analysis. Nevertheless, it is helpful to begin by considering the behavior of two-dimensional suspension-like mechanisms, especially since the interpretation and discussion of actual handling behavior is based largely on two-dimensional motion concepts such as camber and steer. Some principles of kinematics are reviewed here because they provide the key to important later results.

A two-dimensional mechanism is one with all motions parallel to a given plane. The dimension perpendicular to that plane is neglected. This could be said to correspond to a two-dimensional drawing such as a front elevation. To specify the position of any particular object then requires three coordinates in a specified coordinate system, and a freely mobile object is therefore said to have three degrees of freedom when in two-dimensional motion. For example, the position of a link could be specified by two coordinates (x, y) for a given point on the link, plus the angle of the link (θ). If such an object moves without change of the angle θ, it is said to be translating; if it moves with θ changing but the location point remaining at (x, y), then it is said to be rotating about the point (x, y).

Even in complex motions, at any instant it is possible to identify a point that is the center of rotation at that instant. This point is called the instantaneous center, or centro. Imagining the moving object extended as a sheet in all directions, the centro is then that point of the sheet that is not changing its (x,y) coordinates at that instant, i.e., it is the point that is stationary in the selected coordinate system at that instant.

One important property of rotation is that all velocities are perpendicular to the radius from the rotation center, and have a magnitude given by $V = \omega r$ where ω is the angular speed at that moment. This property of perpendicularity is very useful in identifying centros (instantaneous centers). If the velocity directions are known at any two points of an object, then the radii can be drawn, and their intersection must be the centro. These known velocities must be in a specified coordinate system or, equivalently, they must be relative to some other specified object, for example the chassis.

When there are several objects all moving, as in the case of a chassis plus several suspension links and a wheel carrier, then we can direct our attention to any pair of these objects, and that pair will have a particular centro for the motion at that instant, i.e., for one object relative to the other. This is in general different from the centro for any other pair of the objects. However, the centro of A's motion relative to B is the same as that of B's motion relative to A. The centro is a property of the objects as a pair. In some cases it is normal practice for one of the objects to be implied; for example, to speak of the centro of the wheel normally means the centro of the wheel–body combination, and hence of the centro of the wheel motion relative to the body. The centro concept is a powerful tool in suspension analysis.

One special case occurs when the relative motion of the objects is pure translation. Then the constructed radii intended to reveal the centro do not intersect. They are said to meet at infinity (at either side), and this is where the centro is located. This does not cause any practical analytic problems because lines constructed from the centro are simply parallel to the locating radii.

In many practical cases of connected components, the centro location is obvious without formal construction of radii. This is the case, for example, for a radius rod where the rod pivot itself defines the centro for the rod motion relative to the base member.

A property that we shall require in the investigation of roll centers is illustrated in Figure 4.2.1; the centros for the three possible pairs of a group of three objects lie on a straight line. This is known as the Kennedy–Arronhold theorem. In this example AB is pivoted on BC, which is pivoted on CDE. Therefore B is the centro for AB with BC, and C is the centro for BC with CDE. Considering motion relative to link AB, evidently C can move only perpendicularly to the radial line BC. Considering the motion of CDE relative to C, the point E must be moving perpendicularly to the radial line CE. The velocity of E relative to B, $V_{E/B}$, is the vector sum of $V_{E/C}$ and $V_{C/B}$, which are both perpendicular to BCE. Thus $V_{E/B}$ is perpendicular to BCE. Thus the centro of AB with CDE must be somewhere on a line through BC, i.e., the three centros must be on a straight line.

In two-dimensions, the connection of a pair of objects can be classified as either a sliding joint or a rotating joint. In practice a sliding joint is usually straight. Relative to a fixed member, a slider has one degree of freedom, i.e., its relative position can be specified by a single parameter. The pivoting link also has one degree of freedom (1-dof), but in rotation the relative position is specified by a single angle. These elements can be joined serially to allow two degrees of freedom relative to the base member (Figure 4.2.2) where the trunnion (c or d) corresponds closely to the function of a typical suspension strut. The links with two degrees of freedom (2-dof) require two parameters to specify their positions relative to the hatched members; e.g., in (b) two angles, in (d) one angle plus the extension.

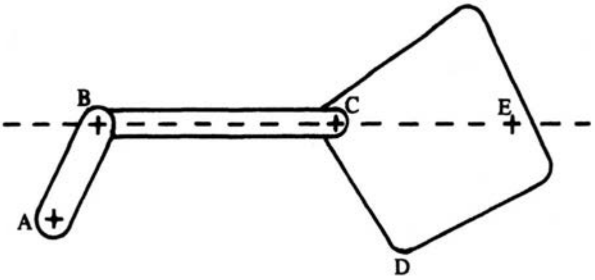

Figure 4.2.1. Kennedy–Arronhold theorem of co-linear centros.

4.3 Straight-Line Mechanisms

It is often desirable to provide a straight motion path for some point of a suspension member, e.g., for lateral location of an axle, and there are several practical ways to achieve this. This section presents several such methods. Analysis of straight-line mechanisms also demonstrates some wider truths that will be relevant later on. In a real suspension, the straight line need only be approximate; precision of the path may be traded-off against other factors, especially cost.

Geometrically, we wish to constrain a given point on body A to move in a straight line relative to body B. Thus there must remain two degrees of freedom for the relative motion. For example, an axle must rise and fall (heave, 1-dof), and have freedom to roll (1-dof), but must be located laterally. For convenience we can assume that the angular rolling freedom is achieved because body B is provided with a pivot hole at the appropriate point to accept a pivot pin; the mechanism to be designed must therefore cause the pin to have a straight-line motion relative to body A.

The most direct solution is to provide a simple slider (Figure 4.3.1). Here the sliding block B has one degree of freedom relative to stationary member A attached to the body. C is the point with straight-line motion. The axle has its second degree of freedom by rotating about C. The locating channel A may alterna-

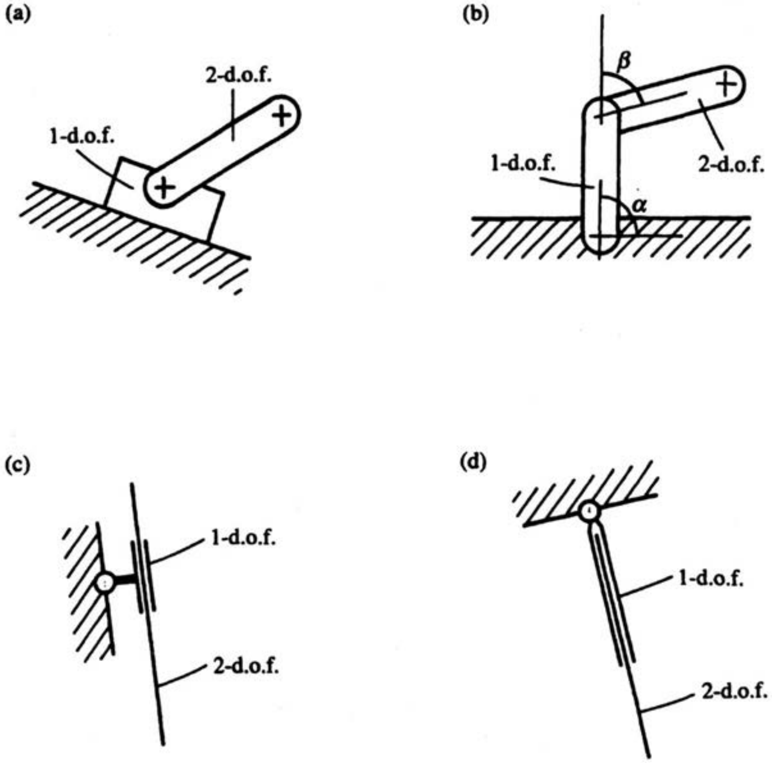

Figure 4.2.2. Serial connection for 2-dof.

tively be fixed to the axle and C to the chassis. This is not entirely equivalent, because when the channel is attached to the rolled body, motion of the axle perpendicular to the road requires some lateral motion of the axle or body; in practice, the slider method of Figure 4.3.1 is not good for passenger cars because of noise transmission and wear, but it is compact and has been used successfully in racing.

The second type of straight-line linkage is the simple radius rod (Figure 4.3.2), known as the Panhard rod (track rod in U.S.) when used for lateral axle location. Of course, in a formal geometric sense, this is anything but a straight-line mechanism, but it is commonly used because its advantages often outweigh the inaccuracy of its straight-line approximation. In seeking to provide a straight line in a given direction it is subject to two kinds of errors. First, the path is nonlinear, having a radius equal to the rod length. Thus a total travel h has a lateral

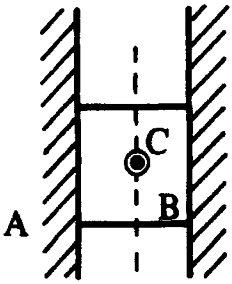

Figure 4.3.1. The slider.

path error $l(1 - \cos\theta)$ where $\sin\theta = h/2l$. This error is approximately $h^2/8l$, showing that the error grows with the square of the travel and inversely with rod length. For a Panhard rod with a practical length of 1 m, a suspension range of 0.2 m gives a rod angle of up to 6°, with an error of 5 mm. The second kind of error arises when the rod is not perpendicular to the desired path, this being equivalent to a misaligned channel in the slider-type mechanism. The influence of body roll is not as clear as in the case of the slider mechanism. Both roll and heave of the chassis will alter the height of the pivot, thus introducing errors of the second kind. Also, the consequences of roll are not symmetrical since the pivot, normally being on one side of the chassis, will rise or fall according to direction of roll. The vertical motion of the pivot of a Panhard rod in roll is eliminated if the chassis pivot is on the vehicle centerline, but this is achieved at the expense of shortening the rod and increasing the curvature errors, and is therefore not normally chosen.

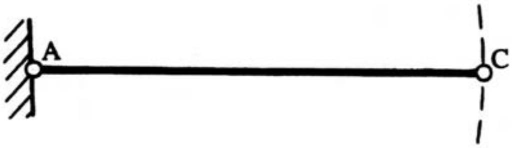

Figure 4.3.2. The Panhard rod (track rod).

A third type of straight-line mechanism is the Watt linkage (Figure 4.3.3). This may be perceived as a logical development of the radius rod, introducing compensating errors. As the link BCD rises or falls, the two equal links AB and DE rotate in opposite senses; C at the mid-point of BD adopts a mean position, resulting in a remarkably good straight line. The errors depend on the length of the short vertical link, as does the total limiting range of vertical motion. For suspension purposes there is negligible error for about half of the total vertical travel, or over a total range of about one-quarter of the total mechanism width, neatly encompassing practical requirements of axle lateral location if the full available width between the wheels is employed. The range of travel can be increased by angling BCD to lengthen AB and DE, the spacing of A to E remaining constant. Beyond about 30°, however, the linearity begins to deteriorate.

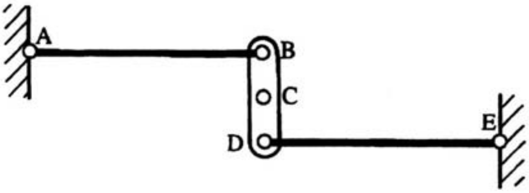

Figure 4.3.3. The Watt linkage.

The Watt linkage can be generalized somewhat; it is not essential for the arms AB and DE to be of equal length provided that C is located at the appropriate point along BD to optimally compensate the errors. Simply stated, C must be nearer to the longer arm, where:

$$\frac{BC}{CD} = \frac{DE}{AB}$$

Alternatively, it is possible to have both arms on the same side of the vertical link (Figure 4.3.4). To retain the error compensation, C must now be on the opposite end from the short link, with the above proportions still applied. This layout often appears in the side elevation of rear-axle locations, and also in the front elevation of independent suspensions, although in this context its relationship to the Watt linkage usually passes unremarked. Where ground clearance is not important, it can be used for solid-axle lateral location to give a low roll center, and has been used in this way as a modification in racing.

A fifth kind is the Roberts straight-line mechanism (Figure 4.3.5). Once again, this can be considered in terms of compensating errors. As C moves up or down, the inclinations of AB and CB to the horizontal are kept approximately equal. For good results, AB, BC, CD and DE should be equal in length and at equal angles to the horizontal in the middle position. Then C is exactly on AE, and also passes directly through A and E. It has very little error over the whole range A to E provided that the initial link inclination θ is kept below about 25°. Thus links of about 300 mm length at 20° will secure a very good motion over

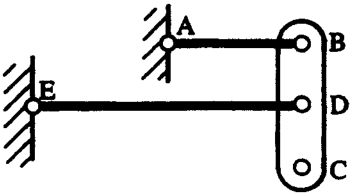

Figure 4.3.4. The modified Watt linkage.

an adequate practical suspension range. Its main problem is the need to provide a low fixture at E; nevertheless it has found application in racing.

This mechanism provides a useful cautionary tale. The instantaneous center F for the triangular plate is easily found by the usual construction of Figure 4.3.5, projecting AB and ED, because B must move perpendicularly to AB so the centro is on AB projected. Thus it is sometimes remarked that this mechanism is equivalent to a Panhard rod of length CF. This is incorrect; the path for a radius rod CF is a very poor competitor to the straight line obtained with the true mechanism. This difference arises because the instantaneous center itself moves as the mechanism moves; indeed the reason for the good straight line is that the centro F keeps pace with C as the latter moves. This keeps CF closely perpendicular to AE so that at every instant the motion of C, perpendicular to CF, has little or no component perpendicular to the desired path AE, which is not the case for the supposedly equivalent radius rod. The truly equivalent radius rod for a given motion must therefore be derived with some caution; this will be relevant later when discussing widely used concepts such as the "equivalent swing arm" for independent suspensions.

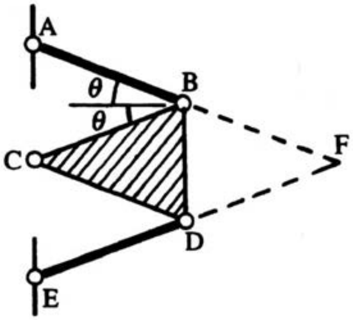

Figure 4.3.5. The Roberts linkage.

The Tchebichef straight-line mechanism (Figure 4.3.6), has a much more limited useful range; C takes the mean lateral position of B and D, which have compensating motions. The Evans mechanism (Figure 4.3.7), in which the inclinations of CD and DE compensate, looks reasonably practicable. The Aston Martin linkage of Figure 4.3.8, which has been used successfully despite its complexity, is well suited to the space that is available adjacent to an axle, and shows how symmetry can be used to obtain a true straight line. The plate FCJ is preferably fixed to the body. Links GK and HK ensure that BFG and DJH, which pivot on FCJ at F and J, must remain symmetrically positioned on FCJ. In a simplified version, G and H are directly linked, necessary compliance being provided by a rubber bush or a simple slot.

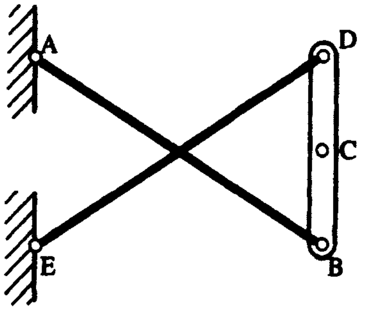

Figure 4.3.6. The Tchebichef linkage

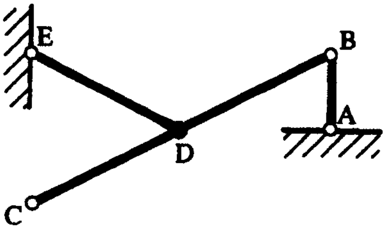

Figure 4.3.7. The Evans linkage

Figure 4.3.9 shows a close relative of the last one, the Mumford linkage, used on Mallock racing cars. Here BFG and HJD are still pivoted on the body, but symmetry is abandoned allowing the simple connecting link GH. Also, by inclining the links AB and DE, a lower roll center is obtained.

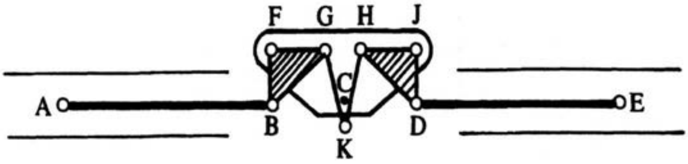

Figure 4.3.8. The Aston Martin linkage.

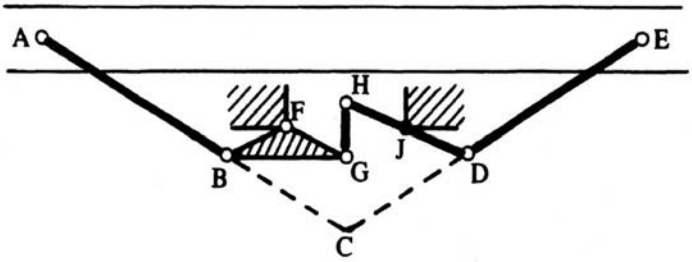

Figure 4.3.9. The Mumford linkage.

Figure 4.3.10 shows the Adex mechanism, which was used in the 1920s and was particularly suited to the chassis construction of that period. Here, DE and EB act to keep B and D symmetrical about the centerline, and BC and CD therefore keep C in the center.

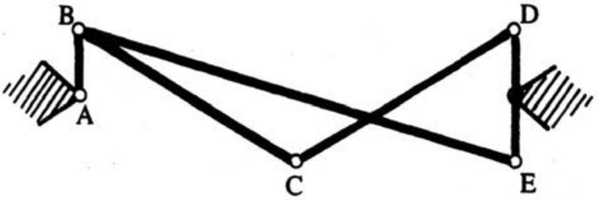

Figure 4.3.10. Adex linkage.

A last example: Taking advantage of the third dimension admits a further solution, the Alfa-Romeo T-bar (Figure 4.3.11), in this case shown in plan view instead of rear view; the locus is a true straight line in rear view, but does have curvature in the side view.

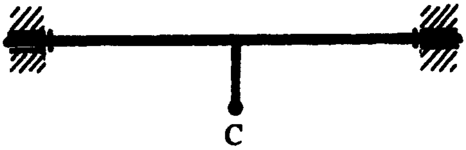

Figure 4.3.11. Alfa-Romeo T-bar (plan view).

4.4 Two-Dimensional Analysis

This section presents a simple analysis of two-dimensonal suspension-like mechanisms. In this case the "wheel" must have one degree of freedom relative to the chassis structure, for vertical motion. This suggests two particularly simple suspensions: a slider and a single pivot (Figure 4.4.1). The slider corresponds to the pillar suspension, now practically extinct. The instantaneous center for the wheel and body is, in this case, at infinity on a line perpendicular to the slider direction. The pivot corresponds to the swing axle, for which the centro is at the pivot.

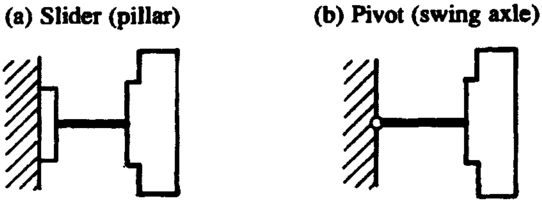

Figure 4.4.1. 2-D suspension.

If we allow the wheel an extra degree of freedom by adding a pivot at the outer end of the swing-axle pivot arm, then an additional radius rod may be added (Figure 4.4.2), corresponding to the three-dimensional two-wishbone (two-A-arm) suspension. The centro of the wheel relative to the body is in this case at the intersection of the radius arm lines, at infinity if they are parallel. Alternatively, a trunnion may be added (Figure 4.4.3); this gives the equivalent of the strut-type suspension. In general the strut slider does not align with the lower outer pivot. It usually does align with the trunnion top pivot, although it need not do so. To find the centro of the wheel relative to the body, the correct radius line for the trunnion is the line perpendicular to the slider line AB and passing through the top pivot point A; the centro of the wheel motion relative to the body is where this line meets CD extended. This should be distinguished from the steering axis, which is line AC that goes from the trunnion point A down to the radius arm outer ball joint C.

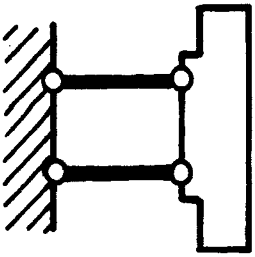

Figure 4.4.2. 2-D suspension using two rods.

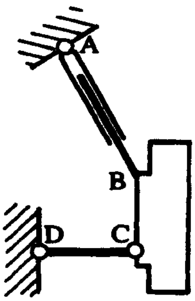

Figure 4.4.3. 2-D suspension using one rod plus one trunnion.

This range of four suspension types realistically exhausts the elementary geometric types within two dimensions. These suspensions can be divided into two types: those in which the location is through a single member (pillar and swing axle), and those in which there are separate upper and lower locations (the double link, and the trunnion with link). The last two types, although somewhat more complex, do permit a much wider choice of location of instantaneous center. Of course, more complex systems can be devised since there is no limit to the number of links in a mechanism having one degree of freedom.

4.5 Independent Systems

In the full three dimensions, an unconstrained object has six degrees of freedom: three of translation and three of rotation. Relative to the chassis, a wheel has two degrees of freedom for a given steering position. One of these is rotation corresponding to normal rolling. The other is for the vertical action of the suspension. The wheel carrier has only one degree of freedom when the steering is fixed. Since an entirely free object has six degrees of freedom, it is necessary to provide constraints to remove five degrees of freedom from the carrier, including the constraint of the steering.

Figure 4.5.1 outlines some constituents of the appropriate constraints. It is convenient to consider these to be built-up in the following way. A spherical (ball) joint (a) allows three degrees of freedom. A radius rod (b), ball-jointed at each end, allows five degrees of freedom, i.e., constrains one degree. The only constraint of such a radius rod on the two objects that it connects is that it prevents relative motion directly along the rod. Two such radius rods will constrain two degrees of freedom. These two rods can be connected together to form a wishbone or A-arm. How the names derived from the shape is visible in Figure 4.5.2, but they are now used interchangeably, with the term "A-arm" favored in U.S. while "wishbone" is used in U.K. The wishbone constraint results in one point on member D being constrained to move in an arc about an axis through the two spherical joints on A, leaving D four degrees of freedom. The same result is obtained by a pivot arm that is ball-jointed to the carrier (Figure 4.5.2(c)). The term wishbone will be used generically for wishbones and A-arms, and pivoted arms with a ball-joint at the end. On the other hand, if member D is simply pivoted directly on member A, equivalent to locking the three degrees of freedom of the spherical joint on D, then only one degree of freedom remains. Evidently this gives a complete suspension unit, i.e., the wheel carrier has a "rigid arm" (as opposed to a wishbone) that is pivoted only on the chassis, for example a trailing arm (Figure 4.5.3).

The wishbone and rigid arm are shown in Figures 4.5.1(c) and (d), respectively. The trunnion connection in three dimensions (e) provides two degrees of constraint – the inner slider (at its notional extended point next to the trunnion pivot) cannot move in either of the two directions perpendicular to the slider alignment. Thus the trunnion constrains two degrees of freedom. The universal joint (f) constrains plunge and rotation. The shaft spline (g) allows plunge but constrains rotation. The plunging universal joint (doughnut) (h) constrains rotation and radial motion in two directions. The sliding pivot (j) is free to slide and

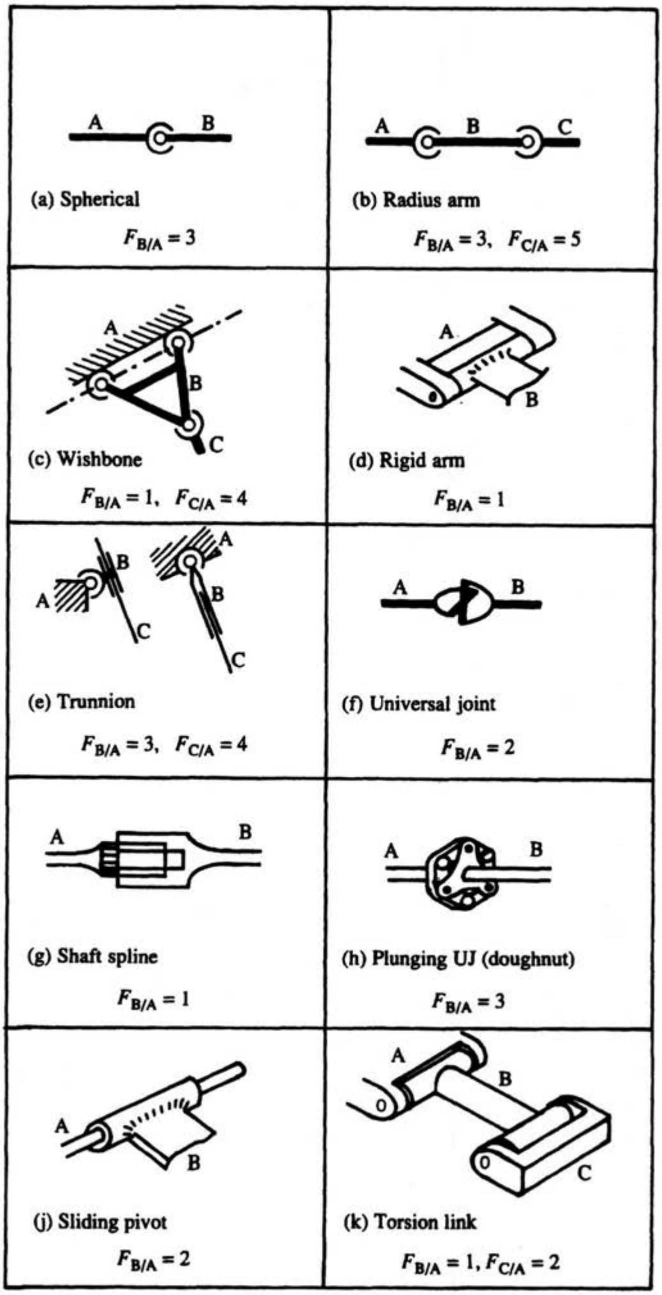
A
B
A
B
C
A
B
C
A
B
A
B
C
A
B
C
A
B
A
B
A
B
A
B
A
B
0
0
C

(a) Spherical

$F_{B/A} = 3$

(b) Radius arm

$F_{B/A} = 3, \ F_{C/A} = 5$

(c) Wishbone

$F_{B/A} = 1, \ F_{C/A} = 4$

(d) Rigid arm

$F_{B/A} = 1$

(e) Trunnion

$F_{B/A} = 3, \ F_{C/A} = 4$

(f) Universal joint

$F_{B/A} = 2$

(g) Shaft spline

$F_{B/A} = 1$

(h) Plunging UJ (doughnut)

$F_{B/A} = 3$

(j) Sliding pivot

$F_{B/A} = 2$

(k) Torsion link

$F_{B/A} = 1, F_{C/A} = 2$

Figure 4.5.1. Various suspension elements.

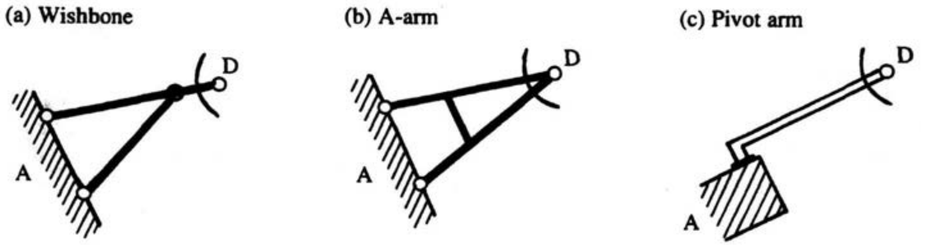
(a) Wishbone

(b) A-arm

(c) Pivot arm

Figure 4.5.2. Plan views: (a) wishbone, (b) A-arm, (c) pivot arm.

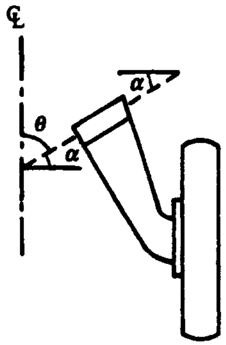

Figure 4.5.3. Rigid semi-trailing arm.

rotate. The torsion link (k), a torsionally rigid link between two pivots, removes four degrees of freedom.

The above classification makes it possible to list the practical range of simple independent suspension types. The practical combinations to constrain five degrees of freedom are presented in Table 4.5.1, showing the constraints in brackets.

It is of course necessary that all alignments are appropriately made so that no members are geometrically redundant. Also, the list is not exhaustive. The twin-trunnion plus rod, for example, is certainly possible, even if unlikely in practice. More complex combinations are, of course, always possible.

Table 4.5.1 Practical Link Combinations

	Combination	Degrees of freedom
(1)	Rigid arm	(5)
(2)	Two wishbones + 1 rod	$(2 \times 2 + 1)$
(3)	One wishbone + 1 trunnion + 1 rod	$(2 + 2 + 1)$
(4)	One wishbone + 3 rods	$(2 + 3 \times 1)$
(5)	One trunnion + 3 rods	$(2 + 3 \times 1)$
(6)	One torsion link + 1 rod	$(4 + 1)$
(7)	Five rods	(5)

The directly pivoted carrier, i.e., the rigid arm of Figure 4.5.3, does not admit the possibility of steering, but is widely used at the rear for both front- and rear-wheel drive. It is mainly characterized by the pivot angle θ to the vehicle centerline. If θ is 90°, it is a plain trailing arm. If θ is 0°, it is a transverse rigid arm, sometimes loosely called a swing axle. In the particular case that the axle, with no plunge freedom, forms part of the arm, then it is a true swing axle. Intermediate values of θ, mostly in the range 15° to 30°, give the semi-trailing arm.

The twin wishbone plus rod suspension is widely used for the front, with the rod controlling the steering. The wishbone pivot axes are usually roughly parallel to the car's centerline. However, pivot axes perpendicular to the centerline give the twin trailing arm (e.g., VW Beetle). There have even been cases of perpendicularity of the two axes in plan view (e.g., Rover 2000). Twin wishbones at the rear is unusual on road vehicles. The all-around wishbone system is the classic and universal method adopted for purpose-designed racing cars in recent years

The combination of trunnion and wishbone is widely used at the front, and is continuing to gain in popularity. This includes the classic Macpherson strut, in which the front member of the effective wishbone is the lever of the anti-roll bar.

The use of a trunnion at the rear is relatively unusual, again tending to be restricted to vehicles aspiring to particular handling qualities. A trunnion plus three rods has been used in some cases. One interesting special case is the Chapman strut, where one of the rods is provided by the fixed-length driveshaft.

Where a wishbone is used at the rear, the wishbone plus toe-control rod can become difficult to distinguish from three rods (Figure 4.5.4). Types (c) and (d) are often referred to as reversed wishbones, since the pivot axis of the "wishbone" is on the wheel carrier rather than the chassis.

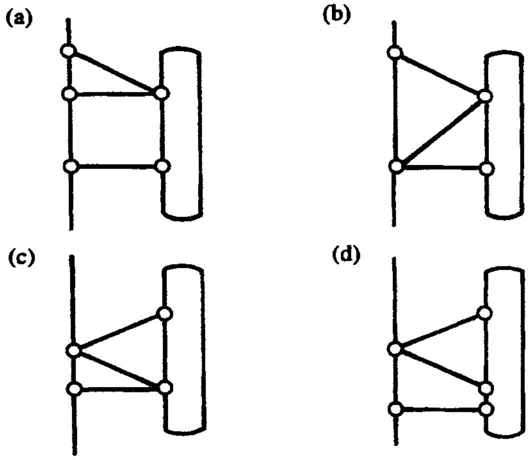

Figure 4.5.4. Rear wishbone plus rod, plan views.

The torsion link plus rod has been used at the rear, with the torsion link below and the fixed length driveshaft acting as the extra rod. In practice the torsion link has inadequate stiffness against tractive forces, so it is supplemented by an additional link forward from the hub.

The five-link independent suspension has only recently come to fruition. It offers the possibility of achieving certain desirable load–distortion properties that will be discussed later. In general, its geometric behavior requires computer analysis. The other systems can be considered as special cases where simple relationships among the links permit a comprehensible analysis. Although the moving two-dimensional body always has an instantaneous center (in a given coordinate system) even if this is at infinity, the motion of a three-dimensional body does not necessarily reduce to rotation about an instantaneous axis – there is in general an axial velocity left in addition to the rotation. In a number of practical suspensions, however, the linkage system is such that there is an instantaneous axis of rotation for the wheel carrier. Generally, this is so if all motion is parallel to a single plane. This is always true for the rigid arm. It is also true for double wishbones provided that the pivot axes are parallel (and that the toe-control rod is in sympathy). Steering permitting, it will be approximately true for the trunnion and wishbone because the trunnion will behave as the notional infinite wishbone with its axis parallel to the bottom wishbone axis.

4.6 Dependent Systems

A dependent (i.e., non-independent) system is one in which the location of one wheel depends in a direct way on its partner on the other side. The dependence must be essentially geometric – an anti-roll bar on an independent system is not considered to make it dependent.

In the normal dependent system, i.e., the axle in its narrower sense, the wheel carriers are rigidly connected together so that the whole can be considered as one unit. Axles are broadly divided into three kinds:

(1) The dead axle – used at the rear with front drive, having undriven wheels.

(2) The live axle – has driven wheels and carries the differential in an integrated unit.

(3) The de Dion axle – has driven wheels but does not carry the differential.

Live and de Dion axles have more stringent location requirements, particularly for rigidity to avoid large displacements or large-amplitude axle vibrations when tractive forces are applied.

The axle must have freedom to heave and roll relative to the body, hence requiring two degrees of freedom, i.e., a four degrees-of-freedom constraint. This can therefore be achieved by four radius rods (Figure 4.6.1(a)). It is common practice to introduce an extra link to provide two links above the axle (Figure 4.6.1(b)). Although this is geometrically redundant, it affects the stiffness and hence the response to forces. The Panhard rod lateral location of Figures 4.6.1 (a), (b) and (c) can, of course, be replaced in any of these examples by an alternative such as a lateral Watt linkage. The upper longitudinal links can be turned around to also give the Watt type linkages (Figure 4.6.1(c)). Alternatively the two top links can be angled to provide lateral location, thus eliminating the need for the Panhard rod and reducing the number of links back to four (Figure 4.6.1(d)).

This upper link pair is sometimes formed into a single wishbone, or a T-bar. The lower links may also be inclined inward (Figure 4.6.1(e)). There are several systems using a single front ball-joint (three degrees of constraint), plus a lateral location. These may be wide-based at the rear (Figure 4.6.1(f)), or the so-called "torque tube" (Figure 4.6.1(g)), a singularly unfortunate name since it does not resist significant engine torque except on those rare cases where it is mounted rigidly to the engine unit, but does oppose axle pitch.

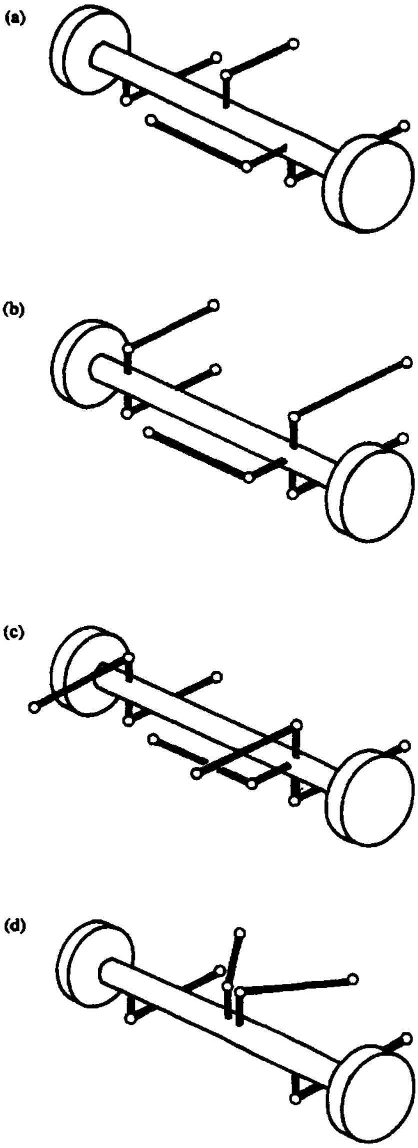

Figure 4.6.1. Axle location systems.

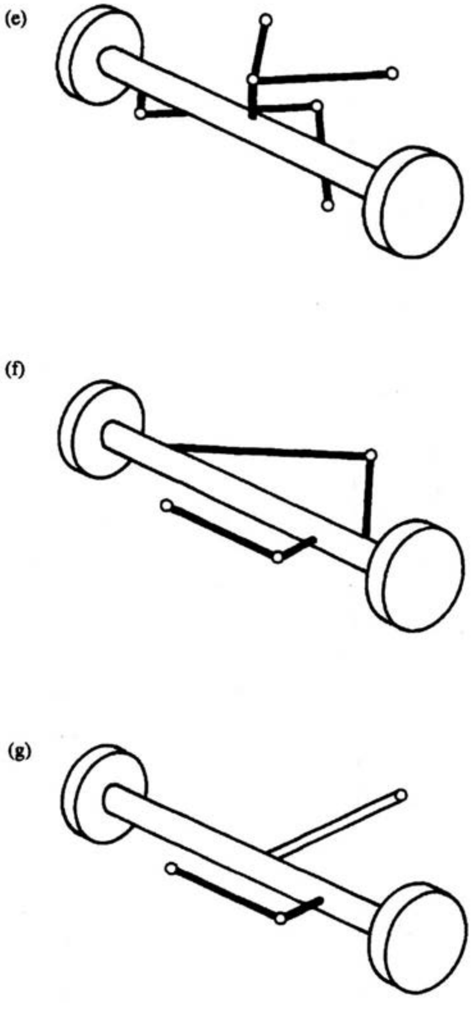

Figure 4.6.1. Axle location systems (continued).

As these examples show, the lateral location of an axle may be achieved as part of the function of a convergent link pair (or pivot arm), or by a dedicated system such as a Panhard rod. The sliding block and channel gives an accurate straight-line path, but there are large lateral forces so it has substantial friction and consequently also wears, although a roller-bearing system might resolve this.

The depth of channel, which must be significantly greater than the total axle movement, would be inconvenient in many cases. The Panhard rod is simple and easily adjustable for suspension tuning, although it gives a relatively poor straight line. It is a likely choice at the rear for a front-wheel-drive vehicle, where it has been demonstrated to be highly successful (Alfa Sud, Saab). However, for rear-wheel drive it does not seem to be so satisfactory, and then one is more likely to find good handling where there is a Watt linkage. The Alfa-Romeo Giulia series used a T-bar with success, although this was later abandoned in favor of the Watt linkage, possibly to achieve a lower roll center. The Roberts mechanism offers good straight line accuracy and is compact laterally, but rather deep. It has found use on some competition cars but does not seem to have found application in quantity production.

4.7 Compliant Link Systems

Although not a new idea, semi-dependent systems have recently come to prominence, particularly at the rear of small front-drive vehicles. Figure 4.7.1 shows a trailing twist axle in which an essential variable is the position of the transverse connecting member. This transverse member is rigid in bending, hence locating the wheels in plan view, but it has torsional compliance, allowing roll and acting as an anti-roll bar. Independent (trailing arm) and dependent (beam axle) represent two particular extreme cases of a continuous range of trailing twist axles. The camber angle of the wheels in single-wheel bump (or when the body is rolled) depends on the geometry and rigidity of all the members. With the cross beam behind the wheel centers it is even possible to camber both wheels into the corner.

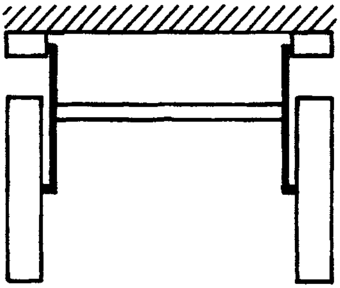

Figure 4.7.1. Trailing twist axle (plan view).

Leaf springs are capable of providing location in both directions perpendicular to the direction of maximum compliance. The use of leaf springs has been reducing over the years on passenger vehicles, although the Hotchkiss drive (live rear axle plus two leaf springs) has been persistent and is still popular on commercial vehicles. New materials such as glass-reinforced plastics for the leaf springs may give it a new lease on life. Two example applications will be considered here: first a cantilever ("quarter elliptic"), and second a typical rear-axle location by a beam spring ("half elliptic") on each side. The term "elliptic" stems from stagecoach days when curved back-to-back beam springs were indeed roughly elliptical. Terms such as semi-elliptic and quarter-elliptic are really misleading because in practice there may be little or no curvature visible.

The cantilever type is exemplified by the front transverse multi-leaf beam clamped rigidly at the center, since this acts as two independent cantilevers. It was also adopted by Bugatti for rear-axle location as a leading arm, presumably for reduced unsprung mass. Since the leaf spring is designed, approximately at least, for uniform surface stress, the radius of curvature under load is roughly constant along its length, while the length itself is hardly changed at all. The geometrically equivalent radius arm length is approximately $0.75l$. The cantilever form finds little application today; it has been superseded by separate geometric location, with a coil spring.

The leaf spring has survived longer at the rear as a complete beam (Figure 4.7.2(a)), in this case often initially curved and with a shackle (short radius arm) at the rear to permit effective length changes. Equivalent linkages can be constructed usually based again on a constant radius model, typically as Figure 4.7.2(b), where the center link remains horizontal. Evidently the equivalent linkage is highly dependent on the particular application. If the leaf is very rigid in front of the axle (a common modification in sedan car racing), then the equivalent linkage is effectively a simple trailing arm with a spring applied at the rear.

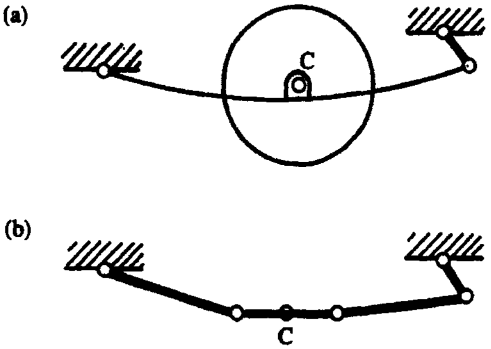

Figure 4.7.2. Full leaf spring and equivalent linkage.

4.8 Spring Types

Springs are components designed to have a relatively low stiffness compared with normal rigid members, thus making it possible to exert a force that varies in a controlled way with the length of the member. Springs are generally classified according to the material used and the way that the forces and corresponding stresses occur. As far as vehicle handling is concerned, it is the apparent properties of the "spring unit" that matter, i.e., force, stiffness, inertia, friction, etc., as felt at the wheel, rather than the precise way in which those results are achieved. Therefore the choice of a springing medium, such as nitrogen, rubber or steel, does not in principle pre-empt the achievement of any particular handling qualities. The wide range of systems in practical use today shows that no overwhelming advantage has been demonstrated for any particular type of spring.

The most obvious first decision is that of the state of the springing medium: solid, liquid or gas. A gas is of course highly compliant, and therefore little mass is required for a given energy storage. Even when the necessary associated containers are included, it is competitive. Typically, nitrogen is used at about 2.5 MPa. Of course, most vehicles are already fitted with four air springs: the tires. Among liquids, oil is relatively compressible and is used in aircraft oleo legs, but is not favored for normal ground transport. Water and water–alcohol mixtures have a relatively small compressibility and are therefore not used as the actual spring medium, although they are commonly used as the working hydraulic fluid for force transfer to a rubber spring, e.g., hydrolastic, or to a gas spring, e.g., hydragas.

Among solids, rubber is pre-eminent in offering a high natural compliance. Indeed, new synthetic materials with high compliance are usually described as rubber, so this is perhaps better seen as a definition of the term "rubber." In order to achieve the extreme fatigue life necessary, rubber is best used in a combination of shear and compression.

For metal, the stiffness in direct compression and tension is very great, so bending or torsion is used. The beam spring (i.e., in bending – the leaf spring) has a rectangular-section bending stiffness of $ab^3E/12$ where b is the dimension perpendicular to the bending axis, and E is the material normal stress modulus (Young's modulus) – about 205 GPa for steel. Figure 4.8.1 is the bending-moment diagram of a typical leaf spring and shows that the strength requirement varies considerably along the beam. Since it is desirable to use a thin beam (small b rather than small a) to give the required compliance, the best shape is a diamond, i.e., one that has a width in proportion to the bending moment, but of constant section depth. This also has excellent rigidity against side forces, i.e., bending about the other axis. Because of the likely inconvenience of the great width at the center, it is usual to "slice up" the diamond shape and to place the slices on top of one another. The bending stiffness in the normal load direction is the same. It is reduced for transverse loads, but still higher by a factor $(a/b)^2$. The bending stress distribution means that the material near the centerline of each leaf is hardly stressed; the leaf is, in practice, too thin to take advantage of the I-section shape prevalent among deeper structural beams. All of the above comments also apply to the cantilever spring, which can be considered to be one-half of a beam spring.

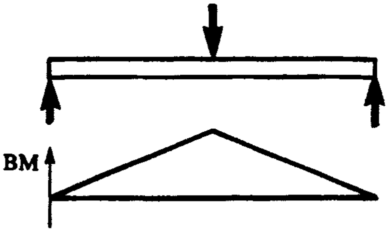

Figure 4.8.1. Bending-moment diagram of beam (leaf spring).

A more efficient utilization of material is achieved by a torsion bar, because with the circular section the bulk of the material is nearer the edge, and is operated nearer to the highest stress. A hollow section may be used, eliminating the relatively understressed core. Controlled overloading and yielding can modify the working stress distribution usefully for solid bars. This reduces the surface stress and hence improves the fatigue life. The angular displacement under a load torque is

$$\theta = \frac{TL}{JG}$$

where G is the shear modulus (80 GPa for steel) and J is the polar second moment of area,

$$J = \frac{1}{2}\pi r_0^4 - \frac{1}{2}\pi r_i^4$$

for a concentric tube. For a solid rod, r_i is zero, and the torsional stiffness varies as the fourth power of diameter.

The coil spring is essentially a coiled torsion bar, as may be seen by observing the loading on a cross-section of the spring wire. As a complete unit it is generally loaded in compression for suspension applications. For a load of this kind, the deflection is given approximately by

$$x = \frac{8FD^3N}{Gd^4}$$

where F is the force magnitude, D is the coil diameter between centers, N is the number of working turns, G is the shear modulus and d is the wire diameter. The stiffness is

$$K = \frac{Gd^4}{8D^3N}$$

Thus the stiffness depends on the fourth power of the wire diameter, and varies inversely with the cube of the spring diameter and inversely with the number of working coils.

The coil spring generally has rather little stiffness laterally and in bending, although these may cause some increase of the effective stiffness for suspension geometries that give large angular changes at the spring seats. The performance of the spring is sometimes varied by designing it with varying coil spacing, varying coil radius or varying wire diameter, so that the spring progressively closes, reducing the number of working turns and increasing the stiffness.

The modern high-quality coil spring is produced on complex automatic machinery. The leaf spring, in contrast, is relatively easily manufactured without special facilities, and this, coupled with the fact that it also provides fore and aft, lateral and pitch angle axle location very cheaply, was the reason for its very widespread use in the early days of motoring. Although the steel leaf spring is generally regarded as rather heavy and inferior to a link and coil system, the use of glass-reinforced plastic leaf springs offers possible weight savings and has resulted in a new interest in this old design. Transverse glass-reinforced plastic (GRP) beam springs with link location have recently been used on a production sports car.

4.9 Spring Linkage Geometry

The spring can be brought to bear on any moving part of the suspension. For the wishbone and trunnion suspension, it is natural to place a coil spring around the trunnion unit, as for example on the Macpherson strut, although the spring is sometimes placed elsewhere. For the double wishbone, common at the front, the spring usually operates on the lower arm since this is more compact overall. When this space is occupied by a driveshaft, the spring can act on top of the upper arm. For many years purpose-designed racing cars usually had the spring unit attached diagonally, acting at the outer end of the lower wishbone. The era of ground-effect aerodynamics called for a reduction in drag and turbulence from the front, so rocker arms, pullrods and pushrods, combined with internal springs, became more popular. For a rigid arm, such as a typical rear trailing arm, the spring unit may operate down on the arm, or is sometimes placed horizontally, acting on a tongue.

In general the spring compression or extension is different from the wheel displacement, and their ratio is not constant. The force at the spring is generally greater than that at the wheel, but because the required range of motion is correspondingly reduced, the energy storage and hence the material requirements of the spring are not dependent on the ratio. The wheel motion ratio may be expressed either as the motion at the spring divided by that at the wheel, or as the motion of the wheel divided by that at the spring. The former will be used here. To achieve a given effective suspension stiffness at the wheel, the spring stiffness required depends on the motion ratio squared. In practice, the motion ratio may be far from constant, and this may be done deliberately to give a rising rate suspension, i.e., an effective stiffness that increases as the wheel rises.

Neglecting detailed arrangements which may have some secondary influence, for example through rubber bush distortion, the important parameters for handling analysis are the force at the wheel and the stiffness at the wheel, which is usually called the wheel rate. It is sometimes considered desirable for the wheel rate to increase as the wheel rises, i.e., for the force to increase nonlinearly, so that when heavily loaded the vehicle has increased wheel rates. This may be achieved by the characteristics of the spring unit. Gas and rubber springs have this kind of behavior due to the material itself. Steel coil springs can do so if the coils are unevenly spaced, or if the wire diameter is tapered, so that they close up progressively. Leaf springs do so if initially curved so as to be separate. Alternatively, it may be achieved through a variable motion ratio of the linkage by having an increasing moment arm for the spring as the wheel deflects. The latter method is more amenable to adjustment and control, and can also give progressive damping.

The use of torsion bars for basic springing requires that space be found for the long bars. This length can be reduced by using a compound rod, i.e., a rod in a tube, fixed together at one end. Alternatively several thin rods in parallel can be used. The rod may be mounted anywhere and connected to the geometric links by a "drop-link" – a short radius rod. In practice there are two typical installations. First, a bottom wishbone (front suspension) will be splined directly to the torsion bar which lies parallel to the vehicle centerline. Second, the rod is transverse, and splined to a trailing arm (rear) or a wishbone with transverse axis (front).

Whatever the means of providing springing, to find the effective force at the wheel generally requires some analysis. For coil spring or equivalent units, the extent of spring compression must be found from a series of position diagrams. The effective spring rate at the wheel for any particular position is related to the actual spring force by the mechanical advantage. If friction is neglected, or dealt with separately, then the mechanical advantage and the motion ratio are reciprocal and may alternatively be found by constructing a velocity diagram. This process can be computerized, of course. This is reasonably easy in two dimensions, but a considerable task in three dimensions if general designs are to be handled. The analysis requires not only the solution of intersecting spheres and circles, and so on, but some logical process to select between alternative solutions to quadratic equations.

There may be some secondary contributions to stiffness. The distortion of rubber bushes is one, adding perhaps 10% to the wheel rate. This can be calculated for some cases, such as simple cylindrical bushes in rotation. Another source of force is the pressurized gas-filled damper. The typical pressure of 2.5 MPa, acting on the piston-rod cross-sectional area, may exert a force of about 200 N which will raise the suspension a few millimetres. This pressure is, however, not highly dependent on position, so the effect on suspension stiffness is small.

Inevitably there are limitations on the possible movement of any suspension. If no explicit provision has been made, then eventually there will be metal-to-metal contact between suspension arms and body, or the wheel will strike the body, or the spring will become coil-bound. In view of the harshness of such occurrences to both passengers and vehicle, it is normal to provide bump and droop stops which soften the final blow. These are usually in the form of a molded rubber block which is squeezed between a suspension arm and the body at an appropriate point.

It is sometimes not possible to provide such a stop, for example for an axle in droop. In such a case the dampers are sometimes allowed to define the limit, or straps may be used.

4.10 Roll and Pitch Springing

The provision of stiffness has so far been examined in the context of a single wheel. However, the position of the body in relation to the road, as far as suspension location is concerned, should also be considered. It is essentially one of heave, roll and pitch.

Body roll is geometrically equivalent to the raising of one wheel and lowering of the other one, while heave is equivalent to equal motion of the two wheels in the same direction. Thus, for conventional suspension, springing at each wheel will contribute to both body heave and body roll stiffnesses. However, the resulting values may not be as required; it may be desired to have more roll stiffness without increasing the heave stiffness, or sometimes vice versa. This can be achieved by appropriate spring design and coupling.

A zero roll-stiffness suspension may be produced by arranging for roll to have no effect on the springs. Figure 4.10.1 shows one example; the spring is connected only to the two parts of the axle, not to the body. The transverse leaf spring can be given this characteristic if provided with a central pivot. The illustration shows a swing-axle type suspension, but equivalent systems for more advanced independent systems or for true axles are easily devised. The use of a swing-axle illustration is in fact appropriate, because they do generally benefit from the use of only a small roll stiffness to reduce load transfer which causes problems for this type of axle. Another possibility is the Z-bar (Figure 4.10.2). Provided that the two lever arms are equal and the suspensions are symmetrical, there is no roll stiffness. The positioning of the body pivots for the Z-bar is not critical but they should be well spaced and symmetrically disposed about the vehicle centerline. Its operation is best imagined by considering the Z-bar rotating – one wheel rises, the other falls; this is equivalent to body roll. Body heave causes opposed motions of the end levers, putting the center section into torsion. Hence the Z-bar gives heave stiffness with no roll stiffness. In practice a zero roll stiffness system is likely to be combined with conventional springing to give the desired overall combination of properties.

It is also possible to devise elements that provide stiffness in roll only, with no heave stiffness. In practice, one particular type is used more-or-less exclusively – the anti-roll bar (Figure 4.10.3). It is a direct corollary to the Z-bar; although shaped as a U it is rarely called a U-bar. The end levers must be of equal length with symmetrical suspension, or a heave stiffness results. Again, in practice the anti-roll bar is combined with conventional springs to give the desired overall properties.

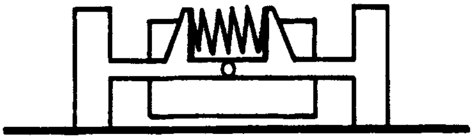

Figure 4.10.1. Zero roll-stiffness suspension (rear view).

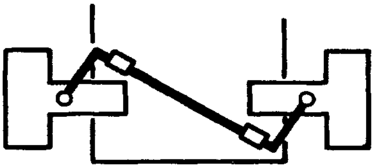

Figure 4.10.2. Z-bar of no roll stiffness (plan view).

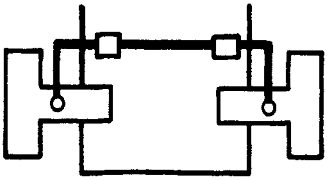

Figure 4.10.3. Anti-roll bar with pure roll stiffness (plan view).

A combination of Z-bar and anti-roll bar can provide any required combination of heave and roll stiffness. In principle either one of them, using unequal lever arms, could provide a required combination, although this is not done. In practice, the usual requirement is for the roll stiffness to exceed that obtained from the springing selected for heave stiffness, so the use of anti-roll bars is common, combined with conventional springs. The opposite case, a requirement for particularly low roll stiffness, seems to be restricted to the virtually defunct swing-axle suspension, and that is where the Z-bar finds its primary evolutionary niche.

Because of their torsion and stiffness, longitudinal leaf springs have an anti-roll effect which can contribute typically 40% to the total body roll stiffness. If there is extra lateral location, for example a Panhard rod at a different height from the leaf springs, then the consequent lateral bending of the leaf springs can give considerable additional roll stiffness.

As will be discussed in more detail later, the distribution of roll stiffness between front and rear axles is used for adjustment of handling qualities. To control the limit handling balance, it is quite common on racing cars to have the roll stiffness at one axle adjustable by the driver without stopping. This is typically done by using an anti-roll bar with one lever arm of thin wide section that can be rotated to change its effective bending stiffness.

In contrast to roll, in pitch the basic springing tends to give rather a high stiffness for comfort, especially for small vehicles. Thus some fore-and-aft interconnection may be used in the furtherance of ride quality if not handling. The front-to-rear Z-bar has been used to provide basic heave springing, coupled with torsion-bar support for pitch springing, plus front and rear anti-roll bars. The transverse anti-roll bars have no effect on pitch or heave at all. Front-to-rear interconnection to reduce pitch stiffness is perhaps more easily achieved with hydraulic suspension systems.

Front-to-rear connection to increase pitch stiffness, for example by longitudinal U-bars, is not used on passenger vehicles. It has, however, been suggested for racing vehicles to reduce the pitching and associated wheel camber changes that are detrimental to braking with modern wide tires, and even more importantly to avoid shift of aerodynamic downforce, which is very pitch-sensitive on many racing cars.

4.11 Damper Types

The damper is commonly known as the shock absorber, although the implication that shocks are absorbed is misleading. Arguably, the shocks are "absorbed" by the deflection of the tires and springs. The purpose of dampers is to dissipate any energy in the vertical motion of body or wheels, such motion having arisen from control inputs or from disturbance by rough roads or winds. As an agglomeration of masses and springs, the car with its wheels constitutes a vibrating system that needs dampers to optimize control behavior by preventing response overshoots, and to minimize the influence of some unavoidable resonances. The mathematical theory of vibrating systems largely uses the concept of a linear damper – with force proportional to extension speed – mainly because it gives equations for which the solutions are well understood and documented, and usually tolerably realistic. There is no obligation on a damper to exhibit such a characteristic; nevertheless the typical modern hydraulic damper does so approximately. This is because the vehicle and damper manufacturers consider this to be desirable for good physical behavior, not for the convenience of the theorist. This characteristic is achieved only by some effort from the manufacturer.

Damper types, which are explained later, can be initially classified as friction (solid elements) or hydraulic (fluid elements), the latter being the only type fitted in recent times. The friction type came originally as sliding discs operated by two arms, and later as a wrapped belt, the "snubber." The hydraulic varieties are lever-arm and telescopic. The lever-arm type uses a lever to operate a vane, now extinct, or a pair of pistons. Telescopics, now most common, are either double-tube or gas-pressurized single-tube.

The history of damper development is virtually as old as that of the car itself. Before 1900, Paris cycle engineer Truffault invented a friction disc system of bronze and oiled hide pressed together by conical disc springs and operated by two arms with a floating body. Between 1900 and 1903, he developed a version for cars at the instigation of Hartford in the U.S., who began quantity production in 1904. In 1901 Horock patented a telescopic hydraulic unit, laying the foundations of the modern type, while in 1902 Mors actually built a vehicle which used simple hydraulic pot dampers. In 1905, Renault patented an opposed-piston hydraulic type, and also patented improvements to Horock's telescopic type, establishing substantially the design used today. Renault used the piston type on his 1906 Grand Prix cars but not on his production cars. Meanwhile Houdaille started to develop his double-arm vane type. Caille proposed the single-lever parallel-piston variety in 1907. In 1909 a single-acting Houdaille vane type was fitted as original equipment, but this was an isolated success for the hydraulic type, the friction-disc type remaining dominant. In 1915 Foster invented the belt "snubber" which had great commercial success in the U.S. The beginning of a turnaround to telescopics was the introduction by Lancia of the double-acting hydraulic unit incorporated in the front independent pillar suspension of the Aurelia in 1924. 1930 saw the issue of Armstrong's telescopic-type patent, and Monroe began manufacture of telescopics in 1934. In racing, at Indianapolis the hydraulic vane type arrived in the late 1920s and was considered a great step forward; the adjustable-piston hydraulic appeared in the early 1930s, but the telescopic was not used there until 1950. In 1947 Koning introduced the adjustable telescopic. The one remaining major advance was the gas-pressurized, single-tube telescopic, invented by de Carbon in the same period and manufactured from 1950.

Each damper type has some advantage, although the hydraulic, particularly telescopic, now reigns supreme. The simple friction-disc was light and cheap and easily adjusted, even remotely while driving. However, its characteristic is that of typical Coulomb friction, reducing with speed. It was sensitive to water or oil contamination, and it is not easy to arrange for controlled asymmetry of force. Perhaps it is fanciful to suggest that materials might be developed with a contact friction rising in a suitable way with sliding speed, although this is not *a priori* impossible. The Coulomb friction gives poor ride and handling by present standards, and there is little incentive to abandon fluid dampers, so the friction-disc damper seems to be defunct.

The belt snubber was a strap wrapped around a pair of spring-loaded wooden blocks and fixed to one of them. Release of tension allowed the block to expand to take up slack. Pulling the strap gave a tension presumably governed by the usual exponential function for wrapping members as applied to drive belts, ropes on bollards and the like. Thus it was single-acting, on rebound only, although still not speed-dependent. SAE defines the term snubber to mean any type of damper using Coulomb friction. It seems unlikely that snubbers will return for basic wheel damping.

Of the hydraulics, the vane type is seriously disadvantaged by the long seal length at the vane edges, giving wear problems, and seems to offer no adequate compensating advantages. This leaves those types based on motion of one or more pistons in cylinders. There are various possible configurations, since all that is fundamentally needed is to move the fluid through a restriction. They fall into two distinct categories: the lever type with two pistons, and the telescopic with one piston. The lever types are opposed piston, parallel piston, and parallel piston operated by involute cams. In practice, to provide different bump and rebound characteristics, two passages and two restriction control valves are generally provided. If the fluid, after its pressure drop, passes directly into the other cylinder, which is the normal arrangement, the same fluid is continuously re-used so good heat transfer around the passages is important to keep temperatures under control. This problem is eased if the fluid is exhausted to the reservoir above the pistons, giving a general circulation, but demanding high-flow replenishment circuits. The small fluid-circuit volume means that lever dampers are sensitive to gas in the circuit, but fortunately the body is mounted to the vehicle sprung mass and the fluid circuit is normally isolated below the pistons, so aeration is minimized.

The telescopic types (Figure 4.11.1) are most easily understood in reverse order of invention. The arrows shown indicate the fluid flow direction when the valve is restricting the flow in a controlled way. The emulsified type (Figure 4.11.1(a)), is simply a piston and rod in a fixed-volume cylinder full of an emulsion of oil and gas (nitrogen). The gas separates out when the car is parked, but re-emulsification is achieved quickly and therefore separation does not seem to be a problem. The piston contains two valves, one that controls the pressure differential across the piston during bump, and the other in rebound. These are calibrated appropriately for the emulsion, not pure oil. During bump (compression) an increasing volume of the piston rod is contained in the cylinder; this causes a pressure rise, and is the reason why it is necessary to have some gas present. This pressure exerts a force on the piston-rod area, trying to expand the damper. Alternatively, the anti-emulsion single-tube damper has the gas separated at one end by a floating piston. Otherwise the function is similar. For these single-tube types there is little problem of reduced effectiveness in sustained use, even on quite rough roads. Hence they are popular in rallying and off-road racing.

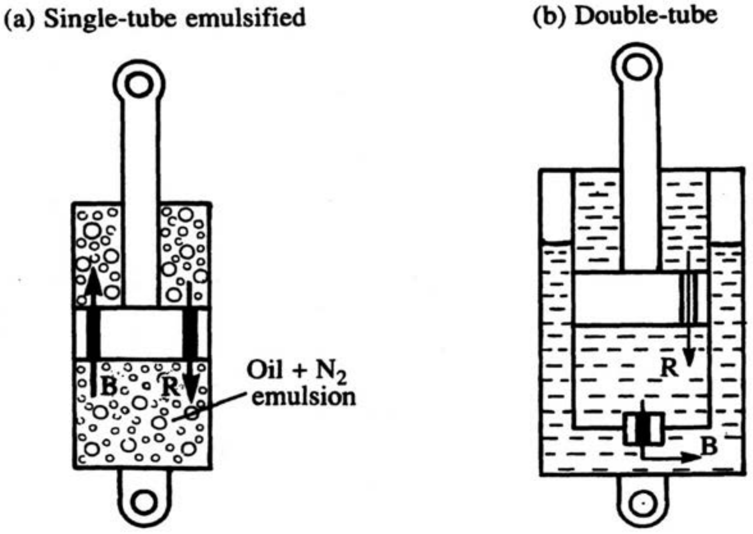
(a) Single-tube emulsified

(b) Double-tube

Figure 4.11.1. Telescopic dampers.

The remote reservoir anti-emulsion type reduces the need for a gas separator piston, especially if the reservoir is chassis-mounted and connected by flexible tubing. This may help cooling in difficult conditions. Arranging the reservoir as an annulus around the main working cylinder gives the double-tube type (Figure 4.11.1(b)). This type is inherently poorer at cooling, although it is improved by arranging some circulation from the top of the inner tube out into the reservoir during rebound. All other types can be mounted upside-down with the lighter piston-rod end on the wheel.

The telescopic damper is not entirely free of problems. The double-tube type must be mounted with the reservoir end on the suspension; this is subject to severe agitation, and although baffles or an annular piston are helpful, aeration is generally a problem in severe conditions. This has been alleviated by anti-foaming agents and solved by the single-tube type. However, the latter type is more prone to damage by stone impact because the active cylinder is exposed. A potential problem with the pressurized type is loss of pressure which may occur over a period of twelve months or so. Oil sealing has been really successful only with the arrival of chromed piston rods of excellent finish running in synthetic rubber seals. Temperature effects have been alleviated by high-viscosity-index oils.

4.12 Damper Characteristics

Hydraulic dampers have substantial advantages in that the damping force can be made a function of speed and direction, and even of position. Positional change of damping effect has rarely been used on cars so far, although it is commonly used on motorcycles to act as a bump stop for the front forks. This can be achieved by placing the bump valve in the side of the working cylinder so that the piston passes it, then forcing fluid through a smaller orifice at the bottom. An important advantage is absence of the bounce that occurs with a rubber stop. One make of damper has used a fluid bypass around the piston central position, with the intention of reducing the damping to improve the ride on smooth roads, while retaining good control of larger suspension excursions. Some positional modification of the damping rate, as seen at the wheel, may be achieved by the connecting linkage geometry, as for springs. Positional variation within the damper itself has been used in racing, but nowadays this is preferably achieved through controlled variation of the motion ratio.

Some advantages may be gained by pressurizing the entire damper, typically to 2.5 MPa cold. This is essential for the anti-emulsion single tube to operate the secondary piston; it is normally done to single tubes, but not to double tubes. Such pressurization means that the flow return valves previously designed to have very low resistance can now contribute to the damping without causing the low pressures (below 100 kPa absolute) liable to cause cavitation. As a consequence of the pressure acting on the piston-rod area, there is a force of typically 300 N attempting to expand the damper, even near full extension, and this increases at about 500 N/m as it shortens. This is at normal temperatures, and may double in severe use.

In order to achieve the desired basic damping characteristic, i.e., the relationship between force and speed, it is necessary to employ a valve system – simple orifices are inadequate. When a fluid passes through a hole or tube there are two contributions to the pressure drop. One is the viscous drag at the walls, which for the usual turbulent flow is roughly proportional to the flow rate squared. The second is dissipated kinetic energy, at the entry and exit, which depends on the density rather than viscosity, and is again proportional to the flow rate squared for a given hole. Use of the second effect in preference to the first would reduce sensitivity to viscosity and hence to temperature. In either case, illustrated in Figure 4.12.1, line A shows the variation of force with velocity for a given hole. The addition of a larger hole B in parallel gives line A + B. By applying to B a valve which opens progressively, a transitional characteristic is obtained. Proper choice of the basic jet sizes A and B and the progressive qualities of the valve enable quite a good straight line, or other desired shape characteristic, to be achieved. These are referred to as stages: stage 1 is valve closed, stage 2 is valve partially open, stage 3 is valve fully open. The valve begins to open at typically 0.1 m/s damper speed, and is completely open at several metres per second.

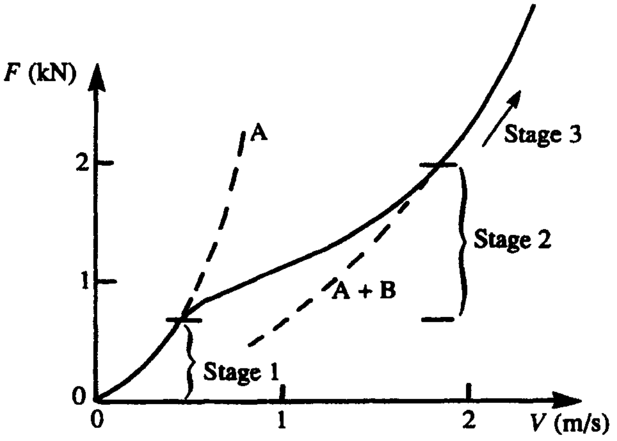

Figure 4.12.1. Damper characteristic.

The typical car damper is designed to exert only about half the force in bump as in rebound. A large rebound coefficient helps to stop the wheel from dropping into potholes. Very early dampers acted only in bump, working as a buffer to discourage bottoming of the suspension (hence the name shock absorber). Some later types operated only in extension. However, it is now considered that the best all-around behavior is achieved if, for a given total damping, 60–70% is on the rebound stroke. This is expressed as, for example, a 30/70 bump to rebound (compression to extension) ratio. The order in which the proportions are quoted is usually bump/rebound, but this is not always so. Fortunately, it is reasonably safe to assume that the larger figure is for extension. In vehicle dynamics analysis, because of this asymmetry a bilinear damper model is frequently used: this is an asymmetric damper with a linear force-velocity relationship but different coefficients for the two directions. With asymmetric rates, oscillating damper motion results in a non-zero mean force which slightly lowers the body, undesirable on a rough road. This is called damper jacking.

Adopting a proportional model, the damper characteristic can be expressed simply by the slope of the force–speed curve, i.e., the damping coefficient c, typically 2 kN/m s^{-1} or 2 kNs/m. For a lever-arm damper this is evidently dependent on the arm length. It is, of course, the effective force at the wheel that matters. It is therefore necessary to establish the motion ratio between wheel displacement and damper length or arm position. This motion ratio R may vary with wheel position – it is typically about 0.7 for a separate damper (there is less damper movement), and near to 1.0 for a damper incorporated in a strut. For a given wheel speed the damper speed and force is thereby reduced, and the damper force itself is further levered down as seen at the wheel; so the damping effect is proportional to R^2, for a linear damper at least, as was found for spring rates. The energy dissipating service required does not depend on R, so it is a matter of providing a larger-diameter shorter-stroke unit for a bigger R.

The damping forces seen at the wheel can be expressed in various ways. For example, dividing the total damping coefficient at the wheels in bump by the vehicle weight gives a characteristic speed, of order 10 m/s, representing a notional steady sink rate at which the car would settle on its suspension when resisted by its dampers without spring support. However, the optimum damping depends not just on the vehicle mass, but on the spring stiffness too, so it is better to refer to the classic vibration concept of damping ratio. This is a poor approximation to apply when damping in the two motion directions is different, but it is useful in a qualitative way. Figure 4.12.2 shows the behavior of a system for various damping ratios, ζ, when released from a deflected position. A damping ratio of 1.0 just prevents overshoot. A more lightly damped vehicle, such as the average car, will have some overshoot, e.g., $\zeta = 0.4$. The average damping ratio for body motion is typically in the range 0.2 to 0.6. Opinions regarding the optimum damping ratio seem to vary over a range of at least 2:1, which is not surprising in view of the subjective nature of ride assessment. Competition vehicles are likely to have twice the damping ratio of a normal passenger vehicle.

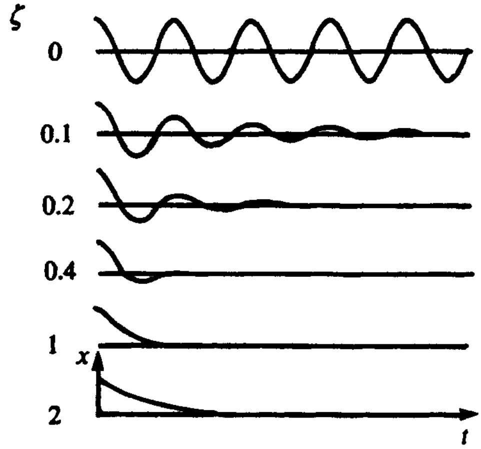

Figure 4.12.2. Free response with various damping ratios in linear damping.

Operation of the damper results in a temperature rise of the fluid, the kinetic energy of motion of the body being dissipated in thermal energy in the fluid. The dampers must not become too hot during the rated sustained operation. Brief intensification of heating is not immediately dealt with by heat transfer to the air, but by a temporary temperature rise according to the thermal capacity of the dampers. Thus the fluid mass and cooling arrangements depend on the vehicle and service requirement. In off-road racing, probably the worst case, water cooling to a radiator with electric water pump and air fan has been used, but multiple dampers to reduce individual heating is the widely adopted solution. For ordinary road use a telescopic piston area of typically 1 to 2 mm^2/per kilogram (10 to 20 cm^2/ton) of wheel load is provided, referred to the wheel, with a fluid volume of 300 to 500 mm^3/kg (300 to 500 cm^3/ton). The temperature rise at a single stroke depends on the pressure drop, and hence speed, and thermal capacity (about 2.5 J/gK) and will be typically in a range up to 0.5°C for the active fluid only. Thus high-frequency short stroking can cause problems if the fluid is not well cooled or circulated.

Manual and automatic electrically adjustable dampers are becoming more common. Adjustability may be applied to any aspect of the valve, so different designs may respond very differently to their adjustments; for example, variations of orifice A or of orifice B or of the valve preload force affect the force-velocity curve quite differently.

Different makes of dampers do not have a large difference in effect in ordinary driving, although optimization is important for competition. The main differences are in life, adjustability, resistance to aeration, and consistency one to another. Like a carburetor, the damper depends on fine control of fluid in small orifices, and production tolerances can result in substantial variation between dampers of the same specification from the same manufacturer, and even greater variations between dampers of the same specification from different manufacturers. The best dampers have well-finished internal surfaces to minimize seal wear, have close tolerances and are individually calibrated, which is expensive.

4.13 Parasitic Friction

Apart from the deliberately introduced damper viscous friction, there are other sources of damping inherent in the system. One is the aerodynamic damping force on the body; this appears to be insignificant for wheeled vehicles. Another is the residual friction in suspension pivots and sliders, driveshaft splines and the like. These generally behave in a Coulomb friction manner. This means that for small changes of vertical wheel force, the suspension remains locked, giving a poor ride quality, e.g., boulevard jerk, a mode where the body and wheels vibrate vertically as one on the tire stiffness. It is also detrimental to handling because it interferes with operation of the suspension and therefore alters the vertical force on the tires. Thus it is generally desirable to minimize such friction.

The total parasitic friction on one wheel is typically equivalent to about ±5 mm of suspension movement, for example ±200 N on a one-ton vehicle, and possibly a good deal worse for a poor design or if there is inadequate lubrication of joints. The friction value of 200 N could result in a diagonal load distribution asymmetry of 400 N, a diagonal bias of about 2%.

The source of this friction is the various sliding joints, including dampers and suspension arms, rubber bushes and especially strut sliders. The friction force depends on the normal forces involved at the sliding face. For example, the main spring may operate on the suspension arm only one-third along; the inner pivot must then support twice the load at the outer ball joint. Loads in the joints are affected by any change of wheel force, especially cornering forces. Again, the leverages involved often give large forces at the joints. An interesting case is the strut and pivot arm suspension. This must transmit, through the guide and piston of the strut damper, a force whose true line of action is through the top bulkhead joint. As a consequence it is desirable to make the strut length as great as possible to maximize the distance between guide and piston. The guide rod itself must be much larger than for an equivalent damper, to spread the load at the guide, and consequently the potential leakage path is also greater. Struts with angled mainsprings have been used to align the spring force with the intersection of the tire and bottom link force; this can eliminate the strut side force in straight running, but at the cost of worse forces in cornering.

The springs themselves can be a source of friction. The coil spring and the torsion bar splined directly to the arm are ideal with respect to friction. The internal friction of metal is entirely negligible. The multi-leaf spring, however, is usually replete with friction because of sliding of the leaves. In the early days this was considered to be useful free damping, although it tends to be rather variable especially when wet; nowadays it is sometimes minimized by the incorporation of plastic spacers. Lubrication does not seem to be very helpful, since it reduces only the dynamic friction and not the static breakout value.

Rubber springs exhibit the usual rubber hysteresis loop. This is not viscous – it is hardly speed-dependent for speeds of interest – but it is not entirely of a Coulomb friction nature either. Therefore, although a rubber-suspended car may exhibit a large friction deadband in suspension height, the ride will not necessarily be as bad as this would suggest.

In order to minimize sliding friction at suspension joints, it is now normal to use a cylindrical rubber bush that distorts in shear as the suspension operates, so most suspensions have an element of rubber type friction and stiffness. A well-lubricated bearing might be better for handling, but rubber bushes are a practical compromise with low cost, low maintenance and good vibration isolation, but generally poorer for handling because of flexibility. In production cars modified for competition, bushes are replaced with harder rubber for rallying, or spherical joints for racing.

The exact influence of all these effective friction sources is not easy to establish, even if the total result as a suspension height deadband is measured directly, because of uncertainty in the influence of vibration from the engine and road roughness. However, since the development of effective hydraulic dampers, there is little to be said in favor of Coulomb friction, and there has been a continuous campaign to reduce it.

A further difficulty arises in the case of the driven wheels, particularly for independent suspension. The suspension geometry generally requires that there is some ability in the driveshafts to extend and contract, usually facilitated by a sliding spline joint. When drive torque is transmitted, or when braking if the brakes are inboard, the splines are subject to considerable friction because of the large torque acting on the splines at a small radius. The consequent binding of the suspension may particularly affect traction on poorer surfaces. There are a number of possible solutions. The effective friction seen at the wheel depends on the motion ratio, so spline sliding should be minimized; this is an unwelcome additional requirement on the geometry. A wire-reinforced flexible "doughnut" can be used for limited plunge. An attractive solution due to Roesch in 1933 is to make the driveshaft of fixed length and to use it as one of the suspension links. The first to actually implement this idea was Chapman on the 1956 Lotus Elite rear suspension, where it was used as part of the bottom arm with a strut above. Various others have used it since; while it solves the friction problem, the driveshaft is not in the most convenient position for a suspension link. A more general solution to this problem is now available – the ball-spline. This uses steel balls to minimize the friction, and is completely effective, although expensive.

4.14 Inertia

The total mass of the vehicle may be considered to be divided into sprung mass and unsprung mass. These terms refer to the component motion relative to the road. Basically the sprung mass is the body and the unsprung mass is the wheels. This distinction is made because it may be necessary to consider the unsprung mass separately, for example for rough roads, or when calculating the load transfer distribution in cornering.

When the road is not smooth, for good handling it is generally desirable to have a small unsprung mass. For a given spring stiffness, a small unsprung mass will follow the contours of the road better with a more uniform vertical force, and hence less lateral force variation and a greater maximum mean cornering force. The choice of suspension spring stiffness is mainly governed by the vehicle body mass, so a useful parameter is the ratio of sprung to unsprung mass. This is usually considered separately for the two ends of the vehicle.

Actually the unsprung mass is not strictly a constant for a given vehicle, but depends on the purpose of the analysis. For example, in single-wheel bump an axle does not exhibit an inertia equal to half of the value for double-wheel bump. The reason for this may be seen by considering a single uniform suspension link. Its weight will be distributed equally between the two ends. However, its angular inertia about one end is $ml^2/3$, so when one end is pivoted and the other end is moved, the apparent inertia there is only $m/3$. An extra point mass only half-way along contributes an inertia at the end of only 1/4 of its mass, i.e., the effective mass contribution depends on the square of the motion ratio. Apart from the case of a live axle, the contribution to the unsprung mass is dominated by the wheel unit, so these effects can usually be neglected, and the links considered to be distributed half as sprung and half as unsprung with little error. Conventional leaf springs are about 2/3 unsprung.

Table 4.14.1 shows representative sprung and unsprung masses for an axle, expressed as a percentage of the total end-mass. The unsprung mass runs from 13 to 26% of the total end-mass, and the sprung to unsprung mass ratio ranges from under 3 to nearly 7. Compared with the minimal set-up of wishbones, coils and inboard brakes, a de Dion axle adds 2%, a differential adds 2%, outboard brakes add 5%, and longitudinal steel leaf springs add 4%. A transverse GRP cantilever leaf spring is as good as coil springs. The quite good showing of the swing axle here has possibly contributed to its use despite its other shortcomings.

Table 4.14.1 Example Unsprung Masses for Heave of an Axle

	Unsprung	Sprung	Sprung/ Unsprung	Unsprung/ Sprung
Type	m_U/m_e (%)	m_S/m_e (%)	m_S/m_U (Ratio)	m_U/m_S (%)
Wishbones, coils, inboard brakes	13	87	6.7	14.9
De Dion, coils, inboard brakes	15	85	5.7	17.6
Wishbones, coils	18	82	4.6	22.0
Swing axle, coils	18	82	4.6	22.0
De Dion, coils	20	80	4.0	25.0
Solid axle, links, coils	22	78	3.5	28.2
Solid axle, leaf springs	26	74	2.8	35.1

The unsprung mass should include an appropriate contribution from all the links, the moving part of the damper, the spring, etc., factored according to the appropriate motion ratio squared. However, as these figures show, these are usually a small proportion of the total, so precise assessment is not important.

The excellent mass ratio of independent systems may appear to account for the widespread use of such systems on the front of cars. This is not entirely so. The success of front independent systems is probably more due to the elimination or reduction of various steering vibration problems, better compatibility with engine space requirements, and better steering geometry which is very difficult to achieve with soft springs and large movements on solid axles.

4.15 Gyroscopic Effects

A rotating wheel also acts as a gyroscope, and any attempt to turn the wheel out of its existing plane of rotation results in a precession effect. For example, if the wheel in bump is cambered a little by the suspension, then it will attempt to rotate about the steering axis. The other wheel will resist, but there will be some effect on the steering. This also arises when the wheels camber in roll. The precession torque is given by

$$T = I\Omega\omega$$

where Ω is the wheel angular speed because of forward motion, and ω is the precession angular speed. I is the second moment of mass about the spin axis, and is typically 0.6 kg m^2 for a passenger car wheel.

4.16 Problems

Q 4.2.1 Explain the Kennedy–Arronhold theorem.

Q 4.3.1 Compare the merits of various straight-line mechanisms in the role of axle lateral location.

Q 4.3.2 Analyze the forces and stresses in the Watt linkage for a lateral force of 6 kN. Choose suitable materials and dimensions. Consider buckling.

Q 4.3.3 Analyze the forces in an Adex linkage for a lateral force of 6 kN.

Q 4.3.4 Analyze the accuracy of the motion of the Watt linkage.

Q 4.3.5 Analyze the accuracy of the motion of the Adex linkage.

Q 4.5.1 List and explain the combinations of links that form the basic independent suspensions.

Q 4.6.1 Describe the basic forms of link combinations for axle location (assume lateral location by a Panhard rod if lateral location is separately provided).

Q 4.7.1 Explain the concept of an equivalent rigid-link system.

Q 4.8.1 Explain the relative merits of the various types of spring and spring materials.

Q 4.9.1 A spring and linear damper both have a motion ratio of 0.80. The damper coefficient in bump is 2.0 kNs/m and the spring stiffness is

9.0 kN/m. Find the effective spring stiffness and damping coefficient values at the wheel.

Q 4.10.1 Explain the various ways in which extra roll stiffness arises as a side effect, beyond that corresponding to the normal spring stiffness.

Q 4.10.2 Explain how roll stiffness may be added.

Q 4.10.3 Describe the various ways in which a very low roll-stiffness suspension may be achieved. Why might this be done?

Q 4.10.4 Describe ways in which a small pitch stiffness may be achieved.

Q 4.11.1 Describe the various damper types and their advantages and disadvantages.

Q 4.12.1 Explain how valving may be used to obtain an approximately linear force–speed relationship for a damper.

Q 4.12.2 A vehicle damper exerts a force of 3 kN at an extension speed of 2 m/s. What is the damping coefficient? Approximately what force would you expect to be required to compress the damper at 1 m/s?

Q 4.13.1 Summarize the methods used to minimize the influence of Coulomb friction in suspension members and driveshafts. Does Coulomb friction have any advantages?

Q 4.13.2 A two-wheel-drive vehicle of mass 1400 kg and wheel radius 0.3 m accelerates at low speed at 8 $\mathrm{m/s^2}$. The driveshafts have splines of effective radius 15 mm, and a coefficient of friction of 1.2. Find the plunge force required to move the splines axially.

Q 4.14.1 Summarize the advantages and disadvantages of keeping the unsprung mass to a small value.

Q 4.14.2 Discuss what can be done to keep the unsprung mass as small as possible.

Q 4.15.1 A wheel with second moment of mass 0.7 kg $\mathrm{m^2}$ about its spin axis, of radius 0.30 m traveling at 50 m/s, is forced to rotate in camber at 20 deg/s as the wheel passes over a bump. What precessional torque must be applied by the steering if the wheel is held rigidly?

Q 4.15.2 Gyroscopic moments are considered in Chapter 5, questions Q 5.10.12 to Q 5.10.15. If you understand lateral load transfer, do those questions now.

5

Suspension Characteristics

5.1 Introduction

This chapter considers characteristics of the suspension as a complete system, in contrast to the previous chapter which considered components in isolation. In particular this chapter presents analysis of chassis heave and roll, the roll center and roll axis, load transfer and the distribution of vertical forces, and the influence of pitching in response to acceleration and braking. This is followed by a look at the geometry of steering systems, at the steering effects of wheel bump and chassis roll, and at the steering effects of wheel forces because of system compliance. These factors are of considerable importance in controlling the behavior and feel of the vehicle, and every one of them must be carefully controlled if the vehicle is to handle well.

The term "axle" is used here in a wide sense to include independent suspension, in which case it means the combination of the wheels, hub carriers and links for the two sides.

5.2 Bump and Heave

The term "ride" is a general one referring to vehicle motions of the sprung and unsprung masses caused by the longitudinal road profile.

Bump is upward displacement of a wheel relative to the car body, sometimes applied more broadly to mean up or down displacement. It is also known as compression or jounce. The opposite, a lowering of the wheel, is called rebound, extension, or droop. Bump is so called because it occurs when a single wheel passes over a bump. When a pair of wheels rises symmetrically this is called double-wheel bump, often referred to simply as double bump. Heave is a vertical upward motion of the body without roll. This is also known as bounce. Double bump is geometrically equivalent to a negative heave of the body, without roll. Bump and heave influence the wheel camber and steer angles relative to the body and road, and also influence the spring and damper forces and hence the tire vertical force. These all influence the tire lateral force. The terms bump and droop may also be applied to velocities to show the direction and motion; in that case it should be borne in mind that a bump velocity may occur in a droop position, and vice versa. Bump velocities also affect the slip angle because of the scrub velocity component. Body roll in cornering gives a combination of bump and droop on opposite wheels, relative to the body. When the car is in combined braking and cornering, the longitudinal and lateral load transfers result in a different combination of heave and bump on each wheel.

The motion ratio (or installation ratio or link ratio) of the spring is the velocity ratio of the spring to the wheel, or the ratio of small displacements for the spring divided by that for the wheel:

$$R_S = \frac{V_S}{V_W} = \frac{dz_S}{dz_W}$$

A similar definition applies for the damper motion ratio:

$$R_D = \frac{V_D}{V_W} = \frac{dz_D}{dz_W}$$

It is the vertical motion of the wheel and the length change of the spring or damper that are relevant. For a complete concentric spring and damper unit as often used on racing cars, or for a strut unit, the spring and damper motion ratios are the same. In the case of a strut the ratio is close to 1.0. For a spring or damper acting part way along the bottom suspension arm, as is common, the ratio may be around 0.7.

The effective suspension stiffness as seen at the wheel, K_W, is called the wheel rate or the suspension rate, and depends on the actual (linear) spring stiffness K_S and the spring motion ratio R_S, provided that this is constant, according to

$$K_W = R_S^2 K_S$$

For a variable motion ratio,

$$K_W = R_S^2 K_S + F_S \frac{dR_S}{dz_S}$$

Similarly, for a linear damper the damping coefficient at the wheel C_W (Ns/m) depends on the actual damper coefficient C_D and the (constant) damper motion ratio:

$$C_W = R_D^2 C_D$$

As far as vehicle dynamics is concerned, it is only the force values at the wheels that are important. A change of spring stiffness or damper coefficient coupled with an appropriate change of motion ratio resulting in unchanged values at the wheel do not in principle change the vehicle dynamics. There may, in practice, be some minor effects, however, because the different internal forces could affect rubber bush distortions or sliding bush friction.

Although the wheel rate for a given spring depends on the local motion ratio, when this is constant, the actual spring force at the wheel still cannot be calculated in this way because it depends on the cumulative spring displacement and therefore on an integral of the motion ratio.

Evaluation of motion ratios may be performed by drawing velocity diagrams for the suspension linkage, or, as is usual nowadays, by computer analysis. A motion ratio is not constant through the range of motion of the suspension, so a graph of the ratio versus wheel bump position is informative.

Modern formula racing cars frequently use a double-wishbone suspension with the spring-damper unit laid horizontally alongside the gearbox or along the top of the front body, operated by a pushrod from the outer end of the bottom wishbone, working via a rocker. The geometry of the rocker, namely the initial moment arms l_1 and l_2 provide a convenient way to introduce a desired motion ratio; the initial angular positions θ_1 and θ_2 of the arms provide a means to vary the motion ratio in a progressive manner.

A similar but more modest rising rate effect may be achieved for a spring acting direct on a suspension arm by angling the spring, inward at the top, so that the effective moment arm increases as the spring is deflected.

For a solid axle with springs of stiffness K_s at spacing S on track T, in double-wheel bump each wheel requires a force equal to the spring force, i.e., in this case the wheel rate equals the spring stiffness (the motion ratio is 1.0):

$$K_W = K_S$$

However, if only one wheel is raised, then by moments

$$K_W = \tfrac{1}{2} K_S \left(1 + \frac{S^2}{T^2} \right)$$

In practice this expression is good for coil springs, but for leaf springs the effective rate is greater because of their torsional stiffness. A representative value of S/T is 0.7. Where coil springs act on links, it is the spacing of the link connection on the axle and the effective stiffness that the spring creates at the link that are relevant.

As an example of independent suspension, consider the double-wishbone system of Figure 5.2.1. The complete range of motion of the wheel can be investigated by position diagrams, or preferably by computer analysis. This will also give the spring length, and hence force. If the forces in the links are found, the bush distortions and torques can be included. Such analysis will reveal the variation in camber angle, and also the variation in track, i.e., the lateral scrub of the center of tire contact F. Scrub is significant when the wheel is moving in bump because there is then a scrub speed; combined with the existing longitudinal speed this scrub speed gives a change of tire slip angle. From the spring and damper force may be found the vertical force at the wheel. The variation of vertical force with vertical position is called the wheel rate. The ride stiffness (or rate) is the wheel rate in series with the tire vertical stiffness, and may be found from the equation

$$\frac{1}{K_r} = \frac{1}{K_W} + \frac{1}{K_t}$$

In Figure 5.2.1, the intersection of AB and CD extended gives point E, the instantaneous center (centro) for the wheel relative to the body (SAE swing center). Thus the direction of motion of F relative to the body is perpendicular to EF. The scrub rate is the rate of change of lateral F position in bump. This is the tangent of the angle between the direction of motion of F and the vertical, which

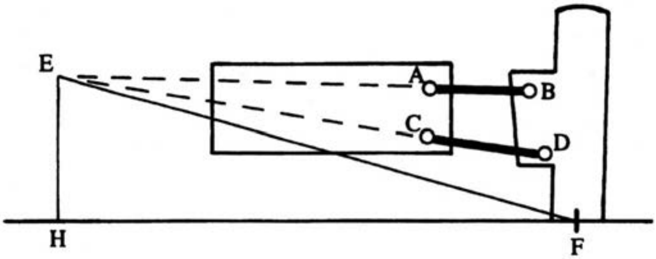

Figure 5.2.1. Double-wishbone suspension in rear view.

equals the angle EFH. Therefore the scrub rate equals EH/HF. Minus twice this value is the rate of track change in heave. The SAE swing arm radius is defined as the horizontal distance from E to F, i.e., the length HF, taken positive if E is on the centerline side of the wheel. This is a rather misleading term because the motion of F does not have a radius of curvature equal to HF, or even EF, because the centro E also moves. This was discussed in Section 4.3. In practice E is typically chosen to be approximately at the opposite wheel. However, in some cases the arms are parallel, giving an infinite swing arm, or E may even be on the other side of the wheel, known as a negative swing arm.

The double-wishbone system is particularly amenable to design adjustments to obtain properties that the designer considers important. Bollée had an unequal wishbone suspension as early as 1878. In the modern phase of wishbone usage, they began with short parallel equal arms. Longer arms were then adopted because these reduce all unfavorable effects. The top arm was made shorter, this leading to negative camber relative to the body in bump which is favorable when the body is rolled in cornering. Nowadays a non-parallel unequal-arm layout is usually favored.

The centro E for other suspensions can also be found quite easily, given the idealization of neglecting bush distortions, and is discussed in more detail later (Fig. 5.5.2). For example, for a Macpherson strut and link, the top line is perpendicular to the slider (not the steering axis) and through the top connection to the body. For pure trailing arms, E is at infinity, with FE parallel to the arm axis in front view. For a semi-trailing arm, projecting the axis of the arm into the transverse vertical plane of the wheel centers gives E. For a true swing axle, it is the axle pivot, usually close to the differential.

Equilibrium analysis of the wheel and links with the spring, bump stops, bushes and static damper force determines the relationship between wheel position and vertical wheel force. (Under dynamic conditions, wheel inertia and damping effects alter the actual vertical force of course.) This is central to handling analysis because it controls the load distribution between the wheels. It is convenient to consider the isolated wheel force with the anti-roll bar disconnected, and to handle the anti-roll bar couple separately. Figure 5.2.2 shows a typical result for wheel force versus bump position, which may be obtained theoretically or experimentally. Point A is the reference standing height and force. The gradient at A is the wheel rate. Moving into bump, if there is an upward curvature then the suspension is rising rate. Point B is the fully loaded condition. In further bump, in due course the bump stop is engaged at C where there may be a discontinuity of stiffness depending on the bump stop design. The force then rises rapidly to the bump limit position D; this is sometimes called the metal-to-metal bump position, although it is rarely literally true because of the presence of bump rubbers. The distance of wheel motion from normal ride height to maximum bump deflection is called the ride bump clearance, often just ride clearance or bump clearance.

Moving from the central position in the droop direction, there is usually a linear or slightly reducing stiffness until the droop stop, also known as the rebound stop, is encountered at E. Again, here there is likely to be a sharp change in stiffness, especially if the limiter is the damper or an axle strap. Point F is the free droop position of zero vertical wheel force, with the droop stop engaged and acting against the main spring. If the wheel is pulled down it can go on to G. This is sometimes called the metal-to-metal droop position, and again is rarely literally true. The distance of wheel motion from normal ride height down to maximum droop deflection is called the ride droop clearance, droop clearance or rebound clearance. The point of engagement and progressiveness of the bump and droop stops varies considerably between vehicles. In some cases the bump stops are already engaged at normal height and are used to provide a steadily progressing stiffness. The curve of Figure 5.2.2 is the mean force for both directions. In practice the curve will exhibit some hysteresis, even for essentially static measurements, because of Coulomb friction or hysteresis for rubber springs.

The spring wheel force may be modeled as nonlinear over a limited range by

$$F_{\mathrm{W}} = F_{\mathrm{W1}} + K_{\mathrm{W}} z_{\mathrm{S}} + K_{\mathrm{r}} z_{\mathrm{S}}^2$$

where z_{S} is the suspension bump deflection.

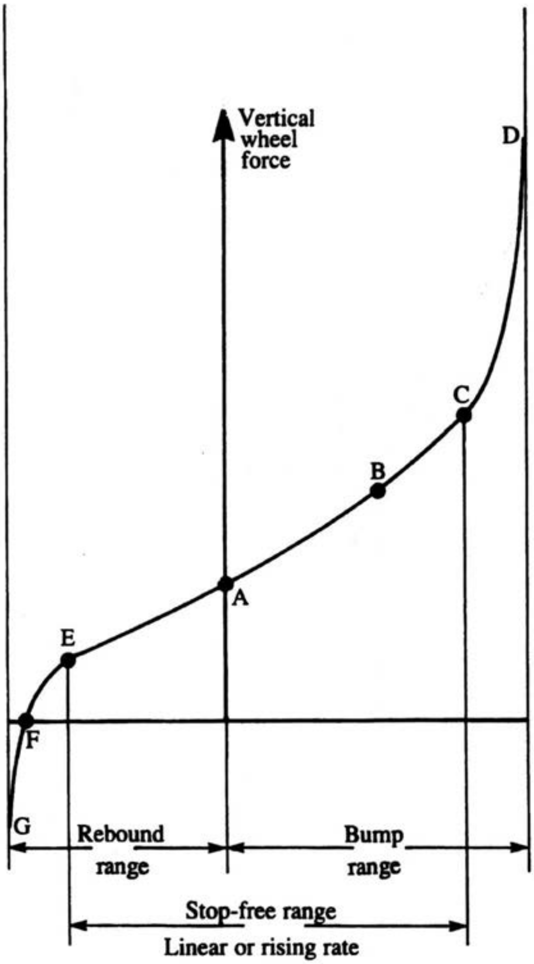

Figure 5.2.2. Wheel vertical force against suspension deflection.

The quadratic stiffness factor K_r [N/m^2] is zero for a linear system. The suspension force rising rate factor f_{sr} is defined by

$$f_{sr} = \frac{K_r}{K_w}$$

This may have a value of around 2/m (2%/cm).

The stiffness at bump z_S is then

$$K_{wz} = \frac{dF_w}{dz_S} = K_w + 2z_S K_r$$
$$= K_w(1 + f_{kr} z_S)$$

where f_{kr} is the suspension stiffness rising rate factor,

$$f_{kr} = \frac{2K_r}{K_w} = 2f_{sr}$$

Figure 5.2.3 shows the rear view of the example double-wishbone suspension again. The forces associated with weight, acceleration and load transfer of the unsprung mass have been subtracted from the tire force, leaving the tire force exerted on the spring and links. The resulting vertical and lateral tire force has been resolved into perpendicular components, F_{R1} and F_{R2} (R for right) where F_{R2} acts through E. Consider an idealized (impractical) case, the idealized spring model, where the suspension spring acts on the wheel carrier directly along the line of action of F_{R1}. The force F_{R1} will then be resisted by the spring and have no effect on the links. F_{R2} will be transmitted by the links and have no effect on the spring because it has no moment about E. Also, considering the link AB, if we neglect its weight and any torques applied by the bushes then it will be in pure tension or compression. Hence the force exerted by the link AB on the body will be along AB. Also the force exerted by CD will be along CD. The total resultant force from the two links must therefore have a line of action through E, because they exert no moment about this point. So, for the idealized spring position the force F_{R2} is transmitted simply by the links, and F_{R1} simply by the spring. F_{R1} and F_{R2} are the net spring force and the net link force. Consider now a more general case of spring position, for example acting part way along a link; then the force F_{R1} will be partly transmitted to the body by the spring and partly by the links. Such a spring position will give rise to forces in the links, but these will be "internal" forces that balance out, not affecting the suspension other than through, for example, rubber-bush distortion. However, the important result is this: F_{R2} will still have no effect on the spring because it acts through E, and F_{R1} is still the force to be balanced by the spring.

The equivalent suspension with a spring acting directly along F_{R1} will be called the idealized spring model. The spring characteristic in this model is chosen to give the correct wheel forces. This model has different internal forces but

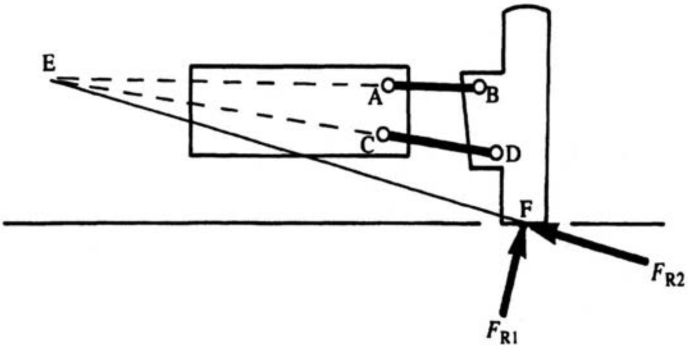

Figure 5.2.3. Resolved forces for double-wishbone, rear view.

the same external effects. In particular, the link forces are simplified and reduced to the transmission of F_{R2}, which is of special significance when investigating roll centers. The idealized spring model is explained further in Section 5.10.

The point E is known as the force center of the links. It is approximately the same as the centro E in Figure 5.2.1, but strictly not identical because different approximations have been made with regard to link stiffness, bush stiffness, link weight and bush torques.

When the car is running straight then there is little lateral force on the tire, in which case F_{R2} is quite small. Nevertheless because of the inclination of FE, some of the vehicle's weight is supported through the links rather than on the springs. Our main interest in the F_{R2} force is when it comes into play in a significant way in cornering. However, it is interesting that when a car is lowered from a central jack, a symmetrical condition with each side like Figure 5.2.3 may occur, with large F_2 forces acting inward on the tires and holding the body in an unusually high position. These forces are relaxed when the car is allowed to move forward. The fact that F_2 can relieve the springs of some of the car's weight comes into play in cornering, giving the link jacking effect.

As in the case of the centro, the force center E for other suspensions can be found quite easily, but now given the idealization of negligible bush torque or friction, discussed later (Figure 5.5.2). For a Macpherson strut, neglecting slider friction the top line is perpendicular to the slider and through the top body connection. For pure trailing arms, E is again at infinity with FE parallel to the arm axis in front view. For a semi-trailing arm, projecting the arm axis into the vertical transverse plane of the wheel centers gives E because there can be no moment exerted about this axis. For the swing axle it is at the pivot near to the differential, again because there can be no moment about this point.

5.3 Roll

Body roll is mainly the result of suspension roll, plus some axle roll from tire deflection:

$$\phi = \phi_S + \phi_A$$

Suspension roll is formally defined (SAE) as rotation of the vehicle sprung mass about a fore–aft axis with respect to a transverse line joining a pair of wheel centers. It is positive for clockwise rotation viewed from the rear. This is unambiguous provided that the ground is flat and that front and rear wheel centers have parallel transverse lines (e.g., that wheels and tires are the same size side-to-side). If the ground is not flat then some mean ground plane must be adopted. The roll angle and roll velocity are in practice fairly clear concepts. Asymmetries, such as the driver, mean that the roll angle is not necessarily zero under reference conditions.

For a torsionally rigid body, the body torsion angle is negligible (applicable to most passenger cars), in which case

$$\phi_f = \phi_{Sf} + \phi_{Af} = \phi_r = \phi_{Sr} + \phi_{Ar}$$

In the case of most trucks, the chassis torsion angle needs to be considered, in which case

$$\begin{aligned} \phi_f &= \phi_{Sf} + \phi_{Af} \\ \phi_r &= \phi_{Sr} + \phi_{Ar} \\ \theta_B &= \phi_f - \phi_r \end{aligned}$$

Roll is geometrically equivalent to bump of one wheel and droop of the opposite one, relative to the body. Thus roll speed generally results in a scrub speed of the tires relative to the ground, causing temporary changes to slip angles and hence to tire forces. In a rolled position, suspension geometry is generally such that there are changes of wheel steer angles relative to the body. This is roll steer, dealt with in Section 5.14. It is equivalent to bump steer for independent suspension, but not for solid axles. The roll gradient is the rate of change of roll angle ϕ with lateral acceleration A:

$$k_\phi = \frac{d\phi}{dA}$$

The total roll gradient is the sum of suspension and axle roll gradients:

$$k_\phi = k_{S\phi} + k_{A\phi}$$

The rolled position also results in wheel camber relative to the body, and more importantly relative to the road, introducing camber forces. In general, in the rolled position the spring stiffnesses on the two sides are different, usually greater on the lower side, so there is some heave of the body as a consequence of roll. This is spring jacking. If a droop stop is engaged first, the body may be lowered. There are other jacking effects through the links in cornering and through damper action which are discussed later.

The vehicle suspension roll couple is the sum of the two suspension roll couples arising because of body roll. The vehicle ride roll stiffness is the sum of the two ride roll stiffnesses. The total ride roll stiffness k_R at each end arises from the suspension roll stiffness k_S acting in series with the axle roll stiffness k_A arising from tire vertical stiffness. Hence

$$\frac{1}{k_R} = \frac{1}{k_S} + \frac{1}{k_A}$$

The suspension roll stiffness is the rate of change of the suspension roll couple with respect to suspension roll angle. For small roll angles the roll couple depends on the main springs and anti-roll bars, while for larger angles the bump and droop stops come into play. Longitudinal leaf springs contribute some roll stiffness of their own because they are in torsion, as does the crossbar of the trailing twist axle, these effects being similar to an anti-roll bar. The roll couple may be found by assuming some angular position and calculating the couple. In general the body heave position varies to keep the total vertical force constant. The total vehicle roll couple may be found experimentally by applying a couple and observing the angle. If all four wheel vertical forces are measured on a flat surface, then an applied body roll angle will show the roll stiffness for each suspension. While doing this the wheels should be free to scrub.

The suspension roll couple is most easily understood for a solid axle with linear spring stiffness K_S, at a spring spacing of S. At a body roll angle of ϕ radians each spring force changes by $\frac{1}{2}K_s\phi S^2$, so there is a couple of moment $\frac{1}{2}K_s\phi S^2$, and the suspension roll stiffness is

$$k_S = \frac{1}{2}K_sS^2$$

This depends on the spring spacing. Where coil springs act on links, it is the spacing of the link connection on the axle and the effective stiffness that the spring creates at the link end that are relevant. For nonlinear springs, or if the bump or droop stops are engaged, it is necessary to find the body heave position first. There may be additional torques arising from torsion in leaf springs or from the bushes of locating links. For a solid axle with coil springs, $\frac{1}{2}K_sS^2$ is the correct basic expression and hence the roll stiffness is less than the effect that the double-bump wheel rate would give if acting at the track spacing. However, for leaf springs the extra torsional stiffness of the leaves is such that the track T may be used as an approximation for the effective spacing instead of the actual spring spacing.

In the case of independent suspension, it is possible to calculate the roll moment by detailing the spring and link forces, but it is much easier to work directly with the wheel forces. Independent suspension can be considered as equivalent to a solid axle with wheel rate springs acting at the full wheel track, giving

$$k = \frac{1}{2}K_wT^2$$

Thus the actual position of the springs does not alter the relationship between roll and vertical stiffnesses, unlike the case of the rigid axle. Independent suspension is also subject to extra torques from rubber bushes in the links, or friction, but this can still be accommodated in terms of the wheel force. Because the spacing of springs on a solid axle is less than the track, the relationship between roll stiffness and heave stiffness is basically inferior to that of independent suspension.

For both solid and independent axles, the axle roll stiffness arising from tire vertical stiffness is given by

$$k_A = \frac{1}{2}K_tT^2$$

Either a solid axle or an independent suspension may be fitted with an anti-roll bar to increase roll stiffness. The effective roll stiffness depends primarily on the torsional stiffness of the active part of the rod, on the length of the lever arms, and on the point of connection of the drop links onto the suspension arms or axle. Secondary factors include the stiffness of the usual bushes, including those where the rod is mounted to the body, and bending of the rod, primarily in the lever arms. In some cases the anti-roll bar has been mounted by strapping directly to the trailing arms giving no contact with the body, i.e., as a nascent trailing twist axle, achieving the anti-roll effect with less noise transmission to the body.

The roll couple or stiffness of each end of the vehicle can be summarized by a roll couple graph (Figure 5.3.1). This is usually roughly symmetrical in roll, but not necessarily exactly so because of suspension asymmetries such as a Panhard rod. The initial position is approximately zero roll, the gradient at A being the initial roll stiffness. There is then typically a constant or rising stiffness until B, where there may be a discontinuity of stiffness where a bump stop is engaged. There may be a further stiffness discontinuity at C where the opposite droop stop is engaged, especially for solid axles. At D the inner wheel is lifted from the ground.

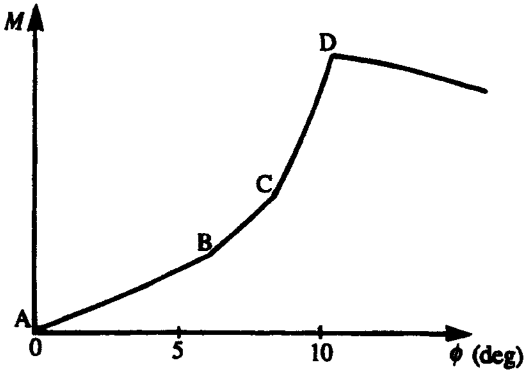

Figure 5.3.1. Roll couple against roll angle.

There is one roll couple graph for each end of the vehicle, and one for the whole vehicle. At any roll angle, the roll couple distribution is the distribution of the total between front and rear, usually expressed as percentages. The roll stiffness distribution is similarly defined. Such distributions may be quoted for the suspension alone, or for the ride roll couple including tire effects. There may be considerable differences, particularly if the suspension bump or droop stops are acting. In fact, the roll stiffness distribution is usually quoted for the zero-roll position, but this is not always satisfactory because the influence of the distribution of roll couple on handling mainly comes into play at medium to large lateral accelerations, when a substantial roll angle has developed, and the roll couple distribution may then be different from the initial value.

5.4 The Roll Center

This section presents the basic theory of the roll center. With detailed computer simulations that consider the forces in the individual suspension links it is not necessary to use the roll center concept. However, the roll center is a very useful idea because the roll center height concisely summarizes the effect of the links. With known roll center heights it is easy to calculate the roll angle and the load transfer at each of the front and rear axles. This is important in handling at large lateral accelerations because it affects the individual tire vertical forces and therefore their lateral forces. Hence the roll center height may be used as a summary of the load transfer characteristics of a suspension found by a detailed suspension analysis, or as the input specification for a simple handling simulation. An explanation of the use of roll centers in lateral load transfer calculation is given in Sections 5.10 and 5.11.

SAE defines the roll center in terms of forces, despite its kinematic name. A definition based on forces will be presented and used here. However, many authors introduce the roll axis as an axis about which the vehicle actually rolls during cornering, the roll axis being the line joining the front and rear roll centers. When a vehicle is actually moving on a road, the concept of a kinematic roll axis is difficult to justify in a precise way, especially for large lateral accelerations. Therefore the idea of the vehicle rolling about such an axis, although useful as a qualitative idea, should be treated rather cautiously, except in the special case of a stationary vehicle subject to loads in the laboratory. From a practical point of view, its kinematic significance is that it permits calculation of the lateral movement of the sprung mass relative to the axle, which affects the load transfer (Figure 5.4.1) and is related to the scrub rate in bump.

The roll center is defined in SAE J670e *Vehicle Dynamics Teminology* (Appendix E) in the following way:

> "The [SAE] roll center is the point in the transverse vertical plane through any pair of wheel centers at which lateral forces may be applied to the sprung mass without producing suspension roll."

This does not call for the roll center to be in the center plane and is therefore ambiguous, although it is usually taken to be there. This is a convenient definition when the roll effect of a force applied externally to the body is required, for example an aerodynamic force. However, the usual application of the roll center is in evaluating the roll angle and the front-to-rear distribution of lateral load transfer during cornering; i.e., it is primarily concerned with the application of forces by the axle to the body, or by the body to the axle. These are action and reaction, which by Newton's third law are equal and opposite and have the same line of action.

The following basic definitions for roll center and roll center height will be adopted initially here:

> The roll center is a point in the center plane and in the vertical transverse plane of the wheel centers, at roll center height.
>
> The roll center height is the height at which lateral forces may be applied to the sprung mass without producing suspension roll.

This is illustrated in Figure 5.4.1 showing the rear-view free-body diagram of an axle in left-hand cornering.

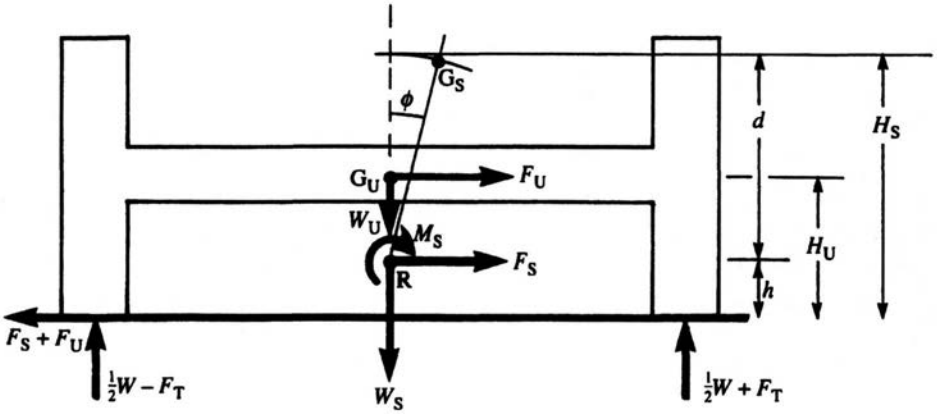

Figure 5.4.1. The free-body diagram of a solid axle in vehicle-fixed axes; rear view in left-hand steady-state cornering.

Figure 5.4.1 actually shows a solid axle; it is permissible for the current purpose to treat the parts of an independent suspension as equivalent to a solid axle. We are here assuming a small lateral acceleration. This is a notional single-axle two-dimensional vehicle; alternatively we could interpret it as a vehicle with identical suspensions front and rear. The real double-axle case is dealt with in Section 5.11. Figure 5.4.1 distinguishes the sprung and unsprung masses m_S and m_U at heights H_S (unrolled) and H_U. The total weight is

$$W = mg = m_S g + m_U g$$

There is a steady-state cornering lateral acceleration A, and the free body is shown in vehicle-fixed axes, so centrifugal compensation side forces are included. The sprung mass with center of mass at the point G_S has rolled by ϕ about the roll axis at point R. There is a total lateral load transfer F_T, so the wheel vertical forces are

$$F_{VR} = \tfrac{1}{2}W + F_T$$
$$F_{VL} = \tfrac{1}{2}W - F_T$$

Acting at the unsprung center of mass is the unsprung weight force, and also the unsprung compensation side force

$$F_U = m_U A$$

The sprung mass compensation side force

$$F_S = m_S A$$

really acts at G_S but it is resisted at the roll center, so the sprung compensation side force F_S is shown acting at the roll center along with a moment M_S. The sprung mass weight force is also transferred to the roll center, and also contributes to M_S, giving a moment

$$M_S = m_S A d \cos\phi + m_S g d \sin\phi$$

where

$$d = H_S - h$$

is the distance of G_S from the roll center. It is the moment M_S that is resisted by the springs and anti-roll bar and creates the suspension roll angle. The sprung mass force F_S acting at the roll center is resisted directly by the links and creates no suspension roll, by definition. Hence the total load transfer can be considered in three factors:

(1) F_{TU} from the unsprung side force

(2) F_{TL} from the sprung side force at the roll center

(3) F_{TM} from the sprung moment

The sprung-mass side force at the roll center is transferred through the links of the idealized spring model. By taking moments about the mid-point between the tire contacts, the load transfer is

$$\begin{aligned} F_T &= F_{TU} + F_{TS} \\ &= F_{TU} + F_{TL} + F_{TM} \\ &= \frac{m_U A H_U}{T} + \frac{m_S A h}{T} + \frac{M_S}{T} \end{aligned}$$

Thus a high roll center increases the load transfer through the links while reducing that through the springs and anti-roll bar, reducing the roll angle.

In the application of roll centers in handling analysis, the load transfer contribution caused by the sprung-mass force at the roll center is calculated from the roll center height, so the relevant equation is

$$F_{TL} = \frac{m_S A h}{T} = \frac{F_S h}{T}$$

This provides an alternative mathematical definition of the roll center height:

$$h = \frac{F_{TL}}{F_S} T$$

To some extent this is a circular definition, because in practice F_{TL} is usually found from h. We could say that F_{TL} is the part of the total sprung-mass load transfer left after F_{TM} is subtracted. For independent suspension, in practice the springs are placed in a way that causes a complex combination of link and spring forces that to a large extent cancel out. However, if we consider the idealized spring model of the suspension, then F_{TL} is simply the load transfer through the links, and F_{TM} is simply the load transfer through the springs and anti-roll bar; these are called the net link load transfer and the net roll load transfer. The idealized spring position model was introduced in Section 5.2, and is further explained in Section 5.10; it has the spring that directly resists F_1 in Figure 5.2.3.

Using the idealized spring model we can define the roll center height using the above equation where F_{TL} is the net link load transfer, or as:

> The roll center height is the load transfer through the links of the idealized spring model, divided by the sprung mass side force, times the track.

We could alternatively think in terms of a non-dimensionalized roll center height, expressed as a fraction of the track. This is simply equal to the load transfer as a fraction of the sprung mass side force, which we can call the load transfer factor, f_{L}:

$$f_{\mathrm{L}} = \frac{h}{T} = \frac{F_{\mathrm{TL}}}{F_{\mathrm{S}}}$$

Hence the load transfer factor is defined in words as follows:

> The load transfer factor is the load transfer through the links of the idealized spring model divided by the sprung-mass side force, and also equals the roll center height divided by the track.

From the above we may deduce two obvious but important equations:

$$h = f_{\mathrm{L}}T$$
$$F_{\mathrm{TL}} = f_{\mathrm{L}}F_{\mathrm{S}}$$

As discussed in Section 5.10, a high roll center reduces the roll angle. The load transfer factor can also be termed the "anti-roll," analogous to anti-dive or anti-squat in longitudinal dynamics. The anti-roll coefficient is

$$J_{\mathrm{AR}} = \frac{h}{H_{\mathrm{S}}}$$

usually quoted as $J_{\mathrm{AR}} \times 100\%$.

5.5 Independent Suspension Roll Centers – Part 1

The load transfer characteristics, and hence the roll center height, may be found by detailed force analysis of the suspension. Figure 5.2.3 showed the force exerted by the ground on the wheel for the case of a double-wishbone suspension. This acts at F, which we can approximate in the usual way as at the center of the contact patch. Given appropriate tire data (overturning moment), a better point could be chosen for F. Here we have already subtracted the part of the force associated with unsprung weight force, unsprung-mass side force and unsprung-mass load transfer, which can be dealt with separately. The force F is resolved into F_1 and F_2 perpendicular and parallel to EF. All further discussion is about the idealized spring model, hence eliminating the internal forces with no net effect. Force component F_1 is the part of the force that has a moment about E, which cannot be transmitted by the suspension links; it is therefore transmitted to the body by the idealized spring. The force F_2 acts through E and has no moment about E, and is therefore the total force exerted by the links of this side of the suspension on the body when the idealized spring is used. This side net total link force therefore has a line of action along EF. This is the basis of the construction of the line EF for a force roll center.

Figure 5.5.1 shows both wheels, with left and right link forces F_{L2} and F_{R2}. Their resultant must act through the intersection of F_{L2} and F_{R2} because they have no moment about this point. Hence this intersection point is the roll center. For a symmetrical vehicle this point is on the centerline. A lateral force applied here can be reacted directly by the links, giving no force in the springs and therefore without resulting in any roll.

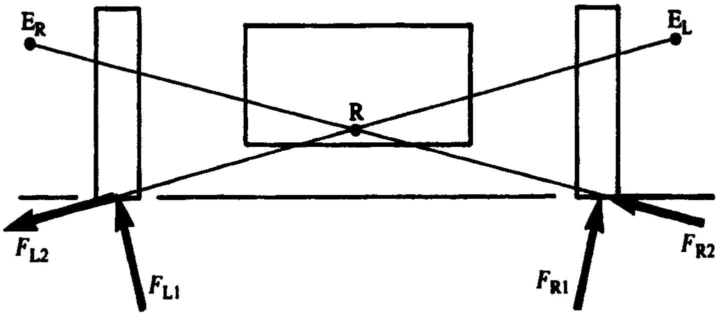

Figure 5.5.1. Independent roll center and forces, rear view.

The above development shows that the roll center can be deduced by an argument based on forces only, without mention of a kinematic roll center. It also shows the real approximations that are usually involved, for example small friction and small bush stiffness, which are quite different from the approximations of the kinematic roll center. In a fully detailed analysis, usually by computer, the roll center height, with the definition adopted here, provides a convenient summary of the load transfer characteristics of the suspension.

From Figure 5.5.1 we can see that a lateral force at the geometric roll center could be exactly equilibrated by suitable magnitudes of F_{L2} and F_{R2}, there being unique values to do this. However, there is no guarantee that this will actually occur, because the magnitudes of F_{L2} and F_{R2} depend on the distribution of tire lateral force on left and right wheels. If they are unequal, with the correct horizontal total, then there will be a residual jacking component.

The presence of friction in the joints, tending to be greater with Macpherson or Chapman strut-type suspensions than with wishbones, introduces an interesting point of principle. There is actually a range of heights over which a side force will cause no roll. The actual line of action of the link forces is uncertain within this band. Thus the force roll center height is also uncertain within this friction band range.

Figure 5.5.2 summarizes the initial roll center constructions (i.e., for small lateral acceleration) for various independent suspensions. With the assumption of symmetry, it is sufficient to draw one side only. For the strut and link (Macpherson) suspension, Figure 5.5.2(b), the upper construction line is perpendicular to the slider, not to the steering axis AD; these are generally different. For the essentially obsolete slider (pillar) suspension, Figure 5.5.2(c), E is at infinity; there is a single construction line from the wheel contact patch perpendicular to the slider direction. For the true swing axle, Figure 5.5.2(d), the roll center is very high. For the transverse rigid arm, the swing arm, Figure 5.5.2(e), sometimes also called a swing axle or pseudo swing axle, it can be made lower.

For a trailing arm or semi-trailing arm suspension, in general the pivot axis should be projected into the vertical transverse plane of the wheel centers. This provides the effective E point because the link cannot exert a moment about this axis, neglecting bush friction and stiffness. If the pivot axis is perpendicular to the vehicle center plane in plan view, i.e., pure trailing arm, then the E point is at infinity, even if it is inclined in front view, Figures 5.5.2(f) and (g). For small lateral acceleration, on the simple trailing arm of Figure 5.5.2(f) the roll center is at ground level, even if the trailing arms are inclined in side view.

If the trailing arm pivot is inclined in front view only, Figure 5.5.2(g), then E is at infinity parallel to the pivot axis. For a semi-trailing arm the pivot axis is not perpendicular to the centerline in plan view, so the axis must be projected into the vertical transverse plane of the wheel centers to find the actual E point which will not be at infinity, Figure 5.5.2(h).

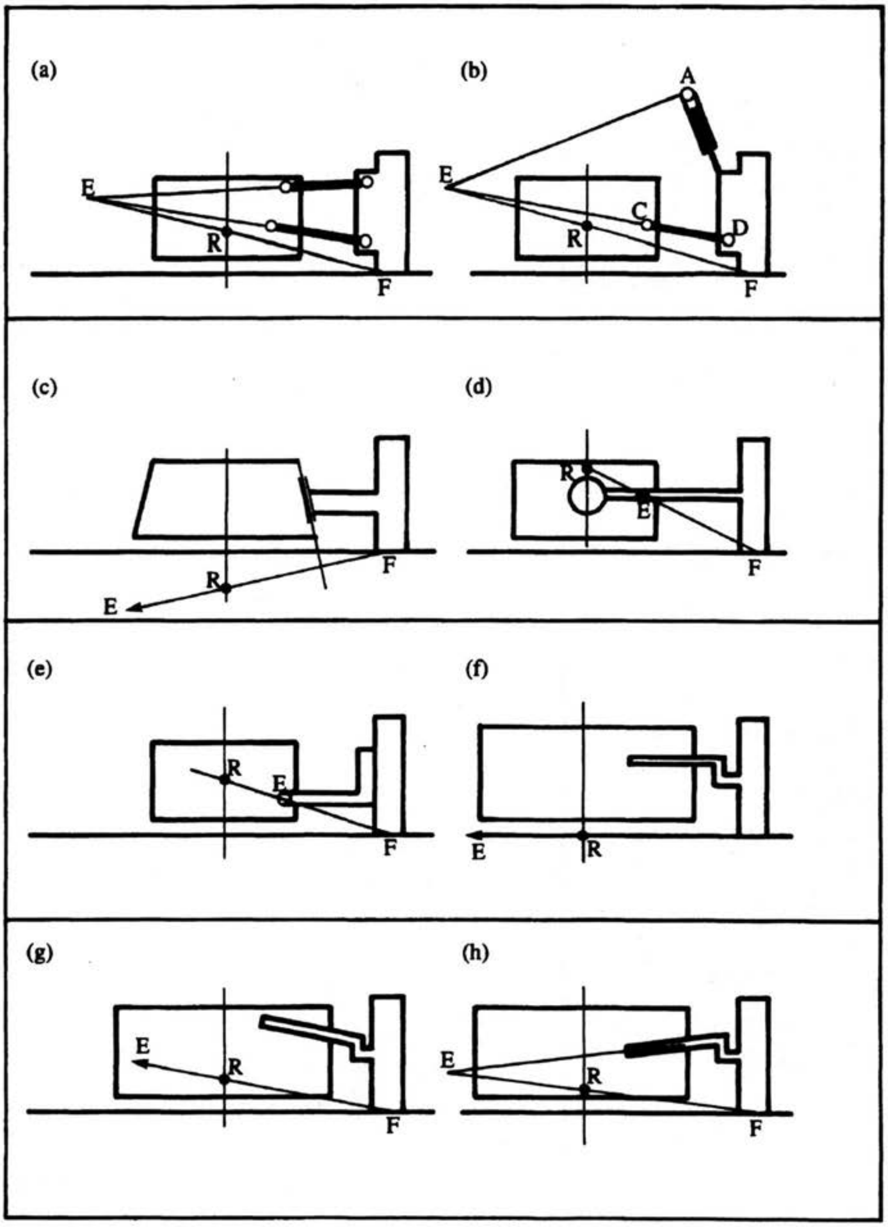
(a)
E
R
F
(b)
A
E
C
R
D
F
(c)
R
F
E
(d)
R
E
F
(e)
R
E
F
(f)
E
R
(g)
E
R
F
(h)
E
R
F

Figure 5.5.2. Basic roll centers for independent suspensions.

An interesting and unusual case of double wishbones that has been used is with the pivot of the upper arm perpendicular to the vehicle centerline in plan view. In front view this gives a straight path of the outer end, at any required angle to the vertical, so that the front view is geometrically rather like a strut suspension, but with the advantage of prospectively lower friction.

With the roll centers determined by the above method, combined with the equations of the previous section, the net link load transfer can be calculated. A high roll center increases the net link load transfer, reducing the net roll load transfer and so helping to reduce the roll angle and roll steer effects. However, a high roll center means a high centro, which means more scrub in bump. Early independent suspension roll centers were at ground level, but the compromise usually found nowadays is a height of 50 to 200 mm.

5.6 Independent Suspension Roll Centers – Part 2

The previous section presented the roll center concept in the degree of detail and accuracy normally applied. However, the load transfer is most important at large lateral accelerations, in which case the body is rolled and the symmetry approximation may not be good. The effective roll center height may then be considerably different from the value in the unrolled position. Therefore this section presents extended analysis of the roll center concept at large lateral accelerations. The explanation is still based on the idealized spring model.

We should make a distinction now between the height at which the link force acts, and the height at which the next increment of force acts, for an increment of lateral acceleration. Such a distinction is routinely made in related fields, such as the center of pressure and the aerodynamic center of a wing. The corresponding terms "roll center" and "incremental roll center" will be used here. The SAE definition does not explicitly address this distinction. The formal definition of the incremental roll center height h_i that will be used here is:

> The incremental roll center height is the rate of change of lateral load transfer through the links of the idealized spring model with respect to the sprung mass side force, multiplied by the track.

Hence

$$h_i = \frac{dF_{TL}}{dF_S} T$$

Differentiating $F_{\mathrm{TL}} = hF_{\mathrm{S}}/T$ with respect to F_{S} and neglecting track change (which is not important in this case), it may be shown by the usual method for a product of variables that

$$h_{\mathrm{i}} = h + F_{\mathrm{S}}\frac{\mathrm{d}h}{\mathrm{d}F_{\mathrm{S}}}$$

It is the incremental roll center heights that determine the front-to-rear distribution of the incremental lateral load transfer. Again, we can define a non-dimensional incremental roll center height, as a fraction of the track, which is the incremental load transfer factor f_{Li}:

> The incremental load transfer factor is the incremental roll center height divided by the track, and equals the rate of change of lateral load transfer through the links of the idealized spring model with respect to the sprung-mass side force.

Hence

$$f_{\mathrm{Li}} = \frac{h_{\mathrm{i}}}{T} = \frac{\mathrm{d}F_{\mathrm{TL}}}{\mathrm{d}F_{\mathrm{S}}}$$

for which

$$f_{\mathrm{Li}} = f_{\mathrm{L}} + F_{\mathrm{S}}\frac{\mathrm{d}f_{\mathrm{L}}}{\mathrm{d}F_{\mathrm{S}}}$$

The position of the incremental force roll center is associated with movement of the force roll center. A high incremental roll center implies a rising roll center. For small lateral acceleration, the roll center height remains approximately constant, and the incremental roll center height equals the roll center height, but this is not so for large lateral acceleration.

In cornering at large lateral accelerations the body is rolled, in which case a symmetry approximation is not appropriate. For example, in the idealized spring model of Figure 5.6.1(a), representing any kind of independent suspension, the positions of $\mathrm{E_L}$ and $\mathrm{E_R}$ depending on the particular geometry, with a total vehicle radial acceleration to the left, the forces resolve as shown, with the link forces directed $\mathrm{F_R}$ to $\mathrm{E_R}$ and $\mathrm{E_L}$ to $\mathrm{F_L}$. The intersection of the EF lines gives a point H on the line of action of the total link force on the body; in general this is not on the vehicle centerline. This total force generally has a vertical upward component, because F_{R2} is different from F_{L2} and θ_{R} different from θ_{L}; this is the jacking force, which partially supports the body weight, relieving the springs and raising the body. From Figure 5.6.1(a), where the total link forces are F_{L2} and F_{R2}, the total jacking force is

$$\begin{aligned} F_J &= F_{R2}\sin\theta_R - F_{L2}\sin\theta_L \\ &\approx 2f(F_{YR} - F_{YL}) \end{aligned}$$

Because the intersection point H is not on the centerline, the jacking force itself is generally distributed unevenly on the two sides, and therefore has some influence on the body roll angle. Actually, for an asymmetric vehicle such as some front-drive vehicles with unequal spring stiffnesses side-to-side, even a central jacking force will result in roll. The vertical line on which a vertical force will cause no roll is called the spring center (SAE). Here we should go further and distinguish between the incremental spring center for a small additional vertical force applied in a given cornering trim, and the (ordinary) spring center which is the place where the vertical component of the total link force can be considered to exert no roll effect.

The point H is not actually the kinematic roll center, that is, it is not the point about which the body rolls relative to the axle. Consider a point M on the centerline at the same height as H. A rotation about H is equivalent to a rotation about M plus a height change. However, the height changes are actually governed by other factors such as jacking force, spring stiffness, etc., not just by the suspension geometry. Therefore the rotation of the body relative to the axle is not constrained to be about H (geometrically there are two degrees of freedom). This is particularly obvious when H moves a long way off to one side, when a roll about H would then demand a very large height change, which simply does not occur. The actual center of roll of the body relative to the axle is offset if there is any jacking, but its position can be found only by first finding the roll angle and heave motion.

Within the approximations stated, the total force exerted on the body by the links acts at H, but not horizontally (Figure 5.6.1(b)). There are points J on the vehicle centerline, K below G, and L on the spring center, all on the line of action of the total link force. If we resolve the total link force into horizontal and vertical (jacking) components at L instead of H, then by definition the jacking component no longer has a rolling effect, and instead the horizontal component now has a different moment because of its new height h_3. In the simplified symmetrical case H, J, K and L are all on the centerline at J.

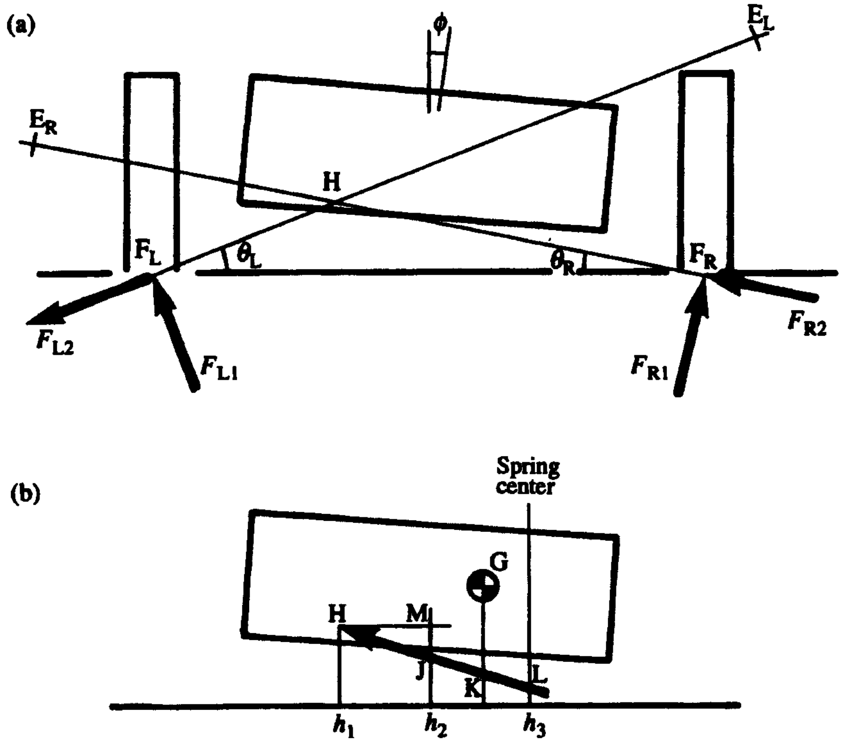

Figure 5.6.1. Roll center at high lateral acceleration.

Where then is the force roll center? Consider the roll center as the point of application of the suspension force to the body. According to this concept, anywhere on the line of action HJKL would do. However, the roll center height is used to calculate the load transfer and the rolling moment, and usually in this process the rolling effect of the jacking force is neglected. In this case we really should use the height of the point L on the spring center. The difference of height between H and L depends on the inclination of the suspension forces, which may be substantial for high lateral acceleration. If we use a point other than L as the roll center, then the moment of the jacking force should be dealt with as a separate item. We may consider the roll center to be on the centerline at the height of L; it need not be considered to be at L itself.

The distinction between H, J, K and L is important in principle, and may also be in practice for large lateral accelerations. In particular, H may move sideways and up or down because of the suspension geometry, and L may move sideways because of nonlinear springs and bump stops.

With the definition of the roll center proposed here, the roll center height in Figure 5.6.1(a) may be determined by force analysis. The definition of link lateral load transfer is:

> The load transfer through the links is one-half of the difference in the vertical upward components of the net forces exerted through the links.

Hence, in Figure 5.6.1(a),

$$F_{TL} = \tfrac{1}{2}(F_{R2}\sin\theta_R + F_{L2}\sin\theta_L)$$

where a plus sign is used because F_{L2} acts downward here with θ_L positive. The roll center height is then found from $h = (F_{TL}/F_S)T$. Of course, having found the load transfer directly, the roll center height need not be found, other than as a matter of record or interest or as a convenient summary of the suspension characteristics.

Two specific examples will be considered here. Figure 5.6.2 shows a parallel equal-arm double-wishbone suspension. In this case the body roll lowers the inside end of the outer (right-hand) side links, the link angle and hence θ depending on the link length and the lateral spacing between the link–body mounting points. In this case

$$F_{TL} = \tfrac{1}{2}(F_{R2}\sin\theta_R - F_{L2}\sin\theta_L)$$

By definition, the total link force from both sides exerts no moment about the roll center for the idealized spring model. In general, at high lateral acceleration $F_{R2} > F_{L2}$, so the roll center will be nearer to the line of action of F_{R2} than that of F_{L2}, i.e., with increasing lateral acceleration and roll, the roll center falls for this kind of suspension; this is generally true of double-wishbone suspensions.

Figure 5.6.3 shows a plain trailing-arm suspension. For this case, with roll angle ϕ,

$$F_{TL} = \tfrac{1}{2}(F_{R2}\sin\phi - F_{L2}\sin\phi)$$

Again, considering the point on the centerline with no moment from F_{L2} and F_{R2} combined, and with $F_{R2} > F_{L2}$, we see that in this case the roll center rises above ground level. It approaches the line of action of F_{R2} as F_{L1}, and hence F_{L2},

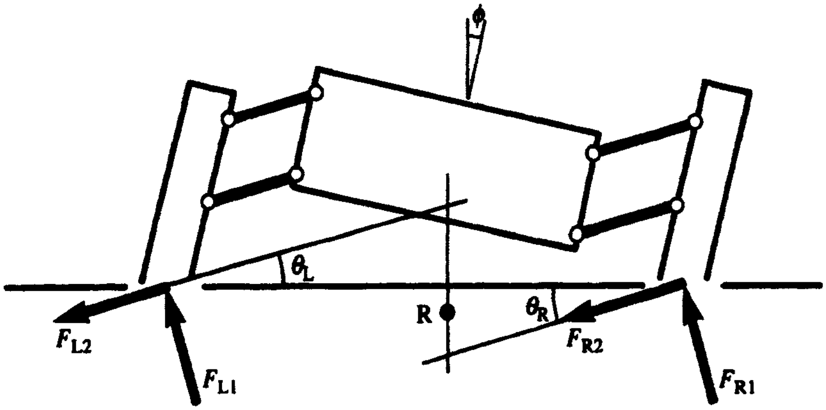

Figure 5.6.2. Rolled equal parallel wishbones.

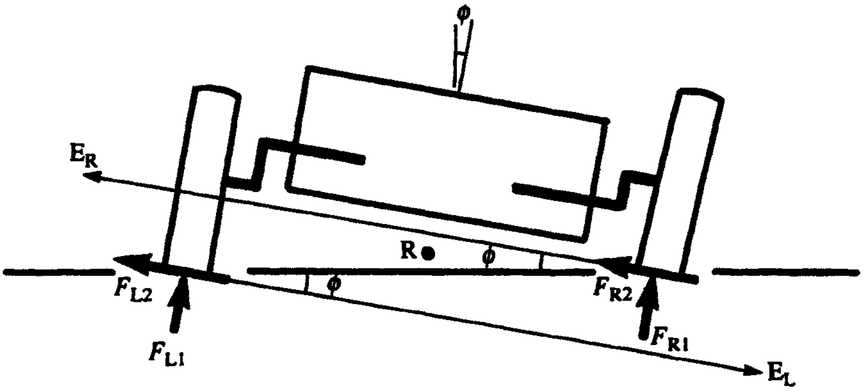

Figure 5.6.3. Plain trailing arms in rolled position.

tends to zero, and therefore may reach 100 mm or more for large lateral accelerations. This is in marked contrast to the usual assumption that it remains at ground level for this kind of suspension. In other words, there is a link load transfer and also a jacking force in contrast to the usual assumption that these are zero. This is easily seen for the extreme case when the inner wheel vertical force goes to zero, leaving a jacking force $F_{R2}\sin\phi$ and link load transfer $\frac{1}{2}F_{R2}\sin\phi$. These are not apparent from the simple theory of Section 5.5 because they develop in a nonlinear way.

For steady-state handling analysis, the roll center height may be represented approximately by

$$h = h_0 + k_{\mathrm{RCA2}} A^2$$

where k_{RCA2} is the quadratic roll center height variation coefficient, with a value possibly around ±0.001 m/(m $\mathrm{s^{-2}})^2$ (0.1 m/g^2).

Because the effect of a rising or falling roll center comes into play only as roll angle develops, it would be possible to treat the roll center height as fixed and to have an extra equivalent anti-roll bar. However, this would have to be nonlinear, probably with moment proportional to roll angle squared, and its properties could be established only by investigating the roll center movement. For a falling roll center it would have negative stiffness.

5.7 Solid-Axle Roll Centers

This section deals with the determination of the roll center for solid axles with rigid link location. Leaf-spring axles are considered in the next section. Figure 5.7.1 shows a general four-link axle. The method is based on studying the support links to find two points A and B where forces are exerted by the axle on the body, the roll center necessarily lying on the line joining A and B, at the point where this line penetrates the transverse vertical plane of the wheel centers. Consider idealized springs at the wheels, or at least springs that do not act on the links. One link pair has an intersection point at A, so the combined force exerted by these links on the body must act through A (neglecting bush torques and link weight). Similarly the other link pair exerts a force through B. The resultant of the two forces at A and B acts through a point somewhere on AB. However, the cornering force acts in the vertical transverse plane of the wheel centers, neglecting pneumatic trail, so the roll center is where AB intersects this plane. The torque due to trail can be dealt with separately.

Suitable points A and B can be found for other axle link layouts. For example, if the lower links are parallel then the point B is at infinity, so AB is parallel to the bottom links. If the bottom link pair is replaced by a torque tube or similar system (Figure 4.6.1(f)), then point B is the front ball-joint. If transverse location is by a Panhard rod, then point A is the point at which the rod intersects the vertical central plane. A characteristic of the Panhard rod is that the roll center rises for roll in one direction, and falls for the other because of vertical motion of the point of connection to the body. For other axle lateral location systems it is similarly necessary to find point A where the line of action of the force intersects the

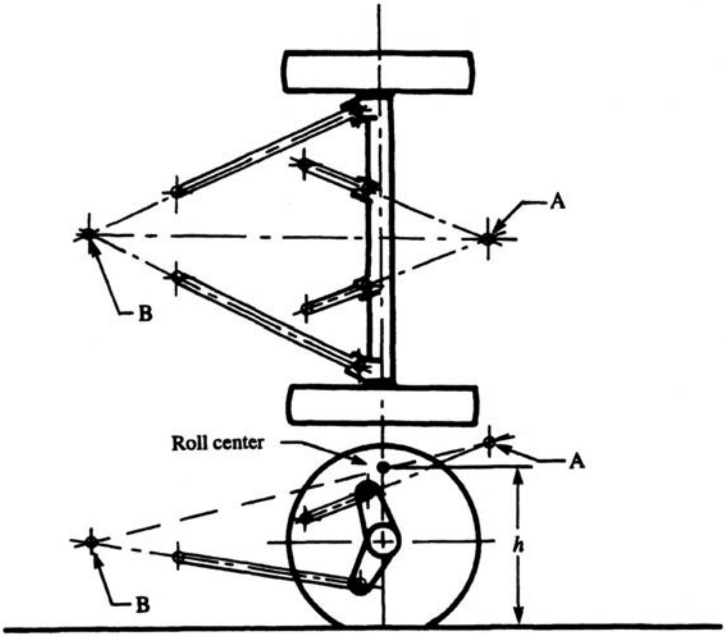

Figure 5.7.1. Roll center for four-link solid axle.

central plane. In the systems described in Section 4.3, this generally corresponds to the pivot pin point C.

The forces exerted on a solid axle are as in Figure 5.4.1. The resolution into components directed along and perpendicular to the line from the contact to the roll center, as in Figure 5.5.1 for independent suspension, is no longer appropriate because the wheels exert forces directly on each other. Hence the solid axle has no link jacking force.

5.8 Compliant-Link Roll Centers

Finding the roll centers of compliant-link systems is especially problematic. In the cases covered so far, the locating links were physically distinct from the springs. The functions of horizontal location and vertical force generation are sometimes combined in single elements, for example the leaf-spring or trailing twist axle. This complicates the issue considerably.

In the case of location by longitudinal leaf-springs, the load transfer properties depend on the bending and torsional stiffness of the springs and bushes, which comes into play only once the body rolls; so it is necessary to separate out the roll stiffness effects as an equivalent anti-roll bar, to leave the effective roll center height. As an example to find a first approximation to the roll center position, consider the simplified case of Figure 5.8.1.

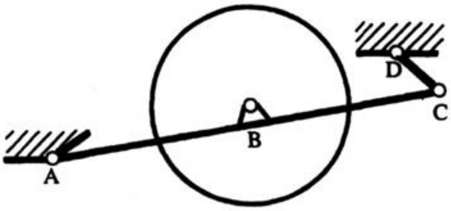

Figure 5.8.1. An idealized leaf-spring axle.

First, consider the case of perfect torsional rigidity of the straight spring ABC, and complete rigidity of link DC and the bushes at A, C and D, other than their basic design motion. In such a case, a force could be applied to the body at any height without any roll rotation being possible. This is equivalent to a perfectly rigid anti-roll bar. To completely eliminate anti-roll bar effects, which must be done to find the roll center, compliance must be introduced into the system, in particular for the bushes about axes AC or AD. In practice, because of the torsional compliance of the leaf-spring, the effective stiffness of bush C will be less than that of D. If we consider bushes A and C to have complete compliance about AC, but D to be rigid, then a side force applied to the body on the line AC can be transmitted to the suspension because DC will act as a rigid cantilever. In this simplified case, the roll center will be at the height of the line AC where it passes the vertical transverse plane of the wheel centers. For other more complex cases, such as curved springs ABC, it is still usual to take this approximation, i.e., to use the line joining the front and rear spring eyes. This is clearly only an approximation because even with a side force applied at roll center height there will be torsion of the spring and additional torque at A and C. In any case, the roll stiffness because of spring torsion with body roll must be treated as an equivalent anti-roll bar.

Because of the lateral compliance of the leaf-spring location system, it is possible to supplement it with a Panhard rod or other lateral location device, as is sometimes done for racing. If the stiffness of the rod with its bushes is sufficient, i.e., much greater than the leaf system, then the rod will be decisive. Otherwise the result will be some intermediate position. If the rod is at a different height from B, this calls for increased lateral deflection of the leaf-springs and therefore results in an additional roll stiffness, which must be treated as an equivalent anti-roll bar.

In the case of the trailing twist axle the crossmember acts in torsion giving an anti-roll bar effect, so to eliminate this we must consider a zero torsion stiffness crossmember, still with bending stiffness. Figure 5.8.2(a) shows a rear view of a simplified case with horizontal arms and small roll angle. The tire lateral forces are L and L'. The crossbeam has the free-body diagram in rear view of Figure 5.8.2(b). The wheel vertical forces are reacted separately by springs on the trailing arms. The tire side forces exert moments Ls and $L's$ on the ends of the beam. For beam rotational equilibrium there must be vertical end forces as shown. This gives the beam the bending-moment diagram of Figure 5.8.2(c).

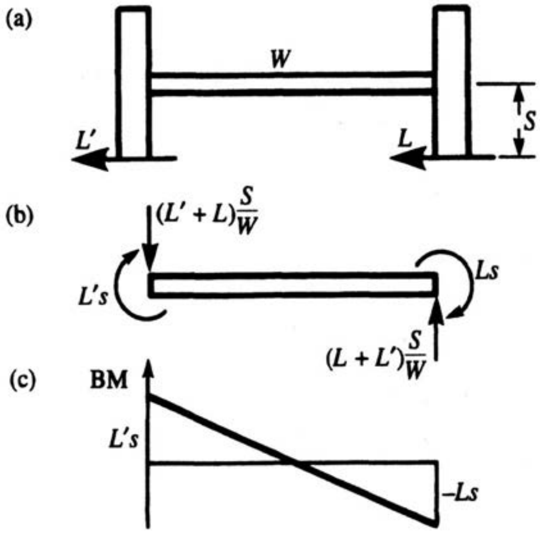

Figure 5.8.2. Trailing twist axle: (a) rear view, (b) beam free-body diagram, (c) bending-moment diagram.

When $L \approx L'$ the central bending moment is small in this view. A similar argument applies in plan view. In conjunction with the zero torsion specification, this means that each half of the suspension exerts negligible moment about an axis from its own front bush through the mid-point of the crossbeam. Therefore this axis can be projected into the transverse plane of the wheel centers to find the force center, as for a trailing arm. The approximations are increasingly in error as the lateral acceleration increases, so this is only the initial position of the roll center.

5.9 Experimental Roll Centers

Various methods have been suggested at times for the experimental measurement of roll center position, none of which are really very satisfactory. One method is the observation of body displacement with application of a lateral force at the center of mass, for example using a laterally slanted ramp, but this is definitely not suitable. The large lateral displacement at the tires is a problem which may be eliminated by using solid wheels, but there will still be inappropriate lateral displacements within the suspension compliances. A correct method of finding the SAE roll center would be to apply lateral forces at various heights. With the lateral force applied at the height of the roll axis, there will be a lateral displacement of the body because of compliances and a vertical displacement because of the jacking force, but no rotation. In this sense, the force roll center is directly analogous to a shear center, which would probably be a better name for it, although the former name is no doubt too entrenched by use to change now.

As in the case of a shear center, there is a more direct method of measurement. If the displacement is observed when a moment is applied, the shear center will be the center of rotation, i.e., the point of zero displacement. The most convenient way to apply a moment is by a couple, for example by a joist through the doors, with a load first on one end then on the other. This does involve a vertical load which is acceptable if the vehicle is to be tested in a loaded condition. Otherwise it is necessary to arrange for a vertical upward force to be applied as half of the couple, say by a hydraulic jack or a weight over a pulley. The actual deflection has been analyzed by double-exposure photographs, but in the interest of accuracy it is much better to take measurements of the displacement of specific points by dial gauges. If these points are not in the vertical transverse plane of the wheel centers, then the data must be used to find the roll axis, and this then used to find the roll axis position at each suspension.

This method is still subject to serious errors and problems. Under real cornering conditions there are actually large forces in the suspension links causing geometric changes through bush distortions. These are largely absent from the test. Any small inappropriate lateral displacement of the body will give a large error in the measured roll center height. The applied couple will change the load on the tires, giving an additional rotation of the complete chassis, including the wheels, about a point at ground level roughly midway between the tires. The result is a false lateral motion of the body at roll center height. This must be guarded against by using solid disc wheels, although this exacerbates the problem of allowing scrub because when finding the roll center for large angular displacements, there will be a consequent track change. This must be permitted, perhaps with air bearing pads, but without allowing any inappropriate lateral motion of the body, which is critical. It is difficult to say how the body should be located.

In summary, it is fairly easy to observe the displacement of a vehicle when it is subject to loads or couples, but it is much more difficult to obtain results that have a worthwhile roll center interpretation, especially for large lateral accelerations. Probably the only satisfactory experimental method is to use an instrumented vehicle in real cornering to find the actual load transfer for each axle with strain gauges on the links, and to deduce the net link load transfer and force roll center height from that, using the equations of Section 5.4.

5.10 Suspension Load Transfer

During cornering, the vertical forces on the outer tires increase at the expense of those on the inner ones. This is vertical force transferred laterally, commonly called lateral load transfer. This section describes lateral load transfer on a single solid or independent axle. A complete vehicle with two axles is examined in the next section.

As perceived in vehicle-fixed axes, the load transfer F_T is accomplished by several simultaneous compensation forces on the axle, referring back to Figure 5.4.1. These are:

(1) The centrifugal force $F_U = m_U A$ on the unsprung end-mass at its G height, giving load transfer F_{TU}.

(2) The centrifugal force $F_S = m_S A$ on the sprung end-mass acting at roll center height through the links, giving the net link load transfer F_{TL}.

(3) The moment M_S resisted by the idealized springs and anti-roll bar, because of roll angle, giving the net moment load transfer F_{TM}.

This gives

$$F_T = F_{TU} + F_{TL} + F_{TM}$$

Actually, the springs normally act on the links in a way that creates additional internal forces in both that have no net effect on the body or axle. Of course, in the investigation of internal effects, e.g., bush distortions, it is necessary to consider the real spring position. However, the important effect of the spring and anti-roll bar is to produce the wheel vertical force, and for handling their exact position is not important provided that the end result is the same. For example, for a given wheel force a spring acting on a wishbone will need to exert a smaller force if it acts closer to the wheel end. Different spring positions for a given wheel force give different spring and link forces, but do not alter the net effect, so it is very convenient to reduce a suspension to the idealized spring model. This has the same links, but the spring and anti-roll bar are deemed to act in a way that creates no link forces; e.g., in Figure 5.2.3 this will mean that the spring force acts directly along the line of action of F_{R1}. In the idealized spring model, the conflicting internal forces are eliminated, leaving only the important net effects.

In Figure 5.5.1, the net link load transfer is the difference of vertical components of F_{L2} and F_{R2}. The net roll load transfer from the springs and anti-roll bar is the difference of vertical components of F_{L1} and F_{R1}. The jacking force is the total vertical force exerted by the links of the model, and so is the sum of the vertical components of F_{L2} and F_{R2}.

Figure 5.10.1(a) shows the rear-view free-body diagram of a highly simplified notional two-dimensional vehicle in steady-state left-hand cornering, in Earth-fixed (inertial) coordinate axes. There are tire lateral forces giving the vehicle a radial acceleration A to the left. Figure 5.10.1(b) shows the free-body diagram in the vehicle-fixed axes. The appropriate compensation force mA has been added at the center of mass, so that the vehicle has no acceleration in this coordinate system. Bearing in mind that the total tire lateral force $F_{YL} + F_{YR}$ equals mA, that the total tire vertical force $F_{VL} + F_{VR}$ equals W, and that there is no roll acceleration, summing moments about the center of mass G for either of these figures gives

$$\sum M = \tfrac{1}{2} F_{VL} T - \tfrac{1}{2} F_{VR} T - (F_{YL} + F_{YR}) H = 0$$

Hence

$$\tfrac{1}{2}(F_{VL} - F_{VR}) T = (F_{YL} + F_{YR}) H = mAH$$

The total load transfer is half of the difference of tire vertical forces:

$$F_T = \frac{F_{VL} - F_{VR}}{2} = \frac{mAH}{T}$$

The wheel vertical forces are therefore

$$F_{\mathrm{VR}} = \frac{W}{2} + \frac{mAH}{T}$$

$$F_{\mathrm{VL}} = \frac{W}{2} - \frac{mAH}{T}$$

The total load transfer depends only on the lateral force *mA*, the center of mass height *H* and the track *T*. This demonstrates that for this model the total load transfer cannot be influenced by adjustment to internal characteristics such as the suspension.

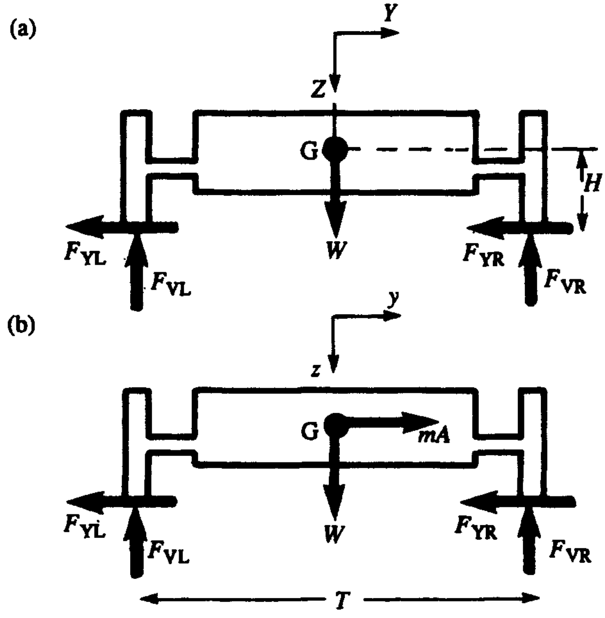
(a)
Y
Z
G
H
F_{YL}
F_{VL}
W
F_{YR}
F_{VR}
(b)
y
z
G
mA
F_{YL}
F_{VL}
W
F_{YR}
F_{VR}
T

Figure 5.10.1. Free-body diagrams: (a) Earth-fixed axes, (b) vehicle-fixed axes.

Actually, this is not exactly true for a body that rolls because the roll angle moves the center of mass out slightly relative to the wheels, depending on the height of G_S above the roll axis, as shown in Figure 5.4.1. At maximum lateral acceleration this lateral motion of G gives a load transfer of about 5% of the total weight, compared with a load transfer of about 35% of the weight from the other factors. It is sometimes stated that a vehicle that does not roll has no load transfer;

this is false. Zero roll will eliminate the small factor because of lateral G movement, but will have no effect on the major factors shown in the zero-roll model above.

It is often convenient to express the lateral load transfer in terms of a non-dimensional vertical force lateral transfer factor e_V. This is defined as

$$e_V = \frac{F_T}{F_{Vi0}}$$

where F_{Vi0} is the static vertical force on the inner wheel. Hence $e_V = 1$ corresponds to inner wheel lift-off.

It is desirable for safety reasons that overturning should not occur before the tire friction sliding limit, placing limits on the relationship between H and T. These limits are met by normal cars but often not met by trucks, especially when loaded. Because of the tire characteristics, the greatest total lateral force can be achieved if the vertical force is as uniform as possible from side to side, giving a strong incentive for racing and sports vehicles to have a low center of mass and a wide track.

Rollover would occur at a lateral acceleration at which the load transfer reduces the inner reaction F_{VL} to zero:

$$A_R = \frac{WT}{2mH} = \frac{gT}{2H}$$

If the maximum lateral acceleration achievable, limited by grip, is A_M, then the safety factor against roll is defined to be

$$S_R = \frac{A_R}{A_M}$$

Using the above expression for the value of A_R, then

$$S_R = \frac{\frac{1}{2}gT/H}{A_M} = \frac{gT}{2A_M H}$$

which is around 1.5 for a conventional passenger car. The simple expression for S_R immediately above can be refined by a more accurate calculation of A_R, including load transfer from body roll (lateral G position), gyroscopic effects, and tire lateral distortion. This gives:

$$A_R = \frac{\frac{1}{2}gT/H}{1 + \dfrac{m_S g(H_S - h)k_\phi}{mH} + \dfrac{m_{4w}k^2}{mHR_e} + \dfrac{mg}{2Hk_y}}$$

where m_{4w} is the mass of the four wheels, k is their radius of gyration, and k_y is the tire lateral stiffness relating the offsetting of F_V to the side force. This more accurate value of A_R is about 20% lower than the simply calculated value, giving a correspondingly much lower calculated S_R.

The steady-state analysis above is useful for basic comparison purposes, but dynamic effects through the sudden or cyclic application of steering can considerably increase the propensity to roll over. Also, many rollovers occur by tripping at a curb. Actual rollovers occur at a rate of around 0.01% per annum for passenger cars. A high S_R value helps to reduce this, but driving style is a major factor. Also rollovers are due to tire, wheel or suspension failure. Heavy trucks are especially prone to roll over because their high center of mass and low natural roll frequency make them especially sensitive to roll resonance problems.

Figure 5.4.1 showed the forces exerted on an axle seen in vehicle-fixed axes, including consideration of separate unsprung and rolling sprung masses. The total tire lateral force is

$$F_S + F_U = m_S A + m_U A$$

The unsprung mass centrifugal compensation force $m_U A$ is applied at the unsprung center of mass height H_U. The sprung-mass centrifugal compensation force, really applied at the sprung center of mass, is shown instead transferred to the roll center, along with a moment. The sprung weight force, now offset because of roll, is also transferred to the roll center and also contributes to the moment. Using

$$d = H_S - h$$

then the moment is

$$M_S = m_S A d \cos\phi + m_S g d \sin\phi$$

In the vehicle-fixed axes, all moments are in equilibrium so setting moments about the mid-point between the tire contacts to zero and dividing by the track T gives the total load transfer:

$$F_T = F_{TU} + F_{TL} + F_{TM}$$
$$= \frac{F_U H_U}{T} + \frac{F_S h}{T} + \frac{M_S}{T}$$

Thus the load transfer arises from three factors: unsprung side force at the unsprung center of mass height, sprung side force through the links at roll center height, and the moment associated with the roll angle. It is usual to treat the two unsprung parts of an independent suspension as having a combined center of mass. For independent suspension, the unsprung load transfer actually results in link forces that affect the sprung mass roll angle slightly, depending on the details of the linkage geometry. This is usually neglected for simplicity.

Part of the total load transfer from the sprung mass is taken by the roll angle acting against the roll stiffness giving F_{TM}, and part is exerted directly by the links giving F_{TL}. The allocation of load transfer to the two methods depends on the roll center height. Usually $0 < h < H_S$, in which case the vehicle rolls outward, and the load transfer by both methods is positive. If $h = H_S$ there will be zero roll angle and all the load transfer is through the links. For a roll center higher than the sprung center of mass ($h > H_S$), not normally met in practice, the links would transfer too much load which would be balanced by a negative load transfer in the springs, and the body would lean into the turn. For a roll center below ground level ($h < 0$), sometimes met in practice, the links have a negative load transfer so the springs and anti-roll bar must have a load transfer exceeding the total. However, whatever the roll center height, the total load transfer is not altered other than that a high roll center helps to reduce the roll angle which reduces the relatively small effect of the lateral movement of the center of mass.

The roll moment produced by the stiffness elements in roll depends on the body roll relative to the axle, i.e., relative to a line joining the wheel centers. This is the suspension roll angle. Because of load transfer on the tire vertical stiffness, typically 250 N/mm, the axle itself, solid or independent, has a small roll angle called the axle roll angle. The body roll is the suspension roll plus the axle roll. Axle roll is typically one-eighth of suspension roll, reaching 1–2°.

5.11 Vehicle Load Transfer

Figure 5.11.1 shows a two-axle vehicle model. This distinguishes the sprung mass m_S from the front and rear unsprung masses m_{Uf} and m_{Ur}, each with its own center of mass. There are different front and rear roll center heights, tracks, etc. The vehicle is in steady-state left-hand cornering. It is convenient to perform this analysis in the accelerating coordinate system *xyz* attached to the vehicle (vehicle-fixed axes), so the centrifugal compensation forces are included at each mass center. In this coordinate system there are no linear or angular accelerations. The sprung-mass weight force is shown; other weights and tire forces are omitted for clarity of the figure. The lateral acceleration considered here is that perpendicular to the vehicle centerline. This is not quite the same as the cornering radial acceleration because the vehicle body has an attitude angle to its direction of travel arising from steering, the slip angle of the rear tires and roll and compliance steer effects, so the vehicle radial acceleration resolves into a lateral acceleration and a longitudinal one. The longitudinal acceleration component causes a front-to-rear load transfer that can be calculated separately. The linear analysis will be presented here in order to illustrate the principles. In practice, the load transfer is important at higher lateral accelerations, in which case nonlinearities may well come into play (for example, bump stops). A good computer simulation can, of course, deal with the nonlinearities.

In these vehicle-fixed coordinate axes, the vehicle is held in equilibrium, with zero acceleration. The forces $m_{Uf}A$ and $m_{Ur}A$ act directly on the front and rear axles, respectively, each transferring load only between its own pair of tires. The effect of the sprung-mass forces m_SA and m_Sg may be determined as before. The distance of the sprung center of mass from the roll axis is $d = H_S - h$. The roll angle is ϕ. The forces m_SA and m_Sg may be replaced by forces at A plus a moment, which is

$$M_S = m_SAd\cos\phi + m_Sgd\sin\phi$$

This moment is reacted by the springs and anti-roll bars, distributed front-to-rear appropriately (according to the distribution of roll stiffness for the linear case for a torsionally rigid body). This determines the suspension roll angle. To find this roll angle, this total applied moment must be matched against the total vehicle roll couple characteristic from Figure 5.3.1. The roll angle is usually small enough for a small ϕ approximation for the applied moment, giving

$$M_S = m_SAd + m_Sgd\phi$$

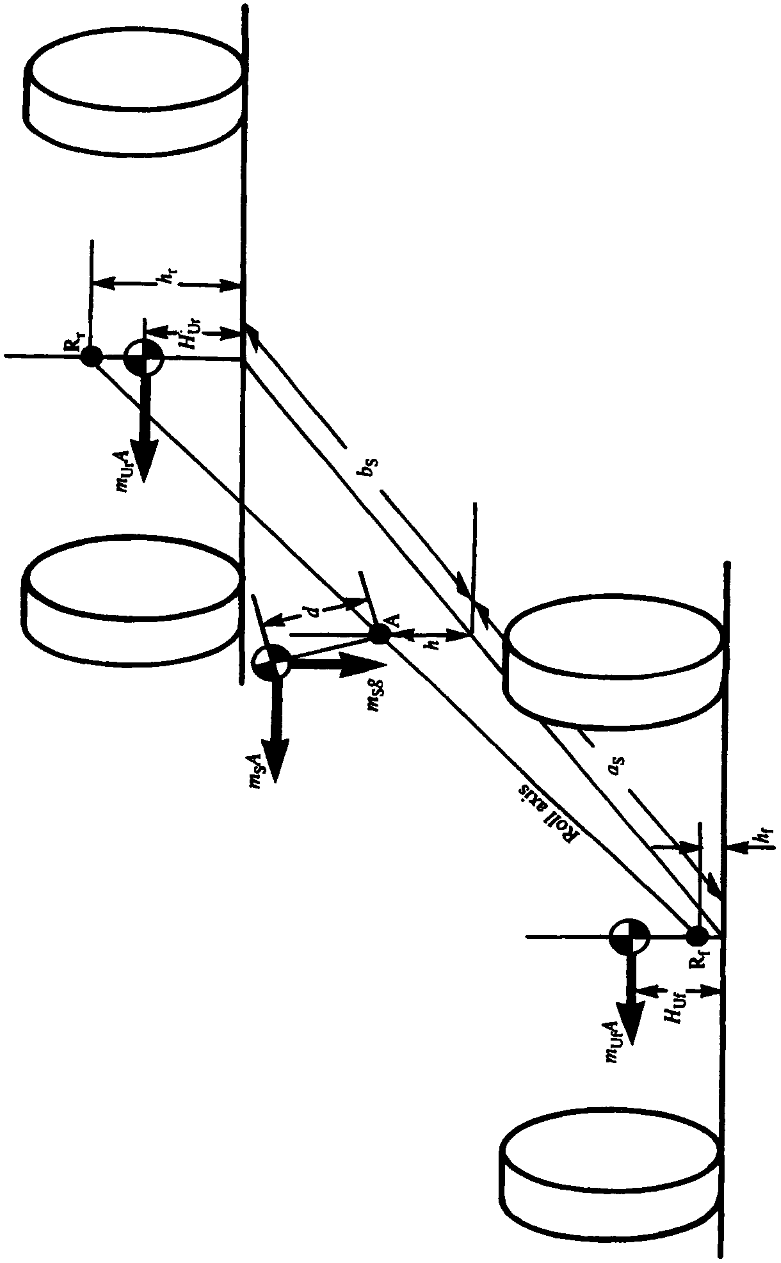
h_r
H_{Ur}
R_r
$m_{Ur}A$
b_S
d
A
h
m_Sg
m_SA
a_S
Roll axis
h_f
R_f
H_{Uf}
$m_{Uf}A$

Figure 5.11.1. Vehicle load transfer model, vehicle-fixed axes.

If the resistance moment is also linearized, which is a more restrictive approximation, then

$$M_\phi = k_{\mathrm{S}}\phi = (k_{\mathrm{Sf}} + k_{\mathrm{Sr}})\phi$$

in which case the roll angle has the simple solution

$$\phi = \frac{m_{\mathrm{S}}Ad}{k_{\mathrm{S}} - m_{\mathrm{S}}gd}$$

Here k_{S} is used, the roll compliance on the tires being neglected for simplicity. In practice it is desirable to include this, especially for higher roll stiffness suspensions.

Consistent units must be used; it is normally necessary to convert $m_{\mathrm{S}}gd$ from Nm/rad to Nm/deg to agree with k, this then giving roll angle in degrees. The roll-angle gradient is

$$k_{\mathrm{f}} = \frac{\mathrm{d}\phi}{\mathrm{d}A} = \frac{m_{\mathrm{S}}d}{k_{\mathrm{S}} - m_{\mathrm{S}}gd}$$

From the known roll angle and the front and rear roll couple graphs or roll stiffnesses, the front and rear load transfer from roll angle may be found. For the linearized case

$$F_{\mathrm{TfM}} = \frac{k_{\mathrm{f}}\phi}{T_{\mathrm{f}}} = \frac{k_{\mathrm{f}}m_{\mathrm{S}}Ad/T_{\mathrm{f}}}{k - m_{\mathrm{S}}gd}$$

$$F_{\mathrm{TrM}} = \frac{k_{\mathrm{r}}\phi}{T_{\mathrm{r}}} = \frac{k_{\mathrm{r}}m_{\mathrm{S}}Ad/T_{\mathrm{r}}}{k - m_{\mathrm{S}}gd}$$

This completes the calculation of roll stiffness load transfer.

The effect of the sprung mass force $m_{\mathrm{S}}A$, which has been transferred to point A on the roll axis, is found by redistributing the side force between the front and rear roll centers according to the position of the unsprung center of mass along the wheelbase. The wheelbase is

$$L = a + b = a_{\mathrm{S}} + b_{\mathrm{S}}$$

where the sprung center of mass is a_S behind the front axle. The front and rear sprung end-masses are:

$$m_{Sf} = \frac{m_S b_S}{L} = m_f - m_{Uf}$$
$$m_{Sr} = \frac{m_S a_S}{L} = m_r - m_{Ur}$$

where m_f and m_r are the total front and rear end-masses:

$$m_f = \frac{mb}{L}$$
$$m_r = \frac{ma}{L}$$

where m is the total mass. At the front and rear axles the sprung end-mass forces are

$$F_{Sf} = m_{Sf} A$$
$$F_{Sr} = m_{Sr} A$$

The sprung end-mass forces F_{Sf} and F_{Sr} each act on the appropriate suspension and cause load transfer on their own end only, according to the roll center height for that end, giving the net link load transfer:

$$F_{TfL} = \frac{m_{Sf} A h_f}{T_f} = m_{Sf} A f_f$$
$$F_{TrL} = \frac{m_{Sr} A h_r}{T_r} = m_{Sr} A f_r$$

where $f = h/T$ is the suspension load transfer factor. This completes calculation of the load transfer from the sprung mass.

The unsprung mass load transfer is simply caused by the height of the centrifugal compensation force on the unsprung center of mass (an approximation for independent suspension), so

$$F_{\mathrm{TfU}} = \frac{m_{\mathrm{Uf}} A H_{\mathrm{Uf}}}{T_{\mathrm{f}}}$$

$$F_{\mathrm{TrU}} = \frac{m_{\mathrm{Ur}} A H_{\mathrm{Ur}}}{T_{\mathrm{r}}}$$

where H_{U} is the unsprung center-of-mass height.

The total load transfer from sprung and unsprung effects at each end is then

$$F_{\mathrm{Tf}} = F_{\mathrm{TfU}} + F_{\mathrm{TfL}} + F_{\mathrm{TfM}}$$

$$F_{\mathrm{Tr}} = F_{\mathrm{TrU}} + F_{\mathrm{TrL}} + F_{\mathrm{TrM}}$$

For the linear case, all this can be summarized by

$$\phi = \frac{m_{\mathrm{S}} A d}{k_{\mathrm{S}} - m_{\mathrm{S}} g d}$$

$$F_{\mathrm{Tf}} = \frac{m_{\mathrm{Uf}} A H_{\mathrm{Uf}}}{T_{\mathrm{f}}} + \frac{m_{\mathrm{Sf}} A h_{\mathrm{f}}}{T_{\mathrm{f}}} + \frac{k_{\mathrm{f}} \phi}{T_{\mathrm{f}}}$$

$$F_{\mathrm{Tr}} = \frac{m_{\mathrm{Ur}} A H_{\mathrm{Ur}}}{T_{\mathrm{r}}} + \frac{m_{\mathrm{Sr}} A h_{\mathrm{r}}}{T_{\mathrm{r}}} + \frac{k_{\mathrm{r}} \phi}{T_{\mathrm{r}}}$$

In this way the front and rear lateral load transfer may be found. The distribution of lateral load transfer moment should be carefully distinguished from the distribution of roll stiffness, even in the linear case. The front load transfer moment distribution factor is

$$d_{\mathrm{f}} = \frac{F_{\mathrm{Tf}} T_{\mathrm{f}}}{F_{\mathrm{Tf}} T_{\mathrm{f}} + F_{\mathrm{Tr}} T_{\mathrm{r}}}$$

with rear factor

$$d_{\mathrm{r}} = 1 - d_{\mathrm{f}}$$

The front and rear load transfer gradients are

$$k_{\mathrm{FTf}} = \frac{\mathrm{d}F_{\mathrm{Tf}}}{\mathrm{d}A}$$

$$k_{\mathrm{FTr}} = \frac{\mathrm{d}F_{\mathrm{Tr}}}{\mathrm{d}A}$$

Where required, the calculation above may be refined by including tire overturning moment, the gyroscopic effect of the wheels, and possibly engine and aerodynamic effects. These may have a substantial cumulative influence.

The procedure for finding the cornering load transfer and its distribution may be summarized as follows:

(1) Find the total applied rolling moment for the sprung mass for each end in terms of ϕ.

(2) Find ϕ using the total roll couple curve or roll stiffness.

(3) Find the roll load transfer for each end using the end roll couple curves or roll stiffnesses.

(4) Find the front-to-rear distribution of side force from the sprung mass.

(5) Find the sprung-mass force load transfer for each end using the roll center heights (net link load transfer).

(6) Find the unsprung-mass load transfer for each end using the unsprung-mass heights.

(7) For each end, sum the load transfers by unsprung-mass side force, net link side force, and the roll stiffness moment.

It is sometimes suggested that account should be taken of the inclination ρ_{ra} of the roll axis, which is usually 6° or less, and 12° in the extreme. Then instead of transferring the sprung side force directly down to the roll axis, it is moved perpendicularly to the roll axis; in practice this means slightly backwards and with a slightly smaller moment arm. However, if this is done then one should also allow for the fact that the moment about the roll axis has a component about a vertical axis, which compensates for the rearward movement. Also, for realistic values of inclination the cosine is so close to 1.0 that the change of moment arm is negligible. Allowing for axis inclination therefore simply complicates the equations without usefully improving the accuracy.

The above analysis assumes that the body is torsionally stiff, to the extent that the torsion angle is much less than the roll angle, i.e., the front and rear suspension roll angles are taken to be equal, which is generally true enough for cars but not so for trucks. If this is not the case, then the moment about the roll axis is distributed front-to-rear in a more complex way. For a torsionally compliant body, attempts to adjust the distribution of roll stiffness by anti-roll bars is ineffective, so this ceases to be an effective tool in handling adjustment. In this context, torsional compliance of the body must be compared with the torsional compliance of the suspension. Also, additional effects may sometimes need to be considered. For example, the center of mass may be off-center, or the ground may be sloping, or aerodynamic forces may be significant.

Tire compliance also has some effect, especially for racing cars. It has relatively little effect on passenger cars, but can be included if desired.

Aerodynamic effects may be added, calculating the forces and moments according to the methods of Chapter 3. The effect of lift and pitch is considered in detail in Section 5.13. Roll, yaw and side lift have some effect on lateral load transfer; this is usually small, but may be significant for some vehicles. For left-hand cornering, as in the rear view of Figure 5.10.1, positive forces act to the right, so the compensation forces are positive and the tire forces are negative, and clockwise moments will be taken as positive. Taking the attitude gradient as positive, the attitude is negative for low speed with front steering, becoming positive for large lateral acceleration. C'_{S}, C'_{R} and C'_{Y} are usually simply given positive values, in which case the side lift, roll moment and yaw moment are

$$
\begin{aligned}
F_{\mathrm{AeS}} &= -C'_{\mathrm{S}}\beta_{\mathrm{Ae}}qA_{\mathrm{F}} \\
M_{\mathrm{AeR}} &= -C'_{\mathrm{R}}\beta_{\mathrm{Ae}}qA_{\mathrm{F}}L \\
M_{\mathrm{AeY}} &= -C'_{\mathrm{Y}}\beta_{\mathrm{Ae}}qA_{\mathrm{F}}L
\end{aligned}
$$

where β_{Ae} is the aerodynamic attitude angle, which in still air is

$$
\beta_{Ae} = \beta = -\frac{b}{R} + k_{\beta}A
$$

The aerodynamic effect on roll angle depends on the aerodynamic roll moment about the roll axis. Considering that the side force acts at the mid-point of the wheelbase, and that the yaw moment has a component about the roll axis, which has inclination

$$\rho_{\mathrm{ra}} = \frac{h_{\mathrm{r}} - h_{\mathrm{f}}}{L}$$

the aerodynamic moment on the sprung mass about the roll axis is

$$M_{\mathrm{SAe,ra}} = M_{\mathrm{AeR}} - \frac{F_{\mathrm{AeS}}(h_{\mathrm{f}} + h_{\mathrm{r}})}{2} + \frac{M_{\mathrm{AeY}}(h_{\mathrm{r}} - h_{\mathrm{f}})}{L}$$

Hence

$$C'_{\mathrm{Rra}} = C'_{\mathrm{R}} - \frac{C'_{\mathrm{S}}(h_{\mathrm{f}} + h_{\mathrm{r}})}{2L} + \frac{C'_{\mathrm{Y}}(h_{\mathrm{f}} + h_{\mathrm{r}})}{L}$$

with a representative value of 0.003 for a sedan. Including consideration of the sprung-mass weight force, this gives an aerodynamic roll angle

$$\begin{aligned}\phi_{\mathrm{Ae}} &= \frac{M_{\mathrm{SAe}}}{k_{\mathrm{S}} - m_{\mathrm{S}}gd} \\ &= \frac{C'_{\mathrm{Rra}}\beta_{\mathrm{Ae}}qAL}{k_{\mathrm{S}} - m_{\mathrm{S}}gd}\end{aligned}$$

which when significant is generally negative, although not invariably so because the attitude angle may be negative with front steering. This roll moment is distributed front-to-rear according to the roll stiffnesses acting against the roll angle.

The side lift force F_{AeS}, acting at the mid-point of the wheelbase, is distributed equally to the front and rear roll centers. Hence the front and rear aerodynamic load transfers are:

$$F_{\mathrm{TfA}} = \frac{F_{\mathrm{AeS}}h_{\mathrm{f}}}{2T_{\mathrm{f}}} + \frac{k_{\mathrm{f}}\phi_{\mathrm{Ae}}}{T_{\mathrm{f}}}$$

$$F_{\mathrm{TrA}} = \frac{F_{\mathrm{AeS}}h_{\mathrm{r}}}{2T_{\mathrm{r}}} + \frac{k_{\mathrm{r}}\phi_{\mathrm{Ae}}}{T_{\mathrm{r}}}$$

where F_{AeS} and ϕ_{Ae} are generally negative when significant. Hence, for positive attitude angle the aerodynamic roll is generally negative, reducing the normal roll slightly, and the aerodynamic roll load transfers are negative. The aerodynamic roll angle is generally less than 1°, and the aerodynamic load transfer reaches 2–3% at high speed for an average sedan.

5.12 Pitch

Vehicle longitudinal dynamics are not of relevance in themselves here, but sometimes need to be considered in conjunction with lateral dynamics, for example during combined braking and cornering or during strong acceleration and cornering, and in racing. Because of aerodynamic pitch moment, or hill climbing, or braking or accelerating, or steady-state cornering with an attitude angle, there will be longitudinal load transfer, i.e., longitudinal transfer of tire vertical force. It is considered positive when the rear reactions are increased. It generally also results in ride height changes at the front and rear suspensions, which may alternatively be considered as a change of height at the center of mass plus a change of pitch angle. This has geometric effects on the wheels, such as camber and steering angle changes, and also affects the caster angles significantly. As in the case of lateral load transfer, the longitudinal load transfer may be achieved partly through the springs and partly through the links. When the linkage arrangements are such as to transfer some of the load through the links rather than through the springs, this is called anti-dive at the front and anti-rise at the rear in the case of braking, and anti-lift at the front and anti-squat at the rear in the case of traction. Having a roll center above ground could correspondingly be described as "anti-roll."

The total longitudinal load transfer moment is

$$M_{\mathrm{TXT}} = mHA_{\mathrm{x}}$$

The load transfer moment on the suspension is

$$M_{\mathrm{TXS}} = m_{\mathrm{S}} H_{\mathrm{S}} A_{\mathrm{x}}$$

The tire pitch stiffness is

$$k_{\mathrm{TP}} = 2a^2 k_{\mathrm{tf}} + 2b^2 K_{\mathrm{tr}}$$

giving an unsprung pitch angle

$$\theta_{\mathrm{U}} = \frac{mHA_{\mathrm{x}}}{k_{\mathrm{TP}}}$$

The suspension pitch stiffness is

$$k_{\mathrm{SP}} = 2a^2 k_{\mathrm{Sf}} + 2b^2 K_{\mathrm{Sr}}$$

giving a suspension pitch angle, for no anti-dive or anti-rise, of

$$\theta_{\mathrm{S}} = \frac{m_{\mathrm{S}} H_{\mathrm{S}} A_{\mathrm{x}}}{k_{\mathrm{SP}}}$$

The body pitch angle, for steady acceleration, is

$$\theta_{\mathrm{B}} = \theta_{\mathrm{U}} + \theta_{\mathrm{S}}$$

with an associated angle gradient around 4 deg/g (longitudinal).

The principle of anti-dive for a twin-wishbone front suspension is shown in Figure 5.12.1. The lines where the planes of the wishbones (i.e., the planes of the pivot points) intersect the plane of the wheel are arranged to converge to a point E, possibly at infinity. The suspension goemetry is characterized primarily by θ_{gf} and by the horizontal arm length l_{ad}. With the usual approximation of zero moment about the pivot axis, the suspension links can exert no moment about E. When, resulting from brake action, a horizontal force is applied by the road to the wheel at the bottom, this can be resolved into components along and perpendicular to AE. The component F_2 perpendicular to AE must be reacted by the springs: at the front it acts downward on the wheel, extending the spring and so opposing the usual compression of the front spring in braking. This is anti-dive.

Figure 5.12.1 assumes that the brakes are outboard. If they are inboard then the torque transferred by the driveshafts means that the brake force is effectively applied at the wheel center height, so it is necessary to arrange for appropriate inclination of line CE instead. Similar principles can be applied to the rear suspension, but in this case the force center must be in front of the wheel to discourage the usual extension of the rear springs in braking or compression in acceleration.

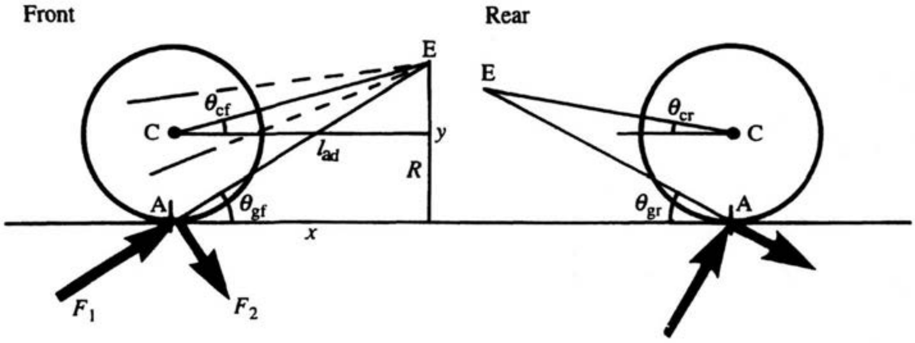

Figure 5.12.1. Anti-dive and anti-squat geometry (only braking forces shown).

The notation for angles in Figure 5.12.1 is that subscripts c and g mean from the center and ground, respectively, and subscripts f and r mean front and rear as usual. The anti-coefficients will be denoted by J (in practice usually expressed as $J \times 100\%$). For example J_{al} is the anti-lift coefficient. Table 5.12.1 summarizes the parameters, showing which angle is relevant to which coefficient. As an aide memoir to distinguish between rise and lift, it is convenient to recall that Rise is at the Rear.

Table 5.12.1. Anti-Dive/Rise/Lift/Squat Parameters

				Relevant angle	
Action	Symbol	Direction	End	Inboard brakes	Outboard brakes
anti-dive	J_{ad}	braking	front	θ_{cf}	θ_{gf}
anti-rise	J_{ar}	braking	rear	θ_{cr}	θ_{gr}
anti-lift	J_{al}	driving	front	θ_{cf}	θ_{cf}
anti-squat	J_{as}	driving	rear	θ_{cr}	θ_{cr}

The total deceleration depends on the total force at both ends, but the horizontal suspension force on each end depends on the braking proportion at that end. Accurate calculation of the anti-dive requires consideration of the proportion of brake force at the front, the sprung and unsprung masses, and the sprung center-of-mass height. The analysis is usually simplified by neglecting the inertial effect of the unsprung mass, as in the following. As an example, consider the braking force

$$F = F_f + F_r = pmA_B + (1 - p)mA_B$$

where p is the proportion of braking at the front, which may be acceleration-dependent, for example if there is a rear pressure limiter. The resulting vehicle deceleration is

$$A_B = \frac{F_f + F_r}{m}$$

The total longitudinal load transfer to the rear is

$$F_{TX} = -\frac{mA_B H}{L}$$

The vertical force exerted by the ground on the front axle is therefore

$$\begin{aligned} F_{Vf} &= W_f - F_{TX} \\ &= W_f + \frac{mA_B H}{L} \end{aligned}$$

The forces on the suspension from the body have no moment about E, so taking moments about E for the front wheel shows the idealized front spring force (two wheels) to be

$$F_S = W_f - W_{Uf} + \frac{mA_B H}{L} - \frac{pmA_B y}{x}$$

Hence the front anti-dive against forces exerted on the wheel at ground level is

$$J_{\mathrm{gf}} = \frac{p(y/x)}{H/L}$$
$$= \frac{\tan\theta_{\mathrm{gf}}}{\tan\theta_{\mathrm{gfi}}}$$

where θ_{gfi} is the "ideal" angle for full anti-dive, given by

$$\tan\theta_{\mathrm{gfi}} = \frac{H}{pL}$$

In braking, with outboard brakes, at the rear the anti-rise is correspondingly given by

$$J_{\mathrm{gr}} = \frac{\tan\theta_{\mathrm{gr}}}{\tan\theta_{\mathrm{gri}}}$$

where

$$\tan\theta_{\mathrm{gri}} = \frac{H}{(1-p)L}$$

In the case of traction, with tractive force

$$F = F_{\mathrm{f}} + F_{\mathrm{r}} = tmA + (1-t)mA$$

where t is the tractive force fraction on the front wheels, the tractive force is produced because of torque in the driveshafts, totaling for both wheels $tmAr$ at the front and $(1-t)mAr$ at the rear (neglecting rotational inertia of the wheels).

This means that the effective line of action of the tractive force is transferred to the center of the wheel. The front anti-lift is

$$\begin{aligned} J_{\mathrm{cf}} &= \frac{t\left[(y-r)/x\right]}{(H/L)} \\ &= \frac{\tan\theta_{\mathrm{cf}}}{\tan\theta_{\mathrm{cfi}}} \end{aligned}$$

where θ_{cf} is the angle of CE at the front:

$$\tan\theta_{\mathrm{cf}} = \frac{y-r}{x}$$

and θ_{cfi} is the angle for full anti-lift, given by

$$\tan\theta_{\mathrm{cfi}} = \frac{H}{tL}$$

The traction anti-squat at the rear is

$$\begin{aligned} J_{\mathrm{cr}} &= \frac{(1-t)\left[(y-r)/x\right]}{(H/L)} \\ &= \frac{\tan\theta_{\mathrm{cr}}}{\tan\theta_{\mathrm{cri}}} \end{aligned}$$

where

$$\tan\theta_{\mathrm{cri}} = \frac{H}{(1-t)L}$$

In the case of inboard brakes, the braking force is associated with a driveshaft torque, so the inclination of CE gives the relevant angle. All of the above equations can be extended to include the effect of the translational and rotational inertia of the unsprung masses. For example, during linear vehicle deceleration, the wheels also have angular deceleration, with angular momentum change that must be provided by the moment of a longitudinal load transfer.

In practice there are objections to anti-dive geometry. It tends to lead to harshness of the front suspension on rough roads because the wheel moves forward as it rises, attacking the bump; it may also cause steering kickback and wander under braking. It also becomes more difficult to achieve good-quality steering geometry, so instead of full anti-dive a proportion is often used, usually expressed as a percentage. Up to 50% anti-dive has been used on passenger cars. Amounts in excess of 50% have been used on ground-effect racing cars because of their extreme sensitivity to pitch angle. However, a large amount may be problematic on small-radius turns, where the large steer angle plus cornering force result in significant jacking forces. The most successful applications of anti-dive seem to be those in which the geometry is arranged to minimize changes of caster angle, and the quantity is more moderate at 20% to 25%.

Considering again Figure 5.12.1, characterized by the angle θ_{gf} and horizontal anti-dive arm length l_{ad}, it is apparent that vertical motion of the wheel (suspension deflection) is liable to give an effective rotation about some point. In the case of a rigid leading arm, this point is simply E, but this is not so for a double wishbone suspension, for which more detailed analysis is required. Any such rotation changes the effective angle of motion θ_{gf} so the anti-dive coefficient will change. The pitch angle of the body (perhaps 4° to 5° in strong braking) will also influence θ_{gf}. Any effective rotation also changes the caster angle; this can be eliminated, if desired, by using parallel arms, although this still leaves the body pitch angle affecting the caster angle, i.e., the anti-dive and the geometric caster change can be chosen independently.

In the case of the pitch-up caused by traction forces, with rear-wheel drive it is quite common to have some anti-squat at the rear. It is not possible to provide anti-rise at the front of a rear-drive vehicle because there is no associated horizontal force applied to the wheel. Anti-squat may have detrimental effects on traction on rough surfaces. Anti-squat effects may also be achieved by other arrangements of the rear suspension, such as a lift bar which is rigidly attached to the rear axle, protruding forward and acting upward on a rubber block on the body; the axle reaction torque therefore provides an upward force on the rear body, depending on the length of the lift bar, relieving the rear springs.

It is sometimes convenient to express the longitudinal load transfer in acceleration in terms of a vertical force longitudinal transfer factor

$$e_{\mathrm{X}} = \frac{F_{\mathrm{TX}}}{N_{\mathrm{f}}}$$

where N_f is the constant-speed front axle reaction, so $e_X = 1$ is front axle lift-off. Correspondingly, the vertical force braking transfer factor is

$$e_B = -\frac{F_{TX}}{N_r}$$

The preceding description and analysis of longitudinal behavior is based on two-dimensional considerations. A precise analysis requires consideration of the suspension in three dimensions. In the case of a solid arm suspension (e.g., a leading arm or trailing arm) then the pivot axis of the arm is well defined (within the limits of compliance effects). Projecting this axis into the transverse vertical plane of the suspension gives the swing arm center E in front view, and hence the roll center. Projecting it into the longitudinal vertical plane of the wheel gives the side-view arm center E (Figure 5.12.1), and hence the anti-dive, etc.

In the case of a double wishbone (A-arm) suspension, each arm has an associated geometric plane defined by three points, usually the outer ball-joint and the two inner pivots. The planes of the two arms intersect in the instantaneous pivot axis. In the case of a strut suspension, the top plane is through the strut top location point, perpendicular to a line from there to the lower ball-joint. The instantaneous pivot axis pierces the vertical transverse suspension plane and the longitudinal wheel plane at the relevant points. When the wheels are steered, then the transverse vertical plane is no longer appropriate, and each wheel needs to be considered independently using the plane perpendicular to the wheel. The distinction between anti-dive and anti-roll can be maintained, of course, but these no longer correspond to the wheel longitudinal and lateral force components, but more nearly to the central and tractive force components.

A full three-dimensional analysis of the suspension, including springs and spring linkages (pushrods, rockers, etc.) is of course feasible, and useful as an adjunct to qualitative understanding. Such programs are far more complex than the relatively easy two-dimensional analysis.

5.13 Wheel Vertical Forces

A statistically determinate system is one in which the forces in the members may be determined by equilibrium analysis. A statistically indeterminate system requires consideration of the deformation of members under load in order to calculate the forces.

The four wheels of a conventional vehicle constitute a statically indeterminate system for the vertical forces at those wheels. There are only three equilibrium equations available: heave, roll and pitch. As a consequence, the distribution of the vertical forces at the wheels depends on the system's internal characteristics. For example, a symmetrical vehicle with center of mass at 46% of the wheelbase from the front, on level ground, would have 27% of the weight supported at each front wheel and 23% at each of the rear wheels, giving 54% total on the front, 46% total on the rear and 50% on each side (Figure 5.13.1(a)). The diagonals D_1 and D_2 are equally loaded, being 50% each. However, because of the indeterminacy, the load on one diagonal can be increased at the expense of the other by adjusting the suspension; this is static diagonal load transfer, usually called diagonal bias. Figure 5.13.1(b) shows a diagonal bias of 6% of the total weight, i.e., the diagonals D_1 and D_2 are 56% and 44%, while the front total, rear total, and side totals remain as before. The convention will be adopted here that a positive diagonal bias means more reaction on the right-front diagonal (D_1).

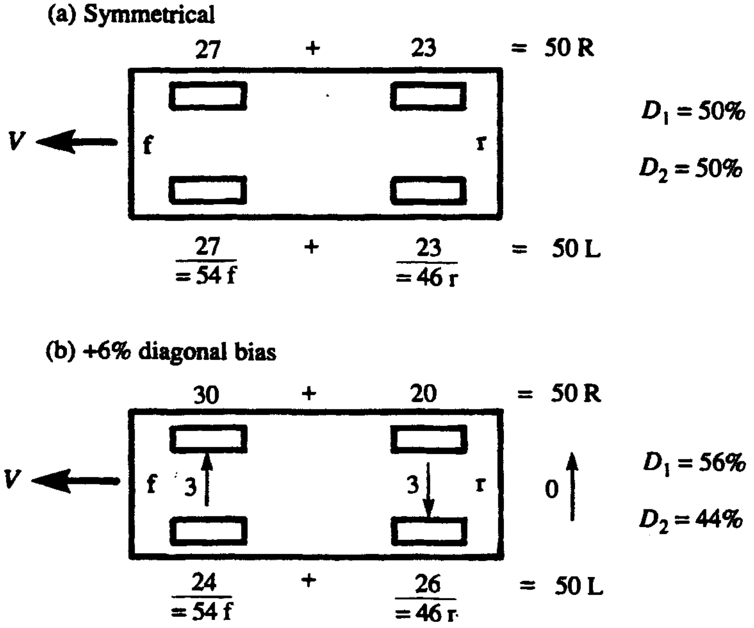

Figure 5.13.1. Wheel vertical forces (static): (a) symmetrical, (b) 6% diagonal bias.

Diagonal bias can be caused by adverse accumulation of production tolerances, operating distortion, incorrectly repaired crash damage, suspension friction or engine torque reaction. Competition vehicles that predominantly run on one-handed tracks are sometimes deliberately adjusted in this way (called weight-jacking in the U.S.), achieved by adjusting the height of a spring seat or the length of an anti-roll bar drop-link.

The distribution of vertical wheel forces is important in handling at higher lateral accelerations. The desired result is achieved by controlling the front-to-rear distribution of lateral load transfer. Figure 5.13.2(a) shows the same car with symmetrical trim, statically as in Figure 5.13.1(a), in left-hand cornering with lateral load transfer equal to 20% of the total weight, where the distribution of lateral load transfer is, in this case, shared equally between front and rear. The front/rear load transfer moment distribution is 50/50. This still leaves the diagonal sums D_1 and D_2 at 50% each. Increasing the lateral load transfer at the front to three-quarters of the total load transfer (load transfer moment distribution 75/25) gives Figure 5.13.2(b), where the diagonal sums are now 60% and 40%.

(a) Load transfer 10 + 10

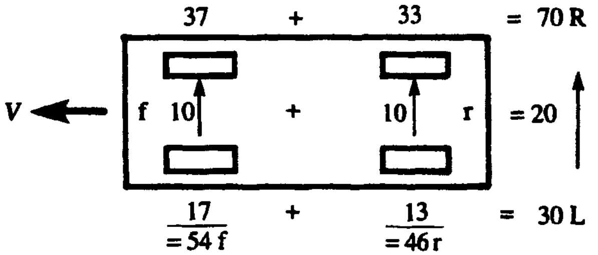

(b) Load transfer 15 + 5

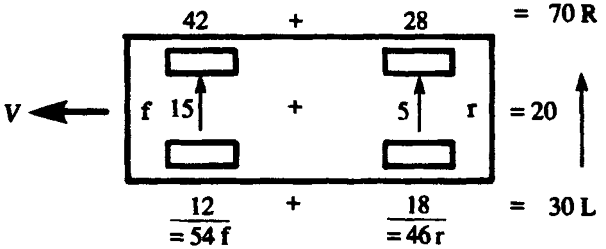

Figure 5.13.2. Wheel vertical forces (cornering): (a) load transfer distribution 50/50 front/rear, (b) distribution 75/25 front/rear.

These effects may be summarized by the following equations, using subscripts L for left, R for right, f for front and r for rear. The diagonal bias is the force transferred diagonally:

$$F_{\mathrm{TD}} = \tfrac{1}{2}\left[\left(F_{\mathrm{Rf}} + F_{\mathrm{Lr}}\right) - \left(F_{\mathrm{Lf}} + F_{\mathrm{Rr}}\right)\right]$$

For zero (static) diagonal bias, the cornering effects give front and rear load transfers

$$F_{\mathrm{Tf}} = \tfrac{1}{2}\left(F_{\mathrm{Rf}} - F_{\mathrm{Lf}}\right)$$

$$F_{\mathrm{Tr}} = \tfrac{1}{2}\left(F_{\mathrm{Rr}} - F_{\mathrm{Lr}}\right)$$

Hence the diagonal bias is

$$F_{\mathrm{TD}} = F_{\mathrm{Tf}} - F_{\mathrm{Tr}}$$

The total lateral load transfer is

$$\begin{aligned} F_{\mathrm{T}} &= \tfrac{1}{2}\left[\left(F_{\mathrm{Rf}} + F_{\mathrm{Rr}}\right) - \left(F_{\mathrm{Lf}} + F_{\mathrm{Lr}}\right)\right] \\ &= F_{\mathrm{Tf}} + F_{\mathrm{Tr}} \end{aligned}$$

The aerodynamic effects on wheel vertical forces may be found as follows, with forces and moments calculated by the methods of Chapter 3 using the coordinate axes of Figures 3.5.1 and 3.5.2. The lift aerodynamic force is

$$F_{\mathrm{AeL}} = C_{\mathrm{L}} q A_{\mathrm{F}}$$

and this acts vertically upward at the center of the wheelbase, this being the aerodynamic coordinate center. Therefore each wheel vertical force is changed by

$$\Delta F_{\mathrm{VAeL}} = \frac{-F_{\mathrm{VAeL}}}{4} = \frac{-C_{\mathrm{L}} q A_{\mathrm{F}}}{4}$$

For passenger vehicles, the lift is usually positive, thus reducing the wheel vertical forces, typically by 5 to 10% at full speed.

A positive pitch moment is defined to give a longitudinal load transfer increasing the rear wheel vertical forces. The pitch-up moment is

$$M_{\mathrm{AeP}} = C_{\mathrm{P}} q A_{\mathrm{F}} L$$

so the total longitudinal aerodynamic load transfer is

$$F_{\mathrm{TXAe}} = \frac{M_{\mathrm{AeP}}}{L} = C_{\mathrm{P}} q A_{\mathrm{F}}$$

and half of the above for each wheel. The pitch coefficient usually causes a longitudinal load transfer of 1% to 2% of total weight at high speed. There may also be a small lateral load transfer from the aerodynamic roll moment.

A diagonal load transfer effect occurs because of the driveshaft torque on a conventional live axle. The driveshaft torque, basically engine torque times the gear ratio less friction (except for rear gearboxes), is as much as 600 Nm for strong acceleration in low gear when the effect is worst. It acts on the axle to give a load transfer. Its reaction acts on the sprung mass and is distributed front-to-rear according to the roll stiffnesses, compensating partially for the direct propshaft torque on the axle. In the case of a three-wheeled vehicle with rear axle, all the body roll stiffness is at the rear, so there is a resulting roll angle but the net load transfer effect is zero. For a four-wheeled vehicle with all the roll stiffness at the front, the full diagonal loading would occur.

The propshaft torque reaction causes a roll angle

$$\phi_{\mathrm{Pr}} = \frac{M_{\mathrm{Pr}}}{k - m_{\mathrm{S}} g d}$$

which is normally positive in left-hand cornering, i.e., it then increases the roll. The propshaft front load transfer is then

$$F_{\mathrm{Tf\,Pr}} = \frac{k_{\mathrm{f}} \phi_{\mathrm{Pr}}}{T_{\mathrm{f}}}$$

The rear load transfer is the negative torque on the axle, plus the body load transfer through the roll stiffness, giving

$$F_{\mathrm{Tr\,Pr}} = -\frac{M_{\mathrm{Pr}}}{T_{\mathrm{r}}} + \frac{k_{\mathrm{r}} \phi_{\mathrm{Pr}}}{T_{\mathrm{r}}}$$

For a vehicle with a live solid rear axle the result is a significant net lateral load transfer at the rear during strong acceleration. This acts to limit traction forces and hence to limit forward acceleration. It is a relatively small asymmetric effect in steady-state cornering, i.e., it has differing effects for different directions of turning. This effect is absent for most front-drive vehicles with the driveshafts from the side of the differential on the sprung mass, or for de Dion rear axles.

For manual computation these effects can best be summarized as in Table 5.13.1, which shows the result corresponding to the diagonal bias of Figure 5.13.1(b) plus the cornering load transfer of Figure 5.13.2(b), and 4% longitudinal load transfer plus example aerodynamic lift and pitch effects.

Table 5.13.1. Example Load Transfer Effects (Percentages of mg)

Wheel	Weight	D. Bias	Lat. LT	Long. LT	Lift	Pitch	Total
Lf	27	−3	−15	−2	−2	+1	6
Rf	27	+3	+15	−2	−2	+1	42
Lr	23	+3	−5	+2	−2	−1	20
Rr	23	−3	+5	+2	−2	−1	24
Totals	100	0	0	0	−8	0	92

It is often convenient to express the vehicle or axle lateral load transfer in terms of the vertical force lateral transfer factors e_{V}, e_{Vf} and e_{Vr}. These are defined as the lateral load transfer divided by the vertical force on the inner wheel(s) before the load transfer. Thus for the case of Table 5.13.1,

$$\begin{aligned} e_{\mathrm{Vf}} &= 15/21 = 0.714 \\ e_{\mathrm{Vr}} &= 5/25 = 0.200 \\ e_{\mathrm{V}} &= 20/46 = 0.435 \end{aligned}$$

The vertical force longitudinal transfer factor is defined in a similar way.

5.14 Steering

5.14.1 Steering Linkage Geometry

Directional control is normally achieved by steering the front wheels, i.e., by rotating them about a roughly vertical axis. The effective steer rotation of the wheels relative to the body is represented by δ (delta). This is mainly the result of steering wheel movement by the driver, but partly the result of suspension characteristics. Rear-wheel steering is inherently unstable at high speeds, but because of its convenience in maneuvering it is sometimes used on specialist low-speed vehicles such as dumper trucks. Recently some interest has been shown in variable rear steering for road cars, coupled with conventional front steering, and this is now commercially available.

In the early days of motoring, various hand controls were tried for the driver. It was Benz who introduced the steering wheel, and this was almost universal by 1900. Tests in other control applications show that the hand wheel is the best way to combine rapid large movements with fine precision. For cars, the road wheels steer through a total of about 70°, and the steering wheel through three and a half turns, requiring a gear ratio of about 18. The average is actually about 17 for power-assisted steering and 21 for unpowered steering. For trucks the steering-wheel movement and gear ratio are about twice those for cars. A high steering gear ratio means a smaller steering force requirement, but it is less favorable for rapid response in emergencies.

The steering of the road wheels is not governed exclusively by the steering hand wheel position. In addition there are:

(1) Toe angle – the initial fixed settings.

(2) Suspension geometric steer arising from vertical wheel motion coupled with the linkage geometry, expressed through bump steer or roll steer.

(3) Suspension compliance steer, resulting from forces or moments and link compliance, mainly in the rubber bushes.

(4) Steering system compliance, mainly in the steering column.

The wheel camber angles are also affected by geometric effects (bump camber and roll camber) and by the flexibility (compliance camber).

The steering system must connect the steering wheel to the road wheels with the appropriate ratio, and also meet other geometric constraints such as limits on bump steer. It is desirable for the forward efficiency of the system to be high in order to keep the steering forces low. On the other hand, a low reverse efficiency helps to reduce the transmission of road roughness disturbances back to the driver, at the cost of some loss of the important feel that helps a driver to sense the frictional state of the road. Hence, there is a conflict in steering design which must be resolved according to the particular application.

For independent suspension there are two principal steering systems in use, one based on a steering box, the other on a rack-and-pinion. In the typical steering box system (Figure 5.14.1), known as the parallelogram linkage, the steering wheel operates the Pitman arm A via the steering box. The box itself is nowadays usually a cam and roller or a recirculating ball worm-and-nut system. The gear ratio of the box alone is usually somewhat less than that of the overall ratio because of the effect of the links. Symmetrical with the Pitman arm is an idler arm B, connected by the relay rod C, so that the whole linkage is geometrically symmetrical, although the forces are introduced on one side. From appropriate points on the relay rod, the tie-rods (track-rods) D connect to the steering arms E. The length and alignment of the tie-rods are critical in controlling bump steer effects. The steering box system has the advantage of a suitable reverse efficiency, but this has become less important than in the earlier days of motoring because of the improved quality of roads.

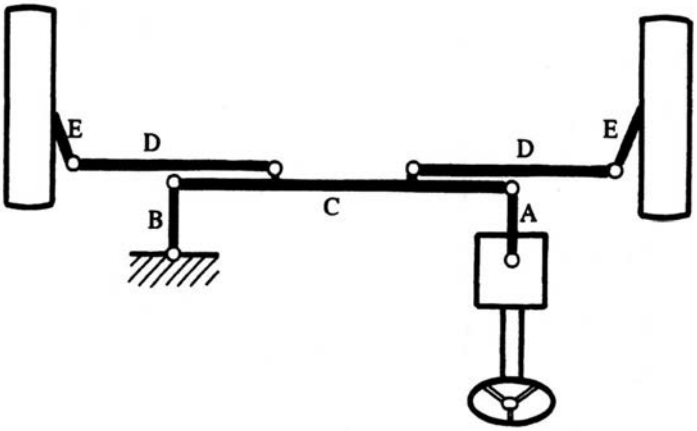

Figure 5.14.1. Steering box system.

In the steering rack system, the steering column is connected directly to a pinion acting on a laterally moving rack. The tie-rods may be connected to the ends of the rack, or they are sometimes attached close to the center where the geometry favors this, for example when the rack is high up with strut suspension. Road shock feedback can be controlled to some extent by choosing a suitable gearing helix angle, minimizing wheel offset, or increasing handwheel inertia. Flexible mounting of the rack has also sometimes been used, but this causes loss of steering precision. A steering damper may also be useful.

Precision is of great importance in the steering system, and the rack system has a superior reputation, although it is quite difficult to observe any substantial difference between a rack and a good box system in comparative driving tests. To prevent play in the various inter-link ball-joints, they are spring-loaded. Where the suspension is mounted on a subframe which has some compliance relative to the body, in the interests of steering precision it is desirable to also mount the steering rack or box on the subframe.

On trucks it is still common to use a rigid axle at the front, mounted on two longitudinal leaf-springs. Usually the wheel steering arms are connected together by a single tie-rod (Figure 5.14.2). Steering is effected by operating a second steering arm A on one of the wheels by the horizontal drag link B from a vertical Pitman arm C. This acts from the side of the steering box which is mounted on the sprung mass.

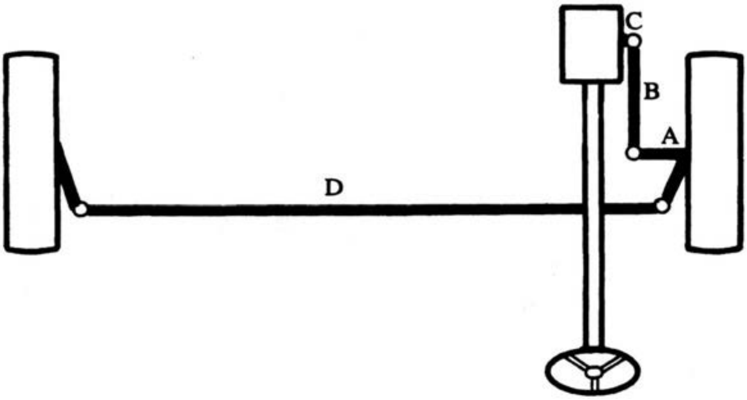

Figure 5.14.2. Truck steering (leaf-spring front axle).

For all systems, the wheels and hubs are pivoted about the kingpin axis (Figure 5.14.3). Nowadays, on cars at least, kingpins are no longer used; the steering axis is now defined by a pair of ball-joints. In front view the axis is at the kingpin inclination θ_k, usually from 0 to 20°, giving a reduced kingpin offset b at the ground. The inclination angle helps to give space for the brakes. Where the steering arms are forward (rack in front of the wheel centers) it also gives room to angle the steering arms for Ackermann geometry. Sometimes a negative offset is used, this giving straighter braking when surface friction varies between tracks. Zero offset is called center-point steering. If the inclination angle is also zero, it is called centerline steering. Center-point steering gives no steering moment from F_X forces; centerline steering gives, in addition, zero moment for rolling resistance forces (at the wheel axle height). This latter effect is important because of the variation of rolling resistance on rough roads.

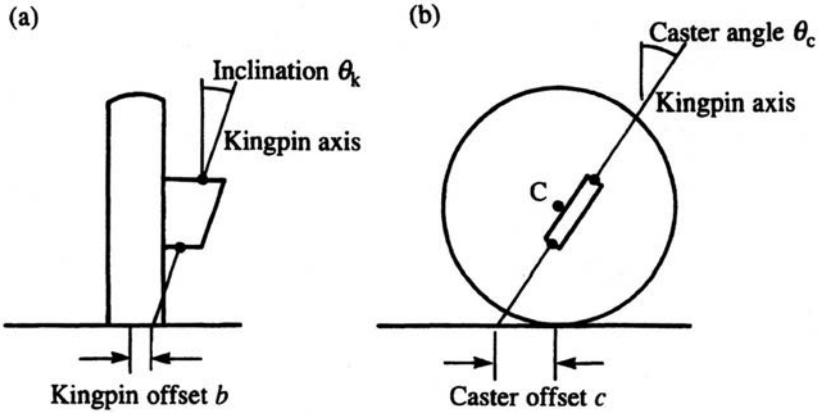

Figure 5.14.3. Geometry of the steering axis of a wheel.

In side view, Figure 5.14.3(b), the kingpin axis is slanted at the caster angle θ_c, usually 0 to 5°. This introduces a mechanical trail, the caster trail (or caster offset), that acts in concert with the tire pneumatic trail. On cars and trucks it is usual for the kingpin axis to pass through the wheel spin axis C in side view, but this is not essential, and some offsetting of the axis from the center enables the caster angle and trail to be independently varied. The caster angle and the associated caster trail are important in the feel of the steering. In general, the caster angle varies with the suspension bump position:

$$\theta_c = \theta_{c1} + \varepsilon_{B\theta C} z_s$$

where $\varepsilon_{B\theta C}$ is the bump caster coefficient (deg/m) (to be distinguished from ε_{BC}, the bump camber coefficient). Bump caster variation acts in addition to the direct effect of the body pitch angle. Caster variation is generally undesirable, but is used deliberately in some cases. The caster angle gives the caster trail, which, in conjunction with the tire pneumatic trail, is very important in giving the steering a suitable feel, and also has a direct effect on stability. The road wheel steer angle δ is the angle between the vehicle longitudinal axis and the line of intersection of the wheel plane and the ground. This is approximately the same as the angle of rotation of the wheel about the inclined kingpin axis. Once the wheel is in a steered position, the caster and kingpin inclination angles affect the camber angle, and this can therefore influence turn-in, and especially influence handling in small-radius corners. For realistic steer angles, a positive kingpin inclination angle causes a positive camber on the outer wheel, growing roughly with the steer angle squared, and is typically 0.15° of camber per degree of inclination at 30° of steer. Positive caster angle causes a negative camber on the outer wheel, approximately proportional to steer angle, and is typically –0.50° of camber per degree of caster at 30° of steer. The actual camber angle is

$$\gamma = \gamma_0 + \arccos(\sin\theta_k \cos\delta) + \theta_k + \arccos(\sin\theta_c \sin\delta) - 180^\circ$$

The dependence of camber angle on steer angle may be represented approximately by

$$\gamma_S = \varepsilon_{SC}\delta + \varepsilon_{SC2}\delta^2$$

where ε_{SC} is the steer camber coefficient, depending on the caster angle ($-\theta_c$ in radians), and ε_{SC2}, the quadratic steer camber coefficient, depends on the kingpin angle ($\frac{1}{2}\theta_k$ in radians) but changes sign with the sign of δ.

The steering wheel angle δ_s is the angular displacement of the handwheel from the straight-ahead position. The overall steering ratio G is the rate of change of steering-wheel angle with respect to the average steer angle of the steered wheels, with negligible forces in the steering system or assuming a perfectly rigid system, and with zero suspension roll:

$$G = \frac{d\delta_s}{d\delta}$$

The mean overall steering ratio is

$$G_m = \frac{\delta_s}{\delta}$$

For a linear system G and G_m are equal and constant. In this case it is sometimes convenient to introduce the reference steer angle

$$\delta_{ref} = \frac{\delta_s}{G}$$

This is not the same as δ because it incorporates the effect of steering compliance. However, it has the advantage over δ_S that it is based on the road wheel angles and therefore it is not very sensitive to G, unlike δ_S.

The steering-wheel angle gradient is the rate of change of steering-wheel angle with steady-state lateral acceleration ($d\delta_S/dA$) in rad/m s^{-2}, deg/m s^{-2} or deg/g, and is a measure of the position control sensitivity. The steering wheel torque gradient is the rate of change of torque T_S with steady-state lateral acceleration (dT_S/dA) typically in Nm/m s^{-2} (Ns^2) or Nm/g, and is a measure of the force control sensitivity.

Steering systems are dynamically complex combinations of components and subject to various modes of vibration. Fortunately, handling effects are essentially low-frequency phenomena, so simple dynamic models usually suffice for handling analysis. The essential inertias are those of the wheels about the kingpin axis, about 1 kg m^2 each, and that of the steering wheel, which for cars is usually in the range 0.025 to 0.065 kg m^2, averaging 0.040 kg m^2. However, they are connected by the overall gear ratio of typically 20, and inertias are factored by the gear ratio squared, so the steering wheel angular inertia referred to the road wheel motion is about 16 kg m^2, which is much greater than that of the road wheels. The dominant compliance is the torsional compliance of the steering column, typically 25 Nm/rad. Depending on the design, sometimes other compliances should be included such as the long tie-rod D on a rigid axle (Figure 5.14.2).

5.14.2 Static Steering Torque

The torque required to steer the road wheels is greatest for static vehicle conditions. Provided that the kingpin axis is not too far from the center of tire contact, for example if it is in the footprint, as it usually is, the following empirical equation gives a fair estimate of the static steering torque at the road wheel:

$$T_{RSt} = \frac{\mu F_V^{1.5}}{3p_i^{0.5}}$$

where p_i is the inflation pressure. The corresponding mean friction radius is

$$R_S = \frac{T_{RSt}}{\mu F_V} = \frac{1}{3}\sqrt{A_i}$$

where

$$A_{\mathrm{i}} = \frac{F_{\mathrm{V}}}{p_{\mathrm{i}}}$$

is the equivalent inflation area.

5.14.3 Aligning Torque

Angular compliance in the steering column proves to be of importance in handling analysis, so it is important to be able to calculate the steering torque about the kingpin axis in dynamic conditions. This comprises a torque to provide wheel angular acceleration (usually small) plus torque to balance the forces exerted by the ground on the tire, and to balance any driveshaft torque, plus the spring torsional stiffness in the case of Macpherson struts.

Driveshaft torque occurs for driven wheels or for inboard brakes. The consequent steering torque is simply the component of the driveshaft torque along the kingpin axis. These ideally balance from side-to-side, but will not do so when the driveshafts are at different angles for any reason, for example because they are of different lengths or because of body roll, or engine torque rock, or when the shaft torques are different as may occur when a limited-slip differential is fitted.

The consequences of the tire forces may be found by considering the three forces and moments at the center of tire contact. The rolling resistance moment and the overturning moment are negligible in this context. The aligning torque, acting about the vertical axis, may easily be resolved into its component about the kingpin axis (Figure 5.14.3). The sum for the two wheels is

$$M_{\mathrm{A}} = (M_{\mathrm{ZL}} + M_{\mathrm{ZR}}) \cos(\phi^2 + \theta^2)^{0.5}$$

This moment attempts to rotate the steering in such a way as to restore straight running. The tire lateral force acts at a distance $c \cos\theta$ from the axis, so the steering moment for the pair of wheels for small θ is

$$M_{\mathrm{L}} = (F_{\mathrm{YL}} + F_{\mathrm{YR}})\, c$$

For positive caster offset c this acts in the same sense as the aligning torque moment, and therefore also has a stabilizing effect.

The tractive force acts at a moment arm of $d \cos\phi$ giving a wheel pair moment for small ϕ of

$$M_T = (F_{XL} - F_{XR})d$$

The two tractive forces balance each other in the symmetrical condition but, as for the driveshaft torques, may be unbalanced with a limited-slip differential, especially on variable surfaces, this leading to the characteristic steering fight of limited-slip front-drive vehicles. Imbalances may also occur for braking on asymmetrical surfaces or for tire deflation, there being some advantage here in avoiding large kingpin offsets.

The influence of the tire vertical force, less the wheel weight, is more difficult to see, and is best considered in two separate parts, one the consequence of kingpin inclination angle, the other of caster angle. As a result of the kingpin inclination angle, there is a component $F_V \sin\phi$ that acts on a moment arm of $b_a \sin\delta$, for small ϕ, when the wheel is steered at angle δ, where b_a is the kingpin offset at wheel axis height perpendicular to the axis. For the two wheels the moment is

$$M_{Vi} = -(F_{VL} + F_{VR})\, b_a \sin\phi \, \sin\delta$$

This is a steering restoring moment independent of load transfer, the wheels acting in the same sense. This moment is often also correctly explained as resulting from the tendency of this geometry to lift the vehicle when steering is performed. It is significant for large steer angles.

As a result of the caster angle, and now neglecting the offset c, there is a force component $F_V \sin\theta$ that, for small θ, acts on a moment arm of $d \cos\delta$. The moment for the pair of wheels is

$$M_{Vc} = (F_{VL} - F_{VR})\, d \sin\theta \, \cos\delta$$

In this case the moments from the two wheels oppose each other, and the net moment depends directly on the load transfer.

To compare the actual size of these torques, consider a medium sedan of total mass 1400 kg with a front weight of 7 kN. The maximum drive thrust is about 7 kN on the two wheels at a radius of 0.35 m, so the shaft torque is 1225 Nm. With 70° between shaft and kingpin axis, the torque component is 420 Nm. Angle asymmetries by roll will cause imbalances of about 40 Nm. With a limited-slip differential, in an extreme case there could be the full 420 Nm difference. The aligning moment will peak at a value of approximately 5000 N on 30 mm giving 150 Nm for the pair of wheels. At 5° caster with the standard geometry, the caster trail c is 30 mm, giving a further 150 Nm from the lateral force. The tractive force, with a limited-slip differential, would give up to 2500 N on a kingpin offset of say 30 mm, giving 75 Nm. For the vertical force effect because of kingpin inclination, an inclination of 15°, b_a is 60 mm, and a maximum steer angle of 35° gives a moment of 60 Nm. Finally, the caster contribution from vertical force, with 5° caster and complete load transfer, at zero steer, is 18 Nm.

These figures illustrate, first, the strong disruptive effect of a limited-slip differential, mainly arising from the direct torque component. With a plain differential, the dominant effect is that of the self-aligning torque and the lateral force. In practice the steering feel is adjusted by the caster offset through the caster angle to obtain a desired relationship between lateral force and total aligning torque, so that the experienced driver can tell from the steering torque when the tires approach their lateral force limit. Adding caster trail moves the maximum steering torque closer to the maximum lateral force, i.e., the steering goes light later.

During cornering, the steering must also support the centrifugal compensation forces on the steering mechanism, for example the rack and the tie-rods. This is called centrifugal caster, and reaches a typical moment about the kingpin of 10 Nm.

On a bumpy road, as the wheel rolls the loaded radius constantly varies. The associated change of effective rolling radius causes changes of wheel angular speed, with associated longitudinal forces on the tire, required to provide the angular acceleration. These forces, of magnitude about 1 kN, act on the hub at wheel axis height, and hence because of the offset b_a disturb the steering. This can be eliminated only by centerline steering.

Another steering disturbance, for front drive, is the side-to-side difference of the component of the driveshaft torque along the kingpin axis; this is a problem where the driveshafts have different inclinations, because they have different lengths, or where they are momentarily differently inclined because of rough roads. This is worst for large torques, and hence during acceleration.

5.15 Turning Geometry

When a vehicle moves in a curved path at a very low speed the lateral acceleration is very small, so the body roll and the axle lateral forces are negligible. Thus the wheel angles are those arising geometrically, not from the need to produce lateral force. There may, however, be opposing slip angles on the two ends of an axle, giving zero net force.

For a normal vehicle with front steering, to turn with zero slip angles means that the turning center C must be in line with the rear axle (Figure 5.15.1). The front wheels must be steered by different amounts, the inner wheel more, in order for both of them to have zero slip angle. The difference between the steer angles for both wheels to have zero or equal slip angles equals the Langensperger angle λ subtended at the turning center by the axle. This is known as the Ackermann steering concept, although actually invented by Langensperger, which we would expect to be desirable for low-speed maneuvering to avoid tire scrub, squeal and wear. Various geometries are used in practice, more or less related to Ackermann geometry. The actual steer angle difference occurring in a given condition is δ_{SD}. For true Ackermann steering,

$$\delta_{SD} = \lambda_0$$

for all steer angles, where λ_0 refers to zero lateral acceleration.

For the actual steering geometry in use, at the mean steer angle δ the difference of steer angles is

$$\delta_{SD} = \delta_L - \delta_R$$

The Ackermann factor is

$$f_A = \frac{\delta_{SD}}{\lambda_0}$$

which is zero for parallel steering, and 1.0 (100%) for true Ackermann. For a real steering arrangement it is only approximately a constant.

The difference between δ_{SD} and λ_0 is sometimes called the tie-rod geometry error:

$$\theta_{TRGE} = \delta_{SD} - \lambda_0 = (f_A - 1)\lambda_0$$

For vehicles that do a great deal of turning or need a very small turn radius, such as purpose-built taxis and urban delivery vehicles, then full Ackermann is often used. The "Lunar Rover" vehicle used on the Moon by Apollo astronauts had four-wheel steering, giving a minimum turn radius equal to the wheelbase of 2.286 m, with close to Ackermann at both front and rear, presumably to minimize resistance in tight turns on the soft ground. The traditional London Taxi has almost perfect Ackermann over its full 60° of inner road-wheel steer angle.

There is less case for Ackermann steering under dynamic cornering conditions. This is because as attitude angle develops, the Langensperger angle λ subtended by the front axle at the turning center reduces. Also, the outer tire has greater vertical force, hence needing a greater slip angle than the inner tire for

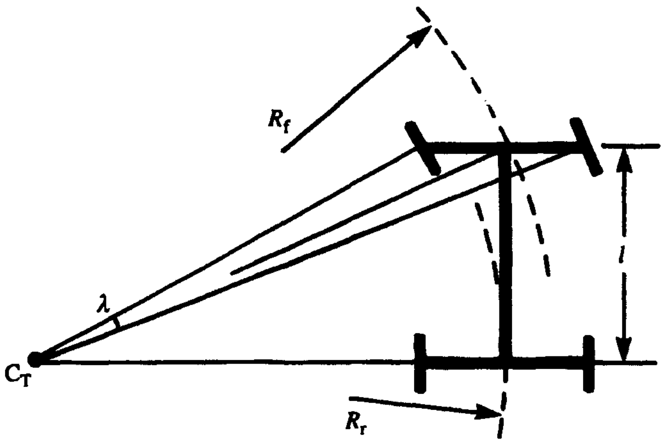

Figure 5.15.1. Turning geometry at very low speed (negligible lateral acceleration).

maximum cornering force. Finally, roll steer effects may give a significant steer angle difference. Even anti-Ackermann (negative f_A) has been used on occasion, and various steering geometries are used in practice. If the steering is not perfect Ackermann, then at low speed each wheel pair must adopt equal and opposite slip angles to give zero net force.

The most convenient way to obtain the different steer angles of the Ackermann layout is to angle the steering arms inward (for a rack behind the kingpins), as in Figure 5.14.1, so that as steer is applied there is a progressive difference in the effective moment arms. This slanting of the arms also helps with wheel and brake clearance. It is widely believed that aligning the steering arms so that their lines intersect at the rear axle will give true Ackermann steering (the Jeantaud diagram). However, this is far from true; the actual Ackermann factor varies in a complex way with the arm angle, rack length, rack offset forward or rearward of the arm ends, whether the rack is forward or rearward of the kingpins, and with the actual mean steer angle. Moving the rack forward or backward to change the tie-rod angles can be a useful way to adjust the Ackermann factor, the most important single variable being the angle between the tie-rod and the steering arm in plan view, the Ackermann factor being proportional to the deviation of this angle from 90°. With straight tie-rods, to obtain an Ackermann factor close to 1.0 may require the projected steering arm intersection point to be at about 60% of the distance to the rear axle.

The attitude angle β is the angle between the vehicle centerline and the velocity vector, which is perpendicular to the radial lines shown in Figure 5.15.1, in which it may be seen that at low speed (negligible lateral acceleration) the attitude angle β_r is zero,

$$\beta_f = -\arcsin\frac{L}{R} \approx -\frac{L}{R}$$

and at the center of mass

$$\beta \approx \frac{b}{L}\left(-\frac{L}{R}\right) = -\frac{b}{R}$$

Hence the attitude angle is negative; however, it is positive-going as lateral acceleration develops.

The two ends of the vehicle corner at different radii (Figure 5.15.1). This is one reason why four-wheel-drive vehicles need a center differential or front overrun clutch. At low speed, with zero slip angles,

$$R_r^2 = R_f^2 - L^2$$

The difference of radii is known as the offtracking:

$$R_f - R_r \approx \frac{L^2}{2R_f} \approx \frac{L^2}{2R}$$

where R is the turn radius of the center of mass. The offtracking can be about 0.4 m for cars, leading to occasional curbing of the rear wheels, or worse. It is more problematic for long trucks, and especially for trailers. It can be obviated by four-wheel steering as is now available for some cars.

The low-speed mean steer angle will here be called the kinematic steer angle:

$$\delta_K = \arctan\left(\frac{L}{R_r}\right) \approx \arctan\left(\frac{L}{R}\right) \approx \frac{L}{R} = \frac{LA}{V^2}$$

At significant speed, when a tire slip angle is required, then attitude angle develops and the offtracking changes. The turning center C_T has now moved forward from the axle line. The condition of zero offtracking will occur when C_T has moved forward half of the wheelbase. This is possible for some particular speed that depends on the cornering radius, according to tire characteristics, etc., and is typically 10 m/s at 30 m radius. For a greater speed, the offtracking becomes negative, the rear following a path of greater radius than the front.

5.16 Bump Steer and Roll Steer

The geometry of the suspension linkages results in small but important changes of the steer angle of the wheels when they move up or down. These angles are represented by δ with an appropriate subscript. Other texts frequently use α, but this is definitely a steer effect not a direct slip angle change, so δ is to be preferred.

The term bump steer means changes of wheel steer angle when the wheel is moved relative to the body in bump and droop. The term roll steer refers to changes of steer of the pair of wheels, i.e., of the axle, when the body rolls. These are obviously related, but bump steer is the basic form of data for independent suspension, and roll steer for solid axles. Some forms of bump- and roll steer can cause poor straight-line stability and very unpredictable and unpleasant vehicle behavior, the handling being sensitive to small changes of wheel steer angles.

The bump steer coefficient $\varepsilon_{\mathrm{BS}}$ is the rate of change of wheel steer angle with vertical wheel position (suspension bump deflection), usually expressed in deg/m. This will be taken as positive for toe-out with a rising wheel. The bump steer angle for one wheel, for a linear model, is

$$\delta_{\mathrm{BS}} = \varepsilon_{\mathrm{BS}} z_{\mathrm{S}}$$

where

$$z_{\mathrm{S}} = z_{\mathrm{W}} - z_{\mathrm{B}}$$

is the suspension bump for the relevant wheel. Bump steer is frequently nonlinear to a significant degree over the full suspension range, so it may be necessary to use

$$\delta_{\mathrm{BS}} = \varepsilon_{\mathrm{BS}}\, z_{\mathrm{S}} + \varepsilon_{\mathrm{BS2}}\, z_{\mathrm{S}}^2$$

The roll steer coefficient $\varepsilon_{\mathrm{RS}}$ is the rate of change of axle mean wheel steer angle with respect to suspension roll angle, and is usually expressed as deg/deg, i.e., it is dimensionless. Hence for small roll, the roll steer angle is given by

$$\delta_{RS} = \varepsilon_{RS}\phi_S$$

For independent suspension, the roll steer coefficient is closely related to the bump steer coefficient, but is also influenced by vehicle track width. For a solid axle it relates to the steer angle of the complete axle, whereas for independent suspension it relates to the mean value for the pair of wheels.

The roll understeer angle δ_{RU} must be clearly distinguished from the roll steer angle δ_{RS}. They are numerically equal but the sign convention is different. The roll understeer angle is positive when it requires increased handwheel angle, i.e., requires increased driver-applied steering. Hence there is a change of sign at the rear:

$$\delta_{RUf} = +\delta_{RSf}$$
$$\delta_{RUr} = -\delta_{RSr}$$

This also applies to the roll understeer coefficients:

$$\varepsilon_{RUf} = +\varepsilon_{RSf}$$
$$\varepsilon_{RUr} = -\varepsilon_{RSr}$$

The advantage of referring to roll understeer coefficients rather than roll steer coefficients is that in evaluating the total understeer coefficient or understeer angle they simply add up without constant consideration of a front/rear sign convention, that is

$$\varepsilon_{RU} = \varepsilon_{RUf} + \varepsilon_{RUr}$$

whereas

$$\varepsilon_{RU} = \varepsilon_{RSf} - \varepsilon_{RSr}$$

Roll steer is a property of an axle, whereas roll understeer is a property of a vehicle, or of an axle in the context of a vehicle.

Derived from the roll steer coefficient, the roll steer gradient k_{RS} in deg/m s^{-2} or deg/g is sometimes used, defined by

$$k_{RS} = \varepsilon_{RS}\frac{d\phi_S}{dA} = \varepsilon_{RS}k_{\phi S}$$

where $k_{\phi S}$ is the suspension roll angle gradient, ϕ_S is the suspension roll angle and A is the lateral acceleration.

The roll understeer gradient is

$$k_{RU} = \varepsilon_{RU} k_{\phi S}$$

The bump steer gradient is

$$k_{BS} = \varepsilon_{BS} \frac{dz_S}{dA}$$

where z_S is primarily governed by the roll angle and track $\left(\pm\frac{1}{2}\phi_S T\right)$ but partly by cornering heave due to suspension jacking (dz_B/dA).

The bump camber angle is

$$\gamma_{BC} = \varepsilon_{BC} z_S$$

where the bump camber coefficient ε_{BC} is positive for positive-going camber on a rising wheel, again with units of deg/m. Although δ was preferred over α for bump steer, there is no accepted symbol for a deliberate alteration of camber angle, since steering is not controlled in that way. Hence, γ is accepted and used here and elsewhere. The distinction should be borne in mind, however, between the effects represented by γ, especially those corresponding to the distinction between δ and α.

The roll camber coefficient ε_{RC} for a single wheel is the camber change with suspension roll, in deg/deg, related to the bump camber coefficient but again depending on the body width between the suspension mountings. For an independent-wheeled axle, the roll camber angle is the mean camber angle for the two wheels, relative to the road. Hence, for small roll, the roll camber is

$$\gamma_{RC} = \varepsilon_{RC} \phi_S$$

The roll camber gradient is

$$k_{RC} = \varepsilon_{RC} k_{\phi}$$

Considering a suspension roll angle ϕ_S, with corresponding suspension bumps $(\pm\frac{1}{2} T\phi_S)$, the camber angles are

$$\gamma_R = +\phi_B + \tfrac{1}{2} T\phi_S\, \varepsilon_{BC}$$

$$\gamma_L = -\phi_B - \tfrac{1}{2} T\phi_S\, \varepsilon_{BC}$$

The mean inclination angle (not camber) is

$$\begin{aligned}\gamma_{\mathrm{m}} &= \frac{1}{2}(\gamma_{\mathrm{R}} - \gamma_{\mathrm{L}}) \\ &= \phi_{\mathrm{B}} + \frac{1}{2}T\phi_{\mathrm{S}}\varepsilon_{\mathrm{BC}} \\ &= \phi_{\mathrm{A}} + \left(1 + \frac{1}{2}T\varepsilon_{\mathrm{BC}}\right)\varphi_{\mathrm{S}}\end{aligned}$$

Hence the relationship between roll camber and bump camber coefficients is

$$\varepsilon_{\mathrm{RC}} = 1 + \tfrac{1}{2}T\varepsilon_{\mathrm{BC}}$$

Bump camber coefficients are usually made negative in order to offset the effect of body roll, reducing $\varepsilon_{\mathrm{RC}}$.

A solid axle is not subject to suspension roll camber, but it does camber in roll because suspension roll leads to axle roll as a result of load transfer on the tire vertical stiffness. Arguably then, a solid axle might be said to have an axle roll camber coefficient, typically of about 0.12 (deg/deg). This is also applicable to independent suspensions.

For a twin-wishbone front suspension (Figure 5.16.1), considering the wheel to move in bump ideally with no steer angle change, then the tie-rod end B should move in an ideal arc with center at A, where the position of A depends on the wishbone geometry. If the tie-rod to rack joint, or tie-rod to relay-rod joint, is actually at A then there will be no bump steer. In practice, there are often deliberate or accidental discrepancies of height e_{H} of the actual joint C, or of length e_{L} of the tie-rod BC. As a consequence there is a first-order bump steer coefficient

$$\varepsilon_{\mathrm{BS}} \approx \frac{e_{\mathrm{H}}}{l_{\mathrm{TR}}l_{\mathrm{SAx}}}$$

and second-order coefficient

$$\varepsilon_{\mathrm{BS2}} \approx \frac{e_{\mathrm{L}}}{2l_{\mathrm{SAx}}\,l_{\mathrm{TR}}^{2}}$$

where l_{SAx} is the longitudinal component of the length of the steering arm, pivot axis to tie-rod end, l_{TR} is the length of the tie-rod, and l_{ITR} is the length of the ideal tie-rod.

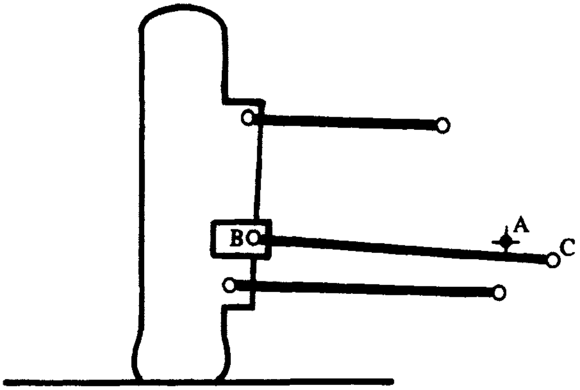

Figure 5.16.1. Wishbone suspension and tie-rod in rear view.

The possibility of achieving an accurate steering motion is an important advantage of independent suspension over a steered solid axle. Predictable and precise handling is particularly important for competition and high-performance vehicles, and in such cases it is considered to be of paramount importance that the rack is mounted at exactly the right height, within 1 or 2 mm, and that the tie-rods should be of the appropriate length. For ordinary road vehicles such complete accuracy is often not attempted. The errors consequently introduced are sometimes claimed to give less wheel response to rough roads or to have handling advantages, although this is a controversial issue.

If the actual wheel steer angle is plotted against bump, a typical result such as Figure 5.16.2 is obtained.

Actually there is normally also a toe angle at zero bump; this is the static toe and does not usually appear in bump steer plots because it is readily adjustable and is measured separately; bump steer is usually measured as the change of angle. It can be characterized in two ways. At zero bump there is a gradient of steer change with bump, in this case about 0.5° toe-out in 75 mm bump, i.e., a bump steer coefficient of 6.7 deg/m. This results from the rack height, say about 7 mm too low in this case with the rack behind the wheels, or high for the rack in front. Second, there is a curvature of the graph. In this case the curvature is toward toe-in, which would result from a tie-rod longer than ideal for a rack

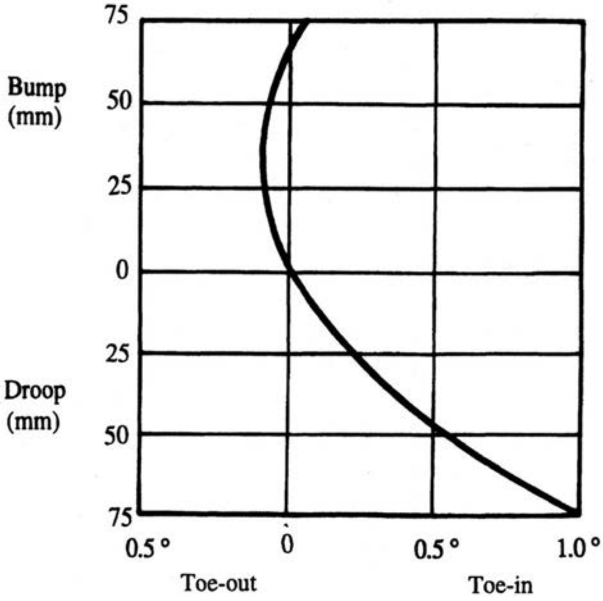

Figure 5.16.2. Example bump steer graph.

behind the wheels, and shorter than ideal for a rack in front of the wheels, as can be seen by imagining the ideal and actual arcs of the tie-rod end. The initial toe-out tendency in bump means that the wheel itself tends to recede from the bump, and so possibly reduces the steering fight on rough roads. The curvature toes-in the inner wheel in cornering, reducing its slip angle. This can help to prevent undue wear because of excessive slip on the lightly loaded tire, an example of the abandonment of ideal Ackermann steering under dynamic conditions.

Considering Figure 5.16.2, evidently a simple linear bump steer representation may not be adequate in the case of substantial suspension deflection. A fuller representation is

$$\delta = \delta_S + \delta_T + \varepsilon_{BS} z_S + \varepsilon_{BS2} z_S^2$$

where δ is the complete wheel angle, δ_S is the steer angle controlled by the handwheel, δ_T is the initial constant toe angle, $\varepsilon_{BS} z_S$ is the linear bump steer, and $\varepsilon_{BS2} z_S^2$ is the quadratic bump steer effect; ε_{BS2} has units expressed as rad/m^2 or deg/m^2.

Because of the nominal symmetry of the whole steering and suspension system, even if the above deliberate steer deviations are adopted, body heave should not cause net steering effects, which is an advantage over a steered solid axle. Nevertheless, the toe-in varies with load, which can affect steering feel and tire wear, for which reason if these effects are used it is best to design them around a light load position. Where present, bump steer is often a palliative for some other fault such as bad weight distribution, and is likely to give poor straight-line stability and tire wear. At best such effects compromise the basic handling in order to gain some rough road or other small advantages, and so should be used with caution.

Many cars are designed with zero theoretical bump steer, but positioning of the steering rack is critical and sufficiently close tolerances are rarely held in production, particularly if this aspect was not considered in the design. Even for a given design, bump steer varies from car to car and even from side to side of one car, sometimes to the extent that one wheel toes-in with bump and the other toes-out. Unequal bump steer left and right, which is heave steer or double bump steer, is especially bad for straight-line stability.

Although the geometry of steering variation is, for independent suspension, expressed by the linear and quadratic bump steer coefficients, from a practical point of view it is the combined action of left and right sides that matters when the body moves in either roll or heave. Hence, it is necessary to deduce the roll steer and the heave steer (double bump steer) from the single bump steer. Of course this may be done by calculating the individual suspension bump values on each side from the suspension roll angle ϕ_S and the suspension double bump z_S (considering a left turn, with clockwise roll seen from the rear to be positive ϕ):

$$
\begin{aligned}
z_{S,R} &= +\tfrac{1}{2}\phi_S T + z_S \\
z_{S,L} &= -\tfrac{1}{2}\phi_S T + z_S
\end{aligned}
$$

and thence finding the bump steer angles from:

$$
\begin{aligned}
\delta_{BS,R} &= \varepsilon_{BS,R}\, z_{S,R} + \varepsilon_{BS2,R}\, z_{S,R}^2 \\
\delta_{BS,L} &= \varepsilon_{BS,L}\, z_{S,L} + \varepsilon_{BS2,L}\, z_{S,L}^2
\end{aligned}
$$

However, it is also of great interest to derive directly the roll steer and heave-steer effects. For a suspension roll angle of ϕ_S with no heave, the individual suspension bump values are

$$\begin{aligned} z_{S,R} &= +\tfrac{1}{2}\phi_S T \\ z_{S,L} &= -\tfrac{1}{2}\phi_S T \end{aligned}$$

The bump steer angles are therefore

$$\begin{aligned} \delta_{BS,R} &= \varepsilon_{BS,R}\left(\tfrac{1}{2}\phi_S T\right) + \varepsilon_{BS2,R}\left(\tfrac{1}{2}\phi_S T\right)^2 \\ \delta_{BS,L} &= \varepsilon_{BS,L}\left(-\tfrac{1}{2}\phi_S T\right) + \varepsilon_{BS2,L}\left(-\tfrac{1}{2}\phi_S T\right)^2 \end{aligned}$$

These bump steers are positive for toe-out on each side, so the equivalent mean roll steer angle for the complete axle is half of the difference of the bump steer angles of the two wheels:

$$\delta_{RS} = \tfrac{1}{2}\left(\delta_{BS,R} - \delta_{BS,L}\right)$$

Since individual toe-out is positive, this gives positive roll steer corresponding to the axle effectively turning out of the curve. Hence this is an understeer effect at the front and oversteer at the rear. Substituting the above expressions, and noting that a negative valve squared is positive, the axle roll steer angle becomes

$$\delta_{RS} = \tfrac{1}{4}\phi_S T\left(\varepsilon_{BS,R} + \varepsilon_{BS,L}\right) + \tfrac{1}{2}\left(\tfrac{1}{2}\phi_S T\right)^2\left(\varepsilon_{BS2,R} - \varepsilon_{BS2,L}\right)$$

The first- and second-order roll steer coefficients are therefore

$$\begin{aligned} \varepsilon_{RS} &= \tfrac{1}{4}T\left(\varepsilon_{BS,R} + \varepsilon_{BS,L}\right) \approx \frac{1}{2}T\varepsilon_{BS} \\ \varepsilon_{RS2} &= \tfrac{1}{8}T^2\left(\varepsilon_{BS2,R} - \varepsilon_{BS,L}\right) \end{aligned}$$

Hence any linear bump steer gives linear roll steer. However, symmetrical second-order bump steer does not give second-order roll steer, which arises only from asymmetrical ε_{BS2}. This will tend to be small since it will usually arise from production tolerances rather than from design intent. One feature that will cause it is unequal tie-rod lengths which have been used on some passenger cars. Symmetrical second-order bump steer actually gives a roll Ackermann effect because it produces a second-order roll steer angle difference (with individual toe-outs positive) of

$$\begin{aligned}\delta_{\mathrm{SDR}} &= \delta_{\mathrm{BS,R}} + \delta_{\mathrm{BS,L}} \\ &= \tfrac{1}{2}T^2\phi_{\mathrm{S}}^2\left(\varepsilon_{\mathrm{BS2,R}} + \varepsilon_{\mathrm{BS2,L}}\right)\end{aligned}$$

In effect then, there is a quadratic roll toe coefficient

$$\varepsilon_{\mathrm{RT2}} = \tfrac{1}{2}T^2\left(\varepsilon_{\mathrm{BS2,R}} + \varepsilon_{\mathrm{BS2,L}}\right)$$

Consider now heave of the body without roll, giving a suspension double bump z_{S}, as might occur on landing after a symmetrical crest. The left and right suspension bumps are

$$z_{\mathrm{S,R}} = z_{\mathrm{S,L}} = z_{\mathrm{S}}$$

The individual bump steer angles are

$$\begin{aligned}\delta_{\mathrm{BS,R}} &= \varepsilon_{\mathrm{BS,R}}\, z_{\mathrm{S}} + \varepsilon_{\mathrm{BS2,R}}\, z_{\mathrm{S}}^2 \\ \delta_{\mathrm{BS,L}} &= \varepsilon_{\mathrm{BS,L}}\, z_{\mathrm{S}} + \varepsilon_{\mathrm{BS2,L}}\, z_{\mathrm{S}}^2\end{aligned}$$

These are both positive for toe-out, so the mean double bump steer angle is given by

$$\delta_{\mathrm{DBS}} = \tfrac{1}{2}\left(\delta_{\mathrm{BS,R}} - \delta_{\mathrm{BS,L}}\right)$$

Hence the mean double bump steer angle is

$$\delta_{\mathrm{DBS}} = \tfrac{1}{2}z_{\mathrm{S}}\left(\varepsilon_{\mathrm{BS,R}} - \varepsilon_{\mathrm{BS,L}}\right) + \tfrac{1}{2}z_{\mathrm{S}}^2\left(\varepsilon_{\mathrm{BS2,R}} - \varepsilon_{\mathrm{BS2,L}}\right)$$

The linear and quadratic double bump steer coefficients are therefore

$$\varepsilon_{\mathrm{DBS}} = \tfrac{1}{2}\left(\varepsilon_{\mathrm{BS,R}} - \varepsilon_{\mathrm{BS,L}}\right)$$

$$\varepsilon_{\mathrm{DBS2}} = \tfrac{1}{2}\left(\varepsilon_{\mathrm{BS2,R}} - \varepsilon_{\mathrm{BS2,L}}\right)$$

Hence both of the double bump steer coefficients depend on the side-to-side difference between the individual bump steer coefficients and on vehicle asymmetries normally arising from production tolerances. The first-order double bump steer coefficient $\varepsilon_{\mathrm{DBS}}$ is the one primarily responsible for bad straight-line behavior on dips and crests.

The roll steer gradient may be deduced from the above; this is controlled almost entirely by the roll steer coefficient, but there is a small contribution from heave because of suspension jacking in cornering; this latter contribution may be important in some cases, e.g., swing axles.

For an independent suspension, calculation of the ideal pivot center A for the tie-rod (Figure 5.16.1) to give zero bump steer is a purely geometrical problem. In the case of strut and link suspension, the ideal link length is highly sensitive to the vertical position of the ball-joint B, tending to infinity when it is at the strut top. A common solution is to use a rack with center-mounted tie-rods, and then to choose a rack height for which these are the correct length, which roughly matches up with the main spring seat. For twin wishbones, the usual rack end connection is suitable. There are various other independent front suspensions, not often seen nowadays, for which there exist suitable ideal steering layouts free of bump steer. The bibliography gives details.

The trailing arm is a common form of rear suspension. For pure trailing arms there is no bump steer. For semi-trailing arms there is often considerable bump steer, depending on the angle of the pivot axis to the vehicle centerline. This is of the second-order (curvature) kind relative to the mid-position, but relative to a loaded position there is usually both static toe-in and a first-order dependence of toe on bump. Although this is a disadvantage, it is often considered an acceptable sacrifice in order to gain the advantage of favorable camber in roll.

Rear solid axles can be considered in two groups: those with link location and those with longitudinal leaf-springs. In the case of link location, the roll center was found by identifying the lateral location points A and B according to the particular linkages (Section 5.7). Because these points define the lateral location of the axle relative to the body, they also define an axis about which the axle will roll relative to the body if the "road" is rolled (subject to the approximations discussed in Section 5.7). If we consider the body to be rolled about a horizontal axis, then if the front point A is lower than the rear point B the different sideways movements of A and B, A more inward, will result in a steer rotation of the axle such that the axle tries to increase its slip angle. This is at the rear, so it is an understeer effect. If the axle axis is inclined at ρ_A radians, positive angle being down at the front, a suspension roll angle of ϕ_S results in a rear axle roll steer angle, out of the curve, of

$$\delta_{RS} = -\rho_A \phi_S$$

The axle is actually turned into the curve, for positive ρ_A, reducing the required attitude angle. This is an understeer effect for a rear axle, so

$$\delta_{RU} = \rho_A \phi_S$$

The roll understeer coefficient (the rate of change of roll understeer with suspension roll angle) is therefore equal to the value of ρ_A in radians, i.e., in this case value of the understeer coefficient is

$$\varepsilon_{RU} = \rho_A \quad \text{[rad]}$$

This is often expressed as a percentage roll understeer, i.e., $100\rho_A\%$.

The variation of roll steer coefficient with axle load is important. This is

$$k_{RUFV} = \frac{d\varepsilon_{RU}}{dF_{VA}}$$

It can be examined easily by considering the change of ρ_A from the motion of A and B with increasing load. If they move equally in the same direction then there is a change of roll center height but no change of roll steer. In some cases, for example the convergent four-link suspension of Figure 5.7.1, when the body moves down, A moves up and B moves down, giving a small change of roll center height but a large change of roll steer coefficient. Some positive sensitivity, i.e., increasing ρ_A, may be desirable to help to compensate for the otherwise general trend toward oversteer with increasing load that occurs because of the tire characteristics. This can help with primary understeer but does not help with final understeer or oversteer.

It might appear in the above discussion that the axle axis angle should be measured relative to the vehicle roll axis rather than to the horizontal. However, as discussed in Section 5.5, the vehicle does not in a real sense roll about its roll axis. Rolling the body about the inclined roll axis implies a roll about a horizontal axis plus a yaw movement which will affect front and rear suspensions equally, and so will have no net result on the steering angle required.

In the case of longitudinal leaf-springs, the roll steer depends on the inclination of the equivalent link AB that describes the motion arc of the wheel center (Figure 5.16.3, considering the figure without the steering system). This equivalent link is directed toward the unshackled end, is about 3/4 of the length of that end of the spring, and is roughly parallel to it. When the body rolls, A rises on the inner side and falls on the outer, thus tending to steer the axle. Horizontal equivalent links give no steer because both sides move forward equally. Having point A higher than B gives roll oversteer for a rear axle, i.e., reduced slip angle tendency; B higher gives roll understeer. For a front axle the effects are opposite. The roll steer coefficient is equal to the AB axis inclination ρ_A, independent of the spring length or separation. On the other hand, the spring length affects the influence of load variation on roll steer coefficient. Too high a coefficient, apart from being bad for handling, also leads to harshness on rough roads because of the wheel path in bump and other problems. Early Hotchkiss axles, pre-1930, were given a negative roll steer coefficient because this resulted in less sensitivity to road roughness. In the early 1930s a positive coefficient was first used (i.e., roll oversteer was replaced by roll understeer) and a dramatic increase in directional stability was found.

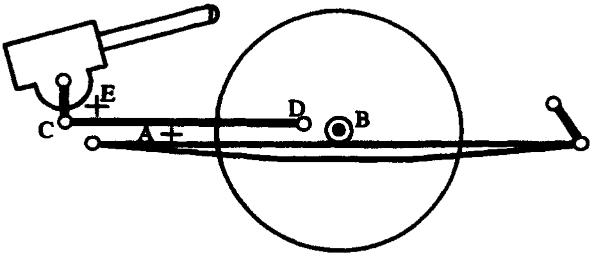

Figure 5.16.3. Steered leaf-spring axle.

When the solid axle with longitudinal leaf-springs is used at the front, as on many trucks, it is subject to all of the effects described above, plus additional effects because of the steering linkage. The critical steering link is always the one that connects the sprung and unsprung parts of the steering. Figure 5.16.3 shows a typical arrangement with front steering and a rear-spring shackle. Here

D is the drag link connection to the wheel hub, and C is its connection to the Pitman arm on the sprung mass. When the axle moves, D has an ideal no-steer arc centered on E. If E and C do not coincide, there will be steering errors. As early as the 1920s, it was attempted to match the E and C positions for roll motions, but with disappointing results. The reason is that the arc of D is different for roll, single-wheel bump, and heave, and different again with braking because of axle wind-up. Also there are differences because of production variability of springs, and variation between spring options. One improvement that is sometimes adopted is to use an unsprung steering box, the sprung to unsprung connecting linkage being through a splined steering column.

The trailing twist rear axle (Figure 4.7.1) is a special case, as usual. In heave the whole axle rotates about the front pivots and there is no steer effect. In single-wheel bump, the other trailing arm remains approximately level so the pivot axis is from the pivot bush of the bumped side to the intersection of the crossbeam with the unbumped arm, equivalent to a semi-trailing arm. For roll, the mid-point of the crossbeam remains approximately stationary, so the pivot axes are from the bush to the center of the beam – a different equivalent semi-trailing arm. The bump and roll steer values follow from these semi-trailing arm equivalents.

Even if the smooth road ideal of zero roll steer is abandoned, there are definite limitations to the degree of roll steer that is acceptable. Roll oversteer of independent front suspension, i.e., wheel toe-in in bump, gives severe wheel fight on rough roads. Roll oversteer of the rear gives increased body attitude angles, a very unpleasant uncertain feeling for the driver, and bad directional response to rough roads and to side winds.

It does not seem to be effective to balance an oversteering rear with an understeering front, and there is little reason to try to do this. In short, there is good reason to avoid roll oversteer at either end. Some would argue for rear roll understeer for its reduced attitude angle and hence possibly faster response, especially for large cars which tend to have a larger dynamic index (I_Z/mab); but this can lead to problems with rough roads or wind, and may result in engine torque steering because of body roll in strong acceleration, unless the power is transmitted through independent or de Dion axles or an offset lift bar is used.

A small static toe-in at the rear often has a surprisingly large effect on handling, increasing understeer; front-wheel-drive vehicles, being lightly loaded at the rear and therefore having a large rear tire cornering stiffness coefficient, are especially sensitive to this. Front toe-out might be expected to have the same effect. However, practical experience shows the reverse: front toe-out gives a vague steering feel whereas front toe-in gives a favorable feel and leads to increased understeer that can be measured on the skid pad. This seems to be caused by the combination of load transfer, aligning torque, lateral force on caster trail, and steering compliance. Too much front toe-in affects corner turn-in, giving an unprogressive and imprecise steering feel.

Static toe settings are governed within quite narrow bands by tire wear. For least wear, toe settings should be arranged to give minimal steer angles when running, regardless of camber. This means a small static toe-in for undriven wheels, and a small toe-out for driven ones, so that free running and tractive forces and compliances act to bring the toe angles to zero when running. Within the allowable band for low wear (a range of about one degree), there is limited scope to use toe angles to tune handling characteristics.

In summary, we have the following main geometric steer and camber coefficients:

(1) δ_{BS}, the bump steer angle

(2) δ_{RS}, the roll steer angle

(3) γ_{BC}, the bump camber angle

(4) γ_{RC}, the roll camber angle

(5) $\varepsilon_{\mathrm{BS}}$, the bump steer coefficient [deg/m]

(6) $\varepsilon_{\mathrm{RS}}$, the roll steer coefficient [deg/deg]

(7) $\varepsilon_{\mathrm{BC}}$, the bump camber coefficient [deg/m]

(8) $\varepsilon_{\mathrm{RC}}$, the roll camber coefficient [deg/deg]

(9) k_{RS}, the roll steer gradient [deg/m s^{-2}]

(10) k_{RC}, the roll camber gradient [deg/m s^{-2}]

5.17 Compliance Steer

Changes of wheel angles, as a result of the tire forces and moments, are known as compliance steer (δ_{C}) and compliance camber (γ_{C}). Related coefficients are represented by η (eta). The compliance may be in the suspension or in the steering linkage. Change of steer and camber angles may in principle result from any of the tire forces or moments. In quoting and using these coefficients it is therefore important to specify the particular force or moment being considered. The main effects are:

(1) Lateral force compliance steer coefficient η_{LCS} (deg/N)

(2) Aligning moment compliance steer coefficient η_{ACS} (deg/Nm)

(3) Lateral force compliance camber coefficient η_{LCC} (deg/N)

(4) Overturning moment compliance camber coefficient η_{OCC} (deg/Nm)

The last of these is usually neglected, and often the last two or three. The actual compliance steer angles are

$$\delta_{\mathrm{LCS}} = \eta_{\mathrm{LCS}} F_{\mathrm{Y}}$$
$$\delta_{\mathrm{ACS}} = \eta_{\mathrm{ACS}} M_{\mathrm{Z}}$$

and the compliance camber angles are

$$\gamma_{\mathrm{LCC}} = \eta_{\mathrm{LCC}} F_{\mathrm{Y}}$$
$$\gamma_{\mathrm{OCC}} = \eta_{\mathrm{OCC}} M_{\mathrm{X}}$$

In the case of compliance camber, some symbol other than γ might be desirable, but there is no commonly accepted symbol. The use of γ is acceptable provided that the preference for δ rather than α is clearly understood in the case of compliance steer.

The total effect of compliance in the linear regime may be summarized by the compliance steer gradient k_{CS} in deg/ms^{-2} or deg/g. Because the lateral force effective in creating distortions is the sprung mass force rather than the total tire force, we have compliance gradients as follows:

$$k_{\mathrm{CS}} = k_{\mathrm{LCS}} + k_{\mathrm{ACS}}$$
$$k_{\mathrm{LCS}} = m_{\mathrm{Sf}}\,\eta_{\mathrm{LCSf}} + m_{\mathrm{Sr}}\,\eta_{\mathrm{LCSr}}$$
$$k_{\mathrm{ACS}} = m_{\mathrm{Sf}}\,t_{\mathrm{f}}\,\eta_{\mathrm{ACSf}} + m_{\mathrm{Sr}}\,t_{\mathrm{r}}\,\eta_{\mathrm{ACSr}}$$

where t is the tire pneumatic trail. Similar equations can be written for the camber. Typical values of compliance understeer gradient are 1.0 deg/g at the front and 0.2 deg/g at the rear. Although these angles are quite small, they are, nevertheless, very important. Sometimes rear compliance oversteer is deliberately introduced. Under tractive or braking forces, there may also be compliant changes of caster angle. These will augment the caster change relative to the ground caused by vehicle pitch due to longitudinal load transfer.

For the design of ordinary passenger vehicles, handling must be seen in the context of the ride/handling compromise. To provide comfort and to avoid noise, vibration and harshness, it is necessary to have considerable compliance of wheel motion, not just vertically but also in longitudinal and lateral directions, achieved by the springs and by the extensive use of rubber bushes. Unfortunately this has generally led to considerable angular compliance of the wheels, resulting in unfavorable or unpredictable handling because of deflection camber and especially because of deflection steer. This conflict is now largely resolvable by allowing the wheel relatively generous movement in translation, but little angular movement in steer or camber for the forces and moments that it actually experiences. The method is to bring the shear center of an independent suspension, in plan view, close to the center of tire contact, or for a solid axle near to the mid-point between the tires. Tire forces then have little moment about the shear center, and so although the wheel still has angular compliance, there is little angular response so that steer angle changes are controlled. Careful location of the shear center can even be used to introduce favorable small deflections. A significant characteristic of compliance steer is that unlike roll steer it occurs almost immediately.

Consider a typical driven semi-trailing arm, supported by two bushes (Figure 5.17.1). If the bushes A and B are of equal stiffness then the shear center lies midway between them. If one is harder then the shear center is closer to that one, but always between A and B. A tractive force on the tire will have a clockwise moment about the shear center, so the wheel will respond by toeing-in. Braking forces will cause toe-out, resulting in some instability under braking. Side force will also cause significant toe changes. If a driver enters a corner under power, the tractive force will contribute a toe-in; if he lifts off the accelerator to slow down, the wheel will make a toe-out change, tightening the curve in a disconcerting manner. This is known as lift-off tuck-in, and is similar to power understeer.

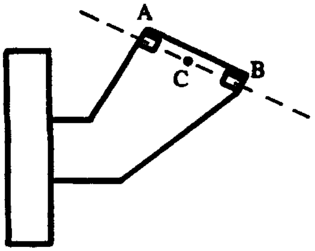

Figure 5.17.1. Plan view of a conventional trailing-arm suspension.

One solution to this problem is the Weissach axle, which has the equivalent plan-view linkage of Figure 5.17.2. With all the usual approximations, the centro of wheel motion relative to the body is at C, and this is also the shear center. Actually wheel motion about this center is resisted by suitable stiffnesses, e.g., the rubber bushes at the link ends. Tractive and braking forces now have the opposite effect to the ordinary semi-trailing arm of Figure 5.17.1, giving toe-out and toe-in, respectively. The stiffnesses are such that the total range of angular motion under cornering and braking forces is a little less than one degree. For outboard brakes, C is the point where the pivot axis intersects the ground plane. For traction, because of driveshaft torque, the total drive force on the suspension acts at wheel center height, so C is the point where the pivot axis intersects the horizontal plane at wheel center height. This distinction permits separate tuning of the response for braking and traction.

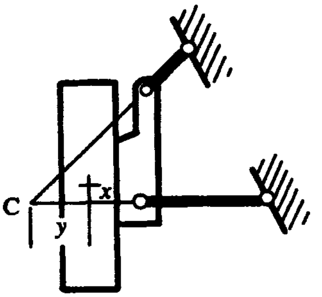

Figure 5.17.2. Plan view of the equivalent linkage of a Weissach axle.

Response to fore–aft forces depends on the lateral position of the shear center relative to the center of tire contact (*y*), whereas response to lateral forces depends on the fore–aft position of the shear center (*x*). It is not possible to achieve completely zero side force steer because the tire pneumatic trail varies with side force. Actually some side force understeer may be desirable on vehicles of large dynamic index (I_z/mab), usually large vehicles, to improve response time and stability in lane change maneuvers, but side force oversteer may give better limit controllability because of more progressive tire breakaway and more controlled response to road roughness or friction variations.

Similar principles are applicable to solid rear axles. For a Panhard rod supported axle, the rod being DE in Figure 5.17.3, the position at which the rod crosses the centerline is the shear center. A side force is opposed by lateral and forward components of force in the rod, for a tilted rod. The forward component

F_1 is then reacted by equal forces at the longitudinal locations at A and B, which cause no steer effect. The couple from the offset force *F* and the wheel side force *F* gives a moment *Fe*, requiring equal and opposite forces *Fe*/*S* at A and B, leading to a steering rotation of the axle. Thus the side force steer depends on the centerline offset *e* of the Panhard rod forward from the tire side force, and on the effective total stiffness *k* of the longitudinal arms, which is basically that of the bushes at A and B and the bushes at the front of the arms. The lateral force compliance understeer coefficient for such an arrangement for a rear axle is

$$\eta_{\mathrm{LCU}} = -\frac{2e}{kS^2} \quad [\mathrm{rad/N}]$$

For a rod forward of the axle the result is side force oversteer. This can be used to give progressive limit state handling. The offset *e* actually varies with the lateral force because of change of pneumatic trail. If the axle is located by a torque tube or equivalent instead of fore-and-aft links at the side, then there is almost inevitably side force oversteer regardless of the lateral location system position.

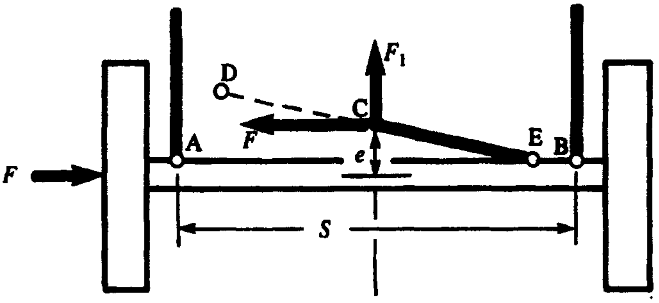

Figure 5.17.3. Compliance steer by Panhard rod, plan view.

One disadvantage of the solid axle compared with an independent system is that different tractive or braking forces side-to-side, e.g., from a limited-slip differential, will cause steer. This will be minimized for a given side force steer if the bushes are stiff and the rod offset large. The solid axle has been very successful for the rear of front-drive vehicles, but these effects suggest that independent suspension may be superior for rear drive in this respect.

Conventional trailing twist axles have a marked side force oversteer because of compliance of the bushes at the front mountings, the shear center being between them. This has been adjusted by using wedged bushes that react to a side displacement with a fore–aft displacement too, essentially as in Figure 5.17.4, where the side force F causes a y displacement of the wedged pivot bolt.

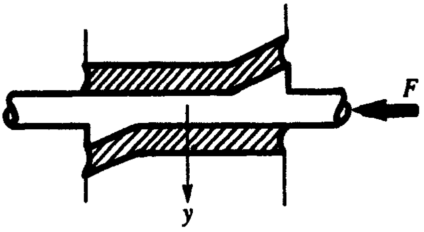

Figure 5.17.4 Radially deflecting bush.

By mounting the trailing twist axle in such bushes, it can be arranged that a side force turns the whole axle in a direction that attempts to oppose the side displacement at the wheels. In effect the shear center is therefore moved rearward from the bushes, and can be placed between the wheels, or as required. A similar effect could be achieved by using conventional bushes with their axes approximately perpendicular to the line from the desired shear center.

With longitudinal leaf springs parallel to the vehicle centerline there is no side force steer effect. However, the spring deflection tends to be perpendicular to the spring, so if the springs are convergent toward the front there will be side force oversteer for a rear axle, and side force understeer for a front axle. Longitudinally split springs have been tried, increasing the lateral compliance, but this leads to a vague steering feel even for parallel springs.

The conventional swing axle is essentially free of side force steer, but is likely to have significant tractive force toe-in, i.e., power understeer and brake oversteer.

The situation at the front of the vehicle is complicated by the steering. The outside wheel in cornering is subject to an inward lateral force, putting the lower wishbone in compression and the upper one in a smaller tension. Because of the bushes this results in a wheel camber. There will be no resultant motion of the wheel at some height between the wishbones, depending on the bush stiffnesses. If the steering arm is at this height then there will be no steering effect from this cause, whether the steering tie-rod is in front or behind the kingpin axis. In plan view the lateral force acts behind the kingpin because of pneumatic and caster trail. For front or rear tie-rods, the steering compliance then results in a side force understeer. This is the most significant of all side force steer effects because of the considerable compliance of the steering column. We can express this relatively high compliance by saying that for side force the shear center (the point where a force will not cause a steer deflection) is a rather small distance behind the kingpin axis. For tractive forces the shear center is again rather closely aligned with the kingpin axis, so in practice steering not far removed from center-point steering is used. For front drive, careful tuning of the system is required to prevent power steer, although the situation is complicated by the dominant influence of the driveshaft torque component (see Section 5.14).

On low-friction surfaces such as ice or snow, the tire characteristics are different and there is a low limit to lateral acceleration, so load transfer distribution becomes less significant and roll steer and side force steer become more critical in determining limit handling, especially at the rear.

5.18 Ride Height

Ride height is the position of the body (sprung mass) above ground level. In general, during acceleration, braking or cornering and on rough roads the ride heights vary continuously and have different values at each wheel. The set-up of the vehicle on an accurate level surface is the static ride height, frequently referred to simply as ride height. Values are specified for the front and rear of the vehicle. Normally it is assumed that the vehicle should have zero body roll in the static position, although some static roll may be specified in special cases, such as racing vehicles on tracks with predominant turns in one direction.

The front and rear ride heights may be specified at any points that are convenient for measurement. Hence particular points on the front and rear fenders may be suitable. However, from the point of view of vehicle dynamics, it is the ride heights at the wheels that are of importance. Hence, for passenger cars it is convenient to measure the ride height at the highest point of the wheel arch opening, the so-called eyebrow level. For ground-effect racing cars, the rules frequently specify a flat, or partially flat, underbody, in which case this flat plane is often used to define the ride heights. Alternatively, measurements may be made to the inner axis of the bottom suspension arm.

Under running conditions, the ride heights or vertical positions of the body (sprung mass), of the wheel and of the local road position are measured from the mean road plane; Figure 5.18.1 shows this for one suspension unit. Hence there are vertical positions Z_B to some reference point on the body, Z_W to the wheel center and Z_R to the road height. Each of these has four values, one at each wheel specified by appropriate subscripts, normally either:

(1) f and r for front and rear, with L and R for left and right, or i and o for inner and outer.

(2) Number 1 to 4 in the order

1 : left front
2 : right front
3 : left rear
4 : right rear

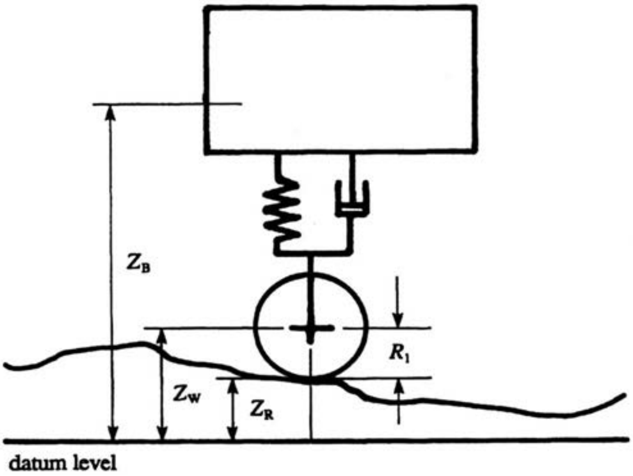

Figure 5.18.1 Body, wheel and road positions.

The static positions are Z_{B1}, Z_{W1}, and Z_{R1}, the last of these being zero by definition. The increase of these in dynamic, running condition compared with the static condition, represented by lower case z, becomes

$$z_B = Z_B - Z_{B1}$$
$$z_W = Z_W - Z_{W1}$$
$$z_R = Z_R - Z_{R1} = Z_R$$

The static tire deflection is then

$$\delta_{t1} = R_u - Z_{W1}$$

so

$$R_u = Z_{W1} + \delta_{t1}$$

The static loaded radius is

$$R_{l1} = Z_{W1} = R_u - \delta_{t1}$$

In running conditions, the loaded radius is

$$R_l = Z_W - Z_R$$

The running tire deflection is

$$\delta_t \equiv R_u - R_l$$

which becomes

$$\delta_t = \delta_{t1} - Z_W + Z_R$$

The increase of tire deflection is simply

$$z_T = z_R - z_W$$

Frequently in handling analysis, the road is deemed to be smooth and level, in which case $z_R = 0$, giving

$$\delta_t = \delta_{t1} - z_W$$
$$z_T = - z_W$$

The suspension deflection (bump) is

$$z_S = z_W - z_B$$

The basic body height is measured at the center of mass, giving a single value for Z_B. Incorporating the body pitch angle θ_B (relative to static θ_1) and the body roll angle ϕ_B (the body assumed torsionally rigid, and static roll assumed to be zero), then changes of body height at the four wheels are

$$
\begin{aligned}
z_{\mathrm{BfL}} &= z_{\mathrm{B}} + a\sin(\theta_{\mathrm{B}} - \theta_{\mathrm{B1}}) + \tfrac{1}{2}T_{\mathrm{f}}\sin\phi_{\mathrm{B}} \\
z_{\mathrm{BfR}} &= z_{\mathrm{B}} + a\sin(\theta_{\mathrm{B}} - \theta_{\mathrm{B1}}) - \tfrac{1}{2}T_{\mathrm{f}}\sin\phi_{\mathrm{B}} \\
z_{\mathrm{BrL}} &= z_{\mathrm{B}} - b\sin(\theta_{\mathrm{B}} - \theta_{\mathrm{B1}}) + \tfrac{1}{2}T_{\mathrm{r}}\sin\phi_{\mathrm{B}} \\
z_{\mathrm{BrR}} &= z_{\mathrm{B}} - b\sin(\theta_{\mathrm{B}} - \theta_{\mathrm{B1}}) - \tfrac{1}{2}T_{\mathrm{r}}\sin\phi_{\mathrm{B}}
\end{aligned}
$$

There are similar expressions, but with some sign changes, for the small deflections of the unsprung mass considered normally in terms of a pitch angle and front and rear roll angles. These are tire, unsprung mass or axle, pitch and roll angles and deflections. In practice they are usually called tire deflections, axle roll angles, and unsprung pitch angle.

The body ride positions are given by equations of the form

$$Z_{\mathrm{BfL}} = Z_{\mathrm{BfL1}} + z_{\mathrm{BfL}}$$

The suspension deflections during running are then of the form

$$z_{\mathrm{SfL}} = z_{\mathrm{WfL}} - z_{\mathrm{BfL}}$$

which is positive for bump (suspension compression).

Similar equations to the above apply for velocities. In a time-stepping computer simulation the velocities will be obtained from displacements over the time increment.

For any given body position (heave, pitch, roll) the four ride heights and ride velocities can be evalulated as above. In a handling analysis, the frequency range considered will normally be below the wheel hop frequency, so the wheel will often be assumed to adopt an equilibrium height according to the body ride height, the suspension stiffness and the tire vertical stiffness. Hence the position and velocities are determined, from which the suspension stiffness and damping forces and tire forces follow.

5.19 Problems

Q 5.2.1 For a spring stiffness of 42 kN/m and a constant spring motion ratio of 0.73, calculate the wheel rate.

Q 5.2.2 A damper has a coefficient of 2.2 kNs/m, and is positioned with a damper motion ratio of 0.82. Calculate the damping coefficient at the wheel.

Q 5.2.3 A spring is to provide a wheel rate of 16 kN/m at a motion ratio of 0.64. Calculate the required spring stiffness.

Q 5.2.4 A wheel damping coefficient of 1.8 kNs/m is required from a damper with coefficient 2.6 kNs/m. Calculate the necessary damper motion ratio.

Q 5.2.5 For a spring acting on the lower suspension arm, specify your own geometry. Draw the velocity diagram to obtain the spring motion ratio (preferably as an approximate algebraic expression).

Q 5.2.6 Repeat Q 5.2.5 for several bump positions and obtain the graph of motion ratio against wheel bump for a full range of wheel motion. Also draw the graph of wheel rate against bump position.

Q 5.2.7 For a spring acting on a bottom arm, it is desired to achieve a rising rate suspension such that the wheel rate is 30% higher at a bump of 100 mm than at normal level. Find a realistic spring position to achieve this.

Q 5.2.8 For a suspension stiffness of 20 N/mm and a tire vertical stiffness of 240 N/mm, what is the ride stiffness?

Q 5.2.9 In Figure 5.2.1, with EH = 300 mm and HF = 2000 mm, what is the rate of track change in heave? What is the value of the SAE equivalent swing arm radius?

Q 5.2.10 Explain, with a diagram, the constructions to find the center E for double-wishbone, Macpherson, trailing arm and semi-trailing arm suspensions.

Q 5.2.11 Draw a typical graph of vertical force against bump position. Describe its features.

Q 5.2.12 Sketch, and justify, the construction to find the force center E for double-wishbone, Macpherson, trailing arm, semi-trailing arm and swing axles.

Q 5.2.13 A wheel has a scrub rate in bump of 0.167, and rises at 3 m/s over a bump on a vehicle traveling at 15 m/s. Calculate the effect of scrub on slip angle.

Q 5.2.14 Obtain an expression for the wheel rate in terms of the idealized spring stiffness. Discuss the result in general terms for a slider and spring for deflections at an angle to the slider motion. (Note that the wheel rate is the rate of change of vertical force with vertical deflection.)

Q 5.2.15 The linear spring stiffness of a suspension, at the wheel, is 15 kN/m. It is desired to have the stiffness increase to 20 kN/m at a bump deflection of 100 mm. Calculate

(1) The required quadratic stiffness factor K_r
(2) The rising rate factor f_{Sr}
(3) The stiffness at a bump of 50 mm
(4) The stiffness at a droop of 80 mm

Q 5.3.1 Describe the problems with the kinematic concept of the roll center.

Q 5.3.2 Explain the difference between body roll, suspension roll and axle roll.

Q 5.3.3 Explain how body jacking can occur because of springs or stops. (After studying the rest of the chapter, compare with link jacking.)

Q 5.3.4 Describe a typical graph of suspension roll moment versus roll angle.

Q 5.3.5 Describe a typical graph of vehicle roll moment versus roll angle (i.e., for two suspensions acting in parallel).

Q 5.4.1 An axle of track 1.48 m has a roll center height of 160 mm. What are the load transfer factor and the net link load transfer at a sprung end-mass side force of 2000 N?

Q 5.4.2 An instrumented vehicle axle is found to have a net link load transfer of 320 N at a sprung side force of 2200 N. The track is 1.44 m. What are the load transfer factor and the roll center height?

Q 5.4.3 Compare and contrast the roll center definitions used here with the SAE definition.

Q 5.4.4 At a lateral acceleration of 7 m/s^2 a suspension of track 1.82 m has a net link lateral load transfer of 680 N for a sprung mass side force of 7 kN, and at 7.5 m/s^2 has 740 N on 7.5 kN. For each case find the roll center height and the load transfer factor.

Q 5.4.5 According to Steeds (1958), if the resisting tire lateral forces are unequal, then a lateral force at roll center height causes a roll angle. Do you agree? Quantify this (if not zero) in terms of the side force transfer factor, i.e., where the inner and outer side forces are $\frac{1}{2}(1-e_S)F$ and $\frac{1}{2}(1+e_S)F$, for a very small roll angle. Do this by considering an independent suspension, with compensation centrifugal force F at the roll center. Draw free-body diagrams of the two sides of the unsprung mass, and taking moments about the instantaneous centers find the effect on the idealized spring forces. Hence find how the effective moment and jacking force on the sprung mass depend on e_S, if either is non-zero.

Q 5.4.6 A vehicle has a sprung center-of-mass height of 0.642 m, 1.422 m back on a 3.141 m wheelbase. The roll center heights are 0.082 m and 0.284 m front and rear. Evaluate the anti-roll coefficient.

Q 5.5.1 Justify the construction of the EF line for a double-wishbone suspension.

Q 5.5.2 Justify each of the constructions of Figure 5.5.2.

Q 5.5.3 Explain with suitable figures how to find the initial roll center of a trailing-arm suspension with pivot axes not perpendicular to the center plane in either front or plan view.

Q 5.5.4 Compare Figure 5.5.2 with other such published figures. Note any discrepancies. Satisfy yourself that Figure 5.5.2 is correct.

Q 5.5.5 Consider a vehicle with three axles, with roll centers that are not colinear. Where is the roll axis? Is this a problem for the kinematic concept of the roll axis? Is it a problem for the force concept of the roll axis?

Q 5.5.6 Draw front views of double-wishbone independent suspensions with a roll center below ground level, one with positive and one with negative SAE swing arm radius.

Q 5.6.1 Explain the concept of the incremental roll center, and compare it with the roll center.

Q 5.6.2 Show that $h_i = h + F_S(\mathrm{d}h/\mathrm{d}F_S)$ and $f_i = f + F_S(\mathrm{d}f/\mathrm{d}F_S)$. Also explain physically why h_i is approximately equal to h for small lateral acceleration.

Q 5.6.3 Explain how the suspension jacking force arises.

Q 5.6.4 For each of the suspensions of Figure 5.5.2, does the roll center rise or fall with increasing lateral acceleration? Can this be stated with confidence without knowing the geometric details?

Q 5.6.5 For the vehicle of Q 5.5.5, find the mean load transfer factor and the mean incremental roll center height for this increment of acceleration.

Q 5.7.1 Explain with diagrams how to find roll centers for rigid link located axles.

Q 5.7.2 In an axle roll center analysis, with track 1.44 m, point A is found 1.20 m behind the suspension plane at a height of 420 mm, and point B is 2.15 m in front at height 220 mm. What are the roll center height, net link load transfer factor and net link load transfer at 3200 N sprung mass side force?

Q 5.7.3 Analyze the effect of vertical load on roll center height for the axles of Figure 4.6.1.

Q 5.7.4 "A solid axle is not subject to the link force jacking effect of independent suspensions." Discuss, with diagrams.

Q 5.7.5 For a four link solid axle (Figure 5.7.1) explain how changes to the lateral spacing of the front ends of the bottom links will affect the roll center height.

Q 5.8.1 Explain the roll center position of a leaf-spring mounted solid axle.

Q 5.8.2 Explain the roll center position of a trailing twist axle.

Q 5.9.1 Discuss various methods of experimental roll center measurement.

Q 5.9.2 For the best method of experimental laboratory roll center measurement, consider the possible inaccuracies in relation to the force roll center for real cornering conditions.

Q 5.10.1 Explain why the total lateral load transfer cannot be altered by suspension adjustments, for a given height of G and track width T, neglecting roll angle.

Q 5.10.2 In load transfer analysis, the axle unsprung masses are treated separately from the sprung mass. Justify the treating of the unsprung mass as a single mass in this context, for an independent suspension.

Q 5.10.3 In steady-state cornering there may be a longitudinal load transfer. List all the possible causes of this, and explain them.

Q 5.10.4 Explain, with equations, how the total lateral load transfer is distributed front and rear.

Q 5.10.5 A vehicle has total mass 1600 kg, lateral acceleration 6.5 m/s^2, $H =$ 550 mm, $a = 0.46l$, track 1.46 m, $h_f = 70$ mm, $h_r = 320$ mm, roll stiffness 350 Nm/deg front, 150 Nm/deg rear. Find the roll angle neglecting the sideways movement of G, the percentage load transfer distribution, and the tire vertical reactions. Neglect the unsprung mass and treat the body as torsionally rigid.

Q 5.10.6 Taking other data from the last question, with front unsprung mass 140 kg at height 280 mm and rear unsprung mass 200 kg at 300 mm, sprung mass 1260 kg at 550 mm height, with $a_s = 0.44l$, find the roll angle allowing for sideways movement of G, and the percentage load transfer distribution.

Q 5.10.7 With the same data as Q 5.10.5, but with a driveshaft torque of 400 Nm exerted by the body on the rear axle, find the roll angle and load transfer because of this.

Q 5.10.8 Repeat Q 5.10.5, allowing for a tire vertical stiffness of 200 N/mm, also finding the two axle roll angles.

Q 5.10.9 Explain the idealized spring model of the suspension, and discuss its advantages.

Q 5.10.10 For a vertical slider pillar suspension, obtain an expression for the real load transfer in the links with the spring acting at the pillar. Compare with the idealized spring model. Where is the roll center? Discuss.

Q 5.10.11 "The roll axis inclination can be neglected in load transfer calculations." Discuss, giving equations and considering the sprung-mass weight and side force.

Q 5.10.12 "The rotation of the wheels gives a gyroscopic effect that affects lateral load transfer in steady-state handling." Explain with equations.

Q 5.10.13 Evaluate the gyroscopic effect of the wheels on lateral load transfer in steady-state handling, as a percentage change, for an ordinary passenger car and for a racing car. See Appendix B for example data.

Q 5.10.14 A racing car designer proposes to improve the cornering performance by eliminating steady-state lateral load transfer. This is to be done by installing a flywheel with axis parallel to the axles. Obtain an algebraic expression for the required angular speed of the flywheel, in terms of car mass, center-of-mass height, flywheel second moment of mass, etc. State the required direction of rotation. What gear ratio is needed if the flywheel is driven from a rear wheel? Comment on the practicality of such a system (giving numerical values). Is the yaw balance of the car directly affected by the flywheel (i.e., is a yaw torque needed)?

Q 5.10.15 Analyze the lateral load transfer effect caused by rotation of a transverse engine. Give values, including the effect of gear ratio.

Q 5.10.16 A vehicle has track 1.440 m, center-of-mass height 640 mm, and maximum lateral acceleration 8.10 m/s^2. Find the rollover lateral acceleration, and the (simply calculated) safety factor against rollover. Give a rough estimate of the probable real value that would be found by more accurate calculation.

Q 5.10.17 Define and explain the vertical force lateral transfer factor e_V.

Q 5.11.1 Derive an expression for the roll angle gradient of a vehicle, neglecting aerodynamics.

Q 5.11.2 Derive an expression for the roll angle gradient, including aerodynamics, for varying radius at constant speed.
[Use $\beta = -(b/R) + (k_\beta / k_\phi)\phi$.]

Q 5.11.3 Explain the effect of tire overturning moment on lateral load transfer for: (1) a solid axle, (2) independent suspension.

Q 5.11.4 In cornering with an independent suspension, there may be a moment (M_X) on the unsprung mass from the couple of compensation force and tire force, from tire overturning moment or from wheel gyroscopic precession. Describe the corresponding lateral load transfer process in detail. Will this cause any roll angle of the sprung mass?

Q 5.11.5 In calculating cornering lateral load transfer from compensation force on the unsprung masses of an independent suspension, can the unsprung masses be treated as a solid axle? Justify your answer in detail.

Q 5.12.1 Describe how complete anti-dive may be achieved for inboard and outboard braked vehicles. What are the problems with such a system?

Q 5.12.2 Describe how anti-squat may be applied to a four-wheel-drive vehicle. Is this compatible with anti-dive, for inboard or outboard brakes?

Q 5.12.3 Analyze the jacking effect resulting from large anti-dive in small radius corners.

Q 5.12.4 Define, explain and give example values for the tire vertical force longitudinal transfer factor in acceleration and braking, e_X and e_B.

Q 5.13.1 Explain why the vertical wheel reactions on a conventional vehicle are statically indeterminate.

Q 5.13.2 Calculate the percentage wheel reactions for a vehicle: (1) with center of mass at 0.44 of the wheelbase, and plus 4% diagonal bias, (2) with center of mass at 0.54 of the wheelbase, and minus 4% diagonal bias (linear springs).

Q 5.13.3 Calculate the percentage wheel reactions for a vehicle in right-hand cornering with center of mass at 0.48 of the wheelbase, with zero static diagonal bias, and 24% lateral load transfer distributed 75% at the front.

Q 5.13.4 Calculate the percentage wheel reactions for a vehicle in left-hand cornering with center of mass at 0.44 of the wheelbase, plus 4% diagonal bias, and 20% lateral load transfer distributed 60% at the front, and 2% longitudinal load transfer.

Q 5.13.5 Apply the vertical force lateral transfer factor e_V to a complete vehicle. Define e_V for the vehicle, and for front and rear suspensions.

Q 5.13.6 For the vehicle of Q 5.13.4, evaluate e_V, e_{Vf} and e_{Vr}.

Q 5.14.1 Describe the merits and demerits of rear-wheel steering.

Q 5.14.2 Describe the most common types of steering system for independent suspension, with diagrams.

Q 5.14.3 Define, explain and give typical values of caster angle, caster offset (trail), kingpin inclination and kingpin offset.

Q 5.14.4 What are the advantages of independently variable caster angle and trail?

Q 5.14.5 Define and explain all terms relating to steer angle and steering gear ratio. Give example values.

Q 5.14.6 Estimate the road wheel torque to statically steer a vehicle with mass 1500 kg, $a = 0.40L$, at 170 kPa inflation pressure with $\mu = 1.1$. With steering ratio of 16 and forward efficiency 85%, what is the steering-wheel torque requirement (unpowered)?

Q 5.14.7 Explain the origin of the most important steering system inertias and compliances, giving example values.

Q 5.14.8 Define and explain the terms steer angle, steering wheel angle, overall steering ratio, reference steer angle and any related terms.

Q 5.14.9 Sketch example curves of δ_S against δ with and without forces in the steering system, for nonlinear steering ratio. Discuss the application of the concept of reference steer angle in such a case.

Q 5.14.10 Explain in detail how braking or driving driveshaft torques affect the steering. Give equations and example values.

Q 5.14.11 Explain in detail how the tire lateral force and aligning moment affect the steering.

Q 5.14.12 Explain in detail how tractive or braking forces affect the steering, with and without a limited-slip differential, on front drive.

Q 5.14.13 Explain in detail how tire vertical forces affect the steering. Give suitable diagrams.

Q 5.14.14 Explain how caster trail is used to give a desired form to the Gough plot.

Q 5.14.15 Explain and give example values for centrifugal caster.

Q 5.15.1 Evaluate the maximum low-speed offtracking for a car, using representative dimensions.

Q 5.15.2 Describe in detail the low-speed offtracking of a two-wheeled trailer on a four-wheel vehicle.

Q 5.15.3 Define the Langensperger angle for an axle, and discuss its significance.

Q 5.16.1 Define and explain bump steer.

Q 5.16.2 Define and explain roll steer.

Q 5.16.3 Define, explain and give example values of bump steer coefficient, bump camber coefficient, roll steer coefficient and roll camber coefficient.

Q 5.16.4 Describe a typical bump steer graph; explain how it might be measured and why certain features may be considered desirable.

Q 5.16.5 In Figure 5.16.2, evaluate the bump steer coefficient at 50 mm droop.

Q 5.16.6 Explain how the link geometry of an axle leads to roll steer, and how this may depend on the vehicle load in a favorable way.

Q 5.16.7 Discuss roll steer of leaf-spring rear axles.

Q 5.16.8 Discuss the extra complications of roll steer on leaf-spring axles at the front rather than the rear.

Q 5.16.9 Explain roll steer of the trailing twist axle.

Q 5.16.10 Discuss the desirability of, and limitations on, deliberate static toe-in and toe-out.

Q 5.16.11 Analyze qualitatively the effect of load on the roll steer coefficient of the axles of Figure 4.6.1.

Q 5.16.12 Is it possible to arrange for no bump steer of a slider (pillar) suspension?

Q 5.16.13 For a rack forward of the steering axis by 120 mm, higher than the steering arm ball-joints by 8 mm, and with tie-rods of length 290 mm against a geometric ideal of 306 mm, calculate the linear and quadratic bump steer coefficients, and draw the bump steer graph.

Q 5.16.14 Explain the relationship between bump steer and roll steer.

Q 5.17.1 Define and explain compliance steer coefficients and compliance camber coefficients.

Q 5.17.2 Explain the principle by which only desirable wheel compliant movements are allowed and undesirable ones minimized.

Q 5.17.3 Considering the two main types of independent suspension, with steering in front and behind the kingpin axis, describe how compliance steer arises. Which force or moment components of tire force are likely to be the main cause of steer effects?

Q 5.17.4 Which components of tire force and moment are likely to be the main cause of compliance steer?

Q 5.17.5 Explain the compliance steer effects that occur on a standard semi-trailing arm because of drive, braking and lateral forces.

Q 5.17.6 Explain the function of the Weissach axle.

Q 5.17.7 Explain how a Panhard rod located dead rear axle can be tuned to give desired compliance steer characteristics. Give relevant equations.

Q 5.17.8 Explain in detail how wedged bushes may be used to eliminate excessive side force steer from a trailing twist axle.

Q 5.17.9 A vehicle has a leaf-spring front axle with the spring divergent at 6° each in plan view, toward the front, spaced at 1.2 m at the axle. Each spring lateral stiffness is 62 kN/m. The front sprung end-mass is 1400 kg. Obtain an expression for the compliance steer gradient ($\mathrm{d}\delta_{\mathrm{CS}}/\mathrm{d}A$) because of this, and evaluate it.

Q 5.17.10 A Panhard rod supported rear axle has a forward offset e of 120 mm, and longitudinal supports at spacing 1.100 m with bushes of stiffness 120 kN/m. The sprung end-mass is 900 kg. Estimate the compliance steer gradient ($\mathrm{d}\delta_{\mathrm{CS}}/\mathrm{d}A$) neglecting pneumatic trail.

Q 5.18.1 Define and explain the term ride height, including equations relating it to the body (sprung mass) position in heave and roll.

Q 5.18.2 A vehicle with independent suspension has a wheelbase of 2.6 m and $a = 1.2$ m, front track 1.6 m and rear track 1.4 m. The front axle roll angle is 1.4°, the rear 1.8°, the front suspension roll is 8.2°. The body is torsionally rigid. The road is smooth. The body pitch angle is 1.7°. The unsprung pitch angle is 0.3°. The heave is 24 mm. Calculate:

(1) The body roll angle

(2) The rear suspension roll angle

(3) The body ride deflections at the four wheels

Q 5.18.3 Obtain algebraic expressions for the tire deflections in terms of the axle roll angles and the unsprung pitch angle.

Q 5.18.4 For the vehicle of Q 5.18.2, calculate the extra tire deflection at each wheel.

Q 5.18.5 For the vehicle of Q 5.18.2, the suspension roll velocity is 8 deg/s. Calculate the resulting suspension bump velocity at the front.

Q 5.19.1 For one of the vehicles specified in Appendix B, apply the theory of each section of this chapter to analyze the suspension.

Q 5.19.2 For vehicle G of Appendix B, calculate the load transfer distribution with and without allowance for tire vertical stiffness.

Q 5.19.3 – 5.19.7

One set of published data for a modern racing car is for a Tyrell F1 on Signes corner of Paul Ricard Circuit in practice for the 1990 French Grand Prix (Curtis, 1990). (This author cannot vouch for the accuracy of the data, which when analyzed gives rise to some doubts, but it is presented here for interest.) Signes is a very fast right-hander, with a recorded speed of 83.4 m/s (186.5 mph) and lateral acceleration of 39.2 m/s^2 (4.0g) at the path radius of 177 m (about 600 ft). The data are:

Mass = 600 kg
Aerodynamic downforce – front wing = 4500 N
– body = 4308 N
– rear wing = 3426 N
Total = 12 234 N
Tire vertical force – front inner = 1667 N
– front outer = 5093 N
– rear inner = 4456 N
– rear outer = 6904 N
Total = 18 120 N
Tire side force – front inner = 3182 N
– front outer = 6998 N
– rear inner = 6166 N
– rear outer = 7144 N
Total = 23 490 N
Typical F1 wheel track – front = 1.804 m
– rear = 1.626 m
Typical F1 wheelbase = 2.800 m

Q 5.19.3 Calculate the front, rear and overall mean tire side force coefficients.

Q 5.19.4 Calculate the longitudinal G position *a/L* using the side forces (neglect steer angle and longitudinal load transfer).

Q 5.19.5 Calculate the front, rear and total vertical force transfer, and the load transfer distribution, the front and rear load transfer factors, and the G height (the result is suspicious).

Q 5.19.6 Calculate the front and rear downforces and the aerodynamic downforce position (using the G position) and the total downforce area.

Q 5.19.7 Analyze the tire maximum cornering force coefficient sensitivity to vertical force.

5.20 Bibliography

For a qualitative discussion of many example suspensions, see Norbye (1980). A more quantitative analysis with many practical examples is given in Bastow (1980 or 1987) and Campbell (1981). For more examples specifically on front-wheel drive see Norbye (1979). Ellis (1969 and 1989) provides a mathematical perspective on suspension analysis, while Segel *et al.* (1980) is a useful reference on the suspension of commercial vehicles.

A full definition of terms is given in SAE J670e *Vehicle Dynamics Terminology* (included here in Appendix E) and MIRA 1965/1 *Definition of Handling Terms*.

A good deal of useful practical information is provided in the popular work by Puhn (1981). Many details of suspension design are discussed in unpublished General Motors reports by Olley (1961a, 1961b, 1962a, 1962b). Reimpell (1982) gives an extensive analysis of suspensions, in German. Large truck suspensions are described by Sternberg (1976). For a more detailed discussion of roll centers for independent suspensions, see Dixon (1987a). Riede *et al.* (1984) have surveyed typical values of vehicle parameters needed for handling analysis.

Although there has been a good deal of discussion elsewhere about active suspension systems they have not so far found great commercial success or shown any consistent advantage in racing. They have the advantage of being able to eliminate roll, even with a ground-level roll center, and to eliminate dive and squat, freeing constraints on the link geometry. They are likely to be rather expensive. Bastow (2nd edition, 1987) gives an introduction. For details, see for example the proceedings of the International Conference on Advanced Suspensions (I.Mech.E. 1988).

6

Steady-State Handling

6.1 Introduction

In a broad sense, the purpose of handling theory is to assist in the design of better vehicles. The first step is to determine if there are optimum or preferred vehicle characteristics. If such characteristics exist, then handling theory should show the designer how to achieve them. In a narrower sense the purpose is to predict the behavior of a vehicle in response to control inputs, or to environmental disturbances such as road roughness or wind. This chapter deals with the theory of response to steady-state control inputs and disturbances.

Two examples of steady-state disturbances are a constant side wind and a constant road camber, i.e., side slope. Later sections deal with the vehicle's response in such cases and with the associated problem of the control inputs required to overcome the disturbance. More attention will be devoted to investigating the steady-state response to control inputs. In this case steady-state is taken to mean the absence of ground or wind disturbances, and fixed controls. This implies constant path radius of curvature, constant translation speed, constant angular speed and constant magnitude of lateral acceleration, although the velocity and acceleration are not constant in direction relative to the ground. The SAE definition of steady-state is:

> "Steady-state exists when periodic (or constant) vehicle responses to periodic (or constant) control and/or disturbance inputs do not

> change over an arbitrarily long time. The motion responses in steady-state are referred to as steady-state responses."

By this definition, regular oscillatory control inputs, for example for a slalom test, would be included in steady-state. Ambiguously, the SAE definition of transient state is:

> "Transient state exists when the motion responses, the external forces relative to the vehicle, or the control positions are changing with time."

The definition adopted here will be that transient states are states that are not steady.

Following aircraft practice, steady-state theory is sometimes said to be a theory of trim states, i.e., of the vehicle response to given control trim conditions. Trim is formally defined by SAE as:

> "...the steady-state condition of the vehicle with constant input which is used as the reference point for analysis of dynamic vehicle stability and control characteristics."

It is sometimes unfortunately said to be the "equilibrium condition"; in general the vehicle is not in equilibrium in Earth-fixed axes, having a non-zero lateral acceleration. The question of the static and dynamic stability of the vehicle at any particular trim state will be considered in the next chapter. This is closely related to the widely used, and often abused, concepts of understeer and oversteer, which are examined in some detail.

Steady-state handling theory can be considered to fall into two main areas. The first area is the representation of the total vehicle handling characteristic, which may be by the sideslip, yaw and steer angles versus lateral acceleration, or by the moment-method graph. Such results may be found by testing. The second area is the prediction of the total vehicle characteristic from its design details such as the tire and suspension characteristics.

6.2 Parameters

The properties of the chassis, the suspension, the tires, the body shape and the environment – i.e., the road surface and the atmosphere – combine to give the vehicle its handling characteristics. The parameters representing the motion state of the vehicle in steady conditions are its forward speed and the path curvature (reciprocal of the path radius of the center of mass). "Steady state" implies constant values for these two variables.

The speed and path curvature are the basic dependent variables that result from the driver control inputs to the system (Figure 1.1.1). These input variables are the steering wheel position, the accelerator position, and the gear-lever position (for automatics the gear is a dependent variable). In a full computer simulation we would expect to find the steering wheel and accelerator positions as real variables, the gear as an integer variable, and the resulting speed and path curvature being deduced as real variables. These are the fundamental control inputs and responses of the system as perceived by the driver.

Even a cursory examination of the research literature quickly shows that handling theory is not actually presented in terms of the above three input variables. Certainly there are innumerable instances of the steering wheel position being considered, but this author cannot recall ever seeing a quantitative, or even qualitative, representation of the accelerator position. As an alternative to the accelerator and gear positions, we could use the effective torque at the rear wheels as an input variable. This is the result of the accelerator position and gear and engine characteristics, environmental conditions, gearbox ratio and friction, and differential and final drive ratio and friction. It also has the advantage of a reduction of the total number of input control variables from three to two, and the elimination of side-effects such as the influence of atmospheric conditions on the engine. Another possible advantage is that "minor" features of the vehicle, such as the throttle linkage, are no longer directly relevant, although experience shows that the apparent response of a vehicle in ordinary driving is governed as much by the progressive action of the throttle linkage as by the maximum engine power; also, for high-powered or competition vehicles the controllability may critically depend on the provision of a good design of throttle linkage, so this simplification is not achieved without some loss of reality. A definite disadvantage is that the driver does not perceive the torque at the rear wheels directly, i.e., it is not strictly a control input, although he does experience it indirectly through the vehicle's speed and acceleration. Again, however, examination of the literature shows that torque at the driven wheels is not normally considered the input variable.

Under steady-state conditions, driven-wheel torque primarily influences the forward speed. It is the steering-wheel position and the forward speed that are generally taken as the basic independent variables of steady-state handling theory. Even this is an oversimplification because the steering wheel angle is often considered after gearing down to the reference steer angle

$$\delta_{\mathrm{ref}} = \frac{\delta_{\mathrm{S}}}{G}$$

In the results of testing, the vehicle speed, angular speed or lateral acceleration may be measured, although it is generally the last of these that is used in graphical results, e.g., Figure 1.13.1. For a speed V and path curvature

$$\rho = \frac{1}{R}$$

the yaw angular speed is

$$r = \rho V = \frac{V}{R}$$

and the lateral acceleration is

$$A = \rho V^2 = rV = \frac{V^2}{R}$$

Hence any two of these four variables suffice to find all four. In practice because the actual vehicle controls are the accelerator and the steering wheel, it is usual to take the speed, plus one of ρ, r or A. Arguably, the path curvature is the most fundamental of these, although each has interesting characteristics in its own right, and will be considered in more detail.

At any particular trim state, the sensitivity of any of the response measures to the steer angle is called a gain. The path curvature gain is

$$G_\rho \equiv \frac{\mathrm{d}\rho}{\mathrm{d}\delta}$$

the yaw velocity gain is

$$G_\mathrm{r} \equiv \frac{\mathrm{d}r}{\mathrm{d}\delta} = V\frac{\mathrm{d}\rho}{\mathrm{d}\delta} = VG_\rho$$

and the lateral acceleration gain is

$$G_\mathrm{A} \equiv \frac{\mathrm{d}A}{\mathrm{d}\delta} = V^2\frac{\mathrm{d}\rho}{\mathrm{d}\delta} = V^2G_\rho$$

By definition, these derivatives are taken at constant speed. The steer angle used may be the steering wheel angle δ_S, the reference steer angle

$$\delta_{\text{ref}} = \frac{\delta_S}{G}$$

or the mean of the front-wheel steer angles, and so should be specified. In principle there are also partial derivatives with respect to speed, keeping steer angle constant, which in practice do not find wide application.

Thinking in terms of force control rather than position control, the input parameter is the steering wheel torque T_S instead of the steer angle. This leads to three new gains, less widely used than the previous ones; the force control lateral acceleration gain $G = \mathrm{d}A/\mathrm{d}T_S$ is perhaps the most common. Sometimes the torque is instead expressed as a force at the steering wheel rim, giving three more gains, e.g., $G = \mathrm{d}A/\mathrm{d}F$.

In practice, various units are used for responses and gains. Because the basic S.I. unit of angle is the radian, with degrees as an allowable alternative, speed in S.I. is m s^{-1} or m/s, although km/h and mi/h (mph) sometimes appear, and acceleration in S.I. is m s^{-2} or $\mathrm{m/s}^2$, but the technical unit of g (equal to 9.81 $\mathrm{m/s}^2$) is convenient and often preferred. An interesting detail is that the units of path curvature are most clearly expressed as rad/m (radians per metre) but are sometimes simplified to m^{-1}, which has the same meaning. In summary the usual expressions are: speed in m s^{-1}, angle in radians or degrees, path curvature in rad/m, yaw velocity in rad/s, lateral acceleration in $\mathrm{m/s}^2$ (m s^{-2}) or g, curvature gain in m^{-1}, yaw velocity gain in s^{-1}, and lateral acceleration gain in m s^{-2}/rad, m s^{-2}/deg or g/deg.

6.3 Basic Handling Curve

The basic handling curve is a plot of the steer angle against lateral acceleration at a given path radius. The steer angle is considered to be the sum of two terms:

$$\delta = \delta_K + \delta_U$$

where δ_K is the kinematic steer angle which is needed for nominally zero lateral acceleration, and δ_U, the understeer angle or dynamic steer angle, is the extra angle required for a given lateral acceleration.

Figure 6.3.1 shows a minimal prototype vehicle without suspension. The properties of the pair of real wheels on each axle are compressed into single wheels on the centerline, thereby simplifying the geometry. This is therefore sometimes known as the bicycle model because it contains only two wheels, but this does not imply that the handling is in any way related to a real bicycle, which banks in corners. In its simplest form there is no suspension, although the front wheel can be steered. Aerodynamic forces are neglected.

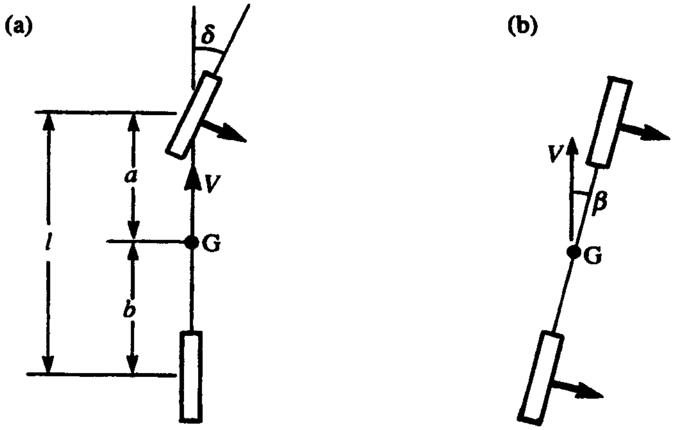

Figure 6.3.1. Bicycle model vehicle: (a) with steer angle only, (b) with yaw angle only.

Figure 6.3.1 actually shows two non-equilibrium conditions of the vehicle. In the first, there is a steer angle but no body yaw, the result being a lateral force and moment. In the second there is a yaw angle with no steer angle. Again there is a lateral force and a moment. In the latter case the total force acts close to the center of mass, usually a little behind it. Thus the moment from yaw can be balanced by a steering moment from a relatively small steer angle. An alternative way to view this is that the yaw angle gives a rear-wheel slip angle, and the steering can be used to give a suitable front slip angle to give zero yaw moment and hence constant yaw speed, i.e., steady state. Thus handling depends on a balance between front and rear.

There are essentially two different approaches to representing the steady-state handling of a vehicle. The first, both the older and more common, we may call the kinematic method because, although forces are considered in the analysis, the result is to relate the response in kinematic terms to the control inputs. Thus path curvature, yaw speed and lateral acceleration are produced as functions of steer angle and forward speed. The second approach, at the same time more difficult and more comprehensive, is called the moment method, and basically considers the total vehicle lateral force and yaw moment as functions of yaw and steer. This gives a handling "portrait" of the vehicle on a plot of moment versus lateral force, with separate plots required for different speeds when speed effects become significant, for example through aerodynamics.

The kinematic method is essentially a steady-state method, whereas the moment method can be used in the prediction of transient behavior. Most of this chapter will be devoted to the kinematic method, although the moment method is introduced later in Section 6.22.

For the model of Figure 6.3.1, with no suspension, no aerodynamic forces and no tractive forces, and small steer angles, the handling characteristics may be deduced in a particularly simple way, from the front and rear tire side force coefficient versus slip characteristics.

The axle characteristics are plotted together in Figure 6.3.2. A given specified lateral acceleration A requires the same F_y/m factor front and rear; the graph then shows the required slip angles α_f and α_r front and rear. For this simple model the vehicle yaw angle equals α_r at the rear axle. If the vehicle is describing a curved path then the yaw angle varies along the vehicle length, being α_r at the rear axle, but $\alpha_r - b/R$ at the center of mass, the point at which it is normally defined. Because of the difference in slip angles required front and rear, the driver must provide an extra steer angle equal to the difference in slip angles. The tire understeer slip angle is

$$\alpha_U = \alpha_f - \alpha_r$$

The driver must apply an extra steer angle to compensate. This extra angle, the understeer angle, is in this case simply

$$\delta_U = \alpha_U = \alpha_f - \alpha_r$$

The total steer angle required in a corner follows from Figure 6.3.3.

Here we see that the total steer angle δ required is a combination of a kinematic angle δ_K because of the path curvature, plus a dynamic steer angle (understeer angle) δ_U required because of the difference of slip angles:

$$\delta = \delta_K + \delta_U$$

(a) Tire characteristics

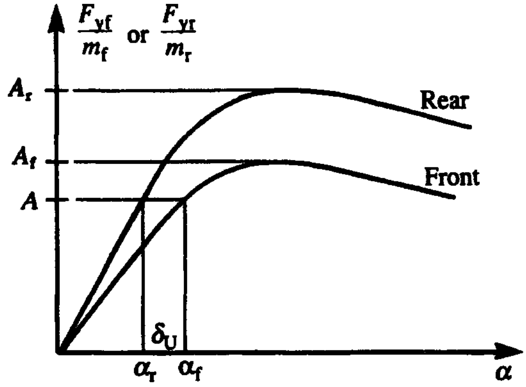

(b) Understeer angle

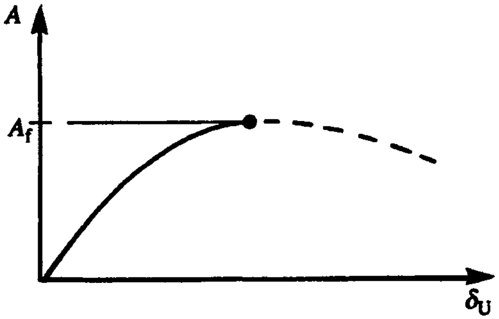

Figure 6.3.2. Vehicle and tire characteristics: (a) tire characteristics, (b) resulting understeer angle.

At very low speed there is negligible lateral acceleration and hence no slip angles, so there is only a kinematic steer angle requirement

$$\delta_K = \frac{L}{R}$$

Sometimes arctan(L/R) is used instead of L/R, but this is not really an improvement. We can now write

$$\delta = \frac{L}{R} + \delta_U$$

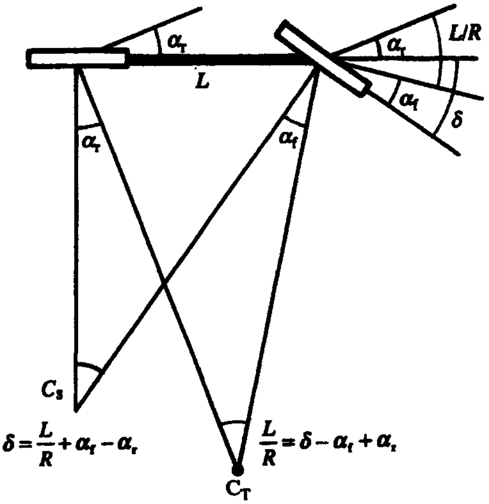
α_r
L
L/R
α_r
α_f
δ
α_r
α_f
C_s
$\delta = \frac{L}{R} + \alpha_f - \alpha_r$
$\frac{L}{R} = \delta - \alpha_f + \alpha_r$
C_T

Figure 6.3.3. Steer angles and slip angles.

where δ_U is the understeer angle arising from the tires and, for a road vehicle, from the suspension characteristics. Rearranging the above, the path radius is

$$R = \frac{L}{\delta - \delta_U}$$

from which it may be seen that the presence of a positive understeer angle δ_U increased the path radius. The total steer angle requirement, for this simple model, is in general therefore

$$\begin{aligned}\delta &= \frac{L}{R} + (\alpha_f - \alpha_r) \\ &= \frac{L}{R} + \alpha_U\end{aligned}$$

Although it is convenient, and common practice, to call $\alpha_f - \alpha_r$ the tire understeer angle, we shall see later that the SAE definition of the understeer condition is not the same as having a positive understeer angle.

In some cases it is convenient to break the kinematic steer angle down into front and rear kinematic steer angles (wheelbase angles):

$$\delta_K = \delta_{Kf} + \delta_{Kr}$$

$$\delta_{Kf} = \frac{a}{R}$$

$$\delta_{Kr} = \frac{b}{R}$$

$$\frac{L}{R} = \frac{a}{R} + \frac{b}{R}$$

Independently of the particular radius, from Figure 6.3.2(a) we can deduce a curve of lateral acceleration against understeer angle; this is the understeer characteristic, as in Figure 6.3.2(b). It is simply the difference of slip angle for the two curves of Figure 6.3.2(a). In this particular, and representative, case this angle smoothly increases and becomes horizontal at a lateral acceleration A_f for which the front tires have their peak side force coefficient.

For lateral accelerations exceeding A_f there is no solution for a front slip angle, so the shape of the rear tire curve at values above the corresponding force coefficient can have no influence on the understeer characteristic. In principle, if the front tire characteristic is peaked, as shown in Figure 6.3.2(a), then a second possible value of α_f occurs for a given lateral acceleration corresponding to a very large steer angle, giving the dashed line of Figure 6.3.2(b). If the rear tire characteristic is highly peaked, falling again into the relevant region below A_f, then there are further possible solutions for δ_U giving additional branches to the A versus δ_U curve. These are interesting in principle, although not of great practical importance. It is also possible for the rear tire characteristic to lie beneath the front tire one, but this is generally undesirable because the understeer angle then reduces with lateral acceleration, the condition known as oversteer.

Figure 6.3.2(b) showed lateral acceleration as the ordinate and steer angle as the abscissa. This is convenient when deducing the curve from the tire characteristics. However, when the steer characteristic is found experimentally it is usually the acceleration that is the abscissa (Figure 6.3.4), with the total steer angle as ordinate. Which way around to plot these curves is a matter of personal taste; more usually acceleration is taken as the abscissa.

In the most common form of handling test, the vehicle is driven at various speeds around a fixed radius, with typical results as in Figure 6.3.4. Curve A is representative of a modern car. Curve B was common on older designs of cars; it would nowadays usually be considered unacceptable for a car, but it is still

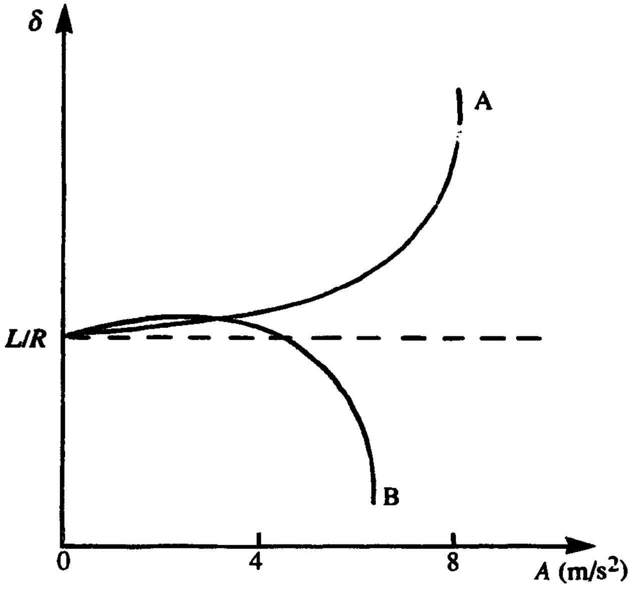

Figure 6.3.4. Example handling (understeer angle) characteristics.

fairly typical of trucks. Curve A is fairly linear up to about 3 m/s^2 (0.3g) lateral acceleration, perhaps as high as 0.45g for a modern high-performance car, and curve B up to about 1 m/s^2. Thus the linear region covers most normal driving conditions, which we may call the primary handling regime. For a typical car, from 3 to 6 m/s^2 constitutes a nonlinear region, the secondary handling regime, where effects such as lateral load transfer become significant. Beyond 6 m/s^2 is the final handling regime where tire frictional effects are paramount. This is the province of desperate accident avoidance for the road vehicle, although entered as a matter of routine in deliberate testing and by competition vehicles. For commercial vehicles all these regions are at lower bands of lateral acceleration. These handling regimes will be considered separately in various sections of this chapter, beginning with the linear region which is the simplest theoretically. From a design point of view, division of the handling curve into three regimes is useful, because the shape in each regime depends on different variables. A thorough understanding of the influence of different parameters on the handing curve is of great value at the design stage, and also, of course, if it is required to modify the behavior of an existing vehicle in a particular way.

6.4 Cornering Forces

Figure 6.4.1 shows the simple "bicycle" model in cornering without tractive forces, rotating about the turn center C_T. Because of the constant angular speed, the slip angles must give no moment about the center of mass G. Rolling resistance and aerodynamic forces are neglected. The tire forces are perpendicular to the wheels and intersect at the force center C_F. Hence the line of action of the resultant force on the vehicle is through G toward the point C_F. This force has the desired centripetal component toward C_T, but also a tire drag component so the tangential speed is not constant. Sometimes it is acceptable to neglect the tractive forces in this way.

Figure 6.4.2 shows a rear-drive vehicle with the required tractive force component F_{xr} to give steady tangential speed. To fit this requirement, the intersection of the total front and rear tire forces F_f and F_r must intersect on the line GC_T. Figure 6.4.3 shows the equivalent force condition for a front-drive vehicle. In this case the intersection of the tire forces occurs to the outside of the vehicle, tractive force F_{xf} having been added to give the required angle to F_f.

The vector force diagrams for rear- and front-drive vehicles appear in Figures 6.4.4 and 6.4.5. These are simply the forces taken from Figures 6.4.2 and 6.4.3. The general form of the diagram as shown corresponds to slip angles larger than a/R and b/R. In the case of small lateral acceleration at a small radius this will not be true, and the form of the vector diagram is significantly changed. The diagram shown assumes a positive understeer angle, i.e., $\alpha_f > \alpha_r$. For the rear-drive vehicle, the steer angle is the angle between F_{yr} and F_f, and for front-drive it is the angle between F_{yf} and F_r.

In each case

$$\begin{aligned}\delta &= \left(\alpha_f + \frac{a}{R}\right) - \left(\alpha_r - \frac{b}{R}\right). \\ &= \frac{L}{R} + (\alpha_f - \alpha_r) \\ &= \delta_K + \delta_U\end{aligned}$$

The diagrams of Figures 6.4.4 and 6.4.5 are easily extended to include additional effects such as aerodynamic forces and rolling resistance.

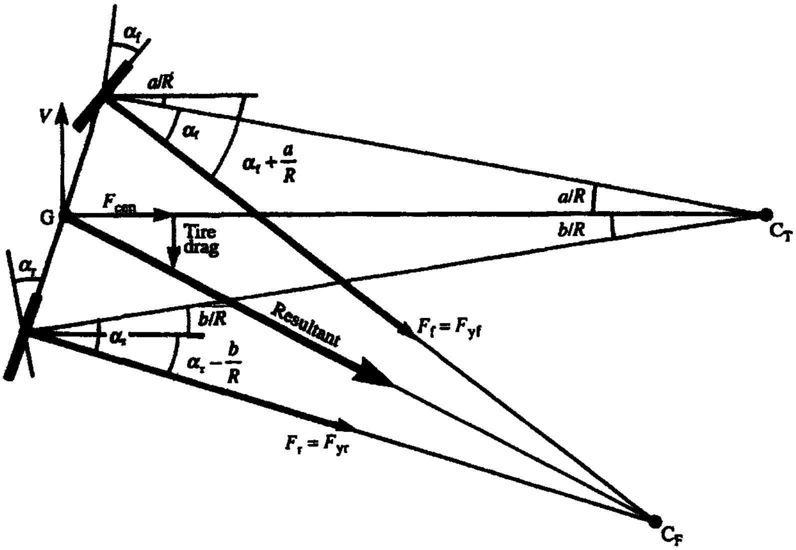
α_f
a/R
V
α_f
$\alpha_f + \frac{a}{R}$
a/R
G
F_{cen}
Tire drag
b/R
C_T
α_r
b/R
Resultant
$F_f = F_{yf}$
α_r
$\alpha_r - \frac{b}{R}$
$F_r = F_{yr}$
C_F

Figure 6.4.1. Plan view free-body diagram for no drive.

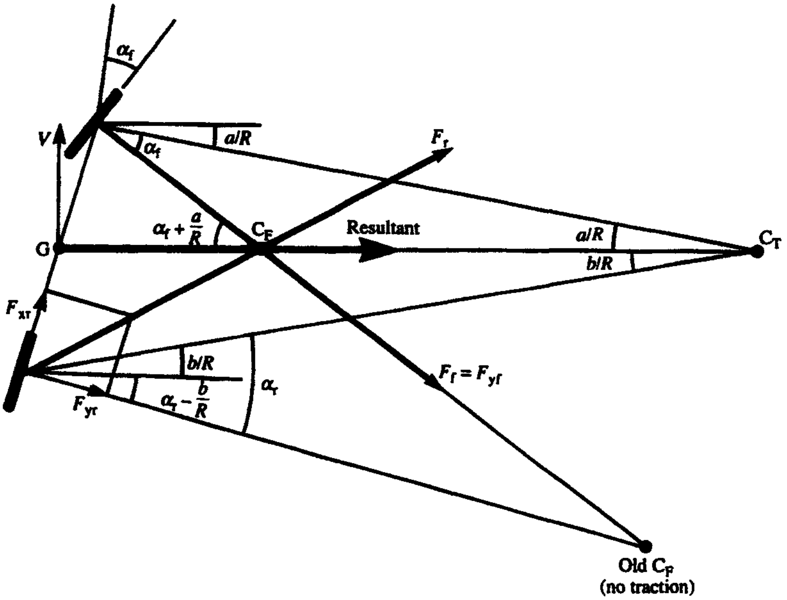
α_f
V
a/R
α_f
F_r
$\alpha_f + \frac{a}{R}$
C_F
Resultant
a/R
C_T
G
b/R
F_{xr}
b/R
α_r
F_{yr}
$\alpha_r - \frac{b}{R}$
$F_f = F_{yf}$
Old C_F
(no traction)

Figure 6.4.2. Plan view free-body diagram for rear drive.

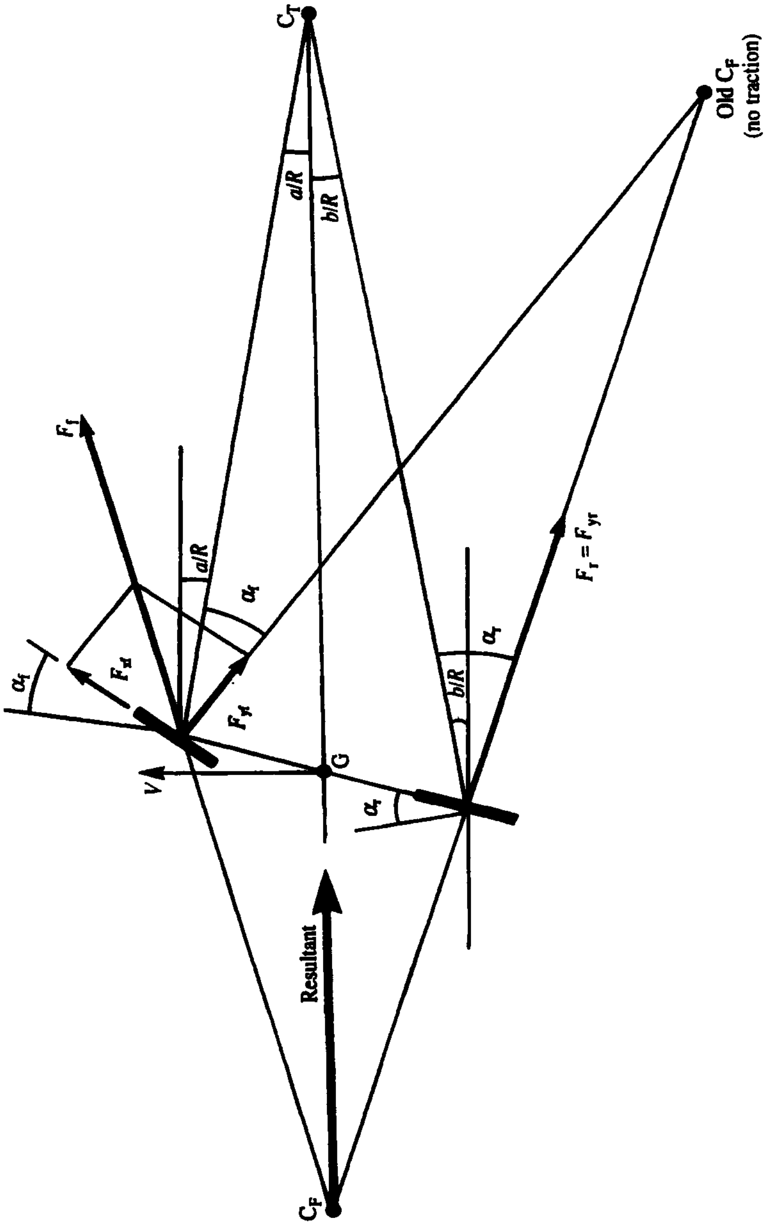
C_T
Old C_F
(no traction)
a/R
b/R
F_f
a/R
α_f
α_f
F_xf
F_yf
F_r = F_yr
α_r
b/R
G
V
α_r
Resultant
C_F

Figure 6.4.3. Plan view free-body diagram for front drive.

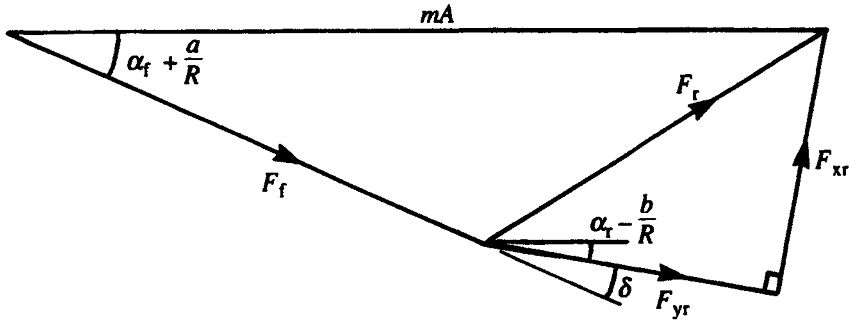
mA
$\alpha_f + \frac{a}{R}$
F_r
F_{xr}
F_f
$\alpha_r - \frac{b}{R}$
δ
F_{yr}

Figure 6.4.4. Force polygon for rear drive.

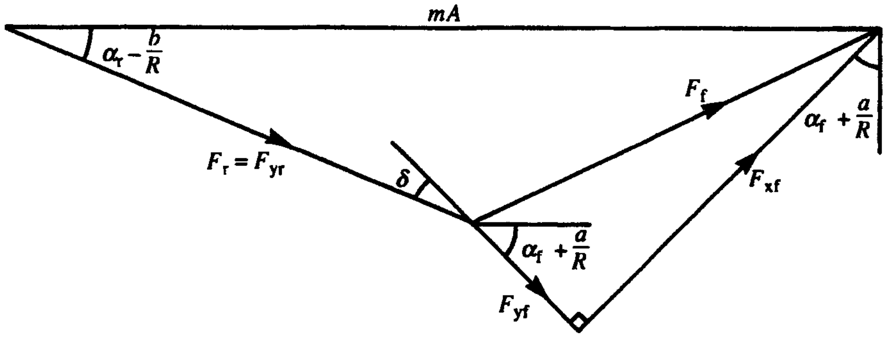
mA
$\alpha_r - \frac{b}{R}$
F_f
$\alpha_f + \frac{a}{R}$
$F_r = F_{yr}$
δ
F_{xf}
$\alpha_f + \frac{a}{R}$
F_{yf}

Figure 6.4.5. Force polygon for front drive.

6.5 Linear Theory

In the primary handling regime, up to about 3 m/s^2 for a typical car, the steer angle changes linearly with lateral acceleration at a given radius (Figure 6.5.1), and hence

$$\delta_U = k_U A$$

$$\delta = \delta_K + \delta_U$$

$$\delta = \frac{L}{R} + k_U A$$

where k_U is called the understeer gradient (or understeer coefficient). Physically, k_U is simply the gradient of the graph of δ against A (Figure 6.5.1). It is expressed in rad/m s^{-2} or deg/m s^{-2} in the S.I. system, although deg/g is convenient and often preferred. A typical value is 5 mrad/m s^{-2} or 3 deg/g. A value of 1.0 deg/g is 0.00178 rad/m s^{-2} or 1.78 mrad/m s^{-2}.

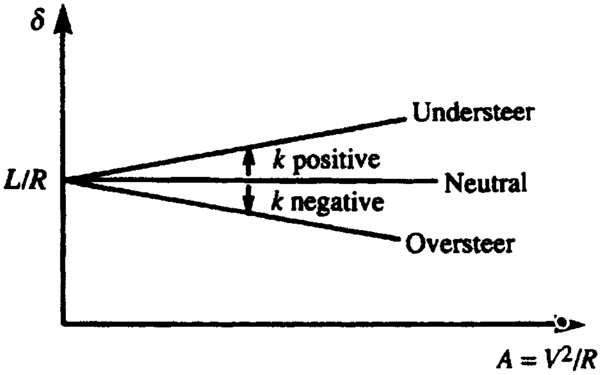

Figure 6.5.1. Simple linear vehicle handling with $\delta = (L/R) + k_U A$ (no suspension steer).

Formally we can define k_U by differentiating the above equations, giving

$$k_U \equiv \frac{d\delta_U}{dA} = \left(\frac{d\delta}{dA}\right)_R$$

where the subscript R means at constant radius. If R is not constant then the kinematic steer angle also changes with A:

$$\delta_K = \frac{L}{R} = \frac{LA}{V^2}$$

The kinematic steer angle gradient (or so-called Ackermann steer angle gradient, although not really connected with Ackermann) is

$$k_K \equiv \frac{d\delta_K}{dA} = \frac{L}{V^2}$$

At constant speed:

$$\delta = \delta_K + \delta_U$$

$$\frac{d\delta}{dA} \equiv \frac{d\delta_K}{dA} + \frac{d\delta_U}{dA}$$

$$= \frac{L}{V^2} + k_U$$

$$= k_K + k_U$$

Where the understeer gradient k_U is positive the total steer angle increases with lateral acceleration, i.e., with increase of speed for a constant-radius test, and the vehicle is described as understeering. For negative k_U the vehicle is described as oversteering. Zero k_U is neutral steer. For a real nonlinear case a vehicle may have different characteristics at different lateral accelerations.

Substituting $A = V^2/R$ into the above equation for δ,

$$\delta = \frac{L}{R} + k_U\left(\frac{V^2}{R}\right)$$

$$= \rho\left(L + k_U V^2\right)$$

where $\rho = 1/R$ is the path curvature. Thus the path curvature response gain for the linear case is

$$G_\rho \equiv \frac{d\rho}{d\delta} = \frac{\rho}{\delta} = \frac{1}{L + k_U V^2}$$

$$= \frac{1}{L}\left(\frac{1}{1 + (k_U/L)\,V^2}\right)$$

Thus, the response gain depends on the speed in a way controlled by k_U/L, i.e., the understeer gradient per unit of wheelbase. It is convenient to define a characteristic speed

$$V_{ch} = \sqrt{\frac{L}{k_U}}$$

so that

$$\frac{\rho}{\delta} = \frac{1}{L}\left(\frac{1}{1 + (V/V_{\mathrm{ch}})^2}\right)$$

If k_{U} is negative then V_{ch} would be imaginary. The $\sqrt{(-1)}$ is then discarded and the result is called the critical speed:

$$V_{\mathrm{cr}} = \sqrt{\frac{-L}{k_{\mathrm{U}}}}$$

In the following, k_{U} will be assumed positive, as is usual in practice; the results are easily adapted to negative k_{U} if required.

Sometimes the above is expressed in terms of the stability factor f_{S}:

$$f_{\mathrm{S}} = \frac{k_{\mathrm{U}}}{L}$$

$$V_{\mathrm{ch}} = \sqrt{\frac{1}{f_{\mathrm{S}}}}$$

$$V_{\mathrm{cr}} = \sqrt{\frac{1}{-f_{\mathrm{S}}}}$$

The velocity-dependent part of the curvature response is called the response factor:

$$f_{\mathrm{R}} = \frac{1}{1 + (k_{\mathrm{U}}/L)V^2} = \frac{1}{1 + (V/V_{\mathrm{ch}})^2}$$

Its reciprocal is called the understeer factor U (to be distinguished from the understeer gradient k_{U}):

$$U \equiv \frac{1}{f_{\mathrm{R}}} = 1 + \left(\frac{k_{\mathrm{U}}}{L}\right)V^2 = 1 + \left(\frac{V}{V_{\mathrm{ch}}}\right)^2$$

These are sometimes given other names. For example, f_R may be called the yaw rate factor, but this is misleading because really it is equally applicable to path curvature, yaw rate and lateral acceleration:

$$G_\rho \equiv \frac{d\rho}{d\delta} = \frac{\rho}{\delta} = \frac{f_R}{L}$$

$$G_r \equiv V\frac{d\rho}{d\delta} = \frac{\rho V}{\delta} = \frac{f_R V}{L} = VG_\rho$$

$$G_A \equiv V^2\frac{d\rho}{d\delta} = \frac{\rho V^2}{\delta} = \frac{f_R V^2}{L} = V^2 G_\rho$$

Furthermore, if we divide the response by the response of a neutral-steer vehicle, in every case the ratio is the response factor f_R. Physically, a large response factor means a large lateral response to a given steer input compared with a neutral vehicle for the prevailing conditions of the test.

Figure 6.5.2 shows how the response factor varies with V/V_c where V_c represents V_{ch} or V_{cr} as appropriate. For understeer the response factor diminishes with speed, being 0.5 at the characteristic speed. For oversteer, the response increases with speed, going to infinity at the critical speed. Thus as the vehicle approaches the critical speed the steering becomes increasingly sensitive and the directional stability diminishes. Beyond the critical speed, f_R is negative, meaning that for a given response the steering angle must be in the opposite direction to that normally expected. In addition, the vehicle is statically unstable, so with a fixed steering position the vehicle will not maintain a steady path, but will spin out. Such a vehicle can be driven, because the system can be stable when the driver response is included, i.e., open-loop instability but closed-loop stability, but naturally this is difficult and tiring for the driver, so the normal car is designed to have an understeer characteristic.

As a matter of interest, for the simple linear vehicle that we are considering, the understeer factor $U = 1/f_R$ plotted against $(V/V_c)^2$ is a simple straight line.

A typical value of k_U is 5 mrad/m s^{-2} (2.8 deg/g), which on a wheelbase of 3 m gives a characteristic speed of 25 m/s. The actual value of the understeer gradient depends on the tire cornering stiffnesses, the center-of-mass position, and

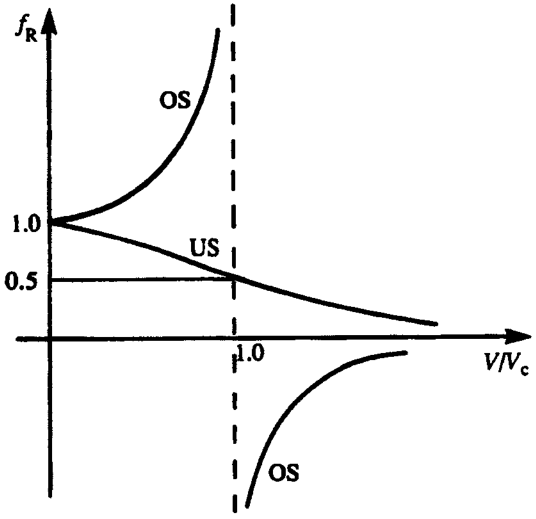

Figure 6.5.2. Linear vehicle response factor.

the suspension geometry and deflection characteristics. This is discussed in detail in Section 6.10. For the linear case the steer angle is

$$\delta = \frac{L}{R} + k_U A = \frac{L}{R} + (\alpha_f - \alpha_r)$$

The vehicle understeer gradient in this case (no suspension effects) is just equal to the tire understeer gradient:

$$k_U = k_{TU} = \frac{d}{dA}(\alpha_f - \alpha_r) = \frac{d\alpha_U}{dA}$$

which for the linear case is

$$k_U = \frac{(\alpha_f - \alpha_r)}{A} = \frac{\alpha_U}{A}$$

For front and rear end-masses m_f and m_r:

$$m_f = \frac{bm}{L}$$

$$m_r = \frac{am}{L}$$

The front and rear lateral forces are

$$m_f A = 2\alpha_f C_{\alpha f}$$

$$m_r A = 2\alpha_r C_{\alpha r}$$

Hence

$$\begin{aligned} k_U &= \frac{m_f}{2C_{\alpha f}} - \frac{m_r}{2C_{\alpha r}} \\ &= \frac{m}{2L}\left(\frac{b}{C_{\alpha f}} - \frac{a}{C_{\alpha r}}\right) \end{aligned}$$

So for the linear suspensionless vehicle, the understeer gradient can be simply related to the tire characteristics, the mass and the position of G on the wheelbase.

For real vehicles, beyond the linear handling regime the understeer gradient depends on the lateral acceleration, as discussed in Sections 6.11 and 6.12.

6.6 Vehicle Cornering Stiffnesses

For the complete simple model vehicle, the moment and side force are related to the vehicle yaw and steer, through coefficients that depend on the tire coefficients and the position of the center of mass on the wheelbase.

Figure 6.6.1 shows the minimal bicycle model vehicle with a steer angle giving a front slip angle (not in steady state). There are two wheels on the front axle, so the front-axle cornering stiffness is $2C_{\alpha f}$ where $C_{\alpha f}$ is the value for one front wheel. For small angles the resulting vehicle lateral force is

$$F_y = 2\alpha_f C_{\alpha f}$$

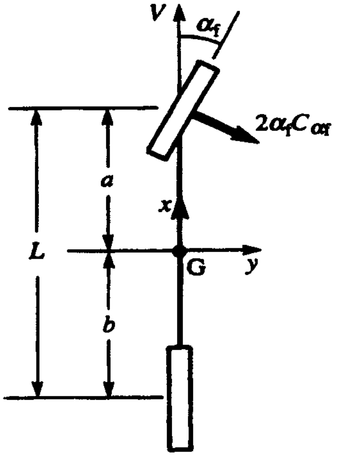

Figure 6.6.1. Bicycle model with steer angle, zero β and r.

As usual, the front axle is a distance a in front of the center of mass G, the rear axle is b behind G, and the wheelbase is

$$L = a + b$$

The moment about G of the front-wheel force, clockwise positive, is

$$M_z = 2a\alpha_f C_{\alpha f}$$

Figure 6.6.2 shows the vehicle with no steer angle and zero angular velocity, but at an angular yaw position β. Front and rear slip angles are equal to the yaw. In this case the total lateral force is

$$F_y = 2\beta C_{\alpha f} + 2\beta C_{\alpha r}$$

so there is a yaw side force stiffness

$$\frac{\mathrm{d}F}{\mathrm{d}\beta} = 2C_{\alpha f} + 2C_{\alpha r}$$

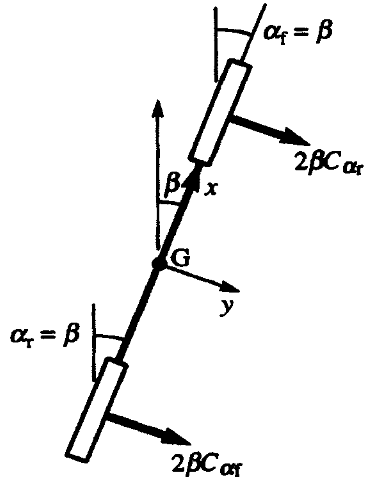

Figure 6.6.2. Bicycle model with yaw angle, zero angular velocity.

The moment about the center of mass, clockwise positive, is

$$M_z = 2a\beta C_{\alpha f} - 2b\beta C_{\alpha r}$$

Thus there is a yaw stiffness

$$\frac{dM}{d\beta} = 2aC_{\alpha f} - 2bC_{\alpha r}$$

Directional yaw static stability requires that this be a restoring moment, i.e., negative (counterclockwise) M for a clockwise β as shown. Thus $dM/d\beta$ must be negative. This requires

$$|bC_{\alpha r}| > |aC_{\alpha f}|$$

Physically, this simply means that for static stability the restoring moment from the rear axle must exceed the disturbing moment from the front axle. If we divide the moment by the total force we get the moment arm of the total force. The moment arm x_s as a distance behind G is $-M_z/F_y$:

$$x_s = -\frac{aC_{\alpha f} - bC_{\alpha r}}{C_{\alpha f} + C_{\alpha r}}$$

This is called the static margin, and is alternatively expressed as a fraction of the wheelbase, x_S/L. For static stability the static margin must be positive, i.e., the force must act behind G. The point at which the total tire force acts is called the neutral steer point, because a small force applied there will cause the vehicle to drift sideways with no change of yaw angle. Actually, because of roll effects there is strictly a neutral steer line in side view, angled back at typically 15° because a force applied high up gives effects such as roll steer, and therefore must generally be more rearward to give a neutral response. In nonlinear analysis the static margin and neutral steer point are defined in terms of increments of force, and the result depends on the trim state, i.e., the reference conditions, but in linear theory the static margin is a constant.

Figure 6.6.3 shows the vehicle with a yaw speed $\dot{\beta} \equiv r$. This gives the velocity diagrams shown, with front and rear slip angles ar/V and br/V (for small r). There is a net lateral force

$$F_y = -\left(\frac{2ar}{V}\right)C_{\alpha f} + \left(\frac{2br}{V}\right)C_{\alpha r}$$

$$= -\frac{2r}{V}(aC_{\alpha f} - bC_{\alpha r})$$

$$\frac{dF_y}{dr} = -\frac{2}{V}(aC_{\alpha f} - bC_{\alpha r})$$

There is a clockwise moment about G of

$$M_z = -\left(\frac{2a^2r}{V}\right)C_{\alpha f} - \left(\frac{2b^2r}{V}\right)C_{\alpha r}$$

$$= -\frac{2r}{V}\left(a^2C_{\alpha f} + b^2C_{\alpha r}\right)$$

$$\frac{dM}{dr} = -\frac{2}{V}\left(a^2C_{\alpha f} + b^2C_{\alpha r}\right)$$

This moment opposes the yawing velocity and therefore has a damping effect on yawing oscillations, and is known as the yaw damping coefficient. It is inversely proportional to speed, but is always opposed to the yaw velocity, i.e., it is always a positive damping.

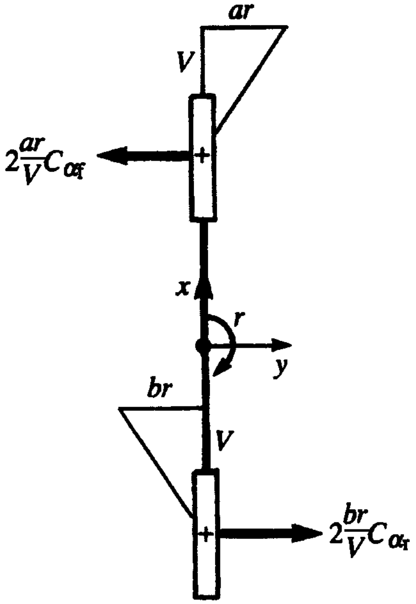

Figure 6.6.3. Bicycle model with yaw speed.

In the above expressions, the vehicle characteristics are expressed in terms of the dimensions a and b and the tire characteristics $C_{\alpha f}$ and $C_{\alpha r}$. The expressions involve the zeroth, first and second moments of the tire coefficients about the center of mass, giving three vehicle cornering stiffnesses:

$$\begin{aligned}C_0 &= 2C_{\alpha f} + 2C_{\alpha r}\\ C_1 &= 2aC_{\alpha f} - 2bC_{\alpha r}\\ C_2 &= 2a^2C_{\alpha f} + 2b^2C_{\alpha r}\end{aligned}$$

Representative values for a medium car would be about 140 kN/rad, –14 kNm/rad and 200 kNm^2/rad, respectively.

These can be expressed in a more general way. For n_A axles, with n_{Wr} wheels and an axle r, at distance x_r in front of the center of mass,

$$C_0 = \sum_{r=1}^{n_A} n_{Wr} C_{\alpha r}$$

$$C_1 = \sum_{r=1}^{n_A} n_{Wr} x_r C_{\alpha r}$$

$$C_2 = \sum_{r=1}^{n_A} n_{Wr} x_r^2 C_{\alpha r}$$

These complete vehicle cornering stiffnesses are sometimes useful to simplify equations, and occur quite frequently in dynamic analysis. For example, the static margin is

$$\begin{aligned} x_s &= -\frac{4LC_{\alpha f}C_{\alpha r}k_U}{mC_0} \\ &= -\frac{C_1}{C_0} \end{aligned}$$

and the yaw damping coefficient is

$$-\frac{dM}{dr} = \frac{C_2}{V}$$

The understeer gradient becomes

$$k_U = \frac{mC_1}{4LC_{\alpha f}C_{\alpha r}}$$

Although developed here in terms of a linear vehicle, the coefficients are easily extended to a nonlinear vehicle, by considering small, and hence linear, deflections from a trim state.

A serious practical limitation in the use of these coefficients is that although they illuminate understanding of the simple vehicle considered, their neglect of the suspension is not generally acceptable. This can be incorporated by using the cornering compliance concept (Section 6.10).

In stability derivative notation, the side force is represented by Y and the moment by N. Derivatives are indicated by a subscript, e.g.:

$$Y_\beta \equiv \frac{\mathrm{d}Y}{\mathrm{d}\beta}$$

In terms of the vehicle coefficients:

$$\begin{aligned} Y_\beta &= C_0 \\ Y_r &= -C_1/V \\ N_\beta &= C_1 \\ N_r &= -C_2/V \end{aligned}$$

Other vehicle cornering stiffnesses that sometimes occur are:

$$\begin{aligned} C_3 &= ml \\ C_4 &= mC_2 + IC_0 \\ C_5 &= mC_2 - IC_0 \\ C_6 &= C_0C_2 - C_1^2 \approx C_0C_2 \approx mC_1V_{\mathrm{ch}}^2 \\ C_7 &= \frac{mC_2 - IC_0}{2mC_1} = \frac{C_5}{2mC_1} \end{aligned}$$

6.7 Nonlinear Trim State

The preceding theory showed that the linear regime of handling can be represented by simple equations. This is not true of the more general nonlinear regime. The trim state, i.e., an output such as path curvature in terms of an input such as steer angle, is not really amenable to an analytical approach, and for detailed representations computer simulations are invariably used. However, small perturbations about a given trim state, for the study of stability of a given cornering condition, can still be treated as linear. Also, the graphical representation of the relationships between control and response, i.e., of the open-loop transfer function, provides an excellent basis for physical understanding of the trim state and is hardly any more difficult than for the linear case.

There are essentially two controls, the lateral (steering wheel) and the longitudinal (accelerator / brake), and for this reason any output variable will generally be a function of these two input variables, and will be represented by a surface on a three-dimensional graph. For example, vehicle yaw angle as output might be represented as a function of steer angle and accelerator position. However, as described earlier, the forward speed is generally preferred to accelerator position as one control variable, as one might prefer path radius or path curvature over steering wheel position. The steering control may be represented by the mean steer angle of the front road wheels δ, the steering wheel angle δ_S, the reference steer angle δ_S/G, the steering wheel torque T_S, or even the tangential steering force at the wheel rim F_S. Possible steady-state output parameters include anything that varies with trim state, such as path curvature, yaw speed, lateral acceleration, roll angle, attitude (yaw) angle, even pitch angle, and so on. As a result of this large number of variables there are many possible interrelationships that could be examined, and many different ways of representing a given result: for example, at a given speed the path curvature, the yaw speed and the lateral acceleration all contain the same information. However, the principal features are the basic lateral motion parameters, namely attitude angle, roll angle, path curvature, speed and steer angle; and the most basic representation is with attitude angle, roll angle and path curvature each as a function of the speed and steer angle.

In practice a different representation is usually adopted, for good reasons. It is more convenient to think of lateral acceleration as a specified variable, and to have a graph showing the required steer angle and the consequent attitude angle and roll angle, as in Figure 1.13.1. Another advantage of this representation is that although the driver seeks to control the path radius directly through the steer angle, he does not seek to control, say, the roll angle directly, i.e., in this sense the roll angle is incidental. However, the relationship between roll angle and lateral acceleration is of importance because it may affect the required steer angle through roll steer, and may be used by the driver as feedback. Speed is retained as the second control variable, and this is satisfactory because in general the effect of speed is secondary in the mid-speed range. However, if it is low then for a given acceleration there may be geometric small-radius effects, and if it is high then aerodynamic and tire speed effects come into play.

For these reasons then, the usual representation of the complete nonlinear characteristics of a vehicle is a series of three-dimensional graphs, one for each variable, e.g., steer angle, shown as a function of lateral acceleration and speed. Of course each of these can be shown as a conventional graph against lateral acceleration for a series of specific speed values, or in the most simplified case for a representative single speed. In the usual constant-radius test, the speed varies with lateral acceleration, but for the usual radius (30 to 40 m) the speed effects are small, so this is not a problem.

Figure 6.7.1 shows a possible surface for understeer angle against V and A. We can note that in the V–A plane there is a minimum V for a given A corresponding to a minimum turning radius. There is also a maximum steady-state A for any given V, reducing with V, e.g., because of aerodynamic lift and because of speed sensitivity of tire friction, and at high speed because of engine power limits. For any particular V there is a curve of δ_U against A, slightly different for each V, the range of V resulting in a complete surface for the understeer angle. For any particular vehicle, similar surfaces exist for the other outputs, e.g., attitude angle. It is only when the speed effect is small that this relatively complex representation can acceptably be reduced to a single curve of δ_U against A.

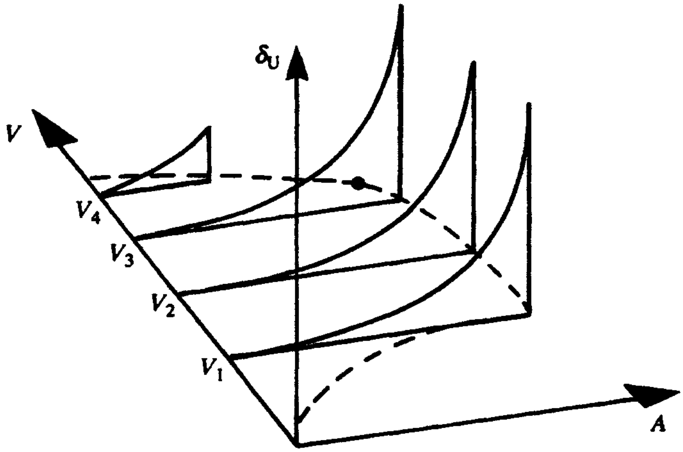

Figure 6.7.1. Understeer angle versus V and A.

6.8 Nonlinear Theory

For small perturbations from a trim state, a vehicle will behave in a linear manner, although with characteristic coefficients quite different from the straight-line case. Hence the linear theory developed in earlier sections is valid in principle, provided that the perturbations are now considered from the particular steady-state condition rather than from the straight-running condition.

The definitions of the various control gains still stand:

$$G_\rho \equiv \frac{d\rho}{d\delta}$$

$$G_r \equiv \frac{dr}{d\delta} = V\frac{d\rho}{d\delta}$$

$$G_A \equiv \frac{dA}{d\delta} = V^2\frac{d\rho}{d\delta}$$

although it is no longer allowable to substitute the linear relationship $d\rho/d\delta = \rho/\delta$. In linear theory we found

$$\delta = \frac{L}{R} + k_U A \quad \text{(linear)}$$

where $k_U = d\delta_U/dA$ is the understeer gradient; in linear theory this is a constant. For the nonlinear case, the concept of the understeer gradient is retained, but it now has a value dependent on the lateral acceleration. The notion of understeer is considered in more detail in the next section.

For the point-specific understeer gradient it is still allowable to calculate a characteristic or critical speed

$$V_{ch} = \sqrt{\frac{L}{k_U}}$$

We can also calculate a response factor

$$f_R = \frac{1}{1 + (k_U/L)V^2}$$

and the various gains

$$G_\rho \equiv \frac{d\rho}{d\delta} = \frac{f_R}{L}$$

$$G_r \equiv V\frac{d\rho}{d\delta} = \frac{f_R V}{L} = VG_\rho$$

$$G_A \equiv V^2\frac{d\rho}{d\delta} = \frac{f_R V^2}{L} = V^2 G_\rho$$

as for the linear case.

The simple expression deduced for a suspensionless vehicle in Section 6.5 for k_U in terms of the tire stiffness and center-of-mass position,

$$k_U = \frac{m}{2L}\left(\frac{b}{C_{\alpha f}} - \frac{a}{C_{\alpha r}}\right)$$

is still appropriate, although now the tire stiffness values must be the ones at the active slip angles, not at zero slip as for the straight-running case. In real cases, however, the suspension is not negligible; its effect on k_U is considered in Section 6.10.

The vehicle cornering stiffnesses C_0, C_1 and C_2 deduced in Section 6.6 remain useful provided that the tire stiffnesses used are the ones effective at the active slip angles. Again, the suspension effects may be incorporated through the cornering compliance concept.

As an alternative to the understeer gradient, the static stability may still be represented by the static margin

$$x_s = -\frac{C_1}{C_0}$$

and the yaw damping coefficient is

$$-\frac{dM}{dr} = \frac{C_2}{V}$$

For a full representation these would be presented as surface plots against V and A. For the typical vehicle with a completely understeer characteristic, the front-axle side force limit is less than the rear, e.g., as in Figure 6.3.2(a); thus the front stiffness coefficient diminishes more rapidly than the rear, and the static margin increases, tending to infinity when the front-axle side force is at a maximum. On the other hand, because the tire stiffnesses reduce at increasing slip, the yaw damping reduces with increased lateral acceleration.

6.9 Understeer and Oversteer

Understeer and oversteer are widely used and often abused terms; their definition will be considered in more detail here.

Two tongue-in-cheek qualitative definitions are perhaps worth mentioning. First: "Understeer is crashing nose first, oversteer is crashing tail first." This is correct in the sense that if the ultimate grip is less at the front then a crash is liable to occur on full lock with the feeling of going straight on, whereas if the ultimate grip is less at the rear then the vehicle will spin. The second definition is "Understeer is when the driver is frightened, oversteer is when the passenger is frightened." This one is more obscure in interpretation. It does reflect the reality that an enthusiastic driver is not necessarily afraid of terminal oversteer, feeling that in such circumstances he can do something about it, i.e., apply opposite lock, whereas in terminal understeer the driver may tend to feel more helpless. This may be true in controlled testing; however, in real crisis situations for a given maximum lateral acceleration it is nearly always preferable for the limit to be understeering so that steering control remains progressive rather than reversing into oversteer.

These popular definitions are in terms of limit behavior, and so are really concerned with the terms called in this book limit understeer and limit oversteer. However, the normal technical definition of understeer and oversteer is not concerned with the limit state. Hence, limit understeer must be firmly distinguished from normal understeer.

As already explained, the basic quantitative definition of understeer is applicable to the low lateral acceleration regime, and comes from the gradient of the steer angle versus lateral acceleration graph, giving the understeer gradient

$$k_{\mathrm{U}} = \frac{\mathrm{d}\delta_{\mathrm{U}}}{\mathrm{d}A} = \left(\frac{\mathrm{d}\delta}{\mathrm{d}A}\right)_{\mathrm{R}}$$

According to the SAE definition, wherever k_{U} is positive, the vehicle is described as understeer; if k_{U} is negative the vehicle is described as oversteering. If k_{U} is zero, the vehicle is neutral steer.

In Figure 6.9.1(a), we see that it is possible for there to be a negative understeer gradient at the same time as a positive understeer angle, or vice versa. It is the gradient that is considered to be decisive, rather than the angle. This is a further distinction between the technical and populist definition of the terms. For $k_{\mathrm{U}} = 0$, the vehicle is said to be neutral. Figure 6.9.1(a) illustrates these conditions for tests at constant radius.

Because speed is normally considered as one of the control variables, it may be better to plot the results instead at constant speed, Figure 6.9.1(b). However, at constant speed the radius changes with lateral acceleration ($A = V^2/R$), so the kinematic steer angle changes too:

$$\delta_K = \frac{L}{R} = \frac{LA}{V^2}$$

$$\frac{d\delta_K}{dA} = \frac{L}{V^2}$$

Hence, for constant speed the kinematic steer angle increases at a rate L/V^2, which is known as the kinematic (SAE Ackermann) steer angle gradient. For neutral steer, i.e., zero rate of understeer angle change, the total steer angle must also change at this rate; for understeer it will increase more quickly, and for oversteer more slowly. This is illustrated in Figure 6.9.1(b). Note that in this case, in contrast to the constant-radius case of Figure 6.9.1(a), the total steer angle starts at zero, because zero acceleration at a given speed corresponds to infinite radius. For a wheelbase of 3.0 m and speed 20 m/s, the kinematic steer-angle gradient is 7.5 mrad/m s^{-2}, 0.43 deg/m s^{-2} or 4.2 deg/g. In Figures 6.9.1(a) and (b), if we were to plot not the total steer angle but only the understeer angle, then in both cases neutral steer occurs at the horizontal point of the graph, and understeer is any point of positive gradient.

So far it has been assumed that the steer angle referred to is the mean steer angle of the front wheels. However, it is also possible to use the actual steering wheel angle δ_S, or the reference steer angle δ_{ref}, as is done in the SAE definitions. Because of steering compliance, there is usually greater understeer for δ_{ref} than for the front wheel angle. It is not fruitful to debate which of these three is the correct understeer value, they are simply parameters of different significance. Steering compliance is sometimes deliberately used to increase the driver's perceived understeer, especially for rear-engined vehicles, when G tends to be more rearward than is desirable. In some cases the steering compliance seems to improve straight-line stability, in others, possibly those with more compliance, it seems to lead to instability and wandering. The situation is clouded by the fact that rear-heavy cars often have considerable roll understeer, which usually has a significant adverse effect on straight-line stability.

Considering the steer angle as a function of both lateral acceleration and speed, it is apparent that instead of keeping the speed constant and looking at understeer with respect to acceleration, we could instead keep the acceleration constant and consider understeer with respect to speed. In this case, if increased speed requires greater dynamic steer angle, this would be understeer with respect to speed. This sort of understeer has been considered in the research literature but has not found engineering application.

(a) Constant radius

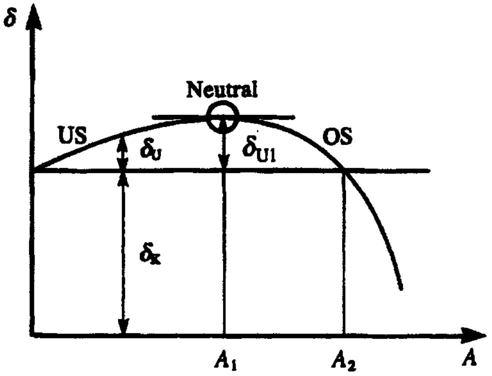

(b) Constant speed

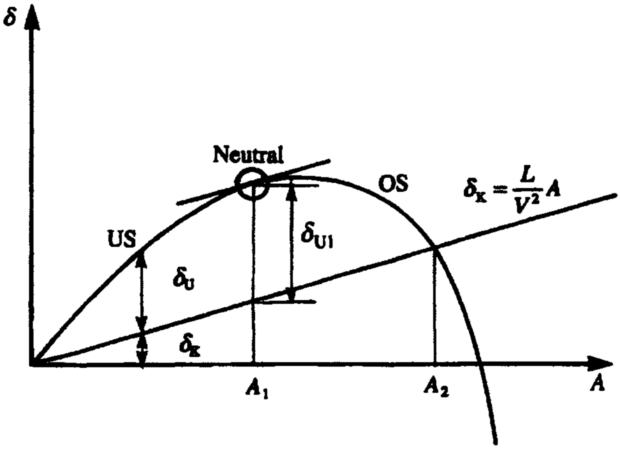

Figure 6.9.1. Steer angle versus lateral acceleration.

6.10 Primary Handling

The primary handling regime is the first stage – that represented adequately by linear relationships. Representation of the vehicle steady-state behavior in this regime essentially reduces to three numbers – the roll gradient, the attitude gradient and the understeer gradient, measuring the constant of proportionality as each of roll angle, attitude angle and understeer angle varies with lateral acceleration:

$$k_\phi = \frac{\mathrm{d}\phi}{\mathrm{d}A}$$

$$k_\beta = \frac{\mathrm{d}\beta}{\mathrm{d}A}$$

$$k_\mathrm{U} = \frac{\mathrm{d}\delta_\mathrm{U}}{\mathrm{d}A}$$

Therefore, for the linear case,

$$\phi = k_\phi A$$

$$\beta = \beta_\mathrm{K} + k_\beta A$$

$$\delta = \delta_\mathrm{K} + k_\mathrm{U} A$$

where it is assumed that the roll angle is zero for zero lateral acceleration. Parameter β_K is the kinematic attitude angle:

$$\beta_\mathrm{K} = -b/R$$

Evaluation of the roll gradient k_ϕ follows from the methods of Chapter 5. Its value depends basically on the height of the sprung center of mass, the roll center heights (the anti-roll) and the total roll stiffness, with a further contribution from axle roll. This section considers how the attitude gradient k_β and the understeer gradient k_U derive from the vehicle and tire design features. The attitude gradient is mainly dependent on the rear-tire cornering stiffness coefficient, although other factors play a part. The understeer gradient depends on many factors including the position of the center of mass, front–rear difference of tire cornering stiffness, roll steer, roll camber, compliance steer, aligning torque compliance steer, and the effect of aligning torque on the vehicle as a rigid body, with further minor effects from such factors as load transfer combined with rolling resistance, static toe and camber, and from axle roll camber. If the differential is not a simple open type, there can be power steer effects because of lateral differences in tractive force acting on the rigid-body vehicle, and from compliance power steer, whether front or rear. If the steering wheel angle or the reference steer angle is being considered, then the steering compliance is also of significance. Aerodynamics may play a part, but this is considered separately in Sections 6.14 and 6.15.

An extremely simple vehicle without suspension was analyzed in Sections 6.4 and 6.5, for which the following simple results were found:

$$\begin{aligned}\delta &= \frac{L}{R} + k_{\mathrm{U}} A \\ &= \frac{L}{R} + (\alpha_{\mathrm{f}} - \alpha_{\mathrm{r}})\end{aligned}$$

$$k_{\mathrm{U}} = \frac{m}{2L}\left(\frac{b}{C_{\alpha\mathrm{f}}} - \frac{a}{C_{\alpha\mathrm{r}}}\right)$$

A more complex vehicle will now be considered, but remaining in the linear range. Figure 6.10.1 illustrates a "bicycle model" vehicle with simple suspension, incorporating suspension understeer effects of δ_{SUf} and δ_{SUr}. With these suspension effects,

$$\delta = \delta_{\mathrm{K}} + \alpha_{\mathrm{U}} + \delta_{\mathrm{SU}}$$

$$\delta = \frac{L}{R} + (\alpha_{\mathrm{f}} - \alpha_{\mathrm{r}}) + (\delta_{\mathrm{SUf}} + \delta_{\mathrm{SUr}})$$

Positive δ_{SUf} and δ_{SUr} are defined to call for an increased δ, i.e., an understeer effect. Hence δ_{SUr} is positive when the rear wheel attempts to increase its cornering force, and δ_{SUf} is positive when the front wheel tries to decrease its cornering force.

The corresponding steer angle gradient is

$$k_{\delta} = k_{\mathrm{K}} + k_{\mathrm{SU}} + k_{\mathrm{TU}}$$

where the suspension understeer gradient k_{SU} is the sum of geometric steer and compliance steer parts:

$$k_{\mathrm{SU}} = k_{\mathrm{SG}} + k_{\mathrm{SC}}$$

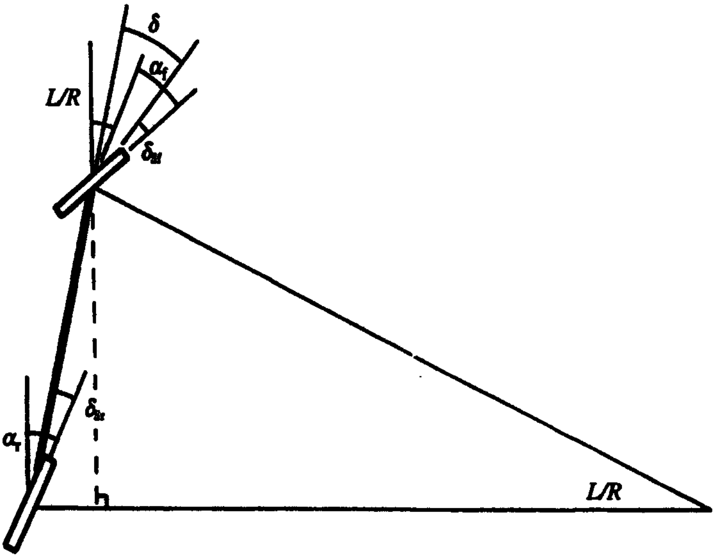

Figure 6.10.1. Bicycle model with suspension steer effects.

and k_{TU} is the tire understeer gradient

$$k_{\mathrm{TU}} = \frac{\mathrm{d}\alpha_{\mathrm{U}}}{\mathrm{d}A}$$

The total steer gradient effect of roll steer and roll camber is the suspension geometric steer gradient

$$k_{\mathrm{SG}} = \varepsilon_{\mathrm{RS}} k_{\phi} + \frac{C_{\gamma}}{C_{\alpha}} \varepsilon_{\mathrm{RC}} k_{\phi}$$

Compliance steer and compliance camber effects accumulate in a similar but more complex way because there are more terms.

Table 6.10.1 lists representative values of the understeer effects for the principal factors for a free-differential vehicle. The sum of the column for each individual axle is called the cornering compliance. Note that understeer tendency effects are positive and increase the cornering compliance for the front, but in tables of this type are given a negative sign for the rear. The tire cornering compliance is the angle for which the side force would give g (9.81 m/s^2) lateral acceleration, i.e., equal to the ground vertical force, if the tire remained linear, i.e., with constant cornering stiffness. It is the reciprocal of the cornering stiffness coefficient expressed in g/deg.

Table 6.10.1. Example primary steer effects (deg/g)

Factor	Front	Rear	F–R
Basic tire compliance	6.0	6.0	0.0
G position	0.6	−0.6	1.2
ΔC_α	−0.3	0.3	−0.6
Roll steer	0.5	−0.5	1.0
Roll camber effect on steer	0.2	0.5	−0.3
Lateral force compliance	0.2	0.2	0.0
Aligning torque compliance	1.1	0.1	1.0
Aligning torque on rigid body	0.1	−0.1	0.2
Cornering compliance	8.4	5.9	
Understeer gradient			2.5

For each row, subtracting the rear value from the front one gives the understeer contribution for that feature (column 4). Summing these contributions, or subtracting the total rear compliance from the front one, gives the understeer gradient for this model vehicle. For constant radius conditions, the attitude gradient k_β is equal to the rear cornering compliance. (For smaller radii, the difference of attitude angles at the rear axle and at G, specifically $\delta_{Kr} = b/R$, is not small, but it is constant.) Thus a table of this kind provides the necessary information to define the parameters of the primary handling regime.

The factors contributing to k_β and k_U will now be considered in more detail. First consider the simplest possible bicycle model with equal tire cornering stiffnesses C_α at each end, i.e., $2C_\alpha$ for an axle, and with G at the wheelbase mid-point, i.e., $a = b$. Then

$$\alpha_f = \alpha_r = \frac{mA}{4C_\alpha}$$

giving

$$k_\beta = \frac{m}{4C_\alpha}$$

$$k_U = 0$$

With $m = 1200$ kg and $C_\alpha = 500$ N/deg, then k_β is 0.6 deg/m s^{-2} or 6 deg/g.

Now consider G to be forward of the mid-point, but with no change to C_α. Considering plan-view moments about the center of the rear wheel:

$$LC_\alpha \alpha_f = bmA$$

$$\alpha_f = \frac{bmA}{LC_\alpha}$$

$$\alpha_r = \frac{amA}{LC_\alpha}$$

giving

$$k_\beta = \frac{am}{LC_\alpha}$$

$$k_U = \frac{d}{dA}(\alpha_f - \alpha_r) = \frac{m(b-a)}{2LC_\alpha}$$

With $a/L = 0.45$, then $k_\beta = 5.4$ deg/g and $k_U = 1.2$ deg/g. Thus the forward G has reduced k_β and increased k_U (Table 6.10.1). This sensitivity to G position is particularly noticeable in practice when a car is loaded at the rear, giving an oversteer increment change. Surprisingly, in practice the opposite sometimes occurs.

In practice a forward G changes the tire vertical reactions, and also usually demands unequal tire pressures; these factors change C_α. This depends on the particular tires and loads; it may result in virtually no change, or there may be a change almost proportional to the normal force. For $a/L = 0.45$ this may as an example lead to $C_{\alpha f} = 525$ N/deg and $C_{\alpha r} = 475$ N/deg. Considering now a model with differing $C_{\alpha f}$ and $C_{\alpha r}$, plan-view moments about the rear wheel give

$$2LC_{\alpha f}\alpha_f = bmA$$

$$\alpha_f = \frac{bmA}{2LC_{\alpha f}}$$

$$\alpha_r = \frac{amA}{2LC_{\alpha r}}$$

This gives

$$k_\beta = \frac{am}{2LC_{\alpha r}}$$

$$k_U = \frac{m}{2L}\left(\frac{b}{C_{\alpha f}} - \frac{a}{C_{\alpha r}}\right)$$

This result was also derived in Section 6.5. With the values mentioned, $k_\beta = 5.7$ deg/g and $k_U = 0.60$ deg/g. Thus the changes to C_α compensate to some extent for the forward G position, in proportion to the C_α sensitivity to F_V.

The effect of roll understeer depends on the roll gradient k_ϕ and the front and rear roll understeer coefficients ε_{RUf} and ε_{RUr}. The actual understeer angle increments are

$$\delta_{RUf} = \varepsilon_{RUf}\, k_\phi A$$
$$\delta_{RUr} = \varepsilon_{RUr}\, k_\phi A$$

Hence the contributions to the attitude gradient and understeer gradient are

$$\Delta k_\beta = -\varepsilon_{RUr}\, k_\phi$$

$$\Delta k_U = \left(\varepsilon_{RUf} + \varepsilon_{RUr}\right) k_\phi$$

where the roll understeer coefficients ε_{RUf} and ε_{RUr} are defined as positive for an understeer contribution at the front or rear. Note that positive rear roll understeer reduces the need for body attitude angle, in which case Δk_β is negative. A typical roll understeer coefficient is 0.1 with k_ϕ up to 10 deg/g so the roll steer may reduce k_β by say 1 deg/g, and this is often done deliberately.

especially on large cars. Rear roll understeer is sometimes combined with front roll oversteer. However, significant amounts of roll steer may create unpleasant handling and so are generally avoided, especially as an oversteer effect.

Suspension roll also causes wheel camber relative to the road. The effect depends upon the roll gradient k_ϕ and the roll camber coefficients $\varepsilon_{\mathrm{RCf}}$ and $\varepsilon_{\mathrm{RCr}}$,

$$\Delta\gamma_{\mathrm{f}} = \varepsilon_{\mathrm{RCf}}\, k_\phi A$$
$$\Delta\gamma_{\mathrm{r}} = \varepsilon_{\mathrm{RCr}}\, k_\phi A$$

These camber changes give forces depending on the tire camber stiffnesses C_γ and consequently there must be changes of slip angles and steer angles to preserve the correct forces. This gives

$$\Delta k_\beta = \left(\frac{\varepsilon_{\mathrm{RCr}} C_{\gamma\mathrm{r}}}{C_{\alpha\mathrm{r}}}\right) k_\phi$$

A positive roll camber coefficient at the rear requires a compensating increase of rear slip angle with an increase of k_β.

$$\Delta k_{\mathrm{U}} = \left(\frac{\varepsilon_{\mathrm{RCf}} C_{\gamma\mathrm{f}}}{C_{\alpha\mathrm{f}}} - \frac{\varepsilon_{\mathrm{RCr}} C_{\gamma\mathrm{r}}}{C_{\alpha\mathrm{r}}}\right) k_\phi$$

where C_γ/C_α is about 0.05 for radial-ply and 0.15 for bias-ply. Positive $\varepsilon_{\mathrm{RC}}$ at the front is an understeer tendency, while at the rear it is on oversteer tendency. In the early days of independent suspension, the front roll camber coefficient was 1.0 and for the rear axle it was zero, and because bias tires were used the camber stiffnesses were large. In this case Δk_{U} from roll camber was typically over 1.0 deg/*g*. However, nowadays front independent suspensions have smaller roll camber coefficients, and radial tires have smaller camber stiffnesses, so with a solid rear axle Δk_{U} is typically 0.2 deg/*g*. With some independent rear suspensions, such as the common trailing-arm type, the roll camber coefficient is 1.0 and there may be a significant k_β effect. If front and rear suspensions are of the same type, this tends to compensate Δk_{U} and make it very small. With a small front roll camber and a large rear one, as on some small front-drive vehicles, the net effect on k_{U} may be –0.3 deg/*g*.

It is difficult to give a useful analytical account of lateral force compliance steer because this depends on small details such as the stiffness of rubber bushes.

Sometimes a compliance steer gradient k_{CS} (deg/m s^{-2}) is used, giving angular deflections

$$\delta_{\mathrm{CSf}} = k_{\mathrm{CSf}}A$$
$$\delta_{\mathrm{CSr}} = k_{\mathrm{CSr}}A$$

Note that the compliance steer gradient k_{CS}, relating the angle to the lateral acceleration, must be distinguished from the compliance steer coefficients η_{CS} relating the angle change to a force or moment on the wheel. The latter causes the former. Compliance camber gradient k_{CC} is often neglected. At the front, because of steering compliance, lateral force compliance steer and aligning torque compliance steer are usually significant, and because of relative stiffness at the rear the effect on k_β is small, but on k_{U} it is substantial, e.g., 2 deg/g. Nowadays compliance steer effects are closely controlled because of their effect on dynamic handling.

The effect of steering-column compliance, i.e., considering the reference steer angle $\delta_{\mathrm{ref}} = \delta_{\mathrm{s}}/G$, can be illustrated by considering the kingpin axes to be rigidly mounted. The self-aligning torque is the front side force times the pneumatic trail, $m_{\mathrm{f}}At$. For an overall steering gear ratio of G_{s} and neglecting friction, the steering-column torque is $m_{\mathrm{f}}At/G_{\mathrm{s}}$; for a column torsional stiffness of k_{sc} the steering column angular deflection is

$$\theta_{\mathrm{sc}} = \frac{m_{\mathrm{f}}At}{G_{\mathrm{s}}k_{\mathrm{sc}}}$$

and the associated front-wheel angular deflection is

$$\delta_{\mathrm{sc}} = \frac{m_{\mathrm{f}}At}{G_{\mathrm{s}}^2 k_{\mathrm{sc}}}$$

Hence

$$\Delta k_{\mathrm{U}} = \frac{m_{\mathrm{f}}t}{G_{\mathrm{s}}^2 k_{\mathrm{sc}}}$$

With $G_{\mathrm{s}} = 16$, $t = 30$ mm and $k_{\mathrm{sc}} = 0.8$ Nm/deg, the result for Δk_{U} is 1.0 deg/g. Actually the effect will be somewhat greater because of the kingpin axis compliance.

The tire lateral force acts much closer to the kingpin axis than to the line of action of the tie-rod, so its effect on steer angles cannot be easily calculated. For a tie-rod positioned rearward of the kingpin axes, the wheel angular deflection depends on the difference between deflections at these two supports. If the tie-rod is in front of the kingpin axes then the deflections both contribute to an angular change.

The aligning torque has some effect on the vehicle considered as a rigid body, i.e., separate from the compliance effects; this is because it effectively moves the tire side force backwards, increasing the static margin. For a mean pneumatic trail t the total plan-view moment is mAt. This requires counteracting side forces at the axles. By moments

$$F = \frac{mAt}{L}$$

so

$$\Delta\alpha_{\mathrm{r}} = -\frac{mAt}{2LC_{\alpha\mathrm{r}}}$$

$$\Delta\alpha_{\mathrm{f}} = +\frac{mAt}{2LC_{\alpha\mathrm{f}}}$$

Hence

$$\Delta k_{\beta} = -\frac{mt}{2LC_{\alpha\mathrm{r}}}$$

$$\Delta k_{\mathrm{U}} = \frac{mt}{2L}\left(\frac{1}{C_{\alpha\mathrm{f}}} + \frac{1}{C_{\alpha\mathrm{r}}}\right)$$

Using the earlier values, and a trail of 30 mm, gives 0.13 deg/g for $\Delta\beta$ and 0.24 deg/g for Δk_{U}.

Considering a four-wheel model instead of the bicycle model, cornering load transfer increases the outer side rolling resistance and reduces the inner one. We consider here only the rolling resistance, not the tire cornering drag which gives a second-order effect (Section 6.11). The load transfer is $F_{\mathrm{T}} = maH/T$, and with rolling resistance μ_{R} this gives a plan view moment about G of

$$M = T\mu_{\mathrm{R}}F_{\mathrm{T}} = \mu_{\mathrm{R}}maH$$

The required rear side force is reduced by F and the front increased by F where

$$F = \frac{\mu_R mAH}{L}$$

Hence

$$\Delta\alpha_f = \frac{\mu_R mAH}{2LC_{\alpha f}}$$

$$\Delta\alpha_r = -\frac{\mu_R mAH}{2LC_{\alpha r}}$$

$$\Delta k_\beta = -\frac{\mu_R mAH}{2LC_{\alpha r}}$$

$$\Delta k_U = \frac{\mu_R mAH}{2L}\left(\frac{1}{C_{\alpha f}} + \frac{1}{C_{\alpha r}}\right)$$

Using $\mu_R = 0.015$ and $h = 0.6$ m, then Δk_β is 0.04 deg/g and Δk_U is 0.07 deg/g, so this is a small effect on passenger cars. However, it may be significant for vehicles with high G and large rolling resistance, such as some military vehicles.

Load transfer will interact with the initial running toe and camber angles to give attitude coefficient and understeer coefficient increments. Denoting the straight running rear toe angle as δ_{Tr}, physically a complete load transfer would be equivalent to δ_{Tr} change of attitude. Denoting the front and rear distribution fractions of load transfer moment as d_f and d_r (i.e., $d_f + d_r = 1$), then

$$\Delta\beta = \delta_{Tr}\left(\frac{mAH}{T}\right)\left(\frac{L}{mgb}\right)d_r$$

$$\Delta k_\beta = -\frac{HLd_r\delta_{Tr}}{Tag}$$

where positive rear toe-in gives reduced attitude angle.

$$\Delta k_U = \frac{HL}{Tg}\left(-\frac{d_r\delta_{Tf}}{b} + \frac{d_r\delta_{Tr}}{a}\right)$$

where front toe-in and rear toe-out give an oversteer effect. For example, with $d_f = 0.8$, $\delta_{Tf} = 1°$ and $\delta_{Tr} = 0$, then Δk_U is -0.6 deg/g, so this is potentially a significant effect. The above analysis refers to the toe angle obtained in running conditions rather than just the static angle. The sensitivity to changes of toe angle remains valid, however. In practice it is particularly noticeable that cars with light rear loading are sensitive to rear toe, probably becuse of the high cornering stiffness coefficient.

A similar analysis for camber gives the result

$$\Delta k_\beta = -\frac{HLd_r\gamma_{Rr}\left(C_\gamma/C_\alpha\right)}{Tag}$$

Positive rear camber gives slightly increased attitude; negative rear camber and positive front camber give increased understeer.

$$\Delta k_U = \left(\frac{HL\left(C_\gamma/C_\alpha\right)}{Tg}\right)\left(\frac{d_r\gamma_{rf}}{b} - \frac{d_r\gamma_{Rr}}{a}\right)$$

Because of the camber/slip stiffness ratio, about 0.04 for radial and 0.15 for bias-ply, the camber effects are much less than the slip angle effects, and generally negligible.

Because of load transfer acting on the tire stiffnesses there is an axle roll angle that results in camber forces. This happens at front and rear, and so has negligible effect on k_U. For a load transfer $F_T = mAH/T$ and tire vertical stiffness K_t the axle roll is

$$\phi_A = \frac{2mAH}{K_tT^2}$$

To preserve the correct tire lateral force, the slip angle must change by

$$\Delta\alpha = \frac{\phi_A C_\gamma}{C_\alpha}$$

$$\Delta k_\beta = \frac{2mH\left(C_\gamma/C_\alpha\right)}{K_tT^2}$$

with a typical value of 0.08 deg/g for radial-ply and 0.20 deg/g for bias-ply, a fairly small effect.

Examining Table 6.10.1 again shows that k_β and k_U are the result of many factors. The attitude coefficient is dominated by the rear tire compliance, and although the center-of-mass position and consequent C_α change largely compensate each other, roll steer and roll camber can be substantial effects and other minor effects may accumulate in a significant way. For the understeer coefficient, again the center-of-mass position and C_α largely compensate, but roll steer, roll camber and steering compliance may be major effects. This table gives a fair indication of the main factors for a typical modern vehicle with open differential at low speed. Other differential types, and aerodynamics, may have significant effects; these are discussed in separate sections later.

6.11 Secondary Handling

The secondary handling regime is the middle range for which the nonlinearities have become significant, but the vehicle has not yet reached the final, purely friction-limited stage. For a car this range typically covers lateral accelerations of $0.3g$ to $0.6g$. The behavior is now much more complex than in the linear regime. In general it cannot be represented by simple equations; it can be modeled by detailed numerical simulations, and the result is still simply represented on a graph of roll angle, attitude angle and understeer angle against lateral acceleration, provided that a simple free differential is used and aerodynamic effects and tire speed effects are neglected.

The roll angle may remain essentially linear. Where it is nonlinear, this is usually because of progressive bump stops coming into operation. There may also be nonlinear springs or bushes. Many factors may produce nonlinearity in the attitude angle and steer angle – essentially any nonlinearity in the variables contributing to the coefficients as listed in Table 6.10.1. The main factor is that the tires now operate on the nonlinear part of the side force versus slip curve. The second major factor is the lateral load transfer. In addition there are many minor factors. The requirement for tractive force affects the tire side forces. The linear roll steer, i.e., a constant roll steer coefficient, may now combine with a nonlinear roll angle. On the other hand, second-order roll steer effects (Section 5.12) tend to cancel out on the axle. Geometry may introduce roll camber nonlinearities, or a constant roll camber coefficient may combine with a nonlinear roll angle. Compliance effects from rubber bushes will diminish as the bushes stiffen rapidly. The aligning torque compliance will be affected by the diminishing pneumatic trail, i.e., the aligning torque itself becomes extremely nonlinear, also diminishing the rigid-body effect. Longitudinal load transfer develops. Jacking causes the nonlinear development of camber, which may be especially significant for a high roll center, e.g., the swing axle.

The first major factor, the attitude angle increment from tire nonlinearity, follows immediately from a comparison of the rear tire characteristic with the linear model. Representing the deviation from linearity as a power model,

$$\Delta\beta = \Delta\alpha_{\mathrm{r}} = C\left(\frac{F_{\mathrm{y}}}{F_{\mathrm{V}}}\right)^{P}$$

Neglecting aerodynamic forces we can simply write

$$\Delta\beta = CA^{P}$$

where P has a typical value of 3.0, and C is 0.0065 deg/(m $\mathrm{s}^{-2})^3$ or 6.5 deg/g^3, giving an increment of 1.4° at 0.6g.

The effect of tire nonlinearity on steer angle depends on the difference between the front and rear increments. Typically the front wheels will be more highly loaded and have a smaller maximum lateral force coefficient. This leads to a steer angle deviation from linearity of similar shape to that for individual tires, but of smaller scale because it is a front-to-rear difference.

The effect of the second major factor, lateral load transfer, is to reduce the cornering force of a pair of wheels, as discussed in Section 2.16. The extra rear slip angle required depends on the load transfer factor (or vertical force lateral transfer factor) e_{V}, i.e., the load transfer divided by the initial vertical force F_{V} for a single wheel

$$e_{\mathrm{V}} = \frac{F_{\mathrm{T}}}{F_{\mathrm{V0}}}$$

and on the particular tire characteristics. This load transfer factor e_{V} must be distinguished from the front and rear load transfer distribution fractions d_{f} and d_{r}. The load transfer will be approximately proportional to the lateral acceleration, giving

$$e_{\mathrm{Vf}} = \frac{F_{\mathrm{Tf}}}{m_{\mathrm{f}}g/2} = \frac{mAHd_{\mathrm{f}}/T}{mbg/2L} = \frac{2AHd_{\mathrm{f}}L}{bgT}$$

$$e_{\mathrm{Vr}} = \frac{2AHd_{\mathrm{r}}L}{agT}$$

where d_f is the front fraction of load transfer moment. The resulting effect on the attitude angle may be modeled by

$$\Delta\beta = C_1 e_{Vr}^P = C_2 A^P$$

where, again, P is typically 3, C_1 is typically 25°, and C_2 is 7 deg/g^3, giving an attitude increment of 1.5° at $0.6g$, similar to the direct effect of the tire F_y–α nonlinearity.

The effect of lateral load transfer on steer angle depends on the front-to-rear difference of lateral load transfer. This effect is controllable, for example by roll center height adjustment, or more readily by redistribution of the anti-roll bar stiffnesses.

An expression for the effect of longitudinal load transfer on steer angle can be obtained by considering the effect of the new vertical forces on the tire cornering stiffness. The resulting effect is small, for example 0.4 deg/g^3.

Thus the principal factors controlling the secondary understeer angle contribution are the center-of-mass position and the distribution of lateral load transfer. In those cases where the tire characteristics are fundamentally different front and rear, for example because of different tire sizes as on racing cars and some sports cars, or multiple tires on trucks, this will also be a major factor.

Tractive forces may be significant in this regime if distributed unevenly side-to-side (Section 6.13), but are not of major importance if a free differential is used. Considering a neutral vehicle, with linear tire characteristics the tractive force must overcome a total drag of

$$D = \mu_R mg + \tfrac{1}{2}\rho V^2 A_D + \frac{m^2 A^2}{4C_\alpha}$$

At 33 m radius and 6 m/s^2 lateral acceleration the average slip angle is about 5°, and the tractive force is typically 600 N, which if demanded at one end of the vehicle is a tractive coefficient $F_x/F_V \approx 0.1$. The total drag will be a little larger at higher speed, on a greater radius, because of the greater aerodynamic drag. It is sometimes said that the total tire drag is greater on a small radius because of the greater steer angle. This is false – it is only the slip angles that contribute to the tire drag, not the kinematic steer angle. This may be seen by taking moments about the center of path curvature, or by considering an energy analysis.

The tractive force, required to maintain speed, affects the tire F_y–α relationship; in some cases there may be a small increase in F_y, but generally, and always for large traction, F_y is reduced and greater slip angle is required. Thus a front-drive vehicle has an increase of steer angle, and a rear-drive one has a decrease; four-wheel drive may remain broadly unaffected if the front-to-rear torque distribution is appropriate. For a traction coefficient of 0.1 on a normal road surface, the effect is in any case rather small, but may become significant at high speed or on low-friction surfaces.

6.12 Final Handling

The final handling regime is the last 25% or so of the handling curve. For passenger cars this corresponds to lateral accelerations from 0.6*g* (6 m/s^2) up to the maximum value of about 0.8*g*. The ultimate value is generally less for commercial vehicles, e.g., 0.5*g*, because of poorer suspension systems, harder-wearing lower-friction tire materials, higher tire–road contact pressures, rollover potential because of high center of mass, and so on. It may exceed 1.0*g* for good sports cars with wide high-grip tires, and may exceed even 3*g* for some racing cars with ultra high-grip tires and aerodynamic downforce.

As far as the handling diagram is concerned, the basic question is whether the vehicle has final understeer or final oversteer, and this depends on which end of the vehicle has the greater ultimate lateral acceleration capability. Neglecting the tractive force requirement, this simply depends on the graph of lateral force over end-mass for the two axles. Referring back to Figure 6.3.2(a), which is representative for a typical modern car with final understeer, the maximum lateral acceleration is achieved at the peak of the curve for the front axle. At this acceleration, the rear axle achieves the required side force at a smaller slip angle. The attitude angle at the limit therefore follows from this rear slip angle plus the roll steer and compliance steer of the rear suspension. The steer-angle curve as a function of acceleration, curve A of Figure 6.3.4, increases extremely steeply near the limit, and may curve back on itself if the tire characteristic is peaked or if account is taken of the tractive requirement for overcoming the tire drag component at high slip angles.

For a final oversteer vehicle, the front suspension has the greater lateral acceleration capability, i.e., the greater side force to end-mass ratio, and the curve labels of Figure 6.3.2(a) are reversed. In the limit the attitude angle grows extremely rapidly, calling for large negative increments of steer angle; the understeer gradient is negative, and the understeer angle and possibly even the total steer angle will become negative (curve B of Figure 6.3.4). Because of this need for steering reversal, final oversteer is generally considered bad; final understeer has the advantage of more progressive and consistent control behavior.

The vehicle final handling behavior can be represented fairly well by just two variables, the front and rear maximum lateral accelerations, A_f and A_r. However, it is more useful to think in terms of the actual vehicle maximum lateral acceleration A_M (which is the lesser of A_f and A_r) and a final handling balance parameter. This is equivalent to using the attitude gradient and the understeer gradient instead of the front and rear compliances for primary handling. This final handling balance parameter should measure the commitment of the vehicle to terminal understeer or oversteer. It would be possible to use A_r minus A_f as a final understeer margin, but this can be non-dimensionalized to give a final understeer number:

$$N_U = \frac{A_r}{A_f} - 1$$

Hence a final understeer vehicle, for which $A_r > A_f$, has positive N_U; final oversteer has negative N_U, and in principle a final neutral vehicle has $N_U = 0$. The typical modern car has a final understeer number of about 0.2, usually somewhat less for rear-drive and more for front-drive. The design factors and operating conditions that contribute to the final understeer number will be considered in this and subsequent sections.

Table 6.12.1 indicates example main contributions to the final understeer number. The changes are considered relative to a vehicle with $a = b$ and equal tires all around.

Table 6.12.1. Example final understeer number effects (front drive), N_U

Factor	$\Delta A_f/A_0$	$\Delta A_r/A_0$	ΔN_U
G at 45% ($a = 0.45L$)	−0.100	+0.100	+0.200
Corresponding N_f, N_r (constant μ)	+0.100	−0.100	−0.200
Friction sensitivity with G posn ($p = -0.15$)	−0.015	+0.015	+0.030
Lateral load transfer 70%/30%	−0.059	−0.011	+0.048
Longitudinal load transfer	−0.029	+0.029	+0.058
Traction (tire drag only, front drive)	−0.040	0	+0.040
Steer angle (6°)	−0.044	0	+0.044
Rolling resistance with load transfer	−0.008	+0.006	+0.014
Totals (front drive)	−0.195	+0.039	+0.234

The principal factors affecting the ultimate ability of each axle are the center-of-mass position, the tire friction coefficient sensitivity to F_V, the lateral load transfer distribution, the longitudinal load transfer, and the tractive force requirements. Roll-steer and compliance steer still have some effect on attitude angle and steer angle, but do not significantly influence the ultimate steady-state cornering ability, other than through the longitudinal load transfer. Camber angles have some effect on maximum cornering force of tires, but this is not well documented.

A forward center of mass increases the front end-mass and increases the axle normal reaction, but it increases the maximum front side force capability in a smaller proportion because the maximum force coefficient reduces. Hence a forward G gives a final understeer tendency. Consider an initially neutral vehicle with G at 50% and four equal tires, and represent this condition with the subscript 0, to give for example a maximum cornering coefficient μ_{C0}. Now move G forward by x. The front axle reaction is

$$N_f = mg\left(\frac{1}{2} + \frac{x}{L}\right)$$

$$\frac{N_f}{N_{f0}} = 1 + \frac{2x}{L}$$

The maximum lateral force coefficient can be represented as being proportional to the vertical force to the power p, where p is found experimentally to be typically −0.15 for passenger car tires and about −0.23 for racing tires. Hence the actual maximum lateral force $F_{Y\max}$ increases with F_V at the power $(1 + p)$, around 0.8. Representing the maximum lateral force coefficient by μ_C,

$$\begin{aligned}\frac{A_{\mathrm{f}}}{A_0} &= \frac{\mu_{\mathrm{Cf}}}{\mu_{\mathrm{Cf0}}}\\ &= \left(\frac{N_{\mathrm{f}}}{N_{\mathrm{f0}}}\right)^p\\ &= \left(1+\frac{2x}{L}\right)^p\\ &\approx 1+\frac{2xp}{L}\end{aligned}$$

$$\frac{\Delta A_{\mathrm{f}}}{A_0} = \frac{2xp}{L}$$

$$\frac{\Delta A_{\mathrm{r}}}{A_0} = -\frac{2xp}{L}$$

For a most extreme likely mass distribution of 70/30, i.e., $x = 0.2L$, this gives $A_{\mathrm{f}}/A_0 = 0.94$, $A_{\mathrm{r}}/A_0 = 1.06$, and $A_{\mathrm{r}}/A_{\mathrm{f}} \approx 1.13$. Thus the maximum side force coefficient of the complete vehicle is 6% less than for an even balance, and there is a strong final understeer tendency with an N_{U} contribution of +0.13. To a good approximation these effects are proportional to x. For negative x (rearward G), the maximum lateral acceleration also deteriorates, but is now limited at the rear so there is a final oversteer tendency. The maximum capability occurs at a central G; it is notable that this is not a curved optimum but a peaked one because of the sharp transition from front limitation to rear limitation. If the tires are different front and rear, the optimum will no longer be a central G, but the sensitivity for deviation from the optimum position will be similar.

The influence of lateral load transfer may be examined by again beginning with an $a = b$ symmetrical vehicle, with lateral load transfer moment distribution factors d_{f} and d_{r}. The individual front-wheel standing reaction without load transfer is

$$N_{\mathrm{f0}} = \tfrac{1}{2} m_{\mathrm{f}} g = \frac{mbg}{2L}$$

The front load transfer is

$$F_{\mathrm{Tf}} = \frac{mAH}{T} d_{\mathrm{f}}$$

giving reaction forces, front inner and front outer, of

$$N_{\mathrm{fi}} = N_{\mathrm{f0}}\left(1 - \frac{2AHLd_{\mathrm{f}}}{Tbg}\right)$$

$$N_{\mathrm{fo}} = N_{\mathrm{f0}}\left(1 + \frac{2AHLd_{\mathrm{f}}}{Tbg}\right)$$

Similar equations may be written for the rear. The axle maximum front cornering force will be

$$\begin{aligned} F_{\mathrm{yf}} &= \mu_{\mathrm{Cfi}} N_{\mathrm{fi}} + \mu_{\mathrm{Cfo}} N_{\mathrm{fo}} \\ &= \mu_{\mathrm{C0}} N_{\mathrm{f0}}\left(\frac{N_{\mathrm{fi}}}{N_{\mathrm{f0}}}\right)^{1+p} + \mu_{\mathrm{C0}} N_{\mathrm{f0}}\left(\frac{N_{\mathrm{fo}}}{N_{\mathrm{f0}}}\right)^{1+p} \end{aligned}$$

The axle maximum lateral acceleration is then given by

$$A_{\mathrm{f}} = \frac{F_{\mathrm{yf}}}{m_{\mathrm{f}}} = \frac{F_{\mathrm{yf}}\, g}{2N_{\mathrm{f0}}}$$

giving

$$\frac{A_{\mathrm{f}}}{\mu_{\mathrm{C0}}\, g} = \frac{1}{2}\left(\frac{N_{\mathrm{fi}}}{N_{\mathrm{f0}}}\right)^{1+p} + \frac{1}{2}\left(\frac{N_{\mathrm{fo}}}{N_{\mathrm{f0}}}\right)^{1+p}$$

Substituting, and using the approximate binomial expansion to the second order, now gives for the acceleration change, with $A_0 = \mu_{\mathrm{C0}}\, g$,

$$\frac{\Delta A_{\mathrm{f}}}{A_0} = 2p(1+p)\left(\frac{AHLd_{\mathrm{f}}}{Tbg}\right)^2$$

For the rear, a similar expression may be obtained, but with d_r and a. With $a = l/2$

$$\frac{\Delta A_f}{A_0} = 8p\,(1+p)\left(\frac{AHd_f}{Tg}\right)^2$$

For representative car values this gives a deterioration of maximum lateral force coefficient of about 4% from lateral load transfer. The effect on the final understeer number is

$$\Delta N_U = 8p\,(1+p)\left(\frac{AH}{Tg}\right)^2 (d_f - d_r)$$

For a representative passenger car this is $\Delta N_U \approx +0.15(d_f - d_r)$.

Thus putting 70% of the load transfer distribution at the front will give a final understeer number contribution $\Delta N_U = 0.06$, another strong final understeer tendency. The load transfer distribution is easily amenable to tuning by the anti-roll bars, and provides an important design variable in this respect.

Perhaps surprisingly, longitudinal load transfer may have a significant effect on N_U. Because of the attitude angle, there is an acceleration component $A \sin\beta$ giving a longitudinal load transfer

$$F_{TX} = \frac{mAH \sin\beta}{L}$$

This influences the axle reactions according to

$$\frac{N_f}{N_{f0}} = 1 - \frac{AH \sin\beta}{bg}$$

$$\frac{N_r}{N_{r0}} = 1 + \frac{AH \sin\beta}{ag}$$

With friction sensitivity *p*,

$$\frac{\Delta A_{\mathrm{f}}}{A_{\mathrm{f0}}} \approx -\frac{(1+p)AH\sin\beta}{bg}$$

$$\frac{\Delta A_{\mathrm{r}}}{A_{\mathrm{r0}}} \approx \frac{(1+p)AH\sin\beta}{ag}$$

$$\Delta N_{\mathrm{U}} \approx (1+p)\left(\frac{AH\sin\beta}{g}\right)\left(\frac{1}{a}+\frac{1}{b}\right)$$

For an example vehicle with $\beta = 6°$ the fractional acceleration changes at each axle are of magnitude 0.029. The total ΔN_{U} of 0.058 resulting from longitudinal load transfer is a large effect.

Traction requirements may have a significant influence on final handling. In this regime slip angles are relatively large, say 10°, and the associated tire cornering drag is substantial:

$$D_{\mathrm{T}} \approx mA\sin\alpha$$

and the traction coefficient for the driven tires for two-wheel drive is

$$f_{\mathrm{T}} = \frac{F_{\mathrm{X}}}{F_{\mathrm{V}}} \approx \frac{D}{mg/2} \approx \frac{2A\sin\alpha}{g} \approx 0.28$$

At the basic test radius of 33 m, 0.8*g* corresponds to 16 m/s, so the aerodynamic drag is relatively small – about 110 N against 2 kN tire cornering drag. Even at 100 m radius and 0.8*g* the aerodynamic drag is only about 350 N, although the force diagram, e.g., as Figure 6.4.2, can easily be amended to include aerodynamic drag and side force, and rolling resistance, if required. The effect of the traction coefficient depends in detail on the tire (Section 2.18), but as a simple approximation the friction ellipse model may be used. A traction coefficient of 0.28 will reduce F_{ymax} by about 4%. This is therefore a significant effect, encouraging final understeer for front-drive and final oversteer for rear-drive.

Because of the steer angle there is a negative contribution to attitude angle at G, giving a forward load transfer. There is also a reduction of the moment arm of the front side force, with a further reduction because of front lateral load transfer. This is discussed in detail in Section 6.16. The outcome for notional infinite radius and 6° final understeer is a ΔN_{U} of 0.037. At 33 m radius this increases by 0.010.

As a result of lateral load transfer there is a rolling resistance understeer moment about G, neglecting the steer angle, of

$$M = \mu_{\mathrm{R}} F_{\mathrm{T}} T = \mu_{\mathrm{R}} mAH$$

This requires counteracting front and rear side forces, and hence

$$\frac{\Delta A_{\mathrm{f}}}{A_0} = \frac{\mu_{\mathrm{R}} mH}{m_{\mathrm{f}} L} = \frac{\mu_{\mathrm{R}} H}{b}$$

$$\frac{\Delta A_{\mathrm{r}}}{A_0} = \frac{\mu_{\mathrm{R}} H}{a}$$

$$\begin{aligned}\Delta N_{\mathrm{U}} &= \mu_{\mathrm{R}} H\left(\frac{1}{a} + \frac{1}{b}\right)\\ &\approx \frac{4\mu_{\mathrm{R}} H}{L}\end{aligned}$$

with a typical value of 0.014.

The maximum lateral force of a tire depends on the camber angle because this controls the presentation of the footprint to the road. Broadly, the best camber angle will be the one that gives the greatest contact area. However, this is not simply zero camber because the tire distorts with side load. Depending on the nature of the distortions, which depend among other things on the rim width, the optimum camber may be a few degrees positive or negative. For conventional passenger car tires the peak is not highly sensitive, although camber angle settings can affect the maximum lateral acceleration by 5% or more, and for the extremely wide tires used in racing camber may be critical. A rigid axle introduces small camber angles equal to the axle roll angle, which is 1 to 2 deg/g. Independent suspensions vary considerably. Simple trailing arms give camber equal to roll. Parallel wishbones may give camber equal to roll, or be arranged at the other extreme to give opposite camber. Thus the suspension camber may be significant in influencing the final cornering limit and the final understeer number, but it is very difficult to make any useful general statements or to quantify the effects in the absence of specific tire and suspension data.

On the basis of force diagrams such as Figure 6.4.2, arguments are sometimes presented to compare the merits of front and rear drive in terms of maximum cornering acceleration. Such analyses do not seem to be borne out by experiment, the most favorable end for traction really depending on many details. Also, from a practical point of view a change of drive implies changes of mass positions, so it is not necessarily useful to compare drives with other things being equal. Rear drive (described by one rally driver as "handling a man can understand") has some controllability advantages at the limit. Four-wheel drive has had only limited success in racing because of controllability problems ("like trying to write your signature with someone jogging your elbow"). The advantage of four-wheel drive lies in its superior traction on poor surfaces, and hence its success in rallying.

6.13 Differentials

In this section, the effect of differentials on the vehicle as a rigid body will be treated. For a non-free differential, there may be different tractive forces on the two sides of the vehicle, giving an understeer or oversteer moment.

With zero net traction, a solid differential will have an inner wheel slip $T/2R$ and outer wheel slip $-T/2R$ (Section 1.9). For a tire longitudinal stiffness C_x (N/unit slip) the forward tractive forces are, for small slip, i.e., $R > 15$ m,

$$F_{xi} = \frac{C_x T}{2R}$$

$$F_{xo} = -\frac{C_x T}{2R}$$

giving an understeer moment

$$M = \left(F_{xi} - F_{xo}\right) T$$

$$= -\frac{C_x T^2}{2R}$$

This moment requires counteracting front and rear slip angle increments to restore steady state. The required axle side force increments are *M/L*. For the linear case

$$\Delta\alpha_f = -\frac{M}{2C_{\alpha f}L}$$

$$\Delta\alpha_r = +\frac{M}{2C_{\alpha r}L}$$

$$\begin{aligned}\Delta\delta = \Delta\alpha_f - \Delta\alpha_r &= -\frac{M}{2L}\left(\frac{1}{C_{\alpha f}} + \frac{1}{C_{\alpha r}}\right)\\ &= \frac{C_x T^2}{4LR}\left(\frac{1}{C_{\alpha f}} + \frac{1}{C_{\alpha r}}\right)\end{aligned}$$

which is typically about $33/R$ degrees. This is valid for the linear tire and lateral acceleration region, i.e., $R > 15$ m and $A < 0.3g$. At the basic test radius of 33 m, $\Delta\delta$ is typically 1°, independent of lateral acceleration.

In the steady state it is necessary only to overcome the vehicle resistance, so the tractive force is generally small and the steer effect fairly small. In transient conditions, such as acceleration out of a corner, there may be strong steer effects from non-free differentials, which vary considerably in their torque distribution characteristics. A simple locking differential may apply all its torque to the inner wheel because of the small angular speed of this wheel. On the other hand an "intelligent" differential seeking to avoid wheel spin might allocate torque in proportion to the tire normal force. The handling contribution of these differentials will be analyzed approximately here for a simple $a = b$ vehicle with equal tire characteristics all around.

The total vehicle drag including tires is D. The simple overrun ratcheting differential, assumed to be applying all its thrust on the inner wheel, gives a tractive understeer moment

$$M = \tfrac{1}{2}DT$$

and hence, arising from the tractive moment, a compensating lateral force is required at each axle of value

$$F = \frac{M}{L} = \frac{DT}{2L}$$

$$\Delta\alpha_{\mathrm{r}} = -\frac{DT}{4LC_\alpha}$$

$$\Delta\alpha_{\mathrm{f}} = \frac{DT}{4LC_\alpha}$$

$$\Delta\delta = \frac{DT}{2LC_\alpha}$$

In the linear regime at moderate speeds the drag is mainly tire drag:

$$\begin{aligned} D \approx D_{\mathrm{T}} &\approx mA\sin\alpha \\ &\approx \frac{m^2A^2}{4C_\alpha} \\ \Delta\delta &= \frac{m^2TA^2}{8LC_\alpha^2} \\ &\approx \left(93\times10^{-6}\right)A^2 \qquad \left(\mathrm{rad}\,/\left(\mathrm{m\,s^{-2}}\right)^2\right) \\ &= 0.6\,A^2 \qquad \left(\mathrm{deg}\,/\,g^2\right) \end{aligned}$$

Hence this type of differential has no effect on the understeer coefficient k_{U} and has a small secondary understeer effect in A^2.

Considering now final handling, the tractive moment influences the axle maximum lateral accelerations:

$$\Delta A_{\mathrm{f}} = -\frac{DT/2L}{m/2} = -\frac{AT\sin\alpha}{L}$$

$$\Delta A_{\mathrm{r}} = \frac{AT\sin\alpha}{L}$$

The change in final understeer number is

$$\begin{aligned}\Delta N_{\mathrm{U}} &= \frac{\Delta A_{\mathrm{r}}}{\mu_{\mathrm{C0}}g} - \frac{\Delta A_{\mathrm{f}}}{\mu_{\mathrm{C0}}g}\\ &= \frac{2AT\sin\alpha}{L\mu_{\mathrm{C0}}g}\\ &= \frac{2T\sin\alpha}{L}\end{aligned}$$

with a value of typically +0.16. Thus there is a very strong final understeer tendency when the traction is on the inner wheel only.

Considering now the "intelligent" differential applying torque proportional to tire vertical force, with load transfer factor d at the powered end, i.e., d_{f} or d_{r} as appropriate, the axle load transfer has inner and outer vertical forces such that

$$\frac{N_{\mathrm{o}}}{N_{\mathrm{i}}} = \frac{1 + CA}{1 - CA}$$

where $C \approx 4Hd/Tg$. The inner and outer tractive forces F_{xo} and F_{xi} give

$$F_{\mathrm{xo}} + F_{\mathrm{xi}} = D$$

and the differential property is

$$\frac{F_{\mathrm{xo}}}{F_{\mathrm{xi}}} = \frac{N_{\mathrm{o}}}{N_{\mathrm{i}}}$$

The result, with some manipulation, is a tractive understeer moment

$$\begin{aligned}M &= -\tfrac{1}{2}DTCA\\ &= -\frac{2mHd\sin\alpha}{g}A^2\end{aligned}$$

In the primary handling regime, $\alpha \approx mA/4C_\alpha$ and the effect on steer angle is

$$\Delta\delta = \frac{M}{LC_\alpha}$$

$$\approx -\frac{m^2 HdA^3}{2gLC_\alpha^2}$$

which is about $-0.50A^3$ (deg/g^3). Thus there is no primary effect, and a small secondary oversteer effect in A^3.

For final handling, we still have

$$M = -\left(\frac{2mHd\sin\alpha}{g}\right)A^2$$

$$\Delta A_f = \frac{M/L}{m/2} = -\left(\frac{4Hd\sin\alpha}{gL}\right)A^2$$

and $\Delta A_r = -\Delta A_f \approx 0.45$ m/s^2.

$$\Delta N_U = \frac{\Delta A_r}{\mu_{C0}g} - \frac{\Delta A_f}{\mu_{C0}g}$$

$$= -\frac{8Hd\sin\alpha\, A^2}{\mu_{C0}g^2 L}$$

which is typically -0.12. Thus there is a very strong final oversteer contribution, in this case with the traction mainly on the outer wheel, not quite as great as for the overrun ratcheting differential understeer because of incomplete load transfer.

6.14 Aerodynamics – Primary

This section discusses the effect of aerodynamics on wind-free steady-state primary handling. As discussed in Chapter 3, the total aerodynamic force on the vehicle may be represented by lift, drag and side force coefficients, and pitching, yawing and rolling moment coefficients.

Table 6.14.1 gives example effects quantified for a representative car at 50 m/s, i.e., at top speed, where aerodynamic effects will be at their most extreme.

Table 6.14.1. Example Primary Aerodynamic Effects (deg/*g* at 50 m/s)

Component			Δk_U	Δk_β
1	Lift – front	$C_{Lf} = 0.1$	+0.22	0.00
2	Lift – rear	$C_{Lr} = 0.1$	–0.14	+0.14
3	Drag (front drive)	$C_D = 0.32$	+0.10	0
4	Side force	$C'_S = 0.04$/deg	+0.06	–0.32
5	Yaw	$C'_Y = 0.01$/deg	–0.32	–0.28
Totals			–0.08	–0.46

At the legal speed limits of most countries these effects will be smaller, but of course it is a manufacturer's responsibility to ensure that a vehicle behaves properly at all speeds of which it is capable. For an aerodynamically bad vehicle the net effect can be significant and bad. For a good one the effects can be controlled and balanced so that there is only a small and possibly even favorable effect. To summarize broadly, the side force contributes directly to lateral acceleration, the yaw moment is usually destabilizing, the lift and pitch affect the tire characteristics, drag affects the tires through traction requirements, and the roll moment gives some load transfer and possible roll steer effects, usually small.

To analyze in more detail, lift and pitching will be taken in terms of front and rear lift. The front lift is

$$F_{\mathrm{AeLf}} = \tfrac{1}{2}\rho V^2 S C_{\mathrm{Lf}}$$

which changes the tire normal reactions and hence the cornering stiffness according to

$$\begin{aligned}\frac{C_\alpha}{C_{\alpha 0}} &= \left(\frac{m_f g - F_{\mathrm{AeLf}}}{m_f g}\right)^f \\ &= \left(1 - \frac{\frac{1}{2}\rho V^2 S C_{\mathrm{Lf}} L}{mbg}\right)^f\end{aligned}$$

which by approximate expansion gives

$$\frac{C_\alpha}{C_{\alpha 0}} = 1 - \frac{f\rho V^2 S C_{\mathrm{Lf}} L}{2mbg}$$

where $m_\mathrm{f} = mb/l$ is the front end-mass and f is an empirical constant for the tire. The change in front cornering compliance is

$$\frac{\Delta D_\mathrm{f}}{D_\mathrm{f}} \approx -\frac{\Delta C_\alpha}{C_{\alpha 0}} = \frac{f\rho V^2 S C_{\mathrm{Lf}} L}{2mbg}$$

with an equivalent expression for the rear. The proportional change in the attitude gradient is

$$\frac{\Delta k_\beta}{k_\beta} = -\frac{\Delta C_{\alpha\mathrm{r}}}{C_{\alpha 0}} = \frac{f\rho V^2 S C_{\mathrm{Lr}} L}{2mag}$$

With $f = 0.5$ this evaluates to $0.22C_{\mathrm{Lr}}$, which could be significant for a bad vehicle, but with $C_{\mathrm{Lr}} = 0.1$ and $k_\beta = 6$ deg/g the result is a negligible 0.14 deg/g change. The change of understeer gradient is

$$\begin{aligned}\Delta k_\mathrm{U} &= \Delta D_\mathrm{f} - \Delta D_\mathrm{r} \\ &\approx \frac{\rho V^2 S L f}{2mg}\left(\frac{C_{\mathrm{Lf}} D_\mathrm{f}}{b} - \frac{C_{\mathrm{Lr}} D_\mathrm{r}}{a}\right)\end{aligned}$$

This is approximately $8C_\mathrm{P}$ (deg/g) which could be significant for a bad vehicle.

The above expressions are for a vehicle with the same tire C_α to F_V sensitivity f value front and rear, but may easily be extended to different values. Typically with a forward G position f_f becomes smaller and f_r larger, making C_{Lr} more important. Even if f_f is close to zero, C_{Lf} may remain important because of attitude changes and consequent coefficient changes, especially to drag which is sensitive to pitch angle.

The aerodynamic drag is

$$F_{\mathrm{AeD}} = \tfrac{1}{2}\rho V^2 S C_\mathrm{D}$$

calling for a traction coefficient

$$f_T = \frac{F_{AeD}}{F_{V0}}$$

where F_{V0} is the vertical reaction of the driven wheels, e.g., for rear drive and no rear lift,

$$F_{V0} = m_T g = \frac{mag}{L}$$

To gain some insight into the likely scale of the consequences of the tractive force, we can use the cornering force ellipse model in the form

$$\frac{C_\alpha}{C_{\alpha 0}} = \sqrt{1 - \left(\frac{f_T}{\mu_L}\right)^2}$$

By approximate expansion

$$\begin{aligned}\frac{\Delta C_\alpha}{C_{\alpha 0}} &= -\frac{1}{2}\left(\frac{f_T}{\mu_L}\right)^2\\ &= -\frac{1}{8}\left(\frac{\rho V^2 S C_D L}{\mu_L mag}\right)^2\end{aligned}$$

For rear drive at 50 m/s a representative result is -0.10 deg/g on both k_β and k_U. For front drive k_β is unchanged, and Δk_U is positive. These values are not large. On the other hand, on a poor friction surface the effects can be substantial.

The aerodynamic side force as a function of aerodynamic yaw angle β_{Ae} is

$$F_{AeS} = \tfrac{1}{2}\rho V^2 S C'_S \beta_{Ae}$$

where

$$C'_S = -\frac{dC_S}{d\beta_{Ae}} \approx 0.04/\text{deg}$$

This contributes a lateral acceleration

$$A'_S = \frac{F'_{AeS}}{m} = \frac{\rho V^2 S C'_S}{2m} \qquad \left(\mathrm{m\,s^{-2}} / \mathrm{deg}\right)$$

By definition of the standard aerodynamic axes, the side force acts at the center of the wheelbase, i.e., there is an equal effective side force at each axle. The required counteracting tire slip angles are therefore

$$\Delta\alpha_f = \frac{F_{AeS}}{4C_{\alpha f}}$$

$$\Delta\alpha_r = \frac{F_{AeS}}{4C_{\alpha r}}$$

Hence

$$\Delta k_\beta = -\frac{\rho V^2 S C'_S k_\beta}{8C_{\alpha r}}$$

$$\Delta k_U = -\tfrac{1}{8}\rho V^2 S C'_S k_\beta \left(\frac{1}{C_{\alpha f}} - \frac{1}{C_{\alpha r}}\right)$$

Representative values are −0.32 deg/*g* for Δk_β, and +0.06 deg/*g* for Δk_U.

Turning now to the aerodynamic yaw moment, as a function of yaw angle this is

$$M_{AeY} = \tfrac{1}{2}\rho V^2 S L C_Y \beta_{Ae}$$

where

$$C'_Y = \frac{dC_Y}{d\beta_{Ae}} \approx 0.01 / \mathrm{deg}$$

The moment requires counteracting forces at the axles, giving

$$\Delta\alpha_{\mathrm{r}} = \frac{M_{\mathrm{AeY}}/L}{2C_{\alpha\mathrm{r}}}$$

Using $\beta_{\mathrm{Ae}} \approx \alpha_{\mathrm{r}}$, this results in

$$\begin{aligned}
\frac{\Delta k_{\beta}}{k_{\beta}} &= -\frac{\Delta\alpha_{\mathrm{r}}}{\alpha_{\mathrm{r}}} \approx -\frac{\Delta\alpha_{\mathrm{r}}}{\beta} = -\frac{M_{\mathrm{AeY}}\Delta\alpha_{\mathrm{r}}}{2LC_{\alpha\mathrm{r}}\beta} \\
&= -\frac{\rho V^2 S C'_{\mathrm{Y}}}{4C_{\alpha\mathrm{r}}} \\
\Delta\delta &= \Delta\alpha_{\mathrm{f}} - \Delta\alpha_{\mathrm{r}} \\
&= -\frac{1}{4}\rho V^2 S C'_{\mathrm{Y}}\beta\left(\frac{1}{C_{\alpha\mathrm{f}}} + \frac{1}{C_{\alpha\mathrm{r}}}\right)
\end{aligned}$$

Using $\beta_{\mathrm{Ae}} = \beta = k_{\beta}A$

$$\Delta k_{\mathrm{U}} = \frac{\Delta\delta}{A} = -\frac{1}{4}\rho V^2 S C'_{\mathrm{Y}} k_{\beta}\left(\frac{1}{C_{\alpha\mathrm{f}}} + \frac{1}{C_{\alpha\mathrm{r}}}\right)$$

For the example vehicle, Δk_{β} is -0.28 deg/g and Δk_{U} is -0.32 deg/g, which are small effects. However, for a vehicle with an unfavorably shaped body and rearward G the effect on the understeer gradient k_{U} may be much larger.

Detailed equations can also be worked out for the effect of the aerodynamic roll moment on lateral load transfer and roll steer; in general for a car such effects are small, although they may be noticeable for high-sided vehicles.

Reconsidering Table 6.14.1, even at 50 m/s the total effects on primary handling are not great, although the effect on understeer coefficient will depend very much on the aerodynamic characteristics of the particular vehicle.

6.15 Aerodynamics – Final

This section discusses the influence of aerodynamics on final steady-state handling, i.e., on the maximum lateral acceleration A_{M} and on the final understeer number N_{U}. Table 6.15.1 indicates example effects quantified for a representative car at 50 m/s.

Table 6.15.1. Example Final Aerodynamic Effects (50 m/s)

Component			ΔA_M (m/s^2)	ΔN_U (–)
1	Lift	$C_L = 0.1$	–0.160	–0.010
2	Pitch	$C_P = 0.1$	–0.320	+0.080
3	Drag	$C_D = 0.32$	0	–0.060
4	Side force	$C'_S = 0.04$/deg	+0.550	+0.030
5	Yaw	$C'_Y = 0.01$/deg	+0.270	–0.070
Totals			+0.340	–0.030

The effects will vary considerably between vehicles. Actually, because of tire cornering drag the maximum steady-state speed at which the lateral acceleration is limited by handling rather than simply speed is usually only about 0.6 times the straight-line maximum speed, and hence typically 30 m/s, corresponding to maximum lateral acceleration at about 110 m radius. However, a vehicle can be turned into a severe corner at its maximum straight-line speed, and although this strictly gives a transient condition it is convenient to adopt it here as the most severe aerodynamic condition. At 30 m/s or legal limit speeds the effects will be substantially smaller.

The basic effect of lift or downforce on the limiting cornering ability may be investigated as follows. For a lift coefficient C_L the total tire vertical reaction is

$$N = mg - \tfrac{1}{2}\rho V^2 S C_L$$

For simplicity, considering first that the maximum cornering force coefficient μ_C is independent of N, the maximum speed V is given by

$$mA = \frac{mV^2}{R} = \mu_Y N$$

For a given radius the maximum speed is then

$$V = \sqrt{\frac{\mu_Y mgR}{m + \tfrac{1}{2}\mu_Y \rho R S C_L}}$$

Without aerodynamics, the maximum lateral acceleration is $\mu_Y g$; by comparison

$$\frac{A}{\mu_Y g} = \frac{1}{1 + (\mu_Y \rho RSC/2m)}$$

Lift reduces the maximum lateral acceleration; but for downforce, which is negative C_L, the maximum A goes to infinity for a radius exceeding

$$R^* = -\frac{2m}{\mu_Y \rho SC_L}$$

This radius was about 180 m for extreme ground-effect Formula 1 racing cars.

Figure 6.15.1 (curve for $p = 0$) shows how the maximum speed for a corner varies with R/R^* for this simple model, where V_0 is the maximum speed with no downforce.

The above analysis neglects the deterioration of maximum side force coefficient with increasing vertical force. In this case, with the usual friction power sensitivity p, and coefficient μ_{Y0} when there is zero aerodynamic lift,

$$\left(\frac{\mu_Y}{\mu_{Y0}}\right) = \left(\frac{N}{N_0}\right)^p$$

where $N_0 = mg$. Then, with lift

$$mA = \frac{mV^2}{R} = \mu_Y N = \mu_{Y0}\left(\frac{N}{mg}\right)^p N$$

$$\frac{V^2}{\mu_{Y0} Rg} = \left(\frac{N}{mg}\right)^{1+p}$$

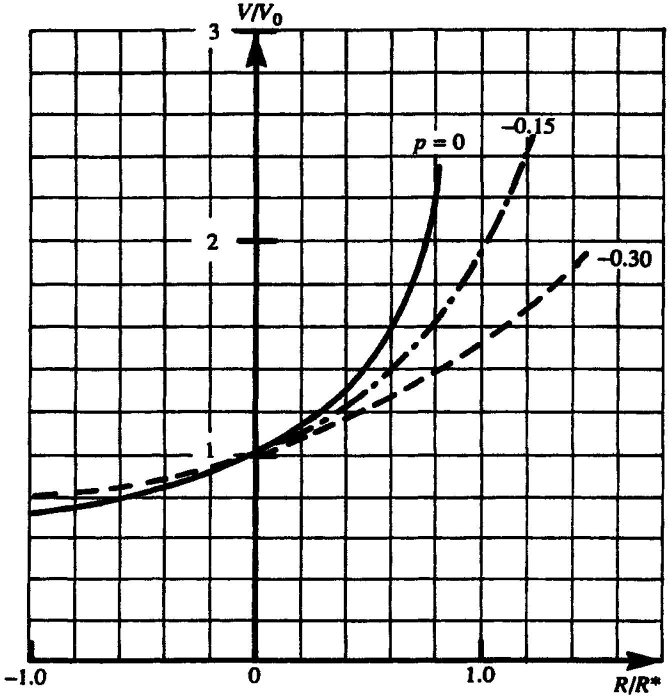

Figure 6.15.1. Downforce effect on maximum cornering speed.

At a given speed, the minimum radius is increased by lift and reduced by downforce. For zero lift, $R_0 = V^2/\mu_{Y0}g$, so

$$\frac{R}{R_0} = \left(1 - \frac{\rho V^2 S C_L}{2mg}\right)^{-(1+p)}$$

$$\frac{R}{R^*} = \frac{V^2}{\mu_{Y0} R^* g}\left(1 - \frac{V^2}{\mu_{Y0} R^* g}\right)^{-(1+p)}$$

Therefore

$$\frac{R}{R^*} = \left(\frac{V}{V^*}\right)^2 \left[1 - \left(\frac{V}{V^*}\right)^2\right]^{-(1+p)}$$

where

$$V^* = \sqrt{\mu_{Y0} R^* g} = \sqrt{\frac{2mg}{\rho S C_L}}$$

which we may call the critical aerodynamic speed. Physically it is the (normally unachievable) speed when lift equals weight. For downforce it is imaginary, but introducing a negative sign it is the speed when downforce equals weight. For Formula 1 racing cars it is about 50 m/s. For a representative passenger car with $C_L = 0.2$ it is 240 m/s. These equations allow us to plot on Figure 6.15.1 how the maximum speed varies with R/R^* for a realistic friction sensitivity of –0.15, and an extreme of –0.30. The maximum speed no longer goes to infinity; the cornering friction deterioration of realistic tires has a surprisingly large effect. For a representative passenger car with $C_L = 0.1$, at 50 m/s the effect on A_M is –0.16 m/s^2; at 16 m/s on the standard 33 m radius it is only –0.02 m/s^2.

By definition the lift acts at the wheelbase mid-point, giving equal lift at the two axles, any difference of lift being reflected in the pitch coefficient instead. The lift alone causes a change of understeer number

$$\Delta N_U = -\frac{(1+p)\rho V^2 S L C_L}{4mg}\left(\frac{1}{a} + \frac{1}{b}\right)$$

This is generally small for road vehicles, e.g., –0.01.

For a pitch coefficient C_P, there is an aerodynamic pitch moment

$$M_{AeP} = \tfrac{1}{2} \rho V^2 S L C_P$$

and a consequent longitudinal load transfer

$$F_{TX} = \frac{M_{AeP}}{L} = \tfrac{1}{2} \rho V^2 S C_P$$

This changes the wheel vertical reactions:

$$\frac{F_{Vf}}{F_{Vf0}} = 1 - \frac{\rho V^2 S L C_P}{2mbg}$$

The maximum lateral acceleration at the front is then given by

$$\frac{A_\mathrm{f}}{A_\mathrm{f0}} = \left[1 - \left(\frac{\rho V^2 SLC_\mathrm{P}}{2mbg}\right)\right]^{1+p}$$

$$\approx 1 - \frac{(1+p)\rho V^2 SLC_\mathrm{P}}{2mbg}$$

$$\frac{\Delta A_\mathrm{f}}{A_\mathrm{f0}} \approx -(1+p)\frac{\rho V^2 SLC_\mathrm{P}}{2mbg}$$

$$\frac{\Delta A_\mathrm{r}}{A_\mathrm{r0}} \approx +(1+p)\frac{\rho V^2 SLC_\mathrm{P}}{2mag}$$

For a final understeer vehicle it will be A_f that controls A_M, giving a reduction of 0.32 m/s^2 for the example case.

$$\Delta N_\mathrm{U} = \frac{\Delta A_\mathrm{r}}{A_\mathrm{r0}} - \frac{\Delta A_\mathrm{f}}{A_\mathrm{f0}}$$

$$= \frac{(1+p)\rho V^2 SLC_\mathrm{P}}{2mg}\left(\frac{1}{a} + \frac{1}{b}\right)$$

This is about 0.08 for $C_\mathrm{P} = 0.1$, and hence aerodynamic pitch may exert a substantial effect on final balance.

The aerodynamic drag combines with the tire drag to require traction. The total drag force is the sum of aerodynamics, tire cornering and rolling resistance:

$$F_\mathrm{D} = F_\mathrm{DAe} + F_\mathrm{DT} + F_\mathrm{DR}$$

$$\approx \tfrac{1}{2}\rho V^2 SC_\mathrm{D} + mA\sin\alpha + \mu_\mathrm{R} mg$$

The tractive coefficient, assuming rear drive, is

$$f_\mathrm{T} = \frac{F_\mathrm{D}}{m_\mathrm{r} g}$$

Using the friction ellipse model, the limiting lateral acceleration is given by

$$\frac{A_T}{A_{T0}} = \sqrt{1 - \left(\frac{f_T}{\mu_L}\right)^2}$$

Rather unrealistically, assuming that sufficient engine power is available to sustain steady-state limit cornering at 50 m/s, with a mean α of 10°, this evaluates to $\Delta A_T = 0.32$ m/s^2 for the tires alone, and $\Delta A_T = 0.76$ m/s^2 for the total drag, i.e., an increment of 0.44 m/s^2 for the aerodynamic drag when added to the existing tire drag. For rear drive and terminal understeer this will have little effect on A_M, and give N_U an increment of -0.06. For final understeer front drive, A_M will be reduced and the final understeer number increment will be positive, i.e., greater understeer.

Considering now the aerodynamic side force, and taking $\beta_{Ae} = \beta$, the side force is F_{AeS} giving an extra lateral acceleration

$$\Delta A_M = \frac{F_{AeS}}{m} = \frac{\rho V^2 S C'_S \beta}{2m}$$

For $C'_S = 0.04$/deg and a final β of 6° this gives $\Delta A_M \approx 0.55$ m/s^2 at 50 m/s, a useful increase of about 7%.

By definition of the standard aerodynamic axes at the wheelbase mid-point, the side forces are equally distributed at the front and rear axles. Hence the change of N_U is given by

$$\Delta N_U = \frac{F_{AeS} L}{2 m A_f}\left(\frac{1}{a} - \frac{1}{b}\right)$$

having a value of typically +0.03 at 50 m/s for a center of mass 5% forward of the mid-point.

Considering now the yaw moment M_{AeY}, for positive yaw coefficient this is a turn-in moment, i.e., an oversteer tendency. The moment changes the required steady-state force at each axle by M_{AeY}/L, giving a limit acceleration increment

$$\Delta A_{\mathrm{f}} = \frac{M_{\mathrm{AeY}}}{Lm_{\mathrm{f}}} = \frac{\rho V^2 SLC'_{\mathrm{Y}}\beta}{2mb}$$

$$\Delta A_{\mathrm{r}} = -\frac{M_{\mathrm{AeY}}}{Lm_{\mathrm{r}}} = -\frac{\rho V^2 SLC'_{\mathrm{Y}}\beta}{2ma}$$

This effect assists the front, and so for terminal understeer there is an improvement in A_{M} of typically about 0.3 m/s^2 (3%) for $C'_{\mathrm{Y}} = 0.01$/deg and $\beta = 6°$.

$$\Delta N_{\mathrm{U}} = \frac{\Delta A_{\mathrm{r}} - \Delta A_{\mathrm{f}}}{A_{\mathrm{f}}}$$

$$\approx -\frac{\rho V^2 SLC'_{\mathrm{Y}}\beta}{2mA_{\mathrm{M}}}\left(\frac{1}{a} + \frac{1}{b}\right)$$

This evaluates to about −0.07 for the example case, illustrating that there may be a substantial oversteer effect from yaw.

Considering broadly the above developments, and Table 6.15.1, it is apparent that at high speed the aerodynamic effects on maximum lateral acceleration may be substantial. The total effect on understeer number for this example is small, but the effect will vary considerably from one car to another because of different aerodynamic coefficients, especially for yaw, lift and pitch. At the basic test radius of 33 m the limiting speed is only about 16 m/s, giving effects only about one-tenth of those of Table 6.15.1; in this case the aerodynamic contribution would usually be negligible, although it is possible that a combination of a strong nose down pitch (negative C_{P}) and positive yaw could become significant. In practice, the minimization of drag does not severely interfere with the trimming of pitch or control of lift, although low-drag vehicles tend to have high yaw coefficients. The oversteer tendency of yaw can be offset by some pitch-up, as can rear-drive effects. On the whole, it is desirable for a vehicle to have greater primary and final understeer at high speed and so some net aerodynamic understeer is preferable. Within legal speed limits such effects remain fairly modest, and unsteady-state problems tend to be more problematic, e.g., wind gust response.

In some of the fields of competition vehicles, aerodynamic effects have become of major importance because of bodywork optimization and higher speeds, as discussed in Section 3.6. Downforce from wings and underbody flow is used to greatly enhance maximum lateral acceleration and traction. To maintain good handling, the position of the center of pressure on the wheelbase, i.e., the front and rear distribution of downforce, must be carefully controlled by adjustment of underbody shape, or by trimming the wing incidences or wing flaps, or even by adjusting the wheelbase by moving the front wheels forward or backward. The optimum position for the total downforce is not simply at the center of mass, but usually farther forward; possibly this is because the smaller front tires have a maximum side force coefficient that diminishes with load more rapidly than the larger rear tires.

For wings, the induced drag increases as the square of the downforce coefficient, so the downforce/drag ratio of a wing deteriorates rapidly as greater downforce is demanded, although because of the irreducible zero-lift drag it may improve for the complete vehicle. Hence the downforce must be optimized, not simply maximized. This optimum depends on the particular circuit, with high mean speeds or long straights tending to favor less downforce and less drag. Of course it is desirable to have minimum drag for given downforce, and venturi underbodies with sealed skirts are much superior to separate wings in this respect.

6.16 Path Radius

Turning radius affects the understeer gradient at small radii. Because the front wheels are (usually) steered, considering a simple bicycle model the moment arm to G for the front tire side force is reduced from a to

$$a' = a \cos\delta_{\mathrm{K}}$$

neglecting the small understeer angle. Hence to preserve moment equilibrium about G, a larger front side force is needed than would otherwise be the case. Compared with the large radius turn, the increase of front slip angle is given by

$$\begin{aligned}\frac{\Delta\alpha_{\mathrm{f}}}{\alpha_{\mathrm{f}}} &= 1 - \cos\delta_{\mathrm{K}} \\ &\approx \frac{1}{2}\left(\frac{L}{R}\right)^2\end{aligned}$$

The effect on steer angle is

$$\Delta\delta = \Delta\alpha_{\mathrm{f}} = \frac{1}{2}\left(\frac{L}{R}\right)^2 \alpha_{\mathrm{f}}$$

$$\Delta k = \frac{\Delta\delta}{A} = \frac{1}{2}\left(\frac{L}{R}\right)^2 D_{\mathrm{f}}$$

This is insignificant at 33 m, but may be as high as 2 deg/*g* at 5 m radius.

For a vehicle with parallel steering (zero Ackermann factor), in a corner the front wheels each have an effective toe-in relative to the direction of travel for low speed of

$$\alpha_{\mathrm{i}} = \frac{T\sin\delta}{2R} \approx \frac{TL}{2R^2}$$

The side force is generally produced more by the outer wheel. Defining a side force transfer factor e_{S}, where $e_{\mathrm{S}} = 0$ represents equal side forces, and $e_{\mathrm{S}} = 1$ represents all force from the outer wheel, then a changed steer angle is required:

$$\Delta\delta = -e_{\mathrm{S}}\alpha_{\mathrm{i}}$$

giving

$$\Delta k_{\mathrm{U}} = -\frac{\mathrm{d}e_{\mathrm{S}}}{\mathrm{d}A}\frac{TL}{2R^2}$$

This is small for 33 m radius, but may be –4 deg/*g* at 5 m radius.

Considering now the effect of radius on final handling, the turning radius affects the understeer number in two main ways: the steering results in a negative attitude angle (front steering) and also in a reduced moment arm for the tire forces on the steered wheels. In addition there may be effects because of cambering of the wheels at large steer angles, but this is hard to quantify because of lack of tire data.

The attitude angles at the center of mass G and at the rear axle differ by the rear kinematic steer angle

$$\delta_{\mathrm{Kr}} = b/R$$

This reduces the attitude angle at G caused by the rear slip angle, which has already been dealt with in Section 6.12. It gives a longitudinal load transfer

$$F_{\mathrm{TX}} = -\frac{mAH\delta_{\mathrm{Kr}}}{L}$$

Adapting the equation derived for slip attitude effects (Section 6.12),

$$\begin{aligned}\Delta N_{\mathrm{U}} &= -(1+p)\left(\frac{AH\delta_{\mathrm{Kr}}}{g}\right)\left(\frac{1}{a}+\frac{1}{b}\right)\\ &= -(1+p)\left(\frac{AH}{Rg}\right)\left(\frac{b}{a}+1\right)\end{aligned}$$

which is an oversteer effect.

Figure 6.16.1 shows a four-wheeled vehicle with steer and slip angles and traction at the rear. The front vertical force lateral transfer factor e_{Vf} results in a front side force transfer factor e_{Sf}. The parameter e_{Sf} is zero for equal side forces

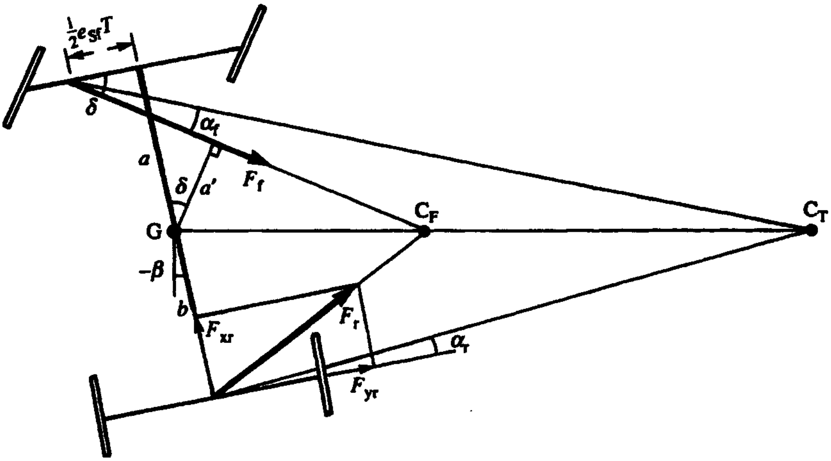
$\frac{1}{2}e_{\mathrm{Sf}}T$
δ
α_{f}
a
δ
a'
F_{f}
$\mathrm{C_F}$
$\mathrm{C_T}$
G
$-\beta$
b
F_{xr}
F_{r}
α_{r}
F_{yr}

Figure 6.16.1. Reduced moment arm of steered-wheel forces.

and unity for all side force on the outer wheel. The moment arm of the front side force is

$$a' = a\cos\delta - \tfrac{1}{2}e_{\mathrm{Sf}}T\sin\delta$$

This causes

$$\begin{aligned}\Delta N_{\mathrm{U}} &= \frac{a-a'}{a'} = \frac{a}{a'} - 1\\ &= \left(\cos\delta - \frac{e_{\mathrm{Sf}}T}{2a}\sin\delta\right)^{-1} - 1\end{aligned}$$

The total radius effect including longitudinal load transfer is therefore

$$\Delta N_{\mathrm{U}} = \left(\cos\delta - \frac{e_{\mathrm{Sf}}T}{2a}\sin\delta\right)^{-1} - 1 - (1+p)\left(\frac{AH}{Rg}\right)\left(\frac{b}{a}+1\right)$$

At a small radius the reduced moment arm effect predominates, and there is a strong understeer tendency

6.17 Banking

Road slopes can be divided into two main types: longitudinal and lateral. Lateral slopes are commonly known as banking, or just as camber in the case of modest slopes used for water drainage. On the straight, banking results in a side force component $mg\sin\theta$ where θ is the road angle. The tire vertical reaction becomes $mg\cos\theta$ which can be approximated as mg for practical camber cases up to 8°. For a primary neutral vehicle, the lateral force at G can be opposed by equal slip angles at the two ends, so the vehicle will drift sideways without rotation, Figure 6.17.1(a). With no control steer change, an understeering vehicle will tend to generate less lateral acceleration at the front, and so will rotate away from the side force, turning down the slope, Figure 6.17.1(b). An oversteer vehicle will initially drift away but will ultimately turn up the slope, Figure 6.17.1(c), because less lateral acceleration is generated at the rear.

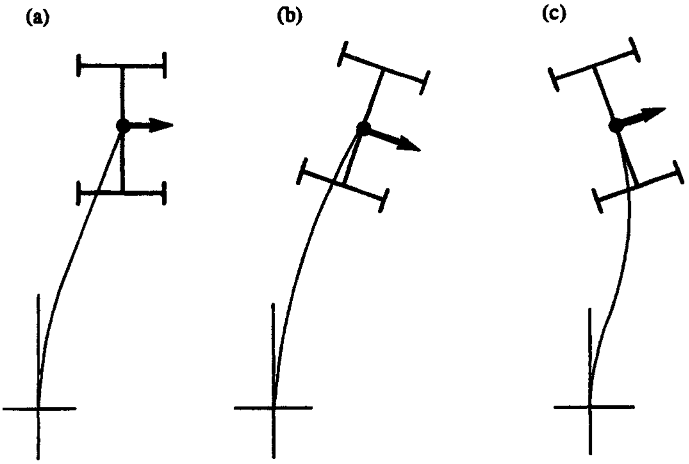

Figure 6.17.1. Effect of side force at G (e.g., on entry to road camber section): (a) neutral steer, (b) understeer, (c) oversteer.

To maintain a straight path in the steady state, the side force acting at G calls for slip angles, but no kinematic steer angle:

$$\alpha_f = \frac{mgb}{2LC_{\alpha f}} \sin\theta$$

$$\alpha_r = \frac{mga}{2LC_{\alpha r}} \sin\theta$$

Allowing for suspension effects using cornering compliance, the attitude angle is

$$\beta = D_r g \sin\theta$$

and the steer angle required is

$$\delta = (D_f - D_r)\, g \sin\theta = k_U\, g \sin\theta$$

where k is the primary understeer gradient. Thus a neutral steer vehicle will be in equilibrium at an attitude angle but zero steer angle. A primary understeer vehicle will need to be steered up the slope, and an oversteer vehicle down it. At the fairly large value of $k_U = 0.5$ deg/m s^{-2} (5 deg/g) and a side slope of 5°, then $\delta = 0.44°$, or about 8° at the steering wheel, and $\beta \approx 0.5°$.

A straight road of banking θ will require a lateral friction coefficient of $\tan\theta$ merely to maintain a straight path. This may be difficult to achieve in icy conditions.

A small amount of banking is also common on corners, and this may be favorable or unfavorable. More extreme banking, sometimes called super-elevation and with angles as great as 40° (Figure 6.17.2), is found on some racing circuits and on high-speed test circuits. In such cases the road cross-section is usually curved with greater angles high up, so that the driver can choose the desired banking angle.

In Figure 6.17.2, a vehicle is cornering with lateral acceleration $A = V^2/R$ at constant height on a banked road. The tire forces required are

$$F = mA\cos\theta - mg\sin\theta$$
$$N = mA\sin\theta + mg\cos\theta$$

The mean required tire cornering coefficient is

$$C_Y = \frac{F}{N} = \frac{A\cos\theta - g\sin\theta}{A\sin\theta + g\cos\theta}$$

Setting F to zero, no tire lateral force will be required if the slope angle is

$$\theta_0 = \arctan\frac{V^2}{Rg}$$

and this condition may actually be achieved on super-elevated circuits. In this case the normal reaction is greatly increased to $mg/\cos\theta$. This is liable to bring a conventional vehicle down onto its bump stops. Vehicles designed for such conditions generally have very stiff or rising-rate suspensions, and appropriately uprated tires.

With a maximum lateral force coefficient μ_Y, the maximum speed on banking is given by

$$V^2 = \mu_Y gR \frac{1 + \dfrac{\tan\theta}{\mu_Y}}{1 - \mu_Y\tan\theta}$$

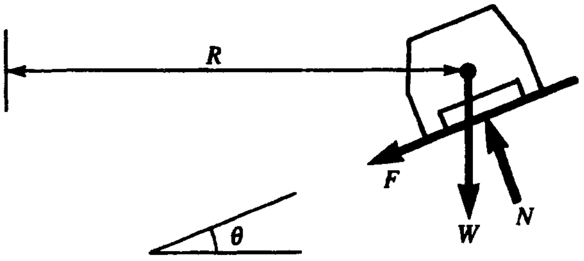

Figure 6.17.2. Free-body diagram for a car on a super-elevated corner.

compared with $V^2 = \mu_Y g R$ on the level.

Even small cambers can be significant with low friction. On ice, taking the maximum lateral force coefficient μ_Y as 0.1, with 5° camber the speed is increased 38% for favorable camber, and reduced 65% for adverse camber. At $\mu_Y = 1$, the changes are +9% and –9%.

Front-to-rear differences of maximum lateral force friction sensitivity p would imply some final handling variation on banking, but this is normally unimportant because the required side force coefficients are generally small. However, there may still be significant changes of primary handling.

6.18 Hills

On longitudinal slopes, uphill at an angle of θ (Figure 6.18.1), at steady speed, there is a front-to-rear load transfer. The axle reactions are

$$N_f = \frac{mgb}{L}\cos\theta - \frac{mgH}{L}\sin\theta$$

$$N_r = \frac{mga}{L}\cos\theta + \frac{mgH}{L}\sin\theta$$

When driving uphill, the load transfer to the rear leads to increased primary understeer and reduced attitude coefficient, but these are not large effects; for example, at 1 in 5 (12°) uphill Δk_β is 0.25 deg/g and Δk is 0.5 deg/g, and the opposite (negative values) downhill. The effect on final handling is more important:

$$\frac{A_f}{A_{f0}} = \frac{\mu_{Cf} N_f}{\mu_{C0} N_{f0}} = \left(\frac{N_f}{N_{f0}}\right)^{1+p}$$

$$= \left(1 - \frac{H}{b}\tan\theta\right)^{1+p}$$

$$\approx 1 - (1+p)\frac{H}{b}\tan\theta$$

$$\frac{A_r}{A_{r0}} \approx 1 + (1+p)\frac{H}{a}\tan\theta$$

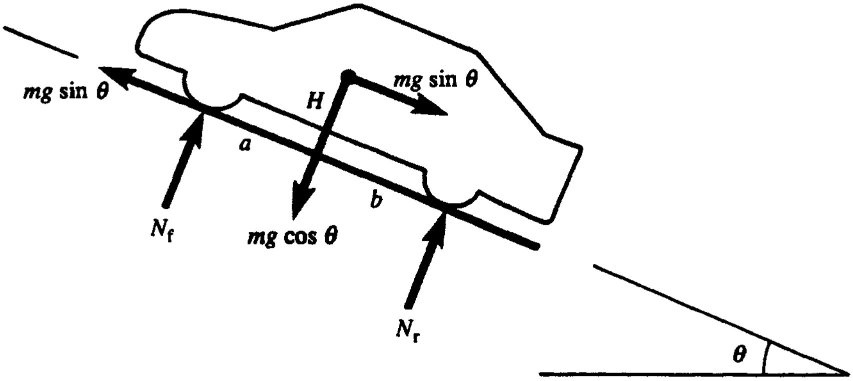
mg sin θ
mg sin θ
H
a
b
N_f
mg cos θ
N_r
θ

Figure 6.18.1. Free-body diagram for a car driving uphill at constant speed, no aerodynamic forces.

For a vehicle which is initially neutral on level ground, for small θ,

$$\begin{aligned}\Delta N_{\mathrm{U}} &= \frac{A_{\mathrm{r}}}{A_{\mathrm{f}}} - 1 \\ &\approx \left(1 + (1+p)\frac{H}{a}\theta\right)\left(1 - (1+p)\frac{H}{b}\theta\right)^{-1} - 1 \\ &\approx (1+p)H\theta\left(\frac{1}{a} + \frac{1}{b}\right)\end{aligned}$$

For $a \approx b \approx L/2$

$$\Delta N_{\mathrm{U}} = 2(1+p)\frac{H\theta}{L}$$

$$\frac{\mathrm{d}N_{\mathrm{U}}}{\mathrm{d}\theta} = 2(1+p)\frac{H}{L}$$

This is about 0.34/rad or 0.006/deg. For 1 in 5 uphill (12°) ΔN_{U} is +0.07, a substantial final understeer effect. Downhill ΔN_{U} is −0.07 which is a readily noticeable effect, and may in some cases change final understeer into final oversteer.

Examining now vertical curves, these are not strictly steady-state but may be analyzed approximately as such. In the vehicle-fixed coordinate system the vehicle has a vertical downward compensation (pseudo) force

$$F_{\mathrm{V}} = \frac{mV^2}{R_{\mathrm{V}}}$$

where R_{V} is the vertical radius of curvature; F_{V} is positive downward for a positive R_{V} which therefore corresponds to a center of curvature above the road, i.e., a trough. Thus tire reaction forces are increased in a trough and reduced over a crest. The main practical consequences are a deterioration of braking and cornering capability over a crest.

6.19 Loading

Adding loads such as passengers, luggage or fuel to a vehicle increases the total mass and moves the center of mass. Usually this movement is rearward and upward; in some cases it may be forward, as in the case of rear engine and front trunk. A higher center of mass means more load transfer and roll. A larger weight increases the suspension deflection, affecting camber and load transfer. Front-to-rear movement of the center of mass affects the relative tire characteristics. This can have complex effects on the handling, and in general it is necessary to analyze the loaded case quite independently of the unloaded case. Of course this is especially true of trucks and commercial vehicles where the load is a large proportion of the unladen weight.

For cars the total maximum load is likely to be about 40% of the curb weight. The driver and front passenger are close to the initial center of mass and so cause little G movement. The rear passengers are usually in front of the rear axle, and for a rear trunk the load is behind the rear axle. Hence a simple indication of the effect of loading on a typical car may be obtained by studying the case of a load m_{ar} added over the rear axle. In any case, an added load may be analyzed as load increments over the two axles.

At the rear the vertical reaction changes in the ratio

$$\begin{aligned}\frac{F_V}{F_{V0}} &= \frac{m_r + m_{ar}}{m_r} \\ &= 1 + \frac{m_{ar}L}{ma}\end{aligned}$$

Denoting the tire cornering coefficient sensitivity to F_V as f then

$$\frac{C_\alpha}{C_{\alpha 0}} = \left(1 + \frac{m_{ar}L}{ma}\right)^f$$

Neglecting suspension, the rear cornering compliance is then given by

$$\begin{aligned}\frac{D_r}{D_{r0}} &\approx \frac{(m_r + m_{ar})/C_\alpha}{m_r/C_{\alpha 0}} \\ &= \left(1 + \frac{m_{ar}L}{ma}\right)^{1-f}\end{aligned}$$

With $m_{ar} = 0.2$ m ($0.4m_r$) and $f = 0.5$, then ΔD_r is 1.1 deg/g. This is an increase of the attitude gradient, and there is also an equal primary oversteer tendency effect, i.e., Δk_U is -1.1 deg/g.

The effect on final handling depends mainly on the reduced rear lateral acceleration limit because of the tire maximum cornering coefficient sensitivity p. At the rear

$$\frac{\mu_Y F_V}{\mu_{Y0} F_{V0}} = \left(1 + \frac{m_{ar} L}{ma}\right)^{1+p}$$

$$\frac{\mu_Y F_V}{m_r + m_{ar}} \, \frac{m_r}{\mu_{Y0} F_{V0}} = \left(1 + \frac{m_{ar} L}{ma}\right)^{p}$$

$$\Delta N_U \approx \frac{p m_{ar} L}{ma}$$

Because p is negative this is an oversteer effect. The equivalent expression for a load increment at the front is

$$\Delta N_U = -\frac{p m_{af} L}{ma}$$

Taking $m_{ar}/m = 0.2$ and $p = -0.15$, this gives $\Delta N_U = -0.06$, a substantial final oversteer tendency. This neglects other possible factors, such as greater rear load transfer because of lowering of the rear suspension toward the bump stops.

The above simple analysis shows how rear loading can result in substantial primary and final oversteer tendencies; these are readily observable in practice. It is common practice for vehicle operating manuals to call for increased rear tire pressures when operating with full load. This limits tire deflections but also generally increases C_α helping to offset the primary oversteer effect, and generally also improves the tire maximum cornering force coefficient with the increased load, helping to offset the final oversteer tendency.

In the case of racing cars with substantial aerodynamic downforce, there may be great sensitivity to changes of mass and to center-of-mass position. Considering first the simplest possible model vehicle (Section 6.15) with no aerodynamics, a mass increase will increase the tire normal forces in proportion, and the maximum lateral acceleration will deteriorate according to the reduction in maximum cornering force coefficient, i.e., it will be directly dependent on the friction sensitivity p. On the other hand, for a vehicle with very large aerodynamic downforce, the maximum lateral acceleration will be inversely proportional to the mass, because the normal forces will not be affected proportionally by a weight change.

The effect of movement of the center of mass on the final balance of a racing car follows a similar pattern. With no aerodynamics, moving the center of mass forward will reduce the front cornering friction and increase it at the rear, according to the sensitivity p. However, with strong downforce, a movement of the center of mass will have much more dramatic effects because the normal forces and maximum cornering forces will hardly be affected. This is one reason for the location of fuel tanks close to the center of mass on downforce racing vehicles, to avoid trim changes as fuel is consumed.

6.20 Wind

In straight running a vehicle may be subject to a side wind, giving a side force and a yaw moment. To maintain the required course an attitude angle and steer angle will be required.

Given the wind speed and direction and the vehicle speed and direction, the relative wind speed V_r and aerodynamic attitude angle β_{Ae} can be calculated (Section 3.4). The resulting dynamic air pressure is

$$q = \frac{1}{2}\rho V_r^2$$

and the side force is

$$F_{AeS} = qC_S S$$

and the yaw moment is

$$M_{AeY} = qC_Y Sl$$

To maintain the required straight course the forces needed at the front and rear axles are

$$F_f = q(C_S + C_Y)S$$
$$F_r = q(C_S - C_Y)S$$

Although there is generally some small aerodynamic roll, the vehicle does not roll as for cornering, so the resulting attitude angle does not depend significantly on the roll steer. On the other hand, suspension compliance may have an effect. But neglecting suspension effects,

$$\Delta\alpha_f = \frac{F_f}{2C_{\alpha f}} \quad \text{and} \quad \Delta\alpha_r = \frac{F_r}{2C_{\alpha r}}$$

Hence the aerodynamic attitude angle is

$$\beta_{Ae} = \alpha_r = \frac{q(C_S - C_Y)S}{2C_{\alpha r}}$$

and the steer angle required toward the wind is

$$\delta = \frac{q(C_S + C_Y)S}{2C_{\alpha f}} - \frac{q(C_S - C_Y)S}{2C_{\alpha r}}$$

$$\delta = \frac{1}{2}qS\left(\frac{C_S + C_Y}{C_{\alpha f}} - \frac{C_S - C_Y}{C_{\alpha r}}\right)$$

From this, the crosswind steer correction coefficient dδ/dw may be found:

$$k_W = \frac{d\delta}{dw} = \frac{1}{2}\rho V\left(\frac{C'_S + C'_Y}{C_{\alpha f}} - \frac{C'_S - C'_Y}{C_{\alpha r}}\right)$$

which may be seen to increase in proportion to the vehicle speed.

For a pure side wind the steer angle is, for the linear case, proportional to $\beta_{Ae}V_r^2$. For a given wind speed, the steer angle increases with vehicle speed. Taking a case with a sidewind speed of 10 m/s and $S = 1.8$ m^2, a vehicle ground speed of 50 m/s gives $\beta_{Ae} = 11.3°$, and typically $C_S = 0.4$ and $C_Y = 0.1$, giving $F_r = 857$ N, $\alpha_r = 0.86°$, $F_f = 1428$ N, $\alpha_f = 1.43°$ and $\delta = 0.57°$. The actual steering wheel deflection will be some 10°. Hence the steady-state effects of wind are not very great. On the other hand, wind gusting is an important unsteady effect.

6.21 Testing

In principle the main result of testing is the path curvature $\rho = 1/R$ as a function of the control inputs δ and V. In practice the required steer input δ is usually plotted as a function of lateral acceleration A, as in Figure 1.13.1 for example. The steer angle is measured at the steering wheel and in some cases also at the road wheels. The lateral acceleration may be found by accelerometer, or from $A = \Omega V$ with a rate gyro measuring the angular speed, or from $A = V^2/R$.

There are three basic forms of the test. These are constant radius, constant speed and constant steer angle, although of course for a full picture of the handling characteristic it is necessary to use a succession of different constant values.

The most common test is the constant radius one, where the speed is varied and the associated required steer angle measured, plus other variables such as attitude angle. The radius chosen is likely to be around 30 m depending on available facilities, but may be 100 m or more if it desired to include aerodynamic effects, if the vehicle has sufficient power, and if a suitable test facility is available. At 33 m the steering kinematic steer angle is only about 5°, thus avoiding extreme steering geometry effects, while for $A = 8$ m/s^2 the speed is 16 m/s, so aerodynamics are usually negligible; hence 33 m radius gives a good reference characteristic. In practice, for a constant-radius test the driver is required to follow a paint line while at the same time keeping the control positions constant; this may be difficult near the limit conditions because of reduced or exaggerated steering response.

In the constant-speed type of test the vehicle is usually tested at various specific radii, and the steer angle, attitude angle, etc., observed. When the steer angle is plotted against lateral acceleration at constant speed, rather than at constant radius, then the kinematic steer angle varies. In this case the understeer coefficient is no longer $\mathrm{d}\delta/\mathrm{d}A$, but it is still $\mathrm{d}\delta_U/\mathrm{d}A$. This is discussed in Section 6.9. An advantage of the constant-speed test is that this is a more realistic representation insofar as aerodynamic effects are concerned. The constant speed is no easier for the driver because the differing lateral accelerations give different tire drags and require different throttle settings.

In the third type of steady-state test, the steer angle is held constant, and a sequence of steady speeds used. This test is the easiest to perform as far as driver skill is concerned because both controls are fixed. It is possible to use a varying speed, but the variation must be fairly slow or else the tractive forces will be sufficiently far from equilibrium to influence the results.

In practice the constant-radius test is most commonly used. For large radii a sufficiently large test pad may not be available, and curved tracks may be used, such as the Dunlop–MIRA handling circuit with its variety of radii of sufficient length to allow steady state to be achieved.

Some description of instrumentation is given in Section 1.13, along with a broader description of testing.

The international standard for steady-state testing is ISO 4138 *Road Vehicles – Steady State Circular Test Procedure*. This requires a constant-radius test, with no particular radius specified other than a minimum of 30 m. The track gradient may not exceed 2%, and the wind speed may not exceed 7 m/s. Tires should preferably be conditioned by normal use for 150–200 km, and warmed-up at the time of test by driving 500 m at a lateral acceleration of 3 $\mathrm{m/s^2}$. Data should be taken at increments not exceeding 0.5 $\mathrm{m/s^2}$, and averaged over 3 s, and the path should be maintained within 0.3 m. The recommended form of presentation of results is separate graphs of steering wheel angle, sideslip angle, roll angle and steering wheel torque, each against lateral acceleration with right turn considered positive lateral acceleration and left turn negative.

The following derived parameters and notation are defined:

(1) steering wheel angle gradient $k_{\delta S} = \mathrm{d}\delta_S/\mathrm{d}A$

(2) sideslip angle gradient $k_\beta = \mathrm{d}\beta/\mathrm{d}A$

(3) roll angle gradient $k_\phi = \mathrm{d}\phi/\mathrm{d}A$

(4) steering wheel torque gradient $k_{TS} = \mathrm{d}T_S/\mathrm{d}A$

(5) steering wheel angle/sideslip gradient $\mathrm{d}\delta_S/\mathrm{d}\beta$

Various normalized parameters are also defined, including:

(1) understeer sideslip gradient $\delta_S/(G\mathrm{d}\beta/\mathrm{d}A)$

(2) steer coefficient $(\mathrm{d}\delta_S/\mathrm{d}A)/GL$

(3) directional coefficient $(\mathrm{d}\delta_S/\mathrm{d}\beta)/GL$

Testing can also be performed by operating the vehicle on a complete chassis handling dynamometer. One such testing system has actually been built, and is described by Odier (1972). There have been other design studies for such systems, including incorporation into a wind tunnel.

6.22 Moment Method

Figure 6.22.1 shows an example plot of total moment coefficient against lateral force coefficient; the vehicle behavior is represented by a carpet plot for various values of steering wheel angle and attitude angle. Here the vehicle is considered to be traveling in a straight line with no lateral or rotational acceleration, i.e., the force and moment are considered balanced by applied external forces. This can be achieved experimentally, but in practice such plots are produced by computer simulation. Also shown are front and rear "construction lines." The front construction line is the locus of points with lateral force at the front axle only. The $\beta = 0$ line diverges from this because of effects such as roll steer. These lines have gradient a/L and $-b/L$, or just a and $-b$ if the plot is of force F_y and moment M_z instead of coefficients F_y/mg and M_z/mgL.

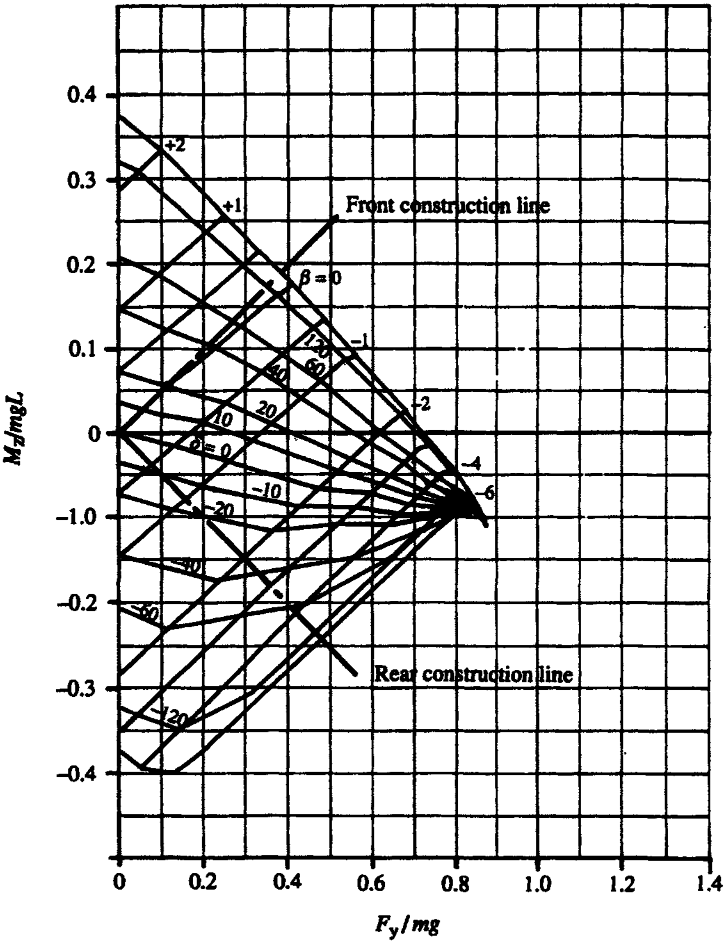

Figure 6.22.1. Moment-method carpet plot.

Considering any particular point, this corresponds to some specific value of moment and force which may be read from the axes. Constructing a parallelogram to the construction lines shows the corresponding front and rear lateral forces. The mesh lines of the carpet plot will show the particular δ_s and β that will give the specified force and moment; usually the values are unique except close to limit conditions. The steer angle derived from this diagram is the understeer angle only; the kinematic steer angle must be considered separately. Actually the exact shape of the diagram will depend on an assumed speed because of the effect on aerodynamics and tires, and of tractive forces. In other words, there are different diagrams for different speeds.

For a given operating point of the diagram, the force and moment may be assigned in various ways, e.g., to oppose applied wind effects, or to maintain a straight course on a camber, or to give accelerations.

The usual definition of steady-state cornering implies zero angular acceleration, and therefore corresponds to points of the mesh lying on the zero-moment line, and with lateral force assigned to producing lateral acceleration. Thus by reading δ and β points from that axis it is possible, although somewhat roughly in practice, to construct the conventional steady-state handling curves of δ and β against A. From Figure 6.22.1, the maximum trimmed lateral acceleration is about $0.73g$, and this occurs with saturation of the front side force rather than the rear, i.e., this vehicle has final understeer.

Evidently the force–moment diagram contains much more information than the usual handling curves which correspond to the force axis points only. On the other hand, the usual handling curves are a clearer representation of their particular state, especially near the limit conditions where there may be overlapping of the δ lines of the mesh. The force–moment diagram is still not a complete representation, but does provide a "portrait" of the vehicle behavior that, to an experienced eye, is very revealing.

6.23 Desirable Results

The essential point of handling theory is to facilitate the design and production of better handling vehicles. An important question, then, is: What is the optimum form of the handling diagram curves? One difficulty here, as discussed in Section 1.12, is that small design changes that have little effect on the theoretical behavior of the vehicle may be strongly noticeable to the driver, and make the difference between good and bad driver-feel, especially dynamically. Furthermore, because handling is so subjective, there are differences of opinion regarding the best behavior. There is therefore scope for disagreement with the following comments. Also, of course, handling cannot in practice be optimized without consideration of other factors such as ride.

For the steering angle versus lateral acceleration curve, the initial slope, i.e., the initial understeer gradient, should be between –1 and +5 deg/*g* at the road wheels. American practice is generally to use the higher values, e.g., 2 to 5 deg/*g*, with European values tending to be lower, e.g., 1 to 3 deg/*g*, with European sports cars sometimes even lower and near neutral at –1 to +1 deg/*g*. Obviously the best understeer gradient depends on driver preference and experience, and very much on the predominant nature of the roads, winding or straight. The graph should then curve smoothly through gradually increasing understeer in the mid-range into final understeer, with a final understeer number of about 0.20. The argument for final understeer is that steering control should be progressive, and not reverse as it does if there is final oversteer. As far as the maximum lateral acceleration is concerned, the greater the better. If a vehicle with final oversteer is altered at the front to reduce the front acceleration ability then the final controllability is improved, but only at the expense of the overall maximum lateral acceleration, so the result is not necessarily a safer vehicle.

For the attitude angle graph, the initial slope, i.e., the attitude gradient or coefficient, should be as small as possible; this mainly depends on the rear tire cornering stiffness. The roll curve is not critical. However, all three curves should be smooth with no irregularities or sharp changes of gradient. Even if power steering is used, it is possibly best to have a steering torque gradient of about 20 Nm/*g*, rather than extremely light steering (position control only). Driver preferences depend to a large extent on previous experience. The actual value of the steering torque gradient is perhaps not as important as the fact that there should be a gradient. Traditional practice in the US, still seen on some European vehicles for the U.S. market, is to have a steep gradient for lateral acceleration up to 0.1*g*, and then zero gradient. Typical European practice is to mimic a manual system, but at lower force levels.

The handling of passenger cars has steadily improved over the last thirty years, and is now generally good. On the other hand, commercial vehicles tend to be rather poor with low limit accelerations and final oversteer. Basically this is because of the low performance limit at the rear because of high loads, and hard tire materials to give good mileage. There are also rollover limitations because of the high center of mass. From a handling point of view, the best solution is a sufficient number of rear wheels and good enough tires to give a rear limit performance close to the roll limit, with a slightly inferior front-end performance to give final understeer without rollover. This is, however, complicated by the proneness of commercial vehicles to dynamic rollover in swerving.

As far as the process of tuning the suspension is concerned, this is basically a matter of achieving the desired understeer gradient and final understeer number. The parameters that the designer can usefully influence have been discussed in some detail in Sections 6.10 and 6.12.

6.24 Problems

Q 6.1.1	Describe the relative merits of various definitions of steady-state vehicle motion.
Q 6.2.1	Give an account of the relative merits of various choices of control parameters.
Q 6.2.2	List, define and explain the steady-state vehicle motion parameters, and any simple relationships between them.
Q 6.2.3	Give the principal alternative units used for the vehicle controls, responses and gains.
Q 6.3.1	Explain, with graphs, how the handling characteristic curves of a simple vehicle can be deduced from the tire force curves.
Q 6.3.2	Define and explain the relationship between steer angle δ, kinematic steer angle, geometric steer angle, Ackermann angle, dynamic steer angle and understeer angle.
Q 6.3.3	Describe the possible shapes of the steer angle curve, as related to the shape and relative position of the tire force curves.
Q 6.3.4	Sketch handling steer curves for a typical modern car and truck, and explain their merits and drawbacks.
Q 6.3.5	Sketch steer curves for vehicles with primary secondary and final steer as follows: (a) under, over, over; (b) under, under, over; (c) over, over, under; (d) over, under, under; (e) under, over, under.
Q 6.4.1	Sketch plan-view free-body diagrams for a "bicycle model" vehicle in cornering without traction, and in steady cornering for front-, rear- and four-wheel drive. Explain them.
Q 6.4.2	Sketch simple plan-view force polygons for front- and rear-drive bicycle model vehicles. Extend them to include rolling resistance and aerodynamic forces.

Q 6.4.3 Draw the plan-view force diagram (as Figure 6.4.2) for rear drive at small *A* and small *R*.

Q 6.4.4 Draw the vehicle with forces (as Figure 6.4.1) for four-wheel drive, for the case with parallel front and rear forces. Discuss alternatives.

Q 6.5.1 Define and explain a linear handling vehicle. What practical conditions are covered?

Q 6.5.2 Define and explain characteristic speed and critical speed for the linear case. Derive equations for them.

Q 6.5.3 For the linear case, define and derive the response factor, also giving graphs, and derive expressions for curvature gain, yaw gain and acceleration gain.

Q 6.5.4 Discuss the problems that would be experienced in driving a linear oversteer vehicle at various speeds in a straight line.

Q 6.5.5 Derive an expression for the understeer gradient for a suspensionless bicycle model vehicle.

Q 6.6.1 Derive expressions for the yaw stiffness and static margin for a simple vehicle. Explain the neutral steer point and line.

Q 6.6.2 Derive an equation for k_U/x_s for a simple suspensionless vehicle.

Q 6.6.3 Explain yaw damping. Give a diagram and derive a suitable equation for a simple linear vehicle.

Q 6.6.4 Obtain an expression for $d\delta/d\beta$ for a simple suspensionless vehicle for steady cornering.

Q 6.7.1 Sketch three-dimensional graphs of understeer angle against speed and lateral acceleration, for a vehicle with primary understeer and final oversteer at low speed and strong aerodynamic understeer effects.

Q 6.8.1 For the nonlinear case, explain understeer angle and understeer gradient/coefficient.

Q 6.8.2 Explain how the idea of characteristic or critical speed can be applied to a nonlinear vehicle in a given trim state.

Q 6.8.3 Plot graphs showing how static margin and yaw damping typically depend on speed and lateral acceleration.

Q 6.9.1 Explain the difference between primary and final understeer.

Q 6.9.2 Describe the concept of understeer gradient for the nonlinear case.

Q 6.9.3 Derive and explain the kinematic steer angle gradient.

Q 6.9.4 Giving example graphs, show how the required steer angle is likely to vary with lateral acceleration at constant radius, and also at constant speed, for cars and for trucks. Explain which regions of the curves represent understeer and oversteer.

Q 6.9.5 Explain the difference between understeer angle and understeer gradient. Explain how a vehicle with positive understeer angle can simultaneously be "oversteer."

Q 6.10.1 Explain, with a diagram, the difference that suspension makes to the linear equation for steer angle.

Q 6.10.2 Give example values of the primary understeer effects, in a table, for a typical modern small front-drive front-wishbone rear plain trailing-arm car, and discuss it.

Q 6.10.3 Explain, with equations and graphs, the effect of G position on k_U and k_β for a vehicle with the same C_α for all tires, and then also for the case when C_α varies with load. Give example values.

Q 6.10.4 Explain the effect of suspension roll steer on primary handling, with equations, and give extreme and representative example values.

Q 6.10.5 Explain the effect of suspension camber on primary handling, with equations and give extreme and representative example values.

Q 6.10.6 Explain the effect of steering-column compliance on primary understeer.

Q 6.10.7 Explain the effect of tire pneumatic trail on primary handling.

Q 6.10.8 Explain the effect of rolling resistance on primary handling.

Q 6.10.9 Cars with lightly loaded rear axles are sensitive to rear toe angle. Explain the effect of front and rear toe on primary handling.

Q 6.10.10 Give an overview, in 1000 words, of the main factors affecting the primary understeer of a modern car.

Q 6.10.11 For an $a = b$ suspensionless vehicle with tire $C_S = 10/\text{rad}$, what are the values of k_U and k_β?

Q 6.10.12 For a suspensionless vehicle with $L = 2.8$ m, $a = 1.3$ m, $C_{\alpha f} = 520$ N/deg, $C_{\alpha r} = 480$ N/deg, $k_f = 9$ deg/g and $m = 1600$ kg, calculate k_U and k_β.

Q 6.10.13 For the vehicle of Q 6.10.12, with front and rear roll understeer coefficients of –0.1 and +0.3, and a roll gradient of 10 deg/g, calculate k_U and k_β.

Q 6.10.14 For the vehicle of Q 6.10.12, with no roll steer, but with front and rear roll camber coefficients of 0.8 and 0.1 and tire $C_\gamma/C_\alpha = 0.15$, calculate k_U and k_β.

Q 6.10.15 For the vehicle of Q 6.10.12, with pneumatic trail of 40 mm, $G = 16$, and a steering column compliance of 4 Nm/deg, compare understeer with respect to δ and δ_{ref}.

Q 6.10.16 For the vehicle of Q 6.10.15, evaluate the pneumatic trail on the rigid-body effect on k_U and k_β.

Q 6.10.17 For the vehicle of Q 6.10.12, with a rolling resistance of 0.03 and a G height of 1.1 m, what is the effect on k_U and k_β?

Q 6.10.18 For steering backlash $\pm\delta_b$ at the front wheels, obtain a simple expression for the range of lateral acceleration in terms of k_U and V. Evaluate this for 0.1° and $k = 0$, at 50 m/s. Find the time to veer 2 m.

Q 6.10.19 Explain the relationship between the lateral force compliance steer and the corresponding compliance steer coefficients η_{LCS} and η_{ACS}.

Q 6.10.20 Explain how the compliance camber gradient arises from compliance camber coefficients.

Q 6.10.21 Explain the effect of compliance camber on the total compliance steer gradient k_{CS}.

Q 6.10.22 Explain how the roll steer gradient k_{RS} is influenced by front and rear roll steer and the roll angle gradient, on a rigid axle.

Q 6.10.23 Explain how the roll steer gradient k_{RS} is influenced by bump steer and bump camber on an all-independent suspension vehicle.

Q 6.10.24 Explain the total roll steer gradient k_{RS} including an allowance for camber effects, and how it arises from roll steer and roll camber coefficients on a rigid axle.

Q 6.11.1 Give an overview of the main factors influencing secondary handling.

Q 6.11.2 Derive an equation representing the effect of longitudinal load transfer on steer angle for moderate A.

Q 6.12.1 Define and explain the term "final handling regime."

Q 6.12.2 Define and explain final understeer number. List the main factors controlling its value.

Q 6.12.3 Give a table showing typical values of N_U contributions to a modern car. Discuss it.

Q 6.12.4 Describe the likely process in a crash because of trying to round a corner too quickly, contrasting final understeer and final oversteer. Compare their merits.

Q 6.12.5 Explain how the effect of G position and tire friction effects influence N_U and A_M. Give an example graph of A_M against G position.

Q 6.12.6 Explain how the distribution of roll stiffness affects N_U.

Q 6.12.7 Compared with $a = b$ at which A_M is $0.8g$, if G is moved forward 120 mm on a wheelbase of 2.8 m, what would be the likely quantitative effect on A_f, A_r, A_M and N_U?

Q 6.12.8 With $p = -0.15$, $A = 0.7g$, $H = 0.8$ m, $T = 1.5$ m, $a = 1.25$ m and $L = 2.7$ m, what will be the effect on N_U of changing the front load transfer fraction d_f from 0.6 to 0.75?

Q 6.12.9 Explain how longitudinal load transfer arises in cornering, and how it affects N_U. Give example values.

Q 6.12.10 For the vehicle of Q 6.12.8, with a final attitude angle of 5.7° what will be the effect of longitudinal load transfer on N_U?

Q 6.12.11 Explain the effect of traction on final handling.

Q 6.12.12 Explain the effect of camber on tire forces and final handling.

Q 6.12.13 Explain the effect on primary, secondary and final handling of adding a stiff front anti-roll bar for vehicles with no roll steer and with

(a) considerable front roll camber, none at the rear,

(b) considerable rear roll camber, none at the front.

Q 6.13.1 Explain the effect of an overrun ratcheting differential on primary and final handling.

Q 6.13.2 Explain the effect on handling of a differential that apportions torque in proportion to tire normal force. Give example values.

Q 6.14.1 Give an overview of the effect of aerodynamics on primary handling.

Q 6.14.2 A rear-drive vehicle at 40 m/s has $S = 2\ \text{m}^2$, $a = 1.26$ m, $L = 2.8$ m, $m = 1500$ kg, tire cornering stiffness sensitivity $f = 0.5$, $D_f = 12$ deg/g, $D_r = 8$ deg/g, $C_{Lf} = 0.1$, $C_{Lr} = -0.2$, $C_D = 0.5$, $C'_S = 0.06$/deg, $C'_Y = 0.02$/deg, and $\mu_L = 0.7$. Evaluate the various aerodynamic effects on k_U.

Q 6.14.3 Give a detailed algebraic development of equations representing the effect of aerodynamic lift (or drag, etc.) on primary handling.

Q 6.15.1 Give a table listing the typical contributions to A_M and N_U for a modern car at maximum speed, and discuss it.

Q 6.15.2 For the vehicle of Q 6.14.2, with a final attitude angle of 7°, a maximum lateral accceleration of $7.5\ \text{m/s}^2$, and a tire friction sensitivity of -0.20, evaluate the effect of aerodynamic yaw moment on N_U.

Q 6.15.3 Show that for a simple vehicle with lift and tire friction sensitivity, the minimum cornering radius is given by

$$\frac{R}{R_0} = \left(1 - \frac{\rho V^2 S C}{2mg}\right)^{-(1+p)}$$

where R_0 is the radius value achievable at zero lift. Explain the idea of a critical aerodynamic speed.

Q 6.15.4 Explain Figure 6.15.1 in qualitative terms.

Q 6.15.5 Explain why, for a racing car with aerodynamic downforce, it becomes even more advantageous to reduce the mass.

Q 6.16.1 Describe the effect of path radius on the understeer coefficient and number.

Q 6.17.1 A straight-running vehicle passes from a level road onto a cambered one. Explain its subsequent path if no control is applied, for understeer, neutral and oversteer cases.

Q 6.17.2 For the vehicle of Q 6.14.2, on a side slope of 6° what will be the required δ and β for straight running?

Q 6.17.3 Explain the principle of super-elevation, with equations, including one for maximum cornering speed. A vehicle of mass 1800 kg has speed 22 m/s at cornering radius 40 m on banking angle 10°. Find the minimum cornering friction coefficient, and the angle for zero lateral force.

Q 6.18.1 Explain longitudinal load transfer on hills, and the consequences for final handling A_M and N_U.

Q 6.18.2 A vehicle with $a = 1.3$ m and $L = 2.8$ m has G height 0.9 m, and $N_U = 0.07$ on level ground. Estimate N_U on a downhill slope of 10°.

Q 6.18.3 A vehicle has a speed of 42 m/s over a crest of radius 300 m. Estimate the proportional deterioration in A_M, compared with the level, assuming constant tire cornering friction.

Q 6.19.1 Explain with equations the influence of adding a load over a rear axle, on primary and final handling.

Q 6.19.2 A vehicle initially with $a/L = 0.46$, $m = 1900$ kg, tire cornering stiffness sensitivity 0.4, $D_f = 10$ deg/g and $D_r = 6$ deg/g has a mass of 300 kg added over the rear axle. Estimate the initial and final k and k_β before and after adding the load.

Q 6.20.1 Explain the effect of side wind on steer and attitude angle for straight running, with equations.

Q 6.20.2 A vehicle has ground speed 40 m/s, frontal area 2.2 m^2, $C'_S =$ 0.07/deg, $C'_Y = 0.02$/deg, $C_\alpha = 500$ N/deg, $G = 20$ and is in a side wind of 8 m/s. Find the effective forces at front and rear axles, and the change of slip angles and steering wheel angle to maintain a straight course.

Q 6.20.3 For a vehicle attempting a steady circular path with modest lateral acceleration, describe the action of the steering wheel required as a result of a steady side wind. Obtain an expression for an estimate of the amplitude of wheel motion.

Q 6.20.4 Derive an equation for the crosswind steer correction coefficient $d\delta/dw$.

Q 6.21.1 Describe the various principal types of steady handling test.

Q 6.21.2 Describe the ISO recommended procedure for a steady-state handling test.

Q 6.21.3 What factors influence the choice of radius for a handling test?

Q 6.22.1 Sketch a representative moment coefficient versus force coefficient plot for a typical car. Describe and explain its main features.

Q 6.22.2 Read the moment-method references, and write a 2000-word review of the method.

Q 6.23.1 Describe the desirable form of the standard handling curves, and discuss the reasons.

Q 6.24.1 For one of the vehicles of Appendix B, apply the theory of each section of this chapter to analyze the steady-state handling.

6.25 Bibliography

Frankly, it is not easy to give a useful bibliography of books for handling theory because the subject has largely been restricted to research papers. One of the few books to tackle the subject at all, and from a quite different perspective from that presented here, is *Road Vehicle Dynamics* by Ellis (1989), a development of the previous book *Vehicle Dynamics* (Ellis, 1969) and revised and republished again as *Vehicle Handling Dynamics,* Ellis (1994). Wong (1978) has a chapter on handling characteristics; see also Steeds (1960). Bastow (1980) has an example numerical calculation of the basic handling curves. More recently, Milliken & Milliken (1995) has a useful amount of material, not entirely overlapping with this volume. Gillespie (1992) has an introductory chapter on steady-state cornering.

For the practical side of suspension modifications to achieve desired handling, Smith (1978) and Puhn (1981) are worth examination.

For terminology, the primary reference is SAE J670e *Vehicle Dynamics Terminology* (see Appendix E), but the ISO will probably soon produce a standard; this will certainly differ from J670e and will be preferred in Europe. See also Hales (1965).

From the research literature, the following can be singled out as particularly relevant or interesting, either expanding slightly on the material here, or giving an alternative perspective: Ellis (1963), Radt & Pacejka (1965), Milner (1967), Bundorf (1967), Grylls (1972), Pacejka (1973), Topping (1974), Bundorf & Leffert (1976), ISO (1982), Dixon (1987b) and (1988).

The moment method is fully described in Milliken *et al.* (1976), Rice & Milliken (1980), and Milliken & Rice (1983). A complete car chassis handling dynamometer is described by Odier (1972).

The influence of aerodynamics on the performance of racing cars is examined in Wright (1983) and Dominy & Dominy (1984).

7

Unsteady-State Handling

7.1 Introduction

This chapter deals with the vehicle in unsteady state, which can be defined as anything other than steady state, i.e., other than a constant speed on a constant path radius, giving constant lateral acceleration. Hence unsteady-state handling includes theory of response to varying control inputs or to disturbances, and covers the natural transient motions after a disturbance. Theory of stability of motion is included here because this is basically the study of the transient motion following a notional small disturbance. The theory of vehicle transient behavior is complex and can be highly mathematical; therefore this chapter is not comprehensive, but serves as an introduction and overview.

Control disturbances may be due to motion of the steering or due to tractive or braking forces. The most basic disturbance is the step-steer input; a practical approximation to this is the ramp-step input. Non-zero longitudinal acceleration is also unsteady, with possible effects from tractive forces unequally distributed side-to-side by non-free differentials, from steer compliance effects, and from tractive force effect on tire characteristics. Of more critical practical importance is longitudinal deceleration combined with cornering, because this is likely to involve large longitudinal forces, and occurs in accident avoidance.

External disturbances arise from wind and road. The classic wind disturbance occurs when suddenly moving into or out of a crosswind; this is a problem of practical importance because it occurs when overtaking or being overtaken on motorways. Road disturbances include anything other than a smooth flat uniform surface, e.g., moving onto a camber, road roughness, or a change of friction coefficient.

The theory of motion stability may be investigated for specific initial conditions by computer, even for large disturbances in the nonlinear regime. However, it is still valuable to have an understanding of the results of the linear mathematical theory, first given by Rocard (1946) for a simple vehicle without suspension or load transfer (two degrees of freedom, yaw and sideslip), and extensively explored by Segel (1957a and 1957b) for three degrees of freedom including roll. Because of the widespread use of computing nowadays, no attempt will be made here to give a full mathematical justification of the linear theory; rather the emphasis is on physical understanding of the results. The chapter begins with the rather unphysical single-degree-of-freedom models of a vehicle, because these, although of little value themselves, throw light on the more complex models.

7.2 1-dof Vibration

Physical interpretation of the equations of motion of the vehicle is enhanced by an understanding of basic stability and vibration theory for a single-degree-of-freedom (1-dof) system, which will therefore be briefly reviewed here. There is an inertia M, stiffness K and damping coefficient C (Figure 7.2.1). When displaced by x there is a stiffness force Kx. If this is a restoring force the system is said to be statically stable; if the stiffness force tends to move the mass farther away from its equilibrium position then it is statically unstable. The damper exerts a force $C\dot{x}$; if this opposes the motion then the damper will remove energy from any motion – this is dynamic stability. If the speed-dependent force acts in the same direction as the motion then it will add energy, giving dynamic instability. The motion of the object after a disturbance will depend on the type of stability (Figure 7.2.2).

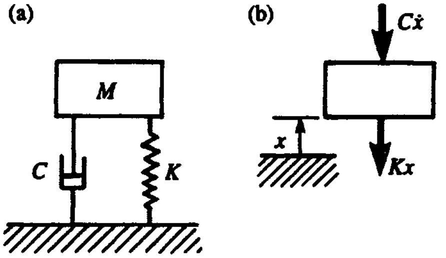

Figure 7.2.1. Single-degree-of-freedom system: (a) system diagram, (b) free-body diagram of mass.

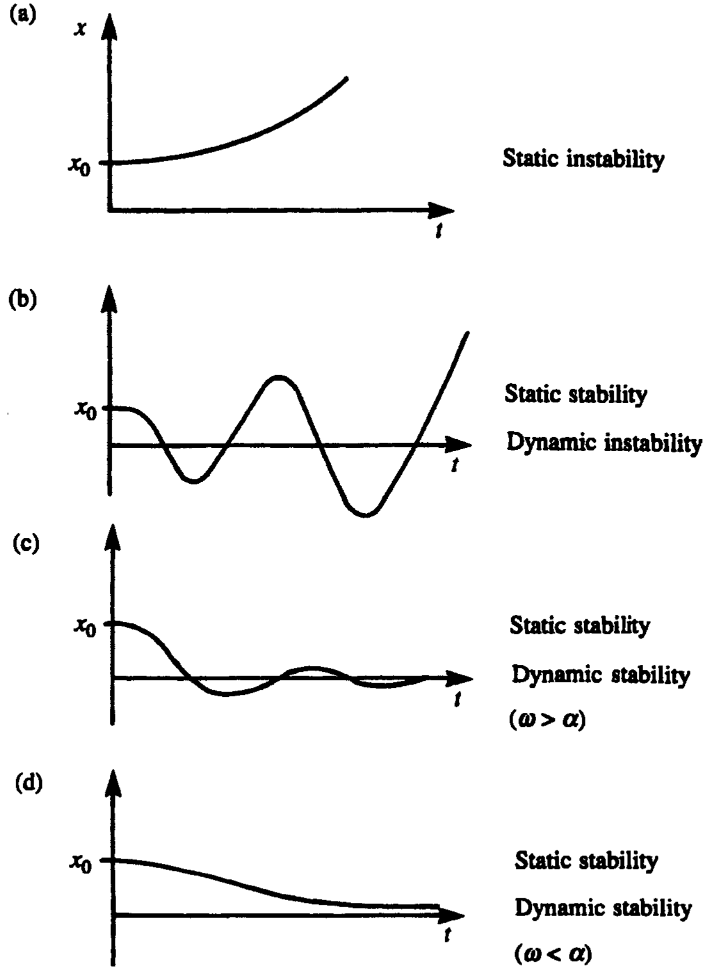

Figure 7.2.2. Possible motions after displacement.

For static instability, regardless of dynamic stability, there is a continuous divergence from the equilibrium position, although this occurs more rapidly if there is also dynamic instability. Static stability coupled with dynamic instability gives an oscillation of growing amplitude. Static stability coupled with dynamic stability gives an oscillation of reducing amplitude; if the damping is sufficient, in excess of critical, then the oscillation is suppressed and there is simply a smooth return to the equilibrium position.

Taking K and C positive for static and dynamic stability, i.e., opposing displacement and velocity (Figure 7.2.1(b)), the equation of motion is

$$\sum F_x = -Kx - C\dot{x} = M\ddot{x}$$
$$M\ddot{x} + C\dot{x} + Kx = 0$$
$$\ddot{x} + \frac{C}{M}\dot{x} + \frac{K}{M}x = 0$$

Using the operational notation D for d/dt, or assuming a solution of the form e^{Dt} and substituting, this becomes

$$D^2x + \frac{C}{M}Dx + \frac{K}{M}x = 0$$

Dividing by x then gives the characteristic equation:

$$D^2 + \frac{C}{M}D + \frac{K}{M} = 0$$

The physical nature of the solution depends on whether D is real (non-oscillatory) or complex (damped oscillatory); D is found by the usual quadratic equation solution:

$$\begin{aligned} D &= \frac{-b \pm \sqrt{b^2 - 4ac}}{2a} \\ &= -\frac{C}{2M} \pm \sqrt{\frac{C^2}{4M^2} - \frac{K}{M}} \\ &= -\alpha \pm \sqrt{\alpha^2 - \omega^2} \end{aligned}$$

where α (units of s^{-1}) is called the damping factor and ω is the undamped natural frequency (rad/s).

The mathematical solution will be complex (which physically means damped oscillatory) if $\omega > \alpha$, in which case we have undamped natural frequency ω, damping ratio ζ and damped natural frequency ω_d according to:

$$\ddot{x} + 2\zeta\omega\dot{x} + \omega^2 x = 0$$

Note the distinction between damping coefficient C (Ns/m), damping factor α (s^{-1}) and damping ratio ζ (non-dimensional).

$$\omega = \sqrt{\frac{K}{M}}$$

$$\zeta = \frac{\alpha}{\omega} = \frac{C}{2M\omega} = \frac{C}{2\sqrt{MK}}$$

$$\omega_d = \sqrt{\omega^2 - \alpha^2} = \omega\sqrt{1 - \zeta^2}$$

The actual displacement is

$$x = X_0 e^{-\alpha t} \sin(\omega_d t + \phi)$$

where α and ω depend on the system properties, and the amplitude X_0 and phase angle ϕ depend on the initial conditions of x and $\dot{x}$.

If $\omega < \alpha$, there will be two real solutions to D, and a non-oscillatory response with two time constants, τ_1 and τ_2:

$$-\frac{1}{\tau_1} = D_1 = -\alpha + \sqrt{\alpha^2 - \omega^2}$$

$$-\frac{1}{\tau_2} = D_2 = -\alpha - \sqrt{\alpha^2 - \omega^2}$$

The actual displacement is then

$$x = X_1 e^{-t/\tau_1} + X_2 e^{-t/\tau_2}$$

where τ_1 and τ_2 depend on the system properties and X_1 and X_2 depend on the initial conditions of x and $\dot{x}$.

The system considered so far has had no additional external forces, so the behavior is called the natural or free response.

If the system of Figure 7.2.1 is subject to an external driving force $F(t)$ then the equation of motion becomes

$$\ddot{x} + \frac{C}{M}\dot{x} + \frac{K}{M}x = \frac{F(t)}{M}$$

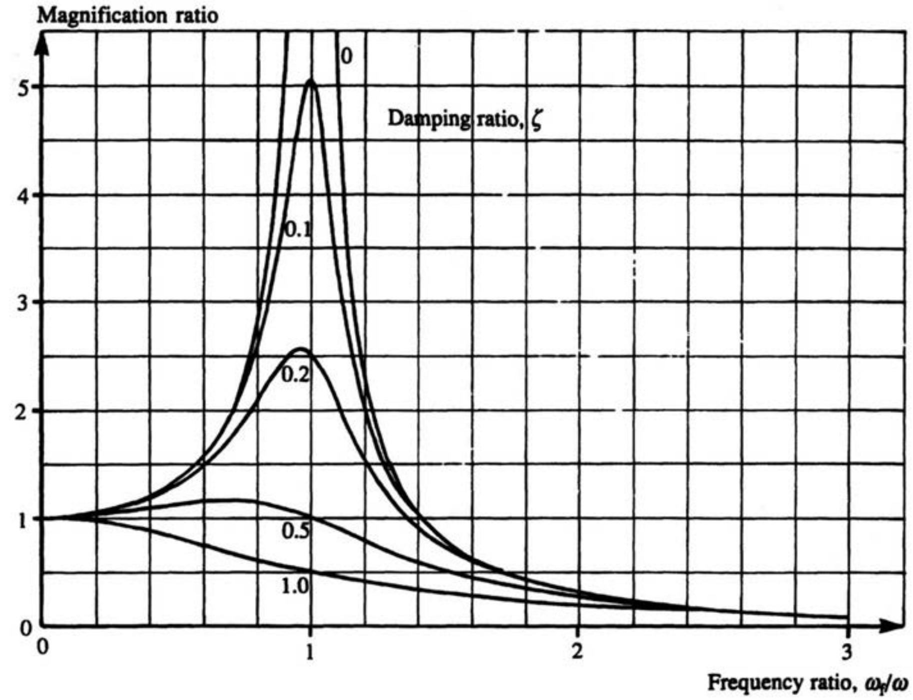

Figure 7.2.3. Magnification ratio versus frequency ratio.

The solution to this is called the forced response. It is mathematically the sum of the complementary function and the particular integral. Physically, it is the sum of the corresponding transient and steady-state solutions. The complementary function represents the transient, and is the natural response with arbitrary constants depending on initial conditions, as before. The particular integral represents the "steady-state" forced response once the starting transient has been damped out. The usual method of solution for the particular integral is to try a solution of the same form as $F(t)$. For example, for $F(t) = F_1 \sin \omega_f t$ where ω_f is the forcing frequency in rad/s and F_1 is the amplitude of the disturbing force, try

$$x = X \sin(\omega_f t + \phi)$$

where X is the displacement amplitude and ϕ is the phase angle of the response. Differentiating, and substituting in the equation of motion, the coefficient of the sine term must be equal for both sides. Assuming an oscillatory natural solution

$$\ddot{x} + 2\zeta\omega\dot{x} + \omega^2 x = 0$$

the response amplitude is given by

$$X = \frac{F_1/K}{\sqrt{\left[1 - (\omega_f/\omega)^2\right]^2 + 2\zeta(\omega_f/\omega)^2}}$$

If the force F_1 were applied steadily to stiffness K then the displacement would be F_1/K. The dynamic effect may be seen by comparing the displacement amplitude X with F_1/K. Figure 7.2.3 shows how the magnification ratio $X/(F_1/K)$ depends on the frequency ratio ω_f/ω for various values of damping ratio ζ. Particularly notable is the resonant response for ω_f close to the natural frequency ω. For road vehicles the yaw damping ratio is generally in the range 0.2 to 1.0, and the yaw natural frequency is typically about 6 rad/s (1 Hz), so there may be observable resonance in yaw behavior.

7.3 1-dof Sideslip

In the one-degree-of-freedom sideslip model the vehicle is considered incapable of yaw; this is of course unrealistic and is investigated here only in order to throw light on the more complex two- and three-degrees-of-freedom models considered later. Figure 7.3.1 shows the bicycle model vehicle with side force $F(t)$ positioned to give zero yaw, with resultant lateral velocity component $\dot{y}$ giving attitude angle β. It is apparent from the figure that a steady $F(t)$ will cause the development of a steady $\dot{y}$ such that β gives adequate tire forces to oppose $F(t)$. Also, because there is a damping force but no stiffness force, there will not be a natural frequency.

$$\alpha_f = \alpha_r = \beta = \frac{\dot{y}}{V}$$

$$\sum F_y = F(t) - 2C_{\alpha f} - 2C_{\alpha r}\alpha_r = m\ddot{y}$$

$$m\ddot{y} + \frac{C_0}{V}\dot{y} = F(t)$$

where C_0 is the zeroth moment vehicle cornering stiffness:

$$C_0 = 2C_{\alpha f} + 2C_{\alpha r}$$

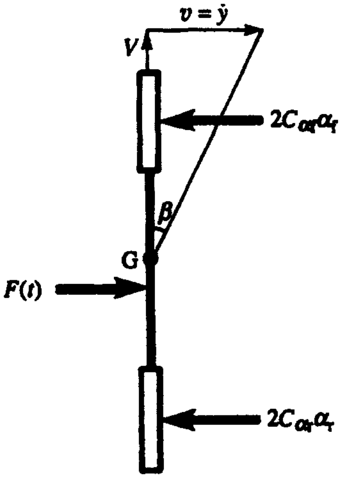

Figure 7.3.1. Single-degree-of-freedom sideslip model.

The characteristic equation of the free motion is

$$D^2 + \frac{C_0}{mV} D = 0$$

$$-\frac{1}{\tau} = D = -\frac{C_0}{mV}$$

$$\tau = \frac{mV}{C_0}$$

This confirms that the natural response is exponential rather than oscillatory. A typical value of τ is 0.2 s at 20 m/s. The solution for y is

$$y = Ye^{-t/\tau}$$

where Y depends on the initial conditions. The forced response to a step input force F is

$$\dot{y} = \frac{FV}{C_0}\left(1 - e^{-t/\tau}\right)$$

The initial lateral acceleration is

$$\ddot{y}_0 = -\frac{FV}{\tau C_0} = \frac{F}{m}$$

as would be expected. The final drift speed is

$$\dot{y}_\infty = \frac{FV}{C_0}$$

which is proportional to V, because this gives the necessary value of $\beta = F/C_0$.

The lateral displacement response to the step force input is found by integrating $\dot{y}$ and evaluating the constant of integration from the initial condition $y = 0$, to give

$$y = \frac{FV}{C_0}\left[t - \tau\left(1 - e^{-t/\tau}\right)\right]$$

In response to a forced displacement held constant at y there is no restoring force. In response to a constant displacement velocity $\dot{y}$ there is an opposing damping force

$$F = C_0\beta = \frac{C_0\dot{y}}{V}$$

Thus the sideslip motion is characterized by no stiffness and no oscillation, but strong positive damping.

7.4 1-dof Yaw

In the one-degree-of-freedom yaw model the vehicle is considered pinned at G; it can yaw but not sideslip. Again, this is unrealistic, but the results help to illuminate the more complex models.

From Figure 7.4.1 the slip angles are

$$\alpha_f = \psi - \frac{ar}{V}$$

$$\alpha_r = \psi + \frac{br}{V}$$

where ψ is the heading angle and $r \equiv \dot{\psi}$ is the yaw angular speed. The equation of motion in yaw is

$$\sum M = 2aC_{\alpha f}\alpha_f - 2bC_{\alpha r}\alpha_r = I\ddot{\psi}$$

$$2aC_{\alpha f}\left(\psi - \frac{a\dot{\psi}}{V}\right) - 2bC_{\alpha r}\left(\psi + \frac{b\dot{\psi}}{V}\right) = I\ddot{\psi}$$

$$I\ddot{\psi} + \left(\frac{2a^2C_{\alpha f} + 2b^2C_{\alpha r}}{V}\right)\dot{\psi} - \left(2aC_{\alpha f} - 2bC_{\alpha r}\right)\psi = 0$$

$$\ddot{\psi} + \frac{C_2}{IV}\dot{\psi} - \frac{C_1}{I}\psi = 0$$

where

$$C_1 = 2aC_{\alpha f} - 2bC_{\alpha r}$$
$$C_2 = 2a^2C_{\alpha f} + 2b^2C_{\alpha r}$$

are the first- and second-moment vehicle cornering stiffnesses.

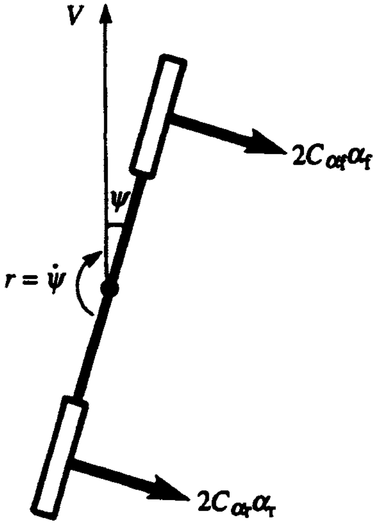

Figure 7.4.1. Single-degree-of-freedom yaw model.

By comparison with the standard one-degree-of-freedom vibration equation of Section 7.2, which was

$$\ddot{x} + \frac{C}{M}\dot{x} + \frac{K}{M}x = 0$$

the yaw stiffness is $-C_1$ and the yaw damping coefficient is C_2/V. For static stability the yaw stiffness should be restoring, i.e., C_1 should be negative. Since, from Chapter 6, the understeer gradient is

$$k = -\frac{mC_1}{4LC_{\alpha f}C_{\alpha r}}$$

static stability requires positive k, i.e., understeer. Dynamic stability requires $C_2/I > 0$, and hence $C_2 > 0$, which will always be the case; i.e., because $C_2 > 0$ there is always positive damping.

If the vehicle is oversteer then the motion will be a non-oscillatory divergence from the equilibrium position. For an understeer vehicle the motion will be a return to the equilibrium position. Whether it is oscillatory or not depends on the characteristic equation:

$$D^2 + \frac{C_2}{IV}D - \frac{C_1}{I} = 0$$

$$D = -\frac{C_2}{2IV} \pm \sqrt{\left(\frac{C_2}{2IV}\right)^2 + \frac{C_1}{I}}$$

In terms of the damping factor α_D and radian natural frequency ω_d, this is the complex solution

$$D = \alpha_D \pm i\omega_d$$

The motion will be oscillatory if D is mathematically complex, i.e., if

$$\left(\frac{C_2}{2IV}\right)^2 + \frac{C_1}{I} < 0$$

$$V^2 > \frac{-C_2^2}{4IC_1}$$

where the right-hand side is positive because C_1 is negative for understeer. Hence there is a transition speed

$$V_t = \sqrt{\frac{-C_2^2}{4IC_1}}$$

below which the response is overdamped. Above this speed there is a natural frequency and damping ratio that may be found by comparing the characteristic equation with this form of the standard single-degree-of-freedom vibration equation:

$$\ddot{x} + 2\zeta\omega\dot{x} + \omega^2 x = 0$$

Hence

$$\omega = \sqrt{\frac{C_1}{I}}$$

which is typically about 10 rad/s (1.6 Hz). The damping ratio is

$$\zeta = \frac{C_2}{2IV\omega} = \frac{C_2}{V\sqrt{4IC_1}} = \frac{V_t}{V}$$

where V_t is the transition speed given by the equation earlier. Hence the damping ratio is inversely proportional to speed. More understeer (greater magnitude of C_1) will increase the natural frequency and reduce V_t, i.e., reduce the damping.

In accordance with standard vibration theory, the damped natural frequency in rad/s is

$$\omega_d = \omega\sqrt{1 - \zeta^2}$$

This is zero at the transition speed.

Thus the single-degree-of-freedom yaw motion is characterized by continuous divergence for oversteer; for understeer it is convergent and possibly oscillatory. There is both stiffness and damping.

7.5 2-dof Model (Vehicle-Fixed Axes)

The equations of motion for the vehicle may be expressed in coordinates fixed to the Earth (*XYZ*) or coordinates fixed to the vehicle (*xyz*); vehicle-fixed axes will be used in this section. First it is necessary to find the vehicle lateral acceleration in terms of the absolute motion. Figure 7.5.1 shows the vehicle in axes *XYZ*, moving substantially in the *X* direction, with angles shown exaggerated. The path angle from the *X*-axis is ν (nu), the heading angle is ψ and the attitude angle is β. The constant total speed V tangent to the path may be resolved into V_{ax} and $V_{\mathrm{ay}} \equiv v$ as used in this section, or into V_{X} and $V_{\mathrm{Y}} \equiv u$ as in the next section.

$$V_{\mathrm{ax}} = V\cos\beta \approx V$$
$$V_{\mathrm{X}} = V\cos\nu \approx V$$
$$V_{\mathrm{ay}} \equiv v \approx \beta V$$
$$V_{\mathrm{Y}} \equiv u \approx \nu V$$

Care is needed here to distinguish angle ν (Greek nu) from speed component v (vee).

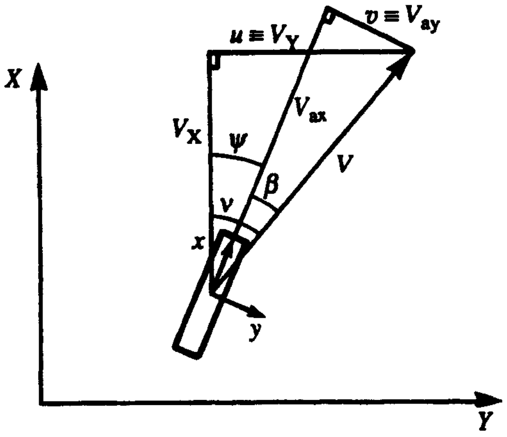

Figure 7.5.1. Angles and velocity components. (Note the distinction between u and v, V_{ax} and V_{X}, and ν and β.)

Here V_{ax} is the component of the absolute velocity in the x direction, in contrast to V_x which would be the component of velocity in xyz, which is zero because xyz are the vehicle-fixed axes. The vehicle has yaw angular velocity $r = \dot{\psi}$ where ψ is the heading angle.

Figure 7.5.2 shows the vehicle position and orientation at time t and $t + \mathrm{d}t$. The relative rotation is $r\,\mathrm{d}t$.

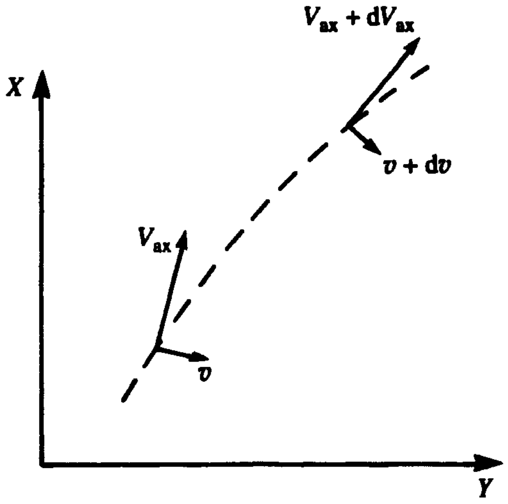

Figure 7.5.2. Velocity components at path points.

The absolute acceleration in the y direction is

$$\begin{aligned} A_{ay}\mathrm{d}t &= \mathrm{d}v\cos(r\,\mathrm{d}t) + V\sin(r\,\mathrm{d}t) \\ &\approx \mathrm{d}v + Vr\,\mathrm{d}t \\ A_{ay} &= \dot{v} + Vr \end{aligned}$$

An alternative approach to developing this expression is to begin with

$$u = Vv$$

With constant V,

$$\begin{aligned} A_{\mathrm{ay}} &= V\dot{v} \\ &= V\left(\dot{\beta} + \dot{\psi}\right) \\ &= V\dot{\beta} + Vr \\ &= \dot{v} + Vr \end{aligned}$$

Hence, the two-degree-of-freedom equations of motion in vehicle-fixed axes for fixed zero control can be expressed as

$$\begin{aligned} &\sum F_{\mathrm{y}} - m(\dot{v} + Vr) = 0 \\ &\sum M - I_{\mathrm{z}}\dot{r} = 0 \end{aligned}$$

Figure 7.5.3 shows the free-body diagram in vehicle-fixed axes, for a bicycle model vehicle, with roll and load transfer being neglected. The vehicle is considered in the accelerating vehicle-fixed axes, so appropriate compensation force and moment (mA_{ay} and $I\dot{r}$) are included (as explained in Chapter 1). The vehicle has been subjected to a small disturbance, now having a lateral velocity component v. As a result there is an attitude angle

$$\beta = \frac{v}{V_{\mathrm{ax}}} \approx \frac{v}{V}$$

Allowing for the attitude angle and the yaw rotation speed r, the slip angles are

$$\begin{aligned} \alpha_{\mathrm{f}} &= \frac{v}{V} + \frac{ar}{V} = \beta + \frac{ar}{V} \\ \alpha_{\mathrm{r}} &= \frac{v}{V} - \frac{br}{V} = \beta - \frac{br}{V} \end{aligned}$$

This is a fixed control analysis; in practice there would still be some control compliance, but this is neglected. Using the linear approximation there are corresponding tire forces of

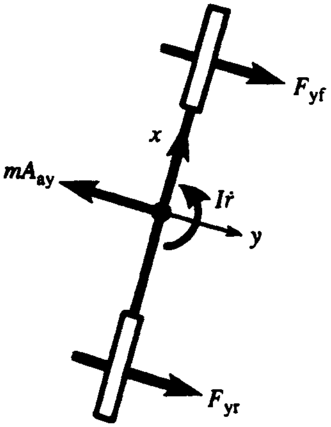

Figure 7.5.3. Vehicle free-body diagram in vehicle-fixed axes.

$$F_{yf} = 2C_{\alpha f}\,\alpha_f$$
$$F_{yr} = 2C_{\alpha r}\,\alpha_r$$

Bearing in mind that the acceleration in the vehicle-fixed axes is zero by definition, the equations of lateral motion for the vehicle of Figure 7.5.3 are

$$\sum F_y = F_{yf} + F_{yr} - mA_{ay} = 0$$
$$\sum M = aF_{yf} - bF_{yr} - I\dot{r} = 0$$

Substituting in the above two equations and collecting terms gives

$$m\dot{v} + \left(\frac{2C_{\alpha f} + 2C_{\alpha r}}{V}\right)v + \left(mV + \frac{2aC_{\alpha f} - 2bC_{\alpha r}}{V}\right)r = 0$$
$$\left(\frac{2aC_{\alpha f} - 2bC_{\alpha r}}{V}\right)v + I\dot{r} + \left(\frac{2a^2C_{\alpha f} + 2b^2C_{\alpha r}}{V}\right)r = 0$$

These equations may be simplified by using the vehicle cornering stiffness constants C_0, C_1 and C_2 (Section 6.6), e.g., $C_0 = 2C_{\alpha f} + 2C_{\alpha r}$. Also introducing

D to represent differentiation with respect to time, the force and moment equations can be represented more concisely as:

$$\left(mD+\frac{C_0}{V}\right)v+\left(mV+\frac{C_1}{V}\right)r=0$$

$$\left(\frac{C_1}{V}\right)v+\left(ID+\frac{C_2}{V}\right)r=0$$

These equations are a representation of the natural motion of the vehicle observed in the vehicle-fixed axes. If there are external forces additionally present, e.g., aerodynamic or steering forces, then these would appear as time-dependent forcing functions on the right-hand side.

Actually these equations can be expressed not only in v and r as above; r may be replaced by $D\psi$. However, it is not useful to replace v by Dy because the cumulative displacement in the varying y direction has no practical significance. A useful alternative form may be found by using the attitude angle $\beta = v/V$, hence expressing the equations in β and r, or in β and ψ.

The characteristic equation for the above pair of simultaneous equations is found by multiplying the first by $(ID + C_2/V)$ and the second by $(mV + C_1/V)$ and subtracting, giving:

$$\left(mD+\frac{C_0}{V}\right)\left(ID+\frac{C_2}{V}\right)-\left(mV+\frac{C_1}{V}\right)\left(\frac{C_1}{V}\right)=0$$

Expanding this gives

$$mID^2+\left(\frac{mC_2}{V}+\frac{IC_0}{V}\right)D+\left(\frac{C_0C_2}{V^2}-mC_1-\frac{C_1^2}{V^2}\right)=0$$

This is the characteristic equation for 2-dof sideslip and yaw. It is the condition for there to be a non-zero solution to the simultaneous differential equations of motion, and therefore tells us the nature of the free response, and in particular tells us the natural frequency and damping of the 2-dof vehicle lateral motion (Section 7.7).

7.6 2-dof Model (Earth-Fixed Axes)

If it is desired to compare theory with data measured by vehicle-fixed instrumentation, e.g., lateral acceleration, then the formulation of the previous section is suitable. However, if it is desired to analyze the vehicle motion as seen in

Earth-fixed coordinates, e.g., to find the amplitude of path oscillations in response to an oscillatory steer input, then the equations of motion should be expressed in Earth-fixed axes.

The equations of motion in Earth-fixed axes are

$$\sum F_y = mA_y = m\dot{u}$$
$$\sum M_z = I_z\dot{r}$$

The slip angles expressed in the variables of the Earth-fixed axis system are:

$$\alpha_f = \frac{u}{V} + \frac{ar}{V} - \psi$$
$$\alpha_r = \frac{u}{V} - \frac{br}{V} - \psi$$

where $r = \dot{\psi}$ is the yaw angular speed. The actual values of the angles are, of course, the same in the two systems. Compared with the slip angle expressions of the last section, the use of u instead of v results in the appearance of ψ in the expressions.

Figure 7.6.1, shows the free-body diagram in the Earth-fixed axes XYZ. These are inertial axes, so compensation forces are not required. From the free-body diagram, the equations of motion in Earth-fixed axes are:

$$\sum F_Y = F_{yf} + F_{yr} = mA_Y$$
$$\sum M = aF_{yf} - bF_{yr} = I\dot{r}$$

Substituting, as in the last section, collecting terms and using the D operator notation gives:

$$\left(mD + \frac{C_0}{V}\right)u + \left(\frac{C_1}{V}D - C_0\right)\psi = 0$$
$$\left(\frac{C_1}{V}\right)u + \left(ID^2 + \frac{C_2}{V}D - C_1\right)\psi = 0$$

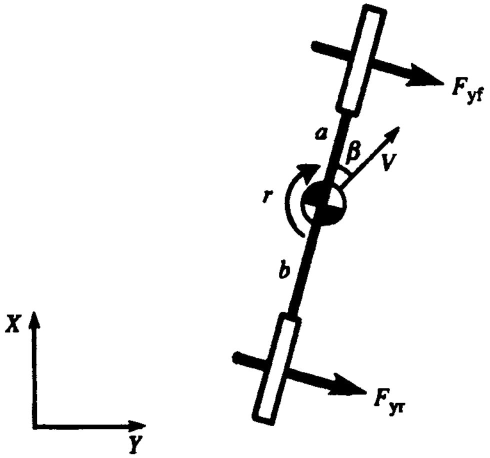

Figure 7.6.1. Vehicle free-body diagram in Earth-fixed axes.

This may also be expressed in other forms, e.g., by using $u = DY$, $r = D\psi$ or $u = vV$. Using the last substitution gives:

$$(mVD + C_0)\, v + \left(\frac{C_1}{V} D - C_0\right) \psi = 0$$

$$(C_1)\, v + \left(ID^2 + \frac{C_2}{V} D - C_1\right) \psi = 0$$

The above equations can be contrasted with the equivalent formulation, in β and ψ, for vehicle-fixed axes from the last section, which were

$$(mVD + C_0)\, \beta + \left(mVD + \frac{C_1}{V} D\right) \psi = 0$$

(vehicle-fixed axes)

$$(C_1)\, \beta + \left(ID^2 + \frac{C_2}{V} D\right) \psi = 0$$

Elimination of v or ψ from the Earth-fixed axes formulation, after cancellation of terms and dividing by VD, gives the following characteristic equation:

$$\left(mD+\frac{C_0}{V}\right)\left(ID^2+\frac{C_2}{V}D-C_1\right)-\left(\frac{C_1}{V}\right)\left(\frac{C_1}{V}D-C_0\right)=0$$

which multiplies out to

$$mID^2+\left(\frac{mC_2}{V}+\frac{IC_0}{V}\right)D+\left(\frac{C_0C_2}{V^2}-mC_1-\frac{C_1^2}{V^2}\right)=0$$

Despite the different starting equations for the Earth-fixed axes, this is the same characteristic equation as was found for the vehicle-fixed axes; physically this is correct because the natural frequency and damping ratio must be the same in both coordinate systems.

If there are additional forces, e.g., aerodynamic or front steer angle, these will appear on the right-hand side of the equations of motion as functions of time.

Eliminating ψ from the various sets of equations will give different results for u and v, as it should, because the different coefficients of ψ for the two sets of axes will affect the right-hand side differently.

7.7 2-dof Free Response

The nature of the free response, i.e., the stability, natural frequency and damping ratio, depends on the characteristic equation as found for both Earth-fixed and vehicle-fixed axes:

$$mID^2+\left(\frac{mC_2}{V}+\frac{IC_0}{V}\right)D+\left(\frac{C_0C_2}{V^2}-mC_1-\frac{C_1^2}{V^2}\right)=0$$

Most 2-dof systems give rise to a quartic (fourth-order) characteristic equation with two modes and two natural frequencies. This is not so here because the system has no true stiffness terms (the vehicle has no spring positioning it laterally), so the third- and fourth-order terms in D disappear, leaving only a quadratic in D.

The conditions for stability of motion can therefore be seen by comparing the characteristic equation with the single-degree-of-freedom vibration equation in the following form, from Section 7.2, where the spring stiffness K is positive for a restoring force (opposing displacement) and C is positive for a positive damping force (opposing velocity):

$$\ddot{x} + \frac{C}{M}\dot{x} + \frac{K}{M}x = 0$$

In the characteristic equation, the inertia term mI is always positive. Dynamic stability requires that the damping coefficient C be positive, i.e., that

$$\frac{mC_2}{V} + \frac{IC_0}{V} > 0$$

This will always be true, so if there is instability it must be static, i.e., due to a negative stiffness. For static stability $K > 0$, so

$$\frac{C_0C_2}{V^2} - mC_1 - \frac{C_1^2}{V^2} > 0$$

requiring

$$C_0C_2 > C_1^2 + mC_1V^2$$

From Chapter 6, the understeer gradient is

$$k_U = -\frac{mC_1}{4LC_{\alpha f}C_{\alpha r}}$$

so for an understeer vehicle C_1 is negative, and, from the previous equation, static stability is assured for all speeds. For an oversteer vehicle (positive C_1) static stability requires

$$V^2 < \frac{C_0C_2}{mC_1} - \frac{C_1}{m}$$

Substituting and simplifying gives

$$V^2 < \frac{4L^2C_{\alpha f}C_{\alpha r}}{mC_1}$$

Hence an oversteer vehicle will be stable up to a critical speed V_{cr} beyond which it will be unstable, where

$$V_{\mathrm{cr}} = \sqrt{\frac{4L^2 C_{\alpha\mathrm{f}} C_{\alpha\mathrm{r}}}{mC_1}} = \sqrt{\frac{L}{-k_{\mathrm{U}}}}$$

$$= \sqrt{\frac{C_0 C_2 - C_1^2}{mC_1}}$$

For understeer, negative C_1, the characteristic speed is

$$V_{\mathrm{ch}} = \sqrt{\frac{-\left(C_0 C_2 - C_1^2\right)}{mC_1}}$$

The undamped natural frequency of the free motion may be found by comparing the characteristic equation with the single-degree-of-freedom vibration equation in the following form, where ω is the undamped natural frequency in rad/s, and ζ is the damping ratio:

$$\ddot{x} + 2\zeta\omega\dot{x} + \omega^2 x = 0$$

Hence the undamped natural frequency in rad/s is given by

$$\omega^2 = \frac{\dfrac{C_0 C_2}{V^2} - mC_1 - \dfrac{C_1^2}{V^2}}{mI}$$

At high speeds, ω tends to the value $\sqrt{-C_1/I}$ which is the value for the single-degree-of-freedom pure yaw model. Hence the sideslip tends to increase the undamped natural frequency, especially at low speed.

Using

$$V_{\mathrm{ch}}^2 = -\frac{C_0 C_2 - C_1^2}{mC_1}$$

then

$$\omega^2 = -\frac{C_1}{I}\left[1+\left(\frac{V_{ch}}{V}\right)^2\right]$$

Expressing ω at infinite speed as ω_∞,

$$\omega_\infty^2 = -\frac{C_1}{I}$$

$$\frac{\omega}{\omega_\infty} = \sqrt{1+\left(\frac{V_{ch}}{V}\right)^2}$$

At $V = V_{ch}$, $\omega/\omega_\infty = \sqrt{2}$, as seen in Figure 7.7.1.

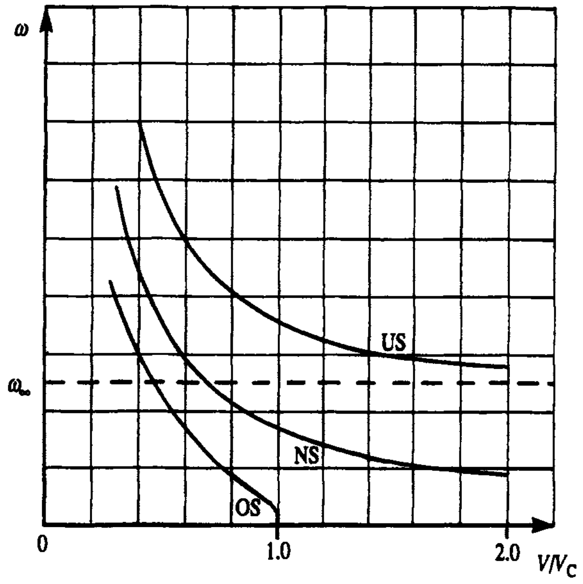

Figure 7.7.1 Undamped yaw natural frequency versus speed.

For a neutral steer vehicle, $C_1 = 0$ and $k = 0$, so $\omega_\infty = 0$ and

$$\omega = \sqrt{\frac{C_0C_2/mI}{V}}$$

tending to zero at infinite speed.

For an oversteer vehicle,

$$\omega^2 = \frac{C_1}{I}\left[\left(\frac{V_{\text{cr}}}{V}\right)^2 - 1\right]$$

and the undamped natural frequency ω goes to zero (Figure 7.7.1) at

$$V = \sqrt{\frac{C_0C_2 - C_1^2}{mC_1}} = V_{\text{cr}}$$

Above this speed the response is non-oscillatory, and there is no natural frequency and no real solution for ω.

The damping coefficient in the characteristic equation is $(mC_2 + IC_0)/V$; this is the sum of the damping coefficients from pure sideslip and pure yaw, and these motions contribute approximately equally to the damping ($a \approx b \approx k_z$, so $mC_2 \approx IC_0$). The damping ratio of the free motion may be found by comparing the characteristic equation with the single-degree-of-freedom vibration equation in the following form, where ζ is the damping ratio:

$$\ddot{x} + 2\zeta\omega\dot{x} + \omega^2 x = 0$$

Hence the damping ratio is given by

$$\zeta = \frac{mC_2 + IC_0}{2mIV\omega}$$

For understeer,

$$\omega^2 = -\frac{C_1}{I}\left[1 + \left(\frac{V_{\text{ch}}}{V}\right)^2\right]$$

so

$$\zeta = \frac{mC_2 + IC_0}{2mI\sqrt{\dfrac{-C_1}{I}}\sqrt{V^2 + V_{ch}^2}}$$

$$= \frac{V_d}{\sqrt{V^2 + V_{ch}^2}}$$

where V_d is the characteristic damping speed:

$$V_d = \frac{mC_2 + IC_0}{\sqrt{-4m^2C_1I}}$$

$$= \frac{C_2 + k_z^2C_0}{\sqrt{-4C_1I}}$$

where k_z is the yaw radius of gyration. Hence

$$\zeta = \frac{V_d/V_{ch}}{\sqrt{1 + \left(\dfrac{V}{V_{ch}}\right)^2}}$$

$$= \frac{\zeta_0}{\sqrt{1 + \left(\dfrac{V}{V_{ch}}\right)^2}}$$

where ζ_0 is the damping ratio at zero speed.

$$\zeta_0 = \frac{V_d}{V_{ch}}$$

$$= \frac{C_2 + k_z^2C_0}{\sqrt{4k_z^2\left(C_0C_2 - C_1^2\right)}}$$

For the neutral steer case, V_{ch} is infinite, and C_1 is zero, so the damping ratio is constant for all speeds, at

$$\zeta = \frac{C_2 + k_z^2 C_0}{\sqrt{4k_z^2 C_0 C_2}}$$

For the oversteer case, an analysis similar to the understeer case may be applied, giving a characteristic damping speed

$$V_d = \frac{C_2 + k_z^2 C_0}{\sqrt{4IC_1}}$$

and a damping ratio

$$\zeta = \frac{\zeta_0}{\sqrt{1 - \left(\frac{V}{V_{\mathrm{cr}}}\right)^2}}$$

The zero-speed damping ratio is

$$\zeta_0 = \frac{V_d}{V_{\mathrm{cr}}}$$

$$= \frac{C_2 + k_z^2 C_0}{\sqrt{4k_z^2 (C_0 C_2 - C_1^2)}}$$

as before.

The possible values of ζ_0 for all cases may be investigated as follows. In practice

$$C_1^2 \ll C_0 C_2$$

and

$$a \approx b \approx k_z$$

so

$$C_2 \approx k_z^2 C_0$$

giving

$$\zeta_0 \approx 1.0$$

Actually, it is possible to place a definite limit on ζ_0 in the following way:

$$\zeta_0 = \frac{C_2 + k_z^2 C_0}{\sqrt{4k_z^2\left(C_0 C_2 - C_1^2\right)}}$$

Hence

$$\zeta_0 > \frac{C_2 + k_z^2 C_0}{\sqrt{4k_z^2 C_0 C_2}} = \frac{\frac{1}{2}\left(C_2 + k_z^2 C_0\right)}{\sqrt{C_2 k_z^2 C_0}}$$

This is the ratio of the arithmetic mean of C_2 and $k_z^2 C_0$ to their geometric mean, which must be greater than or equal to 1.0, so

$$\zeta_0 \geq 1.0$$

Thus $\zeta_0 < 1$ is excluded from physical solutions.

Figure 7.7.2 shows the variation of ζ_0 with radius of gyration k_z for an example case of various C_1 values, for $a = b = 1.5$ m, $C_0 = 120$ kN/rad, and $C_2 = 270$ kNm^2/rad. Again, this indicates that, for the two-degrees-of-freedom model, values of ζ_0 are a little in excess of 1.0, and not below 1.0.

Figure 7.7.3 shows how ζ varies with V/V_c for understeer, neutral and oversteer cases. For understeer, $\zeta = \zeta_0/\sqrt{2}$ at the characteristic speed, and $\zeta_0/\sqrt{5}$ at $2V_{ch}$. For oversteer, ζ goes to infinity at V_{cr}.

From a practical point of view, it is notable that at high speed the damping ratio becomes rather small if there is a large understeer coefficient. To avoid excessive overshoot, V_{ch} should be not less than $\frac{1}{2}V_{max}$, i.e., $\zeta > 0.45$. On a

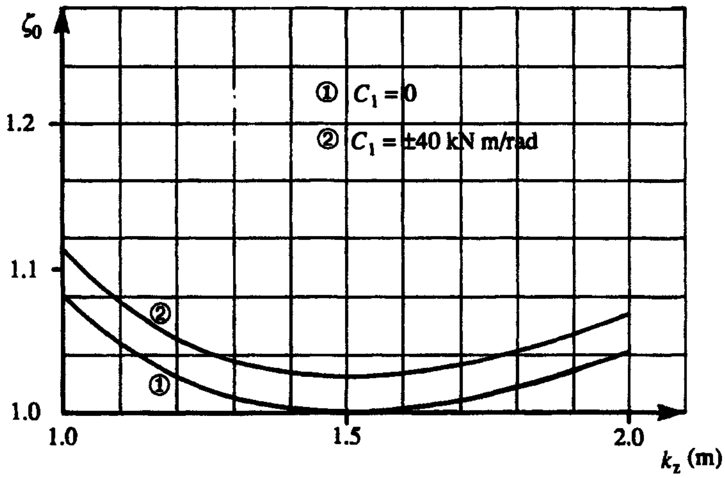

Figure 7.7.2. Initial damping ratio versus radius of gyration.

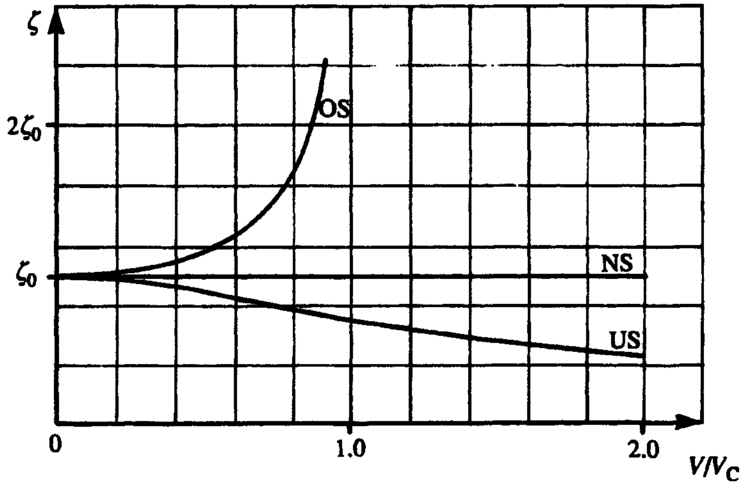

Figure 7.7.3. Damping ratio versus speed.

wheelbase of 2.8 m with a maximum speed of 50 m/s, this implies that the characteristic speed should be at least 25 m/s, and therefore, using

$$V_{ch} = \sqrt{\frac{L}{k_U}}$$

the understeer gradient k_U should preferably not exceed 0.0045 rad/m s^{-2} (2.5 deg/g). High-speed yaw oscillation is dangerous. To obtain good yaw damping at high speed either the tire cornering stiffness must be high or the understeer gradient must not be too large. In other words, too much stability can be as bad as too little because the former can cause low yaw damping.

The damped natural frequency, which is the frequency actually observed, is

$$\omega_d = \omega\sqrt{1 - \zeta^2}$$

The damping ratio is reasonably high except for extreme understeer vehicles, so the damped natural frequency is significantly lower than the undamped one.

For the understeer case

$$\begin{aligned}\frac{\omega_d^2}{\omega^2} &= 1 - \zeta^2 \\ &= 1 - \frac{\zeta_0^2}{1 + \left(\dfrac{V}{V_{ch}}\right)^2} \\ &= \frac{1 + \left(\dfrac{V}{V_{ch}}\right)^2 - \zeta_0^2}{1 + \left(\dfrac{V}{V_{ch}}\right)^2}\end{aligned}$$

Also

$$\frac{\omega^2}{\omega_\infty^2} = 1 + \left(\frac{V_{ch}}{V}\right)^2$$

giving

$$\frac{\omega_d^2}{\omega_\infty^2} = 1 - \left(\frac{V_{ch}}{V}\right)^2\left(\zeta_0^2 - 1\right)$$

where $\zeta_0 \geq 1$. The damped natural frequency is zero at a speed

$$\frac{V}{V_{\mathrm{ch}}} = \sqrt{\zeta_0^2 - 1}$$

Above this speed, the response is oscillatory. It is necessary to distinguish two cases, in principle, according to the value of ζ_0 (Figure 7.7.4). For the limiting case of $\zeta_0 = 1$, ω_d is constant and equal to ω_∞. For $\zeta_0 < 1$, when V/V_{ch} is less than $\sqrt{(\zeta_0^2 - 1)}$ then $\zeta > 1$ and there is no damped natural frequency. For V/V_{ch} greater than $\sqrt{(\zeta_0^2 - 1)}$, ω_d is real, and increases up to ω_∞. This increase occurs because although the undamped natural frequency decreases with speed, the damping ratio also decreases with speed, and the latter is the dominant effect.

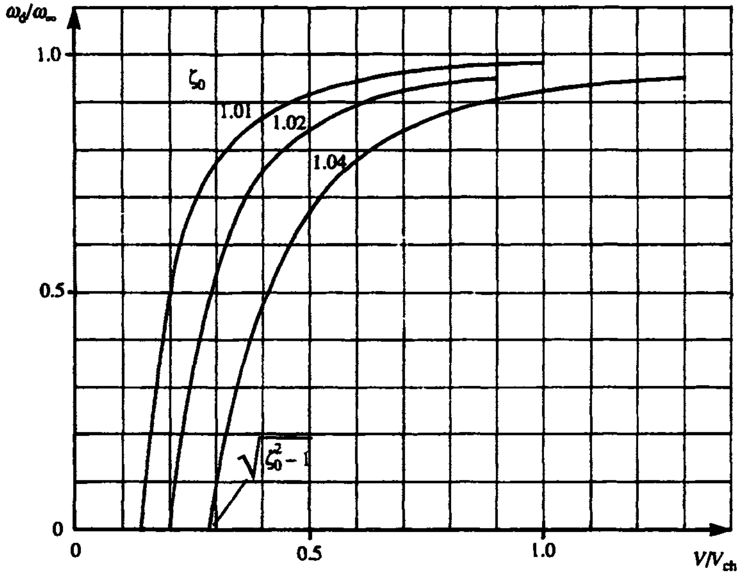

Figure 7.7.4. Damped natural frequency versus speed (understeer).

For a neutral-steer vehicle, the damping ratio always equals ζ_0 which is greater than or equal to 1.0, so the response is always overdamped and there is no real solution for ω_d.

For the oversteer case,

$$\frac{\omega_\mathrm{d}^2}{\omega^2} = 1 - \frac{\zeta_0^2}{1 - \left(\dfrac{V}{V_\mathrm{cr}}\right)^2}$$

There is an oscillatory solution for $V < V_\mathrm{cr}$, with

$$\omega^2 = \frac{C_1}{I}\left[\left(\frac{V_\mathrm{cr}}{V}\right)^2 - 1\right]$$

giving

$$\frac{\omega_\mathrm{d}^2}{C_1/I} = -1 - \left(\frac{V_\mathrm{cr}}{V}\right)^2\left(\zeta_0^2 - 1\right)$$

Thus, since $\zeta_0 \geq 1$, there is no speed with real ω_d, and all responses are overdamped. Above V_cr, of course, the response is divergent.

Knowing the damped natural frequency

$$f_\mathrm{d} = \frac{\omega_\mathrm{d}}{2\pi}$$

then the yaw-sideslip response has a wavelength, along the road, of

$$\lambda = \frac{V}{f_\mathrm{d}} = \frac{2\pi V}{\omega_\mathrm{d}}$$

For example at 50 m/s and 1 Hz this is a wavelength of 50 m.

7.8 Improved 2-dof Model

The accuracy and utility of the various equations involving C_1 found for the two-degrees-of-freedom model may be enhanced by using an effective C_1

deduced from a known understeer gradient or static margin; i.e., instead of the simplistic

$$C_1 = 2aC_{\alpha f} - 2bC_{\alpha r}$$

we may adapt the simple equation for understeer from Chapter 6:

$$k_U = -\frac{mC_1}{4LC_{\alpha f}C_{\alpha r}}$$

to give

$$C_1 = -\frac{4kLC_{\alpha f}C_{\alpha r}}{m}$$

or

$$C_1 = -x_s C_0$$

where k_U or x_s is found from the more extensive steady-state analysis of Chapter 6. In this way, effects such as pneumatic trail, rolling resistance with load transfer, and compliance steer can be incorporated. Roll-steer and roll camber can also be incorporated; in this case the model really requires that the roll natural frequency is substantially higher than that for yaw, which in practice it is for most cars, being about twice the undamped value even for high speed. If it is desired to study the development of roll angle itself, or to more accurately incorporate roll steer and camber and the inertial effects of roll, then the three-degrees-of-freedom model must be used.

7.9 Stability Derivatives

A common alternative representation of the equations of motion uses the stability derivative notation. In this system the side force is represented by Y and the yawing moment by N, and the variation of these with respect to a motion parameter is shown by a subscript; for example, the rate of change of side force with attitude angle is

$$Y_\beta \equiv \frac{\mathrm{d}Y}{\mathrm{d}\beta}$$

Hence the equations of motion may be expressed in the vehicle-fixed axes by

$$\sum Y = Y_\beta \beta + Y_r r + Y - mV\left(\dot{\beta} + r\right) = 0$$

$$\sum N = N_\beta \beta + N_r r + N - I\dot{r} = 0$$

where Y and N are additional forces and moments, either external (e.g., aerodynamic) or steering ($Y_\delta \delta$), and $\dot{\beta} = \dot{v}/V$. As discussed in Section 6.6, the actual derivatives for the two-degrees-of-freedom model are

$$\begin{aligned}
Y_\beta &= -\left(2C_{\alpha f} + 2C_{\alpha r}\right) = -C_0 \\
Y_r &= -\frac{1}{V}\left(2aC_{\alpha f} + 2bC_{\alpha r}\right) = -\frac{C_1}{V} \\
N_\beta &= -\left(2aC_{\alpha f} - 2bC_{\alpha r}\right) = -C_1 \\
N_r &= -\frac{1}{V}\left(2a^2C_{\alpha f} + 2b^2C_{\alpha r}\right) = -\frac{C_2}{V}
\end{aligned}$$

With this notation, the simultaneous differential equations of free motion in the vehicle-fixed axes become

$$(mVD - Y_\beta)\,\beta + (mV - Y_r)\,r = 0$$

$$(-N_\beta)\,\beta + (ID - N_r)\,r = 0$$

and in the Earth-fixed axes they become

$$\left(mD - \frac{Y_\beta}{V}\right)u + \left(-Y_r D + Y_\beta\right)\psi = 0$$

$$\left(-\frac{N_\beta}{V}\right)u + \left(ID^2 - N_r D + N_\beta\right)\psi = 0$$

The characteristic equation for both cases becomes

$$mID^2 - \left(N_r m + \frac{IY_\beta}{V}\right)D + \left(\frac{Y_\beta N_r}{V} + mN_\beta - \frac{Y_r N_\beta}{V}\right) = 0$$

For the two-degrees-of-freedom model there is no great advantage in the use of stability derivatives; in fact rather the contrary because Y_r and N_r vary with speed and hence obscure the effect of speed on the equations. However, the stability derivative notation is useful for the more complex three-degrees-of-freedom model because it is more concise.

7.10 3-dof Model

As discussed in Section 7.8, some of the effects of roll, for example roll steer, can be included indirectly in the two-degrees-of-freedom model. However, a fuller representation requires that roll is included as an explicit variable, usually denoted by ϕ for the roll angle and p for the roll angular speed. This is known as the three-degrees-of-freedom model (sideslip, yaw and roll), and was first systematically investigated by Segel.

The vehicle is considered as two masses – the rolling sprung mass m_S and the unsprung mass m_U. The sprung mass is considered to roll about a longitudinal axis parallel to the ground, at the same height as the "real" roll axis where it meets the vertical z-axis. The origin of the vehicle-fixed xyz axes is not taken at the center of mass but on the roll axis below the center of mass. The basic equations of motion for side force, yaw moment and roll moment, in vehicle-fixed axes, are

$$\sum Y = m(\dot{v} + Vr) + m_S d\dot{p}$$

$$\sum N = I_z\dot{r} + I_{xz}\dot{p}$$

$$\sum L = I_x\dot{p} + m_S d(\dot{v} + Vr) + I_{xz}\dot{r}$$

where I_x is the second moment of sprung mass about the x-axis; because this does not pass through G, this includes an $m_S d^2$ term, where d is the height of G above the roll axis. Roll moment L here is not to be confused with the wheelbase.

In comparison, the 2-dof equations are

$$\sum Y = m(\dot{v} + Vr)$$

$$\sum N = I_z\dot{r}$$

$$\sum L = I_x\dot{p}$$

with the extra 3-dof terms arising from sprung mass roll motion and I_{xz} roll-yaw interaction.

The external forces and moments acting on the vehicle, in stability derivative notation, are

$$\sum Y = Y_\beta\beta + Y_r r + Y_\phi\phi + Y$$

$$\sum N = N_\beta\beta + N_r r + N_\phi\phi + N$$

$$\sum L = L_p p + L_\phi\phi + L$$

where some small terms, e.g., Y_p, are neglected, and Y, N and L are additional applied force and moment, e.g., aerodynamic or steering ($Y_\delta\delta$). The actual values of the stability derivatives depend on the design parameters of the vehicle, but are generally more complex than for the simple two-degrees-of-freedom model, being

$$Y_\beta = -(2C_{\alpha f} + 2C_{\alpha r})$$

$$Y_r = -\frac{2aC_{\alpha f} - 2bC_{\alpha r}}{V}$$

$$Y_\phi = -(2\varepsilon_{Sf}C_{\alpha f} - 2\varepsilon_{Sr}C_{\alpha r}) - (2\varepsilon_{Cf}cC_{\alpha f} - 2\varepsilon_{Cr}cC_{\alpha r})$$

where ε_S is the roll steer coefficient, ε_C is the roll camber coefficient and c is the tire camber/slip stiffness ratio C_γ/C_α.

$$N_\beta = -(2aC_{\alpha f} - 2bC_{\alpha r}) + \frac{dM_{Zf}}{d\alpha_f} + \frac{dM_{Zr}}{d\alpha_r} + \mu_R(2C_{\alpha f}h_f + 2C_{\alpha r}h_r)$$

where M_Z is the tire self-aligning moment, μ_R is the rolling resistance coefficient and h is the height of the roll axis above the ground.

$$N_r = -\frac{2a^2C_{\alpha f} + 2b^2C_{\alpha r}}{V}$$

$$N_\phi = (2a\varepsilon_{Sf}C_{\alpha f} - 2b\varepsilon_{Sr}C_{\alpha r}) - (2a\varepsilon_{Cf}cC_{\alpha f} - 2b\varepsilon_{Cr}cC_{\alpha r}) - \mu_R k_S$$

where k_S is the suspension roll stiffness.

$$L_p = \frac{dL}{dp}$$

which depends primarily on the damper properties, and

$$L_\phi = k_S + m_S g d$$

where $m_S g d$ is the effect of roll in moving G from directly above the roll axis.

In addition, for steering effects:

$$Y_\delta = 2C_{\alpha f}$$

$$N_\delta = 2aC_{\alpha f} - \frac{dM_{Zf}}{d\alpha_f}$$

The equations given above are essentially the equations given by Segel, expressed in slightly different notation.

Knowing these actual values for the stability derivatives, the external forces can be inserted into the equations of motion to yield three simultaneous differential equations for the three independent variables (e.g., lateral speed, yaw angle, roll angle). These are therefore solvable in principle, although analytic solutions are tedious to perform; the Laplace transform method was used by Segel, with results discussed later for various steer inputs.

In comparing this model with the simpler two-degrees-of-freedom model as expressed in Section 7.9 it should be appreciated that it is more complex for two separate reasons. First, it includes more detail, e.g., aligning torque, and second, it includes roll as a separate variable giving three differential equations. This more complex model has been found to give very good agreement with experiment in the linear region of handling.

The natural motion and stability depend on the characteristic equation. For the three-degrees-of-freedom model this is a quartic:

$$A_4 D^4 + A_3 D^3 + A_2 D^2 + A_1 D + A_0 = 0$$

As for the two-degrees-of-freedom model, it is found in practice that for fixed control, dynamic instability does not occur, i.e., that if there is instability it is static, and hence depends simply on the sign of A_0, a positive value being stable, where

$$A_0 = -Y_\beta\left(N_r L_\phi + m_S d V N_\phi\right) - N_\beta\left[L_\phi\left(mV - Y_r\right) - m_S d V Y_\phi\right]$$

There are two principal modes of oscillation having natural frequencies of typically 0.5 Hz and 1 Hz, the lower frequency mode being primarily yawing and sideslipping, the other being primarily roll. Provided that the two natural frequencies are not too close, an approximate factorization of the characteristic equation is reasonably accurate. Ellis developed the following approximation:

$$\left[mVI_zD^2 - \left(I_zY_\beta + mVN_r\right)D + \left(Y_\beta N_r + mVN_\beta - Y_rN_\beta\right) - \frac{m_SdV}{L_\phi}\left(N_\beta Y_\phi - Y_\beta N_\phi\right)\right]$$
$$\times\left[\left(I_x - \frac{m_S^2d^2}{m}\right)D^2 - L_pD - L_\phi\right] = 0$$

where the first major factor corresponds to the yaw motion, and the second to the roll motion. The first factor, compared with the two-degrees-of-freedom characteristic equation, shows approximately how roll affects the yaw natural frequency.

7.11 Step-Steer Response

In practice it is not possible to perform a true step change to the steer angle, a ramp-step being more realistic. However, a step input is particularly simple theoretically. The step-steer response is perhaps the most fundamental transient because it corresponds to simple corner entry or exit conditions. After a step-steer input, there is a new equilibrium state achieved after a transient depending on the natural frequency and damping in yaw. The most general step-steer input is a shift from one corner radius to another, but the case usually analyzed is that starting from straight running.

Figure 7.11.1(a) shows the transient yaw speed response for cases of understeer, neutral and oversteer below critical speed. The attitude response is similar. The best response is that of the neutral vehicle. For understeer there is a response overshoot because of the sub-critical damping, getting worse with increasing speed. For oversteer the damping is good but the response takes a long time to reach equilibrium. Physically, this is because the oversteering vehicle requires a smaller steer input for a given steady state, and the smaller input gives a smaller initial response. The slowness of oversteer vehicles to reach their steady-state levels is one of the factors that makes them generally more difficult to drive. Alternatively, Figure 7.11.1(b) shows the different response to equal steer inputs.

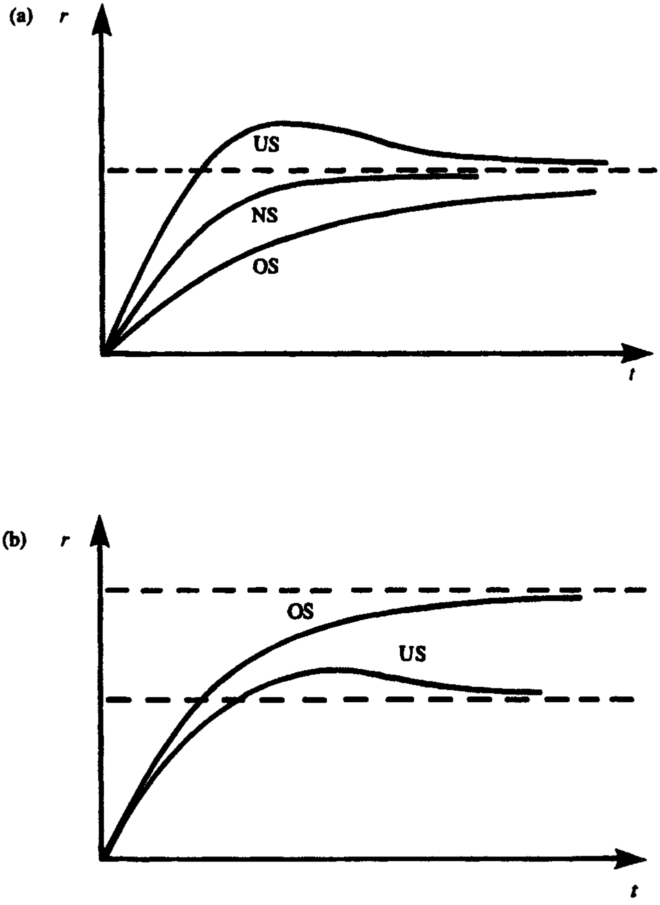

Figure 7.11.1. Yaw speed versus time for steer input: (a) different steer inputs, equal final yaw speeds, (b) equal steer inputs, different final yaw speeds.

Immediately after a step-steer input δ, before any yaw develops there is a front side force $F_y = 2C_{\alpha f}\delta$ and yaw moment $M_z = 2aC_{\alpha f}\delta$. There is a corresponding initial lateral acceleration $A_y = 2C_{\alpha f}\delta/m$ and yaw angular acceleration $\dot{r} = 2aC_{\alpha f}\delta/I$. The yaw angular acceleration creates a yaw speed that gives a slip angle at the rear; this contributes a rear side force that aids the lateral acceleration. On the other hand, the side force induces a side velocity with a corresponding contrary rear slip angle. After a short time t the sideslip velocity and yaw speed are

$$v = \frac{2C_{\alpha f}\delta}{m}t$$

$$r = \frac{2aC_{\alpha f}\delta}{mk_z^2}t$$

where k_z is the yaw radius of gyration. The rear slip angle is therefore

$$\begin{aligned} \alpha_r &= \frac{rb}{V} - \frac{v}{V} \\ &= \frac{2C_{\alpha f}\delta\left(ab - k_z^2\right)t}{Vmk_z^2} \end{aligned}$$

Therefore if $ab < k_z^2$ the rear slip angle will develop initially in the correct direction. If $ab < k_z^2$ it will initially develop in the wrong direction and will undergo a reversal before reaching steady state. Hence a large ab in relation to k_z^2 (a "wheel on each corner") helps to produce an agile vehicle.

The full solution for yaw speed for the three-degrees-of-freedom model is too complex to reproduce here, but the two-degrees-of-freedom analysis is enlightening. After the steer angle step δ, in the vehicle-fixed axes the side force and yaw moment equations of motion are

$$(mVD + C_0)\beta + \left(mV + \frac{C_1}{V}\right)r = 2C_{\alpha f}\delta$$

$$C_1\beta + \left(ID + \frac{C_2}{V}\right)r = 2aC_{\alpha f}\delta$$

Remembering that the initial side force and moment are simply $2C_{\alpha f}\delta$ and $2aC_{\alpha f}\delta$, the initial conditions are

$$\begin{aligned}\beta_0 &= \frac{v_0}{V} = 0\\ \dot{\beta}_0 &= \frac{\dot{v}_0}{V} = \frac{2C_{\alpha f}\delta}{mV}\\ \psi_0 &= 0\\ r_0 &= 0\\ \dot{r}_0 &= \frac{2aC_{\alpha f}\delta}{I}\end{aligned}$$

To find, for example, the yaw speed r we must eliminate β from the equations of motion: to do this multiply the first by C_1 and the second by $(mVD + C_0)$ and subtract, giving

$$mIVf_c(D)\,r = \left[C_1 - (mVD + C_0)a\right]2C_{\alpha f}\delta$$

where $f_c\,(D)$ is the characteristic equation in D with unity coefficient in D^2. On the right-hand side, we can simplify because δ is a constant and so $D\delta = 0$ (hence the simplicity of the step-steer input), giving

$$f_c(D)\,r = (C_1 - aC_0)\frac{2C_{\alpha f}\delta}{mIV} = C$$

where C is constant for the motion. The solution to this differential equation comes in two parts – the particular integral corresponding to the final steady state, and the complementary function corresponding to the transient natural response. For a final steady-state yaw speed r_1, which is a constant, $Dr_1 = 0$ and $D^2r_1 = 0$, so in terms of the undamped natural frequency the particular integral is given by

$$f_c(D)r_1 = \omega^2 r_1$$

$$G_r = \frac{r_1}{\delta} = \frac{(C_1 - aC_0)2C_{\alpha f}}{V\left(\dfrac{C_0C_2}{V^2} - mC_1 - \dfrac{C_1^2}{V^2}\right)}$$

This expression for the yaw speed gain can be compared with that found in Chapter 6.

The solution for the transient is more complex, and depends on whether the vehicle is understeer, neutral or oversteer. In the case of understeer, assume a solution of damped oscillatory form:

$$r = e^{-\zeta\omega t}(A\sin\omega_d t + B\cos\omega_d t) + r_1$$

The initial condition at $t = 0$ is

$$r_0 = 0 = B + r_1$$

Differentiating to find $\dot{r}$, at $t = 0$

$$\dot{r}_0 = \frac{2aC_{\alpha f}\delta}{I} = -\zeta\omega B + A\omega_d$$

Hence

$$B = -r_1$$

$$A = \frac{2aC_{\alpha f}\delta}{I\omega_d} - \frac{\zeta\omega r_1}{\omega_d}$$

This establishes the arbitrary constants, and the complete transient solution is known.

For an oversteer vehicle, the assumed form of solution is

$$r = Ae^{D_1 t} + Be^{D_2 t} + r_1$$

where D_1 and D_2 will be negative. At $t = 0$,

$$r_0 = 0 = A + B + r_1$$

Differentiating to find $\dot{r}$,

$$\dot{r} = D_1 Ae^{D_1 t} + D_2 Be^{D_2 t}$$

At $t = 0$

$$\dot{r}_0 = \frac{2aC_{\alpha f}\delta}{I} = D_1 A + D_2 B$$

This suffices to find A and B, as required.

For the case of a neutral-steer vehicle, the standard solution is

$$r = A\,e^{D_1 t} + Bt\,e^{D_1 t} + r_1$$

At $t = 0$

$$r_0 = 0 = A + r_1$$

Differentiating r above:

$$\dot{r} = AD_1\,e^{D_1 t} + B\,e^{D_1 t} + BD_1 t\,e^{D_1 t}$$

At $t = 0$

$$\dot{r}_0 = \frac{2aC_{\alpha f}\delta}{I} = AD_1 + B$$

This suffices to find A and B for the neutral-steer case.

If it is required to find the attitude angle rather than the yaw speed, then r must be eliminated from the simultaneous differential equations of motion rather than β. To study the path of the vehicle, for example to find the path of G, the Earth-fixed axes formulation must be used. In all cases the method of solution is as above.

For the three-degrees-of-freedom model, the analysis is more complex but gives very similar results.

7.12 Oscillatory Steer Response

The "steady-state" response to an oscillatory (sinusoidal) steer input is not of great practical significance, since this is unlikely to arise in normal operation on the road. However, a sinusoidal steer input is of some theoretical interest for a frequency domain analysis, and can be investigated experimentally.

The three-degrees-of-freedom analysis for this input was first performed by Segel (1955a,b). Figures 7.12.1 to 7.12.3 show how the yaw speed amplitude, roll speed amplitude and lateral acceleration amplitude varied with input frequency. Modern cars and tires tend to give flatter responses up to rather higher frequencies. Modern coaches can produce results much as in these figures. For frequencies below 3 Hz, provided that the speed is not very low, the tire dynamic characteristic (lag between force and angle) can be neglected. As would be expected, the yaw velocity amplitude (Figure 7.12.1), diminishes with frequency, beginning with the steady-state response value. At high frequency it is inertia-limited, so there is only a small yaw amplitude. Neglecting the small response, then evidently the yaw moment tends to $M_z = 2aC_{\alpha f}\delta$, where δ is the applied steer angle amplitude. The yaw acceleration amplitude tends to $A_y = 2aC_{\alpha f}\delta/I$ and the yaw velocity amplitude to $r = 2aC_{\alpha f}\delta/I\omega_f$, where ω_f is the forcing radian frequency of the steering motion. The phase of the response varies from in-phase at low frequency to 90° lag at high frequency.

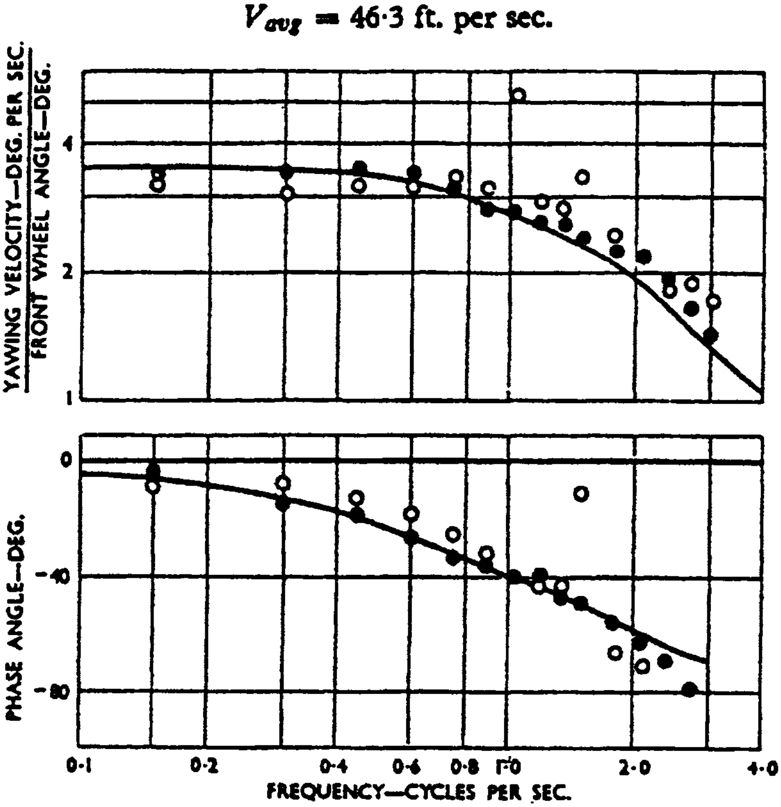

Figure 7.12.1. Yaw speed amplitude and phase: against steer frequency. (Reproduced by permission of the Council of the Institution of Mechanical Engineers, from Segel, L., "Theoretical Prediction and Experimental Substantiation of the Response of the Automobile to Steering Control," Proc. I.Mech.E., *1957.)*

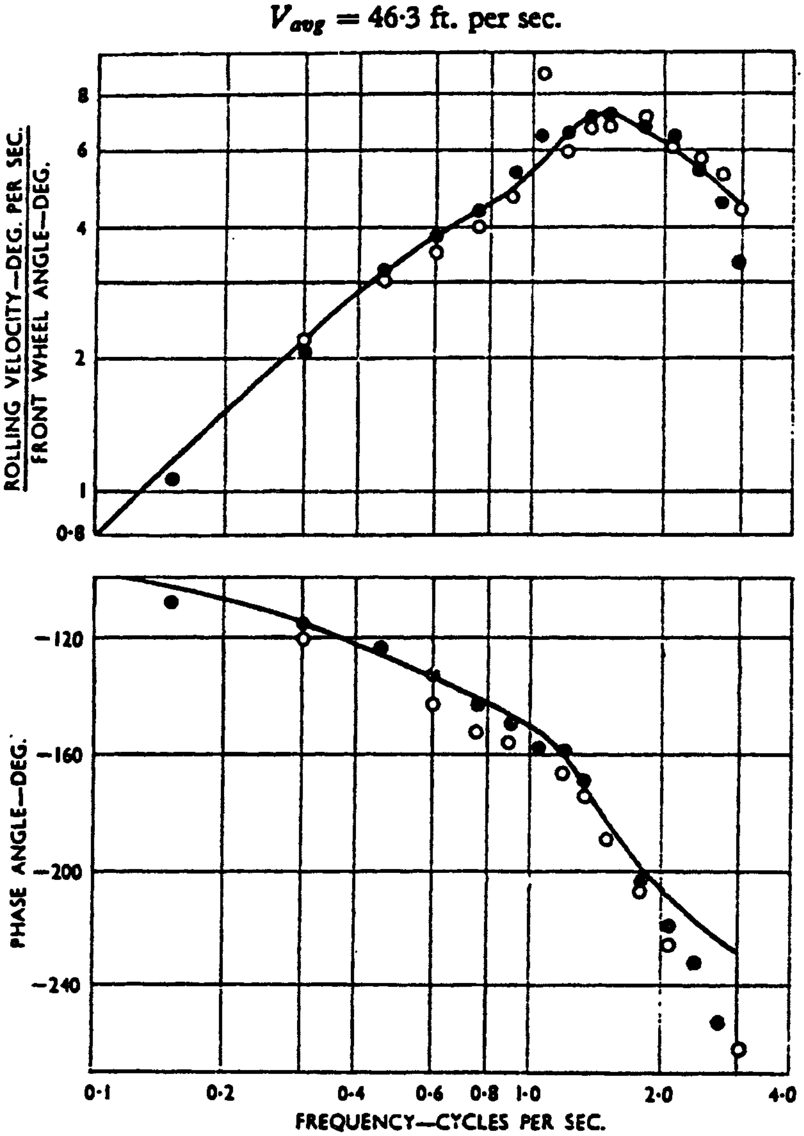

Figure 7.12.2. Roll speed amplitude and phase: against steer frequency. (Reproduced by permission of the Council of the Institution of Mechanical Engineers, from Segel, L., "Theoretical Prediction and Experimental Substantiation of the Response of the Automobile to Steering Control," Proc. I.Mech.E., *1957.)*

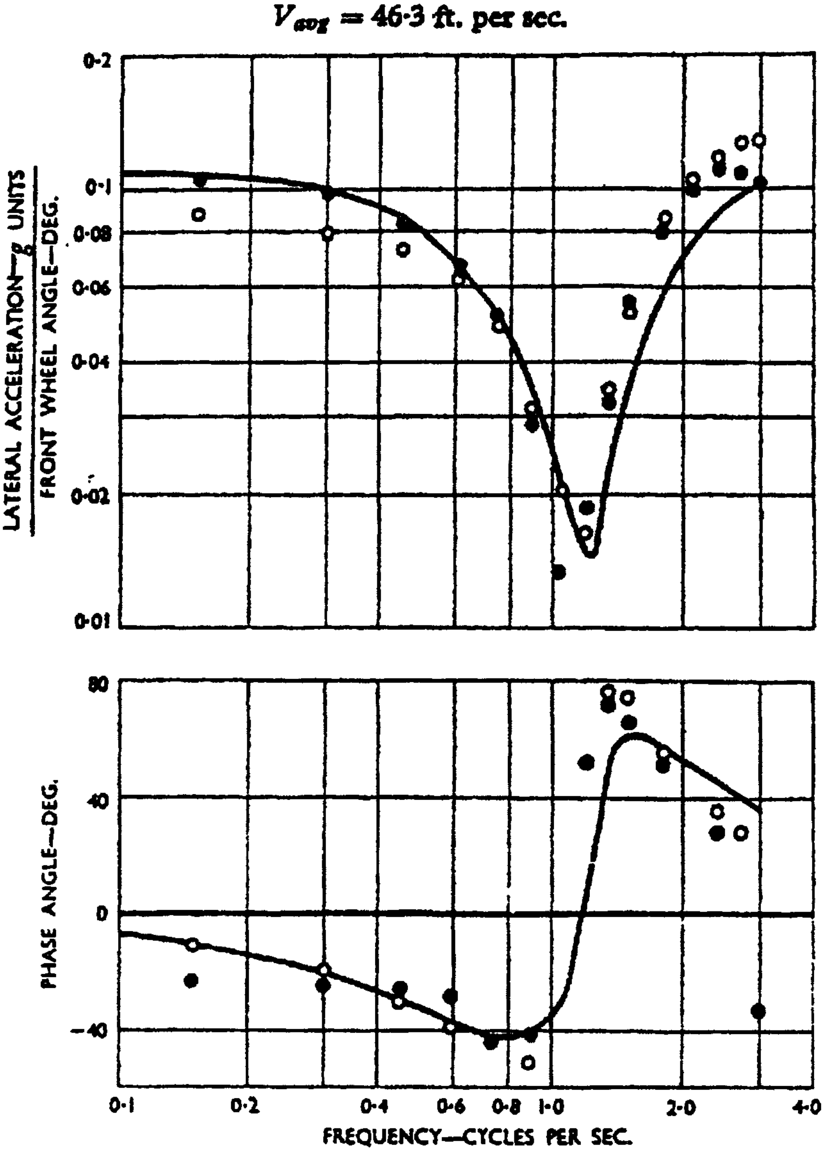

Figure 7.12.3. Lateral acceleration amplitude and phase: against steer frequency. (Reproduced by permission of the Council of the Institution of Mechanical Engineers, from Segel, L., "Theoretical Prediction and Experimental Substantiation of the Response of the Automobile to Steering Control," Proc. I.Mech.E., *1957.)*

The roll velocity response (Figure 7.12.2), begins at zero at low frequency, increases to a peak at around the roll natural frequency, and then declines. The phase lag goes from 90°, through 180° around resonant frequency, to 270° lag at high frequency.

The shape of the lateral acceleration response, Figure 7.12.3, is somewhat unexpected, being rather like an inverted resonance curve. The agreement between theory and practice is, therefore, particularly gratifying. At low frequency the value equals the steady-state response. At high frequency there is little yaw response, so for the 2-dof model the total amplitude side force tends to approximately $F_y = 2C_{\alpha f}\delta$ and the lateral acceleration amplitude to $A_y = 2C_{\alpha f}\delta/m$. In between, there is a minimum. The reason for this shape of curve is that it is the sum of three terms, two decreasing with frequency, and one, the linear lateral acceleration, increasing with frequency. The phase of the response begins at zero, goes to about 45° lead through the resonant frequency, and then declines to zero again.

If the steering forcing frequency is increased beyond about 3 Hz then the tire dynamics will become significant, and there will be a further reduction in response and an extra phase lag.

Instead of using a sinusoidal steering motion of various given frequencies, an alternative frequency domain test is to use a random steer input. The vehicle motion is then the product of the random input spectrum and the vehicle transfer function, so by correlating the output motion with the input steering, the transfer function may be deduced. This is particularly easy if the input is white noise, i.e., having a uniform spectral distribution, at least over the frequency range of interest.

7.13 Power Steer

Previous sections have dealt with the response to steering control, but there may also be steering response to the accelerator or brake, known as power steer and brake steer, respectively. The former must obviously be distinguished from "power steering," i.e., power-assisted steering. Such effects are generally undesirable and are designed out if possible (Section 5.13). The effects may be considered to arise in two ways. The first is by effects that occur on the vehicle considered as a rigid body and include differences in tractive force from side to side, for example because of a limited-slip differential or because of tractive force effects on the tire characteristics. The second is because of vehicle internal compliances.

The dynamic effects are similar to those in the steady state, but may be much greater because the tractive forces are greater. In particular, "lift-off tuck-in" may be very noticeable – really this is the disappearance of power understeer, although nowadays it is known how to control this or to eliminate it if required.

Where a large amount of power is applied then the driven end of the vehicle will inevitably have its cornering ability reduced because of the tire characteristics, giving oversteer for rear drive and understeer for front drive. For more moderate power applications, many details matter and one cannot really generalize. The effect of internal compliance is also very complex and will not be dealt with here, but see Section 5.13.

The effect of a non-free differential on the vehicle as a rigid body may be analyzed in the following way. The tractive force above that required for steady state is $F = mA_X$. Consider a rear-drive vehicle with a tractive force lateral transfer factor e_T:

$$F_i = \tfrac{1}{2}F(1 - e_T)$$

$$F_o = \tfrac{1}{2}F(1 + e_T)$$

With $e_T = 0$ the traction is equally distributed as on a free differential; with $e_T = 1$ all the traction is on the outer wheel. The plan-view moment of the tractive force is

$$M = \tfrac{1}{2}Fe_T T$$

To avoid changing the steady-state cornering radius there must be counteracting side forces at the axles of

$$\frac{M}{L} = \frac{Fe_T T}{2L}$$

The corresponding changes of slip angle are

$$\Delta\alpha_f = -\frac{Fe_T T}{4LC_{\alpha f}}$$

$$\Delta\alpha_r = \frac{Fe_T T}{4LC_{\alpha r}}$$

The change of steer angle required is

$$\Delta\delta = \Delta\alpha_\mathrm{f} - \Delta\alpha_\mathrm{r}$$

$$= -\frac{Fe_\mathrm{T}T}{4L}\left(\frac{1}{C_{\alpha\mathrm{f}}} + \frac{1}{C_{\alpha\mathrm{r}}}\right)$$

which is an oversteer effect for positive e_T. Using $F = mA_\mathrm{x}$, for a car

$$\Delta\delta \approx 0.5A_\mathrm{x}e_\mathrm{T} \quad \text{(deg)}$$

Now since e_T may be in the range 1 to –1 according to the type of differential and the power applied (Section 6.13), then $\Delta\delta$ may be as much as 0.5 deg/m s^{-2} (5 deg/g), a substantial change, potentially much greater than the differential effects in steady state. For good handling, the steer effect should not exceed 1 deg/g of longitudinal acceleration, and therefore non-free differentials may be problematic in this respect.

Power-steer effects are particularly problematic on racing cars for several reasons. The lap time is very sensitive to car acceleration at exit from the corners, with combined lateral and longitudinal accelerations. The high power-to-weight ratios give strong longitudinal acceleration which quickly reveals any handling shortcomings, and, of course, limited-slip differentials are used. Finally, many racing cars have aerodynamic forces that are very sensitive to pitch angle, and particularly to the height of the front wings from the ground.

7.14 Disturbance Response

Transient disturbances include road roughness, changes of surface friction, and wind effects.

Theoretical investigations of road roughness effects have been very limited because of the shortage of data on tire characteristics in conditions of fluctuating normal force. For small fluctuations one might expect the side forces to adjust according to the response distance concept, as they do for varying slip angle, giving little change to the mean force. However, for large fluctuations, if the normal force goes to zero then there will be an immediate loss of side force, not compensated by the slowly growing side force when the normal force becomes large, giving a reduced mean cornering force. Hence the dependence of tire side force on normal force fluctuation amplitude and frequency seems to be an interesting area for investigation and a necessary prerequisite for detailed study of vehicle response in such conditions. Practical results will also depend on how the vertical force actually fluctuates, depending on the suspension characteristics, including the dampers.

The effect of changes of surface friction, for example due to ice patches, is perhaps of wider importance. Again, this is not easily amenable to a useful general analytical approach, but is usually studied by time domain computer analysis.

Transient wind effects are of practical significance – much more so than steady wind effects. They are at their worst at high speed, because although for a given lateral wind speed the aerodynamic attitude angle is less, the dynamic pressure is greater. On motorways, when overtaking or being overtaken, one vehicle may temporarily shield another from a strong side wind, or a large vehicle may subject a small adjacent vehicle to a strong flow even in the absence of wind. The effect of a lateral air speed component may be analyzed in various ways. The consequent lateral force and moment can be inserted into the two-degrees-of-freedom dynamic model; if the vehicle deviation effect on the wind force is neglected, i.e., the force and moment are assumed constant, then this gives a manageable analytical solution. If a computer simulation of the vehicle is available then of course the wind force can be made a function of vehicle lateral speed and yaw angle.

The conclusions of such analysis are fairly simple. The steady-state response is not critical because it simply requires a fixed steering deflection (Section 6.20). The driver response time is about 0.25 s, although experimental results show that the path deviation takes typically 2 s to reach its maximum; it is this maximum that is the important result. This deflection is partly the result of aerodynamic side force but in most cases mainly of the yaw moment; hence a forward center of mass eases the problem. The deflection also depends on the vehicle's handling characteristics, but since these are largely dictated by the wind-free handling requirements, the gust response can really be controlled only by tailoring the aerodynamic characteristics. Essentially this means minimizing the yaw moment, which means keeping the lateral force center of pressure as far back as possible. There is a conflict here, because low-drag shapes tend to have a relatively forward center of pressure and it may be necessary to compromise on the detail design.

7.15 Testing

Unsteady-state testing can conveniently be divided into three types:

(1) Vehicle characteristics

(2) Task performance

(3) Subjective assessment

The first type, vehicle characteristic testing, is open-loop, whereas the last two types, by including the driver performance, are closed-loop tests.

In the open-loop tests, the vehicle motion is studied in response to specified control inputs. The most fundamental test is a step-steer input; in practice a ramp-step is used because the step cannot be achieved instantaneously. This enables the rapidity of response and overshoot to be investigated, giving an experimental measure of the natural frequency and damping ratio. Alternatively a small-amplitude single-cycle steering oscillation (open-loop version of a lane change) or a random steer input (white noise) can be used. The ISO has published draft procedures for these tests. In practice the random steer test seems most practical because it does not require mechanically controlled steering and can be performed on a two-lane-wide road. A variation of the random input test is the steering sweep test, in which a basically sinusoidal steering motion is used, but with smoothly increasing frequency.

Another standard comparison of theory and experiment is the steer pulse, i.e., a sudden deflection of steering and prompt restoration to straight ahead. In Laplace transform analysis the steer deflection can be represented by a succession of three ramps with time delays, and gradients in the ratio 1:–2:1, or by a half period of a sine wave.

The slalom test is distinct from the oscillatory steer test in that the latter uses small steer amplitude and is linear. In the slalom test the vehicle is driven as quickly as possible on a sinuous course on alternating sides of a series of obstacles, and large lateral accelerations are required. Although in principle this is an open-loop test, in practice driver skill plays a significant part. One serious criticism of the slalom test is that comparative ranking of vehicles may vary with the spacing of the obstacles, because of the different vehicle natural yaw and roll frequencies. Hence it has not found wide application. In a variation of the test, the obstacle spacing is progressively reduced and the vehicle is driven at constant speed; this does not overcome the previously mentioned objection.

Little has been published on results of testing on controlled road roughness. The obvious test would be a complete circular test pad with added roughness elements, e.g., radial slats, that can be changed in severity and spacing. A more economical alternative that has been tried is to have a relatively short segment of the circular path slatted, and to drive into the rough region at or near the maximum speed for the smooth section; in such tests the roughness seems to have surprisingly little effect. Tests using a single bump seem to suggest that this is an adequate test of roughness response.

A typical task performance test is the lane-change test. The vehicle is driven at fixed speed toward an obstruction requiring a lane change that could be either right or left; the driver is told as late as possible which way to go. The shortness of time or distance to the obstruction is a measure of the closed-loop lane change performance of the vehicle. This may be quite good for comparative testing of complete vehicles, or for testing detail design changes to the suspension or tires.

Vehicle behavior in side winds can be predicted quite well from wind tunnel yaw data. However, full-scale side wind testing is still sometimes performed, for example by driving the vehicle into a side wind generated by gas turbines exhausting into diffusers to widen the jet, which further expands by mixing with air (at MIRA one engine produces a 40 m wide, 20 m/s jet at the road). To investigate the actual path deviation that will be experienced in practice, the vehicle should be in the side wind for 2 s, the time to maximum deviation. At 20 m/s this requires an exposed path of about 40 m of relatively uniform wind. However, subjective testing is probably best performed in natural wind conditions.

The final test of dynamic handling is of course the subjective general driving test undergone by any new vehicle over a distance of many miles. Although theory is good at predicting the path of a vehicle in response to given control inputs, it is much less good at predicting whether the driver will feel confident in the vehicle. This is because the driver is sensitive to small dynamic effects, e.g., the rigidity of seat mountings. Therefore subjective testing remains of great importance.

7.16 Desirable Results

Various research papers have addressed the question of how the subjective opinion of the driver relates to the dynamic characteristics of the vehicle, and what those characteristics should be for the best subjective and objective performance. Opinions vary. This may be for several reasons: some tests are performed with average drivers, others with experienced test drivers; investigations of a parameter over a limited range may wrongly suggest that it is not important; the test may not be long enough, so potentially superior features are rejected because drivers favor the familiar over the unfamiliar; finally, drivers are inherently highly adaptive, which tends to mask the effect of vehicle characteristics, while at the same time making them generally less critical. A good set of definitive objective tests that predict subjective quality has not yet emerged. On the other hand, there is often agreement as to what constitutes bad dynamic handling, and some conclusions can be drawn. The following indicates some of the results that have been published.

The yaw velocity gain under oscillatory steer conditions is given approximately by the simplified Laplace transfer function

$$G_r = \frac{G_{r\,ss}}{1 + T_r s}$$

where T_r is the effective time constant of the yaw speed behavior, i.e., the lag of the yaw from the steer input. This expression is a reasonable approximation provided that the yaw damping is not too small, i.e., the vehicle is not too understeer. For both expert and average drivers, for a vehicle to be rated as satisfactory requires that $T_r < 0.5$ s, and a good rating requires $T_r < 0.3$ s.

In tests at 23 m/s (50 mph), yaw velocity gains, referred to the handwheel, of 0.2 to 0.4 deg s^{-1}/deg are found to be desirable. This corresponds to understeer gradients of 3.4 deg/g down to zero. The undamped yaw natural frequency should be at least 1 Hz, and the yaw damping ratio at least 0.5 and preferably 1.0. For good yaw damping at high speed the understeer gradient needs to be small, under 2.0 deg/g. Vehicles notable for good handling have been observed to be close to neutral; some would even argue that a small amount of primary oversteer is justified to obtain high yaw damping. Rear roll understeer has, in particular, been implicated in detrimental reduction of yaw damping.

A good correlation has been found between subjective rating, objective performance and the "TB value." This is the product of $T_{\dot\psi}$ and β_{ss} where $T_{\dot\psi}$ is the time from step-steer input to peak overshoot of yaw velocity, and β_{ss} is the steady-state attitude angle, these being measured at a speed of 31.8 m/s (70 mph) and for a steer input sized to give 0.4g steady-state lateral acceleration. In practice, because the steer input is a ramp rather than a true step, time is measured from the moment when the steering is at half of its steady-state value. When a subjective handling poorness rating (1 being very easy handling, 5 being very difficult handling) is used, it is found that the poorness value is proportional to the TB value, reaching 5 at TB = 4.2 deg s.

Thus a TB value of 2 deg s or less is a desirable design target. However, it is not clear that the TB value is really more significant than separately specifying values for $T_{\dot\psi}$ and β_{ss}, both of which should be as small as possible. Also $T_{\dot\psi}$ will be measurable only if there is a distinct yaw velocity overshoot, and this will not be the case if there is good yaw damping – itself desirable.

Good straight running definitely depends on the dynamic characteristics rather than just the steady-state understeer gradient. It is desirable to avoid large amounts of roll steer which can cause weaving. Two vehicles with the same overall understeer gradient may achieve the final value with very different component contributions. Under dynamic conditions, e.g., small wind disturbances or small steer corrections, these differences may manifest themselves when it is generally found that a vehicle with large compensating steady-state effects will not behave well. Good straight running in windy conditions, however, does depend on the steady-state understeer gradient, among other things. Put another way, the relationship between the neutral steer point (the position of which is governed by the center-of-mass position and the understeer gradient) and the aerodynamic center of pressure for side forces is very influential on straight running in gusty conditions.

Another problem with roll steer or bump steer is that it leads to increased tire wear. Nevertheless, many vehicle manufacturers do use roll steer to obtain their desired handling characteristics. Provided that the effects are symmetrical from side to side (a matter of production tolerances) and not excessive, the effect on straight running may be acceptable.

Even if the vehicle itself has good straight-running characteristics, it is possible for the driver to be unhappy, for example in the case of the "oversteering seat" (Grylls 1972). This illustrates the great sensitivity of the driver to relatively small oversteering effects and how a small attitude gradient is important subjectively as well as objectively.

Obtaining good behavior in gusty crosswinds is partly a matter of tuning the aerodynamic coefficients, basically getting the center of pressure as far back as possible, and partly a matter of avoiding suspension arrangements that make the vehicle unduly responsive to wind stimulation.

In the case of racing cars, it is not just a case of obtaining maximum braking, cornering and traction, but also of making the handling predictable so that the driver can extract the full performance; to this end it is usual to eliminate compliance as much as possible, for example by replacing rubber bushes by metal ball-joints. This option is simply not available on passenger cars – the deliberate inclusion of compliance is essential to control noise, vibration and harshness. Until relatively recently the handling engineer saw this mostly as a handling problem with the compliance tolerated; in recent years with growing understanding it has become possible to use compliance advantageously, in the control of power steering and lift-off tuck-in effects, which can now be held to low levels.

As already discussed, there is a correlation between subjective rating and the steering correction required because of braking longitudinal acceleration in a turn. For a good rating, the steer correction should not exceed 1 deg/g at the road wheels, say 20 deg/g at the handwheel, and should preferably be less. Speculatively, a similar quantitative criterion could be applied to power steer on acceleration; in this case, non-free differentials with a steer effect of as much as 5 deg/g at the road wheels are clearly problematic.

7.17 Problems

Q 7.2.1 Explain the difference between the damping coefficient C, the damping factor α_D and the damping ratio ζ.

Q 7.3.1 Establish the equation of motion for a 1-dof sideslip-only model, and show that there is damping but no oscillation.

Q 7.4.1 Establish the equation of motion for a 1-dof yaw-only model, and describe the motion for understeer and oversteer cases.

Q 7.5.1 Establish the differential equations of motion for a 2-dof model in vehicle-fixed axes in v and r.

Q 7.5.2 For a 2-dof model in vehicle-fixed axes, derive the characteristic equation of motion.

Q 7.6.1 Establish the differential equations of motion for a 2-dof model in Earth-fixed axes, in u and ψ.

Q 7.6.2 Derive expressions for the tire slip angles perceived in Earth-fixed axes and vehicle-fixed axes, and discuss the difference.

Q 7.7.1 Deduce the conditions for stable motion from the characteristic equation.

Q 7.7.2 Deduce equations for the damping ratio and damped natural frequency from the characteristic equation. Discuss how these vary with speed.

Q 7.7.3 "Dynamic yaw damping requirements place an upper limit on acceptable understeer gradient." Discuss.

Q 7.7.4 "A neutral steer vehicle has a yaw damping ratio of unity." Discuss.

Q 7.7.5 “Yaw damping is equally due to yaw and sideslip.” Discuss.

Q 7.7.6 When a free yaw oscillation is damped out, the energy of oscillation is dissipated. Where does it go?

Q 7.7.7 For a vehicle with $L = 3$ m, $C_{\alpha f} = 1000$ N/deg, $C_{\alpha r} = 1000$ N/deg, $m = 400$ kg, $I = 2744$ kg m^2, $a = 1.3$ m, at a speed of 22 m/s, find the undamped yaw frequency, damping ratio and damped yaw frequency. Also find the understeer gradient k_U, and V_{ch}.

Q 7.8.1 Explain how factors such as pneumatic trail can be incorporated into an improved 2-dof model.

Q 7.8.2 The vehicle of Q 7.7.7 is found experimentally to have a steady-state understeer gradient of 1.74 deg/g. Suggest an effective value for C_1.

Q 7.9.1 Explain the stability derivative notation, and give expressions for the four stability derivatives for the simple 2-dof model and the improved version.

Q 7.9.2 For the vehicle of Q 7.7.7. evaluate the 2-dof stability derivatives at 15 m/s. State the units in each case.

Q 7.10.1 For the 3-dof model, list all the various possible stability derivatives, and discuss their relative importance. Give representative values.

Q 7.10.2 “The 3-dof model is more complex, more accurate and superior to the 2-dof model.” Discuss.

Q 7.10.3 Under what conditions is the 3-dof model stable?

Q 7.10.4 Explain quantitatively, giving equations and numerical values, how roll affects the yaw natural frequency. Describe the physical features that could be used to achieve this effect. What would be the disadvantages?

Q 7.10.5 Considering the approximate factorization by Ellis, explain the effect of roll on yaw behavior.

Q 7.11.1 Sketch the step-steer response of various understeer, oversteer and neutral-steer vehicles, and discuss their relative merits.

Q 7.11.2 For a step-steer input, explain how the rear slip angle develops for various vehicles.

Q 7.11.3 “Having a ‘wheel on each corner’ results in an agile vehicle.” Discuss.

Q 7.11.4 For an understeer vehicle, applying suitable initial conditions for a step-steer input, derive an expression for the transient solution for 2-dof.

Q 7.12.1 Describe how, for a real vehicle, yaw speed, roll speed and lateral acceleration depend on the frequency of a sinusoidal steer input of fairly small amplitude.

Q 7.13.1 Explain how traction affects transient handling.

Q 7.13.2 Derive equations describing how a limited-slip differential affects transient handling.

Q 7.14.1 Explain the effect of a step change of aerodynamic side force, and how this depends on the aerodynamic static margin.

Q 7.15.1 Give an overview of transient testing.

Q 7.15.2 Explain the difference between slalom testing and an oscillatory steer test.

Q 7.16.1 “It is not possible to have a definitive set of objective transient handling tests because of driver variability.” Discuss.

Q 7.16.2 “For the best overall handling, a vehicle should have a small amount of primary oversteer.” Discuss.

Q 7.16.3 Describe some of the transient handling criteria that have been suggested.

Q 7.16.4 Explain the “TB” value, critically.

Q 7.16.5 “Compensating steer effects may not compensate under transient conditions, giving poor handling.” Discuss.

7.18 Bibliography

As far as books are concerned, some dynamic two-degrees-of-freedom analysis is included in Wong (1978). There is a fairly extensive dynamic analysis of two- and three-degrees-of-freedom models in Ellis (1969) and Ellis (1989). A useful introduction to the three-degrees-of-freedom model is given by Steeds (1960). The transient handling problems that have prevented four-wheel-drive success in racing are discussed by Henry (1975). Gillespie (1992) gives some analysis of rollover.

Of some historical interest, the first paper to study dynamic behavior was by Stonex (1941). An early theoretical analysis was that by Rocard (1946). The real advance in dynamic analysis came in 1957. An extensive list of references up to that time is given in Milliken & Whitcomb (1956). An extensive analysis of the two-dimensional model is given in Whitcomb & Milliken (1957). The three-dimensional model is considered in detail in Segel (1957a and 1957b).

Some of the more interesting papers since that time include: Bergman (1965), Milner (1968), McHenry (1969), Dugoff *et al.* (1971), Carr *et al.* (1973), Bergman (1973), Pacejka (1975), Fancher *et al.* (1976), Bundorf & Leffert (1976), Yoshimori (1976), Good (1977), Weir & Zellner (1977), Chiang & Starr (1978), Weir & DiMarco (1978), Verma & Shepard (1981). The ISO has (unpublished) draft procedures for steer response testing (ISO 1979a,b,c).

The lane-change test has not achieved acceptance as an ISO standard, but there is a technical report ISO TR 3888: Lane Change Test. For braking-in-a-turn testing, see ISO (1985).

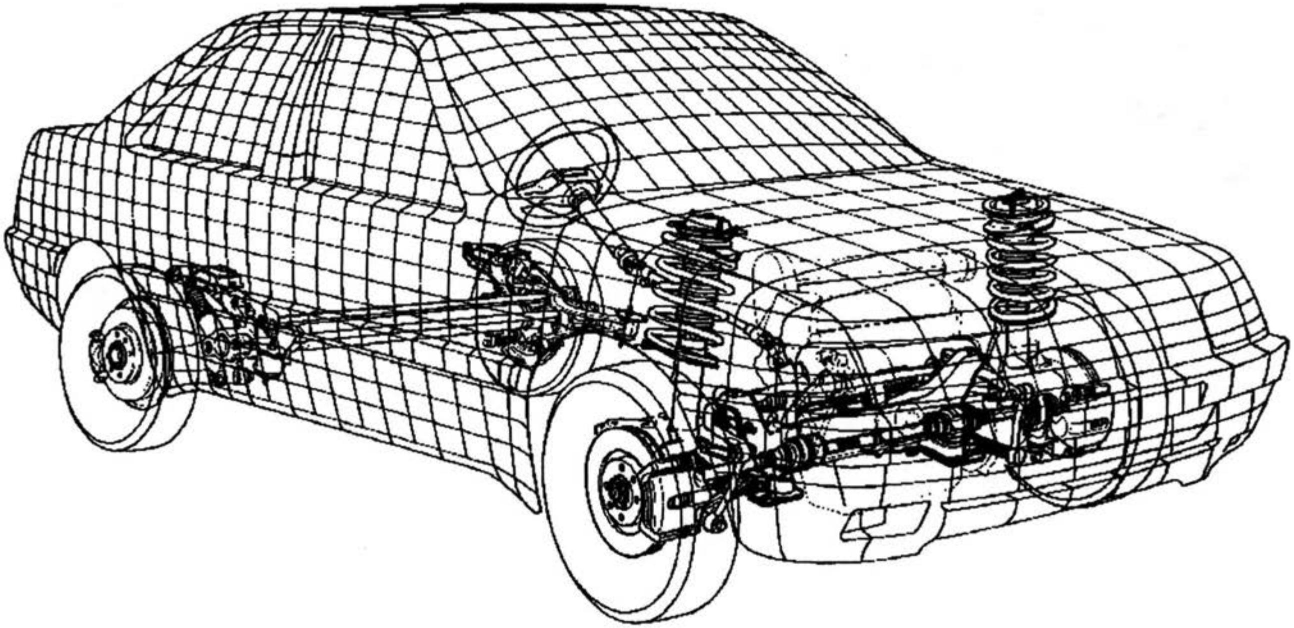

The Peugeot 405 with "Integrated Chassis Design" is broadly representative of modern car suspension designs. It uses struts at the front, but with longitudinal location by a wide-based wishbone rather than by the anti-roll bar which instead acts through drop links (hence strictly not MacPherson struts). The steering is rack-and-pinion, and is mounted on the same sub-frame as the suspension, reducing some adverse steering compliance effects. The rear uses trailing arms, also with anti-roll bar. With many modern cars using a similar layout, the difference between good and bad handling lies in careful optimization of details of the motion geometry of the links (bump steer and bump camber), and of the compliance of the bushes (compliance steer), with a rigid body shell to integrate the whole system. (Courtesy of The Peugeot Talbot Motor Company Ltd.)

Appendix A

Nomenclature

Quantities such as acceleration and force are vector in nature. When the vector nature is implied, such variables are shown in bold type (e.g., **A**, $\mathbf{F}_\mathrm{S}$). Usually, however, the equations use the magnitudes or the scalar components of such vector quantities. These are therefore not vectors and are printed in italic (sloping) type (e.g., A, A_X, F_S). Points are labeled in normal (upright) type. Hence: center-of-mass point G, gear ratio G, linear momentum vector **G**.

Units: Equations are intended to be used in S.I. unit variables, although in many cases they may also be directly applicable in Imperial units. A variable such as understeer gradient is often quoted for convenience in deg/g; its correct S.I. unit is rad/m s^{-2}, which is the unit applicable to numerical values deduced from equations here.

In some cases units are added in brackets. Those shown in square brackets are true S.I. units. Also shown in round brackets are units commonly used to express the value. However, these common units may not be suitable for use in some equations. In particular, angles may need to be in radians.

Normal S.I. units are m for length, s for time, m/s or m s^{-1} for velocity, kg for mass, N (= kg m/s^2) for force, Nm for moment, N/m^2 for pressure (also called pascal, Pa), J for energy, and W for power (J/s). Angles are correctly expressed in rad. Degrees are the common practical unit of course, but rad may be necessary in some equations. Angular speeds should be in rad/s. Frequencies are expressed in rad/s (the radian frequency) or Hz (hertz, cycles/second). Damping coefficients are Ns/m, which is a more concise form of N/m s^{-1}, the latter being a clearer expression of its meaning in a damping context.

Chapter 1 Introduction

a	front axle to G
A	acceleration
A	area
b	rear axle to G
c	dimension
d	dimension
f_N	natural frequency
F	force magnitude
$\mathbf{F}$	force vector
F_{AeD}	aerodynamic drag
F_C	centripetal force
F_D	drag
F_i	static imbalance force
F_R	rolling resistance force
F_S	tire central force
F_T	tire tractive force, tangential force
F_{TCD}	tire cornering drag force
F_{TD}	tire drag force
g	gravitational field strength
$\mathbf{G}$	linear momentum vector [kg m/s]
G	center of mass
H	height of G
$\mathbf{H}$	angular momentum vector [kg m^2/s]
i_Y	dynamic index in yaw
i_P	dynamic index in pitch
i_R	dynamic index in roll
I	second moment of mass [kg m^2]
k	radius of gyration
K	stiffness [N/m]
L	wheelbase
L_P	rotary pendulum length
m_k	mass of kth component
m	vehicle mass
m_S	sprung mass
m_U	unsprung mass
$\mathbf{M}$	moment vector
M	moment magnitude [Nm]
M_i	dynamic imbalance moment [Nm]
N	wheel or axle vertical force
p	roll angular speed [rad/s]
P	power [W, J/s]
q	pitch angular speed [rad/s]
r	yaw angular speed [rad/s]
R	path radius, dimension
R_l	wheel loaded radius
S	tire slip
T	track
T	tension
T_{sw}	steering wheel torque
V	speed
W	weight force
u, v, w	velocity components
xyz	vehicle-fixed axes
X_G	x coordinate of G position
XYZ	Earth-fixed axes
Z	pendulum length
α	tire slip angle [rad] (deg)
β	attitude angle
δ	steer angle
δ_{ref}	reference steer angle
δ_{sw}	steering wheel angle
θ	pitch angle, angle
λ	wavelength
μ_R	rolling resistance coefficient [–]
ν	course angle
ρ	air density
ϕ	roll angle
ψ	heading angle
ω	angular speed [rad/s]
Ω	wheel spin angular speed [rad/s]

Subscripts:

Ae	aerodynamic
C	centripetal, centrifugal, cradle
D	drag
f	front
k	kth component
L	left, lift
M	maximum
m	mean
O	fixed axis
p	principal
P	pitch, pendulum
r	rear
R	right, roll
S	sprung
T	tire, tangential
U	unsprung
V	vehicle
Y	yaw

Chapter 2 The Tire

A	area
c	foundation stiffness [N/m^2]
C	a constant [varies]
C_B	tire braking force coefficient [–]
C_C	tire camber stiffness coefficient [rad^{-1} (deg^{-1})]
C_{FD}	tire drag force coefficient [–]
C_{FS}	tire central force coefficient [–]
C_{FV}	variation of F_Y with F_V [–]
C_{FT}	load transfer sensitivity of axle [–]
C_{MZ}	tire moment "coefficient" M_Z/F_V [m]
C_S	tire cornering stiffness coefficient [rad^{-1} (deg^{-1})]
C_t	tire circumference
C_T	normalized load transfer sensitivity of axle [–]
C_V	load sensitivity of F_Y to F_V [–]
C_W	wave speed [m/s]
C_X	tire longitudinal force coefficient [–]
C_Y	lateral force coefficient [–]
C_α	tire cornering stiffness [N/rad] (N/deg)
C_γ	tire camber stiffness [N/rad] (N/deg)
C_p	tire curvature stiffness [Nm]
d	tread displacement [m]
e_V	vertical force transfer factor [–]
F	force magnitude
F_D	tire drag force
F_R	rolling resistance force
F_S	tire central force
F_V	tire vertical force ($-F_Z$)
F_{VT}	transferred vertical force
F_X, F_Y, F_Z	tire forces on $X'Y'Z'$ axes
F_X	longitudinal force
F_Y	lateral force
F_α	cornering force
F_γ	camber force
I	second moment of mass [kg m^2]
k_{CSFV}	sensitivity of C_S to F_V [–]
k_{CSV}	sensitivity of C_S to V
K_t	tire vertical stiffness
l	tire footprint length
L	relaxation distance
M_X, M_Y, M_Z	tire moments on $X'Y'Z'$ axes
M_X	overturning moment
M_Y	rolling resistance moment
M_Z	aligning moment (torque)
N_{DH}	dynamic hydroplaning number [–]
N_{Dr}	tire tread drainage number [–]
N_T	Turner number [–]
N_{VH}	viscous hydroplaning number [–]
P	contact pressure
p	load sensitivity of μ_Y [–]
R_D	tire test drum radius
p_i	inflation pressure (gauge)
R_e	effective tire rolling radius (V/Ω)
R_l	tire loaded radius

R_u	tire unloaded radius
s	normalized slip (S/S^*) [–]
S	slip [–]
S^*	characteristic slip [–]
t	pneumatic trail [m]
t_C	crown tension per unit width [N/m]
T	temperature [°C]
T	wheel drive torque [Nm]
V	speed
x	position in tire footprint
X	distance rolled
$X'Y'Z'$	wheel-aligned axes
$X''Y''Z''$	motion-aligned axes
α	slip angle [rad] (deg)
α^*	characteristic slip angle
γ	camber angle
θ	slope angle
δ_t	tire vertical compression
λ	wavelength
μ	coefficient of limiting friction [–]
μ_B	maximum braking force coefficient [–]

μ_D	dynamic friction coefficient [–]
μ_R	rolling friction coefficient [–]
μ_S	static friction coefficient [–]
μ_Y	maximum lateral force coefficient (C_{Ymax}) [–]
μ_X	maximum longitudinal force coefficient (C_{Xmax}) [–]
ρ	path curvature ($1/R$) [m^{-1}]
ρ_C	crown density per unit area [$\mathrm{kg/m^2}$]
ρ_W	density of water
τ	water clearance time constant [s]
Ω	wheel spin angular speed [rad/s]

Subscripts:

d	drum
M	maximum
m	mean
t	tire
2	two wheels
α	related to slip angle
γ	related to camber angle

Chapter 3 Aerodynamics

a	wind speed-height exponent [–]
A	reference or frontal area
A_D	drag area
c_p	specific thermal capacity [J/kg K]
c_v	specific thermal capacity [J/kg K]
C_D	drag coefficient [–]
C_{D1}	drag coefficient on 1 m^2 [–]
C_L	lift coefficient [–]
C_P	pitch coefficient [–]
C_R	roll coefficient [–]
C_S	side force coefficient [–]
C_Y	yaw coefficient [–]
F	force magnitude
F_{AeD}	aerodynamic drag force
F_{AeL}	aerodynamic lift force
F_{AeS}	aerodynamic side force
g	gravitational field strength

h	ground clearance
h_A	aerodynamic static margin from wheelbase mid-point [m]
I	turbulent intensity [–]
k	thermal conductivity [W/m.K]
L	wheelbase
m_m	molar mass [kg/kmol]
M	relative molar mass [–]
Ma	Mach number [–]
M_{AeP}	aerodynamic pitch moment
M_{AeR}	aerodynamic roll moment
M_{AeY}	aerodynamic yaw moment
p	atmosphere pressure
P	probability [–]
q	dynamic pressure
R_G	universal gas constant [J/kmol K]
Re	Reynolds number [–]

T_C	temperature (Celsius) [°C]
T_K	absolute temperature (kelvin) [K]
U	wind speed
v	velocity
v_a	ambient wind speed
v_r	relative wind speed
v_v	vehicle speed
V	speed
V_{ch}	characteristic wind speed
V_s	speed of sound
V_S	sustained wind speed
W	turbulent speed deviation [m/s]
x	length dimension
z	altitude from sea level
z_0	altitude constant
xyz	vehicle-fixed axes
XYZ	Earth-fixed axes

α	body pitch angle [rad] (deg)
β	Weibull wind shape factor [–]
β	vehicle sideslip angle
β_{Ae}	aerodynamic sideslip angle

γ	ratio of specific thermal capacities [–]
δ	steer angle
μ	fluid dynamic viscosity [Ns/m^2, Pa s]
ν	fluid kinematic viscosity [m^2/s]
ν_a	ambient wind angle
ν_r	relative wind angle
ν_v	vehicle velocity angle
ρ	air density [kg/m^3]

Subscripts:

Ae	aerodynamic
a	air
D	dry
f	front
M	maximum
m	mean
r	rear, relative
v	vehicle
W	water
0	reference

Chapter 4 Suspension Components

C	damping coefficient [N/m s^{-1}, Ns/m]
d	spring wire diameter
D	spring coil diameter
F	force
$F_{A/B}$	degrees of freedom A from B [–]
G	shear modulus [N/m^2, Pa]
h	suspension travel
I	second moment of mass [kg m^2]
J	polar second moment of mass
L	wheelbase, torsion bar length
m	component mass [kg]
m_e	vehicle end mass (m_f or m_r)
m_S	sprung mass
m_U	unsprung mass
N	number of working coils

r	torsion bar radius
R	motion ratio [–]
T	torque [Nm]
V	speed
$\mathbf{V}$	velocity vector
x	spring deflection
xyz	coordinates

ζ	damping ratio [–]
θ	angle, torsional deflection
ω	angular speed, wheel precession speed [rad/s]
Ω	wheel spin angular speed [rad/s]

Chapter 5 Suspension Characteristics

a	front axle to G
A	lateral acceleration
A_B	braking deceleration
A_F	frontal area
A_M	maximum lateral acceleration
A_R	rollover lateral acceleration
b	rear axle to G, kingpin offset
b_a	kingpin offset at wheel axis height
c	caster offset
C_D	damping coefficient [N/m s^{-1}, Ns/m]
C_F	force center point
C_L	vertical lift coefficient [–]
C_P	pitch coefficient [–]
C_R	roll coefficient [–]
C_Rra	roll coefficient about roll axis [–]
C_S	side lift coefficient [–]
C_T	turning center point
C_W	damping coefficient at the wheel [Ns/m]
C_Y	yaw coefficient [–]
d	height of G_S above roll axis
$d_\mathrm{f}, d_\mathrm{r}$	load transfer moment distribution factors [–]
d_tf	front proportion of tractive force [–]
D_1, D_2	diagonal sums of F_V [N]
e	Panhard rod offset
e_B	tire vertical force braking transfer factor [–]
e_S	tire side force lateral transfer factor [–]
e_V	tire vertical force lateral transfer factor [–]
e_X	tire vertical force longitudinal transfer factor [–]
f_L	load transfer factor (h/T) [–]
f_Li	incremental load transfer factor [–]
f_A	steering Ackermann factor [–]
F	force
F_AeL	aerodynamic lift force
F_AeS	aerodynamic side force
F_AeD	aerodynamic drag force
F_J	jacking force
F_S	sprung mass side force
F_s	spring force
F_T	lateral load transfer
F_TD	diagonal load transfer (diagonal bias)
F_TL	lateral load transfer through suspension links
F_TM	lateral load transfer through sprung mass moment
F_TS	lateral load transfer through sprung mass
F_TU	lateral load transfer through unsprung mass
F_TX	longitudinal load transfer
F_TXAe	longitudinal aerodynamic load transfer
F_U	unsprung mass side force
F_V	wheel vertical force
F_Y	wheel lateral force
g	gravitational field strength
G	center of mass
G_S	overall steering gear ratio [–]
G_m	mean steering gear ratio [–]
h	roll axis height at G_S, roll center height
h_A	roll axis height at aerodynamic side force position
H	height of G
J_AR	anti-roll coefficient [–]
J_ad	front anti-dive coefficient [–]
J_al	front anti-lift coefficient [–]
J_ar	rear anti-rise coefficient [–]
J_as	rear anti-squat coefficient [–]
k	roll stiffness [Nm/rad]
k_A	axle roll stiffness [Nm/rad]
k_β	attitude angle gradient $\mathrm{d}\beta/\mathrm{d}A$ [rad/m s^{-2}] (deg/g)
k_CS	compliance steer gradient [rad/m s^{-2}] (deg/g)

k_{CU}	compliance understeer gradient [rad/m s^{-2}] (deg/g)
k_ϕ	roll angle gradient dϕ/dA [rad/m s^{-2}] (deg/g)
$k_{\phi S}$	axle roll gradient [rad/m s^{-2}] (deg/g)
$k_{\phi S}$	suspension roll gradient [rad/m s^{-2}] (deg/g)
k_R	total ride roll stiffness [Nm/rad] (Nm/deg)
k_{RC}	roll camber gradient [rad/m s^{-2}] (deg/g)
k_{RS}	roll steer gradient [rad/m s^{-2}] (deg/g)
k_{RCA2}	quadratic roll center height variation coefficient [s^4/m = m/(m $s^{-2})^2$] (m/g^2)
k_{RU}	roll understeer gradient [rad/m s^{-2}] (deg/g)
k_{RUFV}	sensitivity of ε_{RU} to axle load [N^{-1}]
k_S	suspension roll stiffness [Nm/rad]
K	stiffness [N/m]
K_r	ride rate [N/m]
K_s	spring stiffness
K_t	tire vertical stiffness
K_W	wheel rate [N/m]
L	wheelbase
m	mass
M	steering moment about kingpin axis [Nm]
M_A	aligning torque steer moment [Nm]
M_{AeP}	aerodynamic pitch moment
M_{AeR}	aerodynamic roll moment
M_{SAe}	aerodynamic roll moment about the roll axis on sprung mass
M_{AeY}	aerodynamic yaw moment
M_L	lateral force steer moment
M_P	propshaft torque
M_{Pr}	propshaft moment
M_S	sprung mass moment
M_T	tractive force steer moment
M_V	vertical force steer moment
M_ϕ	roll moment from springs and anti-roll bar
N_f, N_r	axle vertical force from ground
p	front proportion of brake force [–]
p_i	inflation pressure [N/m^2, Pa]
q	dynamic pressure
R	cornering path radius
R_S	motion ratio of spring [–]
R_D	motion ratio of damper [–]
s	cross beam height
S	spring spacing, link spacing
S_R	safety factor against rollover [–]
T	track
T_R	torque to steer road wheels
T_s	handwheel torque
V	velocity
w	cross beam length
W	weight force
xyz	vehicle-fixed coordinates
XYZ	Earth-fixed coordinates
V	velocity
z	ride displacement from static
z_D	damper deflection from static
z_S	suspension compression (bump) from static position
z_W	wheel deflection from static
Z	ride height or position
β	attitude angle [rad] (deg)
β_{Ae}	aerodynamic attitude angle
γ_{BC}	bump camber angle
γ_{CC}	compliance camber angle
γ_{LCC}	lateral force compliance camber angle
γ_{OCC}	overturning moment compliance camber angle
γ_{RC}	roll camber angle
γ_S	steer camber angle
δ	steer angle
δ_{ACS}	aligning moment compliance steer angle
δ_{BS}	bump steer angle
δ_{CS}	suspension compliance steer angle
δ_{DBS}	double-bump steer angle

δ_{LCS}	lateral force compliance steer angle
δ_{ref}	reference steer angle
δ_{RS}	roll steer angle
δ_{RU}	roll understeer angle
δ_s	steering handwheel angle
ε	suspension geometric steer coefficient [various]
ε_{BC}	bump camber coefficient [rad/m] (deg/m)
ε_{BS}	bump steer coefficient [rad/m] (deg/m)
ε_{DBS}	double-bump steer coefficient [rad/m] (deg/m)
ε_{RC}	roll camber coefficient [–] (deg/deg)
ε_{RS}	roll steer coefficient [–] (deg/deg)
ε_{RU}	roll understeer coefficient [–] (deg/deg)
ε_{SC}	steer camber coefficient [–] (deg/deg)
$\varepsilon_{B\theta C}$	bump caster coefficient [rad/m] (deg/m)
ε_{RT2}	quadratic roll toe-out coefficient [rad/rad^2] (deg/deg^2)
ϕ	roll angle
ϕ_A	axle roll angle
ϕ_{Ae}	aerodynamic roll angle
ϕ_{Pr}	propshaft roll angle
ϕ_S	suspension roll angle
η	suspension compliance steer coefficient [various]
η_{ACS}	aligning moment compliance steer coefficient [rad/Nm] (deg/Nm)
η_{LCC}	lateral force compliance camber coefficient [rad/N] (deg/N)
η_{LCS}	lateral force compliance steer coefficient [rad/N] (deg/N)
η_{OCC}	overturning moment compliance camber coefficient [rad/Nm] (deg/Nm)
λ	Langensperger angle of axle
μ	coefficient of limiting friction [–]
θ_c	caster angle
θ_{cf}	front anti-dive CE line inclination
θ_{cfi}	CE-line inclination for full front anti-dive effect
θ_k	kingpin inclination angle
ρ_A	axle axis inclination
ρ_{ra}	roll axis inclination

Subscripts:

A	axle
Ae	aerodynamic
B	Body
BC	bump camber
BS	bump steer
c	caster
CS	compliance steer
D	diagonal, damper
DBS	double bump steer
f	front
HS	heave steer
i	incremental, inclination
J	jacking
L	left, links
M	maximum
m	mean
P	pitch
Pr	propshaft
R	right, roll
r	rear
ra	roll axis
RC	roll camber
RO	roll oversteer
RS	roll steer
RU	roll understeer
S	sprung, spring
T	transferred
t	tire, tractive
U	unsprung
W	wheel
Y	yaw

Chapter 6 Steady-State Handling

a	front axle to G
a'	front axle effective moment arm when steered
A	acceleration
A_{ax}	absolute acceleration in x direction
A_D	drag area
A_M	tire grip maximum lateral acceleration
A_f	maximum front lateral acceleration
A_r	maximum rear lateral acceleration
A_R	rollover maximum lateral acceleration
b	rear axle to G
C	coefficient [–]
C_D	drag coefficient [–]
$\mathrm{C_F}$	force center point
C_L	lift coefficient [–]
C_R	roll coefficient [–]
C_P	pitch coefficient [–]
C_S	side lift coefficient [–]
$C_S{}'$	$dC_S/d\beta$ [rad^{-1}] (deg^{-1})
C_T	tractive force coefficient [–]
$\mathrm{C_T}$	turning center point
C_x	tire longitudinal stiffness [N] (N/unit slip)
C_Y	yaw coefficient [–]
$C_Y{}'$	$dC_Y/d\beta$ [rad^{-1}] (deg^{-1})
C_0	zeroth moment vehicle cornering stiffness [N/rad] (N/deg)
C_1	first moment vehicle cornering stiffness [Nm/rad] (Nm/deg)
C_2	second moment vehicle cornering stiffness [Nm^2/rad] (Nm^2/deg)
C_α	tire cornering stiffness [N/rad]
C_γ	tire camber stiffness [N/rad]
d_f, d_r	fractions of lateral load transfer [–]
D_f, D_r	axle cornering compliance
e_S	side force transfer factor [–]
e_V	vertical force transfer factor [–]
f	tire C_α sensitivity to F_V [–]
f_R	response factor [–]
f_S	stability factor (k_U/L) [rad/m^2 s^{-2}] (deg/g.m)
F	force
F_{AeD}	aerodynamic drag force
F_{AeL}	aerodynamic lift force
F_{AeS}	aerodynamic side force
F_D	vehicle drag (aero + tire)
F_{DT}	tire cornering drag
F_R	tire rolling resistance
F_s	steering wheel rim force
F_T	lateral load transfer
F_{TX}	longitudinal load transfer
F_X	tire longitudinal (drive) force
g	gravitational field strength
G	center of mass point
G_A	lateral acceleration gain [m s^{-2}/rad] (g/deg)
G_r	yaw velocity gain [rad s^{-1}/rad] = deg s^{-1}/deg)
G_ρ	path curvature gain [m^{-1}/rad] (m^{-1}/deg)
G_S	overall steering ratio [–]
H	height of center of mass
j	load transfer factor [–]
k_β	attitude gradient [rad/m s^{-2}] (deg/g)
k_{CS}	compliance steer gradient [rad/m s^{-2}] (deg/g)
$k_{\delta,W}$	steer angle sensitivity to side wind [rad/m s^{-1}] (deg/m s^{-1})
k_ϕ	roll gradient [rad/m s^{-2}] (deg/g)
k_{GS}	suspension geometric steer gradient [rad/m s^{-2}] (deg/g)
k_K	kinematic steer angle gradient [rad/m s^{-2}] (deg/g)
k_{RS}	roll steer gradient [rad/m s^{-2}] (deg/g)
k_{sc}	steering column torsional stiffness [Nm/rad] (Nm/deg)
k_{SP}	suspension pitch stiffness [Nm/rad]
k_t	tire vertical stiffness

k_{TP}	tire pitch stiffness [Nm/rad]
k_U	understeer gradient [rad/m s^{-2}] (deg/g)
L	wheelbase
m	vehicle mass
m_f, m_r	front and rear endmasses
M_{AeP}	aerodynamic pitch moment
M_{AeR}	aerodynamic roll moment
M_{AeY}	aerodynamic yaw moment
M_{TXS}	sprung mass longitudinal load transfer moment [Nm]
M_{TXT}	total longitudinal load transfer moment [Nm]
n_A	number of axles on vehicle
n_W	number of wheels on axle
M	moment [Nm]
N	total yaw moment
N_f, N_r	axle vertical reactions
N_U	final understeer number [–]
p	tire maximum cornering force sensitivity to F_V [–]
q	dynamic air pressure [N/m^2, Pa]
r	yaw speed
R	path radius
R_V	vertical path radius
R^*	critical path radius
S	frontal or reference area
t	pneumatic trail [m]
T	track
T_s	steering wheel torque
U	understeer factor ($1/f_R$) [–]
V	speed
V^*	critical aerodynamic speed
V_c	V_{ch} or V_{cr} as appropriate
V_{ch}	characteristic speed
V_{cr}	critical speed
V_0	maximum cornering speed with no aerodynamic lift
w	transverse wind speed
x	forward movement of G
x_s	static margin [m]
α	tire slip angle [rad] (deg)
α_U	tire understeer angle [rad] (deg)
β	vehicle attitude angle [rad] (deg)
β_{Ae}	aerodynamic attitude angle [rad] (deg)
β_K	kinematic attitude angle [rad] (deg)
γ	tire camber angle
Δ	change
δ	steer angle of road wheels
δ_b	steering angular backlash [rad] (deg)
δ_K	kinematic steer angle [rad] (deg)
δ_{ref}	reference steer angle [rad] (deg)
δ_s	steer angle of handwheel
δ_{SU}	suspension understeer angle [rad] (deg)
δ_T	toe angle
δ_U	understeer angle [rad] (deg)
ε_{BC}	bump camber coefficient [rad/m] (deg/m)
ε_{BS}	bump steer coefficient [rad/m] (deg/m)
ε_{RC}	roll camber coefficient [–] (deg/deg)
ε_{RU}	roll understeer coefficient [–] (deg/deg)
ϕ	roll angle
ϕ_A	axle roll angle
ϕ_S	suspension roll angle
μ_R	rolling resistance coefficient [–]
μ_X	tire maximum longitudinal force coefficient [–]
μ_Y	tire maximum lateral force coefficient [–]
θ	road slope [rad] (deg)
ρ	path curvature [rad/m]
ρ	air density [kg/m^3]
θ_B	body pitch angle
θ_S	suspension pitch angle
θ_U	unsprung pitch angle

Subscripts:

a	absolute (magnitude in XYZ)
D	driven
f	front
i	inner
K	kinematic
M	maximum
m	mean
o	outer
r	rear
R	running, rolling
T	traction
U	understeer
V	vertical
x,y,z	components
0	reference state

Chapter 7 Unsteady-State Handling

a	front axle to G
A	acceleration
A_f	front maximum lateral acceleration
A_M	maximum lateral acceleration
A_r	rear maximum lateral acceleration
b	rear axle to G
c	tire stiffness ratio C_γ/C_α
C	damping coefficient [Ns/m, N/m s^{-1}]
C_0	zeroth moment vehicle cornering stiffness [N/rad] (N/deg)
C_1	first moment vehicle cornering stiffness [Nm/rad] (Nm/deg)
C_2	second moment vehicle cornering stiffness [Nm^2/rad] (Nm^2/deg)
C_α	tire cornering stiffness [N/rad] (N/deg)
C_γ	tire camber stiffness [N/rad] (N/deg)
d	height of G above roll axis
D	time derivative operator [s^{-1}]
e_T	traction transfer coefficient [–]
e_V	tire vertical force lateral transfer factor [–]
f	frequency [Hz, cycles/s]
f_R	response factor [–]
F	force magnitude
F_{X2}	tractive force of two wheels
G	center of mass
G_r	yaw speed gain [rad s^{-1}/rad, s^{-1}] (deg s^{-1}/deg)
h	height of roll axis
I	second moment of mass
k	radius of gyration
k_s	suspension roll stiffness [Nm/rad] (Nm/deg)
k_U	understeer gradient [rad/m s^{-2}] (deg/g)
k_z	yaw radius of gyration
K	spring stiffness
L	wheelbase
L	roll moment
L_p	dL/dp [Nm/rad s^{-1}]
L_ϕ	dL/dϕ [Nm/rad]
m	vehicle mass
m_S	sprung mass
m_U	unsprung mass
M	moment
M	mass
M_Z	tire self-aligning moment
N	plan-view moment
N_β	dN/dβ [Nm/rad]
N_r	dN/dr [Nm/rad s^{-1}]
p	roll speed $(\equiv \dot{\phi})$ [rad/s] (deg/s)
q	dynamic air pressure [N/m^2, Pa]
r	yaw velocity $(\equiv \dot{\psi})$ [rad/s] (deg/s)
t	time [s]
T	track [m]
T_r	directional time constant [s]
u	Y component of V ($\equiv V_Y$)
v	lateral velocity component $(\equiv \dot{y} \equiv V_y)$

V	vehicle speed
$\mathbf{V}$	vehicle velocity vector
V_c	V_{ch} or V_{cr} as appropriate
V_{ch}	characteristic speed
V_{cr}	critical speed
V_t	transition speed
x_s	static margin
xyz	vehicle-fixed axes
X	amplitude of x
XYZ	Earth-fixed axes
$\dot{y}$	lateral velocity component ($\equiv V_{ay} \equiv \mathrm{v}$)
Y	amplitude of y
Y	side force (F_y)
Y_β	$\mathrm{d}Y/\mathrm{d}\beta$ [N/rad]
Y_r	$\mathrm{d}Y/\mathrm{d}r$ [N/rad s^{-1}]

α	tire slip angle [rad] (deg)
α_D	damping factor [s^{-1}]
β	attitude angle
β_{Ae}	aerodynamic attitude angle
δ	steer angle
ε_{BC}	bump camber coefficient [rad/m] (deg/m)
ε_{BS}	bump steer coefficient [rad/m] (deg/m)
ε_{RC}	roll camber coefficient [–] (deg/deg)
ε_{RS}	roll steer coefficient [–] (deg/deg)
ε_{RU}	roll understeer coefficient [–] (deg/deg)
ϕ	roll angle, phase angle
μ_R	rolling resistance coefficient [–]
ν	path angle
ρ_P	path curvature [rad/m]
τ	time constant [s]
ω	radian frequency [rad/s]
ω	undamped natural radian frequency [rad/s]
ω_d	damped (actual) natural radian frequency [rad/s]
ω_f	forcing radian frequency [rad/s]
ψ	heading angle
ζ	damping ratio [–]

Subscripts:

a	absolute (magnitude in XYZ)
f	front
M	maximum
m	mean
r	rear
s	sprung
u	unsprung
x,y,z	components in vehicle-fixed axes
X,Y,Z	components in Earth-fixed axes
0	reference or specific condition

Appendix B

Properties of Air and Water

B.1 Air

Standard sea-level properties for dry air are given in Section 3.2. In the range of ambient conditions, sufficiently accurate properties of air for engineering purposes may be calculated by the following procedure. All results are in fundamental S.I. units. Temperature T_C (Celsius), absolute pressure P and relative humidity r are measured experimentally. If the data are in Imperial units (Fahrenheit and psi), then

$$T_C = \frac{T_F - 32}{1.8}$$

$$P = P_{psi}\frac{101325}{14.7}$$

The absolute (kelvin) temperature is

$$T_K = 273.15 + T_C \quad [K]$$

The saturated vapor pressure of water at this temperature, P_S, is given by

$$\log_{10} P_S = 3.231 + 0.02807(T_C - 15) - 1.067 \times 10^{-4} (T_C - 15)^2$$

Expressing the relative humidity as a simple decimal value *r*, not as a percentage, the actual absolute water vapor pressure is

$$P_W = rP_S$$

The universal gas constant is

$$R_G = 8314.3 \quad \text{[J/kmol K]}$$

The molar mass for water is

$$m_W = 18.0154 \quad \text{[kg/kmol]}$$

so the specific gas constant for water vapor is

$$R_W = \frac{R_G}{m_W} = 461.51 \quad \text{[J/kg K]}$$

Using the basic gas equation for the water vapor, the absolute humidity, i.e., the actual water vapor density in the air in kg/m^3, is

$$\rho_W = \frac{P_W}{R_W T_K}$$

The absolute pressure of the dry fraction of air is

$$P_D = P - P_W$$

The molar mass of dry air is

$$m_D = 28.965 \quad \text{[kg/kmol]}$$

so the specific gas constant for dry air is

$$R_D = 287.05 \quad \text{[J/kg K]}$$

The density of the dry air fraction is

$$\rho_D = \frac{P_D}{R_D T_K}$$

The total density is then

$$\rho = \rho_D + \rho_W$$

The effective mean molar mass is

$$m_A = \frac{\rho}{\rho_D / m_D + \rho_W / m_W}$$

and the specific gas constant is

$$R_A = \frac{R_G}{m_A} \quad [\mathrm{J/kg\,K}]$$

The dynamic viscosity of dry air, within 0.5% accuracy for the temperature range 250 K to 400 K, is

$$\mu = 17.75 \times 10^{-6} \left(\frac{T_K}{285}\right)^{0.76} \quad \left[\mathrm{Ns/m^2}\right]$$

The kinematic viscosity is

$$\nu = \frac{\mu}{\rho} \quad \mathrm{m^2/s}$$

The ratio of specific heats is

$$\gamma = 1.400$$

The speed of sound is

$$V_s = \sqrt{\gamma R_A T_K} \quad [\mathrm{m/s}]$$

For cooling calculations (tires, engines, dampers) the thermal conductivity, within 1% from 240 K to 500 K, is

$$k = 0.02624\left(\frac{T_K}{300}\right)^{0.8646} \quad [\mathrm{W/m.K}]$$

The specific thermal capacity at constant volume is

$$c_v = 717.8 + 0.07075\,(T_K - 300) + 261.25 \times 10^{-6}\,(T_K - 300)^2 \quad [\mathrm{J/kg\ K}]$$

which is within 0.2% for 275 K to 700 K and 1% for 175 K to 800 K.

The specific thermal capacity at constant pressure is

$$c_p = c_v + R_A$$

Where more accurate expressions are desirable, the dynamic viscosity of dry air is

$$\mu = 1.458 \times 10^{-6}\ \frac{T_K^{1.5}}{T_K + 110.4} \quad \left[\mathrm{Ns/m^2}\right]$$

This is an S.I. version of an equation used to produce reference tables for 100 K to 1800 K.

A more accurate expression for the thermal conductivity is

$$k = \frac{2.646 \times 10^{-3}\ T_K^{1.5}}{T_K + 245.4 \times 10^{(-12/T_K)}} \quad [\mathrm{W/m.K}]$$

Again, this has been used for reference tables, over the range 100 K to 1000 K.

B.2 Water

The fluid dynamic properties of water are relevant for tire hydroplaning. The thermodynamic properties are relevant for cooling of engines, etc.

The density of water is

$$\rho_W = 1001.3 - 0.155\, T_C - 2.658 \times 10^{-3}\, T_C^2 \quad [\mathrm{kg/m^3}]$$

within 0.2% for 0–200 °C (pressurized sufficiently to prevent boiling, of course).

The dynamic viscosity is given by

$$\log_{10} \mu = -2.75 - 0.0141\, T_C + 91.9 \times 10^{-6}\, T_C^2 - 311 \times 10^{-9}\, T_C^3 \quad [\mathrm{Ns/m^2}]$$

This is with 0.5% from 3 to 100 °C.

The specific thermal capacity is

$$c_P = 4209 - 1.31\, T_C + 0.014\, T_C^2 \quad [\mathrm{J/kg\ K}]$$

which is good for 0 to 200°C.

The thermal conductivity is

$$k = 0.5706 + 1.756 \times 10^{-3}\, T_C - 6.46 \times 10^{-6}\, T_C^2 \quad [\mathrm{W/m.K}]$$

again good for 0 to 200°C.

Appendix C

Example Car Specifications

The following tables give some sample data for a variety of cars. The vehicles as a whole do not represent particular real cars, although in many cases some of the data correspond to real cases. In some cases a value has been omitted, either because it is inappropriate or because it is unknown to the author. Of the numerous parameters representing suspension and tires, many have inevitably been omitted (for example, rate of roll center vertical movement in heave, and camber change in bump). Omission is not intended to imply lack of importance.

Overall, the data are intended to indicate realistic values and to provide a source of information for the setting of problems. The passenger car specifications are likely to remain realistic. For racing cars (vehicles G and H) the specifications are sensitive to rule changes and are based on 1990 rules. The C1 sports prototype rules changed significantly with a minimum mass reduction and engine capacity limitation in 1991.

Racing car specifications vary considerably, with a different set-up for each circuit (low-, medium- and high-speed set-up).

Table C.1 Example Car Specifications

Parameter	Symbol		Units	Vehicle							
				A	B	C	D	E	F	G	H
1 Vehicle and type				Sedan	Sedan	Coupe	Sedan	Sedan	Sports	Racing Formula One	Racing C1 Sports Prototype
2 Wheelbase		l	m	2.040	2.398	2.580	2.770	3.075	2.500	2.718	2.910
3 Front track	f	T_f	m	1.206	1.362	1.440	1.480	1.560	1.540	1.804	1.600
4 Rear track	r	T_r	m	1.164	1.324	1.440	1.440	1.540	1.540	1.626	1.524
5 Total mass (part load)		m	kg	727	1045	1175	1435	1945	1600	625	1020
6 G behind front axle		a	m	0.775	1.031	1.161	1.302	1.568	1.250	1.631	1.717
7 G height		H	m	0.550	0.610	0.620	0.635	0.672	0.500	0.280	0.350
8 Yaw dynamic index		i_Y	-	0.860	1.060	0.980	1.030	0.992	0.920	0.650	0.700
Suspension											
1 Wheel rate (no ARB)	f	k_{Wf}	kN/m	16.00	12.40	12.80	12.95	13.40	20.00	300	230
(per wheel)	r	k_{Wr}	kN/m	10.00	10.60	13.80	14.72	17.00	20.00	200	400
2 Roll stiffness of ARB	f	k_{Bf}	Nm/deg	0	146	248	210	205	1000	10000	4000
	r	k_{Br}	Nm/deg	0	0	0	73	0	250	2000	1000

Table C.1 Example Car Specifications (Continued)

Parameter	Symbol		Units	Vehicle							
				A	B	C	D	E	F	G	H
3 Suspension roll stiffness	f	k_{Sf}	Nm/deg	203	347	480	458	490	1414	18520	9140
(springs plus ARB)	r	k_{Sr}	Nm/deg	118	162	250	339	352	664	6611	9107
4 Unsprung mass	f	m_{Uf}	kg	50	80	92	105	115	90	46	70
(per axle)	r	m_{Ur}	kg	40	72	120	110	130	100	60	90
5 Unsprung G height	f	H_{Uf}	m	0.237	0.260	0.290	0.295	0.320	0.300	0.312	0.308
(at loaded radius)	r	H_{Ur}	m	0.237	0.260	0.290	0.295	0.320	0.300	0.320	0.338
6 Roll-center height	f	h_f	m	0.100	0.190	−0.020	0.040	0.062	0.070	−0.005	−0.012
	r	h_r	m	0.0	0.190	0.410	0.080	0.405	0.110	0.050	0.040
7 Roll understeer	f	ε_{RUf}	deg/deg	0.100	−0.08	0.150	0.070	0.000	0.040	0.0	0.0
	r	ε_{Rur}	deg/deg	0.0	0.120	0.040	0.100	0.140	0.020	0.0	0.0
8 Roll camber	f	ε_{RCf}	deg/deg	0.800	0.600	1.000	0.560	0.620	0.820	0.63	0.81
	r	ε_{RCr}	deg/deg	1.000	0.900	0.0	0.840	0.0	0.820	0.51	0.86
9 Lateral force	f	η_{LCUf}	deg/kN	0.100	−0.080	0.060	0.180	−0.120	−0.040	0.0	0.0
compliance understeer	r	η_{LCUr}	deg/kN	−0.360	−0.240	0.120	0.200	0.180	−0.100	0.0	0.0

Table C.1 Example Car Specifications (Continued)

Parameter	Symbol	Units	Vehicle							
			A	B	C	D	E	F	G	H
10 Aligning torque compliance understeer	f η_{ACUf}	deg/ kNm	0.800	1.120	0.650	1.040	0.640	0.200	0.0	0.0
	r η_{ACUr}	deg/ kNm	−0.120	−0.210	−0.080	−0.100	−0.140	−0.020	0.0	0.0
Aerodynamics										
1 Frontal area	A_F	m^2	1.500	1.750	1.850	2.030	2.150	1.700	1.600	2.000
2 Vertical lift	C_L	-	0.610	0.310	0.280	0.120	0.210	−0.040	−2.640	−1.820
3 Pitch	C_P	-	−0.120	−0.060	0.040	0.020	−0.100	0.010	0.268	0.184
4 Drag	C_D	-	0.480	0.410	0.360	0.290	0.400	0.330	1.070	0.420
5 Side lift	C'_S	/deg	0.048	0.039	0.055	0.050	0.042	0.048	*	0.035
6 Yaw	C'_Y	/deg	0.0047	0.0041	0.0061	0.0080	0.0048	0.0065	*	0.003
7 Roll	C'_R	/deg	0.0062	0.0042	0.059	0.0060	0.0082	0.0055	*	0.002
Tires										
1 Cornering stiffness	f C_{Sf}	/deg	0.120	0.168	0.124	0.164	0.171	0.170	0.700	0.500
coefficient (static F_V)	r C_{Sr}	/deg	0.140	0.180	0.140	0.170	0.181	0.170	0.700	0.500
2 Camber stiffness	f C_{Cf}	/deg	0.0175	0.0074	0.0172	0.0072	0.0075	0.0074	*	*
coefficient	r C_{Cr}	/deg	0.0175	0.0074	0.0170	0.0070	0.0071	0.0074	*	*

Table C.1 Example Car Specifications (Continued)

Parameter		Symbol	Units	Vehicle							
				A	B	C	D	E	F	G	H
3 Max lateral force coeff.	f	μ_{Cf}	-	0.900	0.940	0.900	0.880	0.850	1.100	1.60	1.60
(static F_V)	r	μ_{Cr}	-	0.950	0.980	0.930	0.910	0.860	1.100	1.60	1.60
4 C_S sensitivity to F_V	f	k_{CSFVf}	-	0.600	0.580	0.700	0.620	0.520	0.400	*	*
	r	k_{CSFVr}	-	0.500	0.510	0.600	0.600	0.500	0.400	*	*
5 μ_Y sensitivity to F_V	f	p_f	-	−0.14	−0.15	−0.16	−0.18	−0.14	−0.18	−0.24	−0.19
	r	p_r	-	−0.14	−0.15	−0.16	−0.18	−0.14	−0.18	−0.27	−0.24
6 Vertical stiffness	f	K_{tf}	kN/m	120	165	170	180	200	250	228	375
	r	K_{tr}	kN/m	100	150	150	170	200	250	258	398
7 Pneumatic trail	f	t_f	m	0.030	0.035	0.040	0.045	0.044	0.040	*	*
	r	t_r	m	0.025	0.032	0.035	0.043	0.044	0.040	*	*
Dampers											
1 Bump damping	f	C_{WBf}	kNs/m	1.1	1.0	1.0	1.2	1.1	4.1	6	8
	r	C_{WBr}	kNs/m	0.7	0.9	0.8	1.0	1.2	4.1	11	12
2 Rebound damping	f	C_{WRf}	kNs/m	1.5	1.2	2.0	1.8	2.0	5.8	10	12
	r	C_{WRr}	kNs/m	1.1	1.1	1.4	1.8	1.9	5.8	15	16

Table C.2 Indicative Range of Passenger Car Parameter Values

Parameter		Symbol	Units	Lower	Upper
Mass (no load)		m	kg	570	1800
Wheelbase		L	m	2.00	3.00
G longitudinal position		a/L	—	0.33	0.60
G height		H	m	0.43	0.70
Product of inertia		I_{yz}	kg m^2	–200	200
Unsprung end-mass/total mass	f	m_{Uf}/m	—	0.06	0.08
	r	m_{Ur}/m	—	0.06	0.12
Spring stiffness (wheel rate)	f/r	K_w	kN/m	10	30
Roll stiffness	f	k_f	Nm/deg	200	1400
	r	k_r	Nm/deg	180	800
Roll stiffness front fraction		k_f/k	—	0.40	0.80
Roll center height	f	h_f	m	–0.050	0.200
	r	h_r	m	–0.050	0.400
Bump steer coeff (toe-out positive)	f/r	ε_{BS}	deg/m	–40	5
Bump camber coefficient	f/r	ε_{BC}	deg/m	0	500
Roll understeer coefficient	f/r	ε_{RU}	deg/deg	–0.10	0.20

Table C.2 Indicative Range of Passenger Car Parameter Values (Continued)

Parameter		Symbol	Units	Lower	Upper
Roll camber coefficient	f/r	ε_{RC}	deg/deg	0.00	1.00
Lateral force compliance U.S.	f/r	η_{LCU}	deg/kN	–0.30	0.60
Aligning torque compliance U.S.	f/r	η_{ACU}	deg/kNm	0.0	25.0
Lateral force compliance camber	f/r	η_{LCC}	deg/kN	0.20	0.80
Control gains:					
Steering angle gradient		$d\delta_s/dA$	deg/g	–50	200
Understeer gradient		$d\delta_U/dA$	deg/g	–2	10
Body roll angle gradient		$d\phi_B/dA$	deg/g	3	12

Appendix D

Selected Problem Solutions

Chapter 1

Q 1.6.1
$a = 1.545$ m behind front axle
$y = 0.040$ m right of CL

Q 1.6.2
42.18 N
26.36 kg

Q 1.6.3
$a = 1.606$ m
$h = 0.836$ m

Q 1.6.4
$I_v = 8403.3$ kg m^2

Q 1.6.5
$K = 19.96$ kNm/rad
$I = 6012$ kg m^2

Q 1.6.6
$I = 7395$ kg m^2
$k = 2.050$ m
$k^2/ab = 1.87$

Q 1.6.7
$I_P = 2786.3$ kg m^2
$K_T = 37.86$ kNm/rad
$I_T = 13154$ kg m^2
$I_{VG} = 2580$ kg m^2
$k_P = 1.393$ m

Q 1.6.11
$m_f = 899$ kg
$m_r = 851$ kg
$m_S = 1350$ kg
$m_{Sf} = 769$ kg
$m_{Sr} = 581$ kg
$a_S = 1.257$ m
$H_S = 0.833$ m

Q 1.7.1
$a = 1.5794$ m
$h = 0.7053$ m
$I = 3904$ kg m^2

Chapter 2

Q 2.5.5

(1) $F_i = \frac{1}{2\pi} m_p R_u \Omega^2 \sin\theta$

(2) $\left(\frac{l}{2}\right)^2 = z(2R_u - x)$

(3) $F_i = \frac{\sqrt{2}}{2\pi} \frac{m_p V^2}{R_u^{3/2}} z^{1/2}$

Q 2.5.6
509 N

Q 2.6.2
$t = R\,p_i + \rho V^2$
$N_T = V/C = 1$

Q 2.6.3
87 kPa

Q 2.7.3
$\theta = 1.20°$ (in practice a little more, because of other losses, e.g., axle bearings)

Q 2.9.3
$S_1 = 0.0514$
$\alpha = 2.94°$
$C_\alpha = 977$ N/deg
0.204/deg
4067 N
5760 N

Q 2.11.1
42 m/s

Q 2.14.3
Assuming a load sensitivity power of 0.5 gives 0.168/deg.

Q 2.14.4
751 N/deg

Q 2.14.6
(1) 0.205/deg
(2) 0.430/deg

Q 2.14.7
(1) 5405 N
(2) 854 N/deg

Q 2.14.9
(1) 0.25/deg
(2) 0.60
(3) 0.373/deg
(4) 1070 N/deg

Q 2.14.10
(1) 5263 N
(2) 850 N/deg

Q 2.19.2
50 m/s

Q 2.19.4
1.91°
0.3*g*

Q 2.21.2
396 N
1178 N

Q 2.21.3
0.2%

Chapter 3

Q 3.2.1
1.168 kg/m^3

Q 3.2.2
171 kg/m^3

Q 3.3.1
5.95 m/s

Q 3.3.2
7.3 to 20.7 m/s

Q 3.3.3
8%

Q 3.3.4
0.140
0.064%

Q 3.4.4
36.0 m/s
200.5°

Q 3.5.1
$qA = 1185.8$ N
$L = 489$ N
$S = 190$ N
$D = 465$ N
$P = 295$ Nm
$Y = 71$ Nm

Q 3.5.2
$C_{Lf} = 0.289$
$C_{Lr} = 0.123$

Q 3.5.3
$C_f = 0.419$
$C_r = 0.441$

Q 3.7.1
At $C_L = -0.5$, downforce is 20 kN, which equals the weight.
$D = 24.5$ kN = 1.24 × weight

Chapter 4

Q 4.9.1
$C_{Dm} = 1.28$ kN s/m
$K_w = 5.76$ kN/m

Q 4.12.2
$C_e = 1.5$ kN / (m/s)
Assuming typical 30/70 characteristic: 0.64 kN

Q 4.13.2
134 kN

Q 4.15.1
40.7 Nm

Chapter 5

Q 5.2.1
22.4 kN/m

Q 5.2.2
1.48 kNs/m

Q 5.2.3
39.1 kN/m

Q 5.2.4
0.832

Q 5.2.8
18.46 N/mm (kN/m)

Q 5.2.9
−0.3
2.022 m

Q 5.2.13
1.9°

Q 5.2.15
(1) 25 kN/m^2
(2) 1.67/m = 1.67%/cm
(3) 17.5 kN/m
(4) 11.0 kN/m

Q 5.4.1
0.108
216 N

Q 5.4.2
0.145
209 mm

Q 5.4.5
0.0971
177 mm
0.0987
180 mm

Q 5.4.6
$h = 0.1735$ m
$J_{\mathrm{AR}} = 0.270$ (27%)

Q 5.6.5
0.120
218 mm

Q 5.7.2
348 mm
0.242
774 N

Q 5.10.5
9.05°
$F_{\mathrm{Tf}} = 3167 + 269 = 3436$ N
$F_{\mathrm{Tr}} = 1358 + 1049 = 2407$ N
59/41
7674, 802, 6017, 1203

Q 5.10.6
7.215°
$F_{\mathrm{Tf}} = 2525 + 175 + 220 = 2920$ N
$F_{\mathrm{Tr}} = 1082 + 267 + 790 = 2139$ N
58/42

Q 5.10.7
0.8°
$F_{\mathrm{Tf}} = 192$ N
$F_{\mathrm{Tr}} = -192$ N

Q 5.10.14
$\Omega_{\mathrm{f}} = mVH/I$
Opposite rotation to wheels
$G = mR_1H/I$

Q 5.10.16
11.04 m/s^2
$S_{\mathrm{R}} = 1.36$
$S_{\mathrm{R}} \approx 0.8 \times 1.36 = 1.09$

Q 5.12.2
Lf, Rf, Lr, Rr are 26, 30, 24, 20, respectively

Q 5.12.3
8, 44, 18, 30

Q 5.12.4
13, 41, 17, 29

Q 5.13.6

$e_V = 20/50 = 0.40$
$e_{Vf} = 12/25 = 0.48$
$e_{Vr} = 8/25 = 0.32$

Q 5.16.5

16 deg/m

Q 5.16.9

$k_{LCS} = \eta m_S = -m_S \sin\theta/KS$
$= -1.11$ deg/g

Q 5.16.10

0.84 deg/g

Q 5.18.2

(1) $\phi_B = 9.6°$
(2) $\phi_{Sr} = 7.8°$
(3) 199, −68, 92, −142 mm

Q 5.18.4

−26, +13, −15, +29 mm.

Q 5.18.5

0.112 m/s

Q 5.19.3

1.506, 1.172, 1.296

Q 5.19.4

$a/L = 0.567$

Q 5.19.5

$F_{Tf} = 1713$ N
$F_{Tr} = 1224$ N
$F_T = 2937$ N
58.32/41.68 f/r
$e_{Vf} = 0.507$, $e_{Vr} = 0.216$
$H = 0.216$ m (seems a little too low)

Q 5.19.6

$F_{AeLf} = 4209$ N $F_{AeLr} = 8025$ N
$F_{AeLr}/F_{AeL} = 0.656$
$A_L = 2.88$ m^2

Q 5.19.7

$p_f = -0.294$ (possible)
$p_r = -0.664$ (not realistic, one rear tire not limiting?)

Chapter 6

Q 6.10.11

$k = 0$
5.7 deg/g

Q 6.10.12

0.5 deg/g
7.6 deg/g

Q 6.10.13

2.5 deg/g
4.3 deg/g

Q 6.10.14

1.55 deg/g
7.75 deg/g

Q 6.10.15

3.3 deg/g

Q 6.10.16

0.45 deg/g
−0.23 deg/g

Q 6.10.17

0.37 deg/g
−0.19 deg/g

Q 6.12.7
$\Delta A_f = -0.0103g$
$\Delta A_r = +0.0103g$
$\Delta A_M = -0.0103g$
$\Delta N_U = 0.026$

Q 6.12.8
–0.0427

Q 6.12.10
0.0704

Q 6.14.2
$\Delta k = 0.382$ deg/g (lift)
–0.184 deg/g (drag)
–0.0646 deg/g (side force)
–0.422 deg/g (yaw)

Q 6.15.2
–0.099

Q 6.17.2
0.42°
0.84°

Q 6.17.3
$\mu = 0.868$
51°

Q 6.18.2
$N_U = -0.12$

Q 6.18.3
–60%

Q 6.19.2
Initially 6 deg/g, 4 deg/g
Finally 6.75 deg/g, 3.25 deg/g

Q 6.20.2
$F_f = 1867$ N
$F_r = 1037$ N
1.867° 1.037°
$\Delta\delta_s = 16.6°$

Chapter 7

Q 7.7.7
8.96 rad/s, 1.43 Hz
0.900
3.897 rad/s, 0.620 Hz
$k = 1.628$ mrad/(m/s^2) = 0.916 deg/g
$V_{ch} = 42.9$ m/s

Q 7.8.2
–87.1 kNm/rad

Q 7.9.2
$Y_\beta = -229.2$ kN/rad
$Y_r = -3056$ N s/rad
$N_\beta = 45.84$ kNm^2/rad
$N_r = -35.0$ kNm s/rad

Appendix E

The Engineering Society
For Advancing Mobility
Land Sea Air and Space
INTERNATIONAL
400 Commonwealth Drive, Warrendale, PA 15096-0001

SURFACE VEHICLE RECOMMENDED PRACTICE

Submitted for recognition as an American National Standard

SAE J670e

REV. JUL76

Issued 1952-07
Revised 1976-07

Superseding J670d

VEHICLE DYNAMICS TERMINOLOGY

Foreword—This revision of "Vehicle Dynamics Terminology-SAE J670" has been expanded by the Vehicle Dynamics Committee to encompass terminology related to directional control of vehicles. Revisions have also been made to update the original terminology. An alphabetical index is appended to facilitate location of definitions.

The function of uniform terminology is to promote understandable and exact communication. A great deal of effort has been expended to make these definitions suit this purpose. It is recognized that this terminology, like other dictionaries. must be revised periodically to reflect current usage and changing needs. The Vehicle Dynamics Committee therefore solicits suggestions for improvements and additions to be considered in future revisions. Comments should be directed to SAE Headquarters.

TABLE OF CONTENTS

1. MECHANICAL VIBRATION-QUALITATIVE TERMINOLOGY

1.1 Vibration(Oscillation),General 9
1.2 Free Vibration 9
1.3 Forced Vibration 9
1.3.1 Resonance 9
1.4 Self-Excited Vibration 9
1.5 Simple Harmonic Vibration 9
1.6 Steady-State Vibration 9
1.7 Periodic Vibration 9
1.8 Random Vibration 9
1.9 Transient Vibration 9

2. MECHANICAL VIBRATION-QUANTITATIVE TERMINOLOGY

2.1 Period 9
2.2 Cycle 9
2.3 Frequency 9
2.3.1 Natural Frequency 9
2.3.2 Exciting Frequency 10
2.3.3 Frequency Ratio 10
2.3.4 Resonant Frequency 10

SAE Technical Standards Board Rules provide that: "This report is published by SAE to advance the state of technical and engineering sciences. The use of this report is entirely voluntary, and its applicability and suitability for any particular use, including any patent infringement arising therefrom, is the sole responsibility of the user."

SAE reviews each technical report at least every five years at which time it may be reaffirmed, revised, or cancelled. SAE invites your written comments and suggestions.

Copyright 1976 Society of Automotive Engineers, Inc.
All rights reserved.

Printed in U.S.A.

2.4 Amplitude 10
2.4.1 Peak-to-Peak Amplitude (Double Amplitude) 10
2.4.2 Static Amplitude 10
2.4.3 Amplitude Ratio 10
2.5 Velocity 10
2.6 Acceleration 10
2.7 Jerk 10
2.8 Transmissibility 10

3. VIBRATING SYSTEMS 11

3.1 Degree of Freedom 11
3.2 Linear 11
3.3 Nonlinear 11
3.4 Undamped 11
3.5 Damped 11
3.5.1 Viscous Damping 11
3.5.2 Critical Damping 11
3.5,3 Damping Ratio 11
3.5.4 Coulomb Damping 11
3.5.5 Complex Damping 11

4. COMPONENTS AND CHARACTERISTICS OF SUSPENSION SYSTEMS 11

4.1 Vibrating Mass and Weight 11
4.1.1 Sprung Weight 12
4.1.2 Sprung Mass 12
4.1.3 Dynamic Index 12
4.1.4 Unsprung Weight 12
4.1.5 Unsprung Mass 12
4.2 Spring Rate 12
4.2.1 Static Rate 12
4.2.2 Dynamic Rate 12
4.3 Resultant Spring Rate 12
4.3.1 Suspension Rate (Wheel Rate) 12
4.3.2 Tire Rate (Static) 12
4.3.3 Ride Rate 12
4.4 Static Deflection 12
4.4.1 Total Static Deflection 12
4.4.2 Effective Static Deflection 12
4.4.3 Spring Center 12
4.4.3.1 Parallel Springing 13
4.5 Damping Devices 13
4.5.1 Shock Absorber 13
4.5.2 Snubber 13

5. VIBRATIONS OF VEHICLE SUSPENSION SYSTEMS 13

5.1 Sprung Mass Vibration 13
5.1.1 Ride 13
5.1.1.1 Vertical (Bounce) 13

SAE J670e Revised JUL76

5.1.1.2 Pitch 13
5.1.1.3 Roll 13
5.1.2 Shake 13
5.1.2.1 Torsional Shake 13
5.1.2.2 Beaming 13
5.1.3 Harshness 13
5.1.4 Boom 13
5.2 Unsprung Mass Vibrations 13
5.2.1 Wheel Vibration Modes 13
5.2.1.1 Hop 13
5.2.1.1.1 Parallel Hop 13
5.2.1.1.2 Tramp 13
5.2.1.2 Brake Hop 13
5.2.1.3 Power Hop 14
5.2.2 Axle Vibration Modes 14
5.2.2.1 Axle Side Shake 14
5.2.2.2 Axle Fore-and-Aft Shake 14
5.2.2.3 Axle Yaw 14
5.2.2.4 Axle Windup 14
5.2.3 Steering System Vibration 14
5.2.3.1 Wheel Flutter 14
5.2.3.2 Wheel Wobble 14
5.2.3.3 Shimmy 14
5.2.3.4 Wheelfight 14

6. SUSPENSION GEOMETRY 14

6.1 Kingpin Geometry 14
6.1.1 Wheel Plane 14
6.1.2 Wheel Center 14
6.1.3 Center of Tire Contact 14
6.1.4 Kingpin Inclination 14
6.1.5 Kingpin Offset 14
6.2 Wheel Caster 14
6.2.1 Caster Angle 14
6.2.2 Rate of Caster Change 15
6.2.3 Caster Offset 15
6.2.4 Centrifugal Caster 15
6.3 Wheel Camber 15
6.3.1 Camber Angle 15
6.3.2 Rate of Camber Change 15
6.3.2.1 Swing Center 15
6.3.2.2 Swing-Arm Radius 15
6.3.3 Wheel Track (Wheel Tread) 15
6.3.4 Track Change 15
6.3.5 Rate of Track Change 15
6.4 Wheel Toe 15
6.4.1 Static Toe Angle (deg) 15
6.4.2 Static Toe (in (mm)) 15
6.5 Compression 16
6.5.1 Ride Clearance 16

6.5.2 Metal-to-Metal Position (Compression) 16
6.5.3 Bump Stop 16
6.6 Rebound 16
6.6.1 Rebound Clearance 16
6.6.2 Metal-to-Metal Position (Rebound) 16
6.6.3 Rebound Stop 16
6.7 Center of Parallel Wheel Motion 16
6.8 Torque Arm 16
6.8.1 Torque-Arm Center in Braking 16
6.8.2 Torque-Arm Center in Drive 16
6.8.3 Torque-Arm Radius 16

7. TIRES AND WHEELS 16

7.1 General Nomenclature 16
7.1.1 Standard Loads and Inflations 16
7.1.2 Rim Diameter 16
7.1.3 Rim Width 17
7.1.4 Tire Section Width 17
7.1.5 Tire Overall Width 17
7.1.6 Tire Section Height 17
7.1.7 Outside Diameter 17
7.1.8 Flat Tire Radius 17
7.1.9 Deflection (Static) 17
7.1.9.1 Percent Deflection 17
7.1.10 Tire Rate (Static) 17
7.1.11 Sidewall 17
7.1.11.1 Sidewall Rib 17
7.1.12 Bead 17
7.1.12.1 Bead Base 17
7.1.12.2 Bead Toe 17
7.1.13 Tread (Tire) 17
7.1.13.1 Tread Contour 17
7.1.13.2 Tread Radius 17
7.1.13.3 Tread Arc Width 17
7.1.13.4 Tread Chord Width 18
7.1.13.5 Tread Contact Width 16
7.1.13.6 Tread Contact Length 18
7.1.13.7 Tread Depth 16
7.1.13.8 Gross Contact Area 18
7.1.13.9 Net Contact Area 18
7.1.13.10 Tread Pattern 18
7.2 Rolling Characteristics 18
7.2.1 Loaded Radius 18
7.2.2 Static Loaded Radius 18
7.2.3 Spin Axis 18
7.2.4 Spin Velocity 16
7.2.5 Free-Rolling Tire 18
7.2.6 Straight Free-Rolling Tire 18
7.2.7 Longitudinal Slip Velocity 18
7.2.8 Longitudinal Slip (Percent Slip) 18

SAE J670e Revised JUL76

7.2.9 Effective Rolling, Radius 19
7.2.10 Wheel Skid 19
7.3 Tire Forces and Moments 19
7.3.1 Tire Axis System (Fig. I) 19
7.3.2 Tire Angles 19
7.3.2.1 Slip Angle 19
7.3.3 Tire Forces 19
7.3.3.1 Longitudinal Force 19
7.3.3.2 Driving Force 19
7.3.3.3 Driving Force Coefficient 19
7.3.3.4 Braking Force 19
7.3.3.5 Braking Force Coefficient (Braking Coefficient) 19
7.3.3.6 Rolling Resistance Force 19
7.3.3.7 Rolling Resistance Force Coefficient (Coefficient of Rolling Resistance) 19
7.3.3.8 Vertical Force 19
7.3.3.9 Lateral Force Coefficient 19
7.3.3.10 Slip Angle Force 20
7.3.3.11 Camber Force (Camber Thrust) 20
7.3.3.1 2 Normal Force 20
7.3.3.13 Vertical Load 20
7.3.3.14 Central Force 20
7.3.3.15 Tractive Force 20
7.3.3.16 Drag Force 20
7.3.4 Tire Moments 20
7.3.4.1 Overturning Moment 20
7.3.4.2 Rolling Resistance Moment 20
7.3.4.3 Aligning Torque (Aligning Moment) 20
7.3.4.4 Wheel Torque 20
7.3.4.5 Driving Torque 20
7.3.4.6 Braking Torque 20
7.4 Tire Force and Moment Stiffness 20
7.4.1 Cornering Stiffness 20
7.4.2 Camber Stiffness 20
7.4.3 Braking (Driving Stiffness) 20
7.4.4 Aligning Stiffness (Aligning Torque Stiffness) 21
7.5 Normalized Tire Force and Moment Stiffnesses (Coefficients) 21
7.5.1 Cornering Stiffness Coefficient (Cornering Coefficient) 21
7.5.2 Camber Stiffness Coefficient (Camber Coefficient) 21
7.5.3 Braking (Driving) Stiffness Coefficient 21
7.5.4 Aligning Stiffness Coefficient (Aligning Torque Coefficient) 21
7.6 Tire Traction Coefficients 21
7.6.1 Lateral Traction Coefficient 21
7.6.2 Driving Traction Coefficient 21
7.6.3 Braking Traction Coefficient 21
7.6.3.1 Sliding Braking Traction Coefficient 21
7.7 Tire Associated Noise and Vibrations 21
7.7.1 Tread Noise 21
7.7.1.1 Sizzle 21
7.7.2 Squeal 21
7.7.2.1 Cornering Squeal 21
7.7.2.2 Braking (Driving) Squeal 21

7 7.3 Thump 22
7.7.4 Roughness 22
7.7.5 Harshness 22
7.7.6 Slap 22
7.8 Tire and Wheel Non-Uniformity Characteristics 22
7.8.1 Radial Run-Out 22
7.8.1.1 Peak-to-Peak Radial Wheel Run-Out 22
7.8.1.2 Peak-To-Peak Unloaded Radial Tire Run-Out 22
7.8.1.3 Peak-to-Peak Loaded Radial Tire Run-Out 22
7.8.2 Lateral Run-Out 22
7.8.2.1 Peak-to-Peak Lateral Wheel Run-Out 22
7.8.2.2 Peak-to-Peak Lateral Tire Run-Out 22
7.8.3 Radial Force Variation 22
7.8.3.1 Peak-to-Peak (Total) Radial Force Variation 22
7.8.3.2 First Order Radial Force Variation 22
7.8.4 Lateral Force Variation 23
7.8.4.1 Peak-to-Peak (Total) Lateral Force Variation 23
7.8.4.2 First Order Lateral Force Variation 23
7.8.5 Lateral Force Offset 23
7.8.5.1 Ply Steer Force 23
7.8.5.2 Conicity Force 24

8. KINEMATICS: FORCE AND MOMENTS NOTATION 24

8.1 Earth-Fixed Axis System (X, Y, Z) 24
8.2 Vehicle Axis System (x, y, z) 24
8.3 Angular Orientation 24
8.4 Motion Variables 25
8.4.1 Vehicle Velocity 25
8.4.1.1 Longitudinal Velocity 25
8.4.1.2 Side Velocity 25
8.4.1.3 Normal Velocity 25
8.4.1.4 Forward Velocity 25
8.4.1.5 Lateral Velocity 25
8.4.1.6 Roll Velocity 25
8.4.1.7 Pitch Velocity 25
8.4.1.8 Yaw Velocity 25
8.4.2 Vehicle Acceleration 25
8.4.2.1 Longitudinal Acceleration 25
8.4.2.2 Side Acceleration 25
8.4.2.3 Normal Acceleration 25
8.4.2.4 Lateral Acceleration 25
8.4.2.5 Centripetal Acceleration 25
8.4.3 Heading Angle 25
8.4.4 Sideslip Angle (Attitude Angle) 25
8.4.5 Sideslip Angle Gradient 25
8.4.6 Course Angle 26
8.4.7 Vehicle Roll Angle 26
8.4.8 Vehicle Roll Gradient 26
8.4.9 Vehicle Pitch Angle 26

SAE J670e Revised JUL76

8.5 Forces....26
8.5.1 Longitudinal Force....26
8.5.2 Side Force....26
8.5.3 Normal Force....27
8.6 Moments....27
8.6.1 Rolling Moment....27
8.6.2 Pitching Moment....27
8.6.3 Yawing Moment....27

9. DIRECTIONAL DYNAMICS....27

9.1 Control Modes....27
9.1.1 Position Control....27
9.1.2 Fixed Control....27
9.1.3 Force Control....27
9.1.4 Free Control....27
9.2 Vehicle Response....27
9.2.1 Steering Response....27
9.2.2 Disturbance Response....27
9.2.3 Steady-State....27
9.2.4 Transient State....27
9.2.5 Trim....28
9.2.6 Steady-State Response Gain....28
9.2.7 Steering Sensitivity (Control Gain)....28
9.3 Stability....28
9.3.1 Asymptotic Stability....28
9.3.2 Neutral Stability....28
9.3.3 Divergent Instability....28
9.3.4 Oscillatory Instability....28
9.4 Suspension Steer and Roll Properties....28
9.4.1 Steer Angle....29
9.4.2 Ackerman Steer Angle....29
9.4.3 Ackerman Steer Angle Gradient....29
9.4.4 Steering Wheel Angle....29
9.4.5 Steering Wheel Angle Gradient....29
9.4.6 Overall Steering Ratio....29
9.4.7 Understeer/Oversteer Gradient....29
9.4.8 Neutral Steer....29
9.4.9 Understeer....29
9.4.10 Oversteer....29
9.4.11 Steering Wheel Torque....29
9.4.12 Steering W-heel Torque Gradient....29
9.4.13 Characteristic Speed....29
9.4.14 Critical Speed....29
9.4.15 Neutral Steer Line....29
9.4.16 Static Margin....29
9.4.17 Suspension Roll....29
9.4.18 Suspension Roll Angle....30
9.4.19 Suspension Roll Gradient....30
9.4.20 Roll Steer....30
9.4.20.1 Roll Understeer....30

9.4.20.2 Roll Oversteer 30
9.4.21 Roll Steer Coefficient 30
9.4.22 Compliance Steer 30
9.4.2.l Compliance Understeer 30
9.4.21.2 Compliance Oversteer 30
9.4.23 Compliance Steer Coefficient 30
9.4.24 Roll Camber 30
9.4.25 Roll Camber Coefficient 30
9.4.26 Compliance Camber 30
9.4.27 Compliance Camber Coefficient 30
9.4.28 Roll Center 30
9.4.29 Roll Axis 30
9.4.30 Suspension Roll Stiffness 30
9.4.31 Vehicle Roll Stiffness 30
9.4.32 Roll Stiffness Distribution 30
9.5 Tire Load Transfer 31
9.5.1 Tire Lateral Load Transfer 31
9.5.2 Tire Lateral Load Transfer Distribution 31
9.5.3 Tire Longitudinal Load Transfer 31
9.5.4 Overturning Couple 31
9.5.5 Overturning Couple Distribution 31

10. AERODYNAMIC NOMENCLATURE 31

10.1 Aerodynamic Motion Variables 31
10.1.1 Ambient Wind Velocity 31
10.1.2 Ambient Wind Angle 31
10.1.3 Resultant Air Velocity Vector 32
10.1.4 Aerodynamic Sideslip Angle 32
10.1.5 Aerodynamic Angle of Attack 32
10.2 Aerodynamic Force and Moment Coefficient 32
10.2.1 Reference Dimensions 32
10.2.1.1 Vehicle Area 32
10.2.1.2 Vehicle Wheelbase 32
10.2.2 Standard Air Properties 32
10.2.3 Force Coefficients 32
10.2.3.1 Longitudinal Force Coefficient 32
10.2.3.2 Lateral Force Coefficient 32
10.2.3.3 Normal Force Coefficient 33
10.2.4 Moment Coefficients 33
10.2.4.1 Rolling Moment Coefficient 33
10.2.4.2 Pitching Moment Coefficient 33
10.2.4.3 Yawing Moment Coefficient 33

11. MARGINAL INDICIA 33

NOTES 33

VEHICLE DYNAMICS TERMINOLOGY INDEX 36

SAE J670e Revised JUL76

VEHICLE DYNAMICS TERMINOLOGY

NOTE: Italized words and phrases appearing in a definition are themselves defined elsewhere in this Terminology.

1. MECHANICAL VIBRATION-QUALITATIVE TERMINOLOGY

1.1 VIBRATION (OSCILLATION), GENERAL—Vibration is the variation with time of the displacement of a body with respect to a specified reference dimension when the displacement is alternately greater and smaller than the reference. (Adapted from ANS Z24.1-195 1, item 1.040.)

1.2 FREE VIBRATION—Free Vibration of a system is the *vibration* during which no variable force is externally applied to the system. (Adapted from ANS Z24.1-1951, item 2.135.)

1.3 FORCED VIBRATION—Forced vibration of a system is *vibration* during which variable forces outside the system determine the *period* of the vibration. (Adapted from ANS Z24.1-1995 1, item 2.130.)

1.3.1 *Resonance*—A *forced vibration* phenomenon which exists if any small change in *frequency* of the applied force causes a decrease in the *amplitude* of the vibrating system. (Adapted from ANS Z24. 1, item 2.105.)

1.4 SELF-EXCITED VIBRATION—*Vibrations* are termed self-excited if the vibratory motion produces cyclic forces which sustain the *vibration.*

1.5 SIMPLE HARMONIC VIBRATION—*Vibration* at a point in a system is simple harmonic when the displacement with respect to time is described by a simple sine function

1.6 STEADY-STATE VIBRATION—Steady-state vibration exists in a system if the displacement at each point recurs for equal increments of time. (Adapted from ANS Z24 1-1951, items 11.005 and 1.045.)

1.7 PERIODIC VIBRATION—Periodic vibration exists in a system when recurring *cycles* take place in equal time intervals.

1.8 RANDOM VIBRATION—Random vibration exists in a system when the *oscillation* is sustained but irregular both as to *period* and *amplitude.*

1.9 TRANSIENT VIBRATION—Transient vibration exists in a system when one or more component *oscillations* are discontinuous.

2. MECHANICAL VIBRATION-QUANTITATIVE TERMINOLOGY

2.1 PERIOD—Period of an *oscillation* is the smallest increment of time in which one complete sequence of variation in displacement occurs. (Adapted from ANS Z24. 1951, item 1.050.)

2.2 CYCLE—Cycle of *oscillation* is the complete sequence of variations in displacement which occur during a *period.* (Adapted from ANS Z24.1-1951, item 1.055.)

2.3 FREQUENCY—Frequency of *vibration* is the number of *periods* occurring in unit time. (Adapted from ANS Z24.I-1951, item 1.060.)

2.3.1 *Natural Frequency*—Natural frequency of a body or System is a frequency of free vibration. (Same as ANS Z24.I 1951, item 2.140.)

SAE J670e Revised JUL76

2.3.2 *Exciting Frequency*—Exciting frequency is the frequency of variation of the exciting force.

2.3.3 *Frequency Ratio*—The ratio of *exciting frequency* to the *natural frequency*.

2.3.4 *Resonant Frequency*—*Frequency* at which *resonance* exists. (Same as ANS Z24.1-1951, item 2.110.)

2.4 AMPLITUDE—Amplitude of displacement at a point in a *vibrating system* is the largest value of displacement that the point attains with reference to its equilibrium position. (Adapted front ANS Z24.1 - 1951); item 1.070.)

2.4.1 *Peak-to-Peak Amplitude (Double Amplitude)*—Peak-to-Peak amplitude of displacement at a point in a *vibrating system* is the sum of the extreme values of displacement in both directions from the equilibrium position. (Adapted from ANS Z24.1-1951, item 1.075.)

2.4.2 *Static Amplitude*—Static amplitude in *forced vibration* at a point in a system is that displacement of tha point from its specified equilibrium position which would be produced by a static force equal to the maximum value of exciting force.

2.4.3 Amplitude Ratio (Relative Magnification Factor)—The ratio of a forced vibration amplitude to the static amplitude.

2.5 VELOCITY—Velocity of a point in a vibrating system is the time rate of change of its displacement. (Adapted from ANS Z24.1-1951, item 1.345.)

In simple harmonic vibration, the maximum velocity,

$$v_m = \omega x$$

where:

ω = $2\pi f$
f = frequency
x = amplitude

2.6 ACCELERATION—Acceleration of a point is the time rate of change of the *velocity* of the point. (Same as ANS Z24.1-1951, item 1.355.)

In *simple harmonic vibration*, the maximum acceleration,

$$a_m = \omega^2 x$$

2.7 JERK—"Jerk" is a concise term used to denote the time rate of change of *acceleration* of a point.

In *simple harmonic motion*, the maximum jerk,

$$j_m = \omega^3 x$$

2.8 TRANSMISSIBILITY—Transmissibility in *forced vibration* is the ratio of the transmitted force to the applied force.

3. VIBRATING SYSTEMS

3.1 DEGREE OF FREEDOM—The number of degrees of freedom of a *vibrating system* is the sum total of all ways in which the masses of the system can be independently displaced from their respective equilibrium positions.

EXAMPLES: A single rigid body constrained to move only vertically on supporting springs is a system of one degree of freedom. If the same mass is also permitted angular displacement in one vertical plane, it has two degrees of freedom: one being vertical displacement of the center of gravity; the other. angular displacement about the center of gravity.

3.2 LINEAR—Linear *vibrating systems* are those in which all the variable forces are directly proportional to the displacement, or to the derivatives of the displacement, with respect to time.

3.3 NONLINEAR—Nonlinear *vibrating systems* are those in which any of the variable forces are not directly proportional to the displacement, or to its derivatives, with respect to time.

EXAMPLE: A system having a variable *spring rate*.

3.4 UNDAMPED—Undamped systems are those in which there are no forces opposing the vibratory motion to dissipate energy.

3.5 DAMPED—Damped systems are those in which energy is dissipated by forces opposing the vibratory motion.

Any means associated with a *vibrating system* to balance or modulate exciting forces will reduce the vibratory motion, but are not considered to be in the same category as damping. The latter term is applied to an inherent characteristic of the system without reference to the nature of the excitation.

3.5.1 *Viscous Damping*—Damping in which the force opposing the motion is proportional and opposite in direction to the velocity.

3.5.2 *Critical Damping*—The minimum amount of *viscous damping* required in a *linear system* to prevent the displacement of the system from passing the equilibrium position upon returning from an initial displacement.

3.5.3 *Damping Ratio*—The ratio of the amount of *Viscous damping* present in a system to that required for *critical damping*.

3.5.4 *Coulomb Damping*—Damping in which a constant force opposes the vibratory motion.

3.5.5 *Complex Damping*—Damping in which the force opposing the vibratory motion is variable. but not proportional to the *velocity*.

In the field of aircraft flutter and vibration, complex damping is also used to denote a specific type of damping in which the damping force is assumed to be harmonic and in phase with the *velocity* but to have an *amplitude* proportional to the *amplitude* of displacement.

4. COMPONENTS AND CHARACTERISTICS OF SUSPENSION SYSTEMS

4.1 VIBRATING MASS AND WEIGHT

4.1.1 *Sprung Weight*—All weight which is supported by the suspension, including portions of the weight of the suspension members.

In the case of most vehicles, the sprung weight is commonly defined as the total weight less the weight of *unsprung parts*.

4.1.2 *Sprung Mass*—Considered to be a rigid body having equal mass, the same center of gravity, and the same moments of inertia about identical axes as the total *sprung weight*.

4.1.3 *Dynamic Index*—(k^2/ab ratio) is the square of the radius of gyration (k) of the *sprung mass* about a transverse axis through the center of gravity, divided by the product of the two longitudinal distances (a and b) from the center of gravity to the front and rear *wheel centers*.

4.1.4 *Unsprung Weight*—All weight which is not carried by the suspension system, but is supported directly by the tire or wheel, and considered to move with it.

4.1.5 *Unsprung Mass*—The unsprung masses are the equivalent masses which reproduce the inertia forces produced by the motions of the corresponding unsprung parts.

4.2 SPRING RATE—The change of load of a spring per unit deflection, taken as a mean between loading and unloading at a specified load.

4.2.1 *Static Rate*—Static rate of an elastic member is the rate measured between successive stationary positions at which the member has settled to substantially equilibrium condition.

4.2.2 *Dynamic Rate*—Dynamic rate of an elastic member is the rate measured during rapid deflection where the member is not allowed to reach static equilibrium.

4.3 RESULTANT SPRING RATE

4.3.1 *Suspension Rate (Wheel Rate)*—The change of wheel load, at the *center of tire contact*, per unit vertical displacement of the *sprung mass* relative to the wheel at a specified load.

If the *wheel camber* varies, the displacement should be measured relative to the lowest point on the rim centerline.

4.3.2 *Tire Rate (Static)*—The *static rate* measured by the change of wheel load per unit vertical displacement of the wheel relative to the ground at a specified load and inflation pressure.

4.3.3 Ride Rate—The change of wheel load, at the *center of tire contact*, per unit vertical displacement of the *sprung mass* relative to the ground at a specified load.

4.4 STATIC DEFLECTION

4.4.1 *Total Static Deflection*—Total static deflection of a loaded suspension system is the overall deflection under the static load from the position at which all elastic elements are free of load.

4.4.2 *Effective Static Deflection*—Effective Static deflection of a loaded suspension system equals the static load divided by the *spring rate* of the system at that load.

Total *static deflection* and effective static deflection are equal when the *spring rate* is constant.

4.4.3 *Spring Center*—The vertical line along which a vertical load applied to the *sprung mass* will produce only uniform vertical displacement.

SAE J670e Revised JUL76

4.4.3.1 Parallel Springing—Describes the Suspension of a vehicle in which the effective static deflections of the two ends are equal; that is, the *spring center* passes through the center of gravity of the *sprung mass.*

4.5 DAMPING DEVICES—As distinct from specific types of damping, damping devices refer to the actual mechanisms used to obtain-damping of suspension systems.

4.5.1 *Shock Absorber*—A generic term which is commonly applied to hydraulic mechanisms for producing damping of suspension systems.

4.5.1 Snubber—A generic term which is commonly applied to mechanisms which employ dry friction to produce damping of suspension systems.

5. VIBRATIONS OF VEHICLE SUSPENSION SYSTEMS

5.1 SPRUNG MASS VIBRATIONS

5.1.1 *Ride*—The low *frequency* (up to 5 Hz) *vibrations* of the sprung mass as a rigid body.

5.1.1.1 Vertical (Bounce)—The translational component of ride *vibrations* of the *sprung mass* in the direction of the vehicle z-axis. (Fig. 2)

5.1.1.2 Pitch—The angular component of ride *vibrations* of the *sprung mass* about the vehicle y-axis.

5.1.1.3 Roll—The angular component of ride *vibrations* of the *sprung mass* about the vehicle x-axis

5.1.2 *Shake*—The intermediate *frequency* (5-25 Hz) *vibrations* of the *sprung mass* as a flexible body.

5.1.2.1 Torsional Shake—A mode of *vibration* involving twisting deformations of *sprung mass* about the vehicle x-axis.

5.1.2.2 Beaming—A mode of *vibration* involving predominantly bending deformations of the *sprung mass* about the vehicle y-axis.

5.1.3 *Harshness*—The high frequency (25-100 Hz) *vibrations* of the structure and/or components that are perceived tactually and/or audibly.

5.1.4 *Boom*—A high intensity *vibration* (25-100 Hz) perceived audibly and characterized as sensation of pressure by the ear.

5.2 UNSPRUNG MASS VIBRATIONS

5.2.1 Wheel Vibration Modes

5.2.1.1 Hop—The vertical oscillatory motion of a wheel between the road surface and the *sprung mass.*

5.2.1.1.1 Parallel hop is the form of wheel hop in which a pair of wheels hop in phase.

5.2.1.1.2 Tramp is the form of wheel hop in which a pair of wheels hop in opposite phase.

5.2.1.2 Brake Hop—An oscillatory hopping motion of a single wheel or of a pair of wheels which occurs when brakes are applied in forward or reverse motion of the vehicle.

5.2.1.3 Power Hop—An oscillatory hopping motion of a single wheel or of a pair of wheels which occurs when *tractive force* is applied in forward or reverse motion of the vehicle.

5.2.2 Axle Vibration Modes

5.2.2.1 Axle Side Shake—Oscillatory motion of an axle which consists of transverse displacement.

5.2.2.2 Axle Fore-and-Aft Shake—Oscillatory motion of an axle which consists purely of longitudinal displacement.

5.2.2.3 Axle Yaw—Oscillatory motion of an axle around the vertical axis through its center of gravity.

5.2.2.4 Axle Windup—Oscillatory motion of an axle about the horizontal transverse axis through its center of gravity.

5.2.3 *Steering System Vibrations*

5 2.3.1 Wheel Flutter—Forced *oscillation* of steerable wheels about their steering axes.

5.2.3.2 Wheel Wobble—A self-excited *oscillation* of steerable wheels about their steering axes occurring without appreciable tramp.

5.2.3.3 Shimmy—A self-excited *oscillation* of a pair of steerable wheels about their steering axes, accompanied by appreciable tramp.

5.2.3.4 Wheelfight—A rotary disturbance of the steering wheel produced by forces acting on the steerable wheels.

6. SUSPENSION GEOMETRY

6.1 KINGPIN GEOMETRY

6.1.1 *Wheel Plane*—The central plane of the tire, normal to the *spin axis.*

6.1.2 *Wheel Center*—The point at which the *spin axis* of the wheel intersects the *wheel plane.*

6.1.3 *Center of Tire Contact*—The intersection of the *wheel plane* and the vertical projection of the *spin axis* of the wheel onto the road plane. (See Note 1.)

6.1.4 *Kingpin Inclination*—The angle in front elevation between the steering axis and the vertical.

6.1.5 Kingpin Offset—Kingpin offset at the ground is the horizontal distance in front elevation between the point where the steering axis intersects the ground and the *center of tire* contact.

The kingpin offset at the *wheel center* is the horizontal distance in front elevation from the *wheel center* to the steering axis.

6.2 WHEEL CASTER

6.2.1 *Caster Angle*—The angle in side elevation between the steering axis and the vertical. It is considered positive when the steering axis is inclined rearward (in the upward direction) and negative when the steering axis is inclined forward.

SAE J670e Revised JUL76

6.2.2 *Rate of Caster Change*—The change in *caster angle* per unit vertical displacement of the *wheel center* relative to the *sprung mass.*

6.2.3 *Caster Offset*—The distance in side elevation between the point where the steering axis intersects the ground, and the *center of tire contact.* The offset is considered positive when the intersection point is forward of the tire contact center and negative when it is rearward.

6.2.4 *Centrifugal Caster*—The unbalance moment about the steering axis produced by a lateral acceleration equal to gravity acting at the combined center of gravity of all the steerable parts. It is considered positive if the combined center of gravity is forward of the steering axis and negative if rearward of the steering axis.

6.3 WHEEL CAMBER

6.3.1 *Camber Angle*—The inclination of the *wheel plane* to the vertical. It is considered positive when the wheel leans outward at the top arid negative when it leans inward.

6.3.2 *Rate of Camber Change*—The change of camber angle per unit vertical displacement of the *wheel center* relative to the *sprung mass.*

6.3.2.1 Swing Center—That instantaneous center in the transverse vertical plane through any pair of *wheel centers* about which the wheel moves relative to the *sprung mass.*

6.3.2.2 Swing-Arm Radius—The horizontal distance from the *swing center* to the *center of tire contact.*

6.3.3 *Wheel Track (Wheel Tread)*—The lateral distance between the *centers of tire contact* of a pair of wheels. For vehicles with dual wheels, it is the distance between the points centrally located between the *centers of tire contact* of the inner and outer wheels. (See SAE J693.)*

6.3.4 *Track Change*—The change in wheel track resulting from vertical suspension displacements of both wheels in the same direction.

6.3.5 *Rate of Track Change*—The change in *wheel track* per unit vertical displacement of both *wheel centers* in the same direction relative to the *sprung mass.*

6.4 WHEEL TOE

6.4.1 *Static Toe Angle (deg)*—The static toe angle of a wheel, at a specified wheel load or relative position of the *wheel center* with respect to the *sprung mass,* is the angle between a longitudinal axis of the vehicle and the line of intersection of the *wheel plane* and the road surface. The wheel is "toed-in" if the forward portion of the wheel is turned toward a central longitudinal axis of the vehicle. and "toed-out" if turned away.

6.4.2 *Static Toe (in (mm))*—Static toe-in or toe-out of a pair of wheels, at a specified wheel load or relative position of the *wheel center* with respect to the *sprung mass,* is the difference in the transverse distances between the *wheel planes* taken at the extreme rear and front points of the tire treads. When the distance at the rear is greater, the wheels are "toed-in" by this amount; and where smaller, the wheels are "toed-out." (See Note 2.)

---

* Published in the SAE Handbook. available from the Society of Automotive Engineers, Inc., 500 Commonwealth Drive, Warrendale, PA 15096-0001.

SAE J670e Revised JUL76

6.5 COMPRESSION—The relative displacement of *sprung* and *unsprung masses* in the suspension system in which the distance between the masses decreases from that at static condition.

6.5.1 *Ride Clearance*—The maximum displacement in compression of the *sprung mass* relative to the *wheel center* permitted by the suspension system, from the normal load position.

6.5.2 *Metal-to-Metal Position (Compression)*—The point of maximum *compression* travel limited by interference of substantially rigid members.

6.5.3 *Bump Stop*—An elastic member which increases the *wheel rate* toward the end of the *compression* travel.

The bump stop may also act to limit the compression travel.

6.6 REBOUND—The relative displacement of the *sprung* and *unsprung masses* in a suspension system in which the distance between the masses increases from that at static condition.

6.6.1 *Rebound Clearance*—The maximum displacement in *rebound* of the *sprung mass* relative to the *wheel center* permitted by the suspension system, from the normal load position.

6.6.2 *Metal-to-Metal Position (Rebound)*—The point of maximum *rebound* travel limited by interference of substantially rigid members.

6.6.3 *Rebound Stop*—An elastic member which increases the *wheel rate* toward the end of the *rebound* travel. The *rebound stop* may also act to limit the rebound travel.

6.7 CENTER OF PARALLEL WHEEL MOTION—The center of curvature of the path along which each of a pair of *wheel centers* moves in a longitudinal vertical plante relative to the *sprung mass* when both wheels are equally displaced.

6.8 TORQUE ARM

6.8.1 *Torque-Arm Center in Braking*—The instantaneous center in a vertical longitudinal plane through the *wheel center* about which the wheel moves relative to the *sprung mass* when the brake is locked.

6.8.2 *Torque-Arm Center in Drive*—The instantaneous center in a vertical longitudinal plane through the *wheel center* about which the wheel moves relative to the *sprung mass* when the drive mechanism is locked at the power source.

6.8.3 *Torque-Arm Radius*—The horizontal distance from the *torque-arm* center to the *wheel center.*

7. TIRES AND WHEELS

7.1 GENERAL NOMENCLATURE

7.1.1 *Standard Loads and Inflations*—Those combinations of loads and inflations up to the maximum load and inflation recommended by the Tire and Rim Association and published in the yearly editions of the Tire and Rim Association Year Book.

7.1.2 *Rim Diameter*—The diameter at the intersection of the *bead* seat and the flange. (See Tire and Rim Association Year Book.) Nominal rim diameter (i.e., 14, 15, 16.5, etc.) is commonly used.

SAE J670e Revised JUL76

7.1.3 *Rim Width*—The distance between the inside surfaces or the rim flanges. (See Tire and Rim Association Year Book.)

7.1.4 *Tire Section Width*—The width of the unloaded new tire mounted on specified rim, inflated to the normal recommended pressure, including the normal sidewalls but not including protective rib, bars, and decorations. (See Tire and Rim Association Year Book.)

7.1.5 *Tire Overall Width*—The width of the unloaded new tire, mounted on specified rim, inflated to the normal recommended pressure, including protective rib, bars, and decorations. (See Tire and Rim Association Year Book.)

7.1.6 *Tire Section Height*—Half the difference between the tire outside diameter and the nominal rim diameter.

7.1.7 *Outside Diameter*—The maximum diameter of the new unloaded tire inflated to the normal recommended pressure and mounted on a specified rim. (See Airplane Section, Tire and Rim Association Year Book.)

7.1.8 *Flat Tire Radius*—The distance from the *spin axis* to the road surface of a loaded tire on a specified rim at zero inflation.

7.1.9 *Deflection (Static)*—The radial difference between the undeflected tire radius and the static loaded radius, under specified loads and inflation.

7.1.9.1 *Percent Deflection*—The static deflection expressed as a percentage of the unloaded section height above the top of the rim flange.

7.1.10 *Tire Rate (Static)*—See paragraph 4.3.2.

7.1.11 *Sidewall*—The portion of either side of the tire which connects the *bead* with the *tread*.

7.1.11.1 *Sidewall Rib*—A raised circumferential rib located on the sidewall.

7.1.12 *Bead*—The portion of the tire which fits onto the rim of the wheel.

7.1.12.1 *Bead Base*—The approximately cylindrical portion of the *bead* that forms its inside diameter.

7.1.12.1 *Bead Toe*—That portion of the *bead* which joins the *bead base* and the inside surface of the tire.

7.1.13 *Tread (Tire)*—The peripheral portion of the tire, the exterior of which is designed to contact the road surface.

7.1.13.1 *Tread Contour*—The cross sectional shape of tread surface of an inflated unloaded tire neglecting the *tread pattern* depressions.

7.1.13.2 *Tread Radius*—The radius or combination of radii describing the tread contour.

7.1.13.3 *Tread Arc Width*—The distance measured along the tread contour of an unloaded tire between one edge of the tread and the other. For tires with rounded tread edges, the point of measurement is that point in space which is at the intersection of the tread radius extended until it meets the prolongation of the upper sidewall contour.

7.1.13.4 *Tread Chord Width*—The distance measured parallel to the *spin axis* of an unloaded tire between one edge of the tread and the other. For tires with rounded tread edges, the point of measurement is that point in space which is at the intersection of the tread radius extended until it meets the prolongation of the upper sidewall contour.

7.1.13.5 *Tread Contact Width*—The distance between the extreme edges of road contact at a specified load and pressure measured parallel to the Y′ axis at zero *slip angle* and zero *inclination angle*.

7.1.13.6 *Tread Contact Length*—The perpendicular distance between the tangent to edges of the leading and following points of road contact and parallels to the *wheel plane*.

7.1.13.7 *Tread Depth*—The distance between the base of a tire *tread* groove and a line tangent to the surface of the two adjacent *tread* ribs or rows.

7.1.13.8 *Gross Contact Area*—The total area enclosing the pattern of the tire *tread* in contact with a flat surface, including the area of grooves or voids.

7.1.13.9 Net Contact Area—The area enclosing the pattern of the tire tread in contact with a flat surface, excluding the area of grooves or other depressions.

7.1.13.10 *Tread Pattern*—The molded configuration on the face of the *tread*. It is generally composed of ribs, rows, grooves, bars, lugs, and the like.

7.2 ROLLING CHARACTERISTICS

7.2.1 *Loaded Radius*—(R_ℓ) is the distance from the center of tire contact to the wheel center measured in the wheel plane.

7.2.2 *Static Loaded Radius*—The *loaded radius* of a stationary tire inflated to normal recommended pressure. Note: In general, static loaded radius is different from the radius of slowly rolling tire. Static radius of a tire rolled into position may be different from that of the tire loaded without being rolled.

7.2.3 *Spin Axis*—The axis of rotation of the wheel. (See Fig. I.)

7.2.4 *Spin Velocity*—(Ω) The angular velocity of the wheel on which the tire is mounted, about its *spin axis*. Positive spin velocity is shown in Fig. 1.

7.2.5 *Free-Rolling Tire*—A loaded rolling tire operated without application of *driving* or *braking torque*.

7.2.6 *Straight Free-Rolling Tire*—A *free-rolling tire* moving in a straight line at zero *inclination angle* and zero *slip angle*.

7.2.7 *Longitudinal Slip Velocity*—The difference between the *spin velocity* of the driven or braked tire and the *spin velocity* of the *straight free-rolling tire*. Both spin velocities are measured at the same linear velocity at the wheel center in the X′ direction. A positive value results from *driving torque*.

7.2.8 *Longitudinal Slip (Percent Slip)*—The ratio of the *longitudinal slip velocity* to the *spin velocity* of the *free straight-rolling* tire expressed as a percentage.

Note: This quantity should not be confused with the slip number that frequently appears in kinematic analysis of tires in which the spin velocity appears in the denominator.

7.2.9 *Effective Rolling Radius*—(R_e) is the ratio of the linear velocity of the wheel center in the X^1 -direction to the spin velocity. (See paragraph 7.3.1 .)

7.2.10 *Wheel Skid*—The occurrence of sliding between the tire and road interface which takes place within the entire *contact area*. Skid can result from braking, driving and/or cornering.

7.3 TIRE FORCES AND MOMENTS

7.3.1 *Tire Axis System (Fig. 1)*—The origin of the tire axis system is the center of the tire contact. The X^1 -axis is the intersection of the wheel plane and the road plane with a positive direction forward. The Z^1 -axis is perpendicular to the road plane with a positive direction downward. The Y^1 -axis is in the road plane, its direction being chosen to make the axis system orthogonal and right-hand.

7.3.2 *Tire Angles*

7.3.2.1 *Slip Angle*—(α) The angle between the X' axis and direction of travel of the *center of tire contact.*

7.3.2.2 *Inclination Angle*—(γ) The angle between the Z' axis and the *wheel plane.*

7.3.3 *Tire Forces*—The external force acting on the tire by the road having the following components:

7.3.3.1 *Longitudinal Force* (F_x)—The component of the *tire force vector* in the X' direction.

7.3.3.2 *Driving Force*—The *longitudinal force* resulting from *driving torque* application.

7.3.3.3 *Driving Force Coefficient*—The ratio of the *driving force* to the *vertical load.*

7.3.3.4 *Braking Force*—The negative *longitudinal force* resulting from *braking torque* application.

7.3.3.5 *Braking Force Coefficient (Braking Coefficient)*—The ratio of the *braking force* to the vertical load.

7.3.3.6 *Rolling Resistance Force*—The negative *longitudinal force* resulting from energy losses due to deformations of a rolling tire.

Note: This force can be computed from the forces and moments acting on the tire by the road.

$$F_r = \frac{M_y \cos\gamma + M_z \sin\gamma}{R\ell}$$

7.3.3.7 *Rolling Resistance Force Coefficient (Coefficient of Rolling Resistance)*—The ratio of the *rolling resistance* to the *vertical load.*

7.3.3.8 *Lateral Force* (F_y)—The component of the *tire force* vector in the Y' direction.

7.3.3.9 *Lateral Force Coefficient*—The ratio of the *lateral force* to the *vertical load.*

SAE J670e Revised JUL76

7.3.3.10 *Slip Angle Force*—The *lateral force* when the *inclination angle* is zero and *plysteer* and *conicity* forces have been subtracted.

7.3.3.11 *Camber Force (Camber Thrust)*—The *lateral force* when the *slip angle* is zero and the *plysteer* and *conicity* forces have been subtracted.

7.3.3.12 *Normal Force* (F_z)—The component of the *tire force* vector in the Z′ direction.

7.3.3.1 3 *Vertical Load*—The normal reaction of the tire on the road which is equal to the negative of normal force.

7.3.3.14 *Central Force*—The component of the *tire force* vector in the direction perpendicular to the direction of travel of the *center of tire contact*. *Central Force* is equal to *lateral force* times cosine of *slip angle* minus *longitudinal force* times sine of *slip angle*.

7.3.3.15 *Tractive Force*—The component of the *tire force* vector in the direction of travel of the *center of tire contact*. *Tractive force* is equal to *lateral force* times sine of *slip angle* plus *longitudinal force* times cosine of *slip angle*.

7.3.3.16 *Drag Force*—The negative *tractive force*.

7.3.4 *Tire Moments*—The external moments acting on the tire by the road having the following components:

7.3.4.1 *Overturning Moment* (M_x)—The component of the *tire moment* vector tending to rotate the tire about the X′ axis, positive clockwise when looking in the positive direction of the X′ axis.

7.3.4.2 *Rolling Resistance Moment* (M_y)—The component of the *tire moment* vector tending to rotate the tire about the Y′ axis, positive clockwise when looking in the positive direction of the Y′ axis.

7.3.4.3 *Aligning Torque (Aligning Moment)* (M_z)—The component of the *tire moment* vector tending to rotate the tire about the Z′ axis, positive clockwise when looking in the positive direction of Z′ axis.

7.3.4.4 *Wheel Torque* (T)—The external torque applied to the tire from the vehicle about the spin axis; positive *wheel torque* is shown in Fig. 1.

7.3.4.5 *Driving Torque*—The positive *wheel torque*.

7.3.4.6 *Braking Torque*—The negative wheel torque.

7.4 TIRE FORCE AND MOMENT STIFFNESS (may be evaluated at any set of operating conditions).

7.4.1 *Cornering Stiffness*—The negative of the rate of change of *lateral force* with respect to change in slip angle, usually evaluated at zero *slip angle*.

7.4.2 *Camber Stiffness*—The rate of change of *lateral force* with respect to change in *inclination angle*, usually evaluated at zero *inclination angle*.

7.4.3 *Braking (Driving) Stiffness*—The rate of change of *longitudinal force* with respect to change in *longitudinal slip*, usually evaluated at zero *longitudinal slip*.

7.4.4 *Aligning Stiffness (Aligning Torque Stiffness)*—The rate of change of *aligning* torque with respect to change in *slip angle*, usually evaluated at zero *slip angle*.

7.5 NORMALIZED TIRE FORCE AND MOMENT STIFFNESSES (COEFFICIENTS)

7.5.1 *Cornering Stiffness Coefficient (Cornering Coefficient)*—The ratio of *cornering stiffness* of a *free straight-rolling tire* to the *vertical load*.

Note: Although the term cornering coefficient has been used in a number of technical papers, for consistency with definitions of other terms using the word coefficient, the term *cornering stiffness coefficient* is preferred.

7.5.2 *Camber Stiffness Coefficient (Camber Coefficient)*—The ratio of camber stiffness of a *free straight-rolling tire* to the *vertical load*.

7.5.3 *Braking (Driving) Stiffness Coefficient*—The ratio of *braking (driving) stiffness* of a *free straight-rolling tire* to the vertical load.

7.5.4 *Aligning Stiffness Coefficient (Aligning Torque Coefficient)*—The ratio of *aligning stiffness* of a *free straight rolling tire* to the *vertical load*.

7.6 TIRE TRACTION COEFFICIENTS

7.6.1 *Lateral Traction Coefficient*—The maximum value of *lateral force coefficient* which can be reached on a *free-rolling tire* for a given road surface, environment and operating condition.

7.6.2 *Driving Traction Coefficient*—The maximum value of *driving force coefficient* which can be reached on a given tire and road surface for a given environment and operating condition.

7.6.3 *Braking Traction Coefficient*—The maximum of the *braking force coefficient* which can be reached without locking a wheel on a given tire and road surface for a given environment and operating condition.

7.6.3.1 *Sliding Braking Traction Coefficient*—The value of the *braking force coefficient* of a tire obtained on a locked wheel on a given tire and road surface for a given environment and operating condition.

7.7 TIRE ASSOCIATED NOISE AND VIBRATIONS

7.7.1 *Tread Noise*—Airborne sound (up to 5000 Hz) except squeal and slap produced by the interaction between the tire and the road surface.

7.7.1.1 *Sizzle*—*A tread noise* (up to 4000 Hz) characterized by a soft frying sound, particularly noticeable on a very smooth road surface.

7.7.2 *Squeal*—Narrow band airborne tire noise (l50-800 Hz) resulting from either *longitudinal slip* or *slip angle* or both.

7.7.2.1 *Cornering Squeal*—The *squeal* produced by a *free-rolling tire* resulting from *slip angle*.

7.7.2.2 *Braking (Driving) Squeal*—The *squeal* resulting from *longitudinal slip*.

SAE J670e Revised JUL76

7.7.3 *Thump*—A periodic vibration and/or audible sound generated by the tire and producing a pounding sensation which is synchronous with wheel rotation.

7.7.4 *Roughness*—Vibration (15-100 Hz) perceived tactily and/or audibly, generated by a rolling tire on a smooth road surface and producing the sensation of driving on a coarse or irregular surface.

7.7.5 *Harshness*—Vibrations (15-100 Hz) perceived tactily and/or audibly, produced by interaction of the tire with road irregularities.

7.7.6 *Slap*—Airborne smacking noise produced by a tire traversing road seams such as tar strips and expansion joints.

7.8 TIRE AND WHEEL NON-UNIFORMITY CHARACTERISTICS

7.8.1 *Radial Run-Out*

7.8.1.1 *Peak-to-Peak Radial Wheel Run-Out*—The difference between the maximum and minimum values of the wheel *bead* seat redius, measured in a plane perpendicular to the *spin axis* (measured separately for each *bead* seat).

7.8.1.2 *Peak-to Peak Unloaded Radial Tire Run-Out*—The difference between maximum and minimum undeflected values of the tire radius, measured in plane perpendicular to the *spin axis* on a true running wheel.

7.8.1.3 *Peak-to-Peak Loaded Radial Tire Run-Out*—The difference between maximum and minimum values of the *loaded radius* on a true running wheel.

7.8.2 *Lateral Run-Out*

7.8.2.1 *Peak-to-Peak Lateral Wheel Run-Out*—The difference between maximum and minimum indicator readings, measured parallel to the *spin axis* on the inside vertical portion of a rim flange (measured separately for each flange).

7.8.2.2 *Peak-to-Peak Lateral Tire Run-Out*—The difference between maximum and minimum indicator readings, measured parallel to the *spin axis* at the point of maximum *tire section*, on a true running wheel (measured separately for each sidewall).

7.8.3 Radial Force Variation—The periodic variation of the *normal force* of a loaded *straight free-rolling tire* which repeats each revolution at a fixed *loaded radius*, given mean *normal force*, constant speed, given inflation pressure and test surface curvature.

7.8.3.1 *Peak-to-Peak (Total) Tadial Force Variation*—The difference between maximum and minimum values of the *normal force* during one revolution of the tire.

7.8.3.2 *First Order Radial Force Variation*—The peak-to-peak amplitude of the fundamental frequency component of the Fourier series representing *radial force variation*. Its frequency is equal to the rotational frequency of the tire.

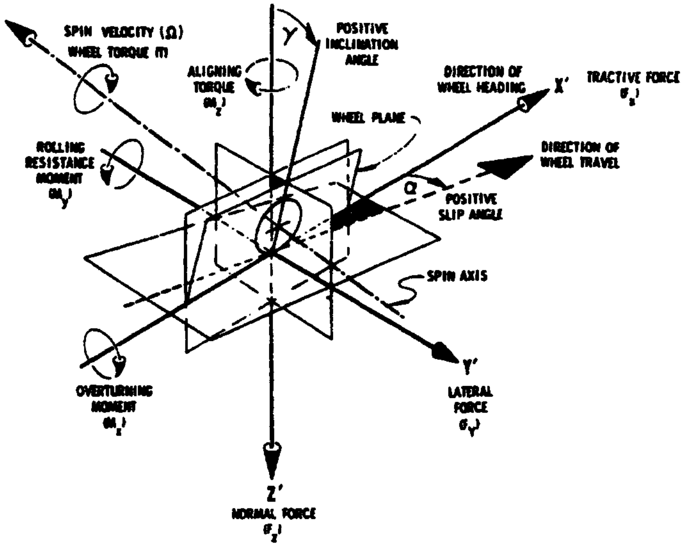
SPIN VELOCITY (Ω)
WHEEL TORQUE (T)
γ
POSITIVE INCLINATION ANGLE
ALIGNING TORQUE (M_z)
DIRECTION OF WHEEL HEADING
X'
TRACTIVE FORCE (F_x)
WHEEL PLANE
ROLLING RESISTANCE MOMENT (M_y)
DIRECTION OF WHEEL TRAVEL
α
POSITIVE SLIP ANGLE
SPIN AXIS
OVERTURNING MOMENT (M_x)
Y'
LATERAL FORCE (F_y)
Z'
NORMAL FORCE (F_z)

Fig. I—Tire Axis System

7.8.4 *Lateral Force Variation*—The periodic variation of lateral force of a *straight free-rolling tire* which repeats each revolution, at a fixed *loaded radius*, given mean *normal force*, constant speed, given inflation pressure and test surface curvature.

7.8.4.1 *Peak-to-Peak (Total) Lateral Force Variation*—The difference between the maximum and minimum values of the *lateral force* during one revolution of the tire.

7.8.4.2 *First Order Lateral Force Variation*—The peak-to-peak amplitude of the fundamental frequency component of the Fourier series representing *lateral force variation*. Its frequency is equal to the rotational frequency of the tire.

7.8.5 *Lateral Force Offset*—The average *lateral force* of a *free straight-rolling tire.*

7.8.5.1 *Ply Steer Force*—The component of *lateral force offset* which does not change sign (with respect to the *Tire Axis System*) with a change in direction of rotation (positive along positive Y' axis). The force remains positive when it is directed away from the serial number on the right side tire and toward the serial number on the left side tire.

7.8.5.2 *Conicity Force*—The component of *lateral force offset* which changes sign (with respect to the *Tire Axis System*) with a change in direction of rotation (positive away from the serial number or toward the whitewall). The force is positive when it is directed away from the serial number on the right side tire and negative when it is directed toward the serial number on the left side tire.

8. KINEMATICS: FORCE AND MOMENTS NOTATION

8.1 EARTH-FIXED AXIS SYSTEM (X, Y, Z)—This system is a right-hand orthogonal axis system fixed on the earth. The trajectory of the vehicle is described with respect to this earth-fixed axis system. The X and Y-axis are in a horizontal plane and the Z-axis is directed downward.

8.2 VEHICLE AXIS SYSTEM (x, y, z)—This system is a right-hand orthogonal axis system fixed in a vehicle such that with the vehicle moving steadily in a straight line on a level road, the x-axis is substantially horizontal, points forward, and is in the longitudinal plane of symmetry. The y-axis points to the driver's right and the x-axis points downward. (See Fig. 2.)

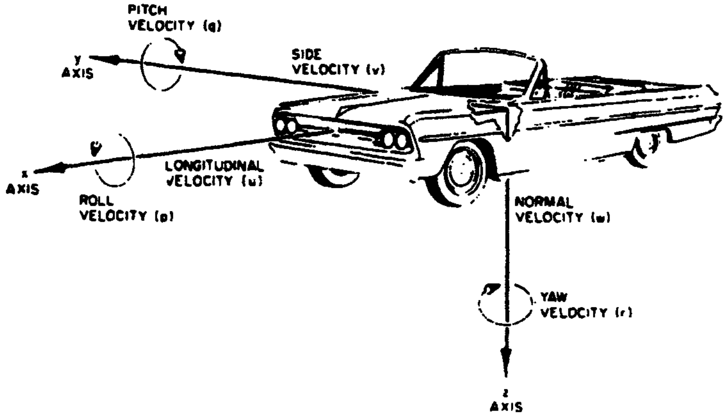

Fig. 2—Directional Control Axis System

8.3 ANGULAR ORIENTATION—The orientation of the *vehicle axis system* (x, y, z) with respect to the *earth-fixed axis system* (X, Y, Z) is given by a sequence of three angular rotations. The following sequence of rotations (see Note 6), starting from a condition in which the two sets of axis are initially aligned, is defined to be the standard:

(1) A yaw rotation, Ψ, about the aligned z and Z-axis.
(2) A pitch rotation, θ, about the vehicle y-axis.
(3) A roll rotation, ϕ, about the vehicle x-axis.

8.4 MOTION VARIABLES

8.4.1 *Vehicle Velocity*—The vector quantity expressing velocity of a point in the vehicle relative to the earth-fixed axis system (X,Y,Z). The following motion variables are components of this vector resolved with respect to the moving vehicle axis system (x,y,z).

8.4.1.1 Longitudinal Velocity (u) of a point in the vehicle is the component of the vector velocity in the x-direction.

8.4.1.2 Side Velocity (v) of a point in the vehicle is the component of the vector velocity in the y-direction.

8.4.1.3 Normal Velocity (w) of a point in the vehicle is the component of the vector velocity in the z-direction.

8.4.1.4 Forward Velocity of a point in the vehicle is the component of the vector velocity perpendicular to the y-axis and parallel to the road plane.

8.4.1.5 Lateral Velocity of a point in the vehicle is the component of the vector velocity perpendicular to the x-axis and parallel to the road plane.

8.4.1.6 Roll Velocity (p)—The angular velocity about the x-axis.

8.4.1.7 Pitch Velocity (q)—The angular velocity about the y-axis.

8.4.1.8 Yaw Velocity (r)—The angular velocity about the z-axis.

8.4.2 *Vehicle Acceleration*—The vector quantity expressing the acceleration of a point in the vehicle relative to the earth-fixed axis system (X,Y,Z). The following motion variables are components of this vector, resolved with respect to the moving vehicle axis system.

8.4.2.1 Longitudinal Acceleration—The component of the vector acceleration of a point in the vehicle in the x-direction.

8.4.2.2 Side Acceleration—The component of the vector acceleration of a point in the vehicle in the y-direction.

8.4.2.3 Normal Acceleration—The component of the vector acceleration of a point in the vehicle in the z-direction.

8.4.2.4 Lateral Acceleration—The component of the vector acceleration of a point in the vehicle perpendicular to the vehicle x-axis and parallel to the road plane. (See Note 7.)

8.4.2.5 Centripetal Acceleration—The component of the vector acceleration of a point in the vehicle perpendicular to the tangent to the path of that point and parallel to the road plane.

8.4.3 *Heading Angle* (Ψ)—The angle between the trace on the X-Y plane of the vehicle x-axis and the X-axis of the earth-fixed axis system. (See Fig. 3.)

8.4.4 *Sideslip Angle (Attitude Angle)* (β) is the angle between the traces on the X-Y plane of the vehicle x-axis and the vehicle velocity vector at some specified point in the vehicle. Sideslip angle is shown in Fig. 3 as a negative angle.

8.4.5 *Sideslip Angle Gradient*—The rate of change of *sideslip angle* with respect to change in steady-state *lateral acceleration* on a level road at a given *trim* and test conditions.

SAE J670e Revised JUL76

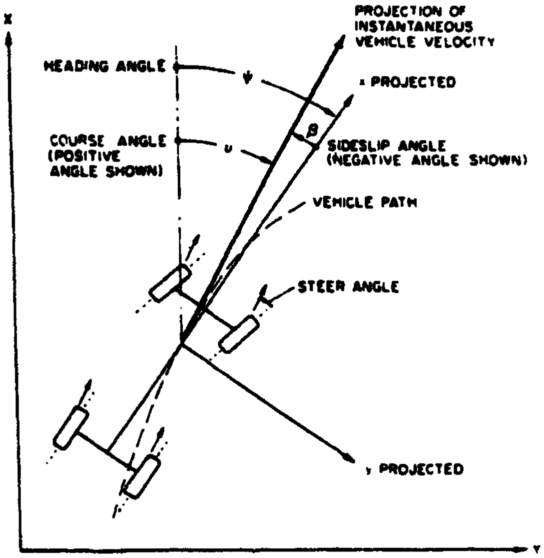
X
PROJECTION OF INSTANTANEOUS VEHICLE VELOCITY
HEADING ANGLE
ψ
x PROJECTED
β
COURSE ANGLE (POSITIVE ANGLE SHOWN)
υ
SIDESLIP ANGLE (NEGATIVE ANGLE SHOWN)
VEHICLE PATH
STEER ANGLE
y PROJECTED
Y

Fig. 3—Heading, Sideslip, and Course Angles

8.4.6 *Course Angle* (v) is the angle between the trace of the vehicle velocity vector on the X-Y plane and X-axis of the earth-fixed axis system. A positive course angle is shown in Fig. 3. Course angle is the sum of heading angle and sideslip angle (v = 41 + 0).

8.4.7 *Vehicle Roll Angle*—The angle between the vehicle y-axis and the ground plane.

8.4.8 *Vehicle Roll Gradient*—The rate of change in *vehicle roll angle* with respect to change in steady-state *lateral acceleration* on a level road at a given *trim* and test conditions.

8.4.9 *Vehicle Pitch Angle*—The angle between the vehicle x-axis and the ground plane.

8.5 FORCES—The external forces acting on the vehicle can be summed into one force vector Driving the following components:

8.5.1 *Longitudinal Force* (F_x) is the component of the force vector in the x-direction.

8.5.2 *Side Force* (F_y) is the component of the force vector in the y-direction.

SAE J670e Revised JUL76

8.5.3 Normal Force (F_z) is the component of the force vector in the z-direction.

8.8 MOMENTS—The external moments acting on the vehicle can be summed into one moment vector having the following components:

8.6.1 *Rolling Moment* (M_x) is the component of the moment vector tending to rotate the vehicle about the x-axis, positive clockwise when looking in the positive direction of the x-axis.

8.6.2 *Pitching Moment* (M_y) is the component of the moment vector tending to rotate the vehicle about the y-axis, positive clockwise when looking in the positive direction of the y-axis.

8.6.3 *Yawing Moment* (M_z) is the component of the moment vector tending to rotate the vehicle about the z-axis, positive clockwise when looking in the positive direction of the z-axis.

9. DIRECTIONAL DYNAMICS

9.1 CONTROL MODES

9.1.1 *Position Control*—That mode of vehicle control wherein inputs or restraints are placed upon the steering system in the form of displacements at some control point in the steering system (front wheels, Pitman arm, steering wheel), independent of the force required.

9.1.2 *Fixed Control*—That mode of vehicle control wherein the position of some point in the steering system (front wheels, Pitman arm, steering wheel) is held fixed. This is a special case of position control.

9.1.3 *Force Control*—That mode of vehicle control wherein inputs or restraints are placed upon the steering system in the form of forces, independent of the displacement required.

9.1.4 Free Control—That mode of vehicle control wherein no restraints are placed upon the steering system. This is a special case of force control.

9.2 VEHICLE RESPONSE—The vehicle motion resulting from some internal or external input to the vehicle. Response tests can be used to determine the stability and control characteristics of a vehicle.

9.2.1 *Steering Response*—The vehicle motion resulting from an input to the steering (control) element. (See Note 8.)

9.2.2 *Disturbance Response*—The vehicle motion resulting from unwanted force or displacement inputs applied to the vehicle. Examples of disturbances are wind forces or vertical road displacements.

9.2.3 *Steady-State*—Steady-state exists when periodic (or constant) vehicle responses to periodic (or constant) control and/or disturbance inputs do not change over an arbitrarily long time. The motion responses in steady-state are referred to as steady-state responses. This definition does not require the vehicle to be operating in a straight line or on a level road surface. It can also be in a turn of constant radius or on a cambered road surface,

9.2.4 *Transient State*—Transient state exists when the motion responses, the external forces relative to the vehicle, or the control positions are changing with time. (See Note 9.)

9.2.5 *Trim*—The steady-State (that is, equilibrium) condition of the vehicle with constant input which is used as the reference point for analysis of dynamic vehicle *stability* and control characteristics.

9.2.6 *Steady-State Response Gain*—The ratio of change in the *steady-state* response of any motion variable with respect to change in input at a given *trim*.

9.2.7 *Steering Sensitivity* (Control Gain)—The change in steady-state *lateral acceleration* on a level road with respect to change in *steering wheel angle* at a given *trim* and test conditions.

9.3 STABILITY—(See Note 10.)

9.3.1 *Asymptotic Stability*—Asymptotic stability exists at a prescribed *trim* if, any small temporary change in disturbance or *control input*. the vehicle will approach the motion defined by the *trim*.

9.3.2 Neutral Stability—Neutral stability exists at a prescribed trim if, for any small temporary change in disturbance or control input, the resulting motion of the vehicle remains close to, but does not return to, the motion defined by the trim.

9.3.3 *Divergent Instability*—Divergent instability exists at a prescribed *trim* if any small temporary disturbance or *control input* causes an ever increasing *vehicle response* without *oscillation*. (See Note 11.)

9.3.4 *Oscillatory Instability*—Oscillatory instability exists if a small temporary disturbance or control input causes an oscillatory vehicle response of ever increasing amplitude about the initial trim. (See Note 12.)

9.4 SUSPENSION STEER AND ROLL PROPERTIES (Fig. 4)—(See Note 13.)

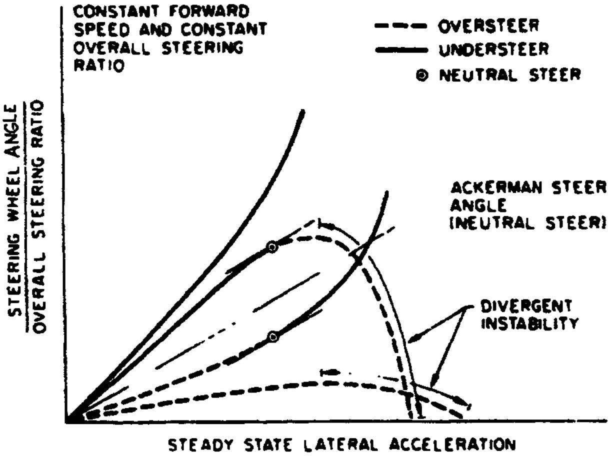

Fig. 4—Steer Properties (See Note 17)

SAE J670e Revised JUL76

9.4.1 *Steer Angle* (δ)—The angle between the projection of a longitudinal axis of the vehicle and the line of intersection of the wheel plane and the road surface. Positive angle is shown in Fig. 3.

9.4.2 *Ackerman Steer Angle*—(δ_a) is the angle whose tangent is the wheelbase divided by the radius of turn.

9.4.3 *Ackerman Steer Angle Gradient*—The rate of change of *Ackerman steer angle* with respect to change in steady-state *lateral acceleration* on a level road at a given *trim* and test conditions. (See Note 14.)

9.4.4 *Steering Wheel Angle*—Angular displacement of the steering wheel measured from the straight-ahead position (position corresponding to zero average steer angle of a pair of steered wheels).

9.4.5 *Steering Wheel Angle Gradient*—The rate of change in the *steering wheel angle* with respect to change in steady-state *lateral acceleration* on a level road at a given *trim* and test conditions.

9.4.6 *Overall Steering Ratio*—The rate of change of *steering wheel angle* at a given steering wheel *trim* position, with respect to change in average *steer angle* of a pair of steered wheels, assuming an infinitely stiff steering system with no roll of the vehicle (Note 15).

9.4.7 *Understeer/Oversteer Gradient*—The quantity obtained by subtracting the *Ackerman steer angle gradient* from the ratio of the *steering wheel angle gradient* to the *overall steering ratio*.

9.4.8 *Neutral Steer*—A vehicle is neutral steer at a given *trim* if the ratio of the *steering wheel angle gradient* to the *overall steering ratio* equals the *Ackerman steer angle gradient*.

9.4.9 *Understeer*—A vehicle is understeer at a given *trim* if the ratio of the *steering wheel angle gradient* to the *overall steering ratio* is greater than the *Ackerman steer angle gradient*.

9.4.10 *Oversteer*—A vehicle is oversteer at a given trim if the ratio of the *steering wheel angle gradient* to the *overall steering ratio* is less than the *Ackerman steer angle gradient*.

9.4.1.1 *Steering Wheel Torque*—The torque applied to the steering wheel about its axis of rotation.

9.4.12 *Steering Wheel Torque Gradient*—The rate of change in the *steering wheel torque* with respect to change in steady-state *lateral acceleration* on a level road at a given *trim* and test conditions.

9.4.13 *Characteristic Speed*—That forward speed for an understeer vehicle at which the steering sensitivity at zero *lateral acceleration* trim is one-half the steering sensitivity of a neutral steer vehicle.

9.4.14 *Critical Speed*—That forward speed for an oversteer vehicle at which the steering sensitivity at zero *lateral acceleration* trim is infinite.

9.4.15 *Neutral Steer Line*—The set of points in the x-z plane at which external lateral forces applied to the *sprung mass* produce no steady-state *yaw velocity*.

9.4.16 *Static Margin*—The horizontal distance from the center of gravity to the *neutral steer line* divided by the wheelbase. It is positive if the center of gravity is forward of the *neutral steer line*.

9.4.17 *Suspension Roll*—The rotation of the vehicle *sprung mass* about the x-axis with respect to a transverse axis joining a pair of *wheel centers*.

SAE J670e Revised JUL76

9.4.18 *Suspension Roll Angle*—The angular displacement produced by *suspension roll.*

9.4.19 *Suspension Roll Gradient*—The rate of change in the *suspension roll angle* with respect to change in steady-state *lateral acceleration* on a level road at a given *trim* and test conditions.

9.4.20 *Roll Steer*—The change in *steer angle* of front or rear wheels due to *suspension roll.*

9.4.20.1 Roll Understeer—*Roll steer* which increases vehicle *understeer* or decreases vehicle *oversteer.*

9.4.20.2 Roll Oversteer—*Roll steer* which decreases vehicle *understeer* or increases vehicle *oversteer.*

9.4.21 *Roll Steer Coefficient*—The rate of change in *roll steer* with respect to change in *suspension roll angle* at a given *trim.*

9.4.22 *Compliance Steer*—The change in *steer angle* of front or rear wheels resulting from compliance in suspension and steering linkages and produced by forces and/or moments applied at the tire-road contact.

9.4.22.1 Compliance Understeer—*Compliance steer* which increases vehicle *understeer* or decreases vehicle *oversteer.*

9.4.22.2 Compliance Oversteer—*Compliance steer* which decreases vehicle *understeer* or increases vehicle *oversteer.*

9.4.23 *Compliance Steer Coefficient*—The rate of change in *compliance steer* with respect to change in forces or moments applied at the tire-road contact.

9.4.24 *Roll Camber*—The camber displacements of a wheel resulting from *suspension roll.*

9.4.25 *Roll Camber Coefficient*—The rate of change in wheel *inclination angle* with respect to change in *suspension roll angle.*

9.4.26 *Compliance Camber*—The camber motion of a wheel resulting from compliance in suspension linkages and produced by forces and/or moments applied at the tire-road contact.

9.4.27 *Compliance Camber Coefficient*—The rate of change in wheel *inclination angle* with respect to change in forces or moments applied at the tire-road contact.

9.4.28 *Roll Center*—The point in the transverse vertical plane through any pair of *wheel centers* at which lateral forces may be applied to the sprung mass without producing *suspension roll.* (See Note 16.)

9.4.29 *Roll Axis*—The line joining the front and rear *roll centers.*

9.4.30 *Suspension Roll Stiffness*—The rate of change in the restoring couple exerted by the suspension of a pair of wheels on the *sprung mass* of the vehicle with respect to change in *suspension roll angle.*

9.4.31 *Vehicle Roll Stiffness*—Sum of the separate *suspension roll stiffnesses.*

9.4.32 *Roll Stiffness Distribution*—The distribution of the *vehicle roll stiffness* between front and rear suspension expressed as percentage of the *vehicle roll stiffness.*

9.5 TIRE LOAD TRANSFER

9.5.1 *Tire Lateral Load Transfer*—The *vertical load* transfer from one of the front tires (or rear tires) to the other that is due to acceleration, rotational, or inertial effects in the lateral direction.

9.5.2 *Tire Lateral Load Transfer Distribution*—The distribution of the total *tire lateral load transfer* between front and rear tires expressed as the percentage of the total.

9.5.3 *Tire Longitudinal Load Transfer*—The *vertical load* transferred from a front tire to the corresponding rear tire that is due to acceleration, rotational, or inertial effects in the longitudinal direction.

9.5.4 *Overturning Couple*—The overturning moment on the vehicle with respect to a central, longitudinal axis in the road plane due to lateral acceleration and roll acceleration.

9.5.5 *Overturning Couple Distribution*—The distribution of the total *overturning couple* between the front and rear suspensions expressed as the percentage of the total.

10. AERODYNAMIC NOMENCLATURE

10.1 AERODYNAMIC MOTION VARIABLES

10.1.1 *Ambient Wind Velocity* (v_a) is the horizontal component of the air mass velocity relative to the earth-fixed axis system in the vicinity of the vehicle.

10.1.2 *Ambient Wind Angle* (v_a) is the angle between the X axis of the *earth-fixed axis system* and the *ambient wind velocity* vector. A positive ambient wind angle is shown in Fig. 5.

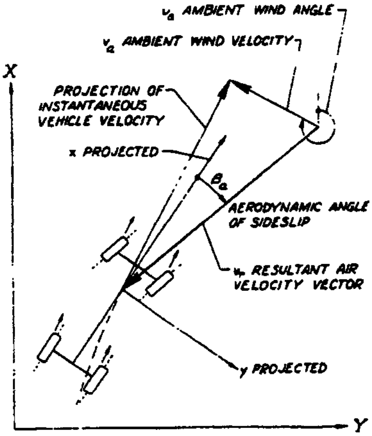
ν_a AMBIENT WIND ANGLE
v_a AMBIENT WIND VELOCITY
X
PROJECTION OF INSTANTANEOUS VEHICLE VELOCITY
x PROJECTED
β_a
AERODYNAMIC ANGLE OF SIDESLIP
v_r RESULTANT AIR VELOCITY VECTOR
y PROJECTED
Y

Fig. 5—Wind Vectors

10.1.3 *Resultant Air Velocity Vector* (v_r) is the vector difference of the *ambient wind velocity* vector and the projection of the velocity vector of the vehicle on the X-Y plane.

10.1.4 *Aerodynamic Sideslip Angle* (β_a) is the angle between the traces on the vehicle x-y plane of the vehicle x-axis and the resultant air velocity vector at some specified point in the vehicle.

10.1.5 *Aerodynamic Angle of Attack* (α_a) is the angle between the vehicle x-axis and the trace of the resultant air velocity vector on a vertical plane containing the vehicle x-axis.

10.2 AERODYNAMIC FORCE AND MOMENT COEFFICIENTS

10.2.1 *Reference Dimensions*

10.2.1.1 Vehicle Area (A) is the projected frontal area including tires and underbody parts,

10.2.1.2 Vehicle Wheelbase (ℓ) is the characteristic length upon which aerodynamic moment coefficients are based.

10.2.2 *Standard Air Properties*

10.2.2.1 The density of standard dry air shall be taken as 2378 X 10^{-6} slugs/ft at 59 F and 29.92 in. Hg.

10.2.2.2 The viscosity of Standard dry air shall be taken 373 X 10^{-9} slugs/ft-sec.

10.2.3 *Force Coefficients*

10.2.3.1 The Longitudinal Force Coefficient (C_x) is based on the aerodynamic force acting on the vehicle in the x direction (as established by paragraph 8.2) and is defined as:

$$C_x = \frac{F_x}{qA}$$

where:

q is dynamic pressure at any given relative air velocity as given by the formula

$$q = \frac{\rho v^2}{2}$$

10.2.3.2 Side Force Coefficient (C_y) is based on the aerodynamic force acting on the vehicle in the y-direction (as established by paragraph 8.2) and is defined as:

$$c_y = \frac{F_y}{qA}$$

where:

q is the dynamic pressure at any given relative air velocity as given by the formula

$$q = \frac{\rho v^2}{2}$$

10.2.3.3 The Normal Force Coefficient (C_z) is based on the aerodynamic force acting in the z direction (as established by paragraph 8.2) and is defined as:

$$C_z = \frac{F_z}{qA}$$

10.2.4 *Moment Coefficients*

10.2.4.1 The Rolling Moment Coefficient (C_{M_x}) is based on the rolling moment deriving from the distribution of aerodynamic forces acting on the vehicle and is defined as:

$$C_{M_x} = \frac{M_x}{qA\ell}$$

10.2.4.2 The Pitching Moment Coefficient (C_{M_y}) is based on the pitching moment deriving from the distribution of aerodynamic forces acting on the vehicle and is defined as:

$$C_{M_y} = \frac{M_y}{qA\ell}$$

10.2.4.3 The Yawing Moment Coefficient (C_{M_z}) is based on the yawing moment deriving from the distribution of aerodynamic forces acting on the vehicle and is defined as:

$$C_{M_z} = \frac{M_z}{qA\ell}$$

11. MARGINAL INDICIA—The ϕ is for the convenience of the user in locating areas where technical changes have been made to the previous issue of the report. If the symbol is next to the report title, it indicates a complete revision of the report.

NOTES

1. The *center of tire contact* may not be the geometric center of the tire contact area due to distortion of the tire produced by applied forces.

2. The static toe (inches) is equal to the sum of the toe angles (degrees) of the left and right wheels multiplied by the ratio of tire diameter (inches) to 57.3.

   If the toe angles on the left and right wheels are the same and the outside diameter of tire is 28.65 in (727.7 mm), the *static toe (inches)* is equal to *static toe angle (degrees)*.

3. It is important to recognize that to make axis transformations and resolve these forces with respect to the direction of vehicle motion, it is essential to measure all six force and moment components defined in paragraphs 7.5.3.1-7.5.3.3 and 7.5.4.1-7.5.4.3.

4. This *rolling resistance force* definition has been generalized so that it applies to wheels which are driven or braked. The *wheel torque* can be expressed in terms of the *longitudinal force*, *rolling resistance force*, and *loaded radius* by the equation

   $$T = (F_x + F_r)R_\ell$$

   For a free-rolling wheel, the rolling resistance force is therefore the negative of the *longitudinal force*.

5. For small *slip* and *inclination angles*, the *lateral force* developed by the tire can be approximated by

   $$F_y = C_\alpha \alpha + C_\gamma \gamma$$

6. Angular rotations are positive clockwise when looking in the positive direction of the axis about which rotation occurs.

7. In steady-state condition, *lateral acceleration* is equal to the product of *centripetal acceleration* times the cosine of the Vehicle's *sideslip angle*. Since in most test conditions the *sideslip angle* is small, for practical purposes, the *lateral acceleration* can be considered equal to *centripetal acceleration*.

8. Although the steering wheel is the primary directional control element it should be recognized that *longitudinal forces* at the wheels resulting from driver inputs to brakes or throttle can modify directional response.

9. Transient responses are described by the terminology normally employed for other dynamic systems. Some terminology is described in the "Control Engineers' Handbook,"* but a more complete terminology is contained in ANS C85.1-1963.**

10. Passenger vehicles exhibit varying characteristics depending upon test conditions and *trim*. Test conditions refer to vehicle conditions such as wheel loads, front wheel alignment, tire inflation pressure, and also atmospheric and road conditions which affect vehicle parameters. For example, temperature may change shock absorber damping characteristics and a slippery road surface may change tire cornering properties. *Trim* has been previously defined as the vehicle operating condition within a given environment, and may be specified in part by *steer angle*, *forward velocity*, and *lateral acceleration*. Since all these factors change the vehicle behavior, the vehicle *stability* must be examined separately for each environment and *trim*.

    For a given set of vehicle parameters and particular test conditions, the vehicle may be examined for each theoretically attainable *trim*. The conditions which most affect *stability* are the *steady-state* values of *forward velocity* and *lateral accelerations*. In practice, it is possible for a vehicle to be stable under one set of operating conditions and unstable in another.

---

* John G. Truxal (Ed.), "Control Engineers' Handbook," New York: McGraw-Hill.

** "Terminology for Automatic Control," ANS C85.1-1963, Published by American Society of Mechanical Engineers.

SAE J670e Revised JUL76

11. Divergent instability may be illustrated by operation above the *critical speed* of an *oversteer* vehicle. Any input to the steering wheel will place the vehicle in a turn of ever decreasing radius unless the driver makes compensating motions of the wheel to maintain general equilibrium. This condition represents *divergent instability*. A linear mathematical analog of a vehicle is *divergently unstable* when its characteristic equation has any positive real roots.

12. Oscillatory instability may be illustrated by the *free control response* following a pulse input of displacement or force to the steering wheel. Some vehicles will turn first in one direction, and then the other, and so on, until the *amplitude* of the motion increases to the extent that the vehicle "spins out." In this event, the vehicle does not attempt to change its general direction of motion, but does not achieve a *steady-state* condition and has an *oscillatory* motion. A linear mathematical analog of a vehicle is *oscillatorily unstable* when its characteristic equation has any complex roots with positive real parts.

13. It is possible for a vehicle to be *understeer* for small inputs and *oversteer* for large inputs (or the opposite), as shown in Fig. 4, since it is a nonlinear system and does not have the same characteristics at all *trims*. Consequently, it is necessary to specify the range of inputs and velocities when making a determination of the vehicle's *steer characteristics*.

    There is a set of equivalent definitions in terms of *yaw velocity* or curvature (reciprocal of radius of curvature), which can be used interchangeably with these definitions. These definitions only apply to two-axle vehicles, since the Ackerman steer angle only applies to two-axle vehicles.

14. *Ackerman Steer Angle Gradient* is equal to the wheelbase divided by the square of the vehicle speed (rad/ft/s^2).

15. For nonlinear steering systems, this ratio should be presented as a function of *steering wheel angle* in order to be compatible with the definition of *understeer/oversteer gradient*.

16. The *roll center* defined in paragraph 9.4.28 constitutes an idealized concept and does not necessarily represent a true instantaneous center of rotation of the sprung mass.

17. Illustration applies only for constant *overall steering ratio*. For other steering systems, refer directly to definitions for interpretation of data.

PREPARED BY THE SAE VEHICLE DYNAMICS COMMITTEE

References

Abbott, I.H. and von Doenhoff, A.E., *Theory of Wing Sections*, Dover, ISBN 486-60586-8, 1959.

Artamonov, M.D., Ilarinov, V.A. and Morin, M.M., *Motor Vehicles – Fundamentals and Design* (Trans. A. Troitsky), M.I.R. Publishers, Moscow, 1976.

Bakker E., Nyborg L. and Pacejka H.B., "Tyre Modelling for Use in Vehicle Dynamics Studies," SAE Paper No. 870421, Society of Automotive Engineers, Warrendale, Pa., 1987

Bastow, D., *Car Suspension and Handling*, Pentech Press, ISBN 0-7273-03050-8, pp. 89–95, 1980.

Bastow, D., *Car Suspension and Handling*, 2nd edition, Pentech Press, ISBN 0-7273-0316-3, 1987.

Bekker, M.G., *Theory of Land Locomotion*, Univ. of Michigan Press, 1956.

Bekker, M.G., *Off-the-Road Locomotion*, Univ. of Michigan Press, 1960.

Bekker, M.G., *Introduction to Terrain-Vehicle Systems*, Univ. of Michigan Press, 1969.

Benzing E., *Wings*, Bruno Alfieri, ISBN 88-85880-38-X, 1991.

Bergman, W., "The Basic Nature of Vehicle Understeer–Oversteer," SAE Paper No. 650085, Society of Automotive Engineers, Warrendale, Pa., 1965.

Bergman, W., "Measurement and Subjective Evaluation of Vehicle Handling," SAE Paper No. 730492, Society of Automotive Engineers, Warrendale, Pa., 1973.

British Standards BS AU 50: Part 2, 1979.

Bundorf, R.T. and Leffert, R.L., "The Cornering Compliance Concept for Description of Vehicle Directional Control Properties," SAE Paper No. 760713, Society of Automotive Engineers, Warrendale, Pa., 1976.

Bundorf, R.T., "The Influence of Vehicle Design Parameters on Characteristic Speed and Understeer," SAE Paper No. 670078, Society of Automotive Engineers, Warrendale, Pa., 1967.

Cain B.S., *Vibration of Rail and Road Vehicles*, Pitman and Sons Ltd, 1940.

Cain T., *Spring Design and Manufacture*, Argus Books, ISBN 0-85242-925-8, 1988

Campbell, C., *Automobile Suspensions*, Chapman and Hall, ISBN 0-412-15820-5, 1981.

Carr, G.W., Rose, M.J. and Smith, N.P., "Some aerodynamic aspects of safety in road vehicles" (in three parts), *Proc. I.Mech.E.* (*A.D.*), Vol. 187, No. 30, pp. 333–360, 1973.

Chiang, S.L. and Starr, D.S., "Using Computer Simulation to Evaluate and Improve Vehicle Handling," SAE Paper No. 780009, Society of Automotive Engineers, Warrendale, Pa., 1978.

Clark, S.K. (ed.), *Mechanics of Pneumatic Tires,* 2nd edition, U.S. Dept of Transportation, 1981.

Cogotti, A., "Aerodynamic characteristics of car wheels," in Dorgham and Businaro, (see below), pp. 173–196, 1983.

Coker A.J., *Automobile Engineer's Reference Book*, George Newnes, 3rd Ed., 1959.

Curtis, A., "Anatomy of the 180 mph corner," *Autocar*, 22 August 1990, pp. 56–59.

Dean-Averns R., *Automobile Chassis Design*, 2nd Ed., Iliffe and Sons Ltd., 1952.

Dixon, J.C., "The roll-center concept in vehicle handling dynamics," *Proc. I.Mech.E.*, Vol. 201, No. D1, 22/87, pp. 69–78.

Dixon, J.C., "Limit steady state vehicle handling," *Proc. I.Mech.E.*, Vol. 201, No. D4, pp. 281–291, 1987.

Dixon, J.C., "Linear and nonlinear steady state vehicle handling," *Proc. I.Mech.E.*, Vol. 202, No. D3, pp. 173–186, 1988.

Dominy, J. and Dominy, R.G., "Aerodynamic influences on the performance of the Grand Prix racing car," *Proc. I.Mech.E.*, Vol. 198, Part D, pp. 87–93, 1984.

Dorgham, M.A. and Businaro, U.L. (eds), *Impact of Aerodynamics on Vehicle Design,* Proc. of the Int. Assoc. for Vehicle Design, SP3, ISBN 0-907776-01-9, 1983.

Dugoff, H., Segel, L. and Ervin, R.D., "Measurement of Vehicle Response in Severe Braking and Steering Manouvers," SAE Paper No. 710080, Society of Automotive Engineers, Warrendale, Pa., 1971.

Durstine J.W., "The Truck Steering System," SAE Paper No. 730039, Society of Automotive Engineers, Warrendale, Pa., 1973.

Ellis J.R., *Vehicle Handling Dynamics*, Mechanical Engg Publications Ltd., ISBN 0-85298-885-0, 1994.

Ellis, J.R., "Understeer and oversteer," *Automobile Engineer*, May 1963.

Ellis, J.R., *Vehicle Dynamics*, Business Books Ltd, ISBN 220-99202-9, 1969.

Ellis, J.R., *Road Vehicle Dynamics*, J.R. Ellis, Akron, Ohio, 1989.

Evans, R.D., "Properties of tyres affecting riding, steering and handling," *SAE Transactions*, Vol. 36, No. 2, pp. 41–49, 1935.

Fackrell, J.E. and Harvey, J.K., "The aerodynamics of an isolated road wheel," in *Proc. A.I.A.A. 2nd Symposium on Aerodynamics of Sports and Competition Automobiles*, 1974.

Fancher, P., Segel, L., Bernard, J. and Ervin, R., "Test Procedures for Studying Vehicle Dynamics in Lane-Change Manouvers," SAE Paper No. 760351, Society of Automotive Engineers, Warrendale, Pa., 1976.

Frank, F. and Hofferberth, W., "Mechanics of pneumatic tyre," *Rubber Chemistry and Technology*, Vol. 40, No. 1, pp. 271–322, February 1967.

French, T., *Tyre Technology*, Adam Hilger, ISBN 0-85274-360-2, 1989.

Frere, P., *The Racing Porsches*, Arco, N.Y., ISBN 0-668-02972-2, 1973.

Gardner, E.R. and Worswick, T., *Trans. Inst. Rubber Industry*, Vol. 27, p. 127, 1951.

Garrett, K., "Traction control differentials," *Automotive Engineer*, pp. 20–26, February 1987.

Giles, J.G. (Ed.), *Steering, Suspension and Tyres*, Iliffe, 1968.

Gillespie T.D., *Fundamentals of Vehicle Dynamics*, SAE R-114, Society of Automotive Engineers, Warrendale, Pa., 1992.

Good, M.C., "Sensitivity of driver–vehicle performance to vehicle characteristics revealed in open-loop tests," *Vehicle System Dynamics*, Vol. 6, pp. 245–277, 1977

Goodsell D., *Dictionary of Automotive Engineering*, 2nd Ed., SAE R-159, Society of Automotive Engineers, Warrendale, Pa., ISBN 1-56091-683-4 1995. (U.K. edition [soft cover], Butterworth-Heinemann, ISBN 0-7506-2795-6.)

Goran, M.B. and Hurlong, G.W., "Determining vehicle inertial properties for simulation studies," *Bendix Technical Journal*, Vol. 6, pp. 53–57, Spring 1973

Grylls, S.H., "Traction v. stability in passenger cars," *Journal of Automotive Engineering*, pp. 8–15, May 1972, also *Proc. I.Mech.E.*, Vol. 186, No. 17, pp. 169–177.

Hales, F.D., *The Handling and Stability of Motor Vehicles, Part 1, Handling, Stability and Control Response Definitions*, MIRA, 1965/1.

Hales, F.D., "Vehicle handling qualities," *Proc. I.Mech.E.*, Vol. 184, Pt 2A, No. 12, pp. 233–248, 1969-70.

Hall, L.C., "The influence of limited slip differentials on torque distribution and steady-state handling of four-wheel drive military vehicles," I.Mech.E. Paper CO5/86, *Proc. I.Mech.E. Conf. on Vehicle Dynamics*, pp. 59–66, 1986.

Hays, D.F. and Browne, A.L. (eds), *The Physics of Tire Traction*, Plenum, N.Y., ISBN 0-306-30806-1, 1974.

Heisler H., *Advanced Vehicle Technology*, Edward Arnold, ISBN 0-7131-3660-X, 1989.

Henry, A., *The 4-Wheel Drives*, Macmillan, ISBN 333-17289-2, 1975.

Hoerner, S.F. and Borst H.V., *Fluid Dynamic Lift*, Hoerner Fluid Dynamics, Brick Town, NJ, LCCC 75-17441, 1975.

Hoerner, S.F., *Fluid Dynamic Drag*, Hoerner Fluid Dynamics, Brick Town, NJ, 1965.

Hogue, J.R., "Aerodynamics of Six Passenger Vehicles Obtained from Full Scale Wind Tunnel Tests," SAE Paper No. 800142, Society of Automotive Engineers, Warrendale, Pa., 1980.

Holthusen, P.J.R., *The Land Speed Record*, Haynes, ISBN 0-85429-499-6, 1986.

Houghton, E.L. and Brock, A.E., *Aerodynamics for Engineering Students*, Edward Arnold, ISBN 7131-3227-2, 1970.

Houghton, E.L. and Carpenter P.W., *Aerodynamics for Engineering Students*, 4th Ed., Edward Arnold, ISBN 0-340-504847-9, 1993.

Howard, G., *Automobile Aerodynamics*, Osprey, ISBN 0-85045-665-, 1986.

Hucho, W.H. (ed.), *Aerodynamics of Road Vehicles*, Butterworths, ISBN 0-408-01422-9, 1987.

Huntingdon, R., *Design and Development of the Indy Car*, HP Books, Tucson, ISBN 0-89586-103-8, 1981.

I.Mech.E., *International Conference on Advanced Suspensions*, Conference Publication C367, 1988.

ISO/TC22/SC9/N185, *Step/Ramp Input*, May 1979.

ISO/TC22/SC9/N194, *Random Input*, May 1979.

ISO/TC22/SC9/N219, *Sinusoidal Input*, June 1979.

ISO 4138, *Road Vehicles – Steady State Circular Test Procedure*, 1982.

ISO 7975-1985, *Road Vehicles – Braking in a Turn – Open Loop Test Procedure*, also issued as BS AU 205: 1986.

ISO 7401, *Road Vehicles - Lateral Transient Response Test Methods.*

ISO 8855, Glossary of Terms for Road Vehicle Dynamics and Road Holding Ability, ISBN 0-580-2083-03 (adopted as a British Standard BS AU 244:1992).

ISO TR 3888, *Lane Change Test.*

Irving, J.S., "The Golden Arrow and the world's land speed record," *Automobile Engineer*, pp. 186–196, May 1930.

Katz J. and Plotkin A., *Low Speed Aerodynamics*, McGraw-Hill, ISBN 0-07-050446-6, 1991

Koenig - Fachsenfeld, F.R., *Aerodynamik des Kraftfahrzeugs*, Umschau Verlag, Berlin, 1951.

Korff, W.H., *Designing Tomorrow's Cars*, M-C Publications, California, ISBN 0-9603850-0-2, 1980.

Lewis, R.P. and O'Brien, L.J., "Limited slip differentials," SAE Paper No. 590028, Society of Automotive Engineers, Warrendale, Pa., 1959.

Ludvigsen, K.E., "The Time Tunnel – A Historical Survey of Automobile Aerodynamics," SAE Paper No. 700035, Society of Automotive Engineers, Warrendale, Pa., 1970.

MIRA, *Definition of Handling Terms*, MIRA 1965/1.

MacAdam C.C., Sayers M.W., Pointer J.D. and Gleason M., "Crosswind Sensitivity of Passenger Cars and the Influence of Chassis and Aerodynamic Properties on Driver Performance," *Vehicle System Dynamics*, V19, 1990.

Massey, B.S., *Mechanics of Fluids*, Van Nostrand Reinhold, ISBN 0-442-30552-4, 1983.

McHenry, R.R., "An analysis of the dynamics of automobiles during simultaneous cornering and ride motions," I.Mech.E. Conference on Handling of Vehicles under Emergency Conditions, in *Computer Aided Design*, Vol. 1, pp. 19–32, Spring 1969.

McLean, W.G. and Nelson, E.W., *Engineering Mechanics; Statics and Dynamics*, Schaum Outline Series, McGraw-Hill, 1962.

Milliken W.F. and Milliken D.L., *Race Car Vehicle Dynamics*, SAE R-146, Society of Automotive Engineers, Warrendale, Pa., 1995.

Milliken, W.F. and Whitcomb, D.W., "General introduction to a programme of dynamic research," *Proc. I.Mech.E. (A.D.)*, pp. 287–309, 1956.

Milliken, W.F. Jr, Dell'Amico, F. and Rice, R.S., "The Static Directional Stability and Control of the Automobile," SAE Paper No. 760712, Society of Automotive Engineers, Warrendale, Pa., 1976.

Milliken, W.F. Jr., and Rice, R.S., "Moment method," *I.Mech.E. Conference on Road Vehicle Handling*, Paper C113/83, 1983.

Milner, P.J., "Steady state vehicle handling," *Automobile Engineer*, October 1967.

Milner, P.J., "Vehicle performance in crosswinds," *Automobile Engineer*, pp. 352–355, August 1968.

Moore, D.F., *The Friction of Pneumatic Tyres*, Elsevier, ISBN 0-444-41323-5, 1975.

Newton K., Steeds W. and Garrett T.K., *The Motor Vehicle*, Butterworths, ISBN 0-408-01802-7, 1989.

Norbye, J.P., *The Complete Handbook of Front Wheel Drive Cars*, Tab Books, ISBN 0-8306-2052-4, 1979.

Norbye, J.P., *The Car and Its Wheels – A Guide to Modern Suspension Systems*, Tab Books, ISBN 0-8306-2058-3, 1980.

Norbye, J.P., *The Michelin Magic*, Tab Books, ISBN 0-8306-2090-7, 1982.

Nye, D., *Theme Lotus*, Motor Racing Publications, London, ISBN 0-900549-40-8, 1978.

Odier, J., "A dynamometer on which the dynamic behaviour of a passenger car can be simulated," *Proc I.Mech.E. (A.D.)*, Vol. 186, No. 7, pp. 87–96, 1972.

Olley, M., "Independent wheel suspension – its whys and wherefores," *SAE Transactions*, Vol. 34, No. 2, pp. 73–81, 1934.

Olley, M., *Notes on Suspensions*, unpublished G.M. report, August 1961.

Olley, M., *Steady State Steering*, unpublished G.M. report, September 1961.

Olley, M., *Notes on Vehicle Handling*, unpublished G.M. report, February 1962.

Olley, M., *Suspension Notes II*, unpublished G.M. report, May 1962.

Pacejka, H.B., "Simplified analysis of steady-state turning behaviour of automobiles," *Vehicle Systems Dynamics*, Vol. 2, pp. 161–172, 173–183 (two parts), 1973.

Pacejka, H.B., "Principles of plane motion of automobiles," *Proc. I.U.T.A.M. Symposium*, pp. 33–59, 1975.

Pershing, B. (ed.), *Proc. A.I.A.A. Symposium on the Aerodynamics of Sports and Competition Automobiles*, 1968.

Pershing, B. (ed.), *Proc. A.I.A.A. Second Symposium on the Aerodynamics of Sports and Competition Automobiles*, 1974.

Pitts S. and Wildig A.W., "Effect of Steering Geometry on Self-Centering Torque and Feel During Low speed Manoeuvres," *Automotive Engineer*, July 1978.

Posthumus, C. and Tremayne, D., *Land Speed Record*, Osprey, London, ISBN 0-85045-641-X, 1985.

Press W.H., Flannery B.P., Teukolsky S.A. and Vetterling W.T., *Numerical Recipes, The Art of Scientific Computing*, Cambridge University Press, ISBN 0-521-38330-7, 1989.

Prevost, R., Letter in *Automobile Engineer*, p. 330, September 1928.

Puhn, F., *How to Make Your Car Handle*, HP Books, ISBN 0-912656-46-8, 1976/1981.

Radt, H.S. and Milliken, W.F., "Non-dimensionalising tyre data for vehicle simulation," *Proc. Conf. on Road Vehicle Handling*, I.Mech.E. Conf. Publ. No. C113/83, 1983.

Radt, H.S. and Pacejka, H.B., "Analysis of the steady-state turning behaviour of an automobile," *Proc. I.Mech.E. Symposium on Control of Vehicles*, 1965.

Rae, W.H. and Pope, A., *Low-Speed Wind Tunnel Testing*, Wiley, ISBN 0-471-87402-7, 1984.

Reimpell, J., *Fahrwerktechnik*, Vogel, Wurzburg, 3 volumes, ISBN 3-8023-0709-7, 1982.

Rice, R.S. and Milliken, W.F. Jr., "Static Stability and Control of the Automobile Utilizing the Moment Method," SAE Paper No. 800847, Society of Automotive Engineers, Warrendale, Pa., 1980.

Riede, P.M., Leffert R.L. and Cobb W.A., "Typical Vehicle Parameters for Dynamics Studies," SAE Paper No. 840561, Society of Automotive Engineers, Warrendale, Pa., 1984.

Robinson, J., *Motorcycle Tuning: Chassis*, Heinemann Newnes, ISBN 0-434-91724-9, 1990.

Rocard Y., *L'Instabilité en Mécanique*, Masson, 1960.

Rocard, Y., "Difficulties arising from auto-oscillation and instability during travel of vehicles," *La Revue Scientifique*, Vol. 84, No. 45, p. 15, 1946.

SAE AE-21, *Spring Design Manual*, Society of Automotive Engineers, Warrendale, Pa., 1996.

SAE XJ266, "Proposed Passenger Car and Light Truck Directional Control Response Test Procedures," Society of Automotive Engineers, Warrendale, Pa., 1985.

SAE J670e, "Vehicle Dynamics Terminology," Society of Automotive Engineers, Warrendale, Pa., 1978.

SAE J1106 (and J1107), "Laboratory Testing Machines (and Procedures) for Measuring the Steady State Force and Moment Properties of Passenger Car Tires," Society of Automotive Engineers, Warrendale, Pa., 1975.

SAE J1594, "Vehicle Aerodynamics Terminology," Society of Automotive Engineers, Warrendale, Pa., 1994.

SAE J2181, "Steady-State Circular Test Procedure for Trucks and Buses," Society of Automotive Engineers, Warrendale, Pa., 1993

SAE J2407, "Tire Performance Terminology," Society of Automotive Engineers, Warrendale, Pa., in draft, due 1997.

SAE SP-878, *Car Suspension Systems and Vehicle Dynamics*, Society of Automotive Engineers, Warrendale, Pa., 1991.

SAE SP-950, *Vehicle Dynamics and Simulation*, Society of Automotive Engineers, Warrendale, Pa., 1993.

SAE SP-952, *Vehicle Suspension and Steering Systems*, Society of Automotive Engineers, Warrendale, Pa., 1993.

Sabey, B.E., "The road surface in relation to friction and wear of tyres," *Road Tar*, Vol. 23, No.1, March 1969.

Sakai, H., "Theoretical and experimental studies on the dynamic properties of tyres, Parts 1–3," *Int. J. of Vehicle Design*, Vol. 2, Nos. 1–3, 1981.

Satchell, T.L., "The Design of Trailing Twist Axles," SAE Paper No. 810420, Society of Automotive Engineers, Warrendale, Pa., 1981.

Scibor-Rylski, A.J., *Road Vehicle Aerodynamics*, 2nd Ed., Pentech Press, London, ISBN 0-7273-1805-5, 1984.

Segel, L., "Theoretical prediction and experimental substantiation of the response of the automobile to steering control," *Proc. I.Mech.E.* (*A.D.*), pp. 310–330, 1957.

Segel, L., "Research in fundamentals of automobile control and stability," *SAE Transactions*, Vol. 65, pp. 527–540, Society of Automotive Engineers, Warrendale, Pa., 1957.

Segel, L., Ervin R. and Fancher, P., *The Mechanics of Heavy Duty Trucks and Truck Combinations*, Int. Assoc. for Vehicle Design, course notes, 1980.

Setright, L.J.K., *Automobile Tyres*, Chapman and Hall, ISBN 412-09850-4, 1972.

Sharp R.S. and Crolla D.A., "Road Vehicle Suspension System Design – A Review," *Vehicle System Dynamics*, V16, No. 3, pp.167-192, 1987.

Shearer, G.R., "The rolling wheel – the development of the pneumatic tyre," *Proc. I. Mech. E. (A.D.)*, Vol. 191, No. 11/77, pp. 75-87, 1977.

Simiu E. and Scanlan R.H., *Wind Effects on Structures*, John Wiley, ISBN 0-

471-02175-X, 1978.

Smith, C., *Tune to Win*, Aero Publishers Inc., USA, LCCC 78-73549, 1978.

Smith, J.G. and Smith, J.E., "Lateral forces on vehicles during driving," *Automobile Engineer*, pp. 510–515, December 1967.

Spiegel, M.R., *Mathematical Handbook*, Schaum Outline Series, McGraw-Hill, 1968.

Steeds, W., "Roll axes," *Automobile Engineer*, pp. 55–58, February 1958.

Steeds, W., *Mechanics of Road Vehicles*, Iliffe, 1960.

Sternberg E.R., "Heavy Duty Truck Suspensions," SAE Paper No. 760369, Society of Automotive Engineers, Warrendale, Pa., 1976.

Stonex, K.A., "Car control factors and their measurement," SAE Paper No. 410092, Society of Automotive Engineers, Warrendale, Pa., 1941.

Taborek J.J., "Mechanics of Vehicles," series of 14 articles in *Machine Design*, published later as a collection, Penton Publ. Co., Cleveland, 1957.

Tidbury G.H., *Advances in Automobile Engineering*, Pergamon, 1963.

Tompkins, E., *The History of the Pneumatic Tyre*, Dunlop Ltd (Eastland Press), ISBN 0-903214-14-8, 1981.

Topping, R.W., "A Primer on Nonlinear Steady-State Vehicle Turning Behaviour," SAE Paper No. 741096, Society of Automotive Engineers, Warrendale, Pa., 1974.

Verma, M.K. and Shepard, W.L., "Comparison of Transient Response Test Procedures for Motor Vehicles," SAE Paper No. 810807, Society of Automotive Engineers, Warrendale, Pa., 1981.

Weir, D.H. and DiMarco, R.J., "Correlation and Evaluation of Driver/Vehicle Directional Handling Data," SAE Paper No. 780010, Society of Automotive Engineers, Warrendale, Pa., 1978.

Weir, D.H. and Zellner, J.W., "The Application of Handling Requirements to an RSV-type Vehicle," SAE Paper No. 770178, Society of Automotive Engineers, Warrendale, Pa., 1977.

Whitcomb, D.W. and Milliken, W.F., "Design implications of a general theory of automobile stability and control," *Proc. I.Mech.E.* (*A.D.*), pp. 367–391, 1957.

Winkler, C.B., "Measurement of Inertial Properties and Suspension Parameters of Heavy Highway Vehicles," SAE Paper No. 730182, Society of Automotive Engineers, Warrendale, Pa., 1973.

Wong, J., *Theory of Ground Vehicles*, Wiley, ISBN 0-471-03470-3, 1978.

Wong, J., *Terramechanics and Off-Road Vehicles*, Elsevier, 1990.

Wright, P.G., "The influence of aerodynamics on the design of Formula One racing cars," in Dorgham and Businaro, (see above), pp. 158–172, 1983.

Yoshimori, K., "Vehicle Controllability and Human Response Characterstics," SAE Paper No. 760780, Society of Automotive Engineers, Warrendale, Pa., 1976.

Index

A-arm. *See* Wishbone
Acceleration
  acceleration components (vectors), 10, 11*f*
  centripetal
    and central force, 80
    maximum (steady-state cornering), 35-36, 36*f*
    and perpendicular tire force, 97
    and vehicle axis systems, 10, 11*f*, 14, 14*f*
    in vehicle-fixed axis system, 10-11, 11*f*
  lateral. *See* Lateral acceleration
Ackermann steering
  Ackermann factor, 293
  Ackermann steer angles, determining, 294
  anti-Ackermann steering, 294
  under dynamic steering conditions, 293-294
  full Ackermann (Lunar Rover, London taxi), 293
  kinematic (Ackermann) steer angle gradient, 346, 363, 364*f*
  understeer and Ackermann steer angle, 363, 364*f*
  see also Steady-state handling
Adex linkage, 191, 191*f*
Aerodynamics
  introduction, 154-155
  of ground vehicles (discussion), 154
  aerodynamic axes, vehicle, 160-162, 161*f*, 162*f*
  aerodynamic force, total
    components of, 159-160
    force coefficients, use of, 155-157
    frontal area, 155
    total force magnitude, 155
  airflow, effects of
    introduction, 165
    aerodynamic coefficients, typical (passenger car), 168, 169*t*
    air dams, use of, 166

Aerodynamics (continued)
  airflow, effects of (continued)
    flow separation, rear, 166
    flow under vehicle, 166
    front shape (box *vs.* wedge), 166
    styling *vs.* airflow, 167
    top (of vehicle) flow, 165-166
  of competition vehicles
    introduction/historical note, 171-173
    downforce in, 404
    drag coefficients, 167, 168*t*
    Golden Arrow (Irving), 171, 172*f*
    ground-effect (venturi) underbodies, 171, 172*f*, 173, 176-177
    Hall fan cars (skirted), 175
    spoilers, 165, 174-175
    see also Downforce; Wings
  downforce. *See* Downforce; *See also* Wings
  drag
    drag areas, typical, 156, 167, 168*t*
    drag coefficients, typical, 167, 168*t*
    drag force, 163
    in primary handling, 393
    tire drag, 33
    wings, induced drag from, 404
  final aerodynamics
    introduction, 396
    aerodynamic effects, discussion of, 403-404
    critical aerodynamic speed, 399
    critical path radius, 398, 399
    drag force, total, 400
    final aerodynamics effects (table of), 397
    lateral acceleration, limiting, 402, 403
    lateral acceleration, maximum, 398, 401, 402
    longitudinal load transfer, 399
    maximum cornering speed downforce, 398-399, 399*f*
    maximum speed for given radius, 397
    maximum steady-state speed (discussion), 397
    pitch coefficient, 399
    tire total vertical force, 397
    tractive force, 401
    understeer number, change in, 399, 401, 402, 403
    wheel vertical reaction, 399
    wings, induced drag from, 404
    see also primary aerodynamics *(below)*
  force coefficients
    adjustment for model tests, 156

Aerodynamics (continued)
  force coefficients (continued)
    airflow, effects of, 165-171
    coordinate system for, 159-160
    lift/pitch/roll, 159-160
    moment coefficients, 159-160
    side force, 161
    and total aerodynamic force, 155, 159
    of typical passenger car, 169*t*
    wheelbase, use of, 159, 160
  ground-effect (venturi) underbodies
    Golden Arrow (Irving), 171, 172*f*
    Prevost proposal, 171, 172*f*
    racing applications of, 176
    wind-tunnel tests of, 178
  lift
    aerodynamic lift force, 281
    front and rear lift, 160
    front lift (in primary handling), 392-393
    lift coefficients, passenger car, 169*t*
    lift coefficients (discussion), 160
    line of action, side lift, 162
    sensitivity to height/incidence, 168
    side lift, 160, 162-163
    terminology of (ambiguity in), 160
  and load transfer, 269-271
    see also Load transfer
  Mach number
    corrections for model tests, 156
  model tests
    force coefficient adjustment for, 156
    Mach number corrections for, 156
    Prandtl's correction, 156
    Reynolds numbers for, 156
  pitch
    pitch coefficients, 160, 169*t*
    pitch moment, 159-160, 163
  primary aerodynamics
    introduction, 391
    aerodynamic drag, 393
    aerodynamic side force, 395
    aerodynamic yaw moment, 395, 396
    attitude gradient, change in, 393, 396
    body shape, importance of, 396
    cornering force (ellipse model), 394
    cornering stiffness, change in, 394

Aerodynamics (continued)
  primary aerodynamics (continued)
    cornering stiffness (normalized), 392-393
    front cornering compliance, change in, 393
    front lift, 392-393
    primary aerodynamic effects (table of), 392*t*
    tire slip angles, counteracting, 395
    traction coefficient, 394
    understeer gradient, change in, 393, 395, 396
    vertical reaction force, 394
    see also final aerodynamics *(above)*
  Reynolds number
    and boundary-layer thickness (on wings), 157
    and edge flow separation, 157
    for model tests, 156
    variation of, 156-157
  roll
    aerodynamic roll moment, 163, 169*t*
    aerodynamic roll moment coefficient, 159-160, 170
  side force
    aerodynamic, expression for, 163-164
    coefficients for, 161, 169*t*
  specifications, car, 510*t*
  spoilers, 165, 174-175
  wheelbase (as reference length), 160-161
  wind
    aerodynamic side force, 415
    aerodynamic yaw moment, 415
    attitude angle, change in, 416
    axle forces (f,r), 415
    crosswind steer correction, 416, 483
    in open-loop testing, 56
    transient wind effects (unsteady-state handling), 479
    vehicle/wind vectors, notation for, 157, 158*f*
    wind testing (vehicle), 481
    see also Atmospherics (wind)
  wind speed
    see under Atmospherics
  yaw
    aerodynamic yaw angle, 164, 170
    aerodynamic yaw moment (in primary handling), 395, 396
    discussion of, 169-170
    yaw coefficients, 161, 164
    yaw moment, 163, 164, 169*t*, 170
  see also Atmospherics; Downforce; Wings
Alfa-Romeo T-bar, 191, 192*f*, 202

Aligning torque. *See* Self-aligning torque
Angular rotations, vehicle (yaw, pitch, roll)
  vehicle-fixed axis systems, 8-11, 9*f*
  see also Body inertia; Roll, body; Roll centers
Angular velocities, vehicle
  vehicle-fixed axis systems, 9*f*, 11-12
Anti-dive/anti-squat, 272-273, 273*ft*, 275
Anti-rise/anti-lift, 273*t*, 275
Anti-roll bars
  and body stiffness, 15, 16
Aquaplaning. *See* Hydroplaning (aquaplaning)
Aston-Martin linkage, 190, 191*f*
Atmospherics
  introduction, 145-146
  atmosphere, properties of
    air, properties of, 147*t*, 501-504
    standard atmospheres (ISO, etc.), 146
  density, dry air
    and perfect gas equation, 148
    vs. temperature/pressure, 148-149
    variation with altitude, 149-150
  gas equation (perfect), 148
  turbulent airflow
    in atmospheric boundary layer, 153
    spatial variations/discontinuities in, 153-154
    turbulent intensity, 152
    vortex shedding, 153
  water
    rain/snow, effects of, 150
    water substance, properties of, 132*t*, 148*t*
    water vapor (humidity), effect of, 146-148
  wind
    introduction, 150-151
    ambient, measurement of, 157
    atmospheric boundary layer, 151
    geostrophic, 151
    gusty crosswinds, handling criteria for, 483
    vehicle/wind force vectors, 157-158, 158*f*
    wind gusts, response to, 157
    wind testing (vehicle), 481
  wind speed
    high, probability of (Weibull equation), 152
    ISO 4138 test limits for, 57
    probability distribution of, 152, 153*f*
    sustained *vs.* height, 151
  see also Aerodynamics

Attitude
  attitude angle
    aerodynamic, 269
    in banking, 408
    in 2-dof model (vehicle-fixed axes), 445
    and load transfer, 374, 378
    and tire nonlinearity, 377
    and turning geometry, 295
    and wind, 416
  attitude gradient
    aerodynamic effects on, 393, 396
    and aligning torque, 373
    and axle roll angle, 375-376
    and camber angle (primary handling), 374-375
    change in (primary aerodynamics), 393, 396
    and cornering load transfer (four-wheel model), 373-374
    effects of roll understeer on, 370-371
    factors affecting (primary handling), 365
    factors affecting (secondary handling), 377
    and load transfer, 374-375
    sensitivity to G position, 369
    and tire cornering stiffness, 369-370
    and toe angle, 374-375
  see also Primary handling; Secondary handling; Final handling
Axis systems
  earth-fixed
    introduction, 7-8, 9*f*
    notational conventions for, 8, 9*f*
    vehicle free-body diagram (2-dof), 449*f*
  tire. *See under* Tire forces
  vehicle-fixed
    acceleration components, 10-11, 11*f*
    angular rotations (yaw, pitch, roll), 9*f*, 9-10
    angular velocities, 9*f*, 11-12
    course angle, defined, 9*f*, 11
    notational conventions for, 8, 9*f*
    sprung-mass moment, 263, 264*f*
    translational velocities, 9*f*, 10
    vehicle free-body diagram (2-dof), 446*f*
    vehicle load transfer model, 264*f*
  see also Free-body diagrams; Vehicle forces, elements of

Baffling, fluid load, 31
Baker Electric Torpedo, 171
Balance, wheel

  static *vs.* dynamic, 44, 45*f*
Banking
  introduction, 407
  attitude angle, 408
  extreme banking (super elevation), 409, 410*f*
  maximum speed, 409-410
  required steer angle, 408
  side force, effect of (at G), 407, 408*f*
  tire cornering stiffness, 409
  understeer *vs.* oversteer, 407, 408*f*
"Belt-snubber" damper (Foster), 212
Benz
  steering wheel, introduction of, 284
Bicycle models
  cornering force free-body diagrams
    front drive, 344*f*
    no drive, 343*f*
    rear drive, 343*f*
  cornering stiffness, steady-state
    bicycle model (with steer angle), 351-352, 352*f*
    bicycle model (with yaw angle), 352, 353*f*
    bicycle model (with yaw speed), 354-355, 355*f*
  1-dof sideslip model, 437, 438*f*
  in steady-state handling
    basic handling curve, bicycle model for, 336*f*, 339*f*
    non-equilibrium conditions for, 336
    slip angle/steer angle, geometry of, 339*f*
    with suspension effects, 366-367, 367*f*
BNP (Bakker-Nyborg-Pacejka) model
  for wet surfaces, 137
Body inertia
  introduction, 17
  center of mass
    empirical determination of (discussion), 18-19, 19*f*
    fuel loads, effect of, 30-31
    general expression for, 17*e*
    lateral position, determining, 19, 19*f*
    load cells, use of, 20
    load shifting, effects of, 17, 21, 31
    longitudinal position, determining, 19, 19*f*
    vertical position, determining, 19*f*, 20-21, 21*f*, 22*f*
  mass, second moment of
    general expression for, 17
    of uniform rectangular solid, 18
  mass, unsprung
    determination of, 21-22, 221

    and suspension system components, 221-222, 222*t*
    see also Sprung/unsprung mass
  mass height, sprung center of, 23-24
  pitch moment
    cradle inertia, determining, 27-28
    pendulum natural frequency, 27
    pitch dynamic index, 29
    pitch inertia, 27, 29
  roll. *See* Roll, body
  yaw moment
    introduction, 24
    aerodynamic, 163, 164, 169*t*, 170
    aerodynamic (in primary handling), 395, 396
    constrained vehicle, pendulum natural frequency, 26-27
    $I_{XZ,}$ determining, 28
    pendulum techniques, structural considerations for, 26
    use in determining pitch second moment, 28
    using quadrifilar pendulum, 25-26
    using trifilar pendulum, 24-25, 25*f*
    yaw dynamic index, 28-29
    yaw moment equations (step-steer, 2-dof), 469-470
    yaw radius of gyration, 28
    see also Yaw
Body stiffness
  and anti-roll bars, 15, 16
  high stiffness, desirability of, 15
  and load transfer, 269
  monocoque *vs.* chassis/body construction, 16
  vs. suspension performance, 15
  torsional stiffness/compliance, 16
Boundary-layer thickness
  and Reynolds number (on wings), 157
Braking
  contact patch (non-sliding braking), 127
  friction *vs.* sliding speed (locked-wheel), 105*f*
  longitudinal force braking torque, 127
  pitch braking force, 274
  pitch vertical force braking transfer factor, 278
"Brush" model (tire), 127-129, 128*f*
Bump and heave
  definitions/derivations
    bump, 226
    damper motion ratio, 226
    damping coefficient (at wheel), 227
    force center (of links), 233, 233*f*
    heave (bounce), 226

    motion ratio (link ratio), 226
    negative swing arm, 229
    quadratic stiffness factor, 231
    rebound, 226
    ride, 226
    ride bump clearance, 230
    ride droop (rebound) clearance, 230
    scrub rate, 228-229
    spring wheel force, 230
    stiffness at bump, 232
    suspension bump deflection, 230
    wheel rate (suspension rate), 226, 227
  double wishbone system
    force resolution, 222-234, 233*f*
    motion of, 228-229, 229*f*
  heave springing (Z-bar), 211
  Macpherson struts
    centro E of, 229
    force center for, 233
  suspension deflection *vs.* vertical force, 230-232, 231*f*
  see also Bump steer/roll steer; Ride height
Bump steer/roll steer
  accurate steering, importance of, 300
  bump steer
    defined, 296
    bump camber angle, 298
    bump camber coefficient, symbol conventions for, 298
    bump steer angle, 296
    bump steer coefficient, 296
    bump steer gradient, 298
    bump steer graph, 300-301, 301*f*
    bump steer variation (car-to-car), 302
    camber angles (from suspension bumps), 298
    complete wheel angle (large suspension deflection), 301
    suspension bump, 296
    vs. toe angle, 300-301, 301*f*
    twin wishbone, bump steer coefficients for, 299-300, 300*f*
  camber angles (with suspension bumps and roll), 298
  double bump steer (heave, no roll)
    bump steer angles, 304
    double bump steer coefficients, 305
    mean double bump steer angle, 304
    roll steer gradient, 305
    suspension bumps (L, R), 304
  double bump steer (heave and roll)
    introduction, 302

Bump steer/roll steer (continued)
  double bump steer (continued)
    axle roll steer angle, 303
    bump steer angles, 302, 303
    equivalent mean roll steer angle, 303
    quadratic roll toe coefficient, 304
    roll steer coefficients, 303
    suspension bump values, 302, 303
    unequal tie-rod lengths, effect of, 304
  ideal pivot center/link length, determining, 305
  independent suspension, advantages of, 300
  leaf springs in (solid axles)
    discussion, 307
    critical steering link, 307-308
    early Hotchkiss axles, 307
    steered leaf-spring axles, geometry of, 307, 307*f*
    unsprung steering box, 308
  rear solid axles (link located)
    introduction, 305-306
    roll steer angle, 306
    roll steer coefficient *vs.* axle load, 306
    roll understeer angle, 306
    roll understeer coefficient, 306
  rear solid axles (longitudinal leaf spring)
    discussion, 307-308
    early Hotchkiss axles, 307
    geometry of, 307*f*
    steering linkage, critical, 307-308
  roll steer
    defined, 234
    axle roll steer angle, 303
    double bump (roll/heave) steer, 302-303
    mean inclination angle, 299
    Olley work on (GM, 1931), 3
    roll camber coefficient, notation for, 298
    roll camber gradient, 298
    roll steer angle, 296-297
    roll steer coefficient, 296
    roll understeer angle, sign conventions for, 297
    roll understeer coefficient, sign conventions for, 297
    roll understeer gradient, 297-298
    solid axle, camber in roll of, 299
  steer/camber coefficients, list of, 309
  toe-in
    bump steer *vs.* toe angle, 300-301, 301*f*
    static (at rear), 308-309

    - and tire wear, 309
    - variation with load, 302
  - trailing arms, bump steer in, 305
  - trailing twist rear axle, 307
  - understeer/oversteer, balancing, 307

- Caille
  - parallel-piston damper development, 212
- Camber
  - in bump steer
    - bump camber angle, 298
    - bump camber coefficient, symbol conventions for, 298
    - bump camber/roll camber coefficients (relationship), 299
    - camber angles (from suspension bumps), 298
  - camber angle
    - and attitude gradient (primary handling), 374-375
    - defined, 77-79*f*, 106
    - typical, 107
  - camber coefficients
    - bump camber coefficients, symbol conventions for, 107-108
    - roll camber coefficient, 298
    - roll camber/bump camber coefficients (relationship), 299
    - *see also* camber stiffness coefficient *(below)*
  - camber deflection
    - of tires (camber distortion), 106*f*
    - of wheels, 45-46
  - camber force, defined, 78, 78*f*, 107
  - camber parameters, summary of, 109
  - camber stiffness
    - defined, 107
    - and lateral force, 107, 109
    - *see also* camber stiffness coefficient *(below)*
  - camber stiffness coefficient
    - defined, 107, 109
    - camber aligning stiffness, 116
    - camber stiffness at large camber angles, 108
    - and design load, 116
    - and lateral force, 107-108
    - in radial-ply motorcycle tires, 107
    - typical values (bias-ply *vs.* radial-ply), 107, 114
  - camber thrust (obsolete), 77, 107
  - conicity (pseudo camber), 112
  - and cornering force
    - camber angle/tire crown, effect of, 118-119
  - and lateral force

Camber (continued)
  and lateral force (continued)
    camber stiffness, 107, 109
    camber stiffness coefficient, 107-108
    conicity (pseudo-camber), 112
    lateral force as camber force, 78, 78*f*
    lateral force *vs.* camber angle, 107, 386
  and path curvature effects, 108-109
  pseudo-camber (conicity), 112
  road camber, spectral analysis of, 51-52
  in roll steer
    roll camber coefficient, 298
    roll camber gradient, 298
    roll camber/bump camber coefficients (relationship), 299
    solid axle, camber in roll of, 299
  and steering geometry
    camber angle (from steer angle), 286, 288
    quadratic steer camber coefficient, 286
    steer camber coefficient, 286
Carbon black
  in tires, 73-74
Caster. *See under* Steering
Center of mass. *See under* Body inertia
Central force
  central/drag force ratio, 100
  defined, 80, 81*f*
  geometry of, 98*f*
  vs. slip angle, 97, 99*f*
Centrifugal force
  as compensation (d'Alembert) force, 14
Centripetal acceleration. *See under* Acceleration
Centro (instantaneous center)
  defined, 183
  in double-wishbone suspensions, 228-229
  properties of, 184
  see also Suspension components
Chapman
  driveshaft as suspension link (Lotus), 221
Chassis/body construction
  torsional stiffness of, 16
Coil springs, 205-206, 208
Collisions
  mean free path between, 47
Compliance
  body torsional stiffness/compliance, 16
  compliance oversteer

      introduction of, 310
      side force (leaf-spring rear axles), 314
      side force (solid axle/Panhard rod), 313
      side force (trailing twist axles), 313-314
      side force (Weissach axle), 312
      trailing twist axles, side force oversteer in, 313-314, 314*f*
   compliance steer
      introduction, 309
      bushes, effects of, 311, 314, 314*f*
      caster angle, compliant changes in, 310
      compliance camber angles, 310
      compliance steer angles, 310
      compliance steer gradients, 310
      effects of, 310
      lift-off tuck-in, 311
      with longitudinal leaf springs, 314
      on low-friction surfaces, 315
      in Panhard rod (track rod), 312-313, 313*f*
      and passenger vehicle handling, 311
      in semi-trailing arm suspension, 311, 311*f*
      shear center, location of, 315
      side force steer, 312-315
      solid rear axles, disadvantages of, 313
      solid rear axles, Panhard rod in, 312-313, 313*f*
      steering geometry dominant compliance, 289
      steering-column angular compliance and self-aligning torque, 290
      steering-column compliance (understeer gradient), 372
      symbol conventions for, 310
      vehicle steering, effects of, 314-315
      Weissach axle, 312, 312*f*
   compliant link suspension systems. *See under* Suspension components
   cornering
      cornering compliance, front (primary aerodynamics), 393
      cornering compliance (rear) and vehicle loads, 413
      front cornering compliance, change in (aerodynamic), 393
   tire compliance and load transfer (four-wheel), 269
   understeer
      compliance steer side force (front axle), 314
      compliance understeer gradient, 310
      steering-column compliance (understeer gradient), 372
Compliant link suspension systems. *See under* Suspension components
Conicity (pseudo camber)
   introduction, 112
Control
   introduction, 6-7
   control gains, definitions for (nonlinear theory), 360

- driver-vehicle system block diagram, 7, 8*f*

Cords, tire, 69

Cornering
- related terms:
  - Aerodynamics
  - Camber
  - Compliance
  - Cornering force
  - Cornering stiffness
  - Final handling
  - Lateral force
  - Primary handling
  - Secondary handling
  - Slip angle
  - Steady-state handling
  - Suspension components
  - Suspension stiffness
  - Tire forces
  - Unsteady-state handling

Cornering force
- defined, 78, 79
- cornering force coefficient
  - *vs.* road surface temperature, 119
  - *vs.* slip angle, 97, 98*f*
  - *vs.* vertical load, 119, 120*f*
  - on wet surfaces, 133-134
- cornering force curve (Evans), 3, 5*f*
- cornering in vehicle tests, 56, 480-481
- cornering performance envelope, 35, 36*f*
- effect on lateral load transfer, 100
- ellipse model (and primary aerodynamics), 394
- free-body diagrams (bicycle model)
  - front drive, 344*f*
  - no drive, 343*f*
  - rear drive, 343*f*
- at large lateral acceleration
  - force roll center, locating, 248, 249*f*
  - ideal spring model, force geometry of, 247-248, 249*f*
  - jacking force, 248, 249*f*, 251, 251*f*
  - kinematic roll center, locating, 248, 249*f*
- and lateral force, 78, 79, 81*f*
- maximum
  - camber angle/tire crown, effect of, 118-119
  - rubber hardness, effect of, 118-119
  - *vs.* slip angle, 97, 98*f*
  - tire speed, effect of, 121-122

    vs. vertical load, 119, 120
  in steady-state handling
    introduction, 342
    bicycle model, geometry of, 336*f*
    free-body diagrams for, 343-344*f*
    steer angle, 342
  and tire footprint/friction, 106, 118-119, 121
  and vertical stiffness, 83
  see also Cornering stiffness; Lateral force
Cornering stiffness
  defined, 95, 98*f*
  on banked roads, 409
  cornering in vehicle tests, 56, 480-481
  cornering performance envelope, 35, 36*f*
  cornering stiffness coefficient, 95-97, 98*f*
  deadband in ("wide center" feel), 112
  high, advantages of, 100
  at large camber angles, 108
  measurement of, 111-115
  in primary aerodynamics, 394
  in steady-state handling
    bicycle model (with steer angle), 351-352, 352*f*
    bicycle model (with yaw angle), 352, 353*f*
    bicycle model (with yaw speed), 354-355, 355*f*
    cornering stiffness coefficients, 355-356, 357
    front wheel force moment, 352
    moments about G, 352-354
    net lateral force (with yaw speed), 354
    side force (in derivative notation), 357
    static margin, 353-354, 356
    total lateral force, 352
    understeer gradient, 356
    yaw damping coefficient, 356, 361
    yaw stiffness, 352-353
    see also Steady-state handling
  tire factors affecting
    bias-ply *vs.* radial-ply, 112, 116
    inflation pressure, 117
    load, 116, 118
    number of plies, 116
    rim width, 117
    section height, 117
    section width, 116
    tire power dissipation, 34-35
    tire-to-tire variability, 112
    tread depth, 118

    tread width/contour, 117
  total cornering stiffness, 35
  on wet surfaces, dynamics of, 135-136
  see also Cornering force; Lateral force
Coulomb friction
  in friction-disc dampers, 213
  in suspension-systems, 219, 220
Course angle
  vehicle-fixed axis systems, 9*f*, 11

Daimler-Benz
  downforce, early work on, 173
d'Alembert forces, 13-14
Dampers
  damper types
    introduction, 211-212
    aeration/foaming, problems with, 215
    "belt-snubber" (Foster), 212, 213
    cooling problems (double-tube type), 214
    Coulomb friction, disadvantages of, 213
    double-tube (telescoping), 214, 214*f*
    friction-disc, 212-213
    historical note, 212
    hydraulic vane, 212, 213
    pressure loss/oil sealing, 215
    single-tube emulsified (telescoping), 213-214, 214*f*
  hydraulic damper characteristics
    introduction, 215
    adjustable dampers, 218
    bump/rebound ratio, 216-217
    damping ratio, 217-218
    force/speed characteristics, 216, 216*f*, 217
    pressurization, advantages of, 215
    surface finish, importance of, 219
    temperature rise, fluid, 218
    valving, 215-216
    variation between makes, 219
    wheel forces, 217
Damping, tire, 83
de Dion axle, 199, 200-201*f*
deCarbon
  gas-pressurized telescopic damper, 212
Deflection, vertical (tire), 82
Degrees-of-freedom. *See under* Unsteady-state handling
Dependent suspension systems. *See under* Suspension components

Differentials
  basic types, 36-37
  characteristics compared, 40, 40*f*
  in four-wheel-drive vehicles, 41
  free (open) differential
    description, 37
    disadvantages of, 37
    speed difference of, 37
  "intelligent" differential
    axle load transfer, 390
    effect on steer angle, 391
    torque allocation in, 388, 390
    tractive forces (inner, outer), 390
    tractive understeer moment, 390
    understeer moment, 391
    understeer number, 391
  limited-slip differential
    applications of, 40-41
    cam-and-pawl type, 39
    clutch type, 39
    cornering breakaway with, 40
    description, 38-39
    disadvantages of, 39-40
  locking differential
    described, 38
    steer effects from, 388
  military vehicles, applications in, 41
  open-center differential, 41
  solid differential
    axle side force increments, 388
    caveats for use on paved roads, 41
    description, 38
    forward tractive forces, 387
    longitudinal slip in, 38
    in military vehicles, 41
    racing applications of, 38
    slip angle increments (f,r), 388
    understeer moment, 387
Disturbance response
  defined, 56
Downforce
  in competition vehicles, 404
  Daimler-Benz work on, 173
  downforce/drag ratio (of wings), 404
  ground-effect (venturi) underbodies, 171, 172*f*, 176, 178
  Hall fan car, 175

- maximum cornering speed downforce (aerodynamic), 398-399, 399*f*
- Mercedes work on, 173
- Porsche work on, 173
- spoilers, 165, 174-175
- suspension requirements of, 177
- and vehicle load (racing cars), 414
- venturi underbodies, advantages of, 404
- *see also* Wings

Drag, aerodynamic. *See under* Aerodynamics

Drag, tire
- aerodynamic, 33
- central/drag force ratio, 100
- cornering (total), 35
- drag force *vs.* slip angle, 97, 99*f*

Drag, vehicle
- total (in secondary handling), 378

Drivers/driver behavior
- car-driver system, introduction to, 52
- design features *vs.* driver "feel," 53-54
- driver behavior *vs.* lateral acceleration, 54, 55*f*
- driver-vehicle system block diagram, 7, 8*f*
- seat design, influence of, 53
- senses, human (and driver responses), 52-53
- test drivers, advantages/disadvantages of, 56, 59
- *see also* Tests

Dunlop-MIRA handling/stability test circuit, 60, 61*f*

Earth-fixed axis system
- introduction, 7-8, 9*f*
- notational conventions for, 8, 9*f*
- vehicle free-body diagram (2-dof), 449*f*

Envirage (slip angle)
- Broulhiet work on, 3

Euler's equations, 12

Evans, R.D.
- cornering force curve, 3, 5*f*
- cornering quotation, 67

Evans linkage, 190*f*

Final handling
- introduction, 379
- axle reaction
  - front axle reaction, normalized, 381
  - G movement, effect of, 381

    - and lateral load transfer, 383
    - and longitudinal load transfer, 384
  - camber angle
    - and lateral tire force, 386
  - final aerodynamics. *See under* Aerodynamics
  - lateral acceleration
    - change (with lateral load transfer), 383-384
    - change (with longitudinal load transfer), 385
    - change (with rolling resistance understeer), 386
    - as critical handling variable, 380
    - mass distribution, effect of, 382
    - maximum (normalized), 3, 382
    - typical range, 379
    - and understeer number, 380
  - lateral force coefficient, maximum, 381
  - load transfer, lateral
    - and acceleration change (f,r), 384-385
    - and axle lateral acceleration, 383
    - effect on understeer number, 384
    - and front load transfer, 383
    - front-wheel standing reaction (no load transfer), 382
    - reaction forces (inner, outer), 383
    - and rolling resistance understeer moment, 386
    - and understeer number, 384
  - load transfer, longitudinal
    - and acceleration change, 385
    - and axle reactions (f,r), 384
    - expression for, 384
    - front load transfer, 385
  - traction coefficient (two-wheel drive), 385
  - understeer
    - final, discussion of, 379
    - *vs.* oversteer, 379
  - understeer number
    - defined, 380
    - factors affecting (table of), 380*t*
    - and lateral acceleration, 380
    - and lateral load transfer, 386
    - and longitudinal load transfer, 385
  - variables affecting, 380
- Flat-run tires
  - divided wheels for, 43
- Footprint, tire
  - contact patch
    - in non-sliding braking, 127
    - with tractive force, 129

    - on wet surfaces, 133, 134
    - and wheel speed, 128
  - and cornering force, 106, 118-119, 121
  - length, typical, 82
  - and rolling resistance, 86
  - sliding/non-sliding *vs.* friction coefficient, 106
- Force control tests, vehicle, 56
- Force roll center
  - at large lateral acceleration, 248, 249*f*
- Forces, tire. *See* Cornering force; Lateral force; Slip angle; Tire forces
- Forces, vehicle. *See* Vehicle forces
- Foster
  - "belt snubber" damper development, 212
- Four-wheel-drive vehicles
  - differentials in, 41
  - secondary handling in, 378
- Free-body diagrams
  - aerodynamic force axes, 161-162*f*
  - banked (super-elevated) corner, 410*f*
  - body-fixed coordinate systems
    - plan view, 13-14, 14*f*
    - rear view, 15, 15*f*
  - car driving uphill, 411*f*
  - for cornering forces (bicycle model)
    - front drive, 344*f*
    - no drive, 343*f*
    - rear drive, 343*f*
  - driven-wheel force vectors, 126*f*
  - Earth-fixed coordinate systems
    - plan view, 13-14, 14*f*
    - rear view, 15, 15*f*
  - of single-axle suspension, 259*f*
  - trailing twist axle, 255*f*
  - for unsteady-state handling
    - 1-dof system, 432*f*
    - 2-dof system (Earth-fixed axes), 449*f*
    - 2-dof system (vehicle-fixed axes), 446*f*
- Friction
  - Coulomb
    - in friction-disc dampers, 213
    - in suspension systems, 219, 220
  - parasitic
    - introduction, 219
    - driven wheels, difficulty with, 220-221
    - driveshaft as suspension link, 221
    - one-wheel total (typical), 219

    - plunge limitation (flexible "doughnut"), 221
    - in rubber snubbers, 220
    - sliding friction, minimizing, 220
    - sources of (general), 219-220
    - from springs, 220
  - surface friction changes (disturbance response), 479
  - tire. *See* Rubber; Tire forces
- Front-drive vehicles
  - cornering force free-body diagram (bicycle model), 344*f*
  - limited-slip differentials in, 41
  - secondary handling in, 378
  - steering disturbance in (aligning moment), 292
  - "wheel fight" in, 40

- Glass fiber
  - in tire construction, 69
- Golden Arrow (Irving), 171, 172*f*
- Gough plot
  - defined, 100, 101*f*
  - and pneumatic trail, 101*f*
  - *see also* Lateral force
- Ground-effect (venturi) underbodies
  - and downforce/drag effects, 404
  - Golden Arrow (Irving), 171, 172*f*
  - Prevost work on, 171, 172*f*
  - in racing cars, 176, 178
  - wind-tunnel tests of, 178
- Gyroscopic effects
  - in suspension components, 223

- Hall, J.
  - downforce wing, use of, 174
  - fan car, introduction of, 175
- Heave. *See* Bump and heave
- Hills. *See under* Steady-state handling
- Historical note, 1-6
- Horock
  - telescopic damper development, 212
- Hotchkiss
  - Hotchkiss axles (bump/roll steer with), 307
  - Hotchkiss drive (on commercial vehicles), 203
- Houdaille
  - vane-type damper development, 212
- Hydroplaning (aquaplaning)

- dynamic hydroplaning number, 134-135
- dynamics of (discussion), 133
- viscous hydroplaning number, 134

Ice
- on road, 52
- and tire friction, 74

Inclination (camber) angle, tire. *See* Camber; Tire forces
Independent suspension systems. *See under* Suspension components
Inertia, body. *See* Body inertia
Inertial (Earth-fixed) axis system (SAE), 7-8, 9*f*
Irving, J.S.
- Golden Arrow, 171, 172*f*

ISO (International Organization for Standards)
- ISO 4138 *Road Vehicles... Test Procedure*
  - discussion of, 418
- proposed tire axis system, 76
- Standard Reference Atmosphere, 146
- wind speed, test limits for (ISO 4138), 57

Jacking force, 248, 249*f*, 251, 251*f*

Kennedy-Arronhold mechanism, 184, 185*f*
Koning, adjustable telescopic damper, 212

Lancia
- hydraulic damper development, 212

Langensperger angle, 292-293
Lateral acceleration
- in basic handling curve
  - influence on understeer/oversteer, 340
  - lateral acceleration gain (linear regime), 349
  - *vs.* slip angle, 338*f*
  - *vs.* steer angle (linear regime), 346*f*
  - *vs.* understeer angle, 338*f*
- cornering (at large accelerations)
  - force roll center, locating, 248, 249*f*
  - ideal spring model, force geometry of, 247-248, 249*f*
  - jacking force, 248, 249*f*, 251, 251*f*
  - kinematic roll center, locating, 248, 249*f*
- and driver behavior, 54, 55*f*
- in final aerodynamics

    limiting, 402, 403
    maximum, 398, 401, 402
  in final handling
    and axle load transfer, 383
    change (with lateral load transfer), 383-384
    change (with longitudinal load transfer), 385
    change (with rolling resistance understeer), 386
    as critical handling variable, 380
    mass distribution, effect of, 382
    typical range, 379
    and understeer number, 380
  on hills, 411
  vs. oscillatory steer frequency (unsteady-state handling), 475*f*, 476
  in steady-state cornering tests, 59-60, 60*f*
  vs. steer angle (understeer), 363, 364*f*
  typical range (in secondary handling), 376
  at vehicle rollover, 260-261
Lateral force
  and camber stiffness, 107, 109
  and camber stiffness coefficient, 108
  and conicity (pseudo-camber), 112
  definitions of
    as camber force, 78, 78*f*, 107
    as cornering (slip-angle) force, 78, 78*f*
    as lateral force, 77*f*, 78, 79*f*, 80, 81*f*
  in elastic foundation model
    discussion (idealized model), 88
    lateral force concentration, 89
    vs. self-aligning torque (Gough plot), 100, 101*f*
    total force magnitude, 89, 92
  force vector geometry
    in SAE axis system, 77*f*
    in tire forces, 32*f*, 79*f*, 80, 81*f*, 91*f*
  lateral force coefficient
    defined, 94, 97
    and camber stiffness coefficient, 108
    and cornering stiffness coefficient, 108
    exponent model for, 114
    linear model for, 113
    vs. longitudinal force coefficient, 129-130, 130*f*
    non-dimensionalization of, 101, 103
    power model for, 114
    vs. slip angle, 94, 97, 98*f*
    vs. vertical force, 119, 120*f*
  lateral/longitudinal force, combined, 129-131
  and ply-steer (pseudo-slip), 112

  vs. slip angle
    at beginning of sliding, 93-94
    for example values, 94, 96*f*
    factors affecting, 93
    maximum force, 92
    at maximum slip angle, 94
    total force magnitude, 92
    typical values, 96*f*
    at various loads, 122, 123*f*
  and sprung/unsprung masses, 261
  vs. vertical force
    expression for, 119E
    load transfer sensitivity (C_{FT}, C_T), 124*f*, 124-125
    small F_V, computer simulation of, 120*f*
    at various slip angles, 122, 123*f*
    vertical force (load) transfer factor, 125
    vertical force sensitivity (C_{FV}), 122
  see also Camber; Cornering force; Cornering stiffness; Slip angle; Tire forces
Leaf springs. *See under* Springs/springing
Linear handling theory. *See under* Steady-state handling
Load shifting (fluid)
  and body inertia, 17, 21
  and center of mass, 31
  and vehicle rollover, 31
  see also Loads, vehicle
Load transfer
  aerodynamic
    introduction, 269
    aerodynamic attitude angle, 270
    aerodynamic load transfer, 271
    aerodynamic moment (sprung mass), 271
    aerodynamic roll angle, 271
    aerodynamic roll/yaw moments, 270
    aerodynamic side force, 270
  in final aerodynamics, 399
  in final handling. *See under* Final handling
  and path radius, 406
  and roll centers
    incremental load transfer factor, 247
    lateral load transfer (idealized spring model), 242
    lateral load transfer (through suspension links), 241
    link lateral load transfer, 250
    link load transfer (parallel wishbone), 250, 251*f*
    link load transfer (plain trailing arms), 250-251, 251*f*
    load transfer, importance of, 246
    load transfer factor, 242

    load transfer factor, incremental, 247
  and rolling resistance understeer moment, 386
  in single-axle (two-wheel) suspensions
    axle forces, introduction to, 257
    body roll, effect of, 259, 260
    factors affecting, 262
    free-body diagram of, 259*f*
    load transfer, defined, 257
    load transfer, total (and tire vertical force), 258
    moments, sum of, 258
    rollover, lateral acceleration at, 260, 261
    rollover safety factor, 260
    spring position, effects of, 257-258
    and suspension stiffness, 262
    tire lateral force, total, 261
    vertical force transfer factor, 260
    wheel vertical force, 259
  and tire forces
    cornering force and overturning moment, 100
    effect on axle lateral force, 124*f*, 124-125
    load transfer sensitivity (C_{FT}, C_T), 124
    vertical force (load) transfer factor, 125
  and understeer number, 384
  in vehicle (four-wheel) suspensions
    introduction, 263
    and body torsional stiffness, 269
    cornering load transfer, procedure for determining, 268
    diagonal load transfer (from cornering effects), 281
    load transfer effects, 283*t*
    load transfer gradients, 268
    load transfer model, geometry of, 264*f*
    moment distribution factors ($d_{f,r}$), 267
    roll angle (from sprung mass), 265
    roll angle gradient, 265
    roll axis inclination, 268-269, 271
    roll moment (from suspension roll stiffness), 265
    from sprung mass only, 266
    from sprung and unsprung mass, 267
    sprung-mass end forces, 266
    sprung-mass moment, 263, 264
    and tire compliance, 269
    total load transfer (from cornering effects), 281
    from unsprung mass, 267
Loads, vehicle
  introduction, 29-30, 412-413
  and camber stiffness

    camber aligning stiffness, 116
    camber stiffness coefficient, 107, 116
  and cornering compliance (rear), 413
  and cornering force
    cornering aligning coefficient *vs.* load, 116
    cornering force coefficient, 119, 120*f*, 413
    cornering stiffness, 107, 116
    maximum cornering force, 119, 120*f*
  lateral center of mass, effect on, 31
  and lateral force
    lateral force coefficients, 113-114, 115*f*
    vs. load (various slip angles), 122, 123*f*
    vs. slip angle (various loads), 122, 123*f*
  longitudinal center of mass, effect on, 30
  maximum, as fraction of curb weight (cars), 413
  and racing cars
    with aerodynamic downforce, 414
    center of mass, movement of, 415
    fuel loads, 30-31
  understeer number, effect on, 414
  and vertical force changes, 413
  see also Load shifting
Longitudinal force
  braking torque, 127
  "brush" model (foundation stiffness), 127-129, 128*f*
  contact patch
    in non-sliding braking, 127
    with tractive force, 129
    and wheel speed, 128
  drive torque
    defined, 126
  driven wheel, free-body diagram for, 126*f*
  geometry of, 77*f*, 77-78, 80, 81*f*
  longitudinal (braking) strain, 127, 129
  longitudinal force coefficient
    vs. lateral force coefficient, 129-130, 130*f*
  longitudinal slip, 127, 129
  longitudinal/lateral force, combined, 129-131
  rolling radius (effective radius), 82, 127
  SAE notation for, 125-126
Lotus
  driveshaft as suspension link (Chapman), 221
  ground-effect underbody, 176
  Lotus 88, 177

Mach number
  corrections for model tests, 156
Macpherson struts
  and aligning torque, 290
  centro location for, 229
  force center location for, 233, 233*f*
  joint friction in, 244, 245*f*
  as suspension components, 229, 233, 244, 245*f*
Mass, center of. *See under* Body inertia
Mercedes
  downforce, early work on, 173
Milliken, William F., 4
MIRA (Motor Industry Research Association)
  Dunlop-MIRA handling/stability circuit, 60, 61*f*
  roll/slip trolley, 59
  steady-state test pad, 57
  tethered testing, 59
Models, tire. *See under* Tires
Moment method
  moment-method carpet plot, 418-420, 419*f*
Moments and forces, tire. *See* Camber; Cornering force; Lateral force; Slip angle; Tire forces
Monocoque construction
  vs. chassis/body construction, 16
  torsional stiffness of, 16
Monroe
  telescopic damper development, 212
Mumford linkage, 190, 191*f*

Non-dimensionalization
  characteristic slip angle, 101-102
  characteristic slip coefficient, 102
  lateral force coefficient, 101, 103
  self-aligning torque, coefficient of, 104
Nonlinear handling theory. *See under* Steady-state handling
Normal force. *See* Tire forces; Vertical force

Odier
  ISO 4138 test system, 418
Opel Rak, 171
Oversteer
  definitions
    as function of understeer gradient (SAE), 347, 362
    tongue-in-cheek, 362
  on banked roads, 407-408, 408*f*

compliance oversteer
    introduction of, 310
    side force (leaf-spring rear axles), 314
    side force (solid axle/Panhard rod), 313
    side force (trailing twist axles), 313-314
    side force (Weissach axle), 312
    trailing twist axles, side force oversteer in, 313-314, 314*f*
  driver sensitivity to, 483
  early work on, 3-4
  and lateral acceleration (basic handling curve), 340
  oversteer effects (in power steer), 478
  side force (in leaf-spring rear axles), 314
  side force (in solid axle/Panhard rod), 313
  side force (in trailing twist axles), 313-314
  side force (in Weissach axle), 312
  understeer/oversteer, balancing, 307
  see also Steering; Understeer
Overturning moment
  defined, 79*f*
  see also Cornering force; Tire forces
Ownership, car
  Europe/world averages, 46

Panhard rod (track rod)
  compliance steer in, 312-313, 313*f*
  equivalence to Roberts linkage, 189
  equivalence to Watt linkage, 199, 200*f*, 201-202
  geometry of, 186-187, 187*f*
Path curvature
  defined, 108
  path curvature stiffness, 108
  and tire lateral force, 108, 109
Path radius
  critical (in final aerodynamics), 398, 399
  effective toe-in (zero Ackermann factor), 405
  force diagram, four-wheeled vehicle, 406*f*, 406-407
  front slip angle increase, 404
  front tire side force, 404
  lateral load transfer, 406
  steer angle, effect on, 405
  understeer gradient, 405
  understeer number, 406, 407
  vertical force lateral transfer factor (front), 406
Pendulums
  constrained vehicle, pendulum natural frequency, 26-27

  - empirical technique using, 26-27
  - pendulum techniques, structural considerations for, 26
  - quadrifilar, 25-26
  - second moment of mass, empirical determination of, 26-27
  - trifilar, 24-25, 25*f*

Peugot
  - Peugot 405 (wire-frame view), 488*f*

Pitch
  - pitch moment, basics of
    - cradle inertia, determining, 27-28
    - pendulum natural frequency, 27
    - pitch dynamic index, 29
    - pitch inertia, 27, 29
    - use of yaw in determining, 28
  - in suspension performance
    - introduction, 271
    - anti-dive geometry, objections to, 277
    - anti-dive/anti-squat, 272-273, 273*ft*, 275-276
    - anti-rise/anti-lift, 273*t*, 275-276
    - body pitch angle, 272
    - braking force, 274
    - double wishbone, discussion of, 278
    - load transfer moment, longitudinal, 271-272
    - longitudinal load transfer, 274
    - pitch-up, tractive, 277
    - suspension deflection, 277
    - suspension pitch angle, 272
    - suspension pitch stiffness, 272
    - tire pitch stiffness, 272
    - tractive force, 275
    - unsprung pitch angle, 272
    - vehicle deceleration, 274
    - vertical force braking transfer factor, 278
    - vertical force (front axle), 274
    - vertical force longitudinal transfer factor (acceleration), 277
  - in vehicle-fixed axis system, 8, 9*f*, 10-11

Ply steer (pseudo-slip)
  - bias-ply *vs.* radial-ply tires, 112
  - genesis of, 112

Pneumatic trail (moment arm)
  - and Gough plot, 101*f*
  - at large slip angles, 95
  - at small slip angles, 93
  - and steering geometry, 287

Porsche
  - downforce, early work on, 173

Position control
  defined, 56
Position control tests, vehicle, 56
Power dissipation (tire), 33
Prandtl's correction
  for model tests, 156
Prevost
  venturi-shaped underbody, 171
Primary handling
  introduction
    attitude gradient, factors affecting, 365, 376
    bicycle model (with simple suspension), 366, 367*f*
    essential three gradients, 364-365
    roll gradient, factors affecting, 365
    steer angle gradient, 366
    steer angle (road wheels), 366
    suspension geometric steer gradient, 367
    suspension understeer gradient, 366
    tire understeer gradient, 367
    understeer effects (free-differential), 367-368, 368*t*
    understeer gradient, factors affecting, 365-366, 376
  attitude gradient
    aerodynamic effects on, 393, 396
    and aligning torque, 373
    and axle roll angle, 375-376
    and camber angle, 374-375
    and cornering load transfer (four-wheel model), 373-374
    effects of roll on, 370-371
    sensitivity to G position, 369
    and tire cornering stiffness, 369-370
    and toe angle, 374
  primary aerodynamics. *See under* Aerodynamics
  understeer gradient
    and aligning torque, 373
    and camber angle, 375
    and cornering load transfer (four-wheel model), 373-374
    effects of roll on, 370-371
    vs. G position, 369-370
    importance of (*vs.* steer angle), 362
    and steering-column compliance, 372
    suspension (k_{SU}), 366
    tire (k_{TU}), 367
    and toe angle, 375
  see also Steady-state handling
Pseudo-camber (conicity), 112

Radius, tire. *See under* Tires
Rain/snow, effects of, 150
Renault
  hydraulic damper development, 212
Reynolds number
  and boundary-layer thickness (on wings), 157
  and edge flow separation, 157
  in model tests, 156
  variation of, 156-157
Ride height
  introduction, 315
  body height changes (four wheels), 318
  body ride positions, 318
  geometry and force diagram for, 316*f*
  handling analysis, special considerations for, 318
  loaded radius (static/running), 317
  nomenclature conventions for, 315-316
  static positions, expressions for, 316
  suspension (bump) deflection, 317
  suspension deflections, 318
  tire deflection, running, 317
  tire deflection, static, 316
Rim width
  and cornering stiffness, 117
Roadholding
  defined, 7
Roads
  general
    introduction, 46
    area density, worldwide, 46
    basic structure, typical, 47
    cars per kilometer (Europe), 46
    mean free path (between collisions), 47
  handling analysis
    road curvature, effect of, 50, 51, 51*f*
    road factors affecting, 50
    road slope, effect of, 50, 51, 51*f*
    steady-state *vs.* unsteady responses, 50
  spectral analysis of
    introduction, 47-48, 48*f*
    camber, 51-52
    curvature, directional conventions for, 50-51, 51*f*
    plan view *vs.* sectional analysis, 49-50
    roughness, 48, 50
    slope, directional conventions for, 50-51, 51*f*

    - undulations, 48, 49, 50
    - wavelengths, significance of, 48
  - surface temperature
    - friction, effect on, 119
  - surface textures
    - controlled road roughness tests, 480-481
    - frictional characteristics, 48, 49, 479
    - ice on road, 52, 119
    - macro/microtexture, 48-49, 49*f*
    - rainfall, drainage of, 51-52
    - roughness, transient effects of, 138, 479
    - surface damage, 51
    - wet roads, influence on, 49
  - wet roads. *See* Wet surfaces, dynamics of
- Roberts straight-line mechanism, 188-189, 189*f*
- Roesch
  - driveshaft as suspension link, 221
- Roll, body
  - definitions/derivations
    - axle roll stiffness, 236*f*
    - roll angle (front, rear, body), 234
    - roll dynamic index, 29
    - roll gradient, 234, 235
    - roll steer, 234
    - suspension roll (SAE), 234
    - suspension roll stiffness, 235
  - effective roll stiffness, 236-237
  - roll couple
    - independent suspension, 236
    - *vs.* roll angle, 237*f*, 237-238
    - solid axle, 235-236
    - total vehicle, 235
  - roll moment and sprung mass angular inertia, 29
  - roll vectors (vehicle-fixed axis system), 8, 9*f*, 10, 11
  - *see also* Load transfer; Roll centers; Suspension stiffness
- Roll centers
  - introduction, 238
  - compliant-link
    - introduction, 253
    - idealized leaf-spring, discussion of, 253-254, 354*f*
    - Panhard rod, use of, 254-255
    - trailing twist axle, 255, 255*f*
  - definitions/derivations
    - lateral load transfer, total, 241-242
    - lateral load transfer (through suspension links), 241
    - link lateral load transfer, 250-251, 251*f*

      - load transfer factor, 242
      - roll center height, defined, 239, 241-242
      - roll center height, determining, 246-249, 249*f*, 252
      - roll center height, incremental, 246-247
      - roll center (SAE), 238-239
      - sprung mass moment, 240
      - sprung mass side force, 240
      - unsprung mass side force, 240
      - weight force, total, 240
      - wheel vertical forces, 240
  - experimental determination of
    - body displacement technique, 256
    - errors and problems with, 256-257
  - force roll center, locating, 248, 249*f*
  - independent suspensions (large lateral accelerations)
    - cornering at large acceleration, 247-248, 249*f*
    - force roll center location, 248-249
    - incremental load transfer factor, 247
    - incremental roll center height, 246-247
    - jacking force, 248, 249*f*, 251, 251*f*
    - kinematic roll center location, 248, 249*f*
    - link load transfer (parallel wishbone), 250, 251*f*
    - link load transfer (plain trailing arms), 250-251, 251*f*
    - load transfer, importance of, 246
    - load transfer factor, incremental, 247
    - roll center height, 252
  - independent suspensions (small lateral acceleration)
    - introduction, 242-243
    - double wishbone, 244, 245*f*, 246
    - friction, joint, 244
    - L/R link forces, intersection of, 243-244
    - roll center and forces (rear view), 243*f*
    - semi-trailing arm, 244, 245*f*
    - slider (pillar), 244, 245*f*
    - strut and link (Macpherson), 244, 245*f*
    - swing arm, 244, 245*f*
    - swing axle (true), 244, 245*f*
    - trailing arm (pivot), 244, 245*f*
    - trailing arm (pure), 244, 245*f*
  - kinematic roll center, locating, 248, 249*f*
  - solid-axle
    - general four-link axle, 252-253, 253*f*
  - *see also* Roll, body
- Roll steer. *See under* Steering
- Rolling radius, 82, 127
- Rolling resistance. *See under* Tire forces

Rollover, vehicle
  and fluid load shifting, 31
  lateral acceleration at, 260, 261
  rollover safety factor, 260
Rubber
  carbon black in, 73-74
  coefficient of friction
    adhesive component of, 75
    friction-speed models, 104-105
    on ice, 74
    against rough surfaces, 73, 74*f*, 75, 75*f*
    vs. sliding speed/temperature (against glass), 72-73, 73*f*
    sliding (*vs.* sliding speed), 105*f*
    WLF transformation for, 72, 73, 74*f*
    see also Tire forces (friction)
  density, typical, 72
  hardness (Shore A Durometer), 76
  oil (in tread rubber), 74
  specific thermal capacity, 76
  as spring material, 204
  thermal conductivity, 76
  types of (in tire carcass/tread), 69, 70, 76
  visco-elastic model for, 72, 73*f*

SAE (Society of Automotive Engineers)
  longitudinal force, notation for, 125-126
  SAE J670e *Vehicle Dynamics Terminology,* 521-556
  steady-state, definition for, 331
  suspension roll, defined, 234
  tire axis system, 76-77, 77*f*
  trim, defined, 332
  understeer/oversteer, definitions of, 347, 362
  vehicle axis systems, 7-12, 9*f*, 11*f*
Seat design
  influence on drivers, 53
Secondary handling
  introduction, 376-377
  attitude angle increment
    and load transfer, 378
    and tire nonlinearity, 377
  drag, total vehicle, 378
  front/rear/four-wheel drive, 378
  lateral acceleration (typical range), 376
  lateral load transfer factor, 377-378
  tire nonlinearity and steer angle, 377

  tractive force, 378-379
Self-aligning torque (aligning moment)
  angular compliance, steering-column, 290
  bumpy road, effect of, 292
  driveshaft torque, effect of, 290
  front drive, steering disturbance in, 292
  geometry of, 77*f*, 77-79, 79*f*
  kingpin axis, torque about, 290
  vs. lateral force (Gough plot), 100, 101*f*
  lateral force steer moment, 290
  limited-slip differential, disruptive effects of, 291, 292
  self-aligning moment coefficient, 103
  vs. slip angle, 93, 95, 96*f*
  test drum curvature, effect on, 110
  tire factors affecting, 116-118
  tractive force steer moment, 290-291
  typical torques (medium sedan), 291-292
  vertical force steer moment, 291
  on wet surfaces, 133
  see also Camber; Cornering; Pneumatic trail, Steering; Tire forces
Shock absorbers. *See* Dampers
Skirts
  in Hall fan car, 175
  in venturi-shaped underbodies, 4404
Slip angle
  axes/notation for, 76-77, 77-79*f*
  centerline displacement, geometry of, 90*f*, 91
  vs. central force, 97, 99*f*
  vs. cornering force, 93-94, 96*f*, 97, 98*f*
  vs. drag force, 97, 99*f*
  envirage, Broulhiet work on, 3
  vs. lateral acceleration (basic handling curve), 338*f*
  vs. lateral force coefficient, 94, 97, 98*f*
  non-dimensionalization of, 101-102
  and pneumatic trail, 93
  pseudo-slip (ply-steer), 112
  vs. self-aligning torque, 93-95, 96*f*
  sinusoidal oscillation of, 137
  slip/steer angle geometry (bicycle model), 339*f*
  tire slip angles, counteracting (aerodynamic), 395
  and turning geometry, 292-293, 336*f*, 339*f*
  see also Cornering force; Steady-state handling; Lateral force
Snow/rain, effects of, 150
Specifications, car
  introduction, 507
  aerodynamics, 510*t*

- passenger car parameters, indicative range of, 512-513*t*
- suspension, 508-510*t*
- tires, 510-511*t*
- wheelbase, 508*t*

Spectral analysis
- of roads, 47-48, 48*f*

Speed limitations, tire. *See under* Tires

Springs/springing
- leaf springs
  - bending-moment of, 204-205, 205*f*
  - cantilever (Bugatti) type, 203
  - and compliant-link roll centers, 253-254, 254*f*
  - in compliant-link system, 203, 203*f*
  - critical steering link (solid axles), 307-308
  - in early Hotchkiss axles, 307
  - "elliptic" terminology in, 203
  - and Hotchkiss drive, 203
  - oversteer side force with (rear axles), 314
  - roll/pitch springing in, 210-211
  - in solid axles, discussion of, 307
  - steered leaf-spring axle, geometry of, 307, 307*f*
  - understeer side force with (front axles), 314
  - unsprung steering box (solid axles), 308
- roll/pitch springing
  - introduction, 209
  - anti-roll bar, 209-210, 210*f*
  - heave stiffness, 211
  - longitudinal leaf springs, 210-211
  - pitch stiffness, 211
  - roll stiffness, front/rear distribution of, 211
  - swing-axle, 209, 210*f*
  - Z-bar, 209, 210, 210*f*, 211
  - zero roll-stiffness suspensions, 209, 210*f*
- spring link geometry
  - introduction, 206-207
  - drop links (for torsion bars), 208
  - effective spring rate (coil springs), 208
  - stiffness, secondary contributions to, 208
  - suspension movement, limitations on, 208
  - torsion bars, compound, 207-208
  - wheel motion ratio, 207
  - wheel rate, 207
- spring types
  - introduction, 204
  - coil springs, 205-206
  - leaf springs, 204-205, 205*f*

    - rubber, 204
    - spring media (solid, gas, etc.), 204
    - torsion bar, 205
  - *see also* Sprung/Unsprung mass
- Sprung/unsprung mass
  - introduction, 21-22, 221
  - sprung mass
    - distance from front axle, 23
    - front and rear end masses, 23
    - sprung center of mass height, 23-24
    - sprung/unsprung mass ratio, 222*t*
    - *vs.* suspension type, 222*t*
    - total, 23
    - *see also* Springs/springing
  - and total tire lateral force, 261
  - unsprung mass
    - introduction, 21-22
    - advantages of (rough roads), 221
    - centers of mass height (f,r), 24
    - front and rear combined, 23
    - sprung/unsprung mass ratio, 222*t*
    - total, 22
    - variability (with suspension system), 221-222, 222*t*
    - *see also* Springs/springing
  - in vehicle load transfer analysis
    - introduction, 263
    - and aerodynamic moment, 270
    - geometry of (vehicle-centered), 264*f*
    - sprung end-mass forces, 266
    - sprung end-masses (F,R), 266
    - sprung mass link load transfer, 266
    - sprung-mass moment, 263, 264*f*
    - total load transfer, 267
    - unsprung mass link load transfer, 267
- Stability, defined, 6
- Stanley Rocket, 171
- Steady-state handling
  - introduction
    - defined, 7
    - equilibrium condition, 332
    - steady-state, defined, 331-332
    - transient states, defined, 332
    - trim, SAE definition of, 332
  - on banked roads. *See* Banking
  - basic handling curve
    - and accident avoidance maneuvers, 341

Steady-state handling (continued)
  basic handling curve (continued)
    axle characteristics, 337, 338*f*
    bicycle model for, 336*f*, 339*f*
    and handling tests, 340-341
    kinematic steer angle, 338, 340
    kinematic *vs.* moment methods, 336-337
    lateral acceleration *vs.* slip and understeer angles, 338*f*
    linear *vs.* nonlinear regions, 341
    path radius, 339
    slip angle/steer angle, geometry of, 339*f*
    steer angle, expression for, 335, 337, 338, 339
    understeer angle, 337
    understeer characteristic, 340-341, 341*f*
    understeer slip angle (tire), 337
  basic parameters
    force control, parameters for, 335
    initial acceleration gain, 334
    lateral acceleration, 334
    of motion state, 332
    path curvature/path curvature gain, 333-334
    rear wheel torque, 333
    reference steer angle, 333, 335
    units for (S.I., etc.), 335
    yaw angular speed, 334
    yaw velocity gain, 334
  bicycle model
    geometry of, 336*f*
    non-equilibrium conditions for, 336
  cornering forces in. *See* Cornering force
  cornering stiffness in. *See* Cornering stiffness
  desirable results
    introduction, 420-421
    attitude gradient (attitude angle graph), 421
    passenger-car handling, discussion of, 421-422
    steering angle *vs.* lateral acceleration, 421
  final handling. *See* Final handling
  on hills
    axle reactions, 410
    free-body diagram for (constant speed uphill), 411*f*
    lateral acceleration, 411
    understeer number, 412
    vertical downward compensation (pseudo) force, 412
  linear theory
    characteristic speed, 347-348
    cornering stiffness. *See under* Cornering stiffness

    critical speed, 348
    kinematic (Ackermann) steer angle gradient, 346
    kinematic steer angle, 346, 347
    lateral acceleration gain, 349
    path curvature response gain, 347, 349
    stability factor, 348
    steer angle (at constant speed), 347
    steer angle *vs.* lateral acceleration, 345, 346*f*, 347
    understeer angle, 345
    understeer factor, 348
    understeer gradient, 346, 349-351
    vehicle response factor, 348, 349, 350*f*
    see also Handling, primary regime
  MIRA ride and handling circuit, 60, 61*f*
  MIRA roll/slip trolley, 59
  moment method
    moment-method carpet plot, 418-420, 419*f*
  nonlinear theory
    introduction, 359
    control gains, definitions for, 361
    cornering stiffness (at active slip angles), 361
    critical speed, 360
    response factor, 360
    static margin, 361
    surface plot representation, 361
    understeer gradient, 360, 361
    yaw damping coefficient, 361
  primary handling. *See* Primary handling
  secondary handling. *See* Secondary handling
  trim state, nonlinear
    introduction, 357
    input-output variables, discussion of, 357-358
    three-dimensional graph, typical, 359, 359*f*
  see also Steering; Unsteady-state handling
Steering
  aligning torque. *See* Self-aligning torque
  bump steer. *See* Bump steer/roll steer
  compliance steer
    introduction, 309
    bushes, effects of, 311, 314, 314*f*
    caster angle, compliant changes in, 310
    compliance camber angles, 310
    compliance oversteer, introduction of, 310
    compliance steer angles, 310
    compliance steer gradients, 310
    effects of, 310

Steering (continued)
  compliance steer (continued)
    lift-off tuck-in, 311
    with longitudinal leaf springs, 314
    on low-friction surfaces, 315
    and passenger vehicle handling, 311
    in semi-trailing arm suspension, 311, 311*f*
    shear center, location of, 315
    side force steer, 312-315
    solid rear axles, disadvantages of, 313
    solid rear axles, Panhard rod in, 312-313, 313*f*
    symbol conventions for, 310
    trailing twist axles, side force oversteer in, 313-314, 314*f*
    vehicle steering, effects of, 314-315
    Weissach axle, 312, 312*f*
  Gough plot, 100, 101*f*
  oversteer. *See* Oversteer
  roll steer. *See* Bump steer/roll steer
  static steering torque
    empirical equation for, 289
    mean friction radius, 289-290
  steering geometry
    introduction, 283-284
    bump caster coefficient, 287
    camber angle (from steer angle), 286, 288
    caster angle (*vs.* bump position), 287
    center-point *vs.* centerline steering, 285-286
    compliance, dominant, 289
    efficiency, forward/reverse, 284
    kingpin inclination angle, 286, 287*f*
    kingpin offset, effects of, 286-287, 287*f*
    overall steering ratio (G, G_m), 288
    precision (box *vs.* rack), 285-286
    quadratic steer camber coefficient, 286
    rear-wheel steering, instability of, 284
    reference steer angle, 288-289
    steer camber coefficient, 286
    steering, factors affecting, 284
    steering box system, 284-285, 285*f*
    steering rack system, 285
    steering systems, dynamic complexity of, 289
    steering wheel, introduction of (Benz), 284
    steering-wheel angle gradient, 289
    trail, caster (and kingpin axis), 287
    trail, pneumatic, 287
    truck steering (solid axle), 285, 285*f*

    steering vibration
        early work on, 3
    turning geometry, 118
        introduction, 292
        Ackermann factor, 293
        Ackermann (Langensperger) concept, 293
        Ackermann steer angles, determining, 294
        anti-Ackermann steering, 294
        attitude angle, 295
        full Ackermann (Lunar Rover, London taxi), 293
        geometry of (no lateral acceleration), 294*f*
        kinematic steer angle, 295-296
        Langensperger angle, 292-293
        offtracking, 295-296
        steer angle difference, 293
        tie-rod geometry error, 293
    understeer. *See* Understeer
    in vehicle testing. *See* Tests, vehicle
    "wide center" feel
        cornering stiffness deadband, 112
    see also Steady-state handling; Unsteady-state handling
Stick-free test (aircraft), 56
Stiffness. *See* Body Stiffness; Camber; Cornering stiffness; Suspension stiffness
Suspension components
    introduction, 181-182
    compliant-link systems
        leaf springs, 203, 203*f*
        trailing twist axle, 202, 202*f*, 313-314, 314*f*
    damper types. *see* Dampers
    dependent systems
        introduction, 199
        axle degrees of freedom in, 199, 200-201*f*
        axle lateral location, 201-202
        de Dion axle, 199, 200-201*f*
        torque tube, 199, 201*f*
        types of, 199
        upper/lower links in, 199, 201*f*
    friction, parasitic. *See under* Friction
    gyroscopic effects in, 223
    independent systems
        degrees of freedom (discussion), 194
        directly pivoted carrier, variations of, 196*f*, 197
        driveshaft as suspension link, 221
        five-link independent suspension, 198
        Macpherson strut, 229, 233, 244
        pivot arm (ball-jointed), 194, 196*f*

Suspension components (continued)
  independent systems (continued)
    plunging U-joint (doughnut), 194, 195*f*, 221
    practical link combinations, 196, 197*t*
    radius rod, 194, 195*f*
    rigid trailing arm, 194, 195*f*, 196*f*, 197
    shaft spline, 194, 195*f*
    sliding pivot, 194-196, 195*f*
    spherical ball joint, 194, 195*f*
    swing axle, 196*f*, 197
    torsion link, 195*f*, 196
    torsion link plus rod, 198
    transverse rigid arm, 196*f*, 197
    trunnion, 194, 195*f*
    trunnion/wishbone combination, 197
    universal joint, 194, 195*f*
    wishbone (A-arm). *See below*
  mobility analysis
    introduction, 182-183
  springs. *See* Springs/springing
  straight-line mechanisms
    introduction, 185
    Adex linkage, 191, 191*f*
    Alfa-Romeo T-bar, 191, 192*f*, 202
    Aston-Martin linkage, 190, 191*f*
    equivalent swing arm, 189
    Evans linkage, 190*f*
    Mumford linkage, 190, 191*f*
    Panhard rod (track rod), 186-187, 187*f*
    Roberts straight-line mechanism, 188-189, 189*f*
    simple slider, 185-186, 187*f*
    Tchebichef linkage, 190*f*
    Watt linkage, 187-188, 188*f*, 189*f*
  two-dimensional
    basic 2-D suspensions (slider/pivot), 192, 192*f*
    2-D rod/trunnion suspension, 192-193, 193*f*
    2-D two-rod suspension, 192, 193*f*
    defined, 183
    instantaneous center (centro), 183
    Kennedy-Arronhold mechanism, 184, 185*f*
    perpendicularity, importance of, 183-184
    serial connections (2-dof), 184-185, 186*f*
    sliding *vs.* rotating joints, 184-185
    suspension types, classification of, 193
  wishbone (A arm)
    bump and heave evaluation of, 228-229, 229*f*

    double, tire force analysis of, 232-234, 233*f*
    geometry of, 194, 195-196*f*
    twin, with arm, 197-198, 198*f*
    wishbone/trunnion combination, 197
  see also Suspension stiffness
Suspension stiffness
  definitions/derivations
    axle roll stiffness, 236*f*
    quadratic stiffness factor, 231
    stiffness at bump, 232
    suspension roll stiffness, 235
  downforce, suspension requirements for, 177
  effective roll stiffness, 236-237
  and load transfer
    single-axle, 262
  roll/pitch springing
    heave stiffness, 211
    pitch stiffness, 211
    roll stiffness, front/rear distribution of, 211
    zero roll-stiffness suspensions, 209, 210*f*
  specifications, car, 508-510*t*
  spring link geometry
    stiffness, secondary contributions to, 208
  see also Load transfer; Ride height; Roll, body; Roll centers; Suspension components

"TB" value
  in vehicle tests, 482-483
Tchebichef linkage, 190*f*
Temperature, tire
  carcass temperature/flexing, effect of, 113
  and coefficient of friction
    against glass, 72-73, 73*f*
    road surface temperature, effect of, 119
Terminology
  SAE J670e *Vehicle Dynamics Terminology,* 521-556
Tests, tire. *See under* Tires
Tests, vehicle
  introduction, 416-417
  closed-loop tests
    defined, 55-56
    subjective (test drivers), 56
  constant-radius tests, 417
  constant-speed tests, 417
  desirable results
    introduction, 481-482

    gusty crosswind behavior, 483
    oversteering effects, driver sensitivity to, 483
    racing cars, special considerations for, 483-484
    steer correction, 484
    straight running, 483
    "TB" value, 482-483
    yaw speed effective time constant, 482
  force control, defined, 56
  open-loop tests
    defined, 55-56
    discussion of, 480
    simplicity/usefulness of, 56
    steer input responses, 56
    "stick-free" test (aircraft), 56
  position control, defined, 56
  steady-state tests
    basics of, 56-57
    with constant steer angle and sequenced speeds, 417
    Dunlop-MIRA handling/stability circuit, 60, 61*f*
    instrumentation for, typical, 57-58, 58*t*
    ISO 4138 *Road Vehicles....* test procedure, 418
    lateral acceleration (in cornering), 59-60, 60*f*
    MIRA ride and handling circuit (suspensions), 60
    MIRA roll/slip trolley, 59
    Odier ISO 4138 test system, 418
    transfer function (from random steer input), 59
    wind speed limits (ISO), 57
  test results, correlation difficulties with, 56
  unsteady-state tests
    automated steering wheel control in, 59
    basics of, 56
    controlled road roughness, 480-481
    lane change/chicane/slalom, 56, 481
    open-loop tests, discussion of, 480
    slalom test, 480
    standardization, lack of, 56-57
    steer pulse test, 480
    subjective evaluation, 481
    wind testing, 481
Thrust power requirements
  and tire cornering forces, 33
Tire axes/notation. *See under* Tire forces
Tire forces
  axes/notation for
    ISO system (proposed), 76
    SAE system, 77, 77*f*, 79*f*

central force, 80, 81*f*, 98*f*
drag
  aerodynamic, 33, 34
  as cornering plus rolling resistance, 33
  total cornering drag, 35
footprint
  and cornering force, 106, 118-119, 121
  length, typical, 82
  and rolling resistance, 86
  sliding/non-sliding *vs.* friction coefficient, 106
force vectors
  "tire force," defined, 79, 81*f*
  camber force, 78*f*
  central force, 80, 81*f*, 98*f*
  cornering force, 32*f*, 78*f*, 98*f*
  inclination (camber) angle, 77*f*
  lateral force, 77*f*, 79*f*, 80, 81*f*
  longitudinal force, 77*f*, 79*f*, 81*f*
  moment about contact patch centerpoint, 90
  normal (vertical) force, 77*f*, 79*f*
  overturning moment, 77*f*, 79*f*
  rolling resistance moment, 77*f*, 79*f*
  self-aligning torque (aligning moment), 77*f*, 79*f*
  slip angle, 77*f*, 79*f*
  tractive force, 81*f*
  wheel [drive] torque, 77*f*
  see also Cornering force; Lateral force; Slip angle
friction
  adhesive component, 75
  cornering force, implications for, 106, 118-119
  footprint, dependency on, 106, 121
  friction-speed models, 104-105, 131
  against glass, 72
  on ice, 74, 119
  against rough surfaces, 73, 74*f*, 75, 75*f*
  and self-aligning torque, 119
  vs. sliding speed (locked-wheel), 105*f*
  vs. sliding speed/temperature, 72-73, 73*f*
  speed, dependency on, 106, 121-122
  WLF transformation for, 72, 73, 74*f*
  see also Rubber
power dissipation
  aerodynamic, 33
  at tire, 33, 34
  vs. vehicle speed, 34
and road surface wear, 47

Tire forces (continued)
  rolling resistance
    introduction, 85, 86*f*
    coefficient of, 87
    components of (hysteresis, friction, etc.), 87
    and drag, 33
    and footprint contact pressure, 86
    representations of (with vertical force), 86*f*
    rolling radius (effective radius), 82, 127
    rolling resistance moment, 77*f*, 79*f*
    and shear stress, 86-87
    vs. tire construction, 86
    and Turner number, 85-86
    on wet surfaces, 136
  thrust power requirements, 34
  tire slip parameters, summary of, 99-100
  tractive force
    and final aerodynamics, 401
    in secondary handling, 378-379
    tire, 80, 81*f*
  transients, effects of
    discussion, 138
    road roughness, 138
    slip angle, sinusoidal oscillation of, 137
    slip angle, step change in, 137
    steering angle, ramp input, 137-138
  vertical force. *See* Vertical force
  on wet roads. *See* Wet surfaces, dynamics of
  see also Camber; Lateral force; Slip angle; Tire models
Tire models
  introduction, 87
  "brush" model, 127-129, 128*f*
  displacement graph of, 88, 89*f*
  finite-element techniques for, 88
  foundation-stiffness (elastic) model, 87, 88*f*
  idealized "transparent" model, 88
  lateral force (discussion), 88
  lateral force concentration, 89
  longitudinal displacement *vs.* slip, 127-128, 128*f*
  moment about contact patch centerpoint, 90
  string *vs.* beam models, 87-88, 88*f*
  see also Lateral force; Slip angle
Tire nonlinearity
  in secondary handling
    attitude angle increment, 377
    effect on steer angle, 377

Tires
  introduction, 67-68
  construction
    bead, 68
    belts, reinforcing, 69, 76
    carbon black, mass of (typical), 76
    the carcass, 68-69
    components of (typical), 76
    cords/cord alignment, 69
    cross-section, typical, 70*f*
    crown/crown angle, 69, 71-72, 121
    oil, mass of (typical), 76
    rayon, mass of (typical), 76
    rubber, types of, 69, 70, 76
    steel, mass of (typical), 76
    tread. *See (below)*
    tubed *vs.* tubeless, criteria for choosing, 71
    see also Rubber
  damping, tire, 83
  deflection, vertical, 82
  design criteria, 71-72
  failure modes for, 71, 72
  flat-run, 43
  inflation pressure
    and cornering stiffness, 117, 119
    and footprint pressure, 121
    load dependency of, 71
    and self-aligning torque, 117
    typical, 68
    and vertical stiffness, 82
  loads
    and cornering stiffness, 116, 118
    design load, 71
    load-time duration, importance of, 71
    optimum pressure, load dependency of, 71
    and tire radius, 80, 81, 82
    and vertical stiffness, 82
    see also Loads, vehicle; Load transfer
  models (elastic, foundation stiffness). *See* Tire models
  puncture resistance
    tubed *vs.* tubeless, 71
  radius
    effective, 82, 83
    loaded, 81, 82
    rolling, 82
    unloaded, 80

Tires (continued)
  radius (continued)
    and vertical deflection, 82, 83
    and vertical stiffness, 82-83
  size
    aspect ratio, 70
    cross-section, typical, 70*f*
    section width, 70
    see also radius *(above)*
  specifications, car, 510-511*t*
  speed limitations
    introduction, 83-84
    energy/heat dissipation, 85
    Turner number, 84, 85, 121
    vertical stiffness, effect on, 82-83
    wave speed (tread waves), 84
    wavelength, predicted (tread waves), 84
  test measurements
    introduction, 111-112
    carcass temperature/flexing, effect of, 113
    and cornering stiffness changes, 113
    cylindrical drum *vs.* belt, 112
    drum curvature, effect on self-aligning torque, 110
    new tires, initial changes in, 112
    road tests, 112
    running-in effect, 112-113
    tread wear, influence of, 110-111
  tread construction
    carbon black, 73-74
    oil, 74
    rubber blends in, 76
    tread friction, 69-70, 72-73
    tread patterns, 69
    wear characteristics, 70
  tread depth/wear
    and aligning torque coefficient, 118
    and aligning torque stiffness, 111
    and cornering stiffness, 118
    influence on test measurements, 110-111
    mold sheen, wear of, 110
    and peak side force, 110-111
    and toe-in, 309
    wear characteristics (wear *vs.* grip), 70
  tread rubber
    oil in, 74
    types of, 69, 70, 76

- tread waves, 84
- tread width/contour
  - and cornering stiffness, 117
- Turner number, 84-85, 121
- vertical deflection, 82
- vertical stiffness, 82
  - cornering force, effect of, 83
  - and inflation pressure, 82
  - and load capacity, 82
  - speed, effect of, 82-83
  - tread and sidewalls, effects of, 82
  - typical values, 82
- *see also* Tire forces

Torque-bias differential. *See* Differentials (limited-slip)
Torque-proportioning differential. *See* Differentials (limited-slip)
Torsion bar, 205, 207-208
Track
- effect of on wet surfaces, 133

Track rod. *See* Panhard rod
Tractive force
- effects of (in power steer), 477
- and final aerodynamics, 401
- in secondary handling, 378-379
- tire, 80, 81*f*
- *see also* Tire forces

Transducers
- in test instrumentation, 58

Translational velocities
- vehicle-fixed axis systems, 9*f*, 10

Tread construction. *See under* Tires
Tread wear. *See under* Tires
Trim state, nonlinear
- introduction, 357
- input-output variables, discussion of, 357-358
- three-dimensional graph, typical, 359, 359*f*

Truffault
- friction-disc damper development, 212

Turner number, 84-85, 121
- defined, 84, 85
- and rolling resistance, 85-86

Understeer
- definitions
  - as function of understeer gradient (SAE), 347, 362
  - limit *vs.* normal, 362

Understeer (continued)
  definitions (continued)
    tongue-in-cheek, 362
  on banked roads, 407-408, 408*f*
  compliance steer side force (front axles), 314
  compliance understeer gradient, 310
  early work on, 3-4
  and kinematic (Ackermann) steer angle, 363
  and lateral acceleration
    influence on understeer/oversteer, 340
    vs. steer angle, 363, 364*f*
    vs. understeer angle, 338*f*
  primary understeer effects (free differential), 367-368, 368*t*
  in roll steer
    roll understeer angle, 297
    roll understeer coefficient, 297
    roll understeer gradient, 297-298
    roll understeer (in primary handling), 370-371
  side force understeer, 314
  in solid rear axles (link located), 306
  understeer damping ratio (2-dof free response), 454-455
  understeer gradient
    defined, 362
    in 2-dof improved model, 462
    in final aerodynamics, 406
    in linear handling, 346, 349, 350, 351
    in nonlinear steady-state handling, 360
    and path radius, 405
    in roll steer, 297-298
  understeer gradient (primary handling)
    and aligning torque, 373
    and camber, 375
    effects of roll on, 370-371
    vs. G position, 369-370
    importance of (*vs.* steer angle), 362
    and load transfer, 375-376
    and primary aerodynamics, 393, 395, 396
    and steering-column compliance, 372
    suspension (k_{SU}), 366
    tire (k_{TU}), 367
    and toe-in, 374
  understeer number, final
    in final aerodynamics, 400, 401, 402, 403
    in final handling, 380, 384, 386, 390
    on hills, 412
    and path radius, 406, 407

  - understeer/oversteer
    - balancing, 307
    - *vs.* speed (2-dof free-response model), 442
  - *see also* Oversteer; Steering
- Unsprung mass. *See* Sprung/unsprung mass
- Unsteady-state handling
  - introduction, 431-432
  - defined, 7
  - disturbance response
    - discussion of, 479
    - road roughness effects, 478-479
    - surface friction changes, 479
    - transient wind effects, 479
  - MIRA ride and handling circuit, 60
  - 1-dof sideslip
    - characteristic equation (of free motion), 438
    - forced response (step input), 438-439
    - lateral displacement (step input), 439
    - opposing damping force, 439
    - sideslip model (1-dof), 437, 438*f*
  - 1-dof vibration
    - characteristic equation, 434
    - displacement (actual), 435
    - equations of motion, 434
    - forced response, 435-437
    - magnification ratio, 436*f*, 437
    - possible motions after initial displacement, 433, 433*f*
    - single-degee-of-freedom system diagram, 432*f*
    - undamped natural frequency, 434, 435
  - 1-dof yaw
    - characteristic equation, 441
    - damped natural frequency, 442
    - damping ratio, 442
    - divergence *vs.* convergence of, 442
    - equation of motion, 440
    - oscillatory motion, criteria for, 441-442
    - single-degee-of-freedom yaw model, 440*f*
    - slip angles, 439-440
    - transition speed (damped *vs.* undamped response), 442
    - understeer gradient, 441
    - vehicle cornering stiffness, 440
  - 2-dof (Earth-fixed axes)
    - introduction, 447-448
    - characteristic equations, 450
    - equations of motion, 448-449
    - slip angles, 448

Unsteady-state handling (continued)
  2-dof (Earth-fixed axes) (continued)
    vehicle free-body diagram, 449*f*
  2-dof free response
    characteristic damping speed, 455
    characteristic equations, 450-451
    critical speed (understeer/oversteer), 452
    damped natural frequency, 459-461, 460*f*
    damping ratio (neutral steer), 456
    damping ratio (oversteer), 456-457
    damping ratio (understeer/oversteer), 454-455
    damping ratio *vs.* radius of gyration, 457, 458*f*
    damping ratio *vs.* speed, 457-459, 458*f*
    stability of motion, conditions for, 451-452
    undamped natural frequency, 452-454, 453*f*
    understeer gradient, 451
    yaw damping, criteria for obtaining, 459
    yaw oscillation, dangers of, 459
    yaw sideslip response (wavelength of), 461
  2-dof improved model
    discussion of, 462
    understeer gradient, 462
  2-dof (vehicle-fixed axes)
    introduction, 443
    absolute acceleration (y direction), 444-445
    angles and velocity vectors, 443*f*, 443-444
    attitude angle, 445
    characteristic equations, 447
    equations of motion, 445
    equations of motion (lateral), 446
    force and moment equations, 447
    slip angles, 445
    tire forces, 445-446
    velocity components (at path points), 444*f*
  3-dof model
    introduction, 464
    characteristic equation, 466
    equations of motion, basic, 464-465
    force derivatives (attitude, yaw, roll), 465
    moment derivatives (attitude, yaw, roll), 465
    oscillation, modes of, 467
    steering effects, 466
  oscillatory steer response
    introduction, 472
    lateral acceleration *vs.* steer frequency, 475*f*, 476

    - random steer input tests, 476
    - roll speed *vs.* steer frequency, 474*f*, 476
  - yaw speed *vs.* steer frequency, 472-473, 473*f*
  - power steer
    - introduction, 476
    - and "lift-off tuck-in," 477
    - oversteer effects, 478
    - racing cars, problems with, 478
    - slip angle changes, 477
    - steer angle changes, 478
    - tractive force, effects of, 477
  - stability derivatives (equations of motion), 462-464
  - step-steer response
    - introduction, 467
    - rear slip angle, 469
    - side force equations (2-dof), 469-470
    - sideslip velocity, 468-469
    - transient solutions (oscillatory, neutral steer), 472
    - transient solutions (oscillatory, oversteer), 471
    - transient solutions (oscillatory, understeer), 471
    - yaw moment equations (2-dof), 469-470
    - yaw speed, 468-469
    - yaw speed response (different steer inputs), 467, 468*f*
    - yaw speed response (equal steer inputs), 467, 468*f*
    - yaw speed/steady-state (final) yaw speed, 470-471

- Vehicle forces, elements of
  - introduction, 12-13
  - body-fixed coordinate systems
    - free-body diagram (plan view), 13-14, 14*f*
    - free-body diagram (rear view), 15, 15*f*
    - rotational moments, 9*f*, 9-10
  - compensation (d'Alembert) forces, 13-14
  - Earth-fixed coordinate systems
    - angular velocity vectors, 9*f*, 11-12
    - free-body diagram (plan view), 13-14, 14*f*
    - free-body diagram (rear view), 15, 15*f*
    - translational velocity vectors, 9*f*, 10
  - Euler's equations, 12
  - vector equations for, 12-13
  - *see also* Axis systems; Free-body diagrams
- Vehicle-fixed axis system, 8-11, 9*f*
- Venturi-shaped underbody
  - and downforce/drag effects, 404
  - Golden Arrow (Irving), 171, 172*f*

  Prevost work on, 171, 172*f*
  in racing cars, 176
  wind-tunnel tests of, 178
Vertical force
  defined, 77*f*, 78, 79*f*
  and cornering force
    cornering force, defined, 77*f*, 78, 79*f*
    and cornering stiffness, 114, 115
    and cornering stiffness coefficient, 114, 115*f*
    vs. maximum cornering force, 119, 120*f*
    in steady-state cornering, 32, 32*f*
  downward compensation (pseudo) force, 412
  vs. lateral force
    expression for, 119E
    lateral force coefficient, 119, 120*f*
    load transfer sensitivity (C_{FT}, C_T), 124*f*, 124-125
    small F_V, computer simulation of, 120*f*
    at various slip angles, 122, 123*f*
    vertical force (load) transfer factor, 125
    vertical force sensitivity (C_{FV}), 122
  lateral transfer factor (front), 406
  in suspension performance
    aerodynamic lift force, 281
    aerodynamic load transfer, 281
    braking transfer factor, 278
    diagonal bias, 281
    diagonal load transfer, 281
    driveshaft front load transfer, 282
    driveshaft rear load transfer, 282
    equilibrium equations for, 278-279
    force resolution, double wishbone suspension, 232-234, 233*f*
    front axle, 274
    lateral transfer factors, 283
    longitudinal transfer factor (acceleration), 277
    pitch-up moment, 281-282
    static force (symmetrical *vs.* diagonal bias), 279*f*, 279-280
    vs. suspension deflection, 230-232, 231*f*
    total load transfer, 281
    total load transfer (from cornering effects), 281
    tractive force, 275
    vertical force, cornering (*vs.* load transfer distribution), 280, 280*f*
    vertical force transfer factor, 125
  and vehicle loads, 413
  see also Loads, vehicle; Load transfer

Water
  rain/snow, effects of, 150
  water substance, properties of, 148*t*, 504-505
  see also Wet Surfaces, dynamics of
Watt linkage
  as dependent system, 199, 202
  as straight-line mechanism, 187-188, 188*f*, 189*f*
Waves, tire tread, 84
Wear, tread. *See under* Tires
Weibull equation
  probability of high wind speed, 152
Weissach axle, 312, 312*f*
Wet surfaces, dynamics of
  introduction, 131
  aligning torque (trail), 133
  BNP model for, 137
  cornering force coefficient *vs.* speed, 133-135, 135*f*
  cornering stiffness, 135-136
  dynamic hydroplaning number, 134-135
  empirical models, use of, 136-137
  gross drainage (at low speed), 134
  hydroplaning, dynamics of (discussion), 133
  lateral water flow, 132
  maximum cornering force, 135
  rain/snow, effects of, 150
  rolling resistance, 136
  speed, effect of, 133, 134, 135*f*
  tire action (discussion), 132
  track, effect of, 133
  tread depth, effect of, 133
  viscous hydroplaning number, 134
  water, properties of, 132*t*, 148*t*
Wheels
  introduction, 41
  light-alloy
    general description, 42-43
    modular wheels, 43
  manufacturing imperfections in, 44
  mounting techniques for
    center-lock, 44
    studs, 43-44
  plastic wheels
    deflection/fatigue in, 46
  solid (high speed racing), 43
  spoked (wire wheel), 42
  steel disc

- camber deflection in, 45-46
- flat base *vs.* wide base, 43
- for flat-run tires, 43
- general description, 42
- removable flange, 43

stresses/load distribution in
- bending moments (cornering), 45
- camber deflection, 45-46
- fatigue stresses, 45
- plastic wheels, deflection/fatigue in, 46
- from tire mounting, 44-45

types of, 41-42

wheel balance
- static *vs.* dynamic, 44, 45*f*

Wind. *See* Aerodynamics; Atmospherics

Wings
- Daimler-Benz T80, 173
- downforce/drag ratio, 54, 55*f*
- early tests of (Hall, McLaren), 174
- European adoption of (ca. 1968), 174
- front wings, use of, 177
- induced drag from (final aerodynamics), 404
- maximum achieved downforce, 177
- McLaren Indy car, 175
- on motorcycles, etc., 178
- racing rules limitations of, 177
- Reynolds number *vs.* boundary-layer thickness, 157
- 1970s developments, 175-176
- *see also* Downforce

Wishbone (A-arm)
- as independent system, 194, 195-196*f*, 197-198, 198*f*

WLF transformation
- for rubber friction coefficient, 72, 73, 74*f*

Yaw
- aerodynamic
  - aerodynamic yaw angle, 164, 170
  - discussion of, 169-170
  - yaw coefficients, 161, 164
  - yaw moment, 163, 164, 169*t*, 170
  - yaw moment (in primary handling), 395, 396
- and steady-state cornering stiffness
  - bicycle model (with yaw angle), 352, 353*f*
  - bicycle model (with yaw speed), 354-355, 355*f*
  - net lateral force (with yaw speed), 354

    yaw damping coefficient, 356
    yaw stiffness, 352-353
  in steady-state handling
    yaw angular speed, 334
    yaw damping coefficient (nonlinear), 361
    yaw velocity gain, 334, 349
  in vehicle-fixed axis systems, 8-10, 9*f*
  yaw inertia, determining
    analytic expression for, 17-18
    I_{XZ}, determining, 28
    using quadrifilar pendulum, 25-26
    using trifilar pendulum, 24-25, 25*f*
    yaw dynamic index, 28-29
    yaw radius of gyration, 28
  yaw speed response (step-steer inputs), 467, 468*f*

Z-bar suspension, 209, 210, 210*f*, 211

Tires, Suspension and Handling

Second Edition

John C. Dixon

This book provides detailed coverage of the theory and practice of vehicle cornering and handling. *Tires, Suspension and Handling* contains a great deal of material not available elsewhere including unique information on suspension analysis, understeer/oversteer, bump steer and roll steer, roll centers, limit handling, and aerodynamics.

Chapters cover:

- **Introduction** - includes basic details on the vehicle body, differentials, wheels, roads, drivers, and testing
- **The Tire** - covers tire materials and construction, speed limitations, rolling resistance, extensive analysis of cornering properties, hydroplaning, and longitudinal forces
- **Aerodynamics** - explains atmospheric influences, wind and turbulence, aerodynamic principles and forces, and coefficient values
- **Suspension Components** - describes straight-line mechanisms, independent and dependent systems, axle location, spring types, damper types, and gyroscopic effects
- **Suspension Characteristics** - discusses bump steer, roll steer, compliance steer, roll centers, roll stiffness, jacking, steering, vertical forces, and load transfers
- **Steady-State Handling** - explains cornering forces, linear and nonlinear theory, understeer and oversteer, and extreme handling
- **Unsteady-State Handling** - describes 1, 2, and 3-degree of freedom models, yaw and sideslip behavior, steer response, power steering, and disturbance response

Each chapter ends with a wide selection of problems, offering an ideal review of concepts covered.

Tires, Suspension and Handling is an excellent resource for vehicle designers and engineering students who want to better understand and analyze the numerous factors affecting vehicle handling.

About the author...

Author Dr. John C. Dixon is a senior lecturer at the Open University, U.K. He has researched vehicle dynamics for more than 15 years, publishing numerous papers and articles on his work. One area in particular that he has made significant contributions to is the theory of suspensions and extreme handling. Dixon has been a consultant to many companies and leading racing teams involved in Formula1, Le Mans, International Touring Cars, Indy, and NASCAR.

R-168

040507

ISBN 1-56091-831-4

9 781560 918318